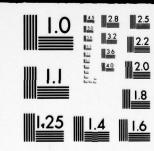


074426



MICROCOPY RESOLUTION TEST CHART



IN-SERVICE IMPROVEMENTS AND MODERNIZATION OF ALL

COMPONENTS OF THE INSTRUMENT LANDING SYSTEMS

VOLUME II - Sections XI and XII

Avionics Engineering Center
Department of Electrical Engineering
Ohio University
Athens, Ohio 45701



JULY 1978

FINAL REPORT

Document is available to the public through the National Technical Information Service Springfield, Virginia 22161

Prepared for

U.S. DEPARTMENT OF TRANSPORTATION FEDERAL AVIATION ADMINISTRATION Systems Research and Development Service Washington, D.C. 20590



A0744

.01

100

DC FILE COPY

NOTICE

This document is disseminated under the sponsorship of the Department of Transportation in the interest of information exchange. The United States Government assumes no liability for the contents or use thereof.

FAA-RD 78-112 2 2	3. Recipient's Catalog No.
N-SERVICE IMPROVEMENTS AND MODERNIZATION OF ALCOMPONENTS OF THE INSTRUMENT LANDING SYSTEMS, YOUME ID SECTIONS XI AND XII.	July 1978 /
7. Author(s) Avionics Engineering Center Staff	8. Performing Organization Report No.
9. Performing Organization Name and Address Avionics Engineering Center / Department of Electrical Engineering Ohio University Athens, Ohio 45701	10. Work Unit No. 11. Contract or Great No. DOT-FA75WA-3549 13. Upe of Report and Pariod Covered
12. Sponsoring Agency Name and Address Department of Transportation Federal Aviation Administration 800 Independence Avenue, S.W. Washington, D.C. 20591	Final Report October 74 - July 14. Sponsoring Agency Code
15. Supplementary Notes	(12) 865.

This final report covering over three-years work on ILS improvement and alternative uses gives results of Ohio University's evaluation of localizer and glide-slope systems emphasizing antenna and monitor performance, terrain effects and the effects of obstructions. Also, details of analyses and flight evaluations of Alford and Hollins localizer systems are provided together with findings during evaluations of the Watts Mark 1, 2, and 3 endfire, glide-slope systems.

Technical results of development and evaluation work on the FAA-suggested techniques for determining range-rate and position during approach using the localizer signal are given.

Non-destructive ILS system fault testing techniques are described, as is a plan for development of an airport systems control/display facility. Further, special devices and techniques for use in ILS field work such as a mini-laboratory for collection of airborne data, digital data collection system, time domain reflectometry, and mathematical modeling to predict localizer and glide slope performance and facilitate setups are discussed.

17. Key Words, ILS, localizer, glide slope, monitor, groundspeed, marker, endfire array, slotted cable, mathematical modeling, terrain effects, flight evaluation 18. Distribution Statement

This document is available to the U.S. public through the National Technical Information Service, Springfield, Virginia 22161.

19. Security Classif. (of this report)

Unclassified

20. Security Classif. (of this page)

Vol. 1 - 598

Vol. 11- 782

21. No. of Pages | 22. Price | Vol. | - 598 |

Form DOT F 1700.7 (0-69)

267 460

1	11231	333	า ใช้ขอมหายหล	£ 28 4 2 5		* # <u># [</u>
	400 M	aquare inches square yards square miles acres	oneces bounds short tons	fluid autores pinta quarts gallona cubic feat cubic yards	Fabranhoit temperatura	<u>.</u>
Maniph by LENGTH	AREA 0.00	, 0.16 1.2 0.4 7) 2.5 MASS (weight)	0.036 2.2 1.1 VOLumin	0.03 2.1 1.06 0.26 35 1.3 TEMPERATURE (exect)	9/5 (then add 32)	0 - 0 - 0 - 0 - 0 - 0 - 0 - 0 - 0 - 0 -
Approximate Conversions from Metric When You Know Multiply by LENGTH	millimeters Continueters meters meters kilometers	square Centimeters square meters square ti (ometers hectares (10,000 m	grams kilograms tonnes (1000 kg)	milititors liters liters liters cubic meters cubic meters	Celsius	0 0 0 0 0 0 0 0 0 0 0 0 0 0 0 0 0 0 0 0
J	1 5 c c 5	F~ £ 2	o 3 -	ǰE°E	ů ů	
22 12 00		91 121 141 151 15	21 11 01 6	8 4 9 5	31 4	
						1 inches
Pirrirri Pirrirri						1 inches
	Continueters Conti	square continuous com square maters millometers millometers millometers to millom	yeans of times of tim	milititers milititers milititers milititers milititers milititers militiers militers	Cotaius ° ° ° ° ° ° ° ° ° ° ° ° ° ° ° ° ° ° °	1 inches
rosartuer : 5 tottgib cibe s ; cr	2.5 continutors cm 2.5 cm		or to the	or yerges you madel-falm s Hawiler richest	(exact) r Colaius no temperatus	1 inches
rotertuer : b lottigilo lothest; cr	inches 12.5 continues 30 contin	equare inches 6.5 square feet 0.09 square yerds 0.5 square miles 2.6 scree 0.4 MASS (vesight)	est bytasto for for on anerty, un	or yerges you madel-falm s Hawiler richest	Cotains	I inches see NBS Misc. Publ. 286, 3.10/286.

TABLE OF CONTENTS

PAS			OLUME 1 - Sections 1 Through	gh X		
60-A			potted their 21 mi votemo	Ref for	Time Donair	PA
(Z-4	list e	of Figures	of ILS System Components			xiv
4-37		f Tables	System runglysis			lxi
12-4	Fore		alysis of RF Combining Bridge	TOR And		lx
4-78	5	omistriA ogo	it Analysis or Fires Office St			
	INTR	ODUCTION	Localizer "DA Study			1-
		Pacifities	gnotures of Commissioned ILS			
	REVI	EW	er 108 Styamers Semples	Loodi	4.65	2-
			ispe TDR Styriature Samples			
AND THE	SUM	MARY		al Conc	19179C	3-
1.5	CEN	ERAL TOPIC	velatio bee for			4-
	GEN	EKAL TOPIC	Lutting ILS Monttoning Sche			4-
5.1.	Α.		iami Airport, Florida, Test Si			4-
	^.	1. Gr	ound Facilities	nivole		4-
4-14				Tortde		4-
M-is			go ingal x		, d	
1-5.	B.	The Mini	ab Airborne Data-Collection	Systems		4-
11-4			rk Minilab) Lil be		4-
1-1-		2. Ma	rk II Minilab			4-
		3. Ma		refore		4-
		enimod?	Introduction	WY WY	49	4-
		b.	Functional Description			4-
al-A		c.	Mechanical Description	a osprv		4-
3 i - h		d.	Specifications .			4-
d=10		e. f.	Antenna Requirements Digital Data Collection Su			4-
de la		1	Digital Data Collection 30	posystem	(0003)	
1-1	c.	Phase-Lo	cked Loop 90 Hz Generator	Commo	.6	4-
4-10			roduction BET			4-
4-16			ic Design			4-
		3. Res	0113	(daga)		4-
al-h			annea Peature	ne in torA	, D	
4-16	D.	The 90-1	50 Hz Phase Measurement Dev	Acces	sion For	1
4		I. Inti	roduction	The second secon	GNA&I	4
(Feel)			cussion Filtering	DDC T	AB A BANK H	4-
		a.		Unann	ounced	4-
		b. c.	Interfacing Phase Detection	Justi	fication	-4
CI-A		c. d.	Amplification and Readout	By	.0	14
CE-D-		e.	Testing	4-5 13-50/8-50	-8	-4
11-0		f./8		STATE OF THE PARTY OF	ibution/	- 4-
				_Avet	ability Codes	
					Avail and/or	
				Dist	special	

4-36
4-37
4-37
4-55
s 4-78
4-106
4-122
4-122
4-132
4-139
4-140
e
4-140
4-140
4-143
4-148
4-150
4-153
4-155
4-156
4-158
4-161
4-161
4-162
4-163
4-163
4-164
4-164
4-165
4-165
4-166
4-169
4-107
4-170
4-170
4-170
4-170
4-173
4-173

\$5-4

			PAGE
		3. The Prototype System Design DAA books to aching heavel	4-17
	+Voice	a. Modification of Standard Marker Beacon Receiver	4-17
79.45		b. Trigger Circuitry	4-17
5-57		c. Flight Evaluation main about 1	4-17
69-5		4. Conclusions staylor A bar Lited 25	4-179
62-3		a. Differential Phase-Measurement System Continuation	4-186
		b. Two-Dimensional Beacon Locator	4-186
50-8		c. Marker Beacon Test Transmitter	4-186
18-6		rating/ successful section, J-art 1	
78-2	His little	Comparison of Common ILS Data Acquired Using a DC-3 and	4 100
		a Beechcraft 35	4-188
		1. Introduction and Summary 2. Background	4-188
1)9-2			4-189
		3. Procedure of Analysis4. Experimental Results	4-190
		5. Conclusions	4-191
	There	I see I be a no Hearth about mered seriford y mountain	T 1/
2-92	1.	References and Bibliography for Section IV	4-20
54-92		notrodection . I	
2-94 \	LOCAL	[1] 10 [2] 11 [10 [2] 12 [2] 12 [2] 12 [2] 12 [2] 12 [2] 12 [2] 12 [2] 13 [2] 13 [2] 14 [2] 15 [2]	5-1
2-94		3. Kesults	
5-134	A.	General another to the second	5-1
5-138	B.	Alford 14-Element Two-Frequency Localizer Systems Tests	5-1
5-136		1. Background restaultants	5-1
5-138		2. Ground-Based Measurements	5-4
		3. Flight Data	5-4
5-143	vesttalic ar	4.elf Conclusions beat beat flowed with a started beat significant.	5-4
Eh i võ	c.	Initial Comparison of Wilcox 14-Element Distribution Unit with	
E&1-0		Alford 12-Element Box	5-14
98.7-2		1. Tests	5-14
941-2		2. Conclusions and Results	5-14
		c Englisher Arroya	
5-155	D.	Final Comparison of Performance of 12-Element V-Ring Array Fed	
)	First with an Alford Distribution Box and Then with a Wilcox	
1-6		Stripline Unit assertant art so owner down systems and agent	5-26
		1. Introduction	5-26
16		2. Discussion of Data allaborated with several and and	5-27
		a. Comments on Data Reduction is about the	5-49
1-5		3. Conclusions becomes and S.	5-54
5-5		3. Avoilable Glide Slaga Mudelt	
H-A	E.	Figure of Merit Analysis for Alford 14/6 Array	5-55
6-12		1. Introduction and assumptions in a transport of the same	5-55
		2. Presentation of Data	5-55
		3. Conclusions	5-57

304

-175

951-

191-

M.

VI

				PAGE
- 1	F.	Inves	tigation of Alford MC 14/6 Two-Frequency Localizer	
	180	Moni	tor Performance Under Attenuation and Phase Fault Condi-	
		tions	b. Taleger Circultre	5-57
		1.	Introduction and thousand the site of the	5-57
		2.	Data and Analysis	5-63
		3.	Tests to Determine Operating Parameters of Equipment	5-63
	G.	Discu	ssion of Total Monitor System Response	5-81
		1.	Pre-Combiner Clearance Monitor	5-81
		2.	Monitor Response to Far-Field Out-of-Tolerance Conditions	5-89
			a. Low Clearance Conditions	5-89
			b. Course Alignment or Course Width Out-of- Tolerance	5-90
		3.	Conclusions	5-90
	н.	1976	Tests of Monitor Performance of the Alford MC 14/6 Two	
			vency Localizer System Under Attenuation and Phase Fault	
		Cond	itions VI national to histography for Section IV.	5-92
		1.	Introduction	5-92
		2.	Data Collection	5-94
		3.	Results	5-94
		4.	Conclusions	5-134
.	ı.	Watt	s-Hollins Small Aperture Slotted-Cable Localizer	5-138
		1.	Introduction	5-138
		2.	Discussion of Data in the Base of the Base	5-138
	J.	Fligh	t Test Results of the Small and Medium Aperture Hollins Slotte	
			e Localizer Antenna Array	5-143
	dish	100	C. Intitut Companion of Wilcows A-Elemen notation	5-143
		2.	Data Collection xxX mand 3-51 band A	5-143
		3.	Results	5-149
		4.	Conclusions attended by and telephone and telephone	5-149
			a. Small Aperture Array	5-149
			b. Medium Aperture Array	5-155
•			NSITIVE MODELING OF ILS SYSTEMS	5-1
	Α.	The (Ohio University ILS Modeling Center	6-1
		1.	Introduction Note Reducti no Introduction	6-1
		2.	Background and industrial and industrial	6-1
		3.	Available Glide Slope Models	6-2
		4.	The Ohio University GTD Glide Slope Model	6-11
			a. Theoretical Background for GTD Model	6-12

Presentation of Date

6-124

45.0

			PAGE				
		b. Ray Geometry for GTD Model	6-16				
		c. Physical Optics and GTD Comparison	6-19				
	5.	OUGSThe Hybrid Glide Slope Program	6-41				
	6.	Localizer Models	6-44				
	7.	Supplemental Data	6-45				
		a. Input Data Format for the OUGS Hybrid Glide					
	RHORE	Slope Terrain Model	6-45				
		b. POSTOUGS Program	6-52				
		c. Mathematical Modeling of Receiver Capture Effect	6-54				
	8.	ILS Modeling Center Facilities	6-69				
	9.	Summary	6-71				
В.	Theo	retical Models Applied to the Kodiak, Alaska Glide Slope	6-71				
Ari	w almone	Airfield Geometry	6-71				
	2.	Calculated Results for Null Reference and Sideband Reference	nce				
		Systems Compared with Flight Measurements	6-72				
	3.	Predicted Results for Possible Future Glide Slape Installation	on				
		at Kodiak	6-79				
	4.	Summary and Conclusions	6-81				
c.	·Valid	Validation of Mathematical Models Using the Kodiak, Alaska					
		A RICE MEAS REMEMBERED ON LOCALIZER SECRETAGOIS OF	6-81				
	1.	Introduction	6-81				
	2.	Results addressed materials A	6-83				
	3.	Data Requirements for Accurate Modeling	6-100				
	4.	Documentation of Data Used in Model Validation	6-103				
		a. Excitation Currents in Antennas	6-103				
		b. Positions of the Radiators	6-104				
		c. Terrain Data 135 - Martin Bernada A 155	6-104				
		d. Aircraft Position Application Application	6-104				
	5.	Summary	6-104				
	6.	Conclusions of economic with to more proceed barranged	6-110				
D.	Math	ematical Prediction of Effects of Hangar Construction on the					
	Denv	ver Stapleton Airport Localizer	6-110				
	1.	Introduction	6-110				
	2.	Results	6-112				
	3.	Summary resitoutered tribility	6-112				
	4.	Conclusions	6-112				
E.		nematical Modeling Applied to Ship Interference with the					
		iam, Washington Localizer	6-116				
	1.	Introduction	6-116				
	2.	Approach and Results	6-116				

July A. 1			PAG
		b. Roy Geometry for GTD Model CD	
61-9		3. Summary and 070 bns with 0 loster!	6-124
6-44		4. Conclusions enals epit a bindy at -42000	6-124
	F.	References for Section VI	6-126
VII	SINGL	E FREQUENCY DISCRIMINATION AGAINST REFLECTIONS	
673.0 - 6 NO - 6	(MULT	D. FOSTOUGS Program (HTAGI	7-1
	A.	General selfill and retrict professory 24	7-1
VIII	SYSTE	M PERFORMANCE STANDARDS	8-1
		S. Theoretical Medals Applied to the Kodiak, Alaska Gligle 3	
	Α.	Proposed Criteria for Classification of Glide Slope Records with	8-1
		Respect to Quality 1. General	3-1
		 General Definition of Classes of Records 	To The A
			8-1
		3. Rationale	8-1
	В.	STI Report	8-4
IX	RANG	E MEASUREMENT FROM LOCALIZER SIGNALS	9-1
	Α.	System Descritpion	9-1
	В.	System Assembly for Concept Demonstration	9-1
601.00	ь.	1. Predicted System Parameters	9-1
		2. Ground Installation	9-4
		3. Airborne Installation - RF	9-8
		4. Airborne Installation - Audio Processor	9-8
101-5			
	C.	Detailed Description of the Airborne Processing Circuitry	9-12
		1. Analog Circuits	9-12
		2. Digital Circuitry	9-12
-111-6		pergeon podres serions served	
	D.	Calibration moltoubortal 1	9-15
6-112	E.	Flight Evaluation	9-19
	F.	Approach Range-Rate and Windspeed: Evaluation and Development	0.25
	n/s	1. General	9-25 9-25
6-116		2. Approach Range-Rate System	9-26
81100		a. Range-Rate System Description	9-26
011-0		b. Initial System Evaluation	9-26
		b. Illindi System Evaluation	9-26
		c. RF-Link Tests	7-20

	TA	BLE OF CONTENTS (CONTINUED)	PAGE
	d.	Individual Module Chackout	9-29
	e.	Preliminary Conclusions from Module Checkout	
		and System Re-Evaluation	9-31
	f.	System Modification and Development	9-31
	g.	Schematics Market American American	9-32
		alog Wind Telemetry System	9-39
	a.	Introduction	9-39
	1 A.A.b.	Ground Installation	9-45
	c.	Airborne Installation	9-45
	d.	Results makey? I show with will be I	9-58
	4. Die	gital Wind Telemetry System	9-58
	a.	Anemometer Transmitter	9-58
	b.	Transmitter Modulator	9-59
	c.	Receiver which has been sent to the sent the sent to t	9-59
	d.	Transmitted Data Format	9-60
	e.	System Schematic Diagrams	9-60
		ta and Discussion	9-60
			0.05
G.	Conclusio	ons and Recommendations	9-85
PROC	ESSING O	FILS FLIGHT DATA	10-1
Α.	General		10-1
~ ·		alog Strip-Chart to Digital Data Translator	10-1
	a.	Introduction	10-1
		Setup and Operating Procedure	10-2
91	c.	Circuit Description	10-5
	d.	Sample Data Sets	10-10
	e.	Recommendations	10-10
	aa. we	The Commence of the American A	10-10
		Perinstance of the contract of	
		VOLUME II - Sections XI and XII	
CHE	E CLORE		
GLIL	E SLOPE		11-1
A.	Compute	er Model for Image Glide Slope Systems	11-1
		eneral 3391 yast shalloulava trigit?	11-1
	2. Th	he Model	11-1
В.	Fault St	udies on a Capture-Effect Glide Slope and Its Computer	
	Model	the second	11-11
	1. In	troduction and Summary	11-11
		nalytical Methods	11-11
		Fround Data	11-12
	4. Pr	reliminary Setup Procedures	11-12
		rror Analysis	11-13
		ness lite	11-15

			PAGE
c.	Eval	uation of Endfire Glide Slope System	11-123
	1.	Introduction and the state of t	11-123
	2.	Watts Mark I System	11-124
		a. Goals matacolyntamal of build palant	11-124
		b. Measurements	11-127
		c. Conclusions Concerning Operation of Mark I	
		Curvi linear System	11-138
	3.	The Watts Mark 2 System	11-138
		a. General	11-138
		b. Data Collection	11-139
		c. Measurements on the Mark 2	11-139
		d. Monitoring of the Watts Mark 2	11-148
	4.	The Mark 3 System Evaluation	11-191
		a. General	11-191
		b. Discussion of Experiments	11-194
		c. Discussion of the Data	11-197
		d. Monitor Investigation for the Mark 3	11-207
		e. Monitor Investigation	11-207
		f. Off-Centerline Path Characteristics for the	X X X
		Mark 3	11-224
		g. Special Tests to Examine Special Characteristics	
		of the Array	11-232
		h. Conclusions Concerning the Mark 3 System	11-239
	5.	Prediction of Performance of the Watts Mark 1 Endfire	207
	٠.	Glide Slope System	11-246
		a. Theory and Analysis of the Effects of Irregular Terrain	
		on Watts Endfire Glide Slope	11-248
		그는 사람들이 많은 사람들이 들어 이렇게 되었다면 하는 것이 살아 아니까 것이 아니라 전혀 들어 없어 사람들이 되었다면 하는데 나를 하는데 하는데 얼마나 없다면 다른데 나를 다 했다.	11-280
			11-200
	6.	Evaluation of the Watts Mark 3 Endfire Glide Slope at	11 205
		Rock Springs, Wyoming	11-285
		a. Introduction b. Background	11-285
			11-285
		c. Flight Evaluation, November 1977	11-285
		d. Flight Evaluation, May 1978	11-297
D.	ILS (Glide Slope Set-Up Measurements Using Thruline Meters	11-321
	1.	General	11-321
	2.	Theory - The A-Ratio	11-321
	3.	Power Measurement - The Thruline Meter	11-322
	4.	Using the Thruline Meter to Set-Up Antenna Current Ratios	11-323
	5.	Experimental Verification of K Equal to 0.80	11-325

1/10	ALE OF CONTENTS (CONTINUED)	PAGE
Monitoring	Tilt of a Null-Reference Glide Slope Mast with	
Near Field	Detectors	11-329
1. Gen	eral and an analysis of the second se	11-329
2. Ana	lysis Documentary Data	11-329
Integral Pa	ath Monitor Test Circuit for Null-Reference Glide Slope	11-339
1. Intro	oduction	11-339
2. Circ	uit Description	11-339
3. Expe	eriment and Results	11-342
4. Con	clusions where the model that	11-342
Effects of	Carrier Sideband Leakage into Sideband Only Signal	
on ILS Gli	de Slope Performance	11-345
		11-345
		11-345
		11-345
Mobile Gl	ide Slope Facility	11-351
On-Site C	Slide Slope Evaluation Activities	11-353
		11-353
		11-353
		11-353
		11-354
		11-355
		11-355
		11-356
		11-356
		11-357
		11-357
		11-357
		11-360
		11-360
	2014 : 과장 및 경우 전에 있는 것이 하고 있다면 하는 것이 없는 것이 없는 것이 없는데 없는데 되었다. 그 사람들은 것이 없는데 없는데 없는데 없는데 없는데 없는데 없는데 없는데 없는데 없다.	11-369
		11-369
n.		11-369
3 Dos	[1] - [1] 전 [1] [1] [1] [1] [1] [1] [1] [1] [1] [1]	11-307
		11-486
		11-486
		11-486
		11-400
Ş.•ic	Systems	11-487
	Monitoring Near Field 1. Gen 2. Ana Integral Po 1. Intro 2. Circ 3. Expe 4. Cone Effects of on ILS Gli 1. Freq 2. Effe and 3. Cone Mobile Gl On-Site Gl 1. Wes a. b. c. d. e. 2. Docc Syst a. b. c. d. e. f. g. h. i. 3. Doc	Monitoring Tilt of a Null-Reference Glide Slope Mast with Near Field Defectors 1. General 2. Analysis Integral Path Monitor Test Circuit for Null-Reference Glide Slope 1. Introduction 2. Circuit Description 3. Experiment and Results 4. Conclusions Effects of Carrier Sideband Leakage into Sideband Only Signal on ILS Glide Slope Performance 1. Frequency Components in Detected SBO + CSB Signals 2. Effect of CSB Leakage into SBO Signal on Null Reference and Capture-Effect Path Width and Symmetry 3. Conclusions Mobile Glide Slope Facility On-Site Glide Slope Facility On-Site Glide Slope Facility On-Site Glide Slope Facility On-Site Glide Slope Evaluation Activities 1. Westinghouse Broadside Glide Slope Array Tests (Lynchburg) a. Mission 1: August 4-6, 1976 b. Mission 2: August 12-13, 1976 c. Mission 3: August 19-20, 1976 d. Mission 4: September 29, 1976 e. Mission 5: October 12, 1976 2. Documentary Flight Data for a Capture Effect Glide Slope System Operating at a Typical Upslope Site (Lawton) a. Introduction b. Glide Slope System Parameters c. Antenna Current Measurements d. Faults e. Terrain Features f. Ground Measurements at the 360° Monitor Point g. Graphical Data Presentation h. Results i. Recommendations 3. Documentary Flight Data for a Capture Effect Glide Slope System Operating at an Unimproved Site a. Introduction b. The Addison System c. Procedures for Probe Measurement Taking on CEGS

			TAGE
		d. Probe Measurement Results	11-488
		e. Terrain and Site Peculiarities	11-489
		f. Data Processing	11-489
		g. Documentary Data	11-492
		h. Comparison of Near-Field Monitor Response	
		with Far-Field Observations	11-492
	4.	Documentary Flight Data for a Capture Effect Glide Slope	
		System Operating with a Truncated Ground Plane (Redbird)	11-531
		a. Optimization	11-531
		b. Perturbational Study	11-540
	5.	Documentary Flight Data for a Capture Effect Glide Slope	11-634
	Lingia y	System Operating with a Two-Level Ground Plane (Columbu	
		a. Introduction	11-634
		b. Equipment	11-634
		c. Procedures for Probe Measurement-Taking on CEGS	
		Systems	11-636
		d. Terrain and Site Peculiarities	11-640
		e. Data Processing	11-640
		f. Documentary Data	11-640
		g. Comparison of Near-Field Alarm Values and Observed	
		For-Field Response	11-641
		Area Company of the State of the State Array Tests	
J.	Mea	surement and Monitoring of Glide Slope Antennas	11-695
	1.	Introduction	11-695
	2.	Relationship Between Radiated Signal and Monitor Port	
		Output	11-695
		a. Single-Element Antennas	11-696
		b. Multi-Element Antennas	11-696
	3.	Recommended Measurement Techniques	11-697
	4.	Hand-Held Probe Performance	11-698
	5.	Development of the Jig-Held Probe	11-703
		a. Probe Placement and Stability	11-703
		b. Experimental Results	11-712
	6.	Far-Field Response to Antenna Currents	11-712
	7.	Multi-Element Antenna Array Radiation Patterns	11- 719
	8.	Antenna Diagnostics	11-725
	9.	Conclusions	11- 72
	10.	Recommendations	11-730
K.	Expe	erimental Investigation of Contemporary Glide Slope Antennas	11-732
	1.	Introduction	11-732
		a. History of Glide Slope Antennas	11-73
		b. History of Signal Sampling for Monitoring	11-73
	2.	Specific Antennos Involved in Tests	11-73

		ASSOCIATE ICI	PAGE
		3. Measurement and Techniques	11-734
		a. Test Range implimed to deprepared to the A	11-734
	2-2	b. Specific Tests	11-735
		4. Matrix of Results	11-738
		a. Baseline Data	11-738
		b. Fault Data on the AIL FA8651	11-752
		5. Correlation of Signal Samples with Monitor Response	11-762
		6. Summary	11-762
		7. Conclusions	11-766
		8. Recommendations	11-767
	L.	Minimum Site Preparation for an Image Glide Slope	11-768
		1. Introduction	11-768
		2. General Case	11-768
		3. Engineering for Minimum Costs	11-769
		a. Reduced Length of Ground Plane	11-772
		b. Reduced Depth of Fill	11-772
		c. Allow Longitudinal Slope of 1 Degree	11- 772
		d. Allow Transverse Slope of 2.5%	11-776
		e. Methods for Additional Cost Savings	11-776
		4. Conclusions	11- 776
		5. Recommendations	11-77
	M.	References for Section XI	11-778
11	INVE	STIGATORS AND ACKNOWLEDGEMENTS	12-1

LIST OF FIGURES

		PAGE
Figure 4-1.	Aerial Photograph of Tamiami Site Prior to Installation of Facilities.	4-2
Figure 4-2.	Ohio University Test Sites - New Tamiami Airport.	4-3
Figure 4-3.	Control Points for ILS Site at New Tamiami Airport, Florida.	4-4
Figure 4-4.	Contour Map, Tamiami, Glide Slope Area.	4-6
Figure 4-5.	Capture-Effect Glide Slope Evaluation Under- way at Tamiami.	4-7
Figure 4-6.	A Ohio University Research Technician Shown Performing Repairs on Monitor Detector at Tamiami, Florida.	4-8
Figure 4-7.	Mark Minilab Showing Typical Aircraft Installation.	4-11
Figure 4-8.	Mark II Minilab Flight Data-Collection Package.	4-11
Figure 4-9.	Mark III Minilab Installed in Beechcraft 35 Bonanza.	4-12
Figure 4-10.	Alarm Panel.	4-13
Figure 4-11.	Mark III Minilab Block Diagram.	4-14
Figure 4-12.	DDCS Block Diagram.	4-18
Figure 4-13.	DDCS Sample CDI Output.	4-19
Figure 4-14.	Analog CDI Test Trace for DDC System.	4-21
Figure 4-15.	PLL 90 Hz Generator.	4-24
Figure 4-16.	Interface Circuit.	4-26
Figure 4-17.	MC 4044P Input/Output Waveforms.	4-28
Figure 4-18.	Plot of Analysis Data.	4-30

		PAGE
Figure 4-19.	Amplification and Readout Circuit.	4-31
Figure 4-20.	Test Circuit Block Diagram.	4-31
Figure 4-21.	Plot of Test Data.	4-33
Figure 4-22.	Schematic of 90-150 Hz Phase Detector.	4-34
Figure 4-23.	Block Diagram, 90-150 Hz Phase Detector.	4-35
Figure 4-24.	Circuit Model for a Short Length of Transmission Line.	4-38
Figure 4–25.	Theoretical TRD Plot of a $50\Omega^{\cdot}$ Line Terminated in 70 Ohms.	4-38
Figure 4-26.	Reflection Diagram for the Quarter-Wave Transformer Matched System.	4-41
Figure 4-27.	TDR Signature and Terminal Voltage Plot for the Quarter-Wave Transformer in Figure 4-26.	4-43
Figure 4-28.	TDR Analysis of Quarter-Wavelength Transformer.	4-44
Figure 4-29.	Graphs Displaying Short, Open, and Properly Terminated 50Ω Cables.	4-45
Figure 4-30.	TDR Graphs Showing Wetted Cable Terminations.	4-46
Figure 4-31.	TDR Graphs Showing Sliced Cables; Dry and Wet.	4-48
Figure 4-32.	Coaxial Cable with Pinhole Fault.	4-49
Figure 4-33.	Corroded Connector Experiment One.	4-50
Figure 4-34.	Corroded Connector Experiment Two.	4-52
Figure 4-35.	Example of Resistive Loss in Cables.	4-54
Figure 4-36.	Capture Effect Glide Slope Antenna and Monitor Cable Traces Obtained at the Tamiami Airport.	4-56

32A1		PAGE
Figure 4-37.	Two Typical Cable Traces Obtained from a Null Reference Glide Slope at Wood County Airport.	4-57
Figure 4–38.	An Example of TDR Analysis of Cable Other than Coaxial.	4-58
Figure 4–39.	Trace of a Glide Path Monitor Cable Used at Tri-State Airport in Huntington, W. Va.	4-59
Figure 4-40.	A Piece of RG-58 (50 Ω) and RG-59 (72 Ω) Cable Spliced Together to Show a Trace of Cables with Different Characteristic Impedances.	4-59
Figure 4-41.	Examples of Cable Faults.	4-60
Figure 4-42.	Tektronic 1502 TDR Measurement of a Sliced Cable Fault.	4-61
Figure 4-43.	Photograph of RF Signal Devices Used in an APCU.	4-63
Figure 4-44.	TDR Signature and Diagram of Test Set-Up for Coaxial Bridge.	4-64
Figure 4-45.	No Fault Bounce Diagram for Bridges of Figures 4–44 and 4–50b.	4-66
Figure 4-46.	TDR Signatures of Faulted Experimental Co- axial Bridge Connections.	4-67
Figure 4-47.	Effect of Shorted Port Connector on TDR Pulse Transmission.	4-68
Figure 4-48.	J2 Open Fault Bounce Diagram for Bridges of Figures 4–46a and 4–50b.	4-70
Figure 4-49.	Shorted Bounce Diagram for Bridges of Figures 4–46b and 4–51c.	4-71
Figure 4-50.	TDR Signature of a Coaxial Bridge on Sideband Input to a Localizer Distribution System.	4-72
00-4		

		PAGE
Figure 4-51.	TDR Signatures of Scanwell Model 110 Bridge.	4-73
Figure 4-52.	TDR Signature and Diagram of Test Set-Up for Scanwell SX-28 Bridge.	4-74
Figure 4-53.	No Fault Bounce Diagram for Scanwell SX-28 Bridge.	4-76
Figure 4-54.	Signatures of Faulted SX-28 Bridge Connections.	4-77
Figure 4-55.	Detailed Diagram of the FA-8976 and Bent Dipole Type Antennas.	4-79
Figure 4-56.	Detailed Diagram of FA-8730 Antenna.	4-80
Figure 4-57.	TDR and TDR Recording of a Scanwell Model 110 Bridge.	4-81
Figure 4-58.	TDR and TDR Chart Recording of the Communications Antenna Shown.	4-82
Figure 4-59.	Probe Measurements of a Scanwell FA-8730 Glide Slope Antenna.	4-83
Figure 4-60.	TDR Antenna Signature Test.	4-86
Figure 4-61.	TDR Pulse Degradation Due to Line Loss.	4-86
Figure 4-62.	Antenna FA-8976 TDR Antenna Signatures of Different Cable Lengths Between TDR and Antenna.	.9%-A 2518 .08-1 4-88
Figure 4-63.	Antenna FA-8976 with Dipoles Individually Opened - Antenna Port Pulsed.	4-89
Figure 4-64.	Antenna FA-8976 with Dipoles Individually Shorted - Antenna Port Pulsed.	4-91
Figure 4-65.	Antenna FA-8976 TDR Signatures – Antenna Port Pulsed.	4-92
Figure 4-66.	FA-8976 Antenna TDR Signatures of Integral Manitor Input Pulsed.	4-93

PAGE		PAGE
Figure 4-67.	Antenna FA-8730 TDR Signatures of Antenna Port with Two Cable Lengths Between TDR and Antenna.	4-95
Figure 4-68.	Bounce Diagram for First Two Feet of TDR Pulse Transmission through the Antenna Port.	4-96
Figure 4-69.	Antenna FA-8730 Antenna Port Pulsed.	4-97
Figure 4-70.	Antenna FA-8730 Antenna Port Pulsed.	4-98
Figure 4-71.	Antenna FA-8730 Antenna Port Pulsed.	4-100
Figure 4-72.	Antenna FA-8730 TDR Signatures of the Inputs of Dipole A1 and J1.	4-101
Figure 4-73.	Antenna FA-8730 TDR Signatures of Integral Manitor Input.	4-104
Figure 4-74.	TDR Signatures of Bent Dipole Type Antenna.	4-105
Figure 4-75.	V-Ring Localizer Antenna Block Diagram.	4-107
Figure 4-76.	V-Ring Localizer Cables.	4-109
Figure 4-77.	V-Ring Antenna Element Construction.	. 4-110
Figure 4-78.	V-Ring Antenna TDR Signature.	. (8-14-11)
Figure 4-79.	Expanded Signature Views of a V-Ring Antenna.	.56-4-112
Figure 4-80.	TDR V–Ring Fault Analysis and Associated VSWR Values.	4-114
Figure 4-81.	V-Ring Antenna 2A(E6), Ohio University Localizer.	4-117
Figure 4-82.	Type FA-8720 V-Ring Monitor Signature and Circuit Diagram.	4-118
Figure 4-83.	V-Ring Localizer APCU Signatures of SB Input (Z3,J1).	4-120

FA-8975 America TDR Signatures of integral

3049		PAGE
Figure 4–84.	V-Ring Localizer APCU Signatures of Power Divider, Z2, Input.	4-123
Figure 4–85.	TDR Signature Example of Traveling Wave Antennas and TWA Monitor.	4-124
Figure 4–86.	Carrier Input for 8-Element TWA Localizer APCU, Raleigh County Airport.	4-127
Figure 4-87.	GRN/27 TWA Localizer Course Antenna Signatures, Detroit Metropolitan Airport.	4-128
Figure 4-88.	Alford Loop Antenna Diagrams.	4-130
Figure 4–89.	Alford Loop Antenna Pair Signatures, Port Columbus Airport.	4-131
Figure 4-90.	Alford Loop Antenna Signatures.	4-133
Figure 4-91.	Glide Slope Antenna Signatures.	4-134
Figure 4-92.	Antenna and Path Monitor Signatures from GRN/27 Glide Slopes.	4-137
Figure 4-93.	O'Hare Runway Map with Monitor Points.	4-141
Figure 4-94.	Future TRACON Configuration at O'Hare.	4-142
Figure 4-95.	Overall System Concept - ASCD.	4-151
Figure 4-96.	Remote Data Processor Block Diagram.	4-154
Figure 4-97.	Configuration for RDP/CP Interface.	4-157
Figure 4-98.	Controller Display When ILS Operating Properly.	4-159
Figure 4-99.	Controller Display After ILS Failure has Occurred.	4-160
Figure 4-100.	Example of Maintenance Feature.	4-167
Figure 4-101.	A.C. Measurements Using High-Speed Sample Capability.	4-168

		PAGE
Figure 4-102.	ILS Middle Marker Beacon Flight Geometry.	4-171
Figure 4-103.	Horizontal Radiation Patterns Obtained from an ILS Marker.	4-172
Figure 4-104.	Simultaneous-Phase-Comparison Radar.	4-174
Figure 4-105.	Differential Phase System.	4-176
Figure 4-106.	Developmental Model - Differential Phase Marker Beacon Locator.	4-177
Figure 4-107.	Differential Phase System - Trigger Circuitry.	4-178
Figure 4-108.	Flight Test #7.	4-180
Figure 4-109.	Flight Test /8.	4-181
Figure 4-110.	Flight Test #9.	4-182
Figure 4-111.	Calibration Pass: Detailed Phase Plot.	4-183
Figure 4-112.	Phase Shift vs. RF Amplitude KR-21.	4-184
Figure 4-113.	Aircraft Angle of Attack Required for Zero Phase Difference.	4-185
Figure 4-114.	Single-Receiver Marker Locator Concept.	4-187
Figure 5–1.	Schematic of Localizer Distribution System for Alford Two-Frequency Array.	5-2
Figure 5–2.	Recording of CDI Observed During Orbit, 6 Miles Range, Elevation 1500 Feet.	5-8
Figure 5-3.	CDI Crossover of Course Array to 45 Degrees.	5-9
Figure 5-4.	CDI Crossover of Clearance Array to 45 Degrees.	5-10
Figure 5-5.	Data Taken During 6-Mile Orbit, 1500 Feet	0(% 511)

		PAGE
SOAT		
Figure 5-6.	Recording of CDI and Differential Amplifier Output Showing Difference Between CDI and Theodolite	
5-35	Track. Track.	5-12
Figure 5-7.	Recording of CDI and Differential Amplifier Approach to Landing Shown in Previous Figure.	5-13
Figure 5-8.	Broad Alarm - CDI - North to South Runs.	5-15
Figure 5–9.	Broad Alarm - CDi - South to North Runs.	5-16
Figure 5-10.	Broad Alarm - Signal Strength - South to North Runs.	5-17
Figure 5-11.	Broad Alarm - Signal Strength - North to South Runs.	5-18
Figure 5-12.	Antenna Feed Line Electrical Length Test Setup.	5-19
Figure 5-13.	Antenna Element Test Setup.	5-20
Figure 5-14.	Alford 12-Element Test Setup.	5-21
Figure 5-15.	Wilcox 14-Element Test Setup.	5-22
Figure 5-16.	Sideband Test Setup.	5-23
Figure 5-17.	Carrier Test Setup.	5-24
Figure 5-18.	System Normal Test Setup.	5-25
Figure 5-19.	Plot of CDI versus Azimuth, Alford Box, 108.5 MHz.	5-28
Figure 5-20.	Plot of CDI versus Azimuth, Alford Box, 109.7 MHz.	5-29
Figure 5-21.	Plot of CDI versus Azimuth, Alford Box, 111.9 MHz.	5-30
Figure 5-22.	Plot of CDI versus Azimuth, Wilcox Box, 108.5 MHz.	5-31
Figure 5-23.	Plot of CDI versus Azimuth, Wilcox Box, 109.7 MHz.	5-32
Figure 5-24.	Plot of CDI versus Azimuth, Wilcox Box, 111.9 MHz.	5-33
Figure 5-25.	Plot of CDI versus Azimuth, Alford and Wilcox Boxes, 108.5 MHz.	5-34

		PAGE
Figure 5–26.	Plot of CDI versus Azimuth, Alford and Wilcox Boxes, 109.7 MHz.	5-35
Figure 5-27.	Plot of CDI versus Azimuth, Alford and Wilcox Boxes, 111.9 MHz.	5-36
Figure 5-28.	Plot of CDI versus Azimuth, Alford Distribution Box, 108.5 MHz, 109.7 MHz, 111.9 MHz.	5-37
Figure 5-29.	Plot of CDI versus Azimuth, Wilcox Distribution Box, 108.5 MHz, 109.7 MHz, 111.9 MHz.	5–38
Figure 5–30.	Plot of Sideband Signal versus Azimuth, Alford and Wilcox Boxes, 108.5 MHz.	5-39
Figure 5-31.	Plot of Sideband Signal versus Azimuth, Alford and Wilcox Boxes, 109.7 MHz.	5-40
Figure 5-32.	Plot of Sideband Signal versus Azimuth, Alford and Wilcox Boxes, 111.9 MHz.	5-41
Figure 5–33.	Plot of Sideband Signal versus Azimuth, Alford Distribution Box, 108.5 MHz, 109.7 MHz, 111.9 MHz.	5-42
Figure 5–34.	Plot of Sideband Signal versus Azimuth, Wilcox Distribution Box, 108.5 MHz, 109.7 MHz, 111.9 MHz.	5-43
Figure 5-35.	Plot of Carrier Strength versus Azimuth, Alford and Wilcox Boxes, 108.5 MHz.	5-44
Figure 5-36.	Plot of Carrier Strength versus Azimuth, Alford and Wilcox Boxes, 109.7 MHz.	5-45
Figure 5–37.	Plot of Carrier Strength versus Azimuth, Alford and Wilcox Boxes, 111.9 MHz.	5-46
Figure 5-38.	Plot of Carrier Strength versus Azimuth, Alford Distribution Box, 108.5 MHz, 109.7 MHz,	
	111.9 MHz.	5-47

		PAGE
Figure 5–39.	Plot of Carrier Strength versus Azimuth, Wilcox Distribution Box, 108.5 MHz, 109.7 MHz, 111.9 MHz.	5-48
Figure 5-40.	Plot of AGC Derived Signal Strength versus Azimuth, Alford and Wilcox Boxes, 108.5 MHz.	5-51
Figure 5-41.	Plot of AGC Derived Signal Strength versus Azimuth, Alford and Wilcox Boxes, 109.7 MHz.	5-52
Figure 5-42.	Plot of AGC Derived Signal Strength versus Azimuth, Alford and Wilcox Boxes, 111.9 MHz.	5-53
Figure 5-43.	Normalized Main Carrier Pattern.	5-56
Figure 5-44.	Normalized Clearance Carrier Pattern.	5-58
Figure 5-45.	Normalized Sideband Difference (NSD) – Main Sideband.	5-59
Figure 5-46.	Normalized Sideband Difference (NSD) - Clearance Sideband.	5-60
Figure 5-47.	Main and Clearance NSD Patterns.	5-61
Figure 5-48.	Criteria for Assessing Acceptability of System Status.	5-63
Figure 5-49.	30° Dephasing, Centerline Readings, Mini-Lab.	5-79
Figure 5-50.	Width Reading of Monitor, Mini-Lab and PFCD for 30° Dephasing at 111.9 MHz.	5-80
Figure 5-51.	Block Diagram - MC-14/6 Alford Array System.	5-82
Figure 5-52.	Block Diagram - MC-14/6 Alford Array System Revised 1976 Tests.	5-93
Figure 5-53.	Run 18-21 (FAA-DC-6), Normal Configuration, ±35° Clearance OrbitMarch 18, 1976.	5-115
Figure 5-54.	Ground Run, 47° Phase Retard in Line A-7, ±35° Clearance OrbitMarch 13, 1976,	5-117

		PAGE
Figure 5-55.	Orbit, 46° Phase Retard in Line A-7, ±35° Clearance OrbitMarch 17, 1976.	5-118
Figure 5-56.	Run 18–18 (FAA–DC–6), 47° Phase Retard in Line A–7, ±35° Clearance Orbit—March 18, 1976.	5-119
Figure 5-57.	Run 18–30 (FAA–DC–6), 31° Phase Retard in M–14 SO Line, ±35° Clearance Orbit—March 18, 1976.	5-121
Figure 5-58.	Run 19–2 (FAA–DC–6), 45° Phase Retard in Line A–7, Broad Course and Clearance Path Widths— March 19, 1976.	5-123
Figure 5-59.	Run 19–8 (FAA–DC–6), 41° Phase Retard in Line A–7, Normal Course and Clearance Path Widths–March 19, 1976.	5-125
Figure 5-60.	Run 19–2 (FAA–DC–6), 51° Phase Retard in Line A–8, Broad Course and Clearance Path Widths––March 19, 1976.	5-127
Figure 5-61.	Run 19–9 (FAA–DC–6), 40° Phase Retard in Line A–8, Normal Course and Clearance Path WidthsMarch 19, 1976.	5-129
Figure 5-62.	Run 19–4 (FAA–DC–6), 36° Phase Retard in M–14 SO Line, Broad Course and Clearance Path Widths— March 19, 1976.	5-131
Figure 5-63.	Run 19–11 (FAA–DC–6), 44° Phase Retard in M–14 SO Line, Normal Course and Clearance Path Widths—March 19, 1976.	5-132
Figure 5-64.	Comparison of 6 and 2-Mile Orbits of Small Aperture Slotted-Cable Localizer.	5-139
Figure 5-65.	Low Approach – Small Aperture Slotted Cable Localizer – January 25, 1976.	5-140
Figure 5-66.	Plot of Localizer CDI vs. Azimuth for a 2 mile run at f= 111.9 on January 27, 1976 of Localizer Array.	5-142
	±35° Clearance Orber-Norch 18, 1870,	

		PAGE
Figure 5-67.	Course Width at Borad Alarm, 1500° Altitude at 6 Nautical Miles for the Medium Aperture Antenna Array at 108.5 MHz.	5–150
Figure 5-68.	Course Width at Broad Alarm, 1500 Altitude at 6 Nautical Miles for the Small Aperture Antenna Array at 111.9 MHz.	5-151
Figure 5–69.	Back Course Orbit, 1000 Altitude at 6 Nautical Miles for the Medium Aperture Antenna Array at 108.5 MHz.	5-152
Figure 5-70.	Back Course Orbit, 1000' Altitude at 6 Nautical Miles for the Small Aperture Antenna Array at 108.5 MHz.	5-153
Figure 5-71.	Structure Runs for the Medium (Top) and Small Aperture Antenna Arrays on 109.7 MHz.	5-154
Figure 6-1.	Examples of Terrain Reflection Mechanisms Normally Neglected in Physical Optics Terrain Models.	6-3
Figure 6-2.	Terrain Approximated as Perfectly-Conducting Plates.	6-5
Figure 6-3.	Geometry of Glide Slope Terrain Problem as Treated by Westinghouse Using Half-Plane Diffraction.	6-7
Figure 6-4.	Geometry of Glide Slope Terrain Problem as Treated by OU Far Zone GTD Model.	6-9
Figure 6-5.	The 8 Types of Ray Contributions Included in the Ohio University GTD Glide Slope Model.	6-10
Figure 6-6.	Wedge Diffraction Geometry and Coordinates.	6-13
Figure 6-7.	Illustration of Diffraction Unit Vectors.	6-13
Figure 6-8.	Diffraction Angle β_0 and Cone of Diffracted Rays.	6-15

		PAGE
Figure 6-9.	Numbering of Terrain Profile Plates and Curves.	6-17
Figure 6-10.	Profile of Terrain in the Reflecting Zone of the Kodiak, Alaska Glide Slope.	6-20
Figure 6-11.	Calculated CDI for 1000 Foot Level Run for Terrain Profile of Figure 6–10.	6-21
Figure 6-12.	Calculated Radiation Pattern for Upper Antenna for Terrain Profile of Figure 6–10.	6-22
Figure 6-13.	Calculated Radiation Pattern for the Lower Antenna for the Terrain Profile of Figure 6–10.	6-23
Figure 6-14.	Profile of Terrain in the Reflecting Zone for Carswell AFB, Texas.	6-24
Figure 6-15.	Calculated CDI for the Terrain Profile of Figure 6-14.	6-25
Figure 6-16.	Calculated Radiation Pattern for the Upper Antenna for the Terrain Profile of Figure 6–14.	6-26
Figure 6-17.	Calculated Radiation Pattern for the Lower Antenna for the Terrain Profile of Figure 6–14.	6-27
Figure 6-18.	Test Profile No. 1.	6-28
Figure 6-19.	Calculated CDI for Test Profile No. 1, Figure 6–18.	6-29
Figure 6-20.	Calculated Radiation Pattern for the Upper Antenna for Test Profile No. 1, Figure 6–18.	6-30
Figure 6-21.	Calculated Radiation Pattern for the Lower Antenna for Test Profile No. 1, Figure 6–18.	6-31
Figure 6-22.	Test Profile No. 2.	6-32
Figure 6-23.	Calculated CDI for Test Profile No. 2, Figure 6–22.	6-33
Figure 6-24.	Calculated Radiation Pattern for the Upper Antenna for Test Profile No. 2, Figure 6–22.	6-34

	are 6-38. Shade Diagram of the Experiment Setup Use Obtain the Magazine Curres of Flaures 3-1	PAGE
Figure 6-25.	Calculated Radiation Pattern for the Lower Antenna for Test Profile No. 2, Figure 6–22.	6-35
Figure 6-26.	Test Profile No. 3.	6-36
Figure 6-27.	Calculated CDI for Test Profile No. 3, Figure 6–26.	6-37
Figure 6-28.	Calculated Radiation Patterns for the Upper Antenna for Test Profile No. 3, Figure 6–26.	6-38
Figure 6-29.	Calculated Radiation Patterns for the Lower Antenna for Test Profile No. 3, Figure 6–26.	6-39
Figure 6-30.	Organization of OUGS and POSTOUGS Programs.	6-43
Figure 6-31a.	Sample Input Data for OUGS Program.	6-46
Figure 6-31b.	Sample Output Data from OUGS Program.	6-47
Figure 6-32.	Coordinate System for Input to OUGS.	6-49
Figure 6-33.	Sample Input Data for POSTOUGS Program.	6-53
Figure 6–34.	Calculated Values of DDM Versus the Ratio of the Clearance Carrier Signal (E _{CC}) to the Course Carrier Signal (E _C) for Various Values of Course Signal Only DDM.	6-55
Figure 6-35.	Calculated Values of DDM Versus the Ratio of the Clearance Carrier Signal (E _C) to the Course Carrier Signal (E _C) for Various Values of Course Signal Only DDM.	6-56
Figure 6–36.	Measured Values of DDM Versus the Ratio of the Clearance Signal (E _{CC}) to the Course Carrier Signal (E _C) for Various Values of Course Signal Only DDM.	6-58
Figure 6–37.	0 . 0 10 10 10 10 10 10	
	Signal Only DDM.	6-59

	WEST AND A SERVICE SOUTH	PAGE
Figure 6-38.	Block Diagram of the Experiment Setup Used to Obtain the Measured Curves of Figures 6-36 and 6-37.	6-60
Figure 6-39.	Block Diagram of the Audio Processor Used to Obtain the Values of DDM Shown in Figures 6–36 and 6–37 and Indicated in the Block Diagram of Figure 6–38.	6-61
Figure 6-40.	Circuit Schematic of the Audio Source Used to Obtain the Values of DDM Shown in Figures 6-36 and 6-37 and Indicated in the Block Diagram of Figure 6-38.	6-62
Figure 6-4].	Calculated Values of DDM Versus the Ratio of the Clearance Carrier Signal (E _{cc}) to the Course Carrier Signal (E _c) for Various Values of Course Signal DDM Calculated Using the Alford Equation.	6-63
Figure 6-42.	Digital Decwriter II 30 Character/Second Terminal and Hewlett-Packard 7203A Graphic Plotter.	6-70
Figure 6-43.	Model of Kodiak Airfield.	6-73
Figure 6-44.	DDM vs. Path Angle for the Kodiak Sideband Reference Glide Slope Calculated Using the GTD Code.	6-77
Figure 6-45.	Calculated Antenna Patterns for the Kodiak Geometry and an Ideal Flat Ground Plane Subtracted to Show Perturbing Effect of Ocean Reflections.	6-78
Figure 6-46.	Calculated Flyability Runs for a Capture Effect System with Antenna Heights of 51°, 34°, and 17° and an A ratio of 0.289.	6-80
Figure 6-47.	Calculated and Measured Curves of CDI vs. Elevation Angle Alpha for a 1000° High Level Run (Pattern B) Flight Measurement Along the Runway Centerline for the Null Reference System at High	[9
Figure 6-48.	Calculated and Measured Curves of CDI vs. Elevation Angle Alpha for a 1000 ⁵ High Level Run (Pattern B) Flight Measurement Along the Runway Centerline for	6-87
	the Null Reference System at Mean Tide.	6-88

		PAGE
Figure 6-49.	Calculated and Measured Curves of CDI vs. Elevation Angle Alpha for a 1000° High Level Run (Pattern B) Flight Measurement Along the Runway Centerline for the Null Reference System at Low Tide.	6-89
Figure 6-50.	Calculated and Measured Curves of CDI vs. Elevation Angle Alpha for a 1000° High Level Run (Pattern B) Flight Measurement Along the Runway Centerline for the Sideband Reference System at High Tide.	6-90
Figure 6-51.	Calculated and Measured Curves of CDI vs. Elevation Angle Alpha for a 1000" High Level Run (Pattern B) Flight Measurement Along the Runway Centerline for the Sideband Reference System at Mean Tide.	6-91
Figure 6-52.	Calculated and Measured Curves of CDI vs. Elevation Angle Alpha for a 1000° High Level Run (Pattern B) Flight Measurement Along the Runway Centerline for the Sideband Reference System at Low Tide.	6-92
Figure 6-53.	Calculated and Measured Curves of CDI vs. Distance for a Pattern A Flight Along the Runway Centerline for the Null Reference System at High Tide.	6-93
Figure 6-54.	Calculated and Measured Curves of CDI vs. Distance for a Pattern A Flight Along the Runway Centerline for the Null Reference System at Mean Tide.	6-94
Figure 6-55.	Calculated and Measured Curves of CDI vs. Distance for a Pattern A Flight Along the Runway Centerline for Null Reference System at Low Tide.	6-95
Figure 6-56.	Calculated and Measured Curves of CDI vs. Distance for a Pattern A Flight Along the Runway Centerline for the Sideband Reference System at	Figur
	High Tide.	6-96

		PAGE
Figure 6-57.	Calculated and Measured Curves of CDI vs. Distance for a Pattern A Flight Along the Runway Centerline for the Sideband Reference System at Mean Tide.	6-97
Figure 6-58.	Calculated and Measured Curves of CDI vs. Distance for a Pattern A Flight Along the Runway Centerline for the Sideband Reference System at Low Tide.	6-98
Figure 6-59.	Ground Profile for Kodiak Modeling Calculations.	6-102
Figure 6-60.	Graph for Experimental Determination of Upper Antenna Height for NR.	6-105
Figure 6-61.	Portion of the Terrain Contour Map for Kodiak Runway 25 Glide Slope.	6-106
Figure 6-62.	Flight Log for Null Reference Tests.	6-107
Figure 6-63.	Tide Plots for NR Tests.	6-108
Figure 6-64.	Tide Plots for SBR Tests.	6-109
Figure 6-65.	Building A Geometry and Relation to Localizer Antenna - Denver Stapleton Runway 26L-8R.	6-111
Figure 6-66.	Calculated Front Course (26L) for Circular Orbit 15,000 Ft. from Localizer Antenna.	6-113
Figure 6-67.	Calculated Back Course (8R) for Circular Orbit 15,000 Ft. from Localizer Antenna.	6-114
Figure 6-68.	Stapleton Field Localizer CDI Envelope for a 2.75° Flight Angle (from Horizontal) Above Run-way Centerline Due to Derogation Caused by Proposed Hangar A.	6-115
Figure 6-69.	Hoquiam, Washington Localizer CDI Envelope for a 3.0° Flight Angle (from Horizontal) Above Runway Centerline.	6-117

	throughton choose to the	PAGE
Figure 6-70.	Hoquiam, Washington Localizer CDI Envelope for a 3.0° Flight Angle (from Horizontal Above Runway Centerline.	6-118
Figure 6-71.	Hoquiam, Washington Localizer CDI Envelope for a 3.0° Flight Angle (from Horizontal) Above Runway Centerline.	6-119
Figure 6-72.	Predicted CDI for Orbital Flight at 1000 Ft. Altitude and 6 Mile Radius with No Ship Present.	6-120
Figure 6-73.	Predicted CDI for Orbital Flight at 1000 Ft. Altitude and 6 Mile Radius with Ship Positioned 2000 ft.	6-121
Figure 6-74.	Predicted CDI for Orbital Flight at 1000 Ft. Altitude and 6 Mile Radius with Ship Positioned 4000 Ft.	6-122
Figure 6-75.	Antenna Radiation Patterns for 14-Element Mark ID LPD Array.	6-123
Figure 6-76.	Ship Modeled Using Five Vertical Plat Plates.	6-125
Figure 9-1.	ILS Distance Measuring System.	9-2
Figure 9-2.	Groundspeed System Block Diagram.	9-5
Figure 9-3.	Pulser No. 1 - Ground.	9-6
Figure 9-4.	Pulser No. 2 - Airborne.	9-6
Figure 9-5.	Transmitter Modulation Generating Circuitry.	9-7
Figure 9-6.	21 KHz Input Conditioning and 5 KHz Phase Detector.	9-9
	Input Conditioning Circuitry for the 5.250 KHz Reference Tone Modulated on the Localizer.	9-10
Figure 9-8.	Directional Phase Detector.	9-11
Figure 9-9.	Processor Control Circuit.	9-13
Figure 9-10.	Groundspeed Computational Circuitry.	9-14

		PAGE
Figure 9-11.	Mixer and Filter for Full Doppler Processing.	9-16
Figure 9-12.	Physical Layout of the Groundspeed Processor.	9-17
Figure 9-13.	Calibration Data for the Flight Tests on July 2, 1978.	9-18
Figure 9-14.	Four Low Approaches from the Flight Test on July 26, 1976.	9-20
Figure 9-15.	360° Turns Made at Ohio University Test Site at Albany, Ohio.	9-21
Figure 9-16.	Two 360° Turns from the Flight Test on July 26, 1976.	9-22
Figure 9-17.	Sample Run from Flight Test on July 26, 1976.	9-23
Figure 9-18.	Initial Test Configuration - Audio Range-Rate System.	9-27
Figure 9-19.	Range-Rate System Tests with RF Generator.	9-28
Figure 9-20.	Revised Synchronous Processing of 1 MHz Data.	9-33
Figure 9-21.	ILS Groundspeed System, Seiko Filter Module, Model SL-62R.	9-34
Figure 9-22.	ILS Groundspeed System 1 MHz Multiplier Detector Module.	9-35
Figure 9-23.	ILS Groundspeed System 5 M Hz Multiplier Detector Module.	9-37
Figure 9-24.	ILS Groundspeed System - Doppler Processor Module.	9-40
Figure 9-25.	ILS Groundspeed System, Fast-Slow Module.	9-41
Figure 9-26.	ILS Groundspeed System Clock Module, Modified.	9-43
Figure 9–27.	Circuit Schematic Anemometer Transmitter Analog Wind Telemetry System.	9-46
Figure 9-28.	Localizer Modulator Circuit.	9-47

		PAGE
Figure 9–29.	Component Layout, Anemometer Transmitter, Analog Wind Telemetry System.	9-48
Figure 9-30.	Circuit Schematic Analog Data Processor, Anal Wind Telemetry System.	9-50
Figure 9-31.	Components Layout, Analog Data Processor, Analog Wind Telemetry System.	9-51
Figure 9–32a.	Circuit Schematic Digital Data Processor, Analog Wind Telemetry System.	9-53
Figure 9–32b.	Circuit Schematic Digital Data Processor, Analog Wind Telemetry System.	9-55
Figure 9–33.	Components Layout, Digital Data Processor, Analog Wind Telemetry System.	9-57
Figure 9-34.	Photograph of Wind Telemetry Anemometer and Transmitter at Ohio University Airport.	9-61
Figure 9-35.	Wind Telemetry System Pictorial.	9-62
Figure 9-36.	Wind Telemetry System Ground Anemometer Transmitter Unit.	9-63
Figure 9-37a.	Wind Telemetry System: Ground Installation at Localizer.	9-64
Figure 9-37b.	Digital Wind Telemetry Receiver Component Layout.	9-65
Figure 9-37c.	Block Diagram: Wind Telemetry Receiver/ Display Module.	9-66
Figure 9-38a.	Anemometer Transmitter: Data Multiplexer and Serializer.	9-67
Figure 9-38b.	Anemometer Transmitter: Data Multiplexer and Serializer.	9-68
Figure 9-39.	Components Layout, Anemometer Transmitter Digital Wind Telemetry System.	9-69

		PAGE
Figure 9-40.	Anemometer Transmitter: Tone Generation and Switching.	9-70
Figure 9-41.	Anemometer Transmitter: lock Generation and Controller.	9-71
Figure 9-42.	Localizer Transmitter: Timing and Synchronizing Tone Generation.	9-72
Figure 9-43.	Localizer Modulator Synchronization Pulse Generation.	9-73
Figure 9-44.	Localizer Modulator: Tone Detection, Tone Generation and Modulation.	9-75
Figure 9-45.	Localizer Modulator and Sync Tone Generator (Viewed from Component Side of Board).	9-77
Figure 9-46.	Groundspeed and Airspeed Traces Using Synchronous Processor with the 5 MHz Detector.	9-79
Figure 9-47.	Groundspeed Outputs Using the 5 MHz Detector and the Non-Synchronous Processor.	9-81
Figure 9-48.	Simultaneous Ground and Aircraft Traces, Digital Wind Telemetry System.	9-83
Figure 9-49.	Simultaneous Wind Telemetry and Groundspeed Outputs.	9-86
Figure 9-50.	Simultaneous Wind Telemetry and Groundspeed Tests with a Change in Airspeed.	9-37
Figure 9–51.	Simultaneous Ground and Aircraft Traces, Analog Wind Telemetry System.	9-88
Figure 10-1.	Analog Strip-Chart to Digital Data Translator.	10-3
Figure 10-2.	Data Translator Operational Setup.	10-4
Figure 10-3.	Remote Manual Sample Control Switch for Analog/ Digital Data Translator.	10-6

			PAGE
Figure	10-4.	Analog/Digital Data Translator Sample Rate Control Circuit.	10-7
Figure	10-5.	Analog/Digital Data Translator Schematic.	10-8
Figure	10-6.	Timing Diagram.	10-9
Figure	10-7.	Data Translator Power Supply.	10-9
Figure	10-8.	Calcomp Plot of Sample Sinusoid and Triangular Waveforms.	10-11
Figure	10-9.	Calcomp Plot of Glide Slope Summer Output.	10-12
Figure	10-10.	Actual Glide Slope Data Used for Data Conversion Comparison.	10-13
Figure	11-1.	Sample Output of Glide Slope Model.	11-9
Figure	11-2.	Example Output: Far Field CDI vs Angle - Capture Effect Glide Slope.	11-10
Figure	11-3.	Near Field (360° Point) CDI vs Angle - Normal Glide Slope.	11-23
Figure	11-4.	Far Field CDI vs Angle - Normal Glide Slope.	11-24
Figure	11-5.	Near Field (360° Point) CDI vs Angle – Sidebands Retarded 20°.	11-25
Figure	11-6.	Far Field CDI vs Angle - Sidebands Retarded 20°.	11-26
Figure	11-7.	Near Field (360° Point) CDI vs Angle – Sidebands Retarded 20°.	11-27
Figure	11-8.	Far Field CDI vs Angle - Sidebands Retarded 20°.	11-28
Figure	11-9.	Near Field (360° Point) CDI vs Angle – Sidebands Retarded 20°.	11-29
Figure	11-10.	Far Field CDI vs Angle - Sidebands Retarded 20°.	11-30
Figure	11-11,	Near Field (360° Point) CDI vs Angle – Sidebands Retarded 30°.	11-31

		PAGE
Figure 11-12.	Far Field CDI vs Angle - Sidebands Retarded 30°.	11-32
Figure 11-13.	Near Field (360° Point) CDI vs Angle – Sidebands Retarded 30°.	11-33
Figure 11-14.	Far Field CDI vs Angle - Sidebands Retarded 30°.	11-34
Figure 11-15.	Near Field (360° Point) CDI vs Angle – Sidebands Retarded 40°.	11-35
Figure 11-16.	Far Field CDI vs Angle - Sidebands Retarded 40°.	11-36
Figure 11-17.	Near Field (360° Point) CDI vs Angle – Sidebands Retarded 50°.	11-37
Figure 11-18.	Far Field CDI vs Angle - Sidebands Retarded 50°.	11-38
Figure 11-19.	Near Field (360° Point) CDI vs Angle – Lower Antenna Advanced 10°.	11-39
Figure 11-20.	Far Field CDI vs Angle – Lower Antenna Advanced 10°.	11-40
Figure 11-21.	Near Field (360° Point) CDI vs Angle – Lower Antenna Advanced 20°.	11-41
Figure 11-22.	Far Field CDI vs Angle – Lower Antenna Advanced 20°.	11-42
Figure 11-23.	Near Field (360° Point) CDI vs Angle – Lower Antenna Advanced 30°.	11-43
Figure 11-24.	Far Field CDI vs Angle – Lower Antenna Advanced 30°.	11-44
Figure 11-25.	Near Field (360° Point) CDI vs Angle – Middle Antenna Retarded 12°.	11-45
Figure 11-26.	Far Field CDI vs Angle – Middle Antenna Retarded 12°.	11-46
Figure 11-27.	Near Field (360° Point) CDI vs Angle – Middle Antenna Retarded 14°.	11-47

25.11	e 11-45. Peer Field (860° Point) CBI vs Angle - Upper Anterno Reforded 50°.	PAGE
Figure 11-28.	Far Field CDI vs Angle - Middle Antenna Retarded 14°.	11-48
Figure 11-29.	Near Field (360° Point) CDI vs Angle – Middle Antenna Advanced 14°.	11-49
Figure 11-30.	Far Field CDI vs Angle - Middle Antenna Advanced 14°.	11-50
Figure 11-31.	Near Field (360° Point) CDI vs Angle – Middle Antenna Retarded 20°.	11-51
Figure 11-32.	Far Field CDI vs Angle - Middle Antenna Retarded 20°.	11-52
Figuré 11-33.	Near Field (360° Point) CDI vs Angle – Middle Antenna Retarded 30°.	11-53
Figure 11-34.	Far Field CDI vs Angle - Middle Antenna Retarded 30°.	11-54
Figure 11-35.	Near Field (360° Point) CDI vs Angle – Middle Antenna Retarded 40°.	11-55
Figure 11-36.	Far Field CDI vs Angle - Middle Antenna Retarded 40°.	11-56
Figure 11-37.	Near Field (360° Point) CDI vs Angle – Middle Antenna Retarded 50°.	11-57
Figure 11-38.	Far Field CDI vs Angle - Middle Antenna Retarded 50°.	11-58
Figure 11-39.	Near Field (360° Point) CDI vs Angle – Middle Antenna Retarded 60°.	11-59
Figure 11-40.	Far Field CDI vs Angle - Middle Antenna Retarded 60°.	11-60
Figure 11-41.	Near Field (360° Point) CDI vs Angle – Upper Antenna Retarded 30°.	11-61
Figure 11-42.	Far Field CDI vs Angle - Upper Antenna Retarded 30°.	11-62
Figure 11-43.	Near Field (360° Point) CDI vs Angle – Upper Antenna Retarded 40°.	11-63
Figure 11-44.	Far Field CDI vs Angle - Upper Antenna Retarded 40°.	11-64

			PAGE
Figure	11-45.	Near Field (360° Point) CDI vs Angle – Upper Antenna Retarded 50°.	11-65
Figure	11-46.	Far Field CDI vs Angle - Upper Antenna Retarded 50°.	11-66
Figure	11-47.	Near Field (360° Point) CDI vs Angle – Upper Antenna Retarded 60°.	11-67
Figure	11-48.	Far Field CDI vs Angle - Upper Antenna Retarded 60°.	11-68
Figure	11-49.	Near Field (360° Point) CDI vs Angle - Upper Antenna Advanced 60°.	11-69
Figure	11-50.	Far Field CDI vs Angle - Upper Antenna Advanced 60°.	11-70
Figure 1	11-51.	Near Field (360° Point) CDI vs Angle – Upper Antenna Retarded 70°.	11-71
Figure 1	11-52.	Far Field CDI vs Angle - Upper Antenna Retarded 70°.	11-72
Figure 1	11-53.	Near Field (360° Point) CDI vs Angle – Upper Antenna Retarded 80°.	11-73
Figure 1	11-54.	Far Field CDI vs Angle - Upper Antenna Retarded 80°.	11-74
Figure 1	11-55.	Near Field (360° Point) CDI vs Angle - Upper Antenna Retarded 90°.	11-75
Figure 1	11-56.	Far Field CDI vs Angle - Upper Antenna Retarded 90°.	11-76
Figure 1	11-57.	Near Field (360° Point) CDI vs Angle – Lower Antenna Attenuated 1 dB.	11-77
Figure 1	11-58.	Far Field CDI vs Angle – Lower Antenna Attenuated 1 dB.	11-78
Figure 1	11-59.	Near Field (360° Point) CDI vs Angle – Lower Antenna Attenuated 3 dB.	11-79
Figure 1	1-60.	Far Field CDI vs Angle – Lower Antenna Attenuated 3 dB.	11-80
Figure 1	1-61.	Near Field (360° Point) CDI vs Angle – Lower Antenna Attenuated 7 dB.	11-81

PAGE.		PAGE
Figure 11-62.	Far Field CDI vs Angle – Lower Antenna Attenuated 7 dB.	11-82
Figure 11-63.	Near Field (360° Point) CDI vs Angle - Middle Antenna Attenuated 1 dB.	11-83
Figure 11-64.	Far Field CDI vs Angle – Middle Antenna Attenuated 1 dB.	11-84
Figure 11-65.	Near Field (360° Point) CDI vs Angle – Middle Antenna Attenuated 2 dB.	11-85
Figure 11-66.	Far Field CDI vs Angle – Middle Antenna Attenuated 2 dB.	11-86
Figure 11-67.	Near Field (360° Point) CDI vs Angle - Middle Antenna Attenuated 4 dB.	11-87
Figure 11-68.	Far Field CDI vs Angle – Middle Antenna Attenuated 4 dB.	11-88
Figure 11-69.	Near Field (360° Point) CDI vs Angle – Upper Antenna Attenuated 3 dB.	11-89
Figure 11-70.	Far Field CDI vs Angle – Upper Antenna Attenuated 3 dB.	11-90
Figure 11-71.	Near Field (360° Point) CDI vs Angle – Upper Antenna Attenuated 6 dB.	11-91
Figure 11-72.	Far Field CDI vs Angle - Upper Antenna Attenuated 6 dB.	11-92
Figure 11-73.	Near Field (360° Point) CDI vs Angle – Upper Antenna Attenuated 10 dB.	11-93
Figure 11-74.	Far Field CDI vs Angle - Upper Antenna Attenuated 10 dB.	11-94
Figure 11-75.	Near Field (360° Point) CDI vs Angle – Lower Antenna Out.	11-95
Figure 11-76.	Far Field CDI vs Angle - Lower Antenna Open.	11-96

PAGE		PAGE
Figure 11-77.	Near Field (360° Point) CDI vs Angle – Lower Antenna Out.	11-97
Figure 11-78.	Far Field CDI vs Angle - Lower Antenna Shorted.	11-98
Figure 11-79.	Near Field (360° Point) CDI vs Angle – Middle Antenna Out.	11-99
Figure 11-80.	Far Field CDI vs Angle - Middle Antenna Open.	11-100
Figure 11-81.	Near Field (360° Point) CDI vs Angle – Middle Antenna Out.	11-101
Figure 11-82.	Far Field CDI vs Angle - Middle Antenna Shorted.	11-102
Figure 11-83.	Near Field (360° Point) CDI vs Angle – Upper Antenna Out.	11-103
Figure 11-84.	Far Field CDI vs Angle - Upper Antenna Open.	11-104
Figure 11-85.	Near Field (360° Point) CDI vs Angle – Upper Antenna Out.	11-105
Figure 11-86.	Far Field CDI vs Angle - Upper Antenna Shorted.	11-106
Figure 11-87.	Near Field (360° Point) CDI vs Angle – Modulation Index = .28.	11-107
Figure 11-88.	Far Field CDI vs Angle - Modulation Index = .28.	11-108
Figure 11-89.	Near Field (360.° Point) CDI vs Angle – Modulation Index = 0.5.	11-109
Figure 11-90.	Far Field CDI vs Angle - Modulation Index = 0.5.	11-110
Figure 11-91.	Near Field (360° Point) CDI vs Angle - No Clearance.	11-111
Figure 11-92.	Far Field CDI vs Angle - No Clearance.	11-112
Figure 11-93.	Near Field (360° Point) CDI vs Angle – Maximum Clearance Modulation.	11-113
Figure 11-94.	Far Field CDI vs Angle - Maximum Clearance Modulation	.11-114

9		PAGE
Figure 11-95.	Far Field CDI vs Angle - Power Divider A+ Clockwise.	11-115
Figure 11-96.	Far Field CDI vs Angle – Power Divider A– Counter- clockwise.	11-116
Figure 11-97.	Far Field CDI vs Angle - Power Divider B+ Clockwise.	11-117
Figure 11-98.	Far Field CDI vs Angle - Power Divider B- Counter- clockwise.	11-118
Figure 11-99.	Far Field CDI vs Angle - Power Divider Carrier +.	11-119
Figure 11-100.	Far Field CDI vs Angle - Power Divider Carrier	11-120
Figure 11-101.	Far Field CDI vs Angle – Z8 Clockwise.	11-121
Figure 11-102.	Far Field CDI vs Angle – Z8 Counterclockwise.	11-122
Figure 11-103.	Watts Mark I Glide Slope Array at New Tamiami, Florida.	11-125
Figure 11-104.	Watts Mark I Antenna Being Lowered for Tests to Determine Path Independence of Antenna Height.	11-126
Figure 11-105.	Antenna Positioning for Seventh Series of Watts Slotted Cable Glide Slope Tests.	11-128
Figure 11-106.	Ground-Based Measurement of Elevation of Zero DDM Line Above Ground at Threshold.	11-129
Figure 11-107.	Flight Recording of Glide Slope CDI Made on a Level Flight Through the Path Structure on Runway Center-	
	line Extended at 1500-feet above the Array.	11-131
Figure 11-108.	Airborne Measurement of Zero DDM Line Made at a Distance of 4.8 Miles from Transmitter Antennas.	11-132
Figure 11-109.	Airborne Measurement of Zero DDM Line Made at a Distance Equal to the Distance of the 100-foot Decision Point on the Glide Slope (ILS Point C).	11-133
Figure 11-110.	Flight Recording of the Mark I, Curvilinear System Made During Low Approach for Landing.	11-134

1		PAGE
Figure 11-111.	a Distance of 4.8 Miles.	11-135
Figure 11-112.	Perpendicular Measurement Subsequent to Figure 11–111 Data But With Sideband Dephased 30 Degrees (advance).	11-136
Figure 11-113.	Measurement of Perpendicular Path Structure with the Sideband Energy Retarded 30 Degrees.	11-137
Figure 11-114.	Tamiami Site Layout for Initial Series of Tests on Watts Mark 2 System.	11-140
Figure 11-115.	Copy of Flight Recording - Level Pass, 1000 Feet.	11-141
Figure 11-116.	Copy of Flight Recording Made During Low Approach for Watts Mark 2 System.	11-142
Figure 11-117.	Three Differential Amplifier Traces Superimposed.	11-144
Figure 11-118.	Copy of Flight Recording, Perpendicular–Cut to Runway Centerline at 5.4 Miles.	11-145
Figure 11-119.	Comparison of Calculated and Measured Cross Sections of the Watts Glide Path.	11-146
Figure 11-120.	Comparison of Calculated and Measured Flyability Runs for Watts Mark 2 System.	11-147
Figure 11-121.	Truck Positions for Fault Tests Mark 2 System.	11-152
Figure 11-122.	Watts Mark II Glide Slope Array with Deliberate Alignment Fault.	11-158
Figure 11-123a	Perpendicular Path Structure from the Watts Array When Fed by the TU-4 and Wilcox Transmitters.	11-161
Figure 11-123b	Perpendicular Path Structure from the Watts Array When Fed by the TU-4 Transmitter.	11-162
Figure 11-124.	Perpendicular Path Structure from the Watts Array Showing the Effects of Antenna Misalianment.	11-164

Made Dietric Law Approach the Landing.

PA		PAGE
Figure 11-125.	Far-Field Monitor *1 RF Level and DDM and Far-Field Monitor *2 DDM responses.	11-169
Figure 11-126.	Watts Mark 2 Glide-Slope Set Up at the Ohio University Test Site, Tamiami, Florida.	11-171
Figure 11-127.	Response of the Integral Monitor, Far-Field Monitor, and the Modulator Carrier to Changes in Transmitter Parameters.	₩613 311-173
Figure 11-128.	Monitor Response for the Period of September 18 to September 21, 1975.	11-175
Figure 11-129a.	Monitor Response, September 18, 1975, from 0630 hours to 0800 hours.	11-176
Figure 11-129b.	Monitor Response, September 18, 1975, from 0930 hours to 1100 hours.	11-177
Figure 11-129c.	Monitor Response, September 19, 1975, from 1400 hours to 1530 hours.	11-178
Figure 11-130.	Far-Field Monitor RF Level, September 18, 1975.	11-180
Figure 11-131.	Effects Due to a Fault in the Monitor Circuit.	11-181
Figure 11-132.	RF Cable Diagram for 2-Antenna End-Fire Glide Slope Junction Box.	11-183
Figure 11-133.	Monitor Response for the Period of September 26 to September 29, 1975.	11-184
Figure 11-134a.	Monitor Response, September 27, 1975, from 0800 hours to 0930 hours.	11-185
Figure 11-134b.	Monitor Response, September 27, 1975, from 1300 hours to 1430 hours.	11-186
Figure 11-134c.	Monitor Response, September 27, 1975, from 1445 hours to 1615 hours.	11-187
Figure 11-134d.	Monitor Response, September 27, 1975, from 2000 hours to 2130 hours.	11-188

M		PAGE
Figure 11-135.	Monitor Response, September 30, 1975, During Varying Rain Conditions.	11-189
Figure 11-136.	Layout of the Watts System at the Tamiami Airport.	11-192
Figure 11-137.	Watts Mark III End-Fire Glide Slope Array Installed at Tamiami.	11-193
Figure 11-138.	Shown in the Foreground are Three Slotted-Cable Monitor Antennas Serving the Rear Antenna Which is Partially Evident.	11-195
Figure 11-139.	Watts Mark III Glide Slope Arrray.	11-196
Figure 11-140.	Level Pass 1000 Feet Above Runway Centerline Extended Normal Daytime Turbulence.	11-198
Figure 11-141.	CDI, Theodolite, and Differential Amplifier Recordings from Run 25–20.	11-199
Figure 11-142.	Completion of a Pattern A Run with the Bonanza 35 Aircraft During Watts Mark III Testing at Tamiami.	11-200
Figure 11-143.	Differential Amplifier Traces from Five Different Runs Made on February 25, 1977.	11-201
Figure 11-144.	Recording of CDI on Transverse Cut to Localizer at 5.2 Miles Range from the Glide Slope Array.	11-203
Figure 11-145.	Comparison of Perpendicular Structures with Different Configurations of the Watts Endfire Glide-Slope Array.	11-204
Figure 11-146.	Comparison of Transverse Patterns from Spinner's Yagi Array in 1956 and the Watts Mark 3 in 1977.	11-205
Figure 11-147.	Transverse Crosspointer Curves Calculated by Watts to Which has been Added the Measured CDI Values During a Perpendicular Cut, Run 25–9.	11-206
Figure 11-148.	Locations of Specific Faults.	11-211
Figure 11-149.	Transverse Path Structure in the Absence of the Clearance Transmitter.	11-213

184

		PAGE
Figure 11-150,	Recording of Glide-Slope CDI During Level Flight Along Localizer Course, 1000 Feet Altitude.	11-217
Figure 11-151.	Recording of Glide-Slope CDI During Level Flight Perpendicular to Localizer, 5.4 Miles from Runway, 1600 Feet Altitude.	11-219
Figure 11-152.	Recordings of CDI and Differential Amplifier Output During Low Approach.	11-221
Figure 11-153.	Recording of Theodolite Trace for FAA Saberliner Flight with a Hand-Calculated Differential Trace Added.	11-225
Figure 11-154.	Effects of Clearance Transmitter Power Level on Perpendicular Structure as Seen at 5.4 Miles, 1600 Feet.	11-227
Figure 11-155.	Composite of Seven Differential Amplifier Traces Taken at Different Azimuth Approach Angles to the Runway.	11-229
Figure 11-156.	Tracings of the Flight Records of Transverse Structure for the Standard and Expanded Aperture for the Watts Mark 3 Endfire Glide Slope Array.	11-234
Figure 11-157.	Plot of CDI Contours in the Vertical Plane Containing the Runway Threshold and Perpendicular to the Run- way Centerline.	11-235
Figure 11-158.	Comparison of Transverse Structure Before and After the Interchange of Single Sections of the Front and Rear Antennas.	11-237
Figure 11-159.	Photograph of Modification of Front Antenna to Lower Its Height Gradually from 42 Inches to 21 Inches at the Runway End.	11-240
Figure 11-160.	Tracing of Two Records Showing the Transverse Path Structures Before and After Lowering of the End Portion of the Front Antenna Element.	11-241
Figure 11-161.	Diagram of Carrier and Sideband Being Fed into the Antenna.	11-247
Figure 11-162.	Relative Slot Excitations of Rear Antenna, Tamiami.	11-250

PAGE		PAGE
Figure 11-163.	Relative Slot Excitations of Front Antenna, Tamiami.	11-251
Figure 11-164.	Watts Slotted-Cable Glide-Slope Layout, Tamiami.	11-252
Figure 11-165.	Relative Slot Excitations of Rear Antenna, Staunton.	11-253
Figure 11-166.	Relative Slot Excitations of Front Antenna, Staunton.	11-254
Figure 11-167.	Watts Slotted Cable Glide Slope Layout, Staunton.	11-255
Figure 11-168.	Terrain Profile of Shenandoah Valley Airport, Staunton.	11-257
Figure 11-169.	Extended Terrain Profile of Shenandoah Valley Airport, Staunton.	11-258
Figure 11-170.	Schematic of Flight Tracks on Watts Slotted-Cable Glide Slope.	11-259
Figure 11-171.	Low Approach, Run 29–5, Tamiami.	11-260
Figure 11-172.	Low Approach, Run 29-6, Tamiami.	11-261
Figure 11-173.	Low Approach, Run 29-8, Tamiami.	11-262
Figure 11-174.	Perpendicular Cut, Altitude 1600°, Run 18–17, Tamiami.	11-264
Figure 11-175.	Perpendicular Cut, Altitude 1700°, N-S, Tamiami.	11-265
Figure 11-176.	Level Pass, Altitude 1000°, Run 18-6, Tamiami.	11-266
Figure 11-177.	Low Approach, Staunton.	11-267
Figure 11-178.	Perpendicular Cut, Altitude 1300°, Run 1-7, Staunton.	11-268
Figure 11-179.	Perpendicular Cut, Altitude 1500°, Run 1-4, Staunton.	11-269
Figure 11-180.	Perpendicular Cut, Altitude 1500°, Staunton.	11-270
Figure 11-181.	Level Run, Altitude 1000°, Staunton.	11-271

	Floure 11-197. Layout of the Warts System of Rock Speke	PAGE
Figure 11-182.	Level Run, Altitude 1500', Run Number 1-8, Staunton.	11-272
Figure 11-183.	Low Approaches 4° South and North of Runway Centerline.	11-273
Figure 11-184.	Low Approach 6° South and North of Centerline.	11-274
Figure 11-185.	Low Approach 8° South and North of Centerline, Tamiami.	11-275
Figure 11-186.	Above and Below .35° Approaches, Tamiami.	11-276
Figure 11-187.	Level Pass, Altitude 1000°, 3° North and South of Centerline.	11-277
Figure 11-188.	Level Pass, Altitude 1000°, 4° North and South of Centerline.	11-277
Figure 11-189.	Level Pass, Altitude 1000 ^s , 5° North and South of Centerline.	11-278
Figure 11-190.	Level Pass, Altitude 1000°, 6° North and South of Centerline.	11-278
Figure 11-191.	Level Pass, Altitude 1000°, 7° North and South of Centerline, Tamiami.	11-279
Figure 11-192.	Level Pass, Altitude 1000 ^s , 8° North and South of Centerline, Tamiami.	11-279
Figure 11-193.	Theoretical Low Approach, 4° North and South of Centerline, Staunton.	11-281
Figure 11-194.	Theoretical Low Approach, 6° North and South of Centerline, Staunton.	11-282
Figure 11-195.	Theoretical Low Approach, 8° North and South of Centerline.	11-283
Figure 11-196.	Diagram to Show the Canical Structure of the Watts Array.	11-284

(0	LIST OF PIGURES (CONTINUES	PAGE
Figure 11-197.	Layout of the Watts System at Rock Springs Airport.	11-287
Figure 11-198.	Level Pass 1000 Feet Above Runway Centerline Extended.	11-289
Figure 11-199.	Differential Amplifier Recording Made During Low Approach at RKS.	11-291
Figure 11-200.	Recordings of CDI on Transverse Cut to Localizer.	11-295
Figure 11-201.	Conceptual Drawing Depicting the Effect of Theodolite Placement on the Measured Path Structure Near Threshold.	11-299
Figure 11-202.	Pertinent Dimensions for Determining and Measuring the Localizer Edge.	11-301
Figure 11-203.	Layout of the Watts System at Rock Springs Airport.	11-302
Figure 11-204.	Level Pass 1000 Feet-Above Runway Centerline Extended.	11-305
Figure 11-205.	Three Differential Amplifier Recordings Made During Low Approaches at Rock Springs.	11-307
Figure 11-206.	Recordings of CDI On Transverse Cut to Localizer.	11-311
Figure 11-207.	Low Angle Transverse Cut to the Localizer.	11-315
Figure 11-208.	Averaged Signal Strength Measured by a 360° Orbit.	11-317
Figure 11-209.	Test Set-Up for Verifying K.	11-328
Figure 11-210.	Phasor Diagram.	11-329
Figure 11-211.	Coordinate System.	11-331
Figure 11-212.	Plots of Path-Width Changes Seen in the Far-Field (30,000 ft.).	11-334
Figure 11-213.	Plots of Path-Width Changes Seen at 5,000 ft. Due to Mast Tilt in the Plane Parallel to Runway Centerline.	11-335
Figure 11-214.	Plots of Changes Seen at 0.7° Below Path at the 180° Proximity Point Due to Mast Tilt in the Plane Parallel to the Runway.	11-336

11-279

		PAGE
Figure 11-215.	Plot of Changes Seen at 0.7° Above Path at the 180° Proximity Point Due to Mast Tilt in the Plane Parallel to the Runway.	11-337
Figure 11-216.	Plot of Near Field Responses at ± 0.7° to Mast Tilt in the Plane Perpendicular to Runway.	11-338
Figure 11-217.	Conventional Null-Reference Monitor System.	11-340
Figure 11-218.	Integral Path and Width Monitor for a Null-Reference System.	11-340
Figure 11-219.	Null-Reference Monitor Test Unit.	11-341
Figure 11-220.	Vertical Labe Structures for Null-Reference and Perturbed Null-Reference Glide Slope.	11-343
Figure 11-221.	Mobile Glide Slope Facility During Tests at Ohio University Airport.	11-352
Figure 11-222.	Lawton, Oklahoma, Municipal Airport, Runway 35.	11-363
Figure 11-223.	Lawton, Oklahoma, Municipal Airport, Runway 35.	11-364
Figure 11-224.	Profile of the Terrain Along a Straight Line Down from the Tower Base to the Middle Marker (Lawton, Oklahoma, Municipal Airport).	11-365
Figure 11-225.	Detailed Terrain Profile Runway 35 Approach Lawton, Oklahoma.	11-367
Figure 11-226.	Ground Data (Commissioned) - Clearance On.	11-370
Figure 11-227.	Ground Data (Commissioned) - Clearance Off.	11-371
Figure 11-228.	Graund Data (Commissioned) –10° Delay in Middle Antenna, Clearance On.	11-372
Figure 11-229.	Ground Data (Commissioned) -10° Delay in Middle Antenna, Clearance Off.	11-373
Figure 11-230.	Ground Data (Commissioned) -10° Advance in Middle Antenna, Clearance Off.	11-374

		PAGE
Figure 11-231.	Ground Data (Commissioned) -10° Advance in Middle Antenna, Clearance On.	11-375
Figure 11-232.	Ground Data (Commissioned) –2 dB Attenuation in Middle Antenna, Clearance On.	11-376
Figure 11-233.	Ground Data (Commissioned) –6 dB Attenuation in Upper Antenna, Clearance On.	11-377
Figure 11-234.	Ground Data (Commissioned) -3 dB Attenuation in Lower Antenna -10° Retard in Middle Antenna, Clearance On.	11-378
Figure 11-235.	Ground Data (Theoretical Phasing) - Clearance Off.	11-380
Figure 11-236.	Ground Data (Theoretical Phasing) - Clearance On.	11-381
Figure 11-237.	Ground Data (Theoretical Phasing) 10° Delay Middle Antenna, Clearance Off.	11-382
Figure 11-238.	Ground Data (Theoretical Phasing) –20° Delay Middle Antenna, Clearance Off.	11-383
Figure 11-239.	Ground Data (Theoretical Phasing) –30° Delay in Middle Antenna, Clearance Off.	11-384
Figure 11-240.	Ground Data (Theoretical Phasing) -10° Advance in Middle Antenna.	11-385
Figure 11-241.	Approach 17-02 BR Commissioned - Normal with Clearance.	11-389
Figure 11-242.	Approach 17-03 BR Commissioned - Normal with Clearance - (Repeat 17-02 BR).	11-390
Figure 11-243.	Approach 17-04 Commissioned - Normal without Clearance.	11-391
Figure 11-244.	Approach 17-05 BR Commissioned - A2 +15 Degrees, Clearance Off.	11-392
Figure 11-245.	Approach 17-06 Commissioned - A2 +15 Degrees, with Clearance.	11-393

		PAGE.
Figure 11-246.	Approach 17-07 BR Commissioned - A2 -15 Degrees, with Clearance.	11-394
Figure 11-247.	Approach 17–08 BR Commissioned – A3 +45 Degrees, with Clearance.	11-395
Figure 11-248.	Approach 17-09 BR Commissioned - A3 -45 Degrees, with Clearance.	11-396
Figure 11-249.	Approach 17-11 BR Theoretical - Normal with Clearance.	11-397
Figure 11-250.	Approach 17–23 BR Theoretical – Without Clearance.	11-398
Figure 11-251.	Approach 17-15 BR Theoretical - A2 +15 Degrees.	11-399
Figure 11-252.	Approach 17-16 BR Theoretical - A2 -15 Degrees.	11400
Figure 11-253.	Approach 17-17 BR Theoretical - Normal - (Repeat 17-12 BR).	11-401
Figure 11-254.	Approach 17-18 Theoretical - A1 -10 Degrees.	11-402
Figure 11-255.	Approach 17-19 BR Theoretical - A1 -20 Degrees.	11-403
Figure 11-256.	Approach 17-20 BR Theoretical - A1 -30 Degrees.	11-404
Figure 11-257.	Approach 17-21 BR Theoretical - A1 +20 Degrees.	11-405
Figure 11-258.	Approach 17-22 BR Theoretical - A2 -10 Degrees.	11-406
Figure 11-259.	Approach 17-23 BR Commissioned - A2 -20 Degrees.	11-407
Figure 11-260.	Approach 17-24 Commissioned - A2 -30 Degrees.	11-408
Figure 11-261.	Approach 17-25 BR Commissioned - A2 +20 Degrees.	11-409
Figure 11-262.	Approach 17-26 BR Commissioned - A2 -40 Degrees.	11-410
Figure 11-263.	Approach 17-27 BR Commissioned - A2 -50 Degrees.	11-411
Figure 11-264.	Approach 17-28 BR Commissioned - A2 -60 Degrees.	11-412

		PAGE
Figure 11-265,	Approach 17-30 BR Commissioned - A3 -30 Degrees.	11-413
Figure 11-266.	. Approach 17-31 BR Commissioned -A3 -40 Degrees.	11-414
Figure 11-267.	Approach 17-32 BR Commissioned - A3 -50 Degrees.	11-415
Figure 11-268.	Approach 17-33 BR Commissioned - A3 -60 Degrees.	11-416
Figure 11-269.	Approach 17-34 BR Commissioned - A3 -70 Degrees.	11-417
Figure 11-270.	Approach 17-35 BR Commissioned - A3 -80 Degrees.	11-418
Figure 11-271.	Approach 17-36 BR Commissioned - A3 -90 Degrees.	11-419
Figure 11-272.	Approach 17-37 BR Commissioned - A3 +60 Degrees.	11-420
Figure 11-273.	Approach 18-01 BR Theoretical - Normal.	11-421
Figure 11-274.	Approach 18-02 BR Theoretical - A2 +10 Degrees.	11-422
Figure 11-275.	Approach 18-03 BR Theoretical - A2 +20 Degrees.	11-423
Figure 11-276.	Approach 18-04 BR Theoretical - A2 +20 Degrees (Repeat 18-03 BR).	11-424
Figure 11-277.	Approach 18-05 BR Theoretical - A2 -10 Degrees.	11-425
Figure 11-278.	Approach 18-06 BR Theoretical - A2 -20 Degrees.	11-426
Figure 11-279.	Approach 18-07 BR Theoretical - Normal (Repeat 18-01 BR).	11-427
Figure 11-280.	Approach 18-08 BR Theoretical - A2 -30 Degrees.	11-428
Figure 11-281.	Approach 18-09 BR Theoretical - A2 -20 Degrees.	11-429
Figure 11-282.	Approach 18-10 BR Theoretical - A2 -40 Degrees.	11-430
Figure 11-283.	Approach 18-11 BR Experimental - Normal.	11-431
Figure 11-284.	Approach 18-12 BR Experimental - Normal (Mod Equality Reset).	11-432

		PAGE
Figure 11-285.	Approach 18-13 BR Experimental - Normal (Repeat 18-12 BR).	11-433
Figure 11-286.	Approach 18-14 BR Experimental - A2 -10 Degrees.	11-434
Figure 11-287.	Approach 18-15 BR Experimental - A2 -20 Degrees.	11-435
Figure 11-288.	Approach 18-16 BR Experimental - A2 -30 Degrees.	11-436
Figure 11-289.	Approach 18-17 BR Experimental - A2 +10 Degrees.	11-437
Figure 11-290.	Approach 18-18 BR Experimental - A3 +40 Degrees.	11-438
Figure 11-291.	Approach 18-19 BR Experimental - A3 -40 Degrees.	11-439
Figure 11-292.	Approach 18-20 BR Experimental - A2 -10 Degrees A1 -1 dB.	11-440
Figure 11-293.	Approach 18-21 BR Experimental - A2 -10 Degrees, A1 -3 dB.	11-441
Figure 11-294.	Approach 18–22 BR Experimental – A2 –10 Degrees, A1 –7 dB.	11-442
Figure 11-295.	Approach 18-23 BR Experimental - A2 -10 Degrees, A1 Shorted.	11-443
Figure 11-296.	Approach 18-24 BR Experimental - A2 -10 Degrees, A1 Open.	11-444
Figure 11-297.	Approach 18-25 BR Experimental - A2 -10 Degrees, A1 -1 dB.	11-445
Figure 11-298.	Approach 18-26 BR Experimental - A1 -10 Degrees, A2 -2 dB.	11-446
Figure 11-299.	Approach 18-27 BR Experimental - A2 -10 Degrees, A2 -4 dB.	11-447
Figure 11-300.	Approach 18-28 BR Experimental - A2 Shorted.	11-448
Figure 11-301.	Approach 18-29 BR Experimental - A2 Open.	11-449

		PAGE
Figure 11-302.	Approach 18-30 BR Experimental - A2 -10 Degrees, A3 -3 dB.	11-450
Figure 11-303.	Approach 18-31 BR Experimental - A2 -10 Degrees, A3 -6 dB.	11-451
Figure 11-304.	Approach 18-32 BR Experimental - A2 -10 Degrees, A3 -10 dB.	11-452
Figure 11-305.	Approach 18–33 BR Experimental – A2 –10 Degrees, A3 Shorted.	11-453
Figure 11-306.	Approach 18-34 BR Experimental - A2 -10 Degrees, A3 Open.	11-454
Figure 11-307.	Approach 18-36 BR Experimental - A2 -10 Degrees (Repeat 18-14 BR).	11-455
Figure 11-308.	Approach 18–37 BR Experimental – A2 –10 Degrees, 20 Degrees SBO Dephase.	11-456
Figure 11-309.	Approach 18–38 BR Experimental – A2 –10 Degrees, 30 Degrees SBO Dephase.	11-457
Figure 11-310.	Approach 18–39 BR Experimental – A2 –10 Degrees, 50 Degrees SBO Dephase.	11-458
Figure 11-311.	Approach 18-40 BR Experimental - A2 -10 Degrees, Clearance -3 dB.	11-459
Figure 11-312.	Approach 18-41 BR Experimental - A2 -10 Degrees, Clearance -6 dB.	11-460
Figure 11-313.	Approach 18-42 BR Experimental - A2 -10 Degrees, Clearance +3 dB.	11-461
Figure 11-314.	Approach 18-43 BR Experimental - A2 -10 Degrees, Clearance = +5.2 dB.	11-462
Figure 11-315.	Approach 18-44 BR Experimental - A2 -10 Degrees,	11-463

		PAGE
Figure 11-316.	Approach 18-45 BR Experimental - A2 -10 Degrees, PWR Divider A Clockwise.	11-464
Figure 11-317.	Approach 18-46 BR Experimental - A2 -10 Degrees, PWR Divider A CCW.	11-465
Figure 11-318.	Approach 18–47 BR Experimental – A2 –10 Degrees, PWR Divider B Clockwise.	11-466
Figure 11-319.	Approach 18-48 BR Experimental - A2 -10 Degrees, PWR Divider B CCW.	11-467
Figure 11-320.	Approach 18–49 BR Experimental – A2 –10 Degrees, Carrier PWR Divider Clockwise.	11-468
Figure 11-321.	Approach 18-50 BR Experimental - A2 -10 Degrees, Carrier PWR Divider CCW.	11-469
Figure 11-322.	Approach 18–51 BR Experimental – A2 –10 Degrees, Control Z8 Clockwise.	11-470
Figure 11-323.	Approach 18–52 BR Experimental – A2 –10 Degrees, Control Z8 CCW.	11-471
Figure 11-324.	Approach 18–53 BR Experimental – A2 –10 Degrees, Normal (Repeat 18–36 BR).	11-472
Figure 11-325.	Approach 18–54 BR Experimental – A2 –10 Degrees, Normal –8 Degree W.	11-473
Figure 11-326.	Approach 19-01 BR Theoretical - Normal.	11-474
Figure 11-327.	Approach 19-03 BR Theoretical - Normal (Repeat 19-01 BR).	11-475
Figure 11-328.	Approach 19-04 BR Theoretical - Normal,	11-476
Figure 11-329.	Approach 19-05 BR Theoretical - Normal, Clearance Off (Repeat 19-04 BR).	11-477
Figure 11-330.	Approach 19-06 BR Theoretical - Normal, Clearance Off (Repeat 19-04 BR).	11-478

PAG		PAGE
Figure 11-331.	Approach 19-07 BR Theoretical - Normal, Clearance Off (Repeat 19-04 BR).	11-479
Figure 11-332.	Approach 19-08 BR Theoretical - A2 -10 Degrees.	11-480
Figure 11-333.	Approach 19-09 BR Theoretical - A2 -20 Degrees.	11-481
Figure 11-334.	Approach 19-10 BR Theoretical - A2 -30 Degrees.	11-482
Figure 11-335.	Approach 19-11 BR Theoretical - A2 -40 Degrees.	11-483
Figure 11-336.	Approach 19–23 BR Theoretical Commissioned – Normal, Clearance Off.	11-484
Figure 11-337.	Approach 19-24 BR Commissioned - Normal, Clearance On.	11-485
Figure 11-338.	Centerline Profile.	11-490
Figure 11-339.	Topographical Map Indicating Terrain Around Glide Slope Reflecting Area.	11-491
Figure 11-340.	Approach 18-2 BR, Normal.	11-495
Figure 11-341.	Approach 18-3 BR, Normal.	11-4%
Figure 11-342.	Approach 18-4 BR, Normal.	11-497
Figure 11-343.	Approach 18-5 BR, Normal.	11-498
Figure 11-344.	Approach 18-6 BR, Normal, No Clearance.	11-499
Figure 11-345.	Approach 18-8 BR, SBO Reduced to Alarm.	11-500
Figure 11-346.	Approach 18-9 BR, SBO Reduced to Alarm.	11-501
Figure 11-347.	Approach 18-11 BR, Normal, 8° West of Centerline.	11-502
Figure 11-348.	Approach 18-12 BR, Normal, 8° East of Centerline.	11-503
Figure 11-349.	Approach 18-13 BR, Middle Antenna Phase Advanced	11-504

OH (Sepace 19-04 BM).

	1,13,000,000,000,000,000,000,000	PAGE
Figure 11-350.	Approach 18-15 BR, Middle Antenna Phase Retarded 14° to Alarm.	11-505
Figure 11-351.	Approach 18–17 BR, Middle Antenna Phase Advanced 28° to Twice Alarm.	11-506
Figure 11-352.	Approach 18–19 BR, Middle Antenna Phase Retarded 28° to Twice Alarm.	11-507
Figure 11-353.	Approach 18-21 BR, Middle Antenna Phase Advanced 28° to Twice Alarm, No Clearance.	11-508
Figure 11-354.	Approach 18–22 BR, Upper Antenna Phase Advanced 22° to Alarm.	11-509
Figure 11-355.	Approach 18–24 BR, Upper Antenna Phase Retarded 22° to Alarm.	11-510
Figure 11-356.	Approach 18–26 BR, Upper Antenna Phase Advanced 44° to Twice Alarm.	11-511
Figure 11-357.	Approach 18–28 BR, Upper Antenna Phase Retarded 44° to Twice Alarm.	11-512
Figure 11-358.	Approach 18–30 BR, Lower Antenna Phase Advanced 15° to Alarm.	11-513
Figure 11-359.	Approach 18–32 BR, Lower Antenna Phase Retarded 10° to Alarm.	11-514
Figure 11-360.	Approach 18–34 BR, Lower Antenna Phase Advanced 30° to Twice Alarm.	11-515
Figure 11-361.	Approach 18-36 BR, Lower Antenna Phase Retarded 20° to Twice Alarm.	11-516
Figure 11-362.	Approach 18-44 BR, Middle Antenna Attenuated 1 dB to Alarm.	11-517
Figure 11-363.	Approach 18-46 BR, Middle Antenna Attenuated 2 dB to Twice Alarm.	11-518
Figure 11-364.	Approach 18-48 BR, Upper Antenna Attenuated 2 dB to Alarm.	11-519

BOA

3(JA)					PAGE
11-505	Figure	11-365.	Approach 18-50 BR, to Twice Alarm.	Upper Antenna Attenuated 4 dB	11-520
308-11	Figure	11-366.	Approach 18-52 BR, to Alarm.	Lower Antenna Attenuated 1 dB	11-521
X02-13	Figure	11-367.	Approach 18-54 BR, to Twice Alarm.	Lower Antenna Attenuated 2 dB	11-522
806-11	Figure	11-368.	Approach 18-56 BR, Alarm.	CSB to SBO Phase Shifted 30° to	11-523
11-509	Figure	11-369.	Approach 18-57 BR, Alarm (Advance).	CSB to SBO Phase Shifted 30° to	11-524
015-11	Figure	11-370.	Approach 18-58 BR,	SBO Power Increased to Sharp Alarm.	11-525
112-11	Figure	11-371.	Approach 19-59 BR,	Normal.	11-526
	Figure	11-372.	Approach 18-60 BR,	Normal.	11-527
916-512	Figure	11-373.	Approach 18-39 AR,	Normal.	11-528
	Figure	11-374.	Approach 18-40 AR,	Normal.	11-529
	Figure	11-375.	Approach 18-41 AR,	Normal.	11-530
11-514	Figure	11-376.	Flight on the Localiz	DI Made with Different Scales on a zer Centerline 1600 Feet Above the	
			Site Elevation.	30° to Twice Alams	11-533
	Figure	11-377.	Redbird Airport CDI	and Differential Amplifier Traces.	11-535
Af6-11	Figure	11-378.	Geometry for Angle	Correction.	11-539
114517	Figure	11-379.	Redbird Profile Start	ing at Center of Tower Base.	11-543
216-11	Figure	11-380.	Topographic Map of at Redbird Airport.	Area Around Glide Slope Antennas	11-544
913-11		11-381.		ographic Map Showing Region in wallel to Centerline.	11-545

HST OF FIGURES (CONTINUED)

PAGE

11-36	Approach 13-13, 8°V/sht.	PAGE
Figure 11-382.	Approach 12-6, Normal.	11-548
Figure 11-383.	Approach 12-7, Normal.	11-549
Figure 11-384.	Approach 12–8, East Localizer Edge.	11-550
Figure 11-385.	Approach 12-9, West Localizer Edge.	11-551
Figure 11-386.	Approach 12–12, 8° East.	11-552
Figure 11-387.	Approach 12-13, 8° West.	11-553
Figure 11-388.	Approach 12-14, Normal.	11-554
Figure 11-389.	Approach 12-15, Normal.	11-555
Figure 11-390.	Approach 12-16, Normal.	11-556
Figure 11-391.	Approach 12-17, Normal.	11-557
Figure 11-392.	Approach 12-18, Normal.	11-558
Figure 11-393.	Approach 12–19, East Localizer Edge.	11-559
Figure 11-394.	Approach 12-20, West Localizer Edge.	11-560
Figure 11-395.	Approach 12-21, 8° West.	11-561
Figure 11-396.	Approach 12-26, Normal, Without Clearance.	11-562
Figure 11-397.	Approach 13-1, Normal.	11-563
Figure 11-398.	Approach 13-8, Normal.	11-564
Figure 11-399.	Approach 13-9, Increasing SBO.	11-565
Figure 11-400.	Approach 13-10, Increasing SBO.	11-566
Figure 11-401.	Approach 13-11, Increasing SBO.	11-567
Figure 11-402.	Approach 13-12, 8° West.	11-568

	TO THE PROPERTY OF THE PARTY OF	PAGE
Figure 11-403.	Approach 13-13, 8° West.	11-569
Figure 11-404.	Approach 13-14, 8° West.	11-570
Figure 11-405.	Approach 13-15, 8° West.	11-571
Figure 11-406.	Approach 13-16, Normal, Without Clearance.	11-572
Figure 11-407.	Approach 13-17, Normal.	11-573
Figure 11-408.	Approach 13–18, Middle Antenna Phase Retarded 15°.	11-574
Figure 11-409.	Approach 13-19, Middle Antenna Phase Retarded 12°.	11-575
Figure 11-410.	Approach 13-20, Normal.	11-576
Figure 11-411.	Approach 13-21, Middle Antenna Phase Advanced 12°.	11-577
Figure 11-412.	Approach 13-22, SBO Decreased to Broad Alarm.	11-578
Figure 11-413.	Approach 13-24, SBO Decreased to Broad Alarm.	11-579
Figure 11-414.	Approach 13–27, Middle Antenna Phase Retarded 11°.	11-580
Figure 11-415.	Approach 13-28, Middle Antenna Phase Advanced 9°.	11-581
Figure 11-416.	Approach 13–29, Middle Antenna Phase Advanced 7°.	11-582
Figure 11-417.	Approach 14-2, Normal.	11-583
Figure 11-418.	Approach 14-3, 8° West.	11-584
Figure 11-419.	Approach 14-4, 8° East.	11-585
Figure 11-420.	Approach 14-5, 8° East.	11-586
Figure 11-421.	Approach 14-7, SBO Decreased to Broad Alarm.	11-587
Figure 11-422.	Approach 14-8, SBO Decreased to Broad Alarm.	11-588
Figure 11-423.	Approach 14-9, Normal.	11-589
Figure 11-424.	Approach 14-10, SBO Decreased to Broad Alarm.	11-590

FAGE		PAGE
Figure 11-425.	Approach 14-11, SBO Decreased to Broad Alarm.	11-591
Figure 11-426.	Approach 14-12, SBO Decreased to Broad Alarm.	11-592
Figure 11-427.	Approach 14-15, SBO Increased to Sharp Alarm.	11-593
Figure 11-428.	Approach 14-18, SBO Phase Retarded 30°.	11-594
Figure 11-429.	Approach 14-19, SBO Phase Advanced 30°.	11-595
Figure 11-430.	Approach 14-20, Middle Antenna Phase Advanced 8°.	11-596
Figure 11-431.	Approach 14-21, Middle Antenna Phase Retarded 8°.	11-597
Figure 11-432.	Approach 14-22, Upper Antenna Phase Advanced 10°.	11-598
Figure 11-433.	Approach 14-24, Upper Antenna Phase Retarded 17°.	11-599
Figure 11-434.	Approach 14-32, Normal.	11-600
Figure 11-435.	Approach 15-3, Normal.	11-601
Figure 11-436.	Approach 15-4, Normal.	11-602
Figure 11-437.	Approach 15-5, SBO Decreased to Broad Alarm.	11-603
Figure 11-438.	Approach 15-6, Lower Antenna Phase Advanced 20°.	11-604
Figure 11-439.	Approach 15-8, Lower Antenna Phase Retarded 8°.	11-605
Figure 11-440.	Approach 15-10, Lower Antenna Phase Advanced 40°.	11-606
Figure 11-441.	Approach 15-12, Lower Antenna Phase Retarded 16°.	11-607
Figure 11-442.	Approach 15–14, Middle Antenna Attenuated 1 dB.	11-608
Figure 11-443.	Approach 15-16, Middle Antenna Attenuated 2 dB.	11-609
Figure 11-444.	Approach 15–18, Upper Antenna Attenuated 1 dB.	11-610
Figure 11-445.	Approach 15-20, Upper Antenna Attenuated 2 dB.	11-611
Figure 11-446.	Approach 15-22, Lower Antenna Attenuated 1 dB.	11-612

PAGE			PAGE
Figure 11-447.	Approach 15-26, Normal.	11-425.	11-613
Figure 11-448.	Approach 15-27, 8° West.	112426,	11-614
Figure 11-449.	Approach 15-28, 8° East.	11-427.	11-615
Figure 11-450,	Approach 15-30, SBO Doubled.		11-616
Figure 11-451.	Approach 15-31, SBO Increased to Sharp Alarm.	11-429.	11-617
Figure 11-452.	Approach 15-32, Normal.	,004-11	11-618
Figure 11-453.	Approach 15-34, Normal.	184-11	11-619
Figure 11-454.	Approach 15-35, Normal.	11-432.	11-620
Figure 11-455.	Approach 2-5, Normal.	11-433,	11-621
Figure 11-456.	Approach 2-6, Normal.	11-434,	11-622
Figure 11-457.	Approach 2-8, SBO Reduced to Broad Alarm.	11-435,	11-623
Figure 11-458.	Approach 2-9, SBO Reduced to Broad Alarm.	.604-61	11-624
Figure 11-459.	Approach 2-10, Normal.	11-437.	11-625
Figure 11-460.	Approach 2–11, Middle Antenna Phase Advanced	13°.	11-626
Figure 11-461.	Approach 2-12, Middle Antenna Phase Advanced	K18% 7.1	11-627
Figure 11-462.	Approach 2-13, Middle Antenna Phase Advanced	ANN 11	11-628
Figure 11-463.	Approach 2–14, Lower Antenna Phase Retarded 18	-55 17	11-629
Figure 11-464.	2 11 10 11 11 11 11 11 11 11 11 11 11 11		11-630
	Approach 2-17, Lower Antenna Attenuated .5 dB.	CV3 54	11-631
	Approach 2-18, Middle Antenna Attenuated .5 db	K5 K - 7 J	11-632
	00 31 debugge	233.77	
Figure 11-467.	Approach 2-19, Lower Antenna Attenuated 1.5 di	ALX 21	11-633
Figure 11-468.	Topographic Map of Columbus 10 R Glide Slope A	rea.	11-635

SOAS		PAGE
Figure 11-469.	Centerline Profile for Port Columbus 10R.	11-637
Figure 11-470.	Approach 19-4BC, Normal.	11-644
Figure 11-471.	Approach 19-6BC, SBO Decreased to Broad Alarm.	11-645
Figure 11-472.	Approach 19–8BC, Middle Antenna Phase Retarded 15°.	11-646
Figure 11-473.	Approach 19–9BC, Middle Antenna Phase Retarded 15°.	11-647
Figure 11-474.	Approach 19-10BC, Middle Antenna Phase Advanced 15°.	11-648
Figure 11-475.	Approach 19-11BC, Middle Antenna Phase Advanced 15°.	11-649
Figure 11-476.	Approach 19-13BC, Normal, Without Clearance.	11-650
Figure 11-477.	Approach 19-21BC, SBO Phase Advanced 30°.	11-651
Figure 11-478.	Approach 19-22BC, SBO Phase Advanced 30°.	11-652
Figure 11-479.	Approach 19-23BC, Middle Antenna Phase Retarded 13°.	11-653
Figure 11-480.	Approach 19-24BC, Middle Antenna Phase Advanced 8°.	11-654
Figure 11-481.	Approach 19-25BC, Middle Antenna Phase Retarded 18°.	11-655
Figure 11-482.	Approach 19-26BC, Middle Antenna Phase Advanced 24°.	11-656
Figure 11-483.	Approach 19-27BC, Lower Antenna Phase Retarded 14°.	11-657
Figure 11-484.	Approach 19–28BC, Lower Antenna Phase Advanced 10°.	11-658
Figure 11-485.	Approach 19–33BC, Upper Antenna Phase Retarded 85°.	11-659
Figure 11-486.	Approach 19–34BC, Upper Antenna Phase Advanced 84°.	11-660
Figure 11-487.	Approach 19–35BC, Upper Antenna Phase Advanced 60° and 3 dB Attenuation in Clearance.	11-661
Figure 11-488.	Approach 19–37BC, Upper Antenna Phase Retarded 58° and 3 dB Attenuation in Clearance.	11-662
Figure 11-489.	Approach 19-38BC, Upper Antenna Attenuated 5 dB.	11-663

		PAGE
Figure 11-490.	Approach 19-39BC, Upper Antenna Attenuated 10 dB.	11-664
Figure 11-491.	Approach 19-41BC, Middle Antenna Attenuated 2 dB.	11-665
Figure 11-492.	Approach 19–43BC, Middle Antenna Attenuated 3 dB.	11-666
Figure 11-493.	Approach 19-44BC, Lower Antenna Attenuated 2 dB.	11-667
Figure 11-494.	Approach 19-45BC, Lower Antenna Attenuated 3 dB.	11-668
Figure 11-495.	Approach 19-17BC, Normal-Low Approach.	11-669
Figure 11-496.	Approach 20-4BC, Normal, Null-Reference.	11-670
Figure 11-497.	Approach 20–5BC, Normal, SBO Adjusted for Normal Width.	11-671
Figure 11-498.	Approach 20-8BC, Normal, Null-Reference.	11-672
Figure 11-499.	Approach 20-9BC, Normal, Aircraft at 500° AGL.	11-673
Figure 11-500.	Approach 20-13BC, System Restored to Normal CEGS.	11-674
Figure 11-501.	Lower Antenna Attenuated 3 dB to Greater than 200% Alarm.	11-675
Figure 11-502.	Phase of Lower Antenna Advanced 15° to Twice Alarm.	11-676
Figure 11-503.	Phase of Lower Antenna Advanced 10° to Alarm.	11-677
Figure 11-504.	Sideband/Carrier Dephasing; -30°.	11-678
Figure 11-505.	Sideband/Carrier Dephasing; +30°.	11-679
Figure 11-506.	Phase of Middle Antenna Advanced 8° to Alarm.	11-680
Figure 11-507.	Phase of Middle Antenna Advanced 24° to Twice Alarm.	11-681
Figure 11-508.	Phase of Lower Antenna Retarded 14° to Alarm.	11-682
Figure 11-509.	Phase of Lower Antenna Retarded 19° to Twice Alarm.	11-683
Figure 11-510.	Phase of Middle Antenna Retarded 13° to Alarm.	11-684

		PAGE
Figure 11-511.	Upper Antenna Retarded 50° to Alarm (Clearance Reduced 3 dB).	11-685
Figure 11-512.	Upper Antenna Advanced 60° to Alarm (Clearance Reduced 3 dB).	11-686
Figure 11-513.	Upper Antenna Attenuated 5 dB to Alarm.	11-687
Figure 11-514.	Upper Antenna Attenuated 10 dB to 133% Alarm.	11-688
Figure 11-515.	Lower Antenna Attenuated 2 dB to 114% Alarm.	11-689
Figure 11-516.	Middle Antenna Attenuated 3 dB to 170% Alarm.	11-690
Figure 11-517.	Middle Antenna Attenuated 2 dB to 128% Alarm.	11-691
Figure 11-518.	Phase of Upper Antenna Advanced 84° to Alarm.	11-692
Figure 11-519.	Normal Run.	11-693
Figure 11-520.	Comparison of Monitor Response to Measured Far- Field Response.	11-694
Figure 11-521.	Configuration for Making Probe Measurements.	11-699
Figure 11-522.	Jog-Held Probe Placement on an FA-8976 Antenna Element.	11-700
Figure 11-523.	Photograph of Magnetic Induction Probe.	11-701
Figure 11-524.	Schematic Representation of Magnetic Induction Probe.	11-702
Figure 11-525.	Element Dimensions for the FA-8976 Glide Slope Antenna.	11-705
Figure 11-526.	Coordinate System for Magnetic Field Analysis.	11-706
Figure 11-527.	Probe Measured Amplitude of Elements of the FA-8976 Antenna Versus Distance.	11-709
Figure 11-528.	Probe Measured Phase of Elements of the FA-8976 Antenna Versus Distance.	11-710

		PAGE
Figure 11-529a.	Isometric Projection of Probe Jig.	11-713
Figure 11-529b.	Drawing of Probe Jig with Dimensions.	11-714
Figure 11-530.	Change in Capture Effect Glide Slope Path Angle (3.0° Normal) Caused by Antenna Dephasing.	11-715
Figure 11-531.	Change in Capture Effect Glide Slope Path Width (.7° Normal) Caused by Antenna Dephasing.	11-716
Figure 11-532.	Change in Capture Effect Glide Slope Path Angle (3.0° Normal) Caused by Signal Attenuation.	11-717
Figure 11-533.	Change in Capture Effect Glide Slope Path Width (.7° Normal) Caused by Signal Attenuation.	11-718
Figure 11-534.	Horizontal Free Space Radiation Pattern for Antenna Array.	11-720
Figure 11-535.	Measured Radiation Pattern for a Typical FA-8976 Antenna Along with FAA Specifications.	11-722
Figure 11-536.	Theoretical Three-Element Array Compared with APC FA-8976 Antenna - Amplitude Horizontal Pattern.	11- <i>7</i> 23
Figure 11-537.	Theoretical Horizontal Phase Pattern for Three- Element Array Compared with Measured Pattern for APC FA-8976.	11-724
Figure 11-538.	Simulated Radiation Pattern for a FA-8976 Antenna with a 3 dB Attenuation in the Third Element.	11-728
Figure 11-539.	Plot of Phase of a Simulated Radiation Pattern for a FA-8976 Antenna with a 3 dB Attenuation in the Third Element.	11-729
(yels: 11-706		
Figure 11-540.	Antenna Test Range Layout.	11-734
Figure 11-541.	The Tamiami Antenna Test Range.	11-735
Figure 11-542.	Impedance and VSWR Test Configuration.	11-735

		PAGE
Figure 11-543a.	The Antenna under Test as seen from the Far-Field Measurement Position.	11-736
Figure 11-543b.	The Far-Field Receiving Dipole as seen from the Far-Field Measurement Point.	11-736
Figure 11-544.	Probe Measurements on the APC FA-8976.	11-738
Figure 11-545a.	Horizontal Radiation Pattern for AIL FA-8651 S/N 126.	11-740
Figure 11-545b.	Horizontal Phase Pattern for the AIL FA-8651 S/N 126.	11-741
Figure 11-546a.	Horizontal Radiation Pattern for AIL FA-8651 S/N 132.	11-742
Figure 11-546b.	Horizontal Phase Pattern for the AIL FA-8651 S/N 132.	11-743
Figure 11-547a.	Horizontal Radiation Pattern for AIL FA-8651 S/N 132.	11-744
Figure 11-547b.	Horizontal Phase Pattern for the AIL FA-8651 S/N 153.	11-745
Figure 11-548a.	Horizontal Radiation Pattern for AIL FA-8651 S/N 160.	11-746
Figure 11-548b.	Horizontal Phase Pattern for the AIL FA-8651 S/N 160.	11-747
Figure 11-549a.	Horizontal Radiation Pattern for SCA FA-8730.	11-748
Figure 11-549b.	Horizontal Phase Pattern for the SCA FA-8730.	11-749
Figure 11-550a.	Horizontal Radiation Pattern for APC FA-8976.	11-750
Figure 11-550b.	Horizontal Phase Pattern for the APC FA-8976.	11-751
Figure 11-551.	Input Port IDR Trace - AIL, FA-8651 S/N 126.	11-753
Figure 11-552.	Input Port TDR Trace - AIL, FA-8651 S/N 132.	11-753
Figure 11-553.	Input Port TDR Trace - AIL, FA-8651 S/N 153.	11-753
Figure 11-554.	Input Port TDR Trace - AIL, FA-8651 S/N 160.	11-754
Figure 11-555.	Input Port TDR Trace, Scanwell FA-8730, S/N 9.	11-754
Figure 11-556.	Input Port TDR Trace, APC FA-8976, S/N C013.	11-754

	The state of the s	PAGE
Figure 11-557a.	"Bubble Pad" Wrapped Around the Center Dipole of the AIL FA-8651 Glide Slope Antenna.	11-757
Figure 11-557b.	Shorted Center Dipole Test of the AIL FA-8651.	11-757
Figure 11-557c.	Spraying the Right Dipole Elements of the AIL FA-8651.	11-758
Figure 11-557d.	Injection of Water in the Feed Area of the Stripline of the AIL FA-8651.	11-758
Figure 11-558.	Polyurethane Foam Being Cut Away.	11-759
Figure 11-559.	Water Corrosion on the Left Dipole of the FA-8651.	11-760
Figure 11-560.	Corrosion on the Stripline Device.	11-761
Figure 11-561.	A Perturbational Influence Impacting the Glide Slope Antenna May be Expected to be Evident in the Far- Field Radiation, the Antenna's Monitor Port, and	
	Possibly at the Input Port.	11-763
Figure 11-562.	Generalized Site in Rolling Terrain with Proposed Runway Extension.	11-770
Figure 11-563.	Generalized Case for Ground Plane Fill.	11-771
Figure 11-564.	Illustration of Truncated and Lowering Ground Plane.	11-774
Figure 11-565.	Illustration of Truncating and Lowering Ground Plane.	11-775

Jour Part 108 Lane - AND PA-8651 SAN 152.

LIST OF TABLES

PAGE			PAGE
Table 4-1.	Harmonics Levels Present in 90 Hz Output.		4-25
Table 4-2.	Analysis Data.		4-29
Table 4-3.	Test Data		4-32
Table 4–4.	List of Faults Induced in the Three Glide Slope Antennas Tested.		4-84
Table 4-5.	Difference Values Observed Between DC-3 and Beechcraft 35.	5-16. 3-17.	4-190
Table 4-6.	Reference Data. 201 parts of supposed northpold	.81-8	4-192
Table 4-7.	Experimental Data.		4-193
Table 5-1.	Data Illustrating Localizer Processor Relative Performance of Collins 51 R-3 and Ohio University		
	Processor Working with a Narco NAV 11.		5-3
Table 5-2.	Clearance System.		5-5
Table 5-3.	Course System.		5-6
Table 5-4.	Course System Carrier Input Fed.		5-7
Table 5-5.	Antenna Feed Line Measurements.		5-19
Table 5-6.	Antenna Element Measurements.		5-20
Table 5-7.	Alford 12-Element Distributions.		5-21
Table 5-8.	Wilcox 14-Element Distributions.	5-26,	5-22
Table 5-9.	Sideband Distributions as Measured on Antennas.		5-23
Table 5-10.	Carrier Distributions as Measured on Antennas.		5-24
Table 5-11.	System Normal - Antenna Amplitudes and Phases.	5-29.	5-25
Table 5-12.	dB Taper for Three Frequencies with Alford and Wild Distribution Systems.	ox -	5-49
	Carrier Equality Unith Measurements.		

		PAGE
Table 5-13.	Microvolts at Receiver Input as Function of Distance from Array Along Extended Centerline at 1500 Feet	Table 4-1,
4-29	Altitude.	5-50
Table 5-14.	Listing of Low Clearance Points.	5-62
Table 5-15.	Monitor Response Data, 108.5 MHz.	5-64
Table 5-16.	Monitor Response Data, 109.7 MHz.	5-65
Table 5-17.	Monitor Response Data, 111.9 MHz.	5-66
Table 5-18.	Monitor Response Data, 108.5 MHz.	5-67
Table 5-19.	Monitor Response Data, 109.7 MHz, May 14, 1975.	5-68
Table 5-20.	Monitor Response Data, 111.9 MHz.	5-69
Table 5-21.	Monitor Response to Phase Lags Just Sufficient to Initiate Alarm, 108.5 MHz.	5-70
Table 5-22.	Monitor Response to Phase Lags Just Sufficient to Initiate Alarm, 109.7 MHz.	5-71
Table 5-23.	Monitor Response to Phase Lags Just Sufficient to Initiate Alarm, 111.9 MHz.	5-72
Table 5-24.	Summary of Monitor Alarms Classified According to Figure 5-43.	5-73
Table 5-25.	Null Checks of Antenna Pairs.	5-74
Table 5-26.	Null Checks of Center Antenna Pairs.	5-75
Table 5-27.	Antenna Feedline Power.	5-75
Table 5-28.	Power at Monitor Box Inputs.	5-76
Table 5-29.	Course Transmitter Phasing.	5-76
Table 5-30.	Clearance Transmitter Phasing.	5-77
Table 5-31.	Carrier Equality Drift Measurements.	5-77

7547

		PAGE
Table 5-32.	Antenna Phase Changes.	5-78
Table 5-33.	Transmitter Power Drift.	5-78
Table 5-34.	Simulated Clearance and Pre-Combiner Clearance Monitor Responses to 3 dB Fault Test at 109.7 MHz.	5-83
Table 5–35.	Simulated Clearance and Pre-Combiner Clearance Monitor Responses to 3 dB Fault at 108.5 MHz.	5-84
Table 5-36.	Simulated Clearance and Pre-Combiner Clearance Monitor Responses to 3 dB Fault Test at 111.9 MHz.	5-85
Table 5-37.	Simulated Clearance and Pre-Combiner Clearance Monitor Response to 30° Phase Fault at 109.7 MHz.	5-86
Table 5-38.	Simulated Clearance and Pre-Combiner Clearance Monitor Response to 30° Phase Fault at 108.5 MHz.	5-87
Table 5-39.	Simulated Clearance and Pre-Combiner Clearance Monitor Response to 30° Phase Fault at 111.9 MHz.	5-88
Table 5-40.	Monitor Alarms for Out-of-Tolerance Conditions of Course Centerline Alginment or Course Width.	5-91
Table 5-41.	Summary of Localizer Standard Flight Check.	5-95
Table 5-42.	Flight Check Results for Selected Faults.	5-96
Table 5-43.	Ground Orbit Results for Those Faults Which Showed Less than 2000 Microamperes Clearance or Excessive Course Width Changes.	5-98
Table 5-44.	Variable Phase Fault Data.	5-101
Table 5-45.	3 dB Attenuation Fault Data.	5-108
Table 5-46.	A Comparison of the Field Responses on Centerline and the Phase Faults Necessary to Produce a Monitor Alarm for the Three Test Frequencies.	5-135
Table 5-47.	Summary of Ohio University Flight Test Results.	5-144

PAGE.

58-2

5-105

		PAGE
Table 5-48.	Data Summary for Small Aperture Array for FAA Flight Test Data.	5-145
Table 5-49.	Data Summary for Medium Aperture Array for FAA Flight Test Data.	5-146
Table 5-50.	Summary of Usable Distance.	5-147
Table 5-51.	Carrier/SBO Dephasing.	5-148
Table 6-1.	Comparisons of CPU Running Time Between the Physical Optics (P.O.) Approximation and the High Frequency Theory of Diffraction Approximation (GTD).	6-40
Table 6-2.	Kodiak Path Angle Calculations by Two Different Methods.	6-74
Table 6-3.	Kodiak Path Width and Symmetry Calculations.	6-75
Table 6-4.	Calculated Path Angles for Untried Capture Effect System.	6-79
Table 6-5.	Comparison of Measured and Calculated Results for Kodiak NR and SBR Tests.	6-83
Table 6-6.	Path Data for Several Untried Systems Calculated Using Physical Optics.	6-84
Table 6-7.	Path Data for Several Untried Systems Calculated Using the Geometrical Theory of Diffraction.	6-85
Table 8-1.	Proposed Criteria for Glide Slope Recordings.	8-2
Table 9-1.	Predicted System Parameters at 110.497 MHz.	9-3
Table 11-1.	Summary of Reaction Time Delays.	11-14
Table 11-2.	Time in Seconds for Selected Angular Intervals of 1000 Foot Level Flight at 140 Kts.	11-14
Table 11-3.	Comparison of Calculated Values for Path Angle and Width to Measured Values.	11-16

	TODORATORO CATRATAO (OL)	PAGE
Table 11-4.	Fault Events.	11-153
Table 11-5.	Monitor Responses and Flight Check Results for 30 Faults Introduced into the Watts Glide-Slape System.	11-154
Table 11-6.	Effects of Changing Transmitters on the Watts System.	11-163
Table 11-7.	Effects of Antenna Misalignment.	11-163
Table 11-8.	Fault Events. 20 > \ 0 0 000 000000000000000000000000	11-166
Table 11-9.	Monitor Response and Flight Check Results for Seven Faults Introduced into the Watts Glide-Slope System.	11-168
Table 11-10.	Responses to System Faults.	11-209
Table 11-11.	Nominal Values for Transverse Path Structure Seen at 5.4 Nautical Mile Range, 1600 Feet Altitude.	11-223
Table 11-12.	Path Angle and Width Values as a Function of Azimuth	. 11-231
Table 11-13.	Listing of Quality Figures for Several Fault Conditions	00-11-231
Table 11-14.	Comparison of Quality Figures for the Standard and Expanded Aperture Versions of the Watts Mark 3 Endfire Glide-Slope Antenna.	11-233
Table 11-15.	Quality Figures Derived from Records Taken of Transverse Path Structures Before and After Changes of Antenna Sections and Antenna Heights.	11-236
Table 11-16.	Figures of Merit for Perpendicular Structure.	11-293
Table 11-17.	Figures of Merit for Perpendicular Cut Data.	11-309
Table 11-18.	Calculated Performance Along Localizer Edge.	11-313
Table 11-19.	Summary of Fault Test Results.	₹E- 11-319
Table 11-20.	Experimental Results.	11-327
Table 11-21.	Path Angle for Zero DDM in Degrees for Indicated Tilt and Displacement of Upper Antenna.	11-333

		PAGE
Table 11-22.	Comparison of Flight Test Data and Monitor Results.	11-342
Table 11-23.	Relative Amplitudes of Frequency Components in Detected SBO + CSB Signal as Function of Co/A Ratio.	11-347
Table 11-24.	Relative Amplitudes of Frequency Components in Detected SBO + CSB Signal as Function of C _a /S Ratio where C _a /< 0.	11-348
Table 11-25.	no Null Reference. and trights brus supposed notino.	11-349
Table 11-26.	Capture Effect.	11-350
Table 11-27.	Antenna Currents.	11-358
Table 11-28.	APCU Calibration.	11-360
Table 11-29.	Ground Monitor Data Site as Commissioned.	11-361
Table 11-30.	Ground Monitor Data Site as Commissioned.	11-362
Table 11-31.	Ground Monitor Data Theoretical Phasing.	11-379
Table 11-32.	Airborne Data.	11-386
Table 11-33.	Comparison of Near-Field/Far-Field Results for Various Fault Conditions.	11-494
Table 11-34.	Fault Data.	11-537
Table 11-35.	Azimuthal Data.	11-538
Table 11-36.	Far-Field and Monitor Response to Certain Fault Conditions.	11-547
Table 11-37.	System Outputs, Columbus 10R.	91-11-639
Table 11-38.	Far-Field Response.	.011-642
Table 11-39.	Hand-Held Probe Measurements Taken from the Lower Antenna of a Commissioned Glide Slope Facility.	11-704

		PAGE
Table 11-40.	Matrix of Characteristics.	11-739
Table 11-41.	Normalized Fault Data for AIL FA-8651 S/N 126.	11-755
Table 11-42.	AlL Mark 1B Monitor Response to Lower Antenna Monitor Line Faults.	11-764
Table 11-43.	AlL Mark 1B Monitor Response to Middle Antenna Monitor Line Faults.	11-765
Table 11-44.	Budget for Reducing Fill.	11-773

XI. GLIDE SLOPE

A. Computer Model for Image Glide Slope Systems.

1. General. This section describes a Fortran program which has been designed as a research tool for use in the study of the effects of various faults on the field patterns of an ILS image glide slope.

Since y is the ongle perween E, and E, this very be written in phases (complex) form

The inputs are complex antenna currents, antenna heights and distances from runway centerline, antenna mast tilt angles, complex dielectric constant of the reflecting surfaces, modulation factors and the observer location.

2. The Model. Since the main output of the program is DDM, this is a logical point of departure for an explanation of the model used.

DDM is defined as the difference between the depths of the 150 Hz and 90 Hz modulations.

$$DDM = M_{150} - M_{90} ag{11.1}$$

$$M_{150} = (E_{cs}_{150} + E_{ss}_{150} + E_{cs}_{150})/E_{c}$$
 (11.2)

where E_{cs}^{150} is the magnitude of the carrier accompanied sidebands for the 150 Hz modulation

E_{ss150} is the magnitude of the suppressed carrier sidebands for 150 Hz modulation

 γ_{150} is the angle between these phasors

E is the magnitude of the carrier.

The reason for the cosine term is that only the component of the sidebands in phase with the carrier produces fundamental amplitude modulation. The quadrature components produce phase modulation and harmonic amplitude modulation.

Similarly,

$$M_{90} = (E_{cs}90 + E_{ss}90\cos\gamma_{90})/E_{c}$$
 (11.3)

Since γ_{90} differs from γ_{150} by 180° this leads to

DDM =
$$(E_{cs}_{150} + E_{ss}_{150}\cos\gamma_{150} - E_{cs}_{90}\cos\gamma_{150})/E_{c}$$
 (11.4)

but
$$E_{cs}90 = E_{cs}150$$
, $E_{ss}90 = E_{ss}150$, and $E_{cs} = mE_{c}$, from which

$$DDM = 2mE_{ss} \cos \gamma / E_{cs}$$
 (11.5)

Since γ is the angle between E_{ss} and E_{cs} this may be written in phasor (complex) form as

 $DDM = Real (2mE_{ss}/E_{cs})$ (11.6)

In general there are six components for each phasor, one from each antenna and one from the image of each antenna. Not all of these components are non-zero for presently used configurations. For example, none of the phasors exists for antenna 3 or its image (3 is the highest antenna) for the null reference system while antenna 1 and its image transmit only E_c and E_{cs} and antenna 2 and its image transmit only E_{ss} . This presents no problem in a computer solution since it is only necessary to enter (0.0,0.0) for those currents (and/or antennas) not present.

To calculate the DDM one must first evaluate various phasors involved, add those of like subscript (cs, cc, ss,) and apply (11.6).

To calculate E in terms of the input data (antenna currents) one assumes that all paths are so nearly the same length that the dependence of magnitude on distance of travel will be negligibly different for all components. Since the fields at any point of interest will be proportional to the antenna currents producing them, the quantity of interest for the waves from the antennas will be the phase delay produced by the path length. Thus

$$\hat{E} = A\hat{l}\exp(-i\beta r) \tag{11.7}$$

where β is in radians per unit distance, or $\beta = 2\pi$ if r is in wavelengths.

For the reflected waves

$$\hat{E} = A\rho \hat{l} \exp(-j\beta r)$$
 (11.8)

where ρ is the complex reflection coefficient for horizontally polarized waves at a horizontal surface. This is given by

$$\rho = \left\{ \cos i - \sqrt{(\varepsilon - \sin^2 i)} \right\} \left\{ \cos i + \sqrt{(\varepsilon - \sin^2 i)} \right\}$$

where i is the angle of incidence (angle between wave and ground normals, or the complement of the angle between the direction of wave travel and the horizontal surface) and ϵ is the relative complex dielectric constant of the reflecting surface.

r is given by

$$r = \sqrt{(x - x_{t} - \epsilon)^{2} + (y - y_{t})^{2} + (z - z_{t})^{2}}$$

where x is the horizontal distance measured normal to the runway centerline from tower base to observer

 x_{\downarrow} is the displacement of the antenna in the x direction due to mast tilt

y is the horizontal distance measured parallel to the runway

y, is the displacement in the y direction due to tilt

z is the vertical distance to the observer from the ground

z, is the antenna height with tilt

e is the antenna offset in the x direction.

Used in conjunction with the carrier sideband and sideband only antenna currents, these formulas permit calculation of the DDM without capture effect. In the capture effect case an empirical formula is used to determine the DDM as a function of the ratio of the main and clearance carrier strengths.

$$DDM_c = ((M_{150} - DDM)/(1 + Q^{-2.5})) + DDM$$

where DDM is the DDM including the effect of the clearance signal

Q is the ratio of the clearance carrier magnitude to the main carrier magnitude

M₁₅₀ is the modulation index of the clearance signal.

DDM is calculated as 2 times the modulation index (M) times the real part of the complex ratio of $E_{\rm SS}$ to $E_{\rm CS}$. Due to faults introduced, $E_{\rm CS}$ may become very much smaller than $E_{\rm SS}$ at some locations in the field. This gives rise to very large DDM values (when the angles are such that the real part becomes very large). Such large DDM's are false results since a DDM greater than 2M indicates over-modulation and the accompanying distortion. In order to avoid such results, each DDM is tested and if it is greater than 2M, DDM is set equal to 2M (which in this case is 0.8). This result is not to be taken literally but merely as an indication of a high DDM.

In order to make the results more useful in capture effect studies, the calculated DDM without clearance signal is saved as UDDM and printed out along with the DDM with clearance. A printout of the program with comments appears on the following pages, with an example of output in Figures 11-1 and 11-2.

The columns of output data are identified as:

alpha = elevation angle base of pole to observer

μA = CDI in microamperes (static)

DDM = DDM with clearance signal

Phase = angle between E and E phasors

UDDM = DDM without clearance signal

Q = ratio of clearance carrier amplitudes to main carrier

Input data is given as:

```
real component of complex sideband phasor on antenna 1 (lowest)
ISI R
        imaginary component of complex sideband phasor on antenna 1
ISI IM
IS2 R
IS2 IM
        as above for antenna 2 (middle) and antenna 3 (upper)
IS3 R
1S3 IM
ICI R
ICI IM
1C2 R
        as above but for complex carrier sideband phasors
IC2 IM
IC3 R
IC3 IM
CEC R
        real component of complex dielectric constant
CEC IM
        imaginary component of complex dielectric constant
HI U
        height of lower antenna in wavelengths
HI L
        height of image of lower antenna below ground
H2 U
        as above for middle antenna
H2 L
H3 U
        as above for upper antenna
H3 L
EPSI 2
        offset of middle antenna wrt lower antenna
EPSI 3
        offset of upper antenna wrt lower antenna
Y
        horizontal distance to observer along centerline in wavelengths
X
        horizontal distance from pole to centerline in wavelengths
        antenna tilt from vertical
Theta
        direction of antenna tilt (0° for tilt toward runway)
Phi
        modulation factor
M
        clearance modulation factor
MC 150
ICC1 R
ICCI IM
ICC2 R
        complex clearance phasor components
ICC2 IM
ICC3 R
ICC3 IM
```

3. FORTRAN Program Listing

```
CALCOMP.PLOTT
GENERALIZED COMPUTER PROGRAM TO DETERMINE THE EFFECTS ON THE ILS
RESULTING FROM FAULTS INTO THE SYSTEM INCLUDING ANTENNA SHIFTS
AND CHANGING COMPLEX DIELECTRIC COEFFICIENTS.
0000
            IMPLICIT REAL*8(A,9.D-H.N.C-Z).COMPLEX*16(C)
COMPLEX*16 IS1.IS2.IS3.IC1.IC2.IC3.ICC1.ICC2.ICC3.FSS.ECS.ECC.
RHO1.RHO2.RHO3.TIA.TIE.TIC.TID.TIE.TIF.TIG.TIH.TII
DIMENSION FEL(17.2.2).A(17.2)
REAL*4 TTL(80).TTL2
REAL BXX(6).BXY(6)
            REAL *4 AXX(490), AXY(490)
DIMENSION BUF(5000)
DATA TTL2/' '/
             DATA TTL2/
            CALL PLOTS(BUF.20000.10)
ALL PARAMETERS SUCH AS ANTENNA FEED, ANTENNA HEIGHTS. COMPLEX
DIELECTRIC COEFFICIENTS. ETC.. ARE READ INTO THE PRIGRAM AS DATA
                      INDIVIDUAL CARDS.
             GO TO 17
         1 CUNTINUE
             READ(5,2) (((FEL(K1.K2.K3).K3=1.2).K2=1.2).K1=1.17)
         2 FURMAT (4A3)
         PI = 3.14159265358979323846264
3 READ(5.4.END=29) ((A(J1.J2).J2=1.2).J1=1.17)
        3 READ(5.4.END=29) ((A(J1.J2).J2=1.2).J1=1.17)
4 FURMAT(2F10.3)
EQUIVALENCE (A(8.1).H1U).(A(8.2).H1L).(A(9.1).H2U).(A(9.2).H2L).
> (A(10.1).H3U).(A(10.2).H3L).(A(11.1).EPS12).(A(11.2).EPS13).
> (A(12.1).Y).(A(12.2).X).(A(13.1).THETA).(A(13.2).PHI).(A(14.1).
> M).(A(14.2).MC150)
ISI = DCMPLX(A(1.1).A(1.2))
IS2 = DCMPLX(A(2.1).A(2.2))
IS3 = DCMPLX(A(3.1).A(3.2))
IC1 = DCMPLX(A(3.1).A(3.2))
IC2 = DCMPLX(A(4.1).A(4.2))
IC2 = DCMPLX(A(4.1).A(4.2))
IC3 = DCMPLX(A(6.1).A(6.2))
CEC = DCMPLX(A(15.1).A(15.2))
ICC1 = DCMPLX(A(15.1).A(15.2))
ICC2 = DCMPLX(A(16.1).A(16.2))
ICC3 = DCMPLX(A(16.1).A(16.2))
ICC3 = DCMPLX(A(17.1).A(17.2))
X=155.46
             X=155.46
Y=10000.0
CCC
             PRINT OUT OF INPUT DATA.
            PRINT 5
        5 FORMAT ( THE INPUT DATA IS AS FOLLOWS )
        WRITE(6.6) (A(KV.1).(FEL(KV.1.KC).KC=1.2).A(KV.2).(FEL(KV.2.KB).
> KB=1.2).KV=1.17)
6 FORMAT(* *.F10.3.2X.2A3.4X.F10.3.2X.2A3)
         PRINT 7.Y
7 FORMAT( THE DISTANCE OUT FROM THE ANTENNA.
         8 FURNAT( *OALPHA * . 1x . *UA* .6x . * DDM* .5x . * PHASE* .4x . *UDDM* . 3x . *Q*)
             GO TO 22
         9 CONTINUE
             D = DSQRT(X*X+Y*Y)
             THETA = THETA+PI/180.0
PHI = PHI+PI/180.0
            DO 15 J=1.61
               COMPUTATION OF ELEVATION ANGLE IN ONE TENTH OF DEGREE STEPS.
             ALPHA = (J-1.0)/10.0
AP = ALPHA+PI/180.
             Z = D+DTAN(AP)
CCC
             COMPUTATION OF ANTENNA TILT.
                                                                                              THIS PAGE IS BEST QUALITY PRACTICAL
             TMA = DSIN(THETA)
             TMB = TMA+DCOS(PHI)
TMC = TMA+DSIN(PHI)
                                                                                               TROM GOPY PURMISHED TO DDC
                    = DCOS ( THE TA)
                    = HIU+TMB
```

```
X2T = H2U*TMB
                                                   X3T = H3U*TMB
                                                   YIT = HIU*TMC
                                                                        =
                                                                                     H2U*TMC
                                                   Y3T = H3L*TMC
                                                   ZIT
                                                                      = H1U*TMD
                                                   ZZT = HZU#TMD
                                                   Z3T = H3U+TMD
               000
                                                  COMPUTATION OF DISPLACEMENT FROM ANTENNA ELEMENT TO OBSERVER.
                                                 TMA = (X-X1T)**2+(Y-Y1T)**2

TMB = (X-X2T-EPSI2)**2+(Y-Y2T)**2

TMC = (X-X3T-EPSI3)**2+(Y-Y3T)**2

R1U = DSQRT(TMA+(Z-Z1T)**2)

R3U = DSQRT(TMB+(Z-Z2T)**2)

R3U = DSQRT(TMC+(Z-Z3T)**2)

R1L = DSQRT(TMA+(Z+Z1T)**2)

R2L = DSQRT(TMB+(Z+Z2T)**2)
                                                 R2L = DSURT(TM8+(Z+Z2T)**2)
R3L = DSURT(TMC+(Z+Z3T)**2)
                                                  COMPUTATION OF REFLECTION COEFFICIENT FOR ANTENNA NO. 1
                                                   BETAL = DARCGS(D/RIL)
                                                  SI1 = PI/2.0D0-BETA1
CSIN1 = DCMPLX(DSIN(SI1)**2.0.0D0)
                                                  CSUM1 = CEC-CSIN1
CRUDT1 = CDSQRT(CSUM1)
                                                 CCUS1 = DCMPLX(DCGS(SI1),0.0D0)
CN1 = CCGS1-CRUGTI
CD1 = CCGS1+CRUGTI
                                                                                                                                                               GIALLICE LA CONTRACTOR DE LA CONTRACTOR 
                                                   RHC1 = CN1/CD1
                                                 COMPUTATION OF REFLECTION COEFFICIENT FOR ANTENNA NO. 2
                                                   BETA2 = DARCOS(D/R2L)
                                                 BETA2 = DARCOS(D/R2L)
SI2 = FI/2.0D0-BETA2
CSIN2 = DCMPLX(DSIN(SI2)**2.0.0D0)
CSUM2 = CEC-CSIN2
CROOT2 = CDSQRT(CSUM2)
CCOS2 = DCMPLX(DCDS(SI2).0.0D0)
CN2 = CCOS2-CROOT2
CD2 = CCUS2+CROOT2
RHO2 = CN2/CD2
               CCC
                                                   COMPUTATION OF REFLECTION COEFFICIENT FOR ANTENNA NO. 3
                                                   BETA3 = DARCOS (D/R3L)
                                                  BETA3 = DARCOS(D/R3L)
SI3 = P1/2.0D0-BETA3
CSIN3 = DCMPLX(DSIN(SI3)**2.0.0D0)
CSUM3 = CEC-CSIN3
CROUT3 = CDSQRT(CSUM3)
CCUS3 = DCMPLX(DCOS(SI3).0.0D0)
CN3 = CCCS3-CROUT3
CD3 = CCUS3+CROUT3
PHO3 = CN3/CD3
PLEMBISHED TO DOG
                                                   RHO3 = CN3/CD3
               c
                                                   COMPUTATION OF EPSILON(JBR)
                                                                                   2.D0*PI*R1L
                                                   TMB = 2.00*P1*R2U
                                                   TMC = 2.00*PI*R3U
TMD = 2.00*PI*R1L
                                                                                                                                                                                                                                                                                   THE IS STATE OF THE TAPE (180.0)

THE IS SELECTION OF THE PARTY OF THE
                                                                     = 2.D0 *PI*R2L
= 2.DC *PI*R3L
                                                   THE
                                                 TMF = 2.0C*PI*R3L

CIU = DCMPLX(DCOS(TMA).-DSIN(TMA))

C2U = DCMPLX(DCOS(TMB).-DSIN(TMB))

C3U = DCMPLX(DCOS(TMC).-DSIN(TMC))

CIL = DCMPLX(DCOS(TMC).-DSIN(TMD))

C2L = DCMPLX(DCOS(TME).-DSIN(TME))

C3L = DCMPLX(DCOS(TMF).-DSIN(TMF))
                                                 COMPUTATION OF SIDERANC ANTENNA PATTERNS.
                                                                                                                                                                                                                                                                                                      THA STREET HERE
THE CONTROL OF THE STREET
                                                                     # 1510C1U+RHO10151+C1L
```

est quality practicable

TE 29

11-6

```
THIS PAGE IS BEST QUALITY PRACTICABLE
FROM GOFY PURMISHED TO DDC
```

```
ESS = TIG+TIH+TII
MESS = CDABS(ESS)
CCC
          CCMPUTATION OF CAPRIED ANTENNA PATTERNS.

TIA = IC1*C1U+RH01*IC1*C1L

TIB = IC2*C2U+RH02*IC2*C2L

TIC = IC3*C3U+PH03*IC3*C3L
          TIB. = IC2*C2U+RH02*IC2*C2L
TIC = IC3*C3U+PH03*IC3*C3L
           G1 = CDABS(TIA)
           G2 = CDABS(TIB)
          G3 = CDABS(TIC)
ECS = TIA+TIH+TIC
           MECS = CDABS(ECS)
          COMPUTATION OF CLEARANCE SIGNAL PATTERNS
          TIA = ICC1*C1U+R+01*ICC1*C1L
TIB = ICC2*C2U+R+U2*ICC2*C2L
TIC = ICC3*C3U+R+U3*ICC3*C3L
           CC1 = CDABS(TIA)
          CC2 = CDABS(TIA)
CC3 = CDABS(TIC)
ECC = TIA+TIB+TIC
MECC = CDABS(ECC)
          TIA = ESS/ECS
PHASE = DATAN2(DIMAG(TIA), DREAL(TIA))
PHASE = PHASE*18C.C/PI
DDM = 2.0DO**DREAL(TIA)
          TMG = M*2.0D0
TMH = DABS(DDM)
           IF(TMH.GT.TMG) GO TO 10
     GO TO 11
10 DDM = IMG*DDM/TMH
     11 CONTINUE
          UDOM = DDM

GAPTURE EFFECT CALCULATIONS
           0 = (MECC/MECS)
          IF(Q.LT.0.1) GC TO 12
DDM = DDM+(MC150-DDM)/(1+Q**(-2.5))
     12 UA = DDM*78./.091
PRINT 13.ALPHA.UA.DDM.PHASE.UCDM.Q
13 FURMAT(' '.2X.F3.1.1X.F7.1.1X.F7.3.1X.F8.3.1X.F7.3.1X.F6.4)
          GO TO 24
     14 CONTINUE
     15 CONTINUE
     GO TO 25
          GO TO 3
COCCOCC
     **
     **
                   THIS IS THE CALCOMP SERVICING PORTION OF THIS PROGRAM
                                                                                                                           **
     **
                                                                                                                           **
            IF FOR ANY REASON. YOU DO NOT WISH CALCUMP GRAPHS TO BE MADE. YOU MAY DISABLE THE CALCUMP PORTION OF THIS PROGRAMBY PLACING AN ASTERIX IN COLUMN EIGHTY OF YOUR CONTROL CARDS
     **
                                                                                                                           **
                                                                                                                           **
          CONTINUE
          DO 20 INN=1.61
           INK = INJ+61
INL = INK+61
IJJ = INL+61
           IJK = [JJ+61
          IJL = IJK+61
IF(INN.GT.30) GD TO 18
AXY(INL) = 888.0
AXY(INK) = 868.0
          AXY(INJ) = 888.0
GD TO 19
AXY(INL) = -500.0
          AXY(INJ) = -500.0
AXY(INK) = -500.0
     19 CONTINUE

AXX(INJ) = 2.3

AXX(INK) = 3.0

AXX(INL) = 3.7

AXY(IJJ) = 150.0

AXY(IJK) = 0.0
```

```
AXY(IJL) = -150.0

AXX(IJJ) = (INN-1.0)/10.0

AXX(IJK) = (INN-1.0)/10.0

AXX(IJL) = (INN-1.0)/10.0
    20 CONTINUE
        NPT = 61
        NPL = 8
    RE AD(5,21) BXX.BXY
21 FORMAT(12A4)
GO TO 1
    22 CONTINUE
    119 = 0
READ(5.23) TTL
23 FORMAT(80A1)
                                    COMPUTATION OF CLEARANCE STONAL PARTICIPAL.
        GO TO 9
    24 CONTINUE
        II9 = II9+1
UDUA = UDDM*78./.091
        AXX(119) = ALPHA
AXY(119) = UA
        AXX(119+61) = ALPHA
AXY(119+61) = UDUA
GU TU 14
   25 CUNTINUE
        DO 28 1=1.429
IF(AXY(1).LT.888.0) GO TO 26
AXY(1) = 888.0
   26 IF(AXY(I).GT.-500.C) GG TG 27
AXY(I) = -500.C
27 CONTINUE
        CONTINUE
        IF(TTL(2).EQ.TTL2) GO TO 16
CALL PLOTT(AXX.AXY.NPT.NPL.BXX.BXY.TTL)
GO TO 16
    **
0000
                            END UF CALCOMP PACKAGE
    **
    ************
    29 CONTINUE
        STOP
        END
```

Malegar Trought Principle State St 2015 5145

```
THE INPUT DATA IS AS FOLLOWS
-1.000 IS1 R
2.000 IS2 R
0.342 IS3 R
-0.6.514 IC1 R
0.0 IC3 R
0.0 IC3 R
10000.000 CEC R
                                                                                                            0.0
                                                                                                                                         151
                                                                                                                                         152
                                                                                                                                                         IM
                                                                                                        -0.939
                                                                                                                                         153
                                                                                                                                         1C1
1C2
1C3
                                                                                                                                                         1 .
                                                                                                             0. C
                                                                                                             0.0
                                                                                                                                                         IM
                                                                                                                                                                                                                                  MIS PAGE IS BEST QUALITY PROPINGES
                                                                                                             0.0
                                                                                                                                                         IN
                                                                                                             0.0
                                                                                                                                         CEC
                                                                                                                                                         IM
                                                                                                        4.777
9.554
14.330
                    4.777
                                                 HIU
                                                                                                                                         HIL
                                                H2U
                 14.330
                                                 H3U
                                                                                                                                         H3L
                                                EPS12
                                                                                                             0.420
                                                                                                                                         EPS 13
      10 CC 0.000
C.400
                                                                                                      155.460
                                                                                                                                         PHI
                                                 THETA
                                                                                                            0.0
                                                                                                                                                                                                                                         THOU GOPY PUNEISHED TO DOG
                                                                                                             0.900
                                                                                                                                         MC150
                                                 ICC1 R
                                                                                                                                         ICC SIM
                                                                                                             C.C
                      3.220
                     0.0
                                                                                                             0.0
                 -1.101
                                                                                                             3.025
                                                                                                                                         ICC3IN
                                                                                                                                                                 Y= 1000.000
THE DISTANCE OUT FROM THE ANTENNA.
                                                                                        PHASE
-56.243
30.509
 ALPHA
                                                                                                                            UDDM 0
0.228 0.5670
                                                                0.359
0.900
0.900
0.900
0.900
0.900
                                307.7
771.4
771.4
         0.0
        0.2
                                                                                                                                     C. 800
                                                                                                                                    C.80C *****
G.800 *****
O.800 *****
                                                                                            -6.140
-21.19C
                                771.4
                                                                                                                                     0.800
                                                                                           -26.905
-29.389
-30.498
                                                                                                                                                          *****
        0.4
                                                                                                                                     0.800
                                771 · 3
771 · 2
770 · 3
                                                                                                                                                          ****
                                                                                                                                     0.800
                                                                                                                                                          5.9794
                                                                                                                                     0. 600
         0.6
                                                                 0.899
                                                                                                                                                           6.9999
                                                                                            -30.896
         0.7
                                                                                                                                     0.800
                                                                 0.898
                                                                                            -30.858
                                 770.0
                                                                                                                                                          5.0723
         0.8
                                                                                                                                     C. 800
                                768.4
                                                                 0.896
                                                                                                                                    C.80C 3.7596
C.80C 2.8310
                                                                                            -30.511
         0.9
                                                                 0.893
         1.0
                                                                                            -29.909
                                 760.5
                                                                                                                                                           2.1553
         1 -1
                                                                 0.867
                                                                                            -29.074
                                                                                                                                     0.800
         1.3
                                 752.5
                                                                 0.878
                                                                                            -28.001
                                                                                                                                     0.800
                                                                                                                                                           1.6538
                                                                                                                                                          1.2771
                                 741.3
                                                                 0.865
                                                                                            -26.666
                                                                                                                                     0.800
                                                                                                                                                         0.7820
0.6282
                                                                                            -25.026
-23.008
         1 . 4
                                 728.2
                                                                 C.850
                                                                                                                                     0.800
         1.5
                                 715.8
                                                                 0.835
                                                                                                                                     0.800
                                                                                           -20.498
-17.316
-13.159
-7.501
0.623
         1.6
                                                                 0.762
                                                                                                                                     0.719
0.566
                                 653.3
                                                                                                                              0.719 0.6282
0.566 C.5218
0.440 0.4536
0.334 0.4145
0.245 0.3952
0.170 0.3874
0.107 0.3850
0.052 0.3840
0.006 0.3822
-0.034 0.3722
-0.098 0.3632
                                 532.4
         1.8
                                 424.9
                                                                 0.496
                                                                 0.390
         1.9
                                 334.6
                                                           0.390
0.304
0.233
0.123
0.080
0.042
-0.024
-0.053
-0.079
-0.104
-0.147
                                260.4
        2.0
                                                                                                    0.623
                                                                                                13.004
32.423
59.623
86.852
                                 199.3
        2.1
         2.2
                                 148.6
                                 105.6
                               105.6
68.4
35.7
6.2
-20.6
-45.3
-68.1
        2.5
                                                                                            106.468
119.298
128.116
134.697
140.000
                                                                                                                               -0.098 0.3632
-0.123 0.3518
-0.144 0.3379
-0.163 0.3220
-0.175 0.3044
         2.8
        3.0
                            -89.1
-105.4
-125.9
                                                                                            144.545
148.632
152.440
156.079
159.618
         3.1
                                                                                                                               -0.179 0.3044
-0.192 0.2853
-0.204 0.2651
-0.214 0.2442
-0.222 0.2231
-0.229 0.2021
-0.234 0.1817
-0.239 0.1627
         3.2
                                                            -0.147
                           -141.8
                                                            -0.165
                                                           -0.165 | 156.079 | 159.618 | 163.098 | 166.541 | 169.958 | 173.346 | 176.697 | 176.697 | 176.697 | 176.696 | 167.696 | 167.696 | 167.696 | 167.696 | 167.696 | 167.696 | 167.696 | 167.696 | 167.696 | 167.696 | 167.696 | 167.696 | 167.696 | 167.696 | 167.696 | 167.696 | 167.696 | 167.696 | 167.696 | 167.696 | 167.696 | 167.696 | 167.696 | 167.696 | 167.696 | 167.696 | 167.696 | 167.696 | 167.696 | 167.696 | 167.696 | 167.696 | 167.696 | 167.696 | 167.696 | 167.696 | 167.696 | 167.696 | 167.696 | 167.696 | 167.696 | 167.696 | 167.696 | 167.696 | 167.696 | 167.696 | 167.696 | 167.696 | 167.696 | 167.696 | 167.696 | 167.696 | 167.696 | 167.696 | 167.696 | 167.696 | 167.696 | 167.696 | 167.696 | 167.696 | 167.696 | 167.696 | 167.696 | 167.696 | 167.696 | 167.696 | 167.696 | 167.696 | 167.696 | 167.696 | 167.696 | 167.696 | 167.696 | 167.696 | 167.696 | 167.696 | 167.696 | 167.696 | 167.696 | 167.696 | 167.696 | 167.696 | 167.696 | 167.696 | 167.696 | 167.696 | 167.696 | 167.696 | 167.696 | 167.696 | 167.696 | 167.696 | 167.696 | 167.696 | 167.696 | 167.696 | 167.696 | 167.696 | 167.696 | 167.696 | 167.696 | 167.696 | 167.696 | 167.696 | 167.696 | 167.696 | 167.696 | 167.696 | 167.696 | 167.696 | 167.696 | 167.696 | 167.696 | 167.696 | 167.696 | 167.696 | 167.696 | 167.696 | 167.696 | 167.696 | 167.696 | 167.696 | 167.696 | 167.696 | 167.696 | 167.696 | 167.696 | 167.696 | 167.696 | 167.696 | 167.696 | 167.696 | 167.696 | 167.696 | 167.696 | 167.696 | 167.696 | 167.696 | 167.696 | 167.696 | 167.696 | 167.696 | 167.696 | 167.696 | 167.696 | 167.696 | 167.696 | 167.696 | 167.696 | 167.696 | 167.696 | 167.696 | 167.696 | 167.696 | 167.696 | 167.696 | 167.696 | 167.696 | 167.696 | 167.696 | 167.696 | 167.696 | 167.696 | 167.696 | 167.696 | 167.696 | 167.696 | 167.696 | 167.696 | 167.696 | 167.696 | 167.696 | 167.696 | 167.696 | 167.696 | 167.696 | 167.696 | 167.696 | 167.696 | 167.696 | 167.696 | 167.696 | 167.696 | 167.696 | 167.696 | 167.696 | 167.696 | 167.696 | 167.696 | 167.696 | 167.696 | 167.696 | 167.696 | 167.696
         3.4
                                                            -0.182
                            -168.1
-178.6
         3.5
         3.6
         3.7
                            -187.4
                                                                                                                              -0.234 0.1627
-0.239 0.1627
-0.243 0.1458
-0.246 0.1321
-0.250 0.1189
-0.251 0.1189
-0.252 0.1247
-0.252 0.1342
-0.252 0.1342
-0.252 0.1745
-0.252 0.1745
-0.252 0.1745
-0.251 0.2167
-0.251 0.2167
-0.251 0.2167
-0.251 0.2167
-0.2549 0.2598
-0.249 0.2598
-0.248 0.2778
-0.248 0.2778
-0.248 0.2778
         3.8
                            -194.5
                            -200.2
         3.9
         4.0
                            -204.4
                            -207·4
-209·3
        4.1
         4.3
                            -210.2
         4.4
                            -210.3
         4.5
                             -209.6
                            -208.2
-206.1
         4.6
                                                                                                                                                                                          Figure 11-1. Sample
         4 . 7
        4 .8
                            -203.5
                                                                                                                                                                                          Output of Glide
         4.9
                            -200.5
                           -197.2
-193.7
                                                                                                                                                                                           Slope Model.
        5.0
        5.1
                            -190.1
                           -190.1
-186.6
-183.3
-187.7
-177.7
-175.5
-174.0
-173.0
-175.2
        5.4
                                                                                                                                -0.248
                                                                                                                                                             0.2815
                                                                                                                                -0.262 0.3072
```

CAPTURE EFFECT A3
FAR FIELD NO MAG.CHANGE
110 DEGREES PHASE SHIFT

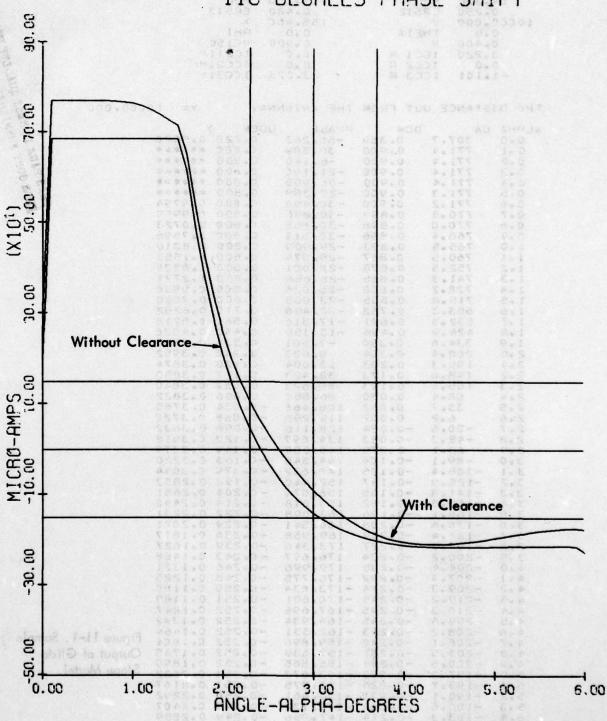


Figure 11-2. Example Output: Far Field CDI vs. Angle - Capture Effect
Glide Slope. 110 Degrees Phase Shift in Upper Antenna Line.

B. Fault Studies on a Capture-Effect Glide Slope and Its Computer Model.

1. Introduction and Summary. This section is a report of tests involving a capture-effect glide slope that was set up at Ohio University's test facility at Tamiami Airport, Miami, Florida on which extensive fault studies were made. Perturbations employed include phase delays and advances, changes in modulation indices for main and clearance signals, attenuation in antenna lines and resetting of power dividers in the APCU.

The transmitter used was a Wilcox Mark 1C solid-state with 3 element colinear antennas in corner reflectors Type FA8976 manufactured by Antenna Products Company.

In most cases theoretical (predictive) computer modeling was performed using the computer program described in Section XI.A.

In-flight measurements were made using the Mark II Minilab in a Beechcraft Model 35 Bonanza flying a level pattern on the localizer on-course at 1000 feet altitude (above ground). A theodolite was used to mark the elevation angle of the plane by signaling as it passed through the crosshair with the theodolite preset to each tenth of one degree.

For selected faults the near-field monitor in combination with a PIR (Portable ILS Receiver) was used to gather measured data at the 360° point. For each computable run, near-field values were calculated and are presented preceding the corresponding level run graph.

Figures 11-3 through 11-102 present a graphical story of the tests.

2. Analytical Methods. The program used in calculating the DDM and CDI to be expected in a given set of conditions is based on a number of assumptions which seem to be well met at the Tamiami site. These are (a) a flat, smooth, horizontal reflecting plane of extent sufficient to cover all significant Fresnel zones, (b) a sufficiently uniform earth dielectric constant (or one sufficiently high so that it appears uniform) and (c) all field points of interest far enough from the sources to permit use of the plane wave approximation.

Given these assumptions the program uses the image principle to calculate the fields due to the antennas and their images at the point of observation, working from the complex values of the various antenna current components. Adjustment of the phase of each field component is made using the calculated distance of travel and, in the case of the images, due to the reflection coefficients calculated for each point of reflection from incidence angles and complex dielectric constant of the earth (if known or assumed).

The complex fields are then added to produce total sideband only, total carrier sideband, and total clearance fields. From these, DDM and CDI are calculated. The main course fields are combined with the clearance fields according to an empirical

formula for capture-effect and the results are printed out as DDM without clearance signal, DDM with clearance signal, and the corresponding CDI. The ratio of clearance to main signal strength is also indicated.

If these results are to predict CDI values obtained in flight measurements, it is necessary further to alter them to correspond to values obtainable with practical receivers. The Mark II Minilab employs a Narco UGR2 receiver which responds well to DDM producing CDI between +80 microamperes (150 Hz) and -80 microamperes (90 Hz) but whose response falls off rapidly outside this range. Extensive testing of the UGR2 has yielded a correction curve which has been used to alter the calculated data so that it can predict the CDI values seen by the Minilab.

Data listed and values plotted on the accompanying figures have been so adjusted for far-field plots (level runs) but not for the 360° point data since this is not read by the UGR2 but by the monitor-PIR combination for which there is presently no calibration curve over the whole range of CDI values.

3. Ground Data. The CEGS (capture-effect glide slope) transmitter used in these experiments was a Wilcox Mark 1C feeding the three Antenna Products Company 3-element colinear arrays in comer reflectors through RG-214 cables.

The antenna tower was located 461.5 feet from the runway centerline with the upper antenna offset 12.4 inches toward the runway and the lower antenna offset 7.5 inches away from the centerline. Antenna heights were adjusted to 14.18, 28.36, 42.54 feet to produce a 3° glide path angle. Operating frequency was assigned as 331.1 MHz with the main course signal 4 KHz above and the clearance signal 4 KHz below this value.

Transmitter carrier power was set at 2.9 watts, sideband power adjusted to 37.5 milliwatts and clearance power at 0.29 watt.

This data was entered in the program after conversion of the distances to wavelengths and the powers to relative equivalent antenna currents.

4. Preliminary Setup Procedures. Relative antenna currents and powers were determined and adjusted in accordance with the Mark 1C installation handbook values. The procedure was modified to include the use of a hand-held probe and a Hewlett-Packard Model 8405A vector voltmeter.

With the sideband only (SBO) feedline to the APCU dummied, carrier and sideband (CSB) energy was fed to the SBO input. The clearance transmitter was de-energized and the CSB input jack dummied. This applied carrier and sidebands to all three antennas through the SBO channels of the APCU.

In order to balance out the termperature-induced errors in the voltmeter probe cables, the middle antenna monitor port was chosen for the voltmeter reference probe and the probe cables made as nearly equal in length and temperature as possible.

With the hand-held probe on the middle antenna, the voltmeter was adjusted to read zero phase difference. Then with the probe on the upper antenna, the phase was adjusted until the meter read 180°. This was repeated for the lower antenna. The reference was checked between readings to check the stability of the measurements.

Power levels were set using the in-line wattmeters. The use of this type of meter on the ILS waveforms is covered in Section XI.D.

5. <u>Error Analysis</u>. Certain errors arise in the measurements of any physical quantity. In a process as dynamic as flight measurements of field quantities these errors must be analyzed and either systematically corrected for or shown to be of negligible significance.

Calibration of the receiver and recorder used in the Mark II Minilab has been accomplished and is used in modifying the calculated (predicted) response. Such errors are effective only in the regions of high DDM (CDI greater than 75 microamps).

Errors in determining and recording the position of the aircraft and errors due to dynamic response time of the Minilab need to be considered. Aircraft elevation angle is recorded by the event marker on the margin of the recorder chart through a ground-to-air link involving the action of the theodolite operator who closes a push-button switch when he sees the target aircraft arrive at the horizontal crosshair of his prepositioned instrument. This causes an audio beep to sound in the plane to which the airbome instrument man responds by pushing a button to close the marker circuit switch momentarily (the Mark III Minilab will eliminate the on-board operator from this link by using the incoming signal directly to actuate the marker).

To evaluate the effect of human reaction times in this link a series of controlled experiments was performed. These showed that a skilled theodolite operator could use anticipatory cue to eliminate the delay in his response almost entirely since he watches the plane approach the target at a reasonably uniform rate even in fairly rough weather. The operator in the plane, however, has no such visual cue and exhibits a lag in response of about 0.3 second. Time constants of the instruments are much shorter especially in flight where the constant vibration supplies an automatic keep-alive action. Table 11-1 gives the CDI error in microamps caused by the operator reaction times for various elevation angles of a 1000-foot altitude level run. Later developments in the Mark III Minilab allowed automation of the function and the elimination of the error.

Table 11-2 shows the time for 0.1 degree intervals as a function of the elevation angle. Since the theodolite operator must reset his instrument precisely and also return his attention to the field of view during this interval, the necessity of using skilled personnel for this job is evident.

From the foregoing it can be seen that the errors introduced by these delays are of no great significance.

Angle	Onboard Delay	Theodolite Delay	Total Delay	Degrees
1.0 pove	0.260	0.052	0.312	0.0014
1.5	0.59	0.12	0.71	0.0033
2.0	1.05	0.21	1.26	0.0059
3.0	2.35	0.47	2.82	0.013
4.0	4.20	0.85	5.05	0.024
5.0	6.56	1.31	7.87	0.037

σ Normal glide slope. Altitude 1000 feet. Groundspeed 140 Kts.

accomplished and is used in modifying the calculated (prediction) response. Such errors are effective only in the regions of high DDM (CD) greater than 75 microamps).

to dynamic response time of the Minflob need to be considered. Afrerest elevation

prevaltioned instrument. This course an audio been to sound in the place to which

this link by using the in

aspertments was parforme

the plane approach the M

The operator in the plane

flight where the constant

DDI a to seigno nationals

are of to great, significance,

To evaluate the a

Table 11-1. Summary of Reaction Time Delays.

Angular Interval	Time in Seconds
1.0-1.1	rolltages at 22 to to
1.5-1.6	10.1
2.0-2.1	5.8
2.5-2.6	3.7
3.0-3.1	2.6
3.5-3.6	1.9
4.0-4.1	1.5
4.5-4.6	1.3
5.0-5.1	0.95

redtpow doubt vi

times for vestious

sendagen ni pol p si

Table 11–2. Time in Seconds for Selected
Angular Intervals of 1000 Foot
Level Flight at 140 Kts.

From the foregoing it can be seen that the error introduced by these deleres

Table 11-2 shows the time for 0.1 degree intervals as a function of this elevation

6. Results. Results of the tests are presented in Figures 11-3 through 11-102. An important purpose of these experiments was to lay the groundwork for specifying a setup procedure designed to minimize flight test time in commissioning glide slopes. Close agreement between predicted and measured results exists.

In Table 11-3 calculated values for path angle and width are compared to measured values with a percentage difference calculated. Provided the mathematical model is a good means of representing the glide slope performance, one would expect good agreement, particularly since the near-ideal site at Tamiami offers no complications. A careful inspection of the tables does indeed show this to be the case. The difference is typically one percent or less.

Data is also available for the near-field monitor condition. For some of the perturbations field measurements were made with the monitor detector probe being moved physically up and down from its normal position at the 360-degree proximity point. The angular position where the zero DDM value was obtained was recorded. Calculations were made for most of the perturbations and when possible a comparison was made and a percentage difference calculated. Again, results were quite encouraging. The reader must, of course, remember that the ground plane was essentially ideal with no problems such as snow cover.

A final comparison is given for cases when data was available to determine how well the measured monitor (second choice, calculated) predicted the observed far-field values. For these cases the agreement is not as good.

	Lower 75µA	75µA	Upper 7	75µA	Wid	Width °	Structure Angle	bre le °	P. P.	Far-Field Path Angle°		Z&	Near-Field Path Angle®		% Diff. (Path Angle)
Condition	Meas.	Calc.	Meas.	Calc.	Meas.	Calc.	<	Calc.	Meas.	Calc.	% Diff.	Meas.	Calc.	% Diff.	FF-NF × 100
Normal	2.63	2.66	3.34	3.37	17.0	17.0	2.13	2.06	2.98	3.01	1.01	2.99	3.00	0.33	0.34
Phase Perturbations							li bota	,	erurano explication explication	h-dugne Ined va	noi .n	at acios	ed the e, ener	a Filluasi	I amus weigh
Sidebands							ang (bi		g saure Luaen va Eg hosso	de edit da edit	oit ibrios	eint we	Provi Province	Constitution in	filmi ba Fiyot o est tea
-20° (Run 1)	2.57	2.63	3.35	3.39	0.78	0.76	2.09	2.04	2.97	3.0	1.01	eb ene eta beeb	3.00	sea bree	rrais o u saw eti
-20° (Run 2)	2.59	2.63	3.35	3.39	0.76	0.76	2.10	2.04	2.98	3.0	0.7		3.00	Alena sa	ne joo wang siming
-20° (Out- bound)	2.62	2.63	3.41	3.38	0.79	0.75	is Empai mulates	2.04	2.99	3.0	0.33	en em e refulsts seal no i	3.00	g Daawi	0
-30° (Run 1)	2.51	2.60	3.38	3.42	0.87	0.82	2.02	2.01	2.95	3.0	121d	2.98	3.00	0.7	1.02
-30° (Run 2)	2.54	2.60	3.38	3.42	0.84	0.82	2.05	2.01	2.98	3.0	0.7	2.98	3.00	0.7	0
-40°	2.49	2.54	3.42	3.47	0.93	0.93	2.01	1.97	2.96	3.0	do 1.0	ichaela ichaela ologiui	3.00	610 1	yl o oqmi as quisa e

Table 11–3. Comparison of Calculated Values for Path Angle and Width to Measured Values.

	Lower 75µA	75µA	Upper 7	75µA	Wio	Width.	Structure Angle	ure le °	F S	Far-field Path Angle°	0	Z &	Near-Field Path Angle	P %	% Diff. (Path Angle)
Condition	Meas.	Calc.	Meas.	Calc.	Meas.	Glc.	Meas.		Mea	Calc.	% L	Meds.	Calc.	% Diff.	FF-NF × 100
-50	2.40	2.46	3.49	3.56	1.09	1.10	1.95	1.93	2.92	3.0	2.7	11	3.00		0
D Lower Ant.		9	3						3				2		
+10•	2.58	2.63	3.33	3.36	0.75	0.73	2.03	2.00	2.98	3.0	0.7	1	3.01	:	0.33
+20°	2.47	2.55	3.33	3.36	0.86	0.81	1	1.81	2.96	2.97	0.34	I.	3.03		2.02
+30								•	•••			1	3.06		
● Middle Ant.												r, İ	3,01		
-12°	2.63	2.64	3.33	3.37	0.7	0.73	2.03	1.98 3.0	3.0	3.01	0.33		3.01	:	0
-14	2.61	2.63	3.30	3.37	0.69	0.74	1.98	1.95	2.99	3.01	0.77	1	3.01	:	0
+14°	2.63	2.63	3.32	3.37	0.69	0.74	2.03	1.94	1.94 3.01	3.01	0	1	3.00	il	0.33

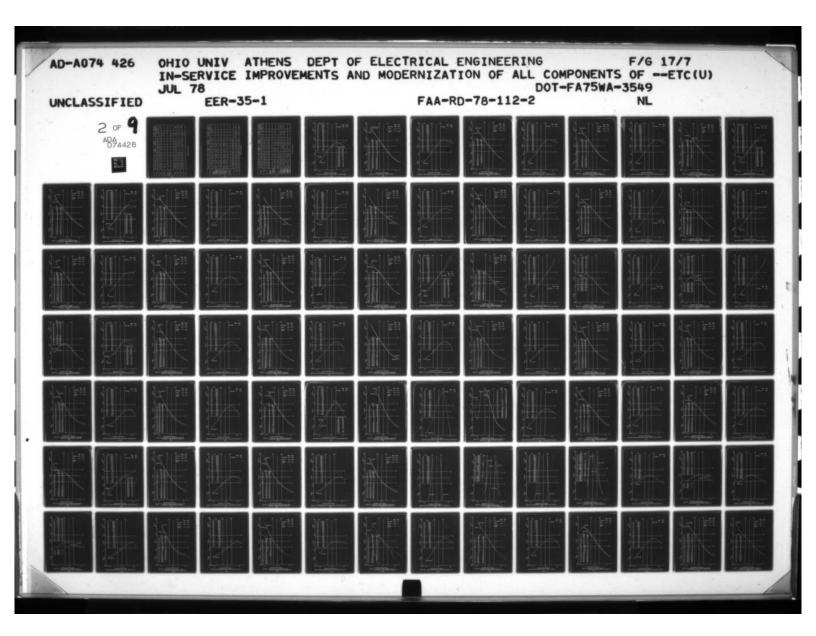
Table 11-3. (Continued)

	Lower 75µA	75µA	Upper	75µA	Wid	Width *	Structure Angle	ure e °	P. P.	Far-field Path Angle°	0	Z&	Near-Field Path Angle	e q	% Diff. (Path Angle)
Condition	Meas.	Calc,	Meas.	Calc.	Meas.	Calc.	Meas.	Calc.	Calc. Meas.	Calc.	% Diff.	Meas.	Cale.	% Diff.	FF-NF × 100
-50%	2.63	2.60	3.36	3.38	0.73	0.78	1.8	-	3.02	3.01	0.33	- 1	3.01		0
-30°	2.44	2.44	3.36	3.39	0.92	0.95	2 12	. !	3.01	3.01	0	2.96	3.01	1.7	1.66
-40		:	V.					•		i	:	i	3.01	•	
-50	10					:				:		1	3.01	· i	•
. 09-										i		i 1	3.01		
Upper Ant.	78. 1	2	en en	8	0.83	0		0	8	76 76	6	100	8 1		30.9
-30	2.63	2.60	3.31	3.31	0.68	0.71	2.14	2.06	2.98	2.95	1.01	2.94	3.04	3.4	1.34
-40	2.60	2.57	3.29	3.29	69.0	0.72	2.13	2.04	2.97	2.92	1.7	1	3.11		6.51
-20	2.56	2.54	3.26	3.25	0.70	0.71	2.12	2.06	2.90	2.88	0.7	1	3.16	1	9.72
							1		1						

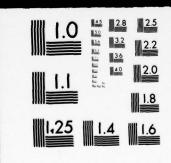
Table 11-3. (Continued)

Condition Meas. Ca -60° 2.61 2. +60° 2.49 2. -80° 2.48 2. -90° 2.40 2.			Ardc/			Angle	ွချ	Pa	Path Angle	0	Pc	Path Angle°	e o	(Path Angle)
2.49	Calc.	Meas.	Calc.	Meas.	Calc.	2	Calc.	Calc. Meas.	Calc.	% Diff.	Meas.	Calc.	% Diff.	FF-NF × 100
2.49	2.51	3.20	3.21	0.59	0.70	2.13	2.06	2.86	2.84	0.2	1	3.21	:	13.03
2.49	2.52	3.28	3.22	0.75	0.7	2.14	2.06	2.84	2.85	0.3	4		7:	
2.40	2.48	3.17	3.16	0.68	0.68	2.11	2.05	2.80	2.79	0.4	1	3.27	:	17.20
2.40	2.43	3.13	3.08	0.65	0.65	2.11	2.05	2.80	2.71	3.2	1	3.39		25.09
Attenuation	2.43	3.08	3.06	0.68	0.63	2.09	2.05	2.74	2.71	- 2	1	3.40		25.46
• Lower Ant.														
0	:	:	:	:	:	:			:			8,31	:	
148 2.77 2.7	2.76	3.41	3.37	0.64	19.0	2.34	2.23	3.05	3.06	0.3	1	2.94		3.92

Table 11-3. (Continued)



2 OF ADA 074426



MICROCOPY RESOLUTION TEST CHART

	Lower 75µA	75µA	Upper	75,A	Wid	Width	Structure Angle	ture le °	P. P.	Far-Field Path Angle°	, a	Z&	Near-Field Path Angle°	, o	% Diff. (Path Angle)
Condition	Meas.		Calc. Meas.	Calc.	Meas.	Calc.	Calc. Meas.	Calc.	Calc. Meas.	Calc.	% Diff.	Meas.	Calc.	% Diff.	FF-NF × 100
348 348	2.93	2.89	3.36	3.37	0.43	0.48	2.59	2.50	3.14	3.12	9.0	2.76	2.85	3.3	12.10
gPZ			•				:	:		•		* 1	2.71		
8		:		:	·		i	:	:			:			•
• Middle Ant.															
0	00	22	8:	30.8	00 00 00 00 00 00 00 00 00 00 00 00 00		\$ 09	\$ 98	N :	:		1. 1	2.91		35.88
∯P I	2.58	2.59	3.36	3.39	0.78	0.8	1.98	1.90	3.01	3.01	0	- 1	3.00		0.332
2dB	2.47	2.49	3.39	3.43	0.92	0.94		& 1 	3.00	3.01	.3	1	3.00		0.332
4d8	2.08	2.00	3.43	3.48	1.35	1.48	51	% I	3.00	3.01	0.3	: 1	3.00		0.332
8	50 141	fe s	3.30	3.21	0.59	07.0	2.13	30.12	Or 07- 1/2	57 60 2-3	22	1	2.91		8

Table 11-3. (Continued)

Condition Mears Calc. Mears Mears Mears Mears Calc.		Lower 75µA	75µA	Upper 75µA	75µA	Wig	Width	Structure Angle	ure le °	Fc	Far-Field Path Angle°	_ o	Z &	Near-Field Park Angle	e e	% Diff. (Path Angle)
2.66 3.34 0.68 2.25 2.98 2.74 3.42 0.68 2.23 3.07	Condition	Meas.	Calc.	Meus.	Calc.	Meas.	Calc.	Meas.	Cale.	Meas.	Calc.	% Diff.	Meas.	Calc.		
2.74 3.42 0.68 2.23	Power divider carrier -	2.66		3.34	1	0.68	1	2.25	1	2.98	1	1				
2.48 3.38 0.90 1.95	Z8 Counter- clockwise	2.74	1 %	3.42	1	89.0	1 0 V	2.23	1 10	3.07	100	1				928. O
2.52 3.26 0.75 2.10 2.87	Power div. A+, c lock- wise	2.48	is	3.38		0.00	ı	1.95	l	2.99	l i	l				35.0
2.55 3.34 0.79 1.91 2.95	Power div. B+, clock- wise	2.52	1	3.26	ı	0.75	1	2.10	1	2.87	1	1				
2.42 2.38 3.03 2.95 0.61 0.57 2.11 2.08 2.70 2.62 3.0 2.54 2.52 3.20 3.23 0.66 0.71 2.12 2.05 2.85 2.84 0.4 3.08 3.24 5.2 2.48 2.47 3.12 3.15 0.64 0.68 2.12 2.06 2.77 2.78 0.4 3.46	Power div. carrier +	2.55	1	3.34	1	0.79	1	1.91	I	2.95	ľ	I	1 1			
2.42 2.38 3.03 2.95 0.61 0.57 2.11 2.08 2.70 2.62 3.0 3 2.54 2.52 3.20 3.23 0.66 0.71 2.12 2.05 2.85 2.84 0.4 3.08 3.24 5.2 2.48 2.47 3.12 3.15 0.64 0.68 2.12 2.06 2.77 2.78 0.4 - 3.46	Upper Ant.															
3.54 2.52 3.20 3.23 0.66 0.71 2.12 2.05 2.85 2.84 0.4 3.08 3.24 5.2 2.48 2.47 3.12 3.15 0.64 0.68 2.12 2.06 2.77 2.78 0.4 3.46	0	2.42	2.38		2.95	19.0	0.57	2.11	2.08	2.70	2.62	3.0	:			
2.48 2.47 3.12 3.15 0.64 0.68 2.12 2.06 2.77 2.78 0.4 3.46	998	2.54	2.52	3.20	3.23	99.0	0.71	2.12	2.05	2.85	2.84	0.4	3.08	3.24	5.2	8.07
	898	2.48	2.47	3.12	3.15	0.64	0.68		2.06	2.77	2.78		The contract of the contract o	3.46	ä	24.46

Table 11-3. (Continued)

	Lower 75µA	75µA	Upper 7	75µA	Wid	Width	Structure Angle	e ° e	P. P.	Far-Field Path Angle°	0	Z&	Near-Field Path Angle	e° e	% Diff. (Path Angle)
Condition	Meas.	Calc.	Calc. Meas.	Calc.	Meas.	Calc.	Meas.	c.	Meas.	Calc.	% Diff.	Meas.	Cale.	% Diff.	FF-NF × 100
10dB	2.47	2.43	3.07	3.08	09.0	0.65	2.13	2.05	2.74	2.71	-		5		•
8	2.42	2.38	2.95	3.0	0.53	0.62	2.11	2.08	2.67	2.62	1.9		:		:
Discretes															
Modulation Index .28	2.63	+	3.31	+	0.68	+	2.12	+	2.97	+	+	1	+	:	:
5.	2.62	+	3.32	+	0.7	+	2.13	+	2.97	+	+	1	· c		•
No Clearance	2.62	2.66	3.34	3.37	0.72	0.71	L	1	2.98	3.01	1.0	1	3.00	:	0.332
Maximum Clearance Modulation	2.61	2.66	3.32	3.37	12.0	0.71	2.14	2.08	2.98	3.01	1.0	1	3.00	:	0.332
Power Div. A- counter- clockwise	2.68	1	3.32	1	0.64		2.26	1	2.99	1	1				
Power Div. B-, counter- clockwise	2.80	1	3.46	1	99.0	1	2.17	1	3.13	1	1				

Table 11-3. (Continued)

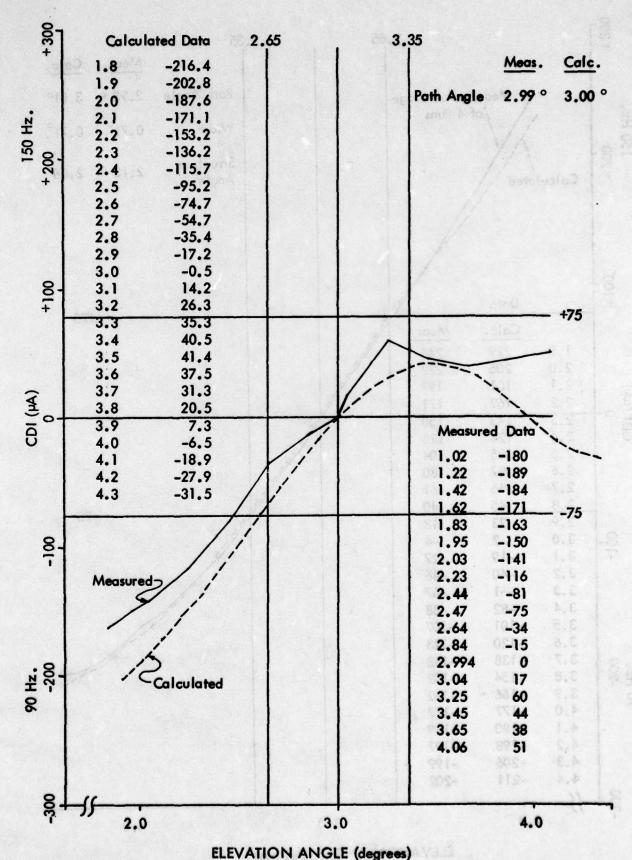


Figure 11-3. Near Field (360° Point) CDI vs Angle - Normal Glide Slope.

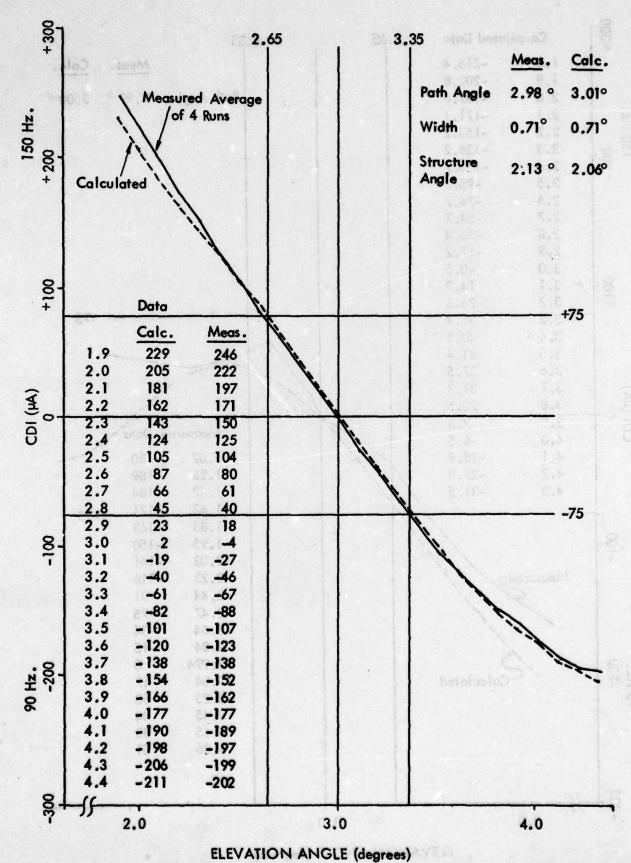


Figure 11-4. Far Field CDI vs Angle - Normal Glide Slope.

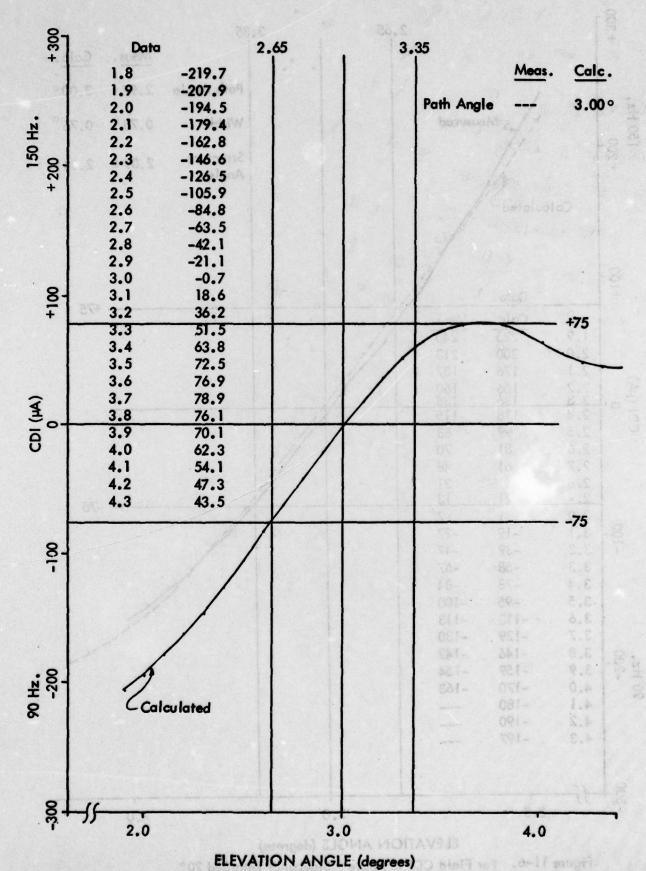


Figure 11-5. Near Field (360° Point) CDI vs Angle - Sidebands Retarded 20°.

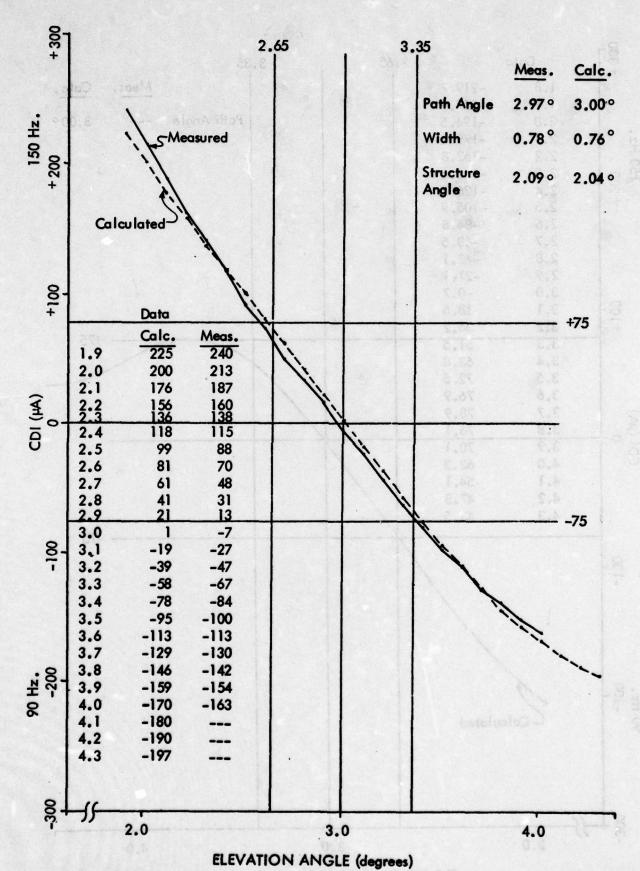


Figure 11-6. Far Field CDI vs Angle - Sidebands Retarded 20°.
Horizontal Run at 1000 Feet Altitude, 1 September 1976.

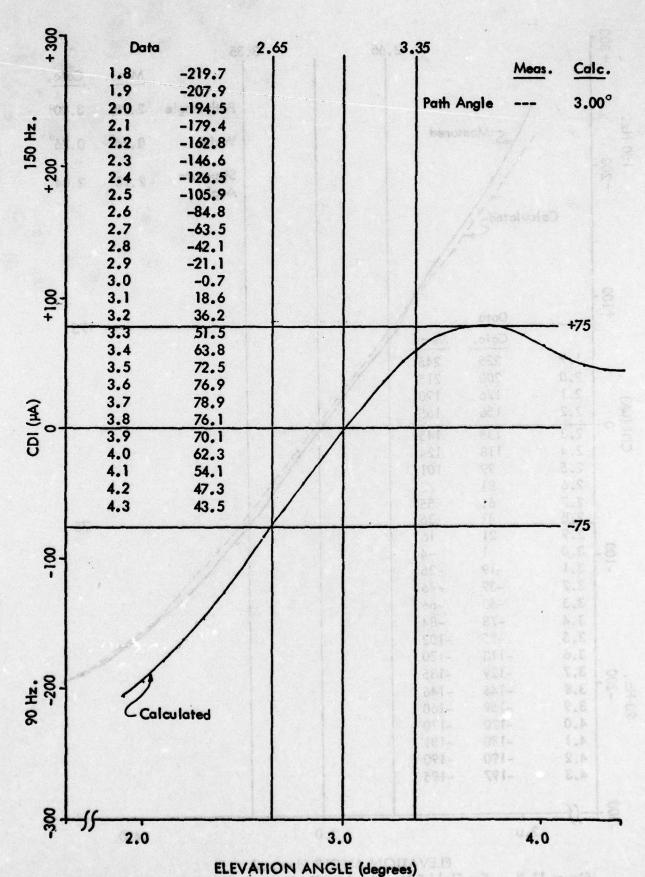
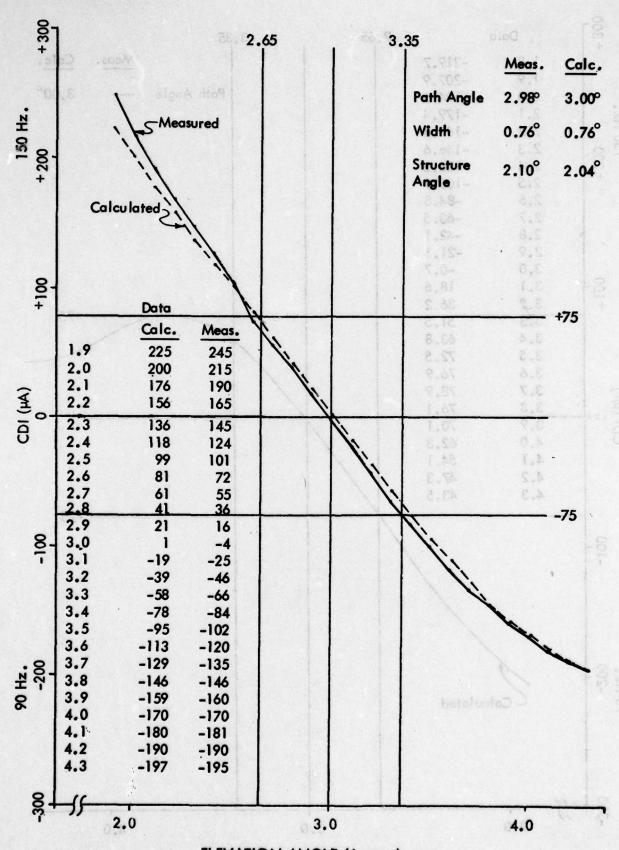


Figure 11-7. Near Field (360° Point) CDI vs Angle - Sidebands Retarded 20°.



ELEVATION ANGLE (degrees)
Figure 11-8. Far Field CDI vs Angle - Sidebands Retarded 20°.
Horizontal Run at 1000 Feet Altitude, 2 September 1976.

11-28

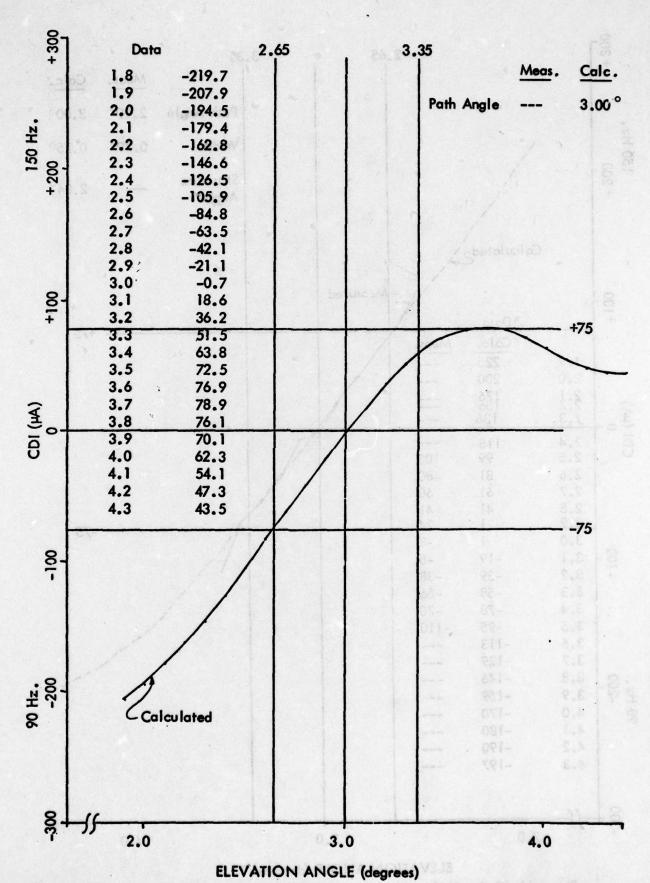


Figure 11-9. Near Field (360° Point) CDI vs Angle - Sidebands Retarded 20°.

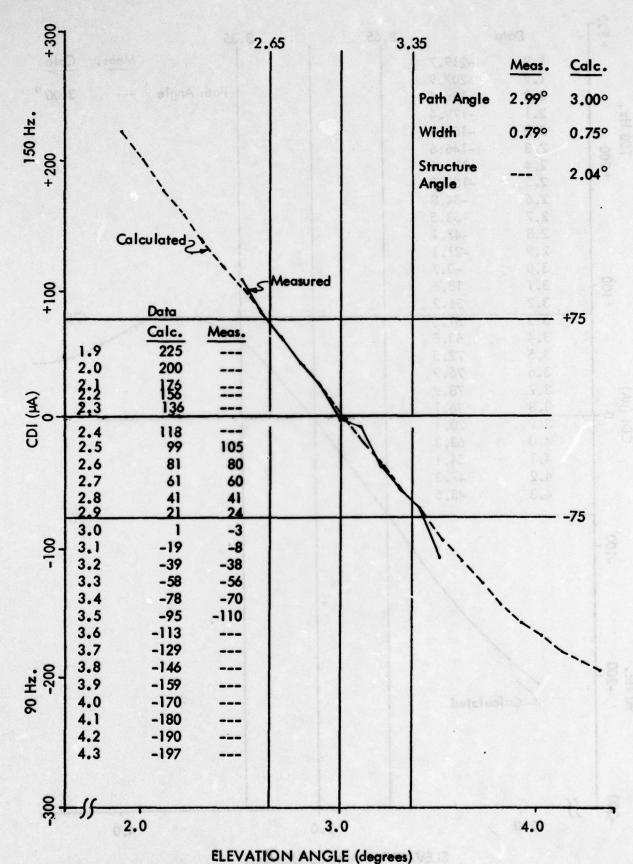


Figure 11–10. Far Field CDI vs Angle – Sidebands Retarded 20°.

Horizontal Run at 1000 feet Altitude Outbound, 2 September 1976.

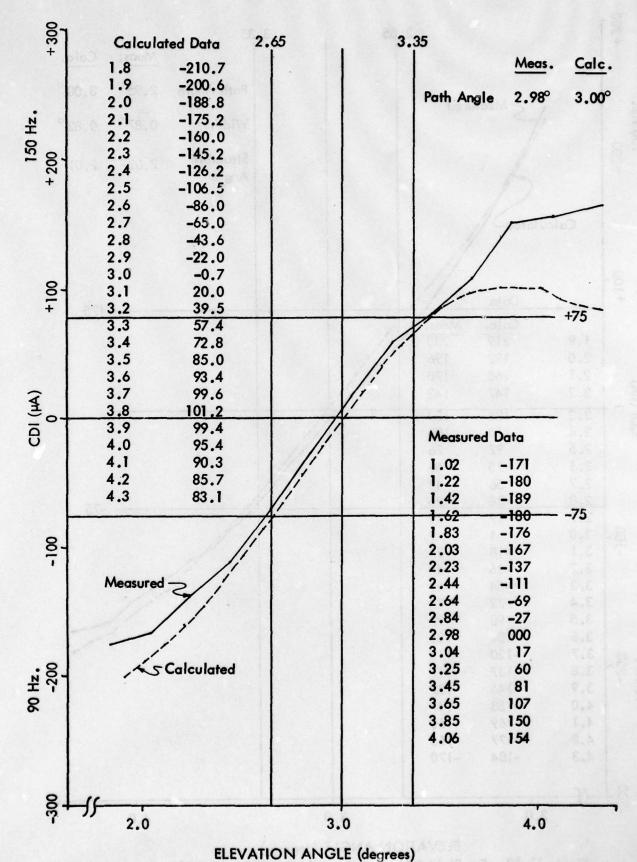


Figure 11-11. Near Field (360° Point) CDI vs Angle - Sidebands Retarded 30°.

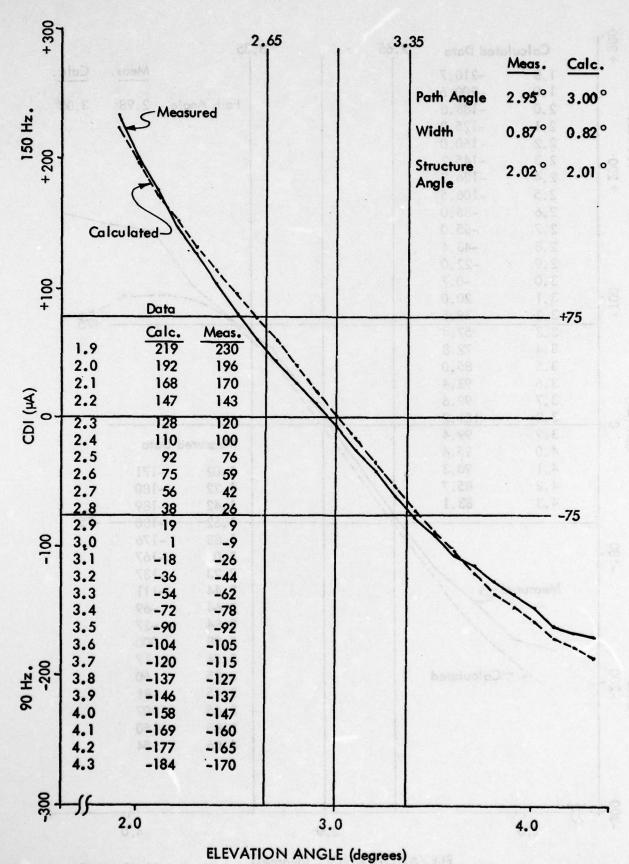


Figure 11-12. Far Field CDI vs Angle - Sidebands Retarded 30°.

Horizontal Run at 1000 Feet Altitude, 1 September 1976.

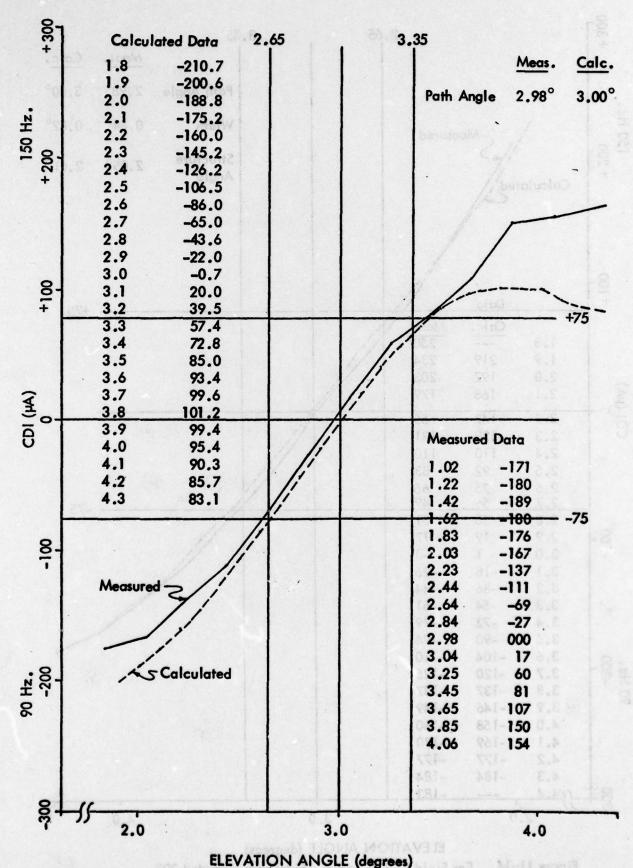


Figure 11-13. Near Field (360° Point) CDI vs Angle - Sidebands Retarded 30°.

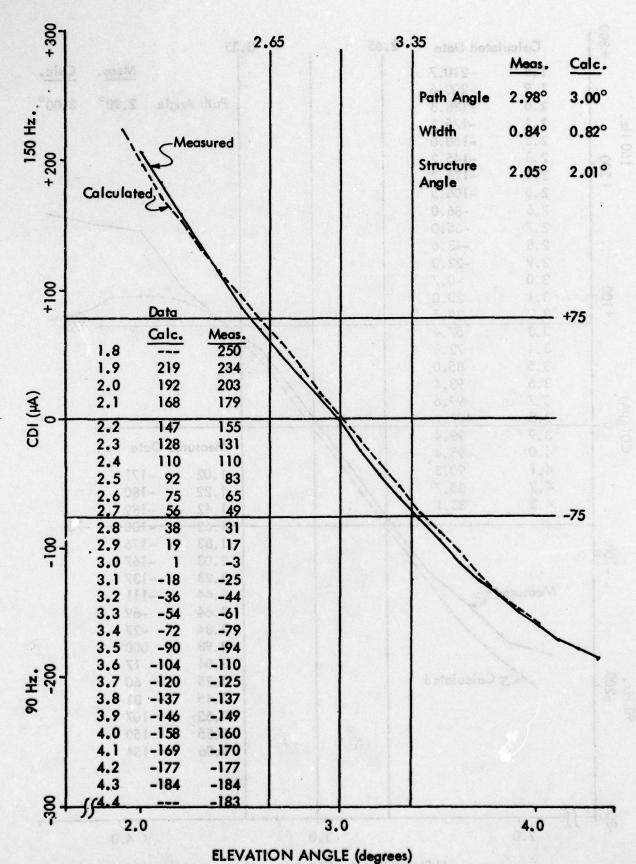


Figure 11-14. Far Field CDI vs Angle - Sidebands Retarded 30°.
Horizontal Run at 1000 Feet Altitude, 2 September 1976.

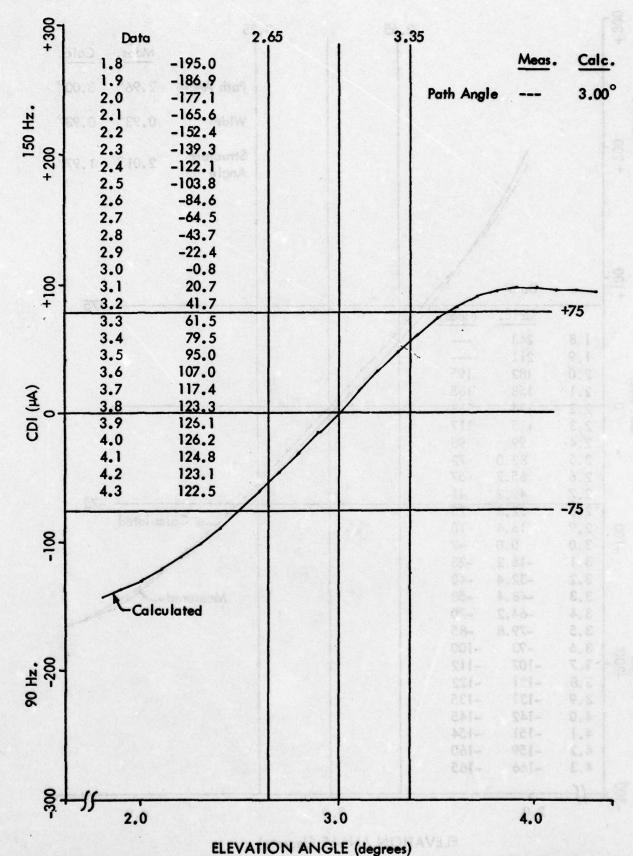


Figure 11-15. Near Field (360° Point) CDI vs Angle - Sidebands Retarded 40°.

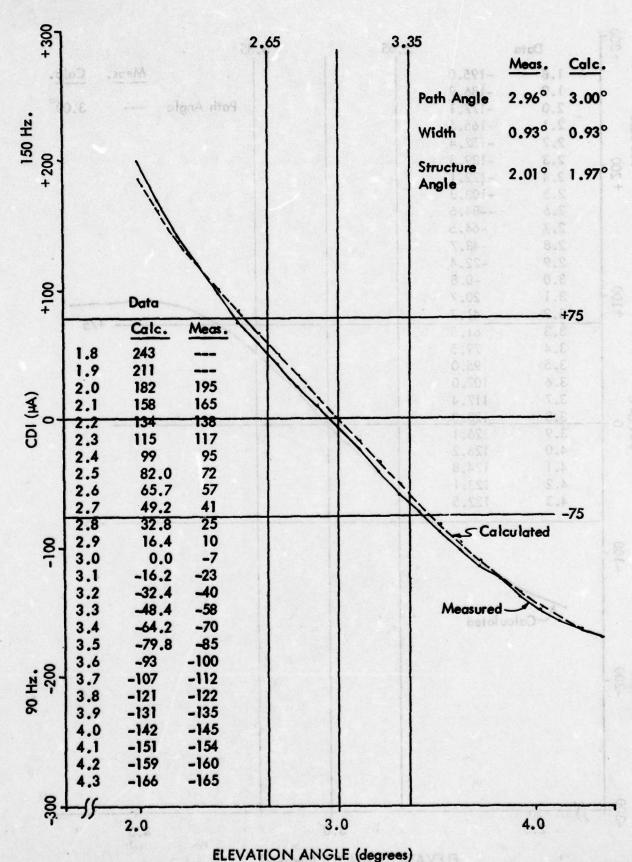


Figure 11–16. Far Field CDI vs Angle – Sidebands Retarded 40°.
Horizontal Run at 1000 Feet Altitude, 2 September 1976.

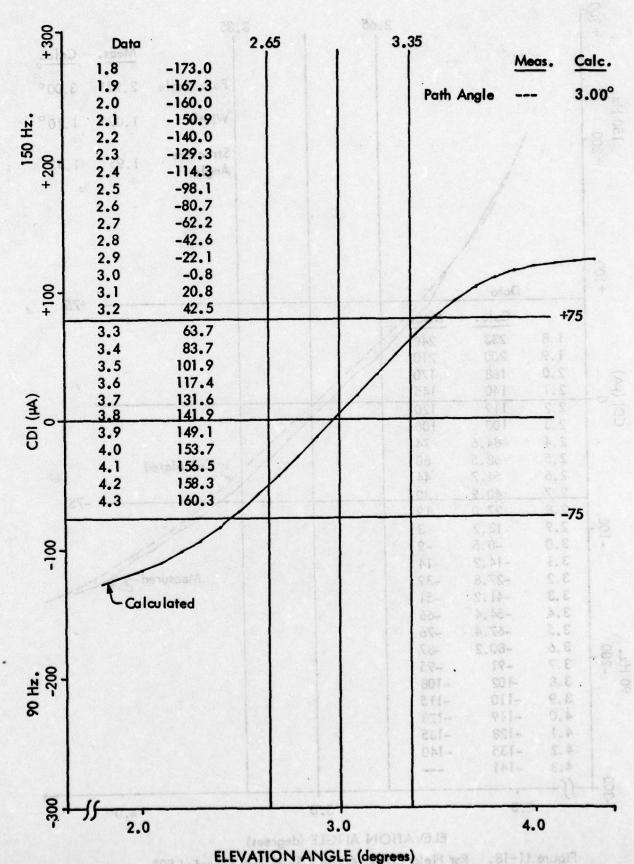


Figure 11-17. Near Field (360° Point) CDI vs Angle - Sidebands Retarded 50°.

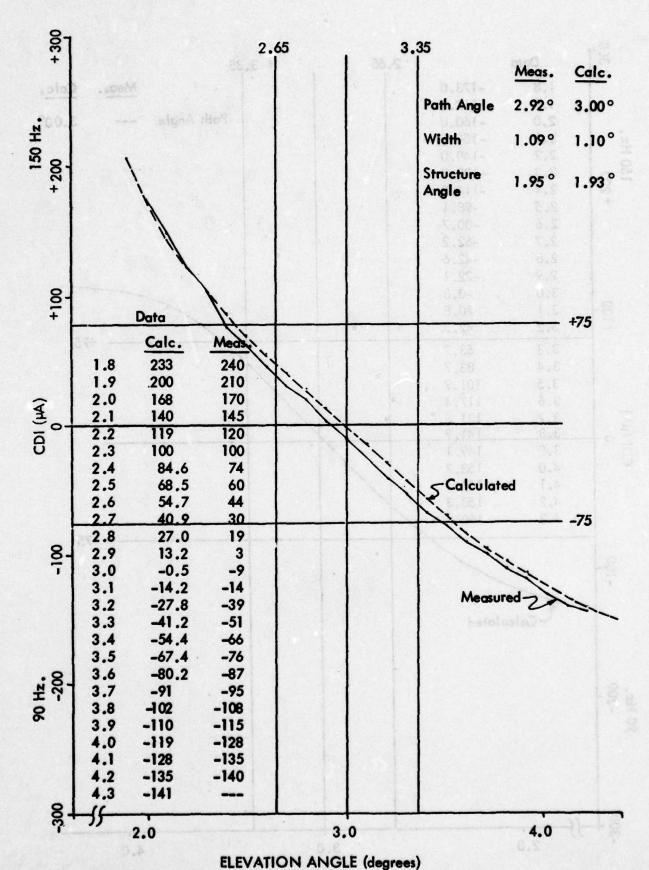


Figure 11-18. Far Field CDI vs Angle - Sidebands Retarded 50°.
Horizontal Run at 1000 Feet Altitude, 2 September 1976.

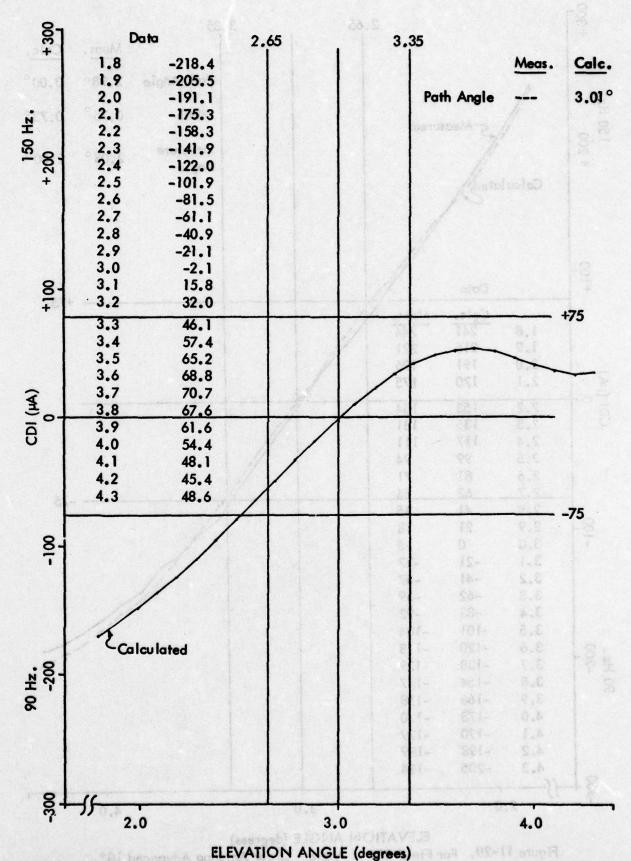


Figure 11-19. Near Field (360° Point) CDI vs Angle - Lower Antenna Advanced 10°.

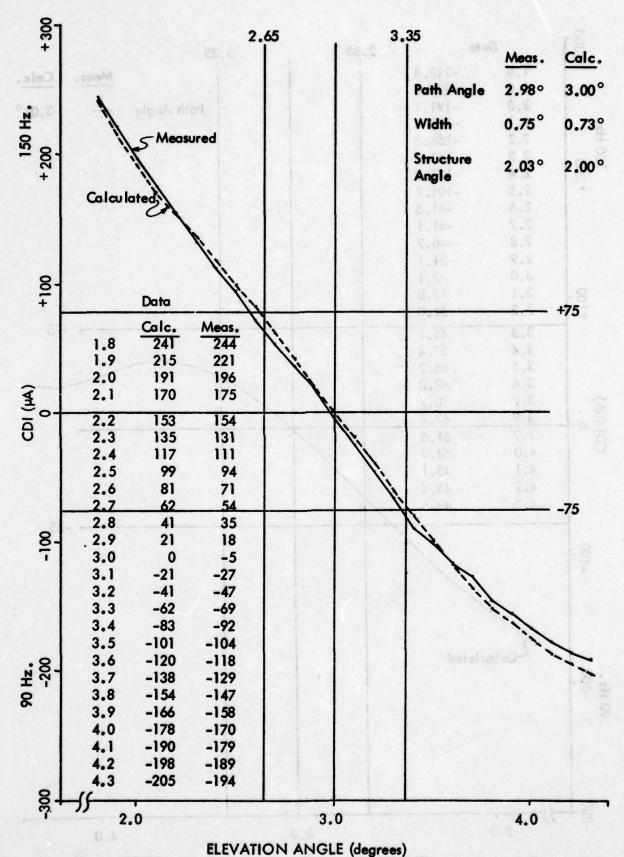


Figure 11-20. Far Field CDI vs Angle - Lower Antenna Advanced 10°.
Horizontal Run at 1000 Feet Altitude, 31 August 1976.

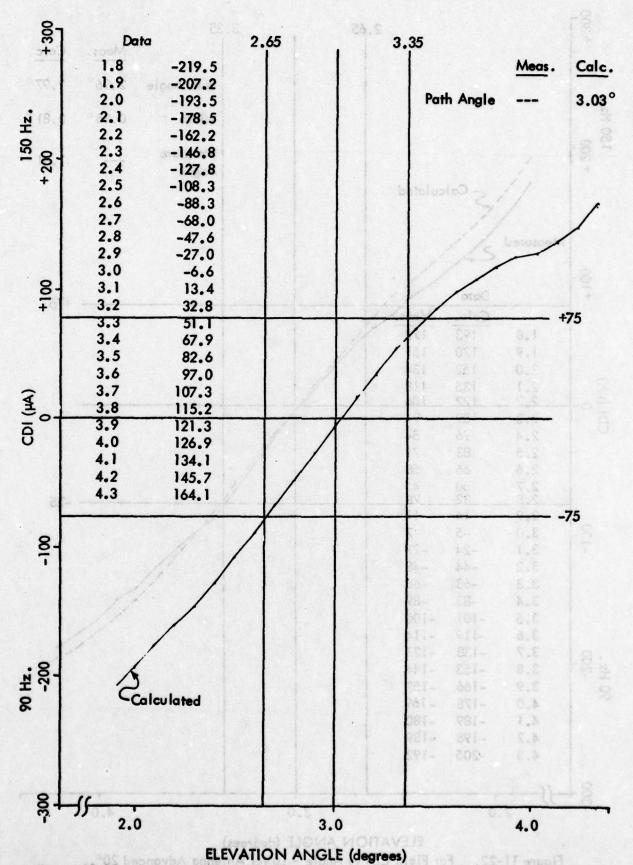


Figure 11-21. Near Field (360° Point) CDI vs Angle - Lower Antenna Advanced 20°.

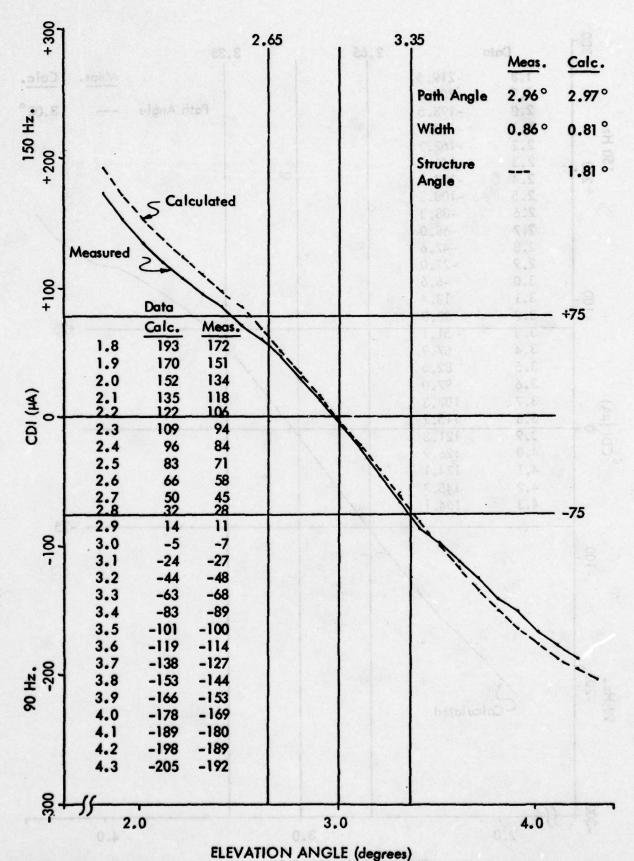


Figure 11-22. Far Field CDI vs Angle - Lower Antenna Advanced 20°. Horizontal Run at 1000 Feet Altitude, 31 August 1976.

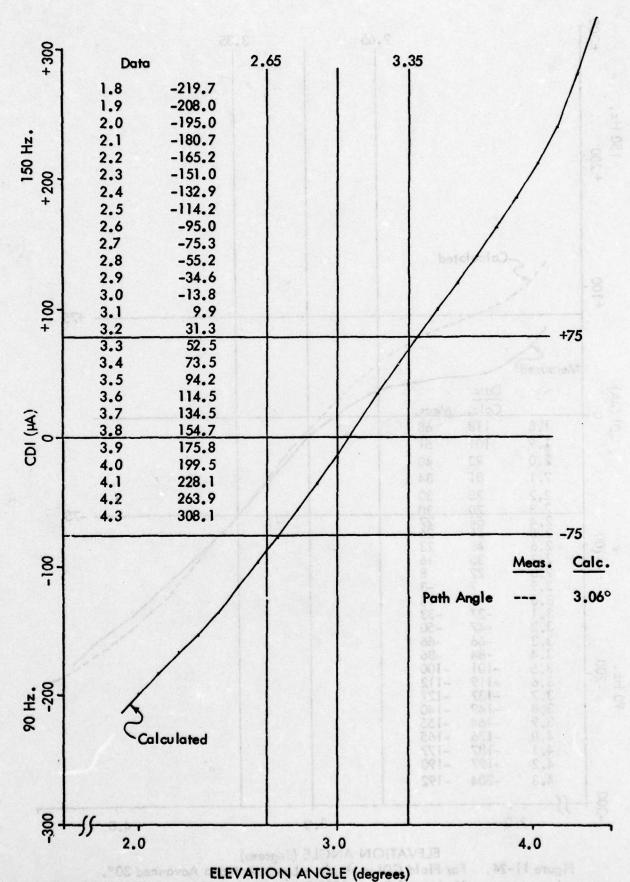


Figure 11-23. Near Field (360° Point) CDI vs Angle - Lower Antenna Advanced 30°.

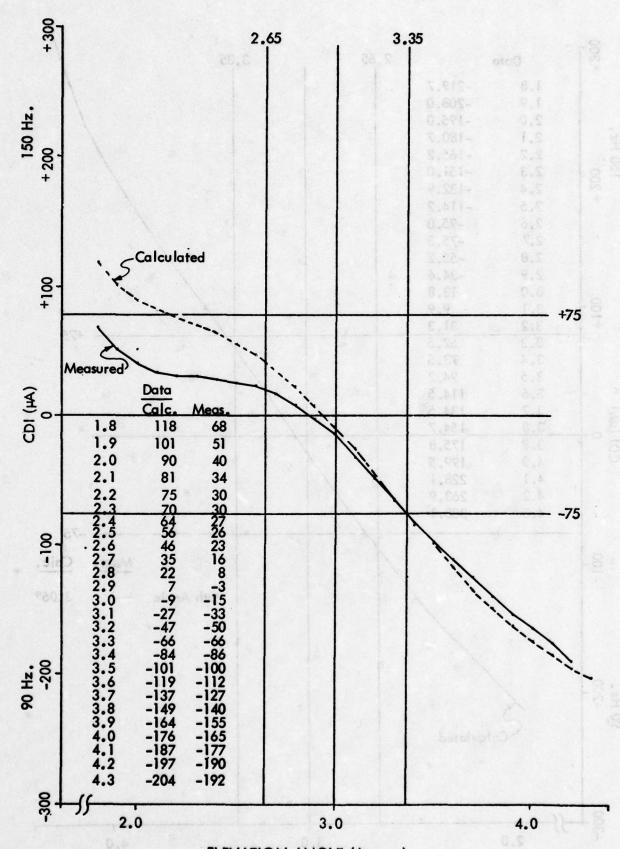


Figure 11-24. Far Field CDI vs Angle – Lower Antenna Advanced 30°. Horizontal Run at 1000 Feet Altitude, 31 August 1976.

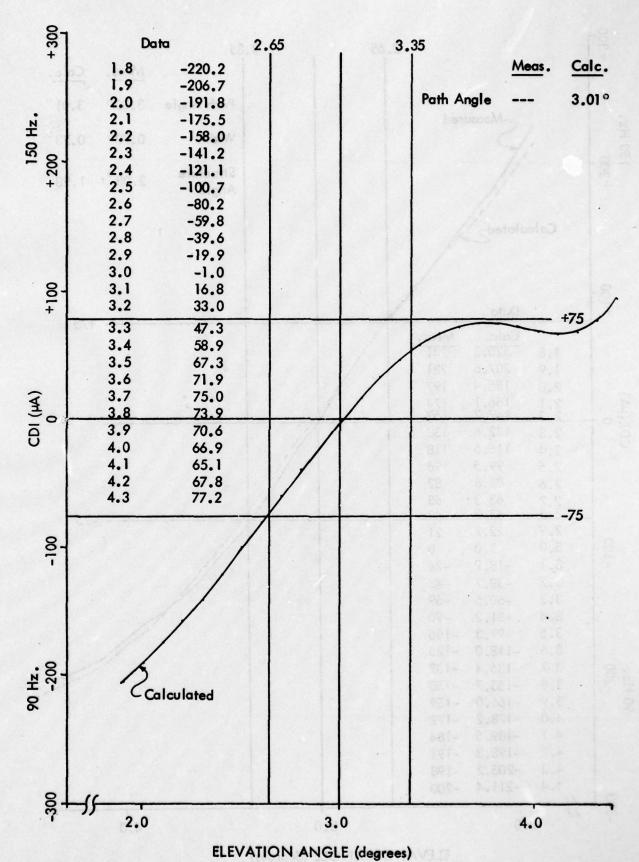
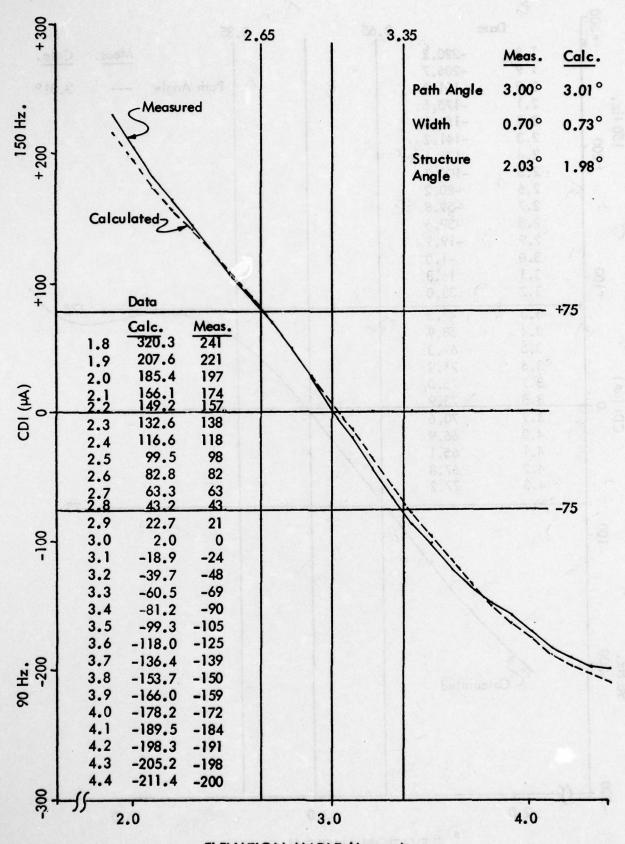


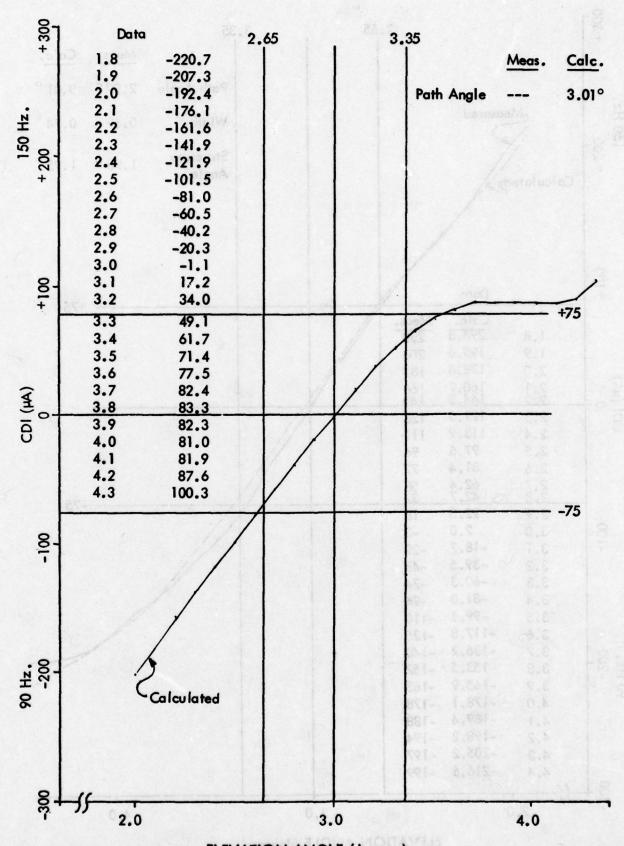
Figure 11-25. Near Field (360° Point) CDI vs Angle - Middle Antenna Retarded 12°.



ELEVATION ANGLE (degrees)

Figure 11–26. Far Field CDI vs Angle – Middle Antenna Retarded 12°.

Horizontal Run at 1000 Feet Altitude, 31 August 1976.



ELEVATION ANGLE (degrees)
Figure 11-27. Near Field (360° Point) CDI vs Angle - Middle Antenna Retarded 14°.

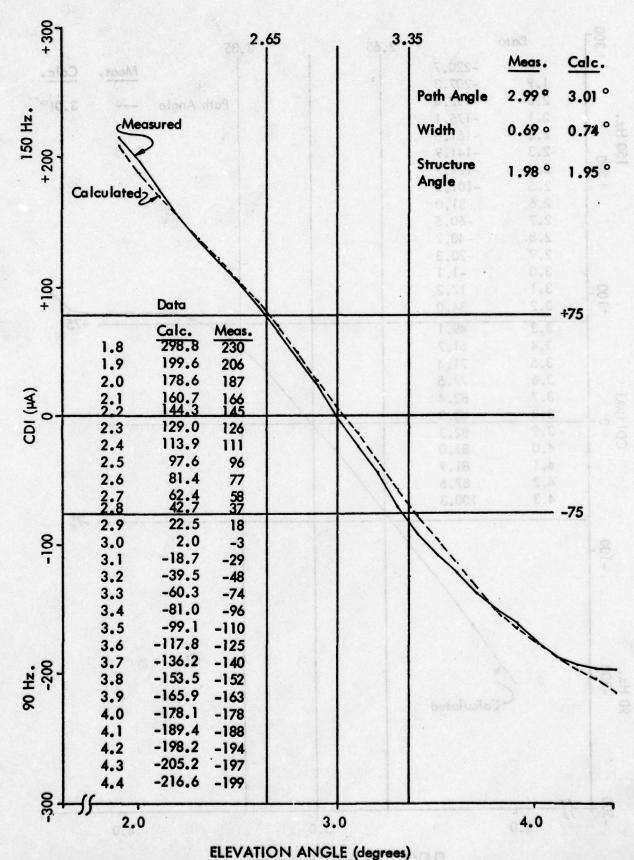


Figure 11-28. Far Field CDI vs Angle - Middle Antenna Retarded 14°. Horizontal Run at 1000 Feet Altitude, 31 August 1976.

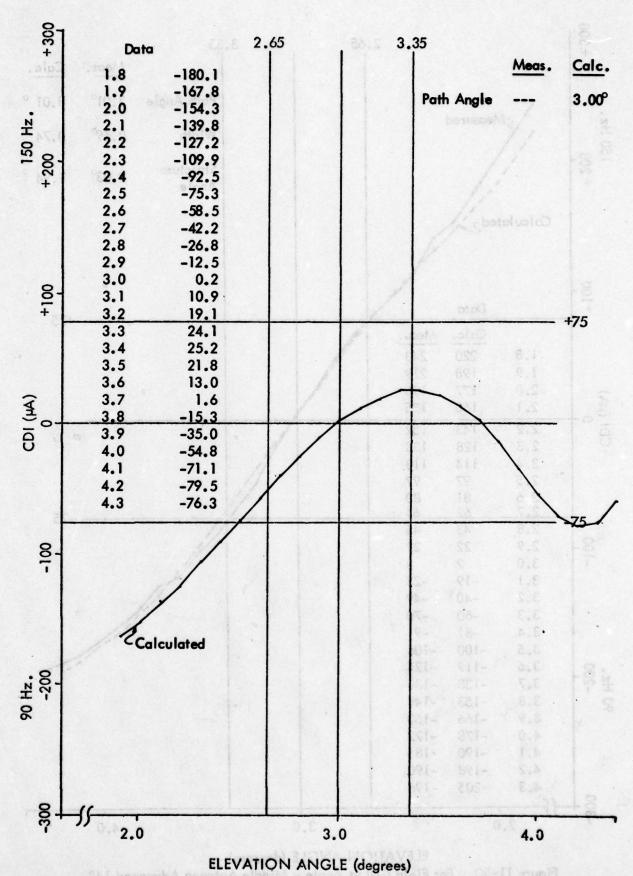


Figure 11-29. Near Field (360° Point) CDI vs Angle - Middle Antenna Advanced 14°.

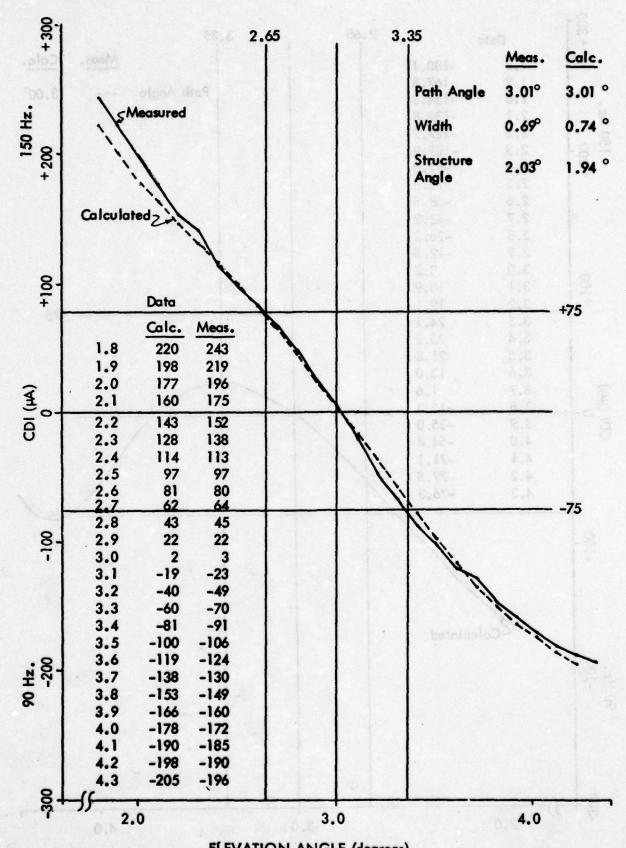


Figure 11-30. Far Field CDI vs Angle - Middle Antenna Advanced 14°.
Horizontal Run at 1000 Feet Altitude, 31 August 1976.

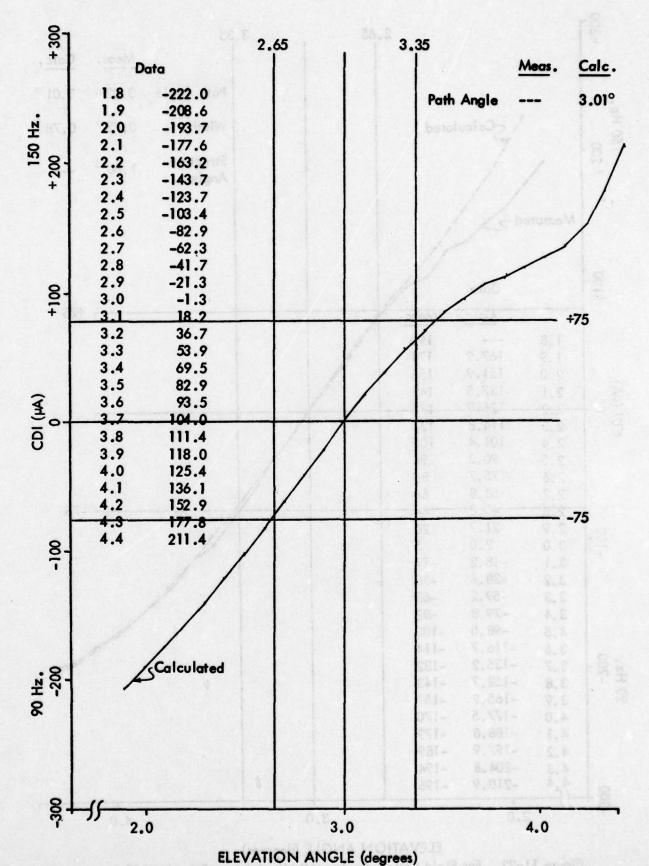


Figure 11-31. Near Field (360° Point) CDI vs Angle - Middle Antenna Retarded 20°.

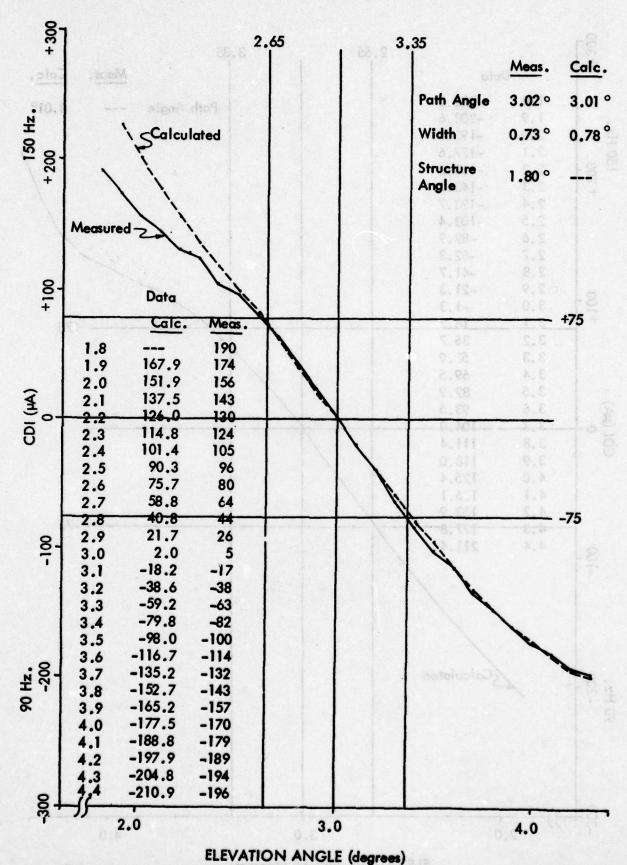
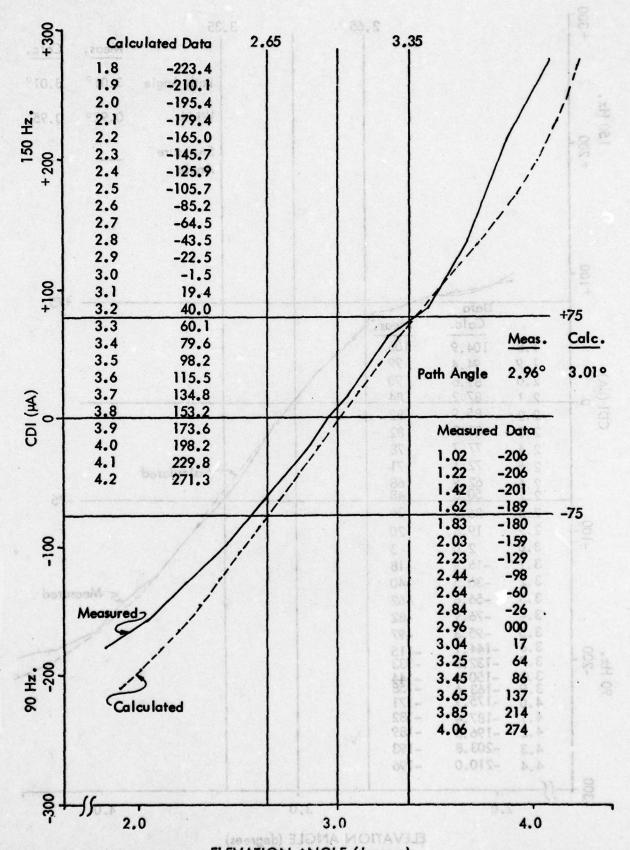


Figure 11-32. Far Field CDI vs Angle - Middle Antenna Retarded 20°.
Horizontal Run at 1000 Feet Altitude, 31 August 1976



ELEVATION ANGLE (degrees)
Figure 11-33. Near Field (360° Point) CDI vs Angle - Middle Antenna Retarded 30°.

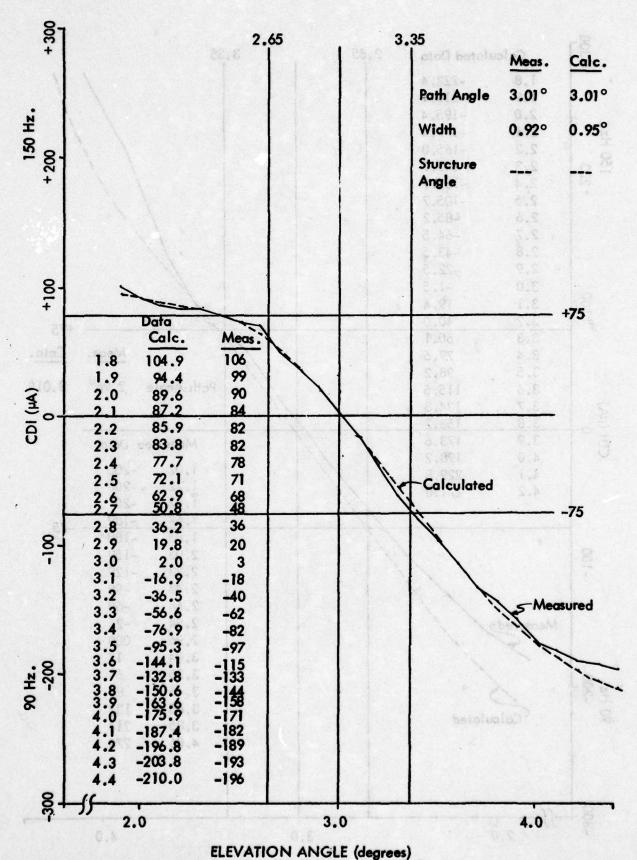
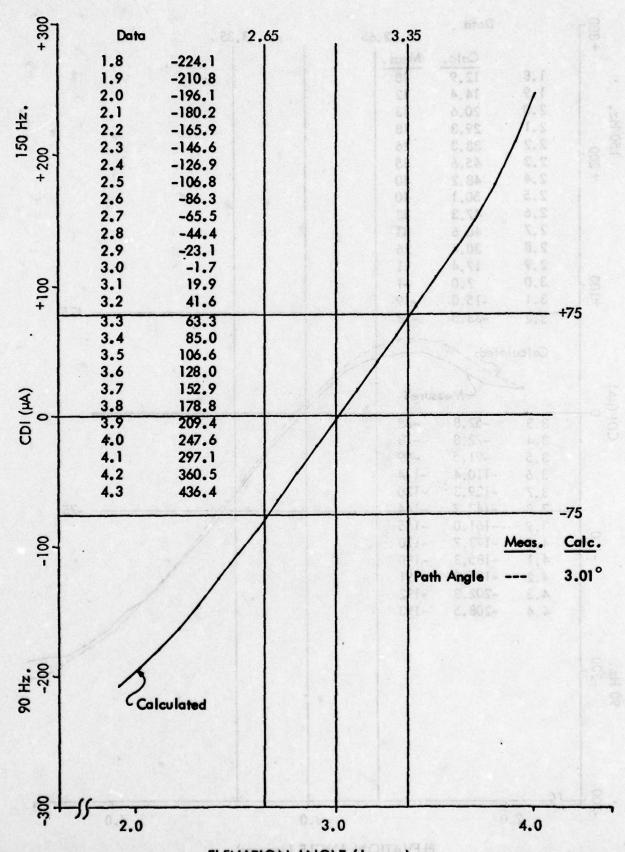


Figure 11-34. Far Field CDI vs Angle - Middle Antenna Retarded 30°. Horizontal Run at 1000 Feet Altitude, 31 August 1976.



ELEVATION ANGLE (degrees)

Figure 11-35. Near Field (360° Point) CDI vs Angle - Middle Antenna Retarded 40°.

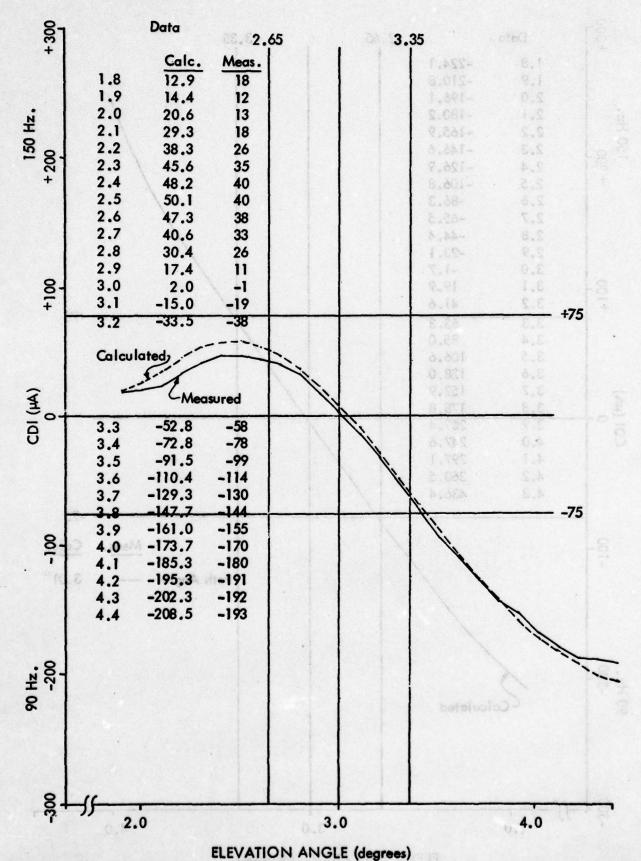
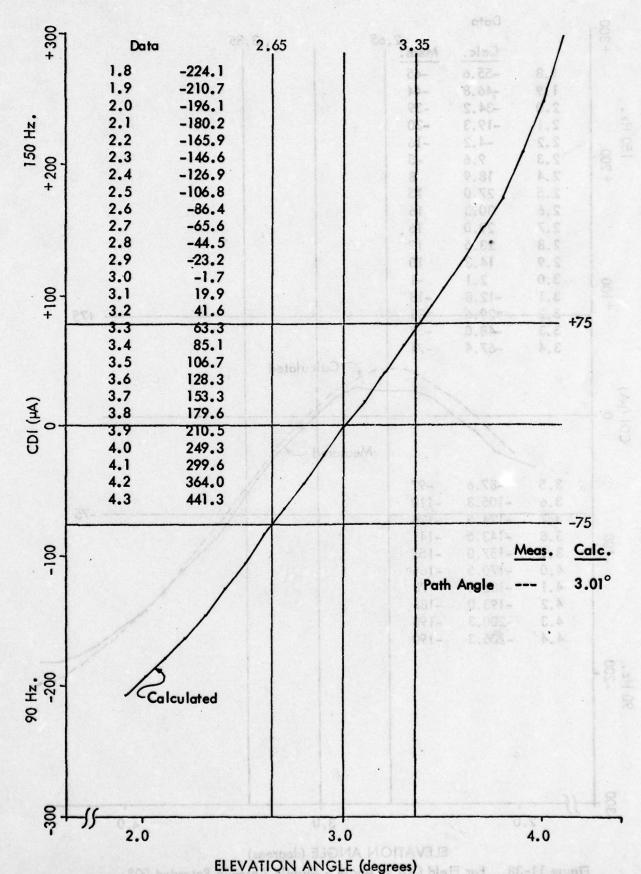


Figure 11–36. Far Field CDI vs Angle – Middle Antenna Retarded 40°. Horizontal Run at 1000 Feet Altitude, 31 August 1976.



ELEVATION ANGLE (degrees)

Figure 11-37. Near Field (360° Point) CDI vs Angle - Middle Antenna Retarded 50°.

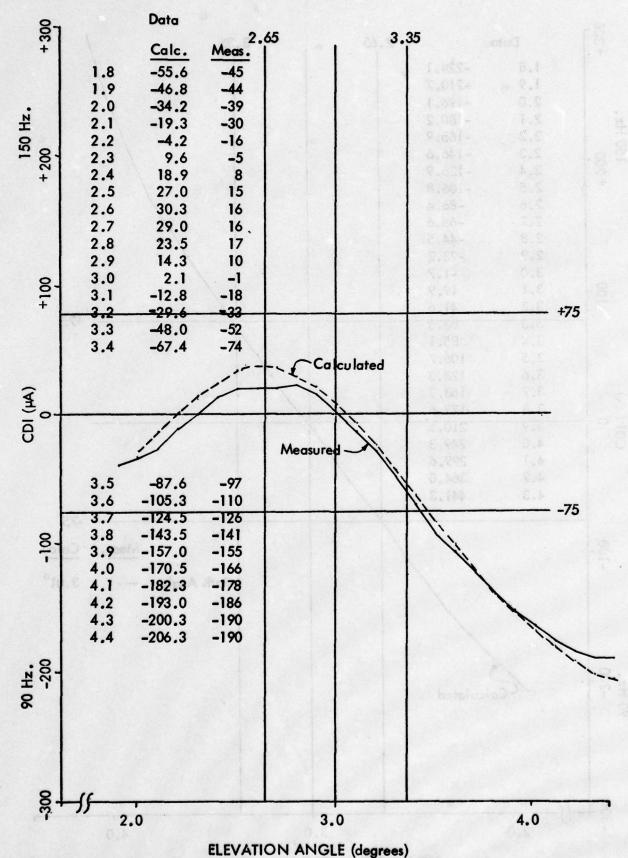
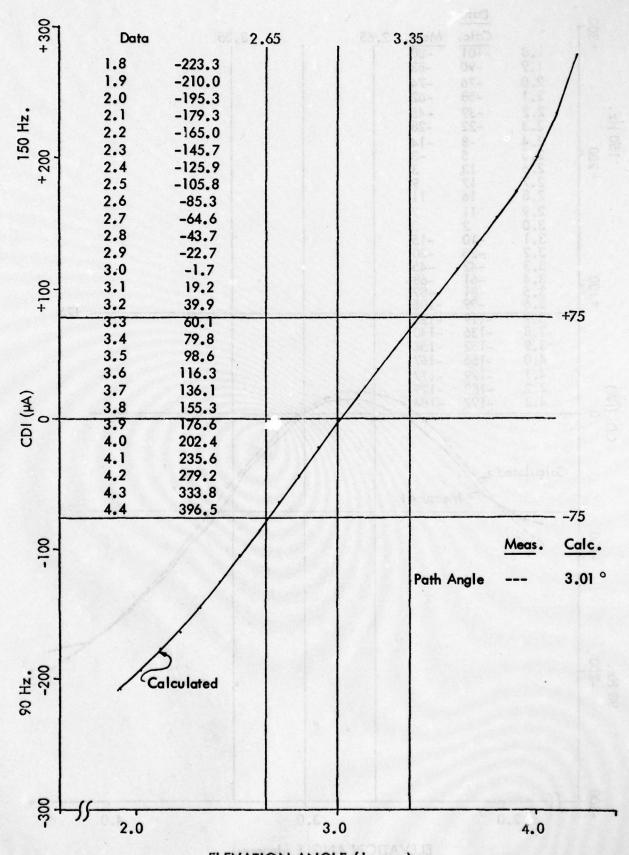


Figure 11-38. Far Field CDI vs Angle - Middle Antenna Retarded 50°.
Horizontal Run at 1000 Feet Altitude, 31 August 1976.
11-58



ELEVATION ANGLE (degrees)
Figure 11-39. Near Field (360° Point) CDI vs Angle - Middle Antenna Retarded 60°.

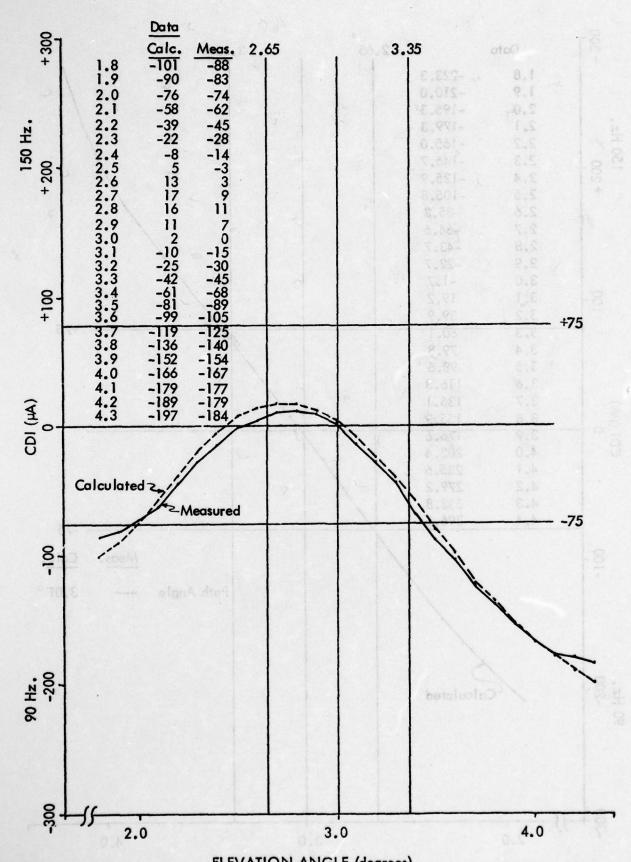


Figure 11-40. Far Field CDI vs Angle - Middle Antenna Retarded 60°. Horizontal Run at 1000 Feet Altitude, 31 August 1976.

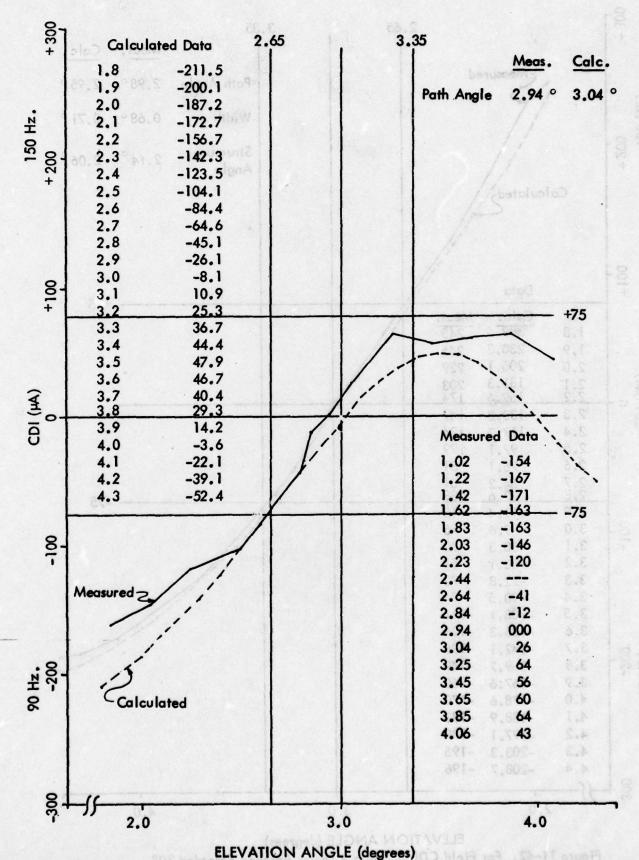


Figure 11-41. Near Field (360° Point) CDI vs Angle - Upper Antenna Retarded 30°.

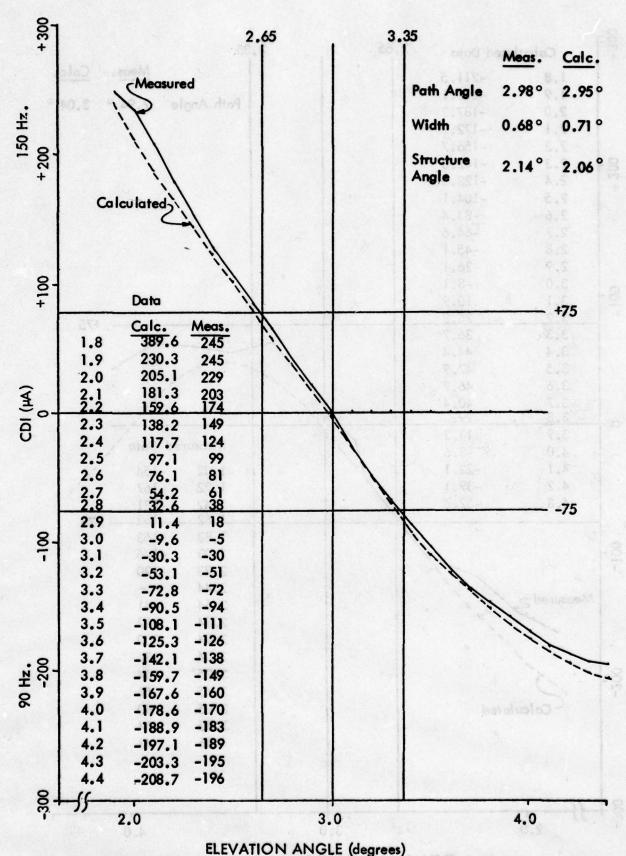
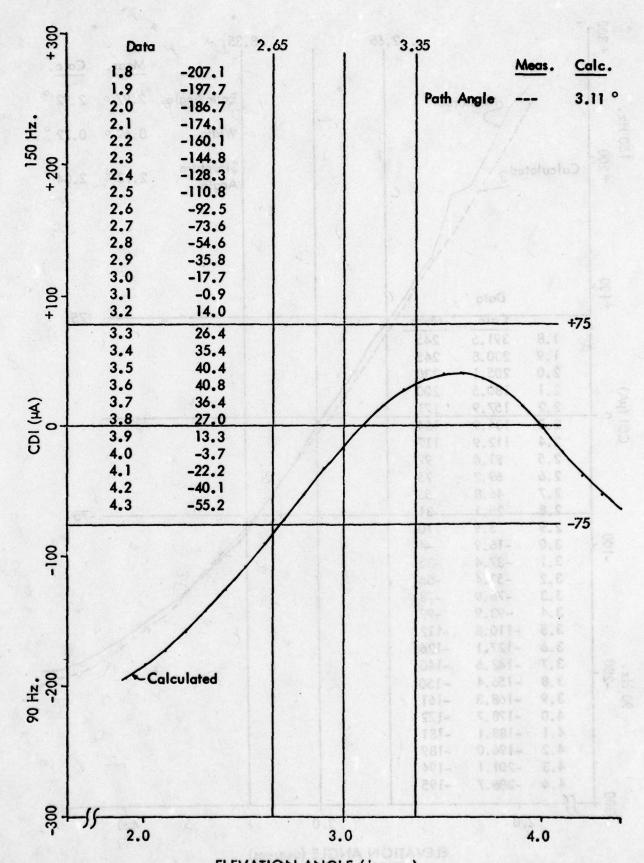


Figure 11-42. Far Field CDI vs Angle - Upper Antenna Retarded 30°.
Horizontal Run at 1000 Feet Altitude, 31 August 1976.



ELEVATION ANGLE (degrees)
Figure 11-43. Near Field (360° Point) CDI vs Angle - Upper Antenna Retarded 40°.

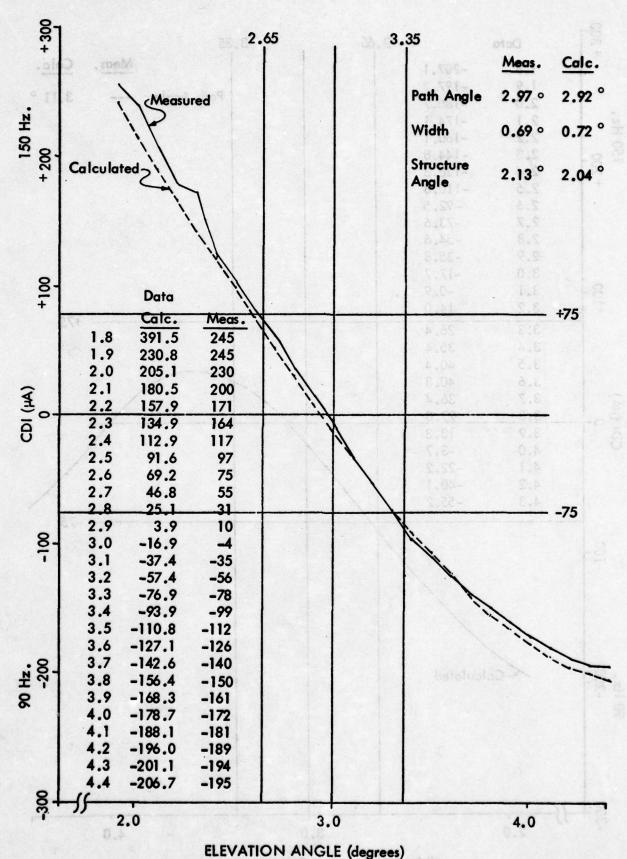


Figure 11-44. Far Field CDI vs Angle - Upper Antenna Retarded 40°.
Horizontal Run at 1000 Feet Altitude, 31 August 1976.

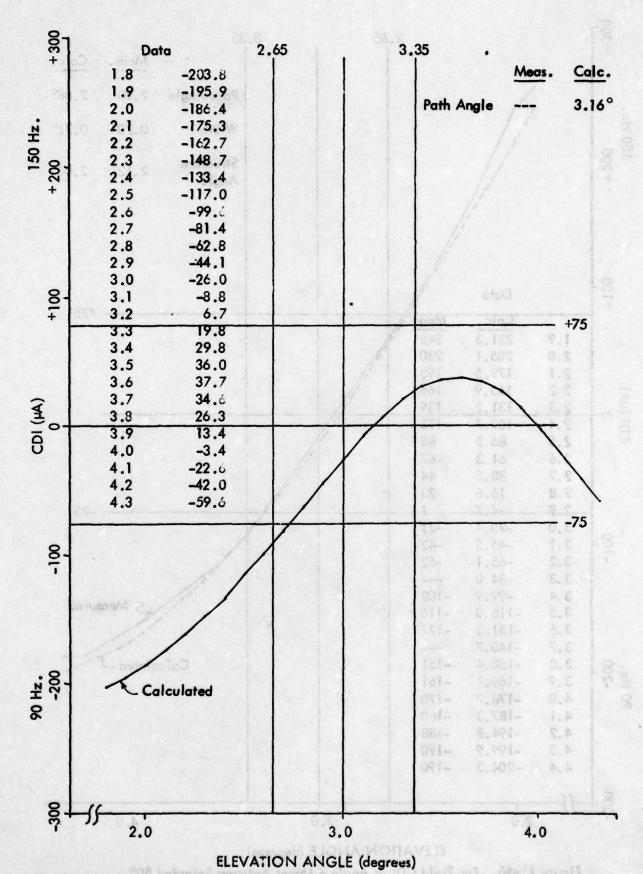


Figure 11-45. Near Field (360° Point) CDI vs Angle - Upper Antenna Retarded 50°.

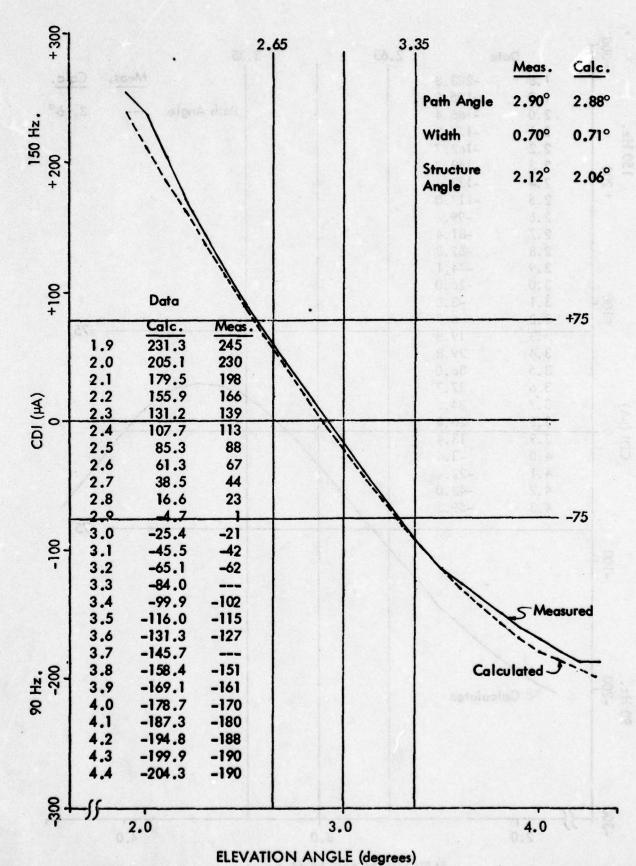


Figure 11–46. Far Field CDI vs Angle – Upper Antenna Retarded 50°. Horizontal Run at 1000 Feet Altitude, 31 August 1976.

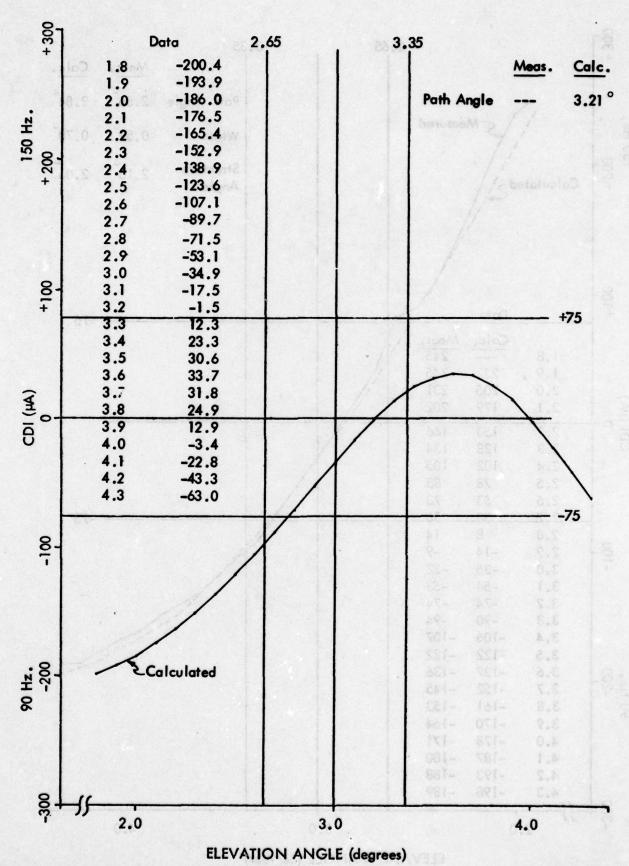


Figure 11-47. Near Field (360° Point) CDI vs Angle - Upper Antenna Retarded 60°.

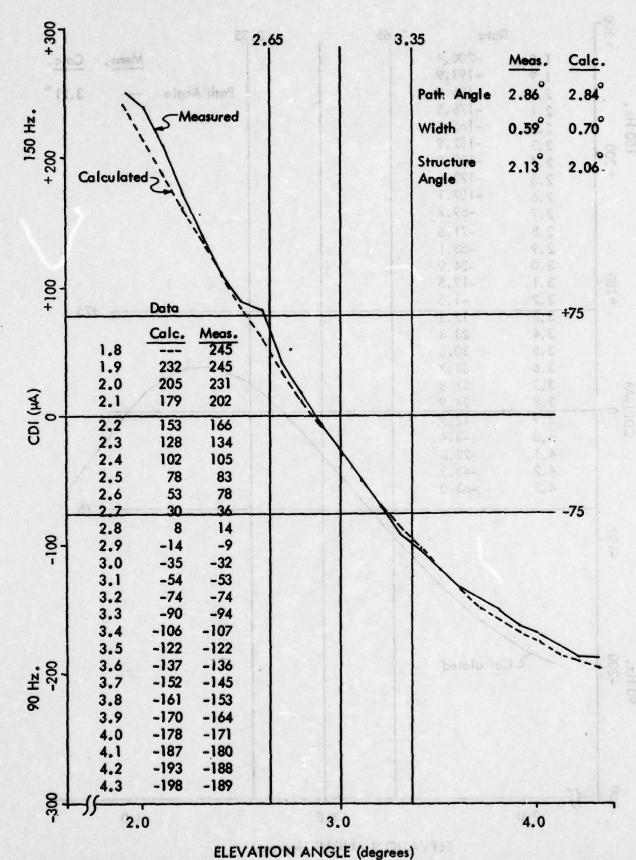


Figure 11–48. Far Field CDI vs Angle – Upper Antenna Retarded 60°. Horizontal Run at 1000 Feet Altitude, 31 August 1976.

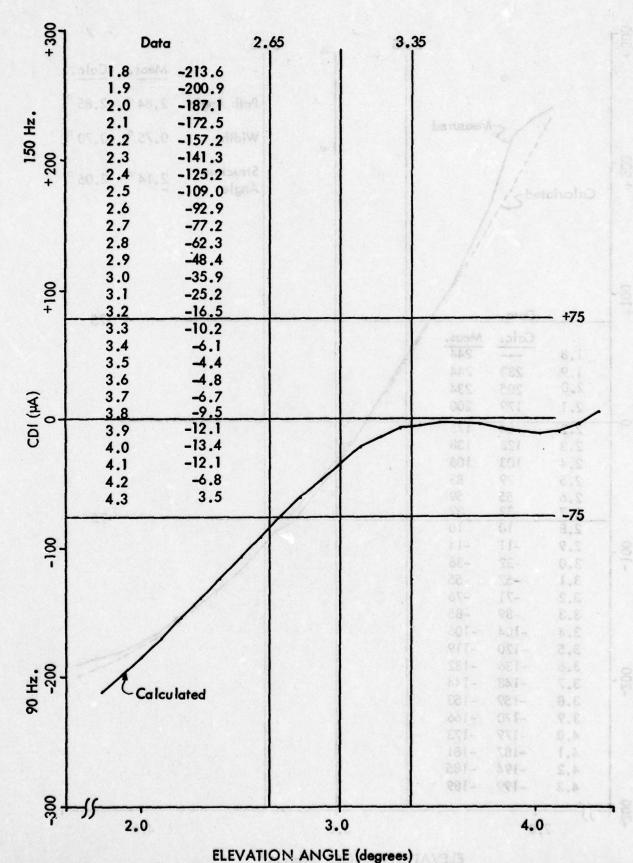


Figure 11-49. Near Field (360° Point) CDI vs Angle - Upper Antenna Advanced 60°.

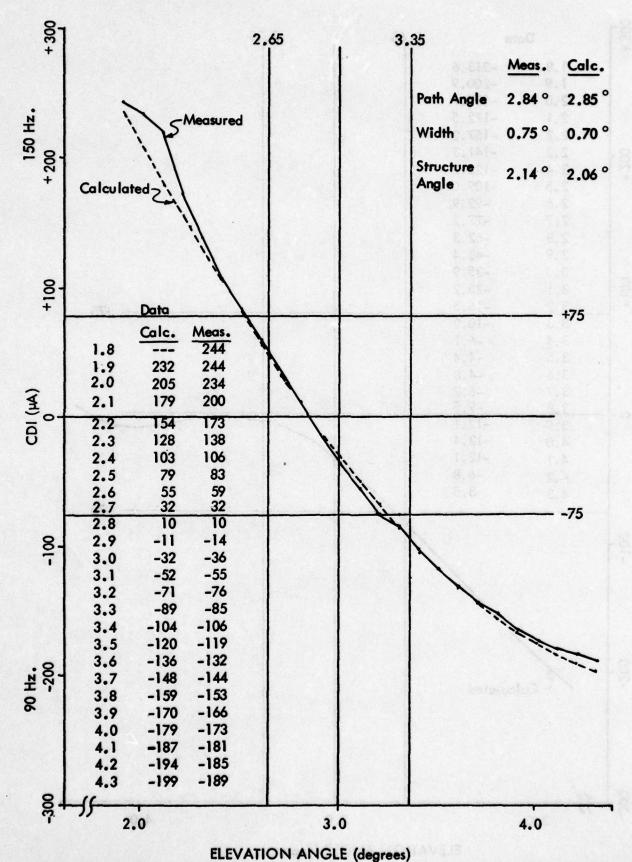


Figure 11-50. Far Field CDI vs Angle - Upper Antenna Advanced 60°.
Horizontal Run at 1000 Feet Altitude, 31 August 1976.

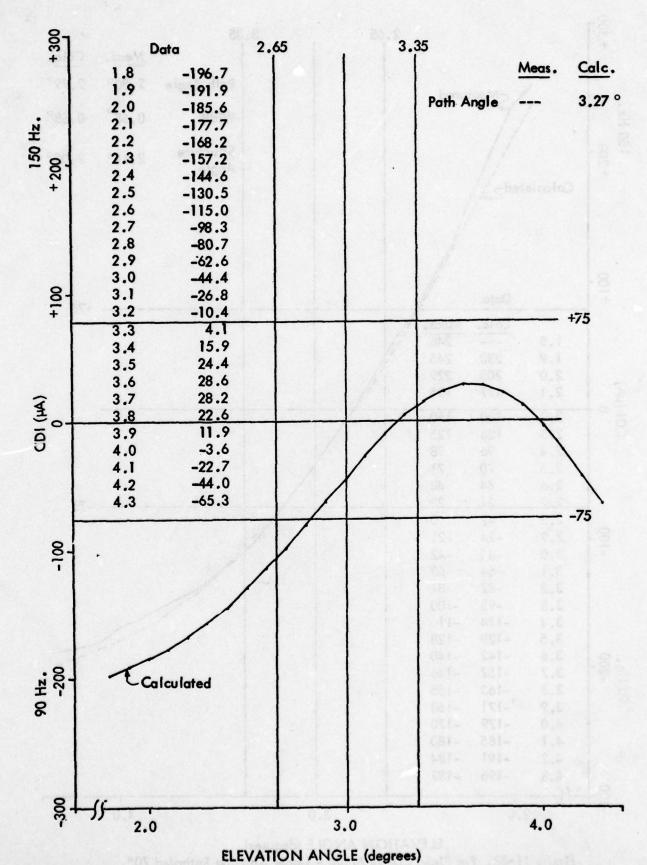
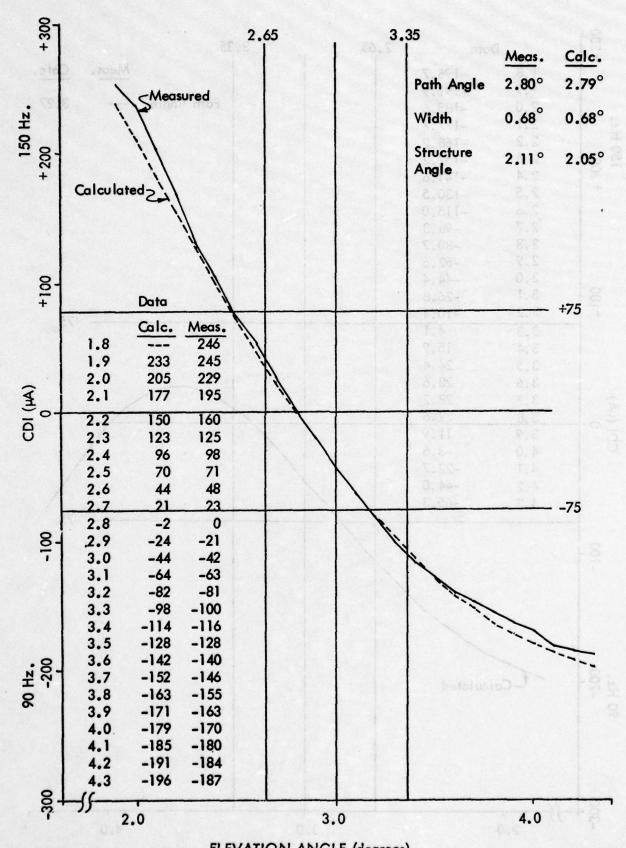


Figure 11-51. Near Field (360° Point) CDI vs Angle - Upper Antenna Retarded 70°.



ELEVATION ANGLE (degrees)

Figure 11-52. Far Field CDI vs Angle - Upper Antenna Retarded 70°.

Horizontal Run at 1000 Feet Altitude, 31 August 1976.

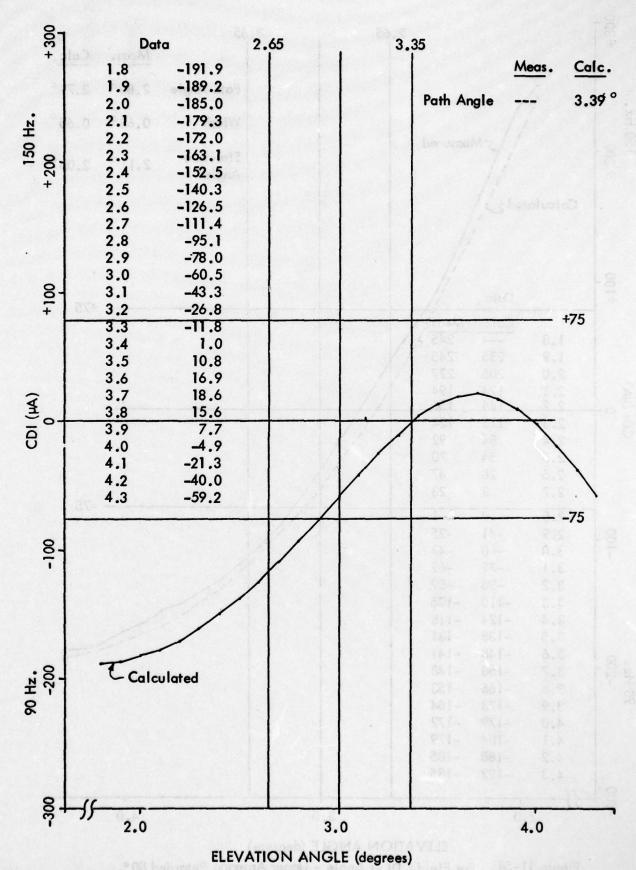


Figure 11-53. Near Field (360° Point) CDI vs Angle - Upper Antenna Retarded 80°.

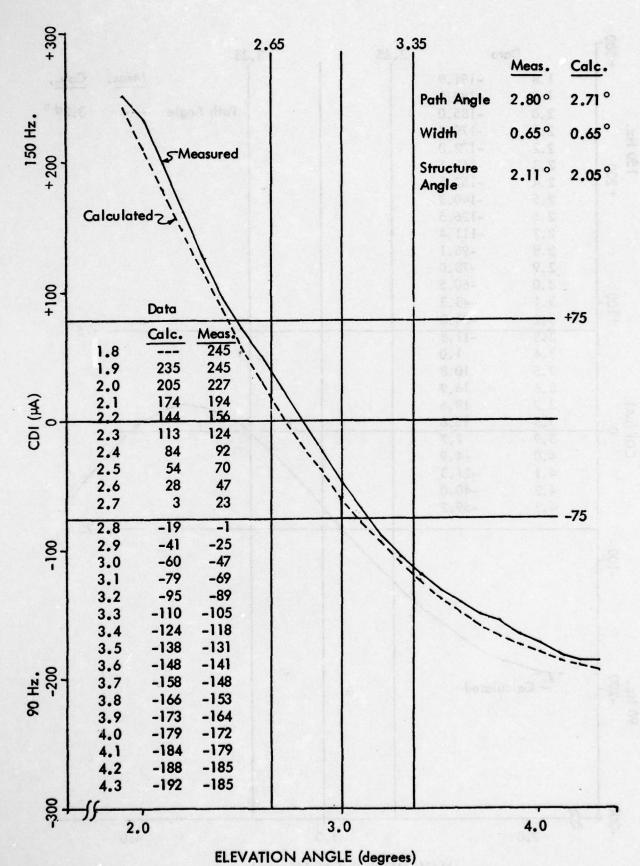


Figure 11-54. Far Field CDI vs Angle - Upper Antenna Retarded 80°. Horizontal Run at 1000 Feet Altitude, 31 August 1976.

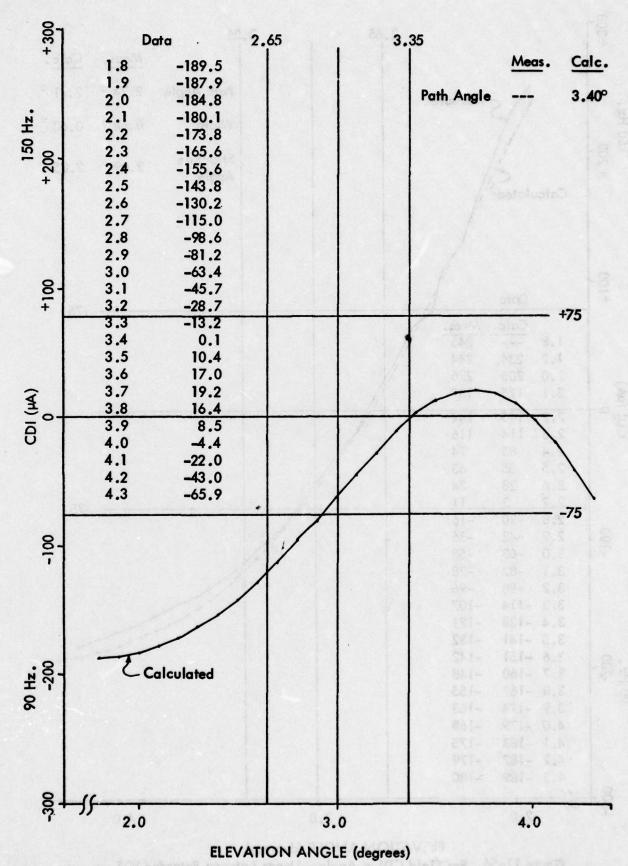


Figure 11-55. Near Field (360° Point) CDI vs Angle - Upper Antenna Retarded 90°.

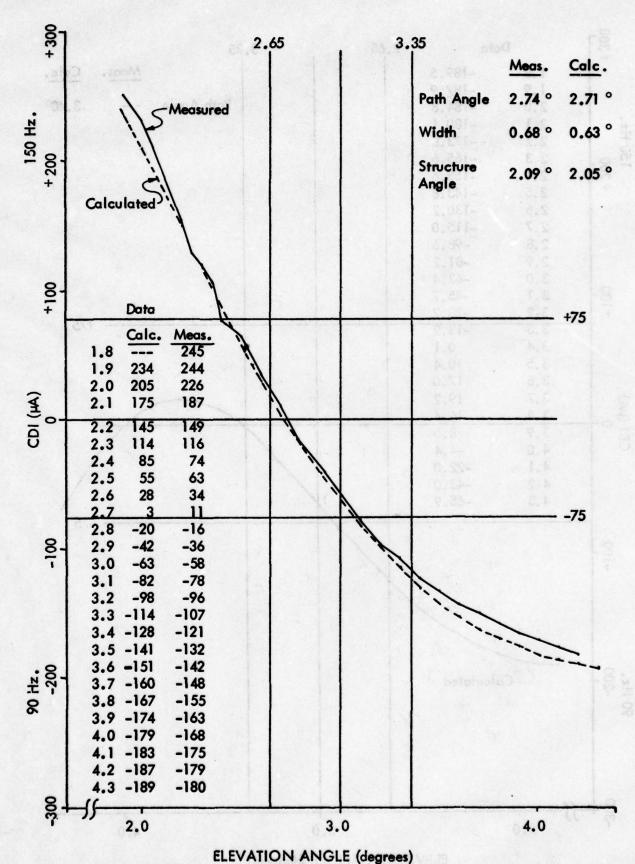


Figure 11-56. Far Field CDI vs Angle - Upper Antenna Retarded 90°.

Horizontal Run at 1000 Feet Altitude, 31 August 1976.

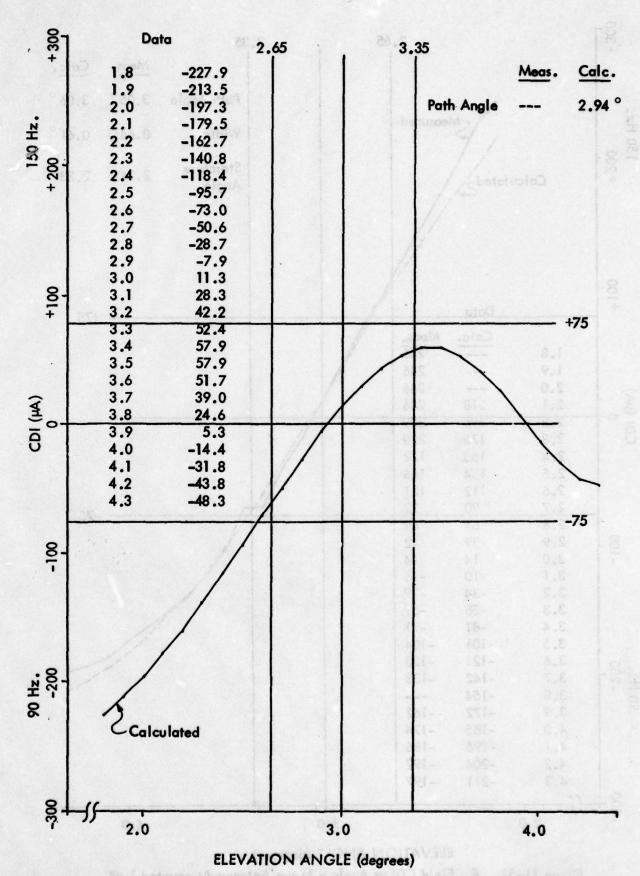


Figure 11-57. Near Field (360° Point) CDI vs Angle - Lower Antenna Attenuated 1 dB.

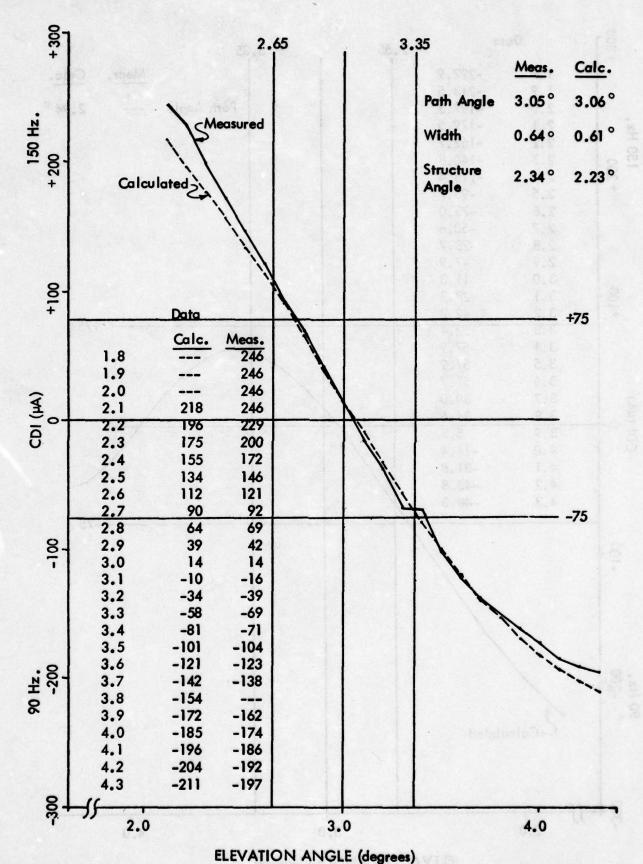


Figure 11-58. Far Field CDI vs Angle - Lower Antenna Attenuated 1 dB. Horizontal Run at 1000 Feet Altitude, 31 August 1976.

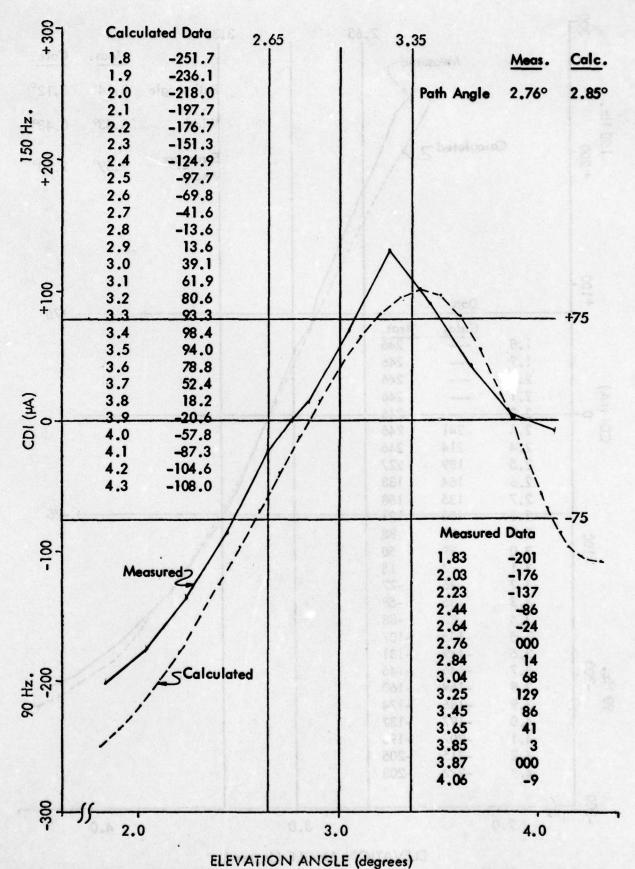


Figure 11-59. Near Field (360° Point) CDI vs Angle - Lower Antenna Attenuated 3 dB.

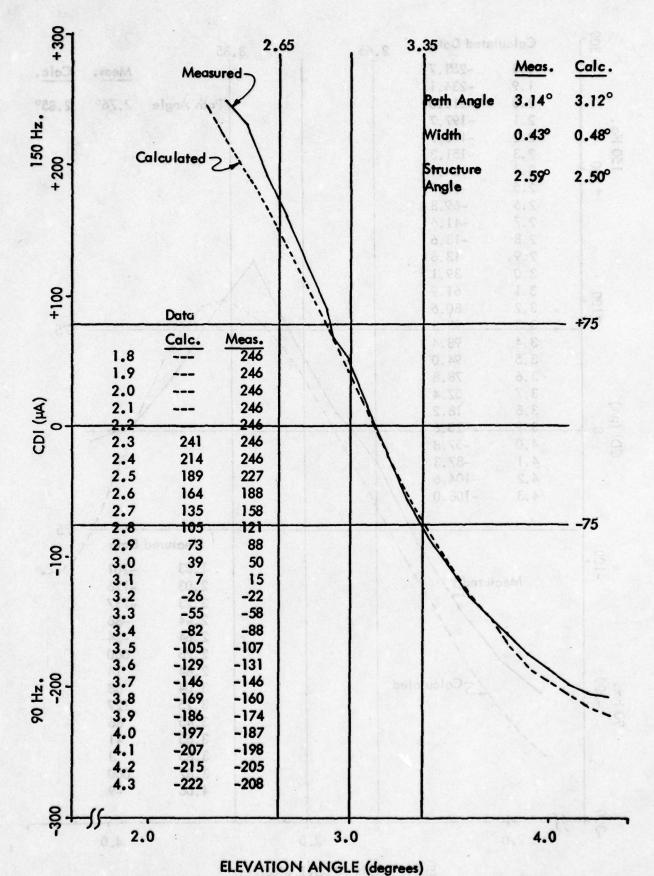


Figure 11–60. Far Field CDI vs Angle – Lower Antenna Attenuated 3 dB. Horizontal Run at 1000 Feet Altitude, 31 August 1976.

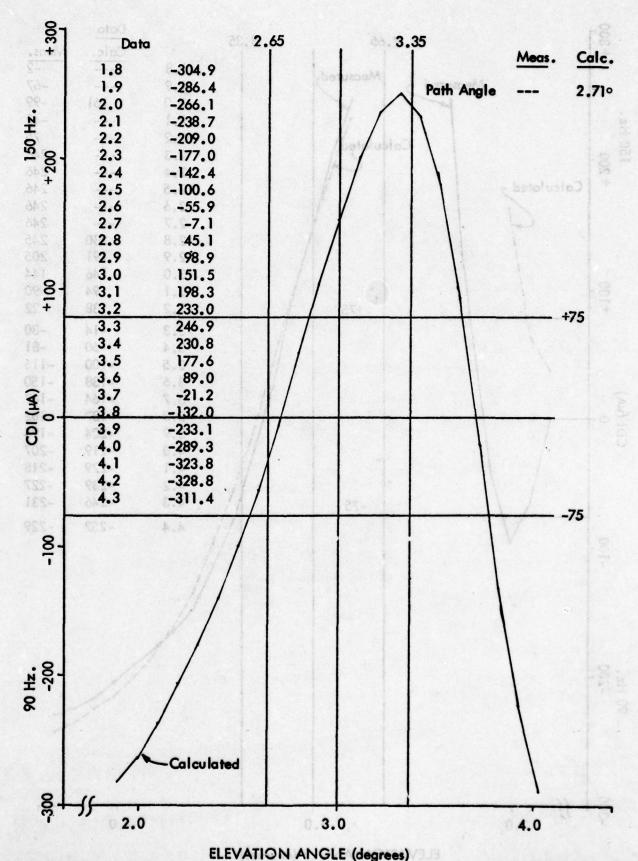


Figure 11-61. Near Field (360° Point) CDI'vs Angle - Lower Antenna Attenuated 7 dB.

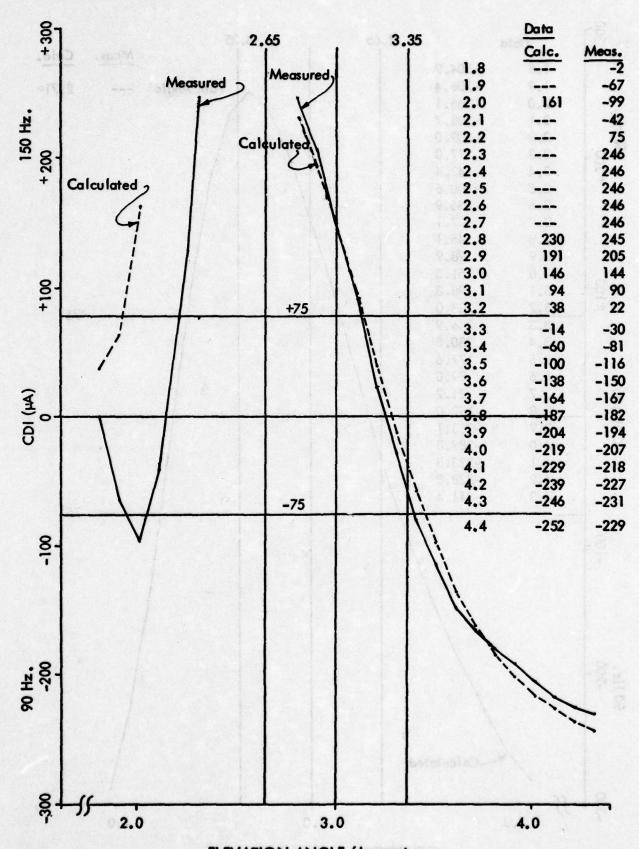


Figure 11–62. Far Field CDI vs Angle – Lower Antenna Attenuated 7 dB. Horizontal Run at 1000 Feet Altitude, 31 August 1976.

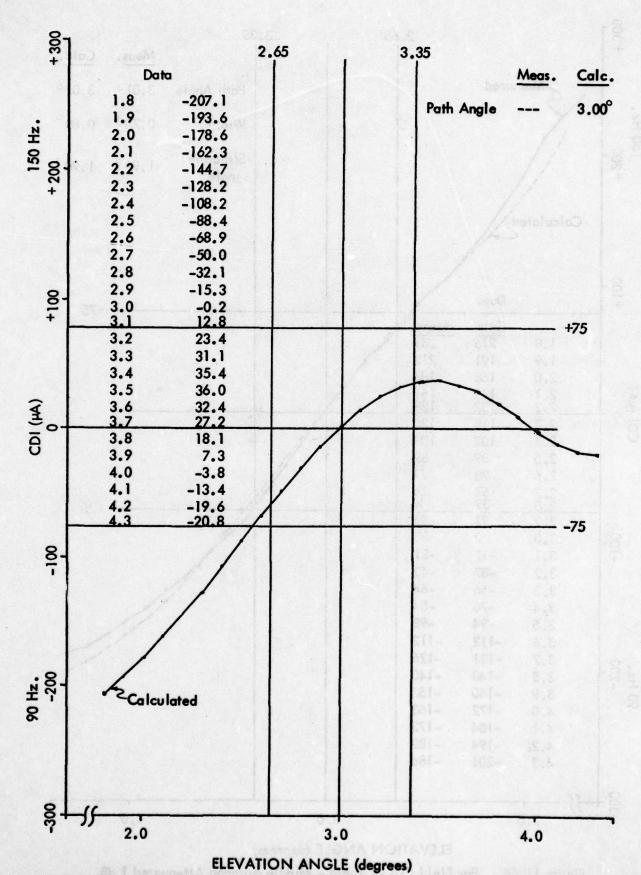


Figure 11-63. Near Field (360° Point) CDI vs Angle - Middle Antenna Attenuated 1 dB.

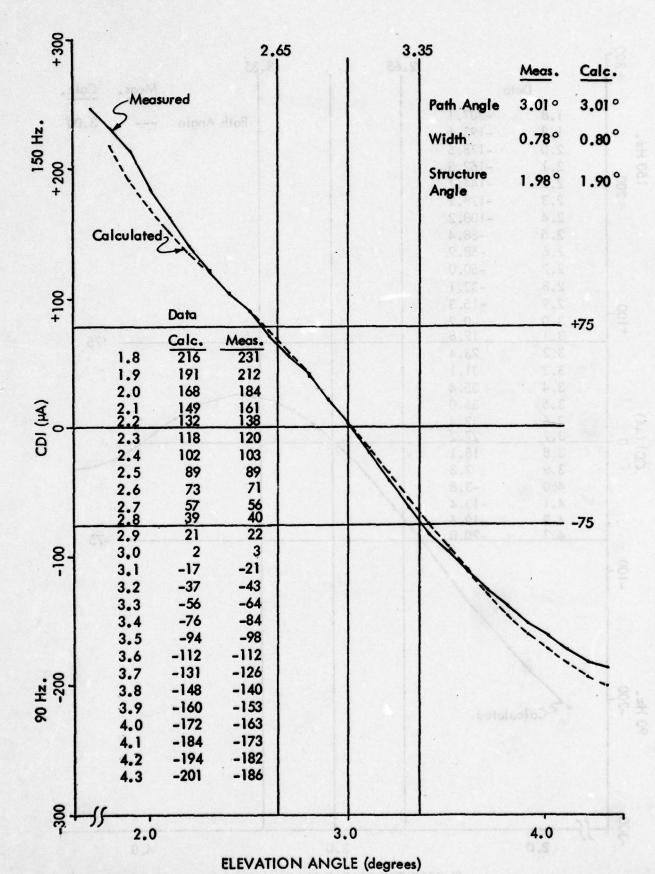


Figure 11-64. Far Field CDI vs Angle - Middle Antenna Attenuated 1 dB. Horizontal Run at 1000 Feet Altitude, 31 August 1976.

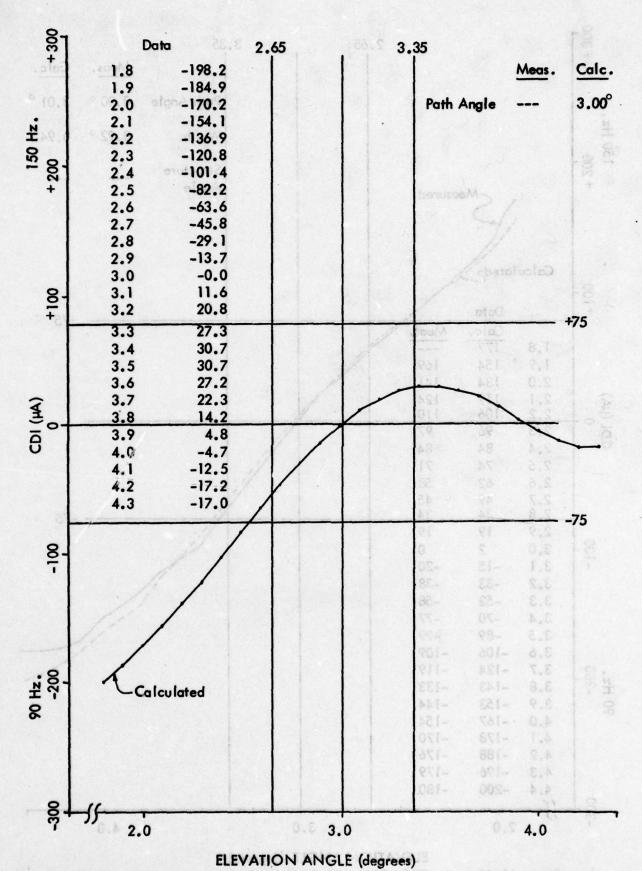


Figure 11-65. Near Field (360° Point) CDI vs Angle - Middle Antenna Attenuated 2 dB.

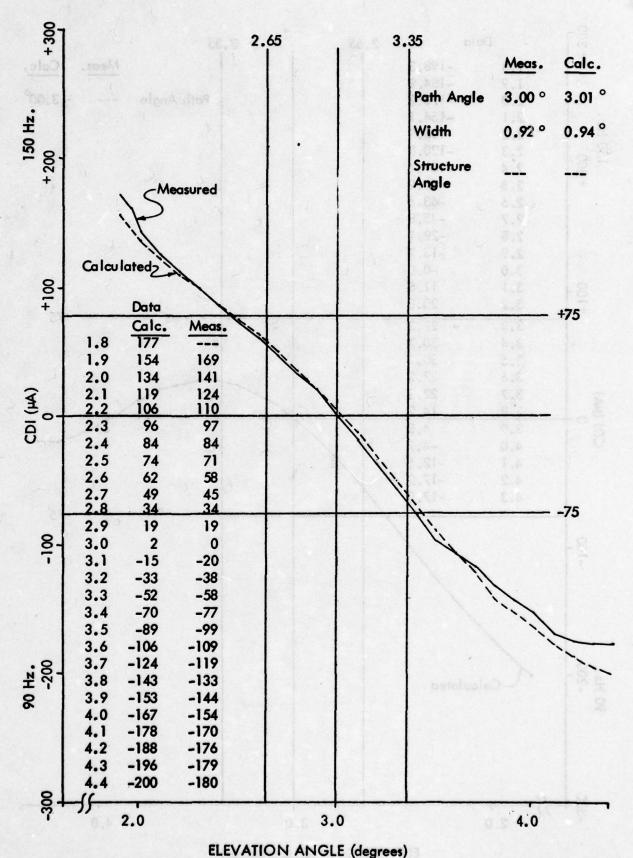


Figure 11-66. Far Field CDI vs Angle - Middle Antenna Attenuated 2 dB. Horizontal Run at 1000 Feet Altitude, 31 August 1976.

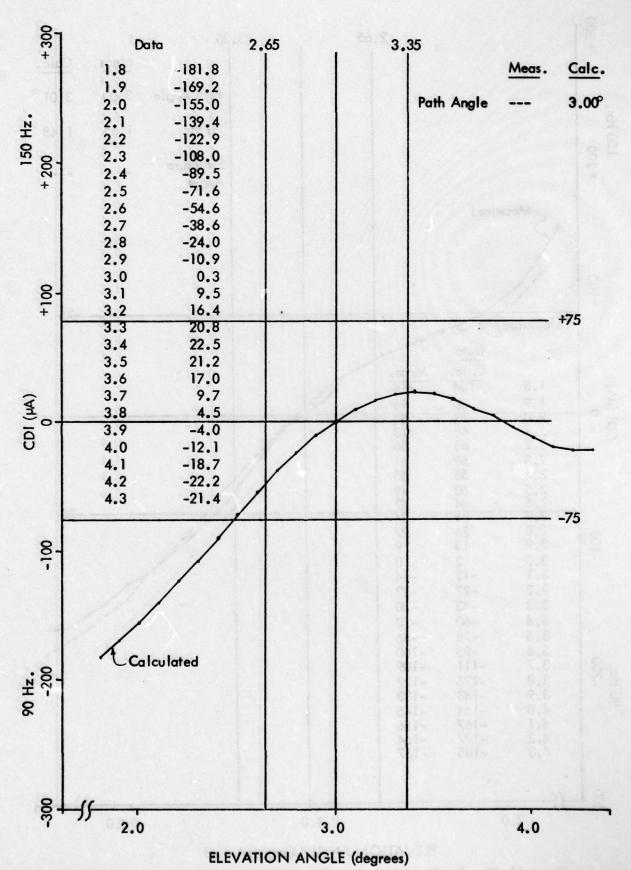


Figure 11-67. Near Field (360° Point) CDI vs Angle - Middle Antenna Attenuated 4 dB.

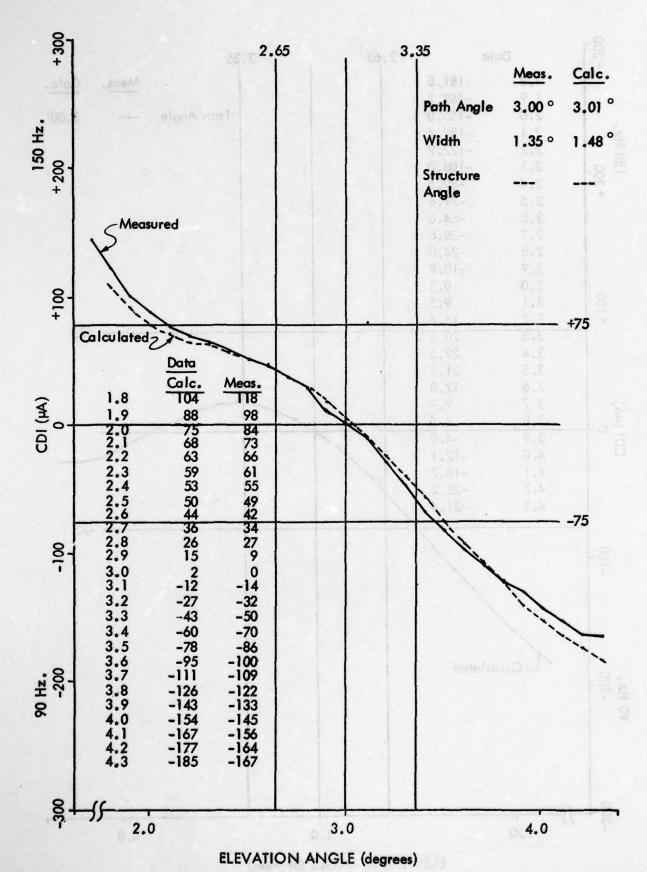
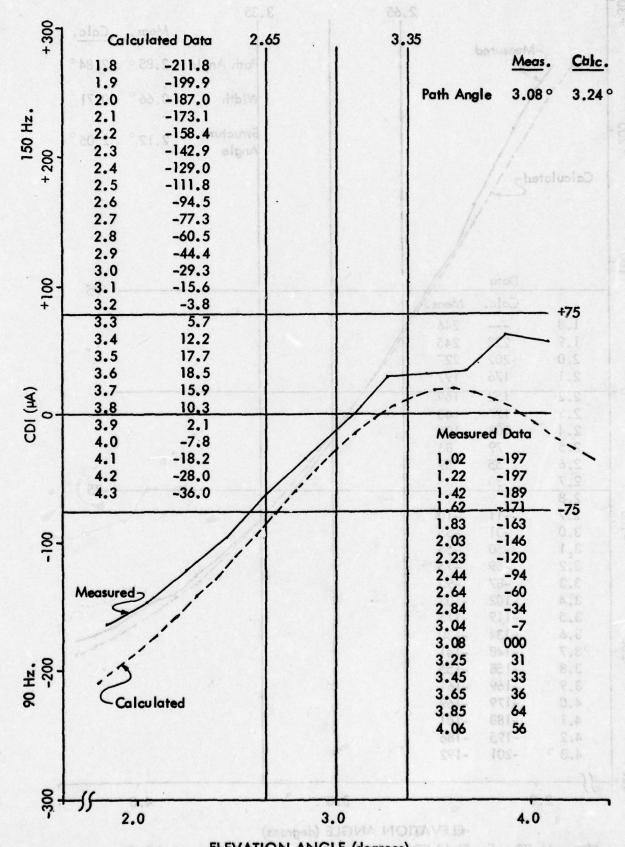


Figure 11-68. Far Field CDI vs Angle - Middle Antenna Attenuated 4 dB. Horizontal Run at 1000 Feet Altitude, 30 August 1976.



ELEVATION ANGLE (degrees)
Figure 11-69. Near Field (360° Point) CDI vs Angle - Upper Antenna Attenuated 3 dB.

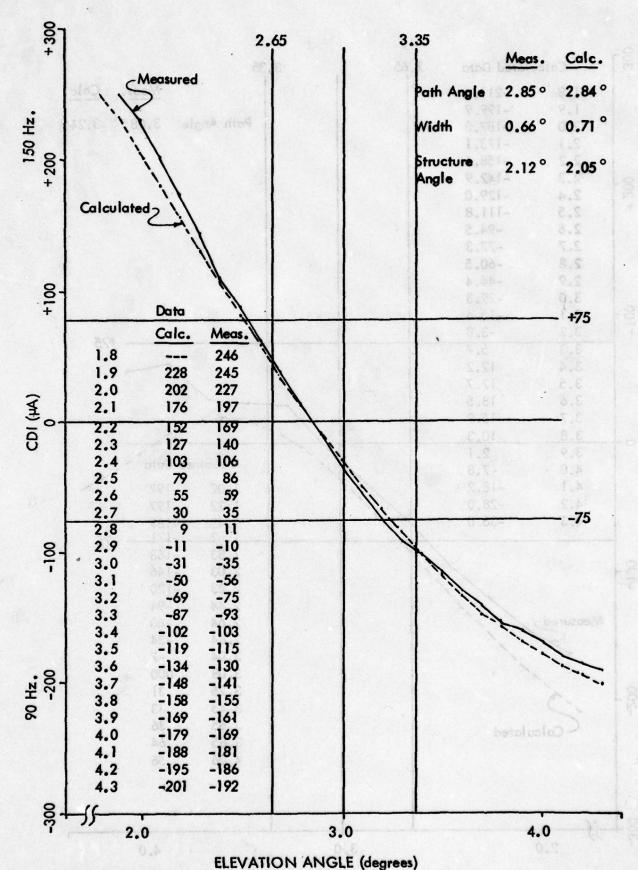


Figure 11–70. Far Field CDI vs Angle – Upper Antenna Attenuated 3 dB. Horizontal Run at 1000 Feet Altitude, 31 August 1976.

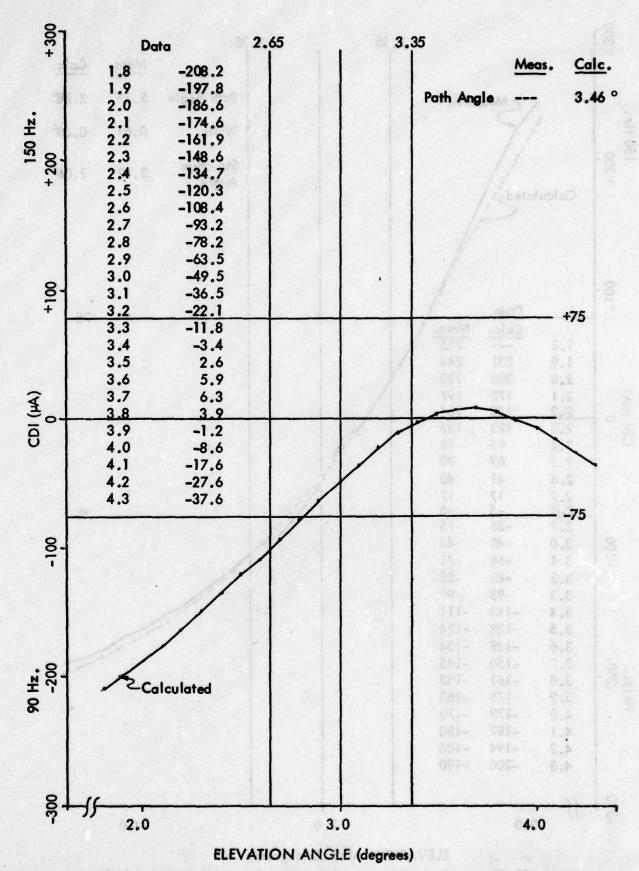


Figure 11-71. Near Field (360° Point) CDI vs Angle - Upper Antenna Attenuated 6 dB.

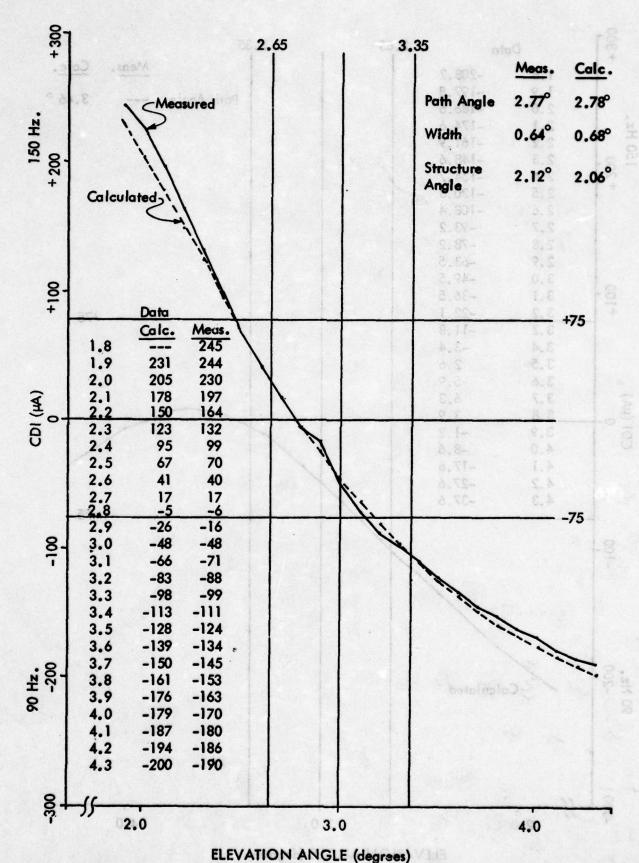


Figure 11–72. Far Field CDI vs Angle – Upper Antenna Attenuated 6 dB. Horizontal Run at 1000 Feet Altitude, 31 August 1976.

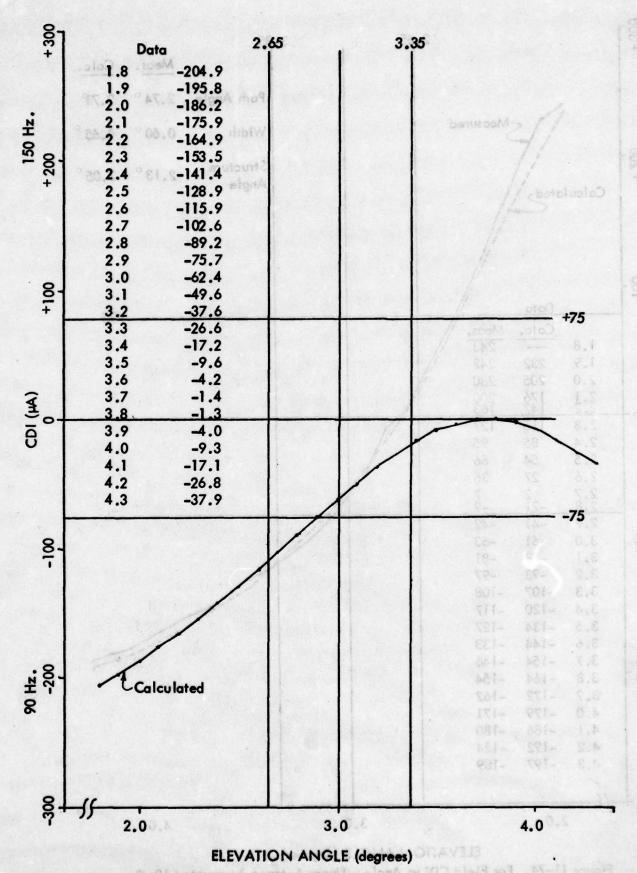


Figure 11-73. Near Field (360° Point) CDI vs Angle - Upper Antenna Attenuated 10 dB.

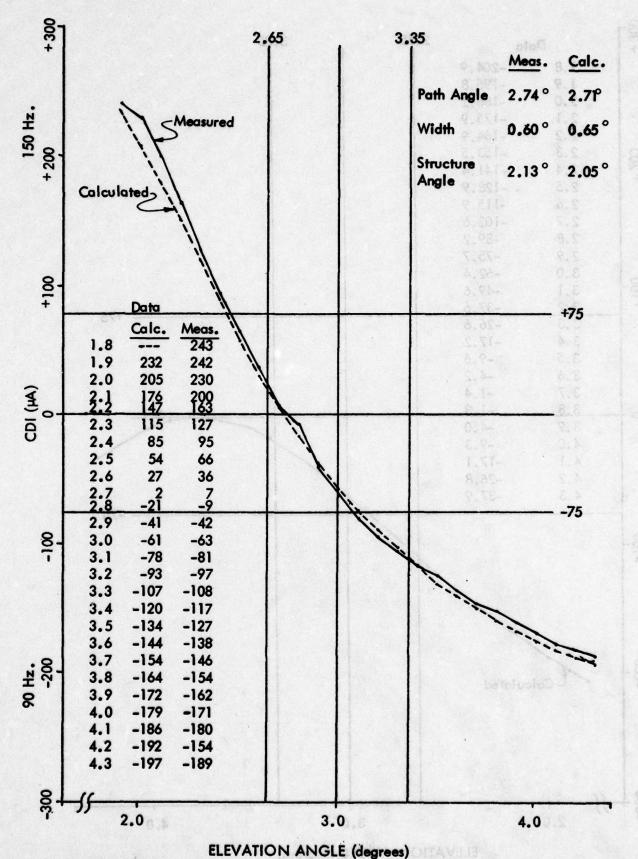
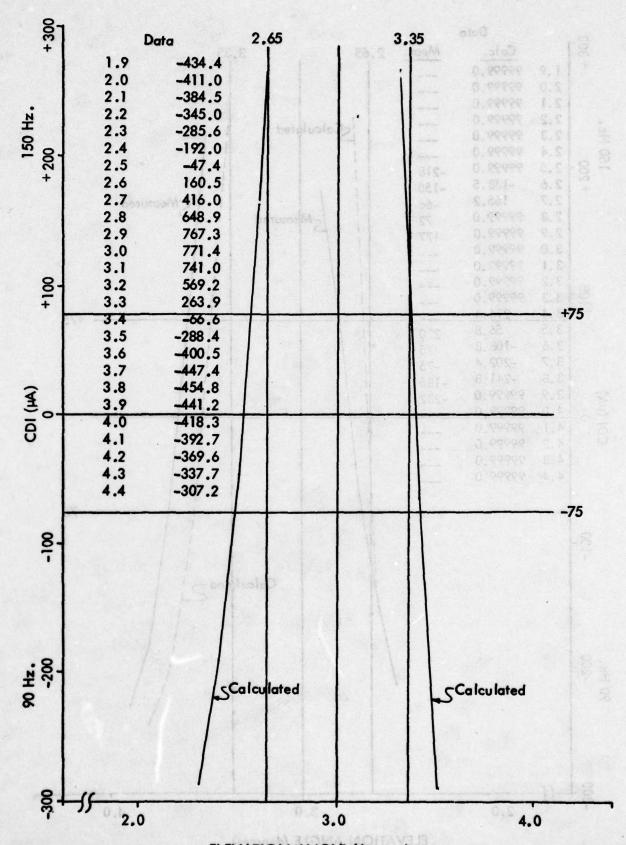


Figure 11-74. Far Field CDI vs Angle - Upper Antenna Attenuated 10 dB. Horizontal Run at 1000 Feet Altitude, 31 August 1976.

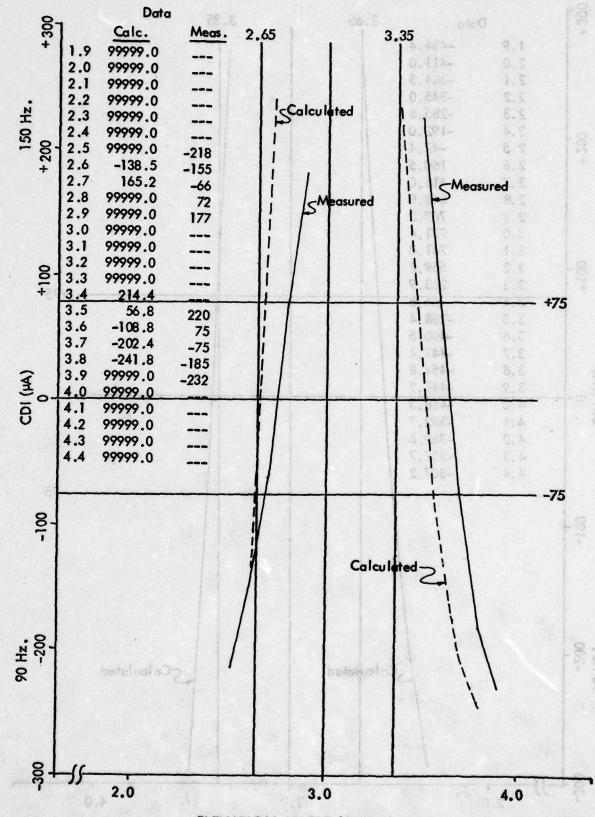
11-94



ELEVATION ANGLE (degrees)

Figure 11-75. Near Field (360° Point) CDI vs Angle – Lower Antenna Out.

11-95

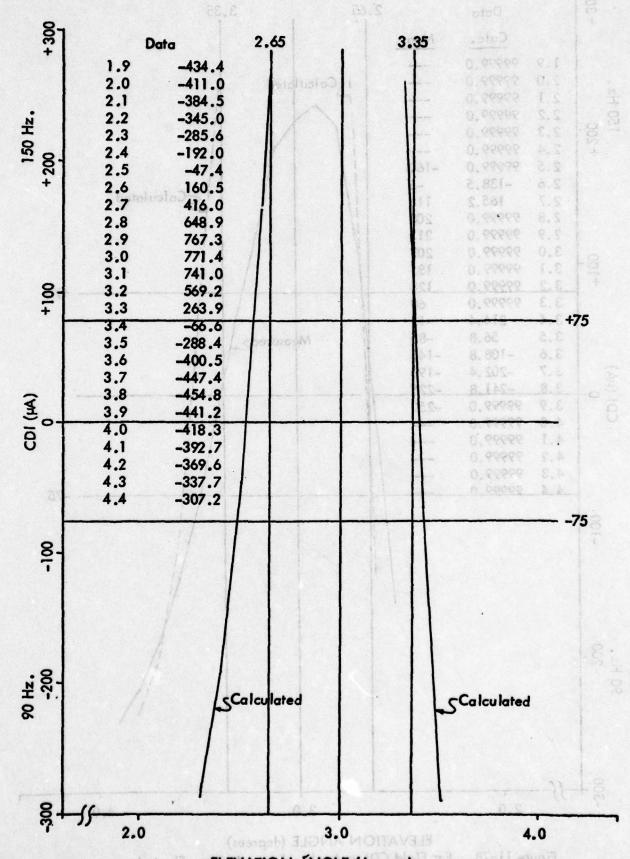


ELEVATION ANGLE (degrees)

Figure 11–76. Far Field CDI vs Angle – Lower Antenna. Open.

Horizontal Run at 1000 Feet Altitude, 1 September 1976.

11–96.



ELEVATION ÁNGLE (degrees)

Figure 11-77. Near Field (360° Point) CDI vs Angle – Lower Antenna Out.

11-97

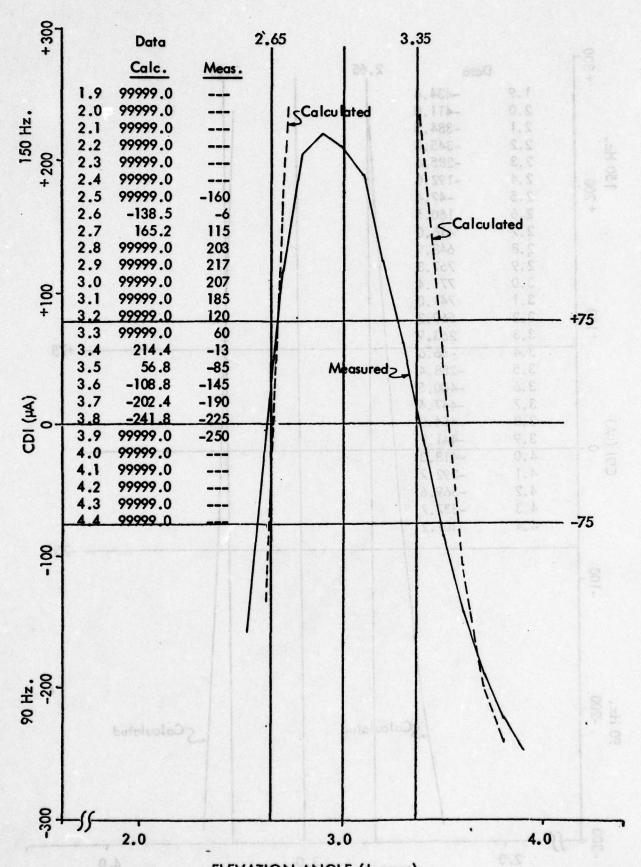


Figure 11-78. Far Field CDI vs Angle - Lower Antenna Shorted.
Horizontal Run at 1000 Feet Altitude, 1 September 1976.

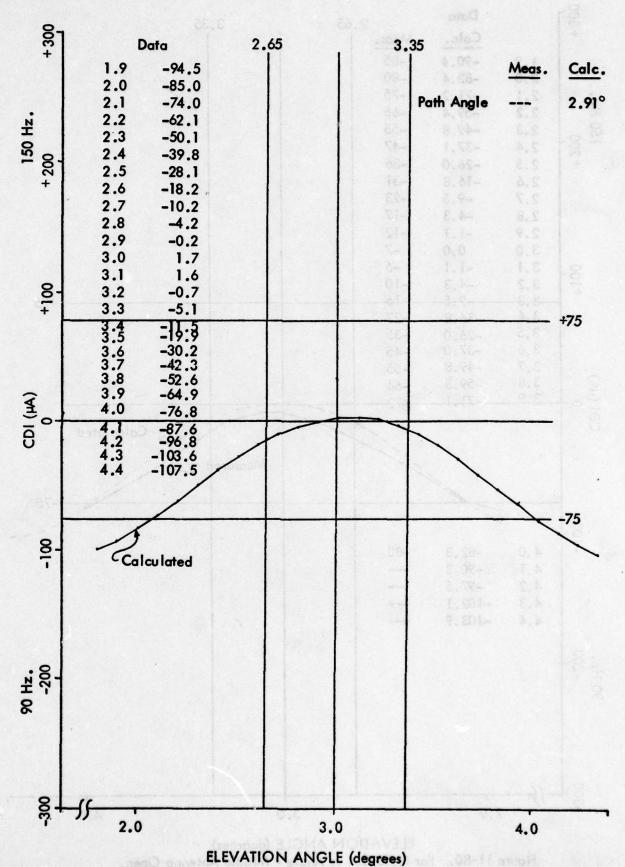


Figure 11-79. Near Field (360° Point) CDI vs Angle - Middle Antenna Out.
11-99

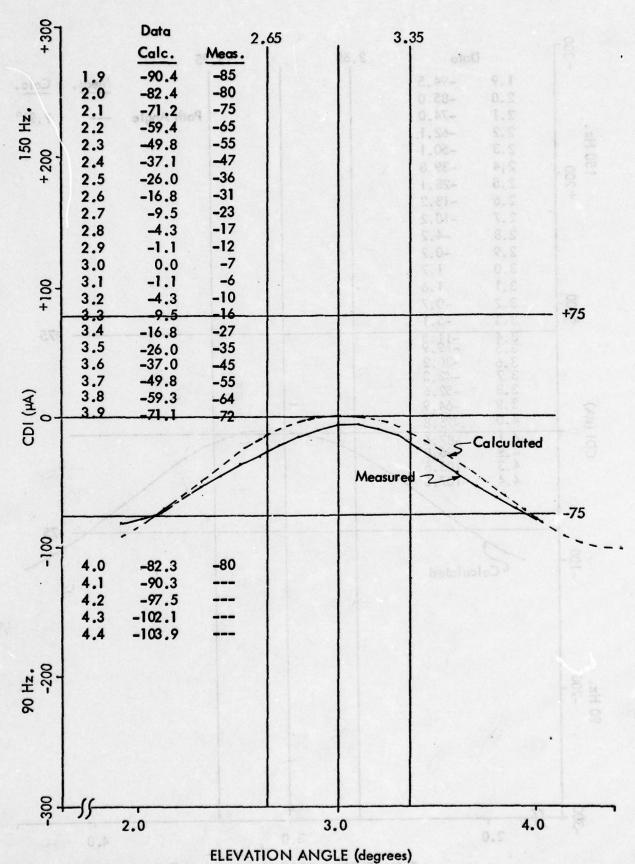


Figure 11-80. Far Field CDI vs Angle - Middle Antenna Open.
Horizontal Run at 1000 Feet Altitude, 1 September 1976.

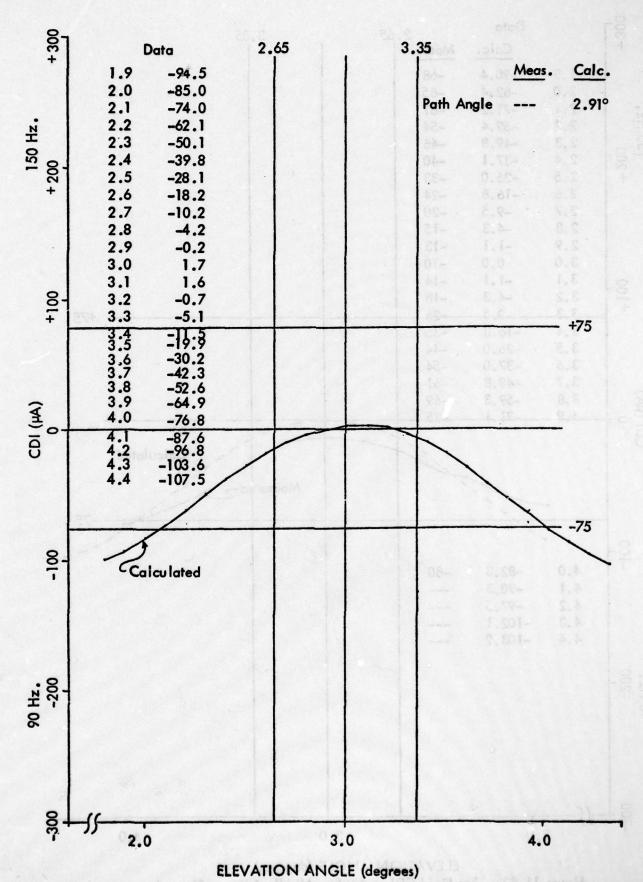
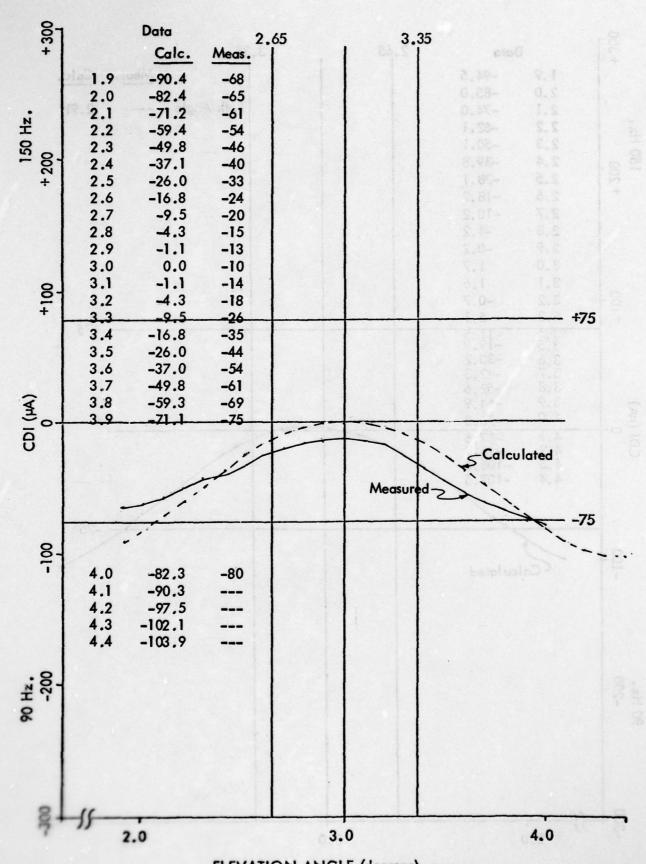


Figure 11-81. Near Field (360° Point) CDI vs Angle - Middle Antenna Out.



ELEVATION ANGLE (degrees)

Far Field CDI vs Angle - Middle Antenna Shorted.

Horizontal Run at 1000 Feet Altitude, 1 September 1976.

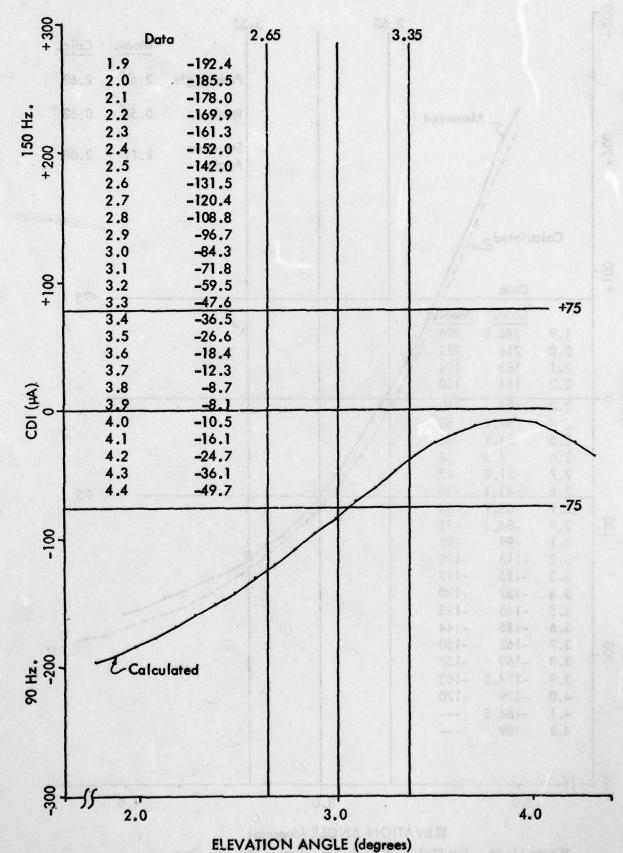


Figure 11-83. Near Field (360° Point) CDI vs Angle - Upper Antenna Out.

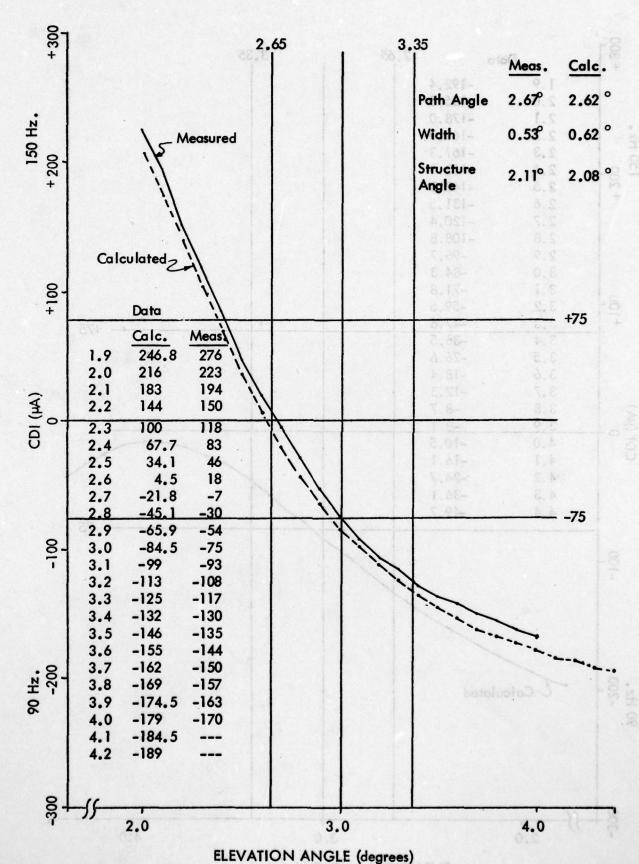


Figure 11–84. Far Field CDI vs Angle – Upper Antenna Open. Horizontal Run at 1000 Feet Altitude, 1 September 1976.

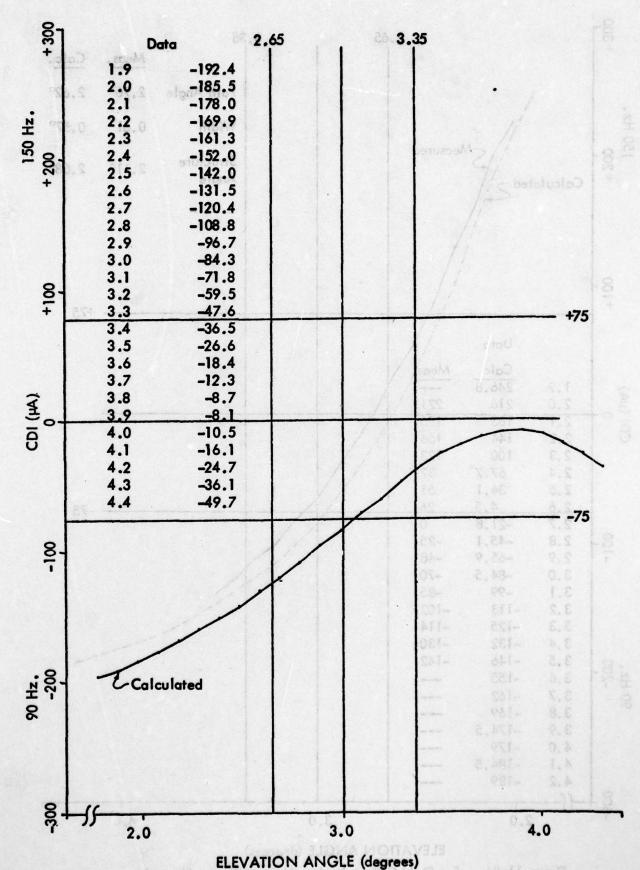


Figure 11-85. Near Field (360° Point) CDI vs Angle - Upper Antenna Out.

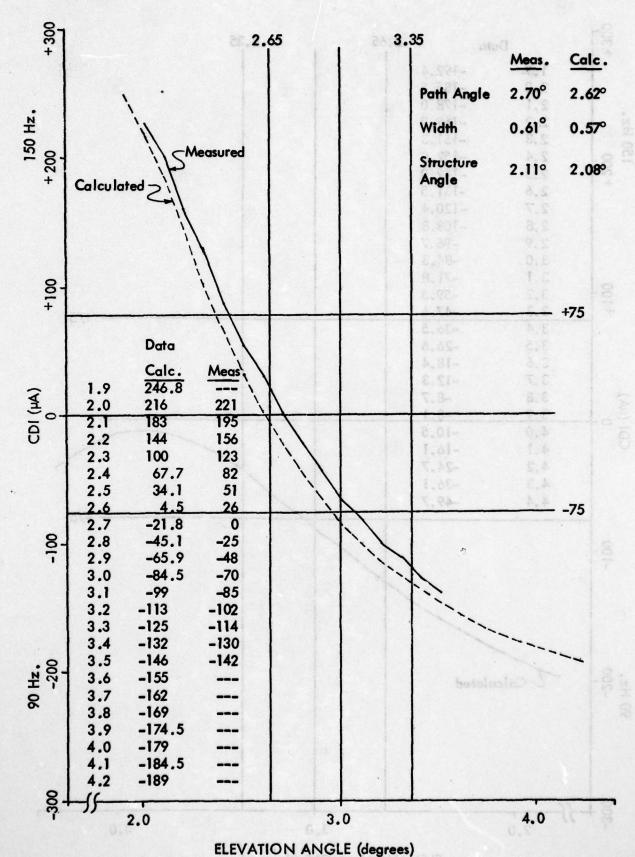


Figure 11–86. Far Field CDI vs Angle – Upper Antenna Shorted.
Horizontal Run at 1000 Feet Altitude, 1 September 1976.

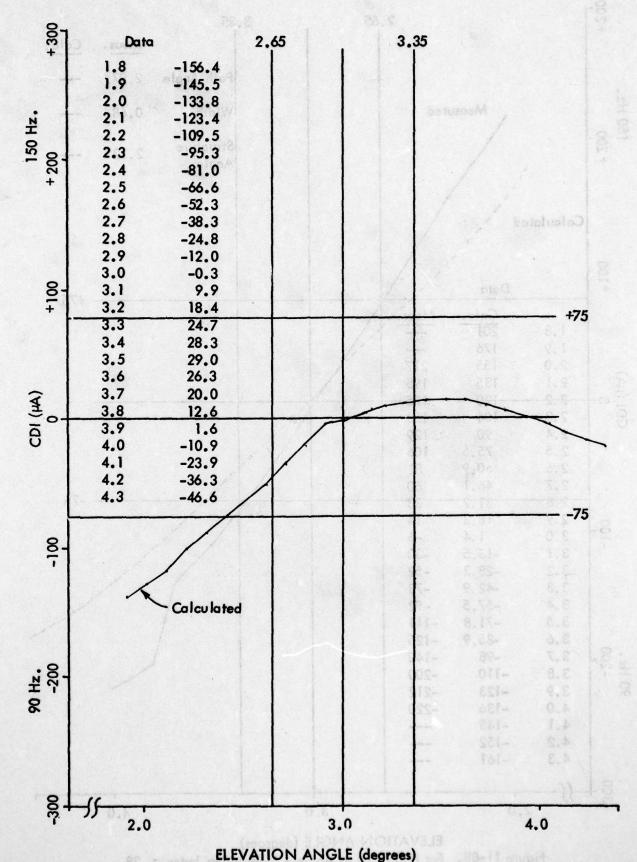


Figure 11-87. Near Field (360° Point) CDI vs Angle - Modulation Index = .28.

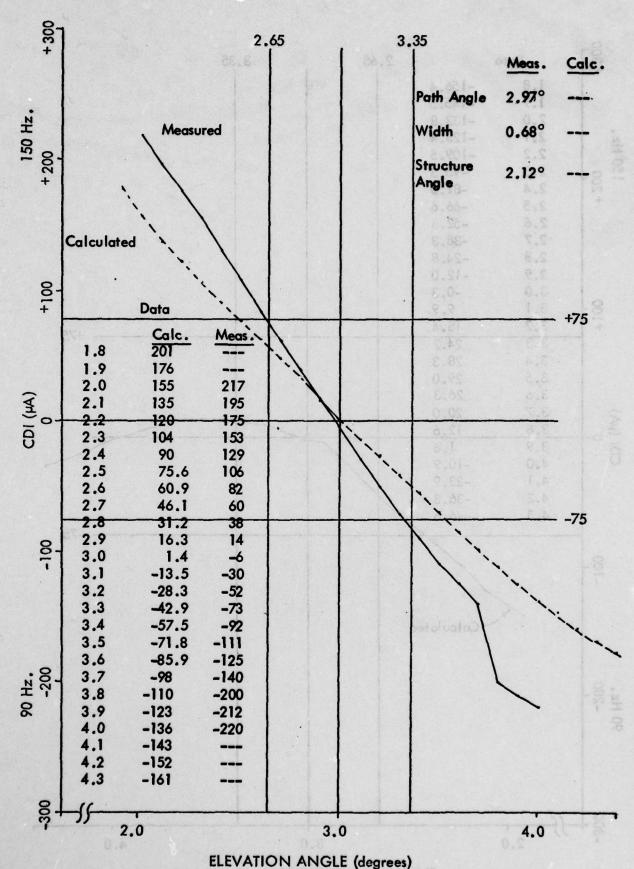


Figure 11-88. Far Field CDI vs Angle - Modulation Index = .28.

Horizontal Run at 1000 Feet Altitude, 1 September 1976.

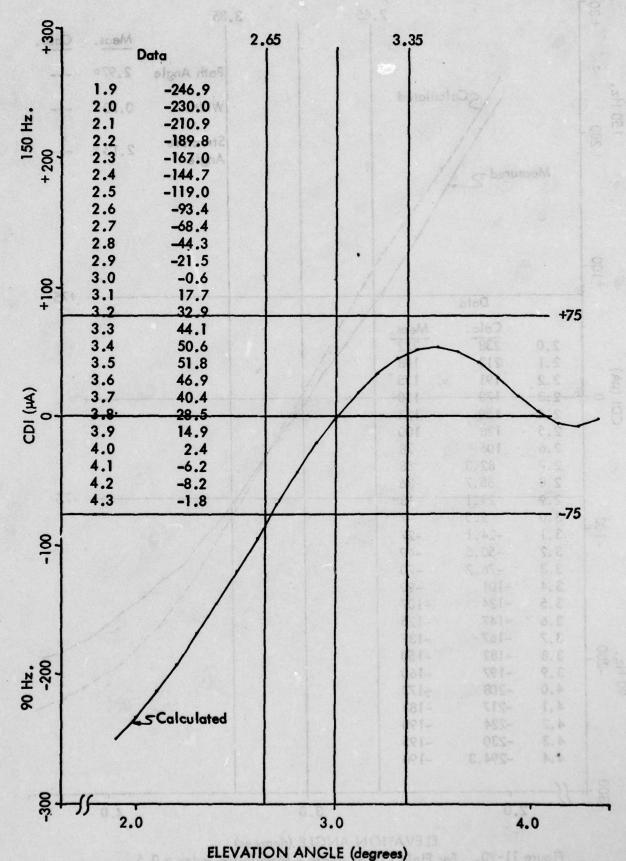
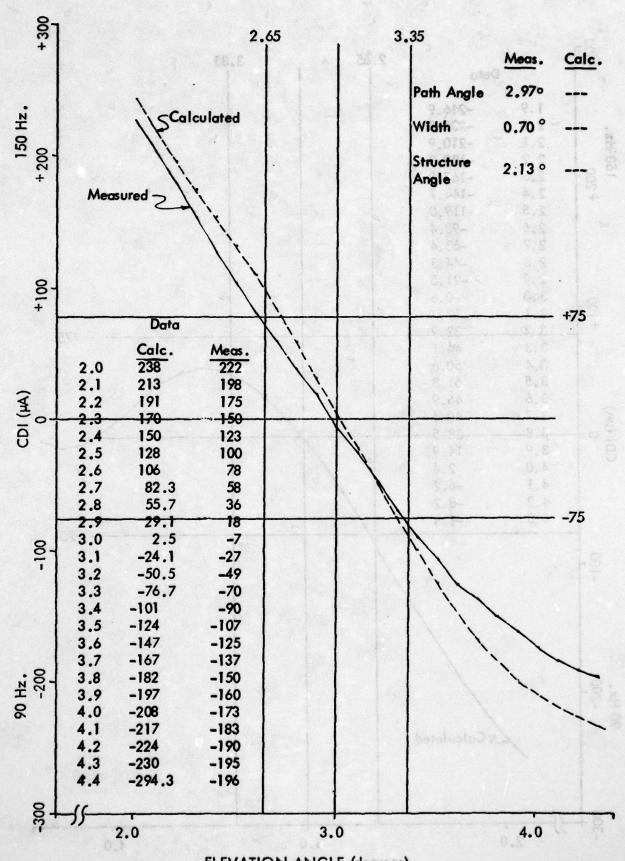
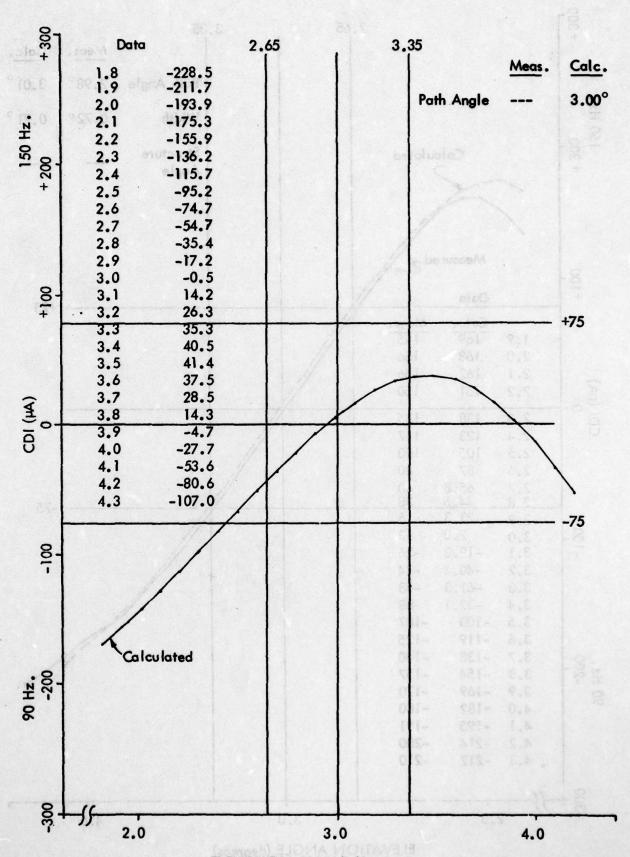


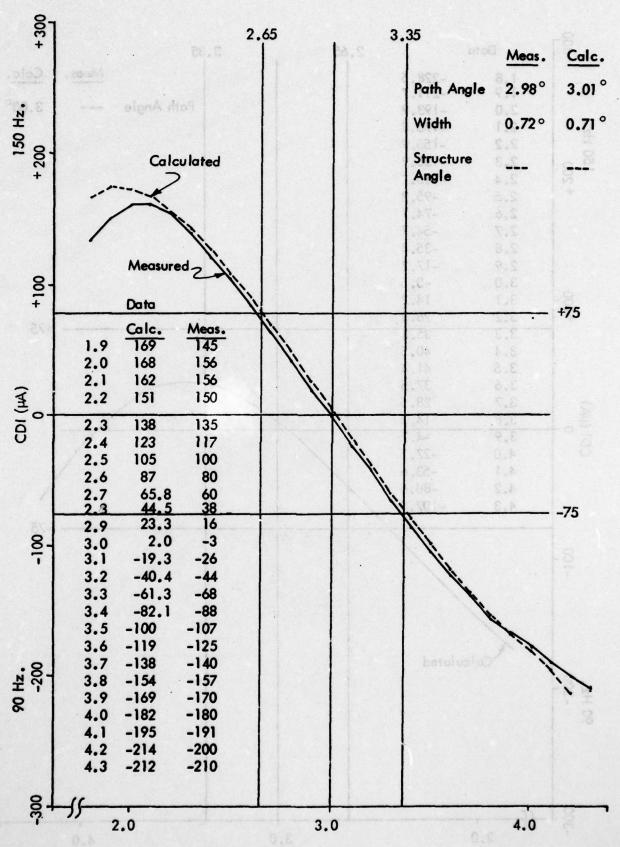
Figure 11-89. Near Field (360° Point) CDI vs Angle - Modulation Index = 0.5.



ELEVATION ANGLE (degrees)
Figure 11-90. Far Field CDI vs Angle - Modulation Index = 0.5.
Horizontal Run at 1000 Feet Altitude, 1 September 1976.



ELEVATION ANGLE (degrees)
Figure 11-91. Near Field (360° Point) CDI vs Angle - No Clearance.



ELEVATION ANGLE (degrees)

Figure 11–92. Far Field CDI vs Angle – No Clearance. Horizontal Run at 1000 Feet Altitude, 1 September 1976. 11–112

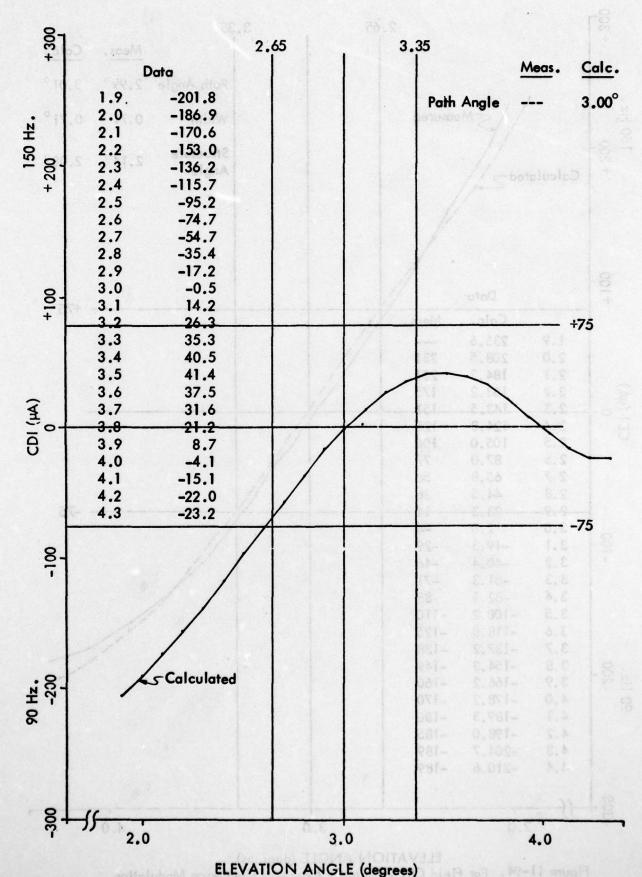


Figure 11-93. Near Field (360° Point) CDI vs Angle - Maximum Clearance Modulation.

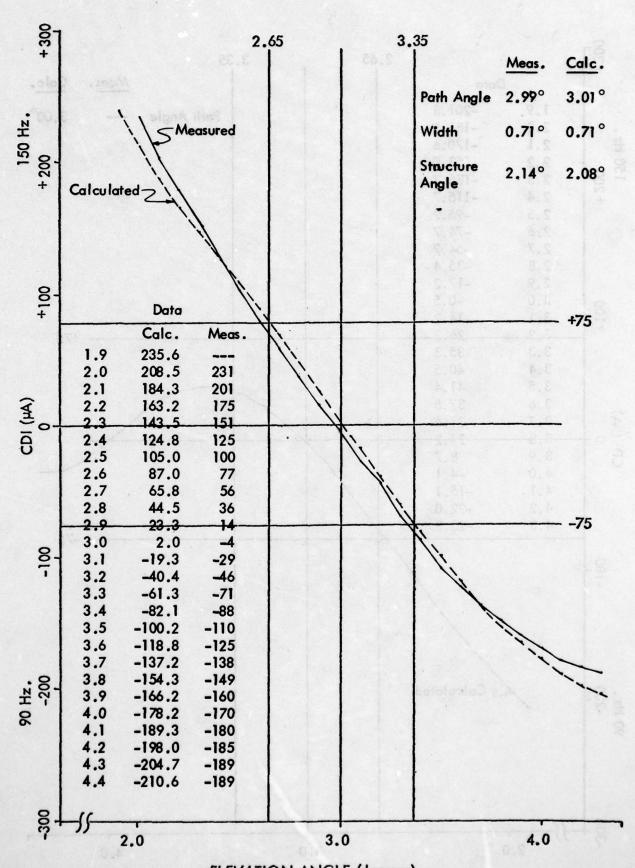


Figure 11-94. Far Field CDI vs Angle - Maximum Clearance Modulation.
Horizontal Run at 1000 Feet Altitude, 1 September 1976

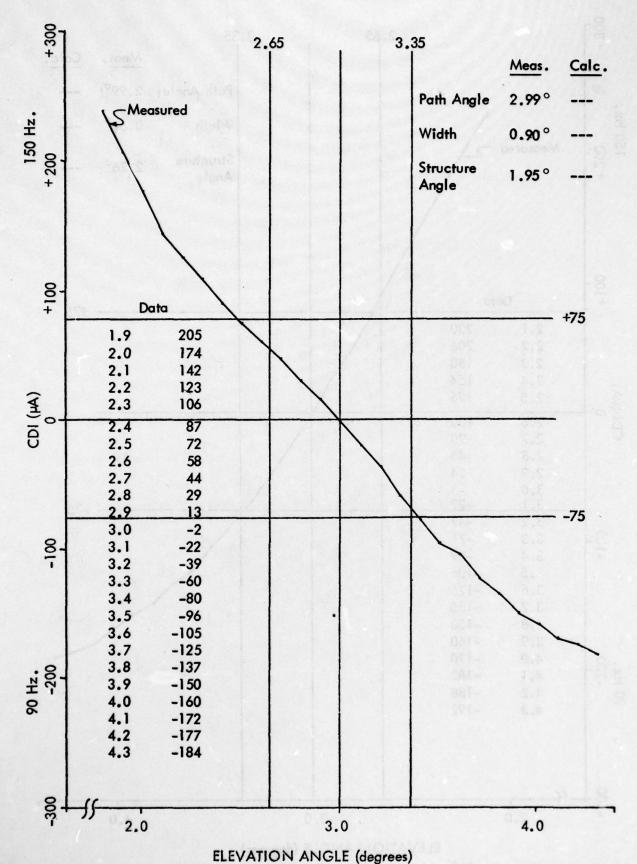
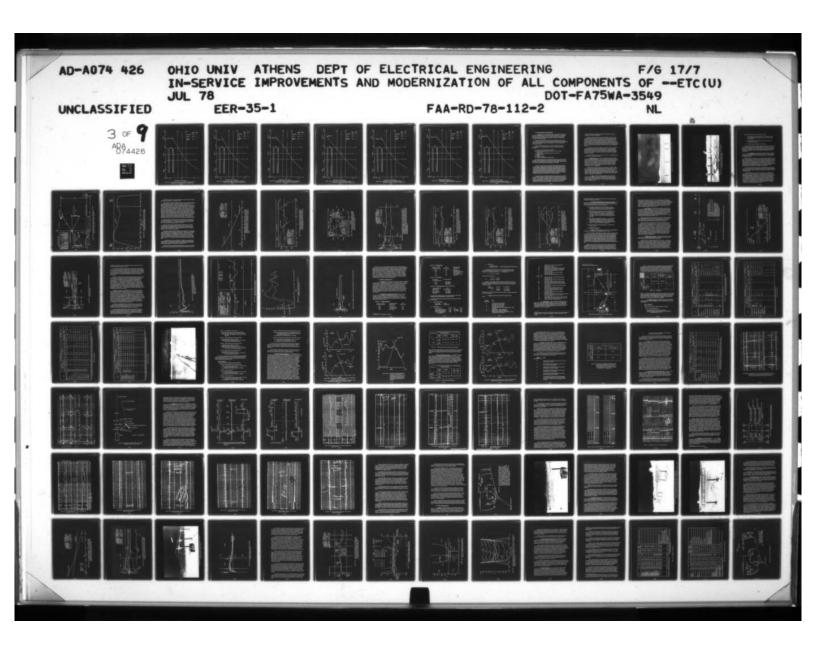
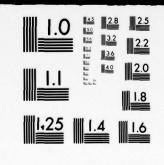


Figure 11-95. Far Field CDI vs Angle - Power Divider A+ Clockwise.
Horizontal Run at 1000 Feet Altitude, 1 September 1976.
11-115





MICROCOPY RESOLUTION TEST CHART

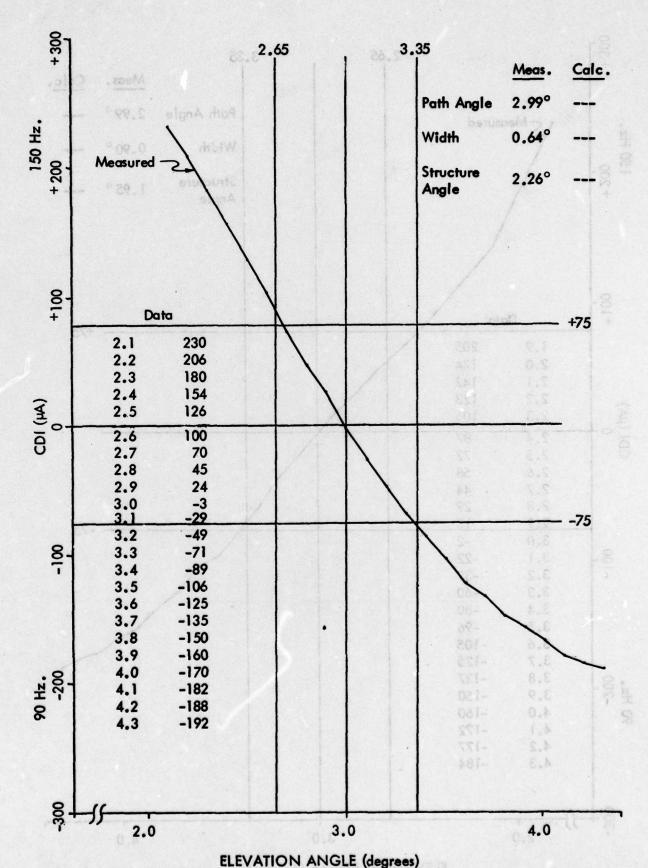


Figure 11-96. Far Field CDI vs Angle - Power Divider A- Counterclockwise.

Horizontal Run at 1000 Feet Altitude, 1 September 1976.

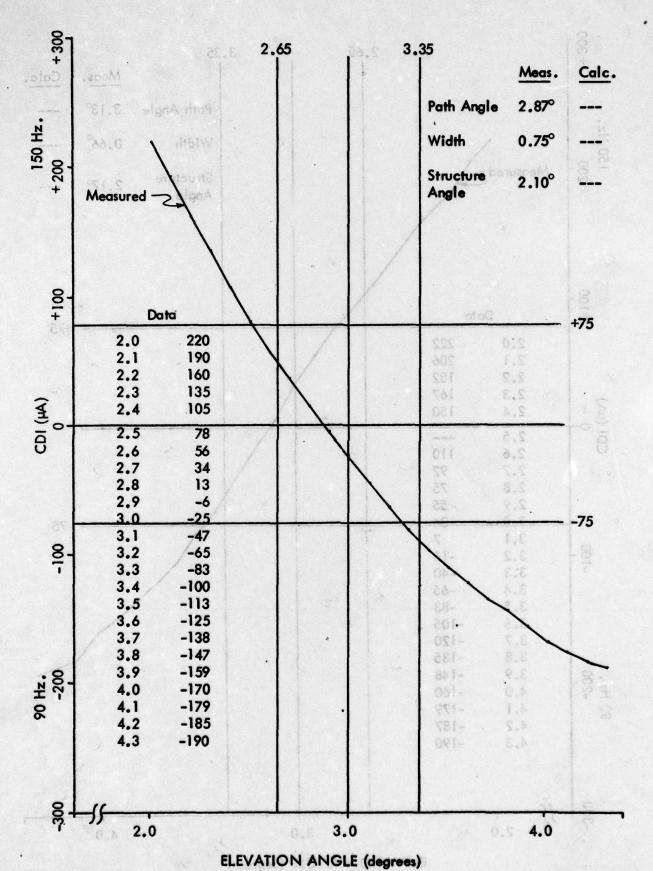


Figure 11-97. Far Field CDI vs Angle - Power Divider B+ Clockwise.

Horizontal Run at 1000 Feet Altitude, 1 September 1976.

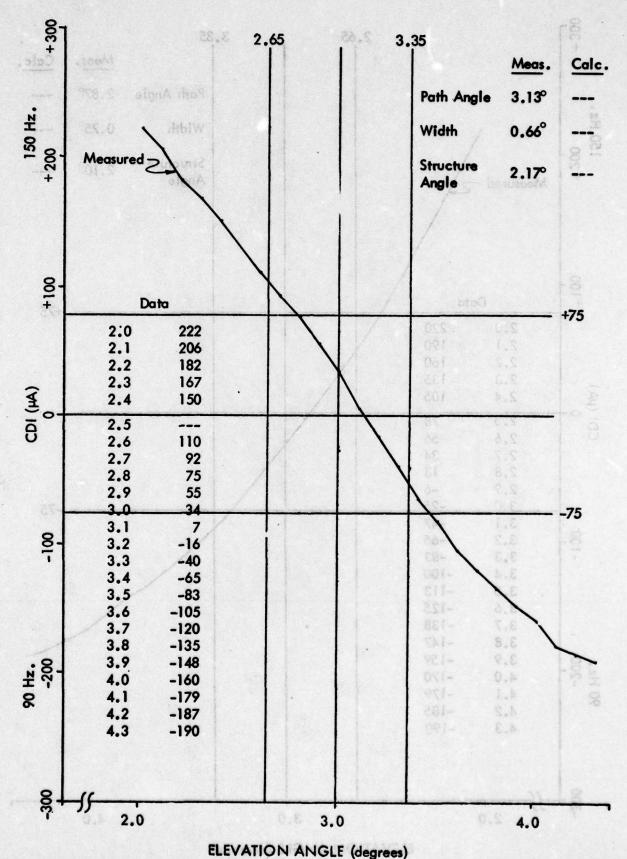


Figure 11-98. Far Field CDI vs Angle - Power Divider B- Counterclockwise.

Horizontal Run at 1000 Feet Altitude, 1 September 1976.

11-118

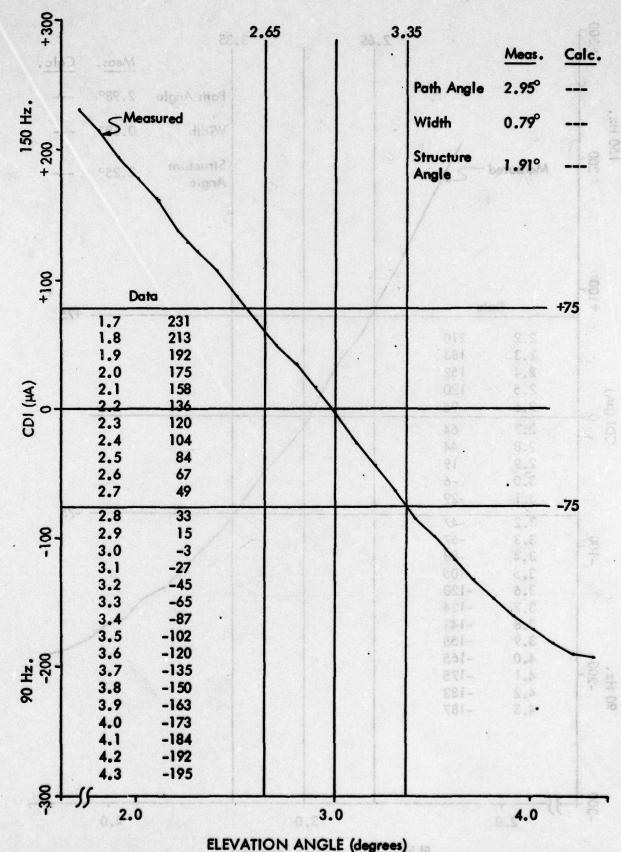
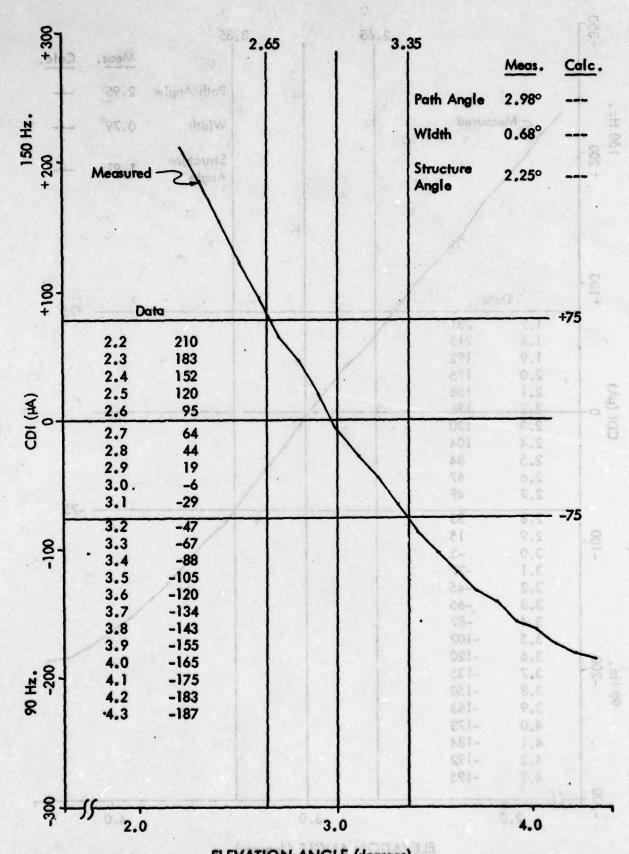


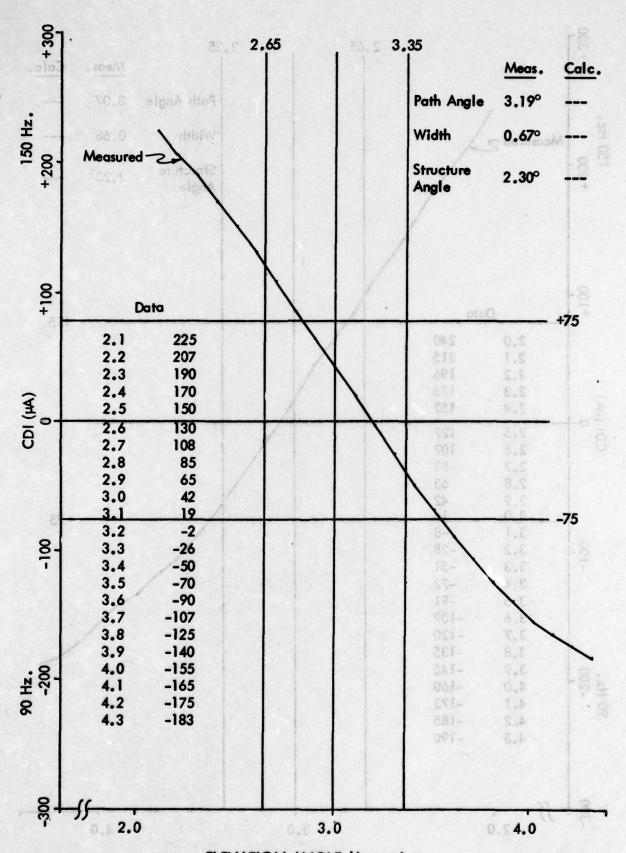
Figure 11-99. Far Field CDI vs Angle - Power Divider Carrier +.
Horizontal Run at 1000 Feet Altitude, 1 September 1976.



ELEVATION ANGLE (degrees)

Figure 11-100. Far Field CDI vs Angle - Power Divider Carrier -.

Horizontal Run at 1000 Feet Altitude, 1 September 1976.



ELEVATION ANGLE (degrees)
Figure 11–101. Far Field CDI vs Angle – Z8 Clockwise.
Horizontal Run at 1000 Feet Altitude, 1 September 1976.

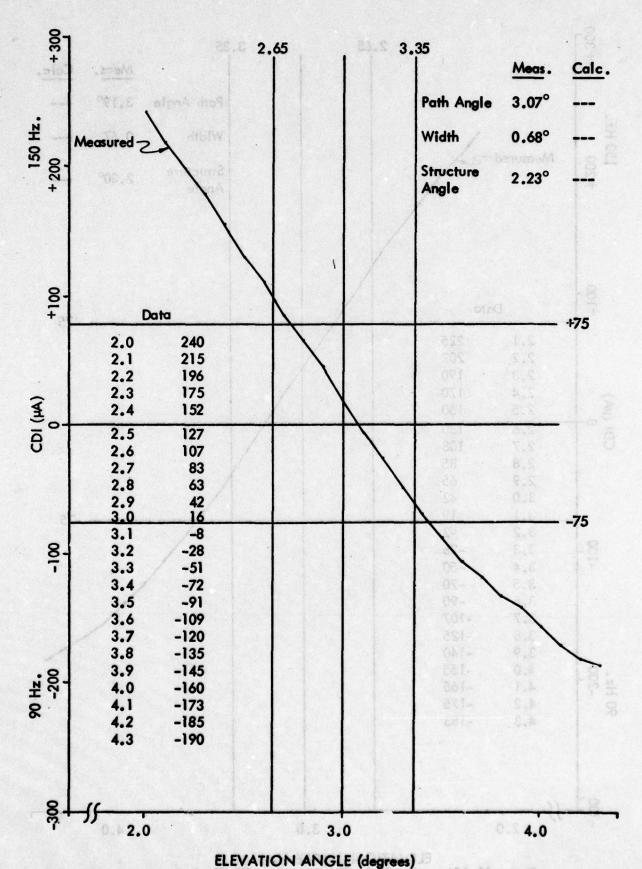


Figure 11–102. Far Field CDI vs Angle – Z8 Counterclockwise. Horizontal Run at 1000 Feet Altitude, 1 September 1976. 11–122

C. Evaluation of Endfire Glide Slope System.

1. Introduction. Ohio University has been in the process of evaluating the performance of several models of slotted cable endfire, glide slope arrays developed by the Watts Prototype Company since 1973. Results of initial tests were reported in Technical Report FAA-RD-75-153 with subsequent activities and findings being described in these following pages.

Substantial improvements have been made in the slotted cable system which clearly overcome the inherently narrow endfire pattern constraints and other deficiencies of earlier endfire systems to produce what is judged to be a very satisfactory glide slope structure in space.

Problem areas with endfire systems have long been identified and there is general agreement on the improvements that are needed. Briefly these problems have been:

(a) Very narrow on-course structure in azimuth

(b) Fly-down commands (existing to the side of the main on-course (localizer) area

(c) Inadequate signal strength due principally to required long transmission lines

(d) Stability

(e) Adequate monitoring

(f) Adequate smoothness in transverse direction.

Major system changes which were tested during the first period of this contract included a change in array spacing from near 600 to 450 feet, shorter and lower loss feed cables, and implementation of a reflector for the slotted cable antennas, change of the slotted cable antennas from linear orientation to curvilinear.

Following an analysis of the results obtained from extensive measurements on this first system, the Watts Company redesigned the slotted cable antennas to produce a Mark 2 system. In addition to the new design for the antennas which provided more precise amplitude and phase control along the aperture, the Mark 2 system was novel in that it used reflectors that increased gain 5 dB, it used plastic supports to minimize effects of moisture below the slotted cables with 7/8 inch air-filled lines feeding the antennas, and it provided for the inclusion of far-field monitor pickups to augment the integral monitors associated with the slotted cables.

The design approach for the Mark 2 by Watts was to obtain improved transverse path smoothness with better control of the aperture illumination from linear antenna elements. It turned out that a significant penalty was incurred with the requirement that each antenna section of which there were 14 were different resulting in potential logistics and test problems. The Mark 3 design, which followed 15 months later, was produced to allow for maximum duplication in sections through the use of

uniform slot spacing and excitations for all but the end elements. These were organized in a curvilinear configuration.

The Mark 3, which is the final version, has some other new features. It has an auxiliary transmitting system which is provided to fill the regions either side of the localizer course with fly-up command signals and thus eliminate variable flag and fly-up, fly-down conditions evidenced in the earlier endfire systems. This auxiliary system makes use of the clearance transmitter of a capture effect transmitting system together with two slotted cable sections located near the mid area of the main array. Special monitoring has been added to the Mark 3 to observe the clearance signal. Radiation from the main antennas is monitored with a set of 6 slotted cable antennas.

The end result of several years of design and testing is very good. A quality glide slope signal is provided in space which to the user will not be distinguishable from that radiated by a conventional image system. The path is sufficiently broad in azimuth with a smooth structure extending from the threshold to a minimum usable distance of 10 miles. Fault testing of the monitors indicates that adequate protection is available.

Following are discussions which relate with somewhat of a chronological theme the details of the Watts system evaluation.

2. Watts Mark I System. In May, 1974, following testing of the Watts Slotted Cable Endfire Glide Slope Array at the Shenandoah Valley Airport, Staunton, Virginia, several conclusions were reached by the Federal Aviation Administration. These were that the signal strength in the far-field was insufficient when a contemporary solid state transmitter was used as a source and the azimuth coverage was marginal. Further, it became evident with the upslope present at Staunton that vertical directivity would be desirable for such sites. Finally, a complete monitoring had yet to be accomplished.

Following shipment of the Watts antennas from Staunton to NAFEC, Atlantic City, New Jersey, the antennas were returned to the Ohio University Test Site at the New Tamiami Airport, Miami, Florida, October, 1974 for the purpose of experimentally determining the results of redesign of the array by Mr. Watts. The redesign included a change in spacing and orientation of the slotted cables, shorter and lower loss feed cables, and implementation of a reflector for the slotted cable radiators. See Figures 11–103 and 11–104.

a. Goals. As a result of observations made in the past with the Watts system and because of lack of precise specifications from ICAO or other sources in June, 1974, Flight Standards of the FAA promulgated guidelines for azimuth coverage with the glide slopes. These guidelines have been adopted as goals for the endfire system.

was produced to allow for croximum ductionline in sections through the

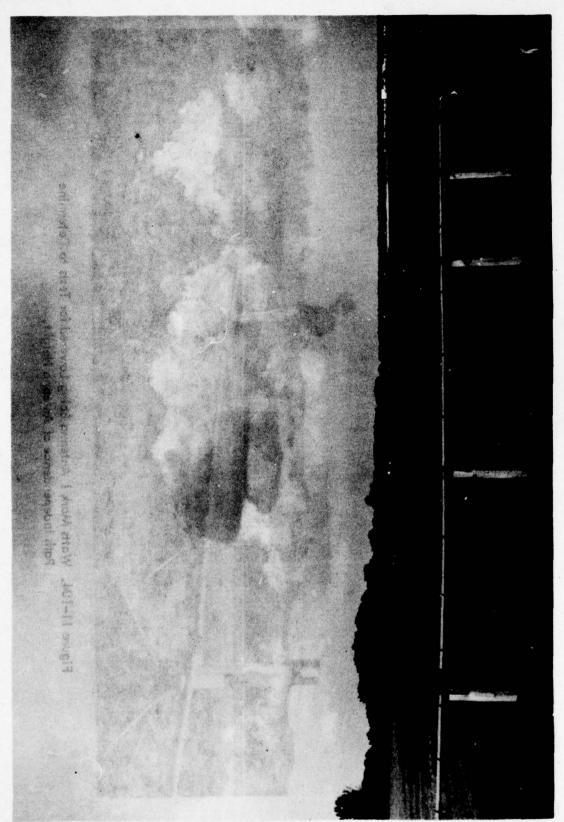


Figure 11-103. Watts Mark I Glide Slope Array at New Tamiami, Florida.

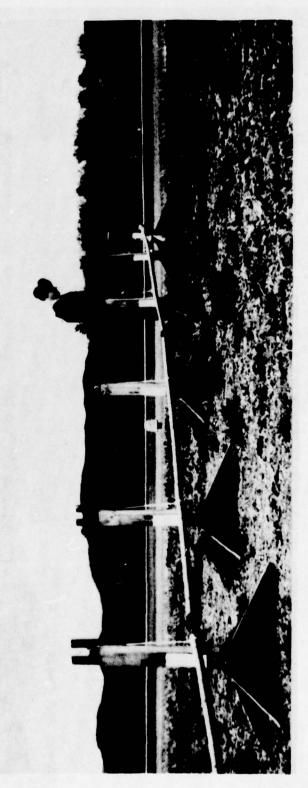


Figure 11–104. Watts Mark I Antenna Being Lowered for Tests to Determine Path Independence of Antenna Height.

With respect to azimuth coverage the following is given:

- 1. Precise guidance is to be available over a ± 5° (total 10° azimuth sector measured from the touchdown point on the centerline of the runway (GPIP)).
- 2. Precise guidance or a fly-up command must be available from 5° to at least 8° on both sides.
- 3. No flag alarms are permitted in the ± 8° sector.

With respect to coverage in range these signals just described must extend to a minimum of 10 nautical miles, measured at 1500 feet above the site. This is construed to mean a minimum of 15 microvolts of signal, referenced to FAA calibration on their DC-3 flight check aircraft. Minimum range for requiring acceptable path performance is considered to be the 100 foot decision point 900 feet in front of the threshold.

b. Measurements. The Watts Slotted Cable Antennas were installed as shown in Figure 11–105 and defined as Position Number 8 by the Watts Company. Note that the linear antennas are now both skewed and bowed. Height remains at 42 inches above ground.

Because the lower-loss cables were not initially available, measurements were begun using the original one-half inch spiroline cable fed from 60 feet of RG-214/U cable. This cable produced a 12.6 dB power loss going to the Watts distribution box, located 410 feet from the original position of the glide slope transmitter hut. For these tests this loss was not significant; however, for the final evaluation the transmitter building will be repositioned as shown in Figure 11-105 to eliminate this power loss and make the installation more representative of an operational facility. Frequency of operation was 331.1 MHz, with a TU-4 transmitter.

This work was considered as a first phase of a three-phase measurement exercise, the second phase would involve checking the system with the lower loss cables, relocated transmitter, reflectors installed, and the final phase would be a monitor validation exercise.

The objectives of the initial tests of the first phase were to determine the path structure produced by the new array. Ground data were first taken using a portable tower to produce a DDM profile in the vertical plane cutting the runway at the 1000 foot threshold. This is shown in Figure 11–106. Flight measurements were then made with a Beechcraft Model 35 and the Ohio University Minilab. Level transitions, perpendicular cuts at and below path at 1900 feet and 29,000 feet from the array, normal approaches for flyability, below path clearance runs, and usable range were obtained. A radio telemetering theodolite was used for a reference. The vertical path width was set at 0.79° between 75 microampere points and the path angle was established at 3.00°.

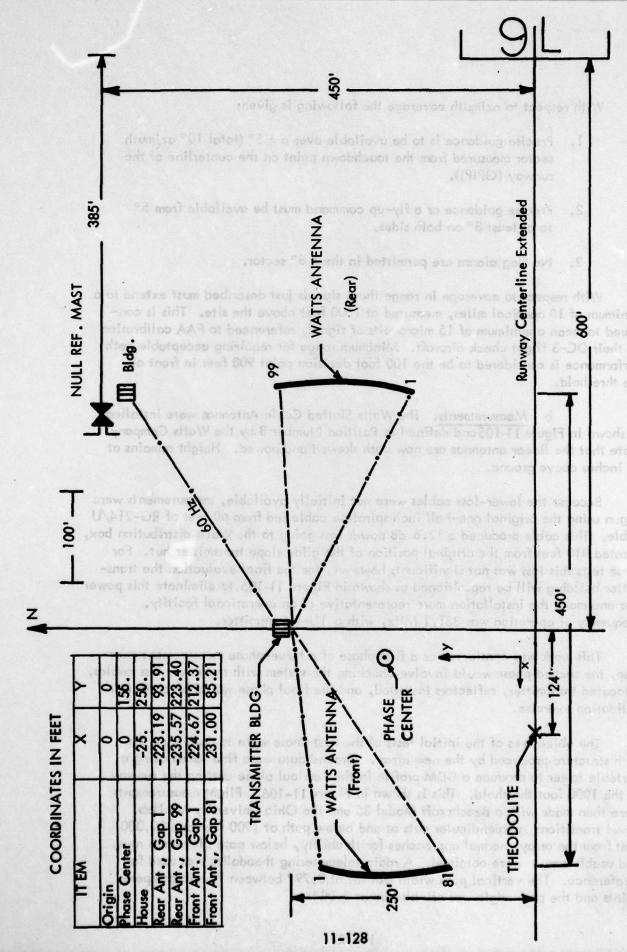
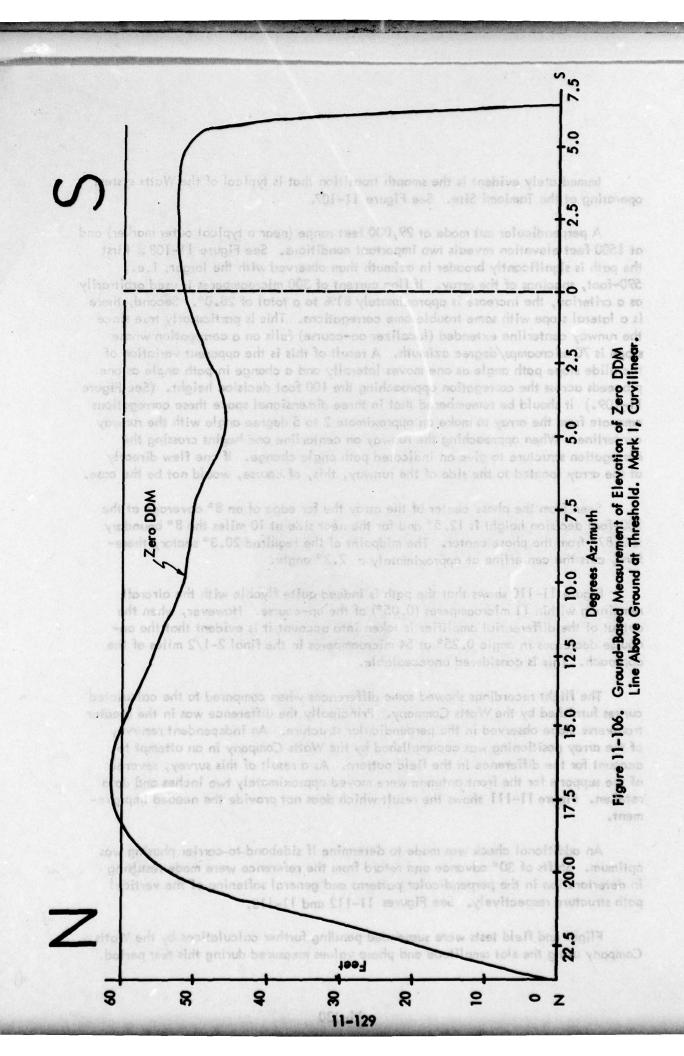


Figure 11–105. Antenna Positioning for Seventh Series of Watts Slotted Cable Glide Slope Tests. Position Number 8. Mark I, Curvilinear.



Immediately evident is the smooth transition that is typical of the Watts system operating at the Tamiami Site. See Figure 11-107.

A perpendicular cut made at 29,000 feet range (near a typical outer marker) and at 1500 feet elevation reveals two important conditions. See Figure 11–108. First the path is significantly broader in azimuth than observed with the larger, i.e., 590-foot, spacings of the array. If flag current of 300 microamperes is used arbitrarily as a criterion, the increase is approximately 81% to a total of 28.0°. Second, there is a lateral slope with some troublesome corregations. This is particularly true since the runway centerline extended (localizer on-course) falls on a corregation whose slope is 70 microamps/degree azimuth. A result of this is the apparent variation of the glide slope path angle as one moves laterally and a change in path angle as one proceeds across the corregation approaching the 100 foot decision height. (See Figure 11–109.) It should be remembered that in three dimensional space these corregations emanate from the array to make an approximate 2 to 5 degree angle with the runway centerline. When approaching the runway on centerline one begins crossing the corregation structure to give an indicated path angle change. If one flew directly at the array located to the side of the runway, this, of course, would not be the case.

Seen from the phase center of the array the far edge of an 8° coverage at the 100-foot decision height is 12.5° and for the near side at 10 miles the 8° boundary is 7.87° from the phase center. The midpoint of the required 20.3° sector, therefore, cuts the centerline at approximately a 2.3° angle.

Figure 11-110 shows that the path is indeed quite flyable with the aircraft remaining within 11 microamperes (0.05°) of the on-course. However, when the output of the differential amplifier is taken into account, it is evident that the on-course decreases in angle 0.25° at 54 microamperes in the final 2-1/2 miles of the approach. This is considered unacceptable.

The flight recordings showed some differences when compared to the calculated curves furnished by the Watts Company. Principally the difference was in the greater transverse slope observed in the perpendicular structure. An independent resurvey of the array positioning was accomplished by the Watts Company in an attempt to account for the difference in the field pattern. As a result of this survey, several of the supports for the front antenna were moved approximately two inches and data retaken. Figure 11-111 shows the result which does not provide the needed improvement.

An additional check was made to determine it sideband-to-carrier phasing was optimum. Shifts of 30° advance and retard from the reference were made resulting in deterioration in the perpendicular patterns and general softening of the vertical path structure respectively. See Figures 11-112 and 11-113.

Flight and field tests were suspended pending further calculations by the Watts Company using the slot amplitude and phase values measured during this test period.

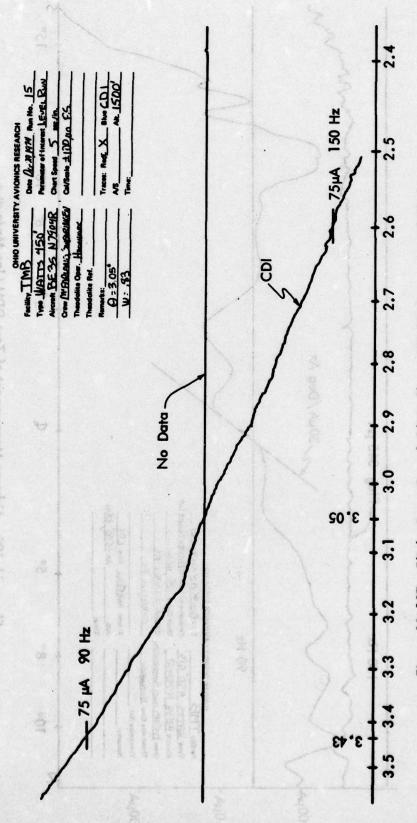
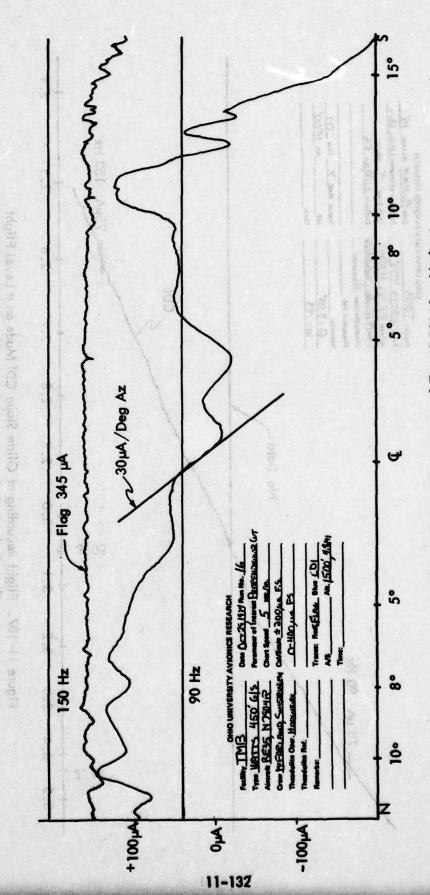


Figure 11-107. Flight Recarding of Glide Slope CDI Made on a Level Flight Through the Path Structure on Runway Centerline Extended at 1500-feet above the Array. The Path Angle is Indicated to be at 3.05° with a Width of 0.83° between 75 microampere points.



Through the Path Structure on femury Centerline Extended or

of beroeibni si elignA ritor pall , which art sweets to see on 2,05° with a Width of 0,83° belower 23 microampers

DOMESTS.

Figure 11–108. Airborne Measurement of Zero DDM Line Made at a Distance of 4.8 Miles from Transmitting Antennas on a Track Perpendicular to the Runway Centerline.
Altitude 1500 feet above array. Mark I, Curvilinear.

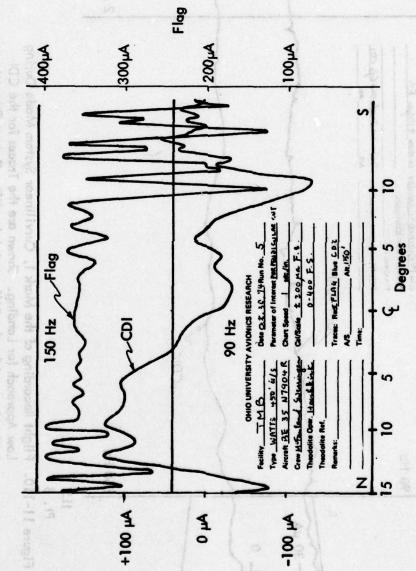
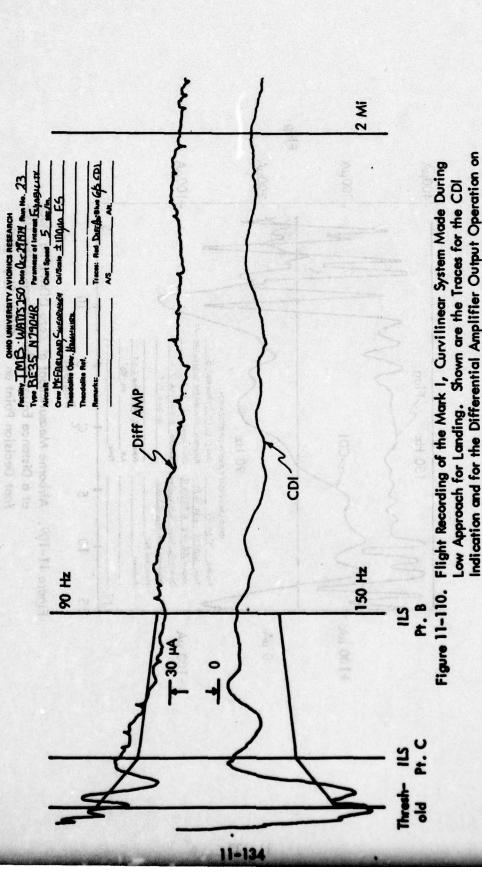


Figure 11–109. Airborne Measurement of Zero DDM Line Made at a Distance Equal to the Distance of the 100–foot Decision Point on the Glide Slope (ILS Point C). Mark I, Curvilinear.



the Theodolite and CDI Data. Note that Although the Zero DDM Line is Tracked Rather Closely by the Aircraft, the Glide Slope is Continually Decreasing.

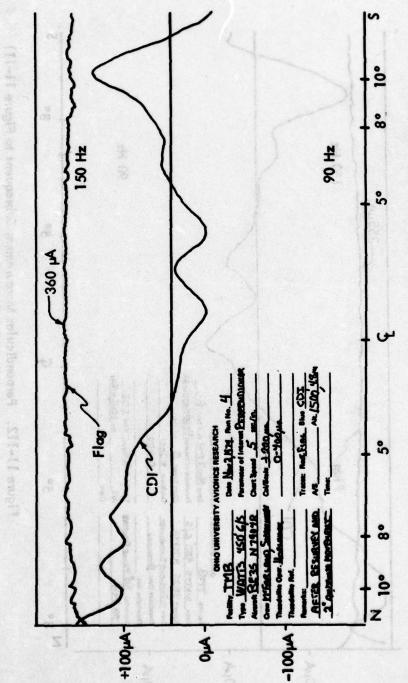
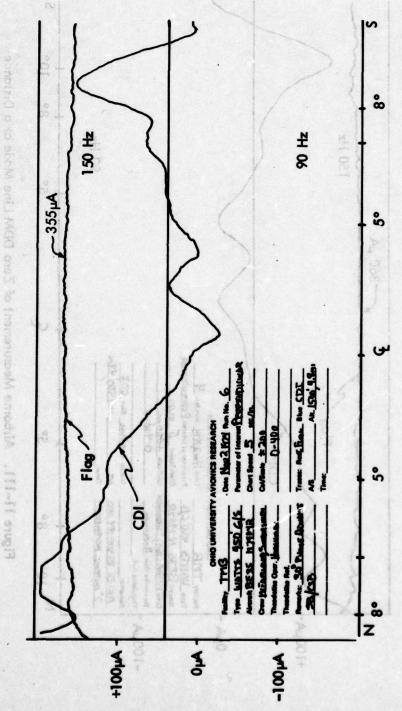


Figure 11–111. Airborne Measurement of Zero DDM Line Made at a Distance of 4.8 Miles From Transmitting Antennas Similar to That Shown in Figure 11–108 but With Front Antenna of Array Adjusted in Position Approximately 2 inches.



of A.B. Miles From Indicate Proof Antenna Similar to That Shown in Pigure 11-108 but With Front Antenna of Arroy Adjusted in

dadrion specializately 2 inches

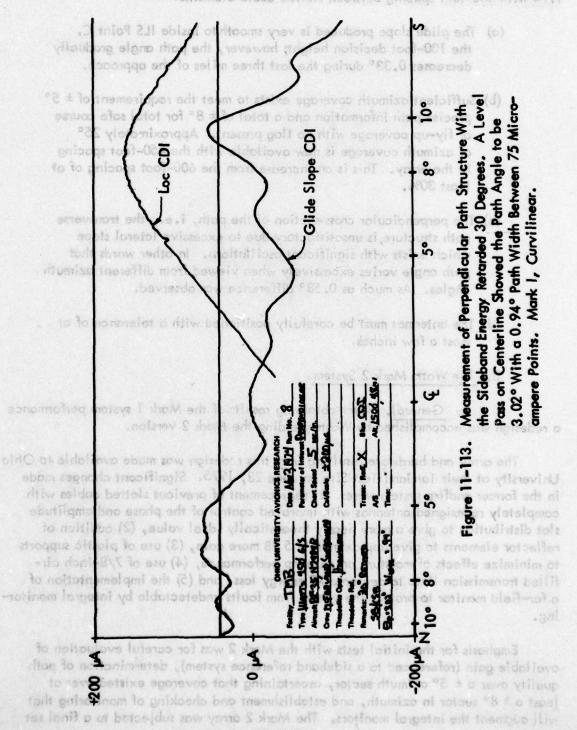
Figure 11–112. Perpendicular Measurement Subsequent to Figure 11–111 Data But With Sideband Dephased 30 Degrees (advance).

No Vertical Path Width Measurement Was Made of This Condition. Mark I, Curvilinear.

From these colculations it is expected that changes in the array can be effected to produce better transverse path statemen.

. 6

c Conclusions Concerning Operation of Work I Curvilling System. The following comments are based on measurements used on the Work I curvillinger system that had been reinstabled at the Chip University Textiami Test Site in October, 1974 with 450-fact spacing between slotted cable elements.



From these calculations it is expected that changes in the array can be effected to produce better transverse path structure.

- c. Conclusions Concerning Operation of Mark I Curvilinear System. The following comments are based on measurements made on the Mark I curvilinear system that had been reinstalled at the Ohio University Tamiami Test Site in October, 1974 with 450-foot spacing between slotted cable elements.
 - (a) The glide slope produced is very smooth to inside ILS Point C, the 100-foot decision height; however, the path angle gradually decreases 0.33° during the last three miles of the approach.
 - (b) Sufficient azimuth coverage exists to meet the requirement of ± 5° precise path information and a total of ± 8° for total safe course or fly-up coverage with no flag present. Approximately 25° of azimuth coverage is now available with the 450-foot spacing in the array. This is an increase from the 600-foot spacing of at least 30%.
 - (c) The perpendicular cross-section of the path, i.e., the transverse path structure, is unsatisfactory due to excessive lateral slope which exists with significant oscillations. In other words that path angle varies excessively when viewed from different azimuth angles. As much as 0.58° difference was observed.
 - (d) The antennas must be carefully positioned with a tolerance of at most a few inches.
 - 3. The Watts Mark 2 System.
- a. General. After obtaining results of the Mark 1 system performance a redesign was accomplished by Watts yielding the Mark 2 version.

The array and hardware resulting from this redesign was made evailable to Ohio University at their Tamiami Test Site on June 23, 1975. Significant changes made in the former endfire system were: (1) replacement of previous slotted cables with completely redesigned antennas with improved control of the phase and amplitude slot distribution to give a more nearly theoretically ideal value, (2) addition of reflector elements to give approximately 5 dB more gain, (3) use of plastic supports to minimize effects of moisture on antenna performance, (4) use of 7/8-inch air-filled transmission lines to decrease RF energy loss, and (5) the implementation of a far-field monitor to protect the system from faults undetectable by integral monitoring.

Emphasis for the initial tests with the Mark 2 was for careful evaluation of available gain (referenced to a sideband reference system), determination of path quality over $a \pm 5^{\circ}$ azimuth sector, ascertaining that coverage existed over at least $a \pm 8^{\circ}$ sector in azimuth, and establishment and checking of monitoring that will augment the integral monitors. The Mark 2 array was subjected to a final set

of fault tests on November 22 and 23, 1975. The specific faults investigated were truck positions in front of, and between, the antenna elements, and wet cloths both spread out along, and lumped over the antenna elements. Also checked with differences in glide path signal quality as generated using a Wilcox solid state glide slope transmitter and a TU-4 glide slope transmitter, and the effects to the glide path signal quality as caused by an approximate three inch horizontal displacement to the end of the rear antenna nearest the runway centerline.

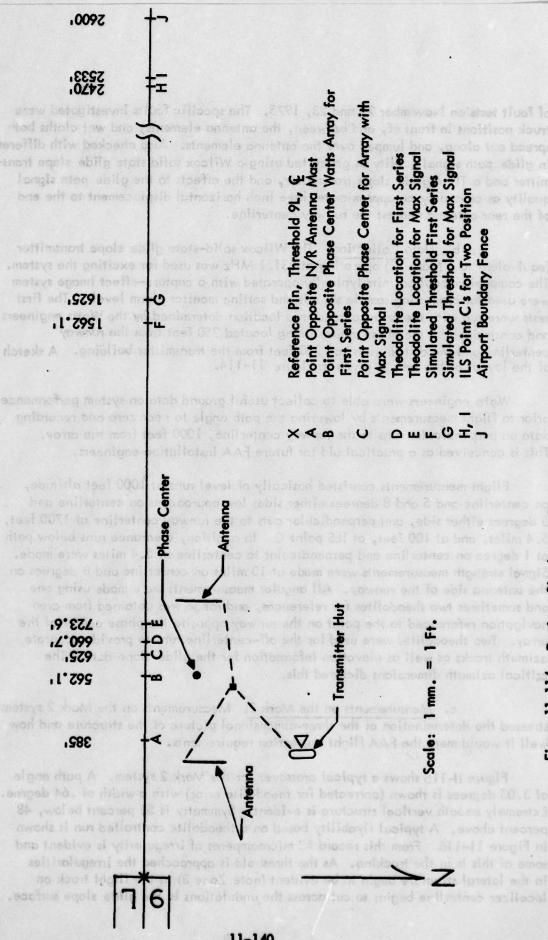
b. Data Collection. The Wilcox solid-state glide slope transmitter (equivalent to a Mark IC) operating at 331.1 MHz was used for exciting the system. The companion monitor units typically operated with a capture-effect image system were used for processing sample signals and setting monitor alarm levels. The first tests were run with the array placed in a location determined by the Watts engineers and constrained by the phase center being located 250 feet from the runway centerline and the distribution box 250 feet from the transmitter building. A sketch of the layout of the tests is given in Figure 11-114.

Watts engineers were able to collect useful ground data on system performance prior to flight measurements by lowering the path angle to near zero and recording data on perpendicular runs to the runway centerline, 1000 feet from the array. This is conceived as a practical aid for future FAA installation engineers.

Flight measurements consisted basically of level runs at 1000 feet altitude, on centerline and 5 and 8 degrees either side; low approaches on centerline and 5 degrees either side, and perpendicular cuts to the runway centerline at 1700 feet, 5.4 miles, and at 100 feet, at ILS point C. In addition, clearance runs below path at 1 degree on centerline and perpendicular to centerline at 5.4 miles were made. Signal strength measurements were made at 10 miles on centerline and 8 degrees on the antenna side of the runway. All angular measurements were made using one and sometimes two theodolites for references, and range was obtained from area navigation referenced to the point on the runway opposite the phase center of the array. Two theodolites were used for the off-centerline runs to provide accurate azimuth tracks as well as elevation information for the glide slope data. The critical azimuth dimensions dictated this.

c. <u>Measurements on the Mark 2</u>. Measurements on the Mark 2 system stressed the determination of the three-dimensional picture of the structure and how well it would meet the FAA flight inspection requirements.

Figure 11–115 shows a typical crossover for the Mark 2 system. A path angle of 3.03 degrees is shown (corrected for theodolite error) with a width of .64 degree. Extremely smooth vertical structure is evident. Symmetry is 52 percent below, 48 percent above. A typical flyability based on a theodolite controlled run is shown in Figure 11–116. From this record ±3 microamperes of irregularity is evident and some of this is in the tracking. As the threshold is approached the irregularities in the lateral structure begin to be evident (note Zone 3) as the flight track on localizer centerline begins to cut across the undulations in the glide slope surface.



Tamiami Site Layout for Initial Series of Tests on Watts Mark 2 System

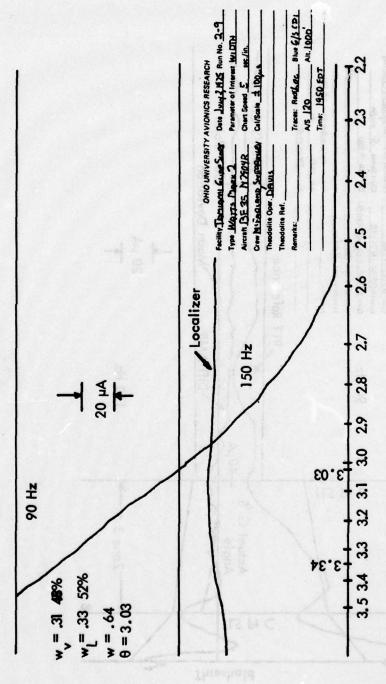


Figure 11-115. Copy of Flight Recording - Level Pass, 1000 Feet.

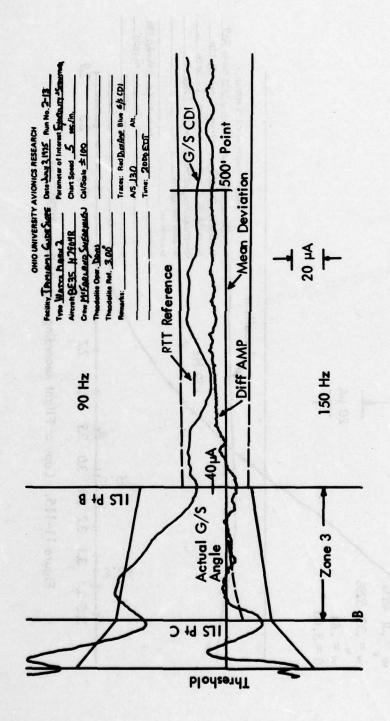


Figure 11–116. Copy of Flight Recording Made During Low Approach for Watts Mark 2 System.

Nevertheless, Category II structure and alignment tolerances are obtained in spite of the non-optimum lateral course structure.

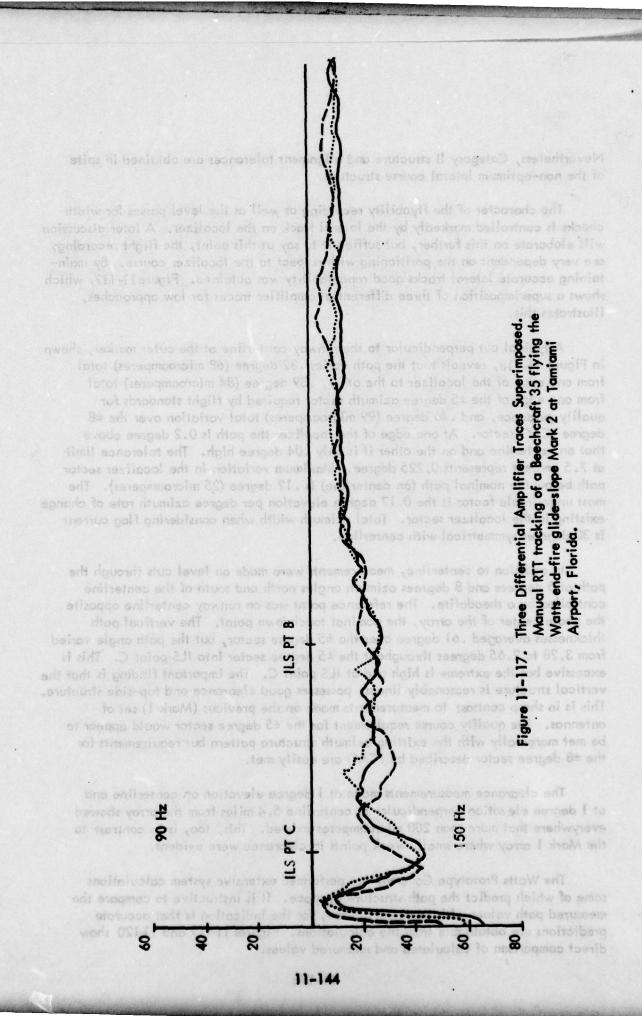
The character of the flyability recording as well as the level passes for width checks is controlled markedly by the lateral track on the localizer. A later discussion will elaborate on this further, but suffice it to say at this point, the flight recordings are very dependent on the positioning with respect to the localizer course. By maintaining accurate lateral tracks good repeatability was obtained. Figure 11–117, which shows a superimposition of three differential amplifier traces for low approaches, illustrates this.

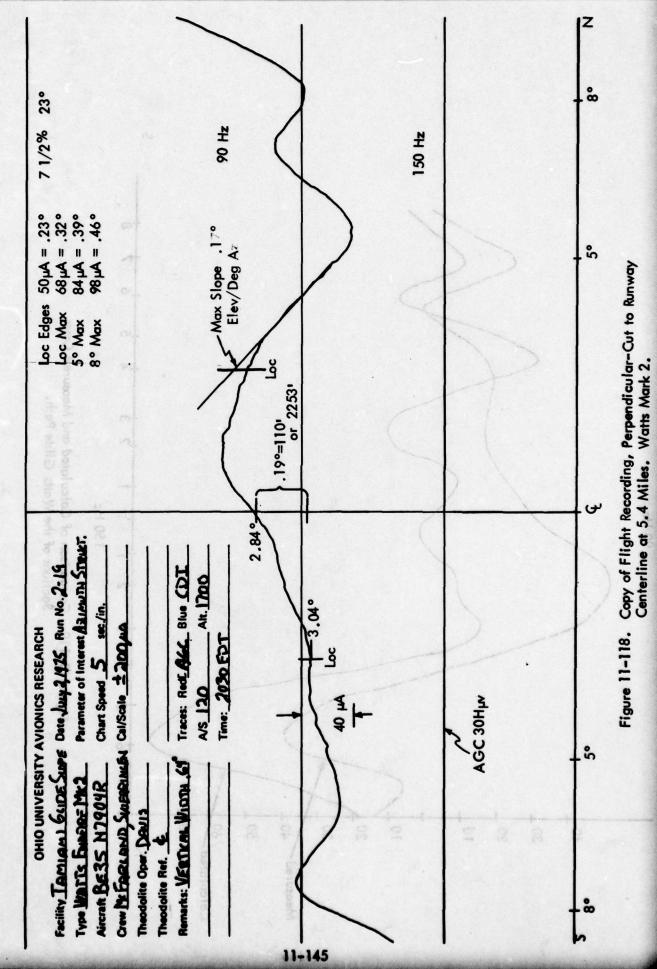
A typical cut perpendicular to the runway centerline at the outer marker, shown in Figure 11–118, reveals that the path varies .32 degree (68 microamperes) total from one edge of the localizer to the other, .39 degree (84 microamperes) total from one edge of the ±5 degree azimuth sector required by flight standards for quality guidance, and .46 degree (99 microamperes) total variation over the ±8 degree ICAO sector. At one edge of the localizer the path is 0.2 degree above that on centerline and on the other it is only .04 degree high. The tolerance limit at 7.5 percent represents 0.225 degree. Maximum variation in the localizer sector path below the nominal path (on centerline) is .12 degree (25 microamperes). The most undesirable factor is the 0.17 degree elevation per degree azimuth rate of change existing in the localizer sector. Total azimuth width when considering flag current is 30 degrees symmetrical with centerline.

In addition to centerline, measurements were made on level cuts through the path at 5 degrees and 8 degrees azimuth angles north and south of the centerline controlled by a theodolite. The reference point was on runway centerline opposite the phase center of the array, the nominal touchdown point. The vertical path thicknesses averaged .61 degree over the ±5 degree sector, but the path angle varied from 3.28 to 2.65 degrees throughout the ±5 degree sector into ILS point C. This is excessive but the extreme is high and at ILS point C. The important finding is that the vertical structure is reasonably linear, possesses good clearance and top-side structure. This is in sharp contrast to measurements made on the previous (Mark 1) set of antennas. The quality course requirement for the ±5 degree sector would appear to be met marginally with the existing azimuth structure pattern but requirements for the ±8 degree sector described by ICAO are easily met.

The clearance measurements made at 1 degree elevation on centerline and at 1 degree elevation perpendicular to centerline 5.4 miles from the array showed everywhere that more than 200 microamperes existed. This, too, is in contrast to the Mark 1 array where small, weak points in clearance were evident.

The Watts Prototype Company has performed extensive system calculations some of which predict the path structure in space. It is instructive to compare the measured path values with those calculated, for the indication is that accurate predictions are obtainable from the calculations. Figures 11–119 and 11–120 show direct comparison of calculated and measured values.





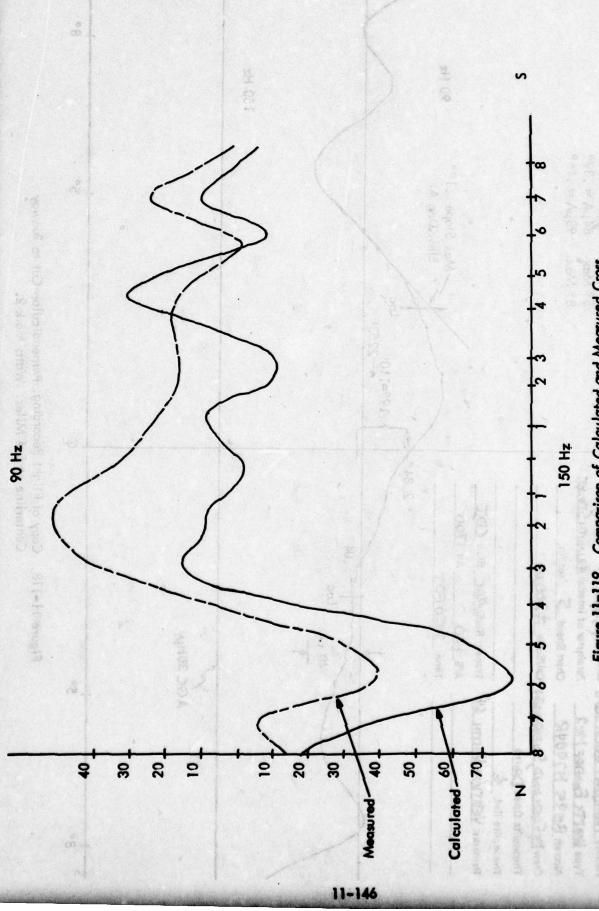
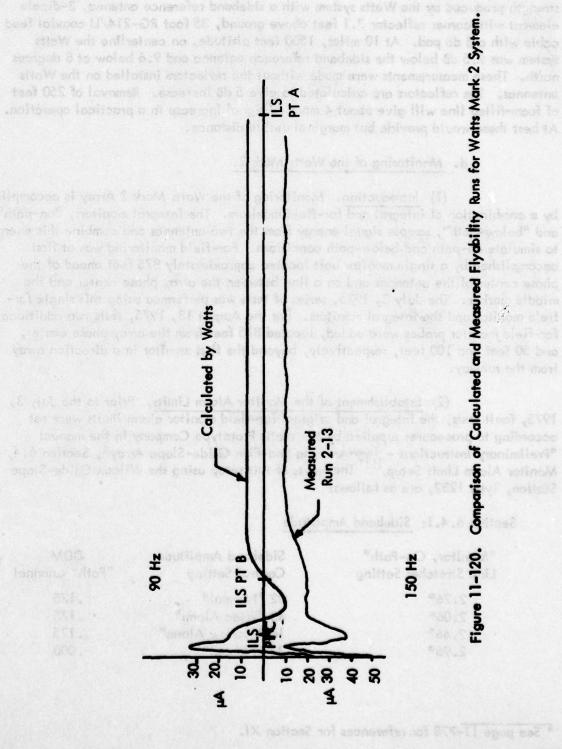


Figure 11-119. Comparison of Calculated and Measured Cross Sections of the Watts Glide Path.



Because of a lack of a field strength standard and a good comparison presently between receiver terminal voltages as they are read by the FAA and by Ohio University, signal strength measurements and reports are confined to readings comparing the signal strength produced by the Watts system with a sideband reference antenna, 3-dipole element with corner reflector 7.1 feet above ground, 35 foot RG-214/U coaxial feed cable with a 3 dB pad. At 10 miles, 1500 feet altitude, on centerline the Watts system was 9.5 dB below the sideband reference antenna and 9.6 below at 8 degrees north. These measurements were made without the reflectors installed on the Watts antennas. The reflectors are calculated to give 5 dB increase. Removal of 250 feet of foam-filled line will give about 4 more dB signal increase in a practical operation. At best these would provide but marginal usable distance.

d. Monitoring of the Watts Mark 2.

(1) Introduction. Monitoring of the Watts Mark 2 Array is accomplished by a combination of integral and far-field monitors. The integral monitors, "on-path" and "below-path", sample signal energy from the two antennas and combine this energy to simulate on-path and below-path conditions. Far-field monitoring was at first accomplished by a single monitor unit located approximately 875 feet ahead of the phase center of the antennas and on a line between the array phase center and the middle marker. The July 3, 1975, series of tests was performed using this single far-field monitor and the integral monitors. For the August 13, 1975, tests two additional far-field monitor probes were added, located 875 feet from the array phase center, and 50 feet and 100 feet, respectively, beyond the first monitor in a direction away from the runway.

(2) Establishment of the Monitor Alarm Limits. Prior to the July 3, 1975, fault tests, the integral and original far-field monitor alarm limits were set according to procedures supplied by the Watts Prototype Company in the manual "Preliminary Instructions - Two-Antenna End-Fire Glide-Slope Array", Section 6.4, Monitor Alarm Limit Setup. The results of this setup using the Wilcox Glide-Slope Station, Type 1232, are as follows:

Section 6.4.1: Sideband Amplitude

"Monitor, On-Path" Line Stretcher Setting	Sideband Amplitude Control Setting	DDM "Path" Channel
2.26°	32 "Normal"	.175
2.06°	43 "Wide Alam"	.175
2.46°	16 "Narrow Alarm"	.175
2.96°	32 "Normal"	.000

^{*} See page 11-778 for references for Section XI.

Section 6.4.2: Sideband Phase

"Monitor, On-Path" Line Stretcher Setting	DDM . "Path" Channel	"Sideband-Phase" Control Setting
m blait-12.26 of Hibbs awt a	175 LEL 180	5 Advance
-rot loni 2:06° t to scott do to rottopiloni at	to the 1.175 mil media A liet a tel ter atom !	45 Advance (Wide Alarm Dephase Advance)
2.06°	.175	12 Retard (Wide Alarm Dephase Retard)
2.96°	.002	5 Advance

Co Filight Check

Section 6.4.3: Path Channel

	th-Angle" e-Stretcher Setting	Path Channel DDM
fiel.	102.960 and amountibre	.004 (150Hz)
odt r	2.76°	.046 (90Hz)
f me	3.16° 1 10 . stew 210	.056 (150 Hz)

Section 6.4.4: Width Channel (Monitoring Far-Field Signal)

"Sideband-Amplitude"	DI	M
Control Setting	Far-Field	Channel
Wide Alarm (43)	.320	(150Hz)
Narrow Alarm (17)	.550	(150Hz)
Normal (32)	.404	(150Hz)

The width channel DDM dial was set to zero, the DDM meter, and the alarm indicators set to give the proper alarm condition operation.

The conditions existing at the glide slope station at the outset of the testing on July 3, 1975, were:

A. Glide Slope Transmitter

Carrier Power	4 Watts
Sideband Power	340 Milliwatts

B. Monitor Panel Smartha scall or sail cost mode

Monitor Channel	RF Level	DDM	% Mod.
Path (Integral Path Monitor)	0 dB	.002 (150Hz)	93%
Width (Far-Field Monitor)	0 dB	.410 (150Hz)	98%
Clearance (Integral Below- Path Monitor)	0 dB	-	100%

C. Flight Check

Path Angle = 3.01° } { average values determined by flight checks.

Prior to the August 13, 1975, fault tests two additional far-field monitors were installed and their alarm limits set to match those of the original far-field monitor, i.e., the DDM meter set for a full scale indication of

$$\pm .075 \times 2 = \pm .150 DDM$$

The alarm indicators were set at

$$+.075 \times 2 = +.150 DDM$$

and $-.040 \times 2 = -.080 DDM$

Note that, under normal (no fault) conditions, the three far-field monitors detected different values of DDM. With all three needles zeroed on the DDM meters, the respective settings on the digital DDM dials were, at the start of the August 13, 1975 tests, as follows:

Monitor #1	444 DDM	(2 x 222 DDM)
(original unit)	ACICL	
# 2	420 DDM	(2 x 210 DDM)
*3	410 DDM	$(2 \times 205 DDM)$

This response is indicative of the non-uniform path structure in a direction perpendicular to the runway centerline.

(3) <u>Faults.</u> The faults introduced into the system are listed below:

the conditions existing at the glide stone existion at the outset of the testing

Number	Fault 1999W CARL C YOUL
(July 3, 1975)	A. Gilde Slope Transmitter
1	Open feed line to Front antenna
3	Open feed line to Rear antenna
3	Short feed line to Front antenna
4	Short feed line to Rear antenna
5 MGd	Decrease Sideband Power for broad alarm (340> 200 milliwatts)
rule on one	Sideband Phase - Retard (12R setting)
7.007	Sideband Phase - Advance (45A setting)
8	Decrease Percent Modulation (95% to 70% on Integral Path Monitor % Mod. Channel)

9	Unbalance Tone - 90 Hz high (unbalance until
	reach alarm condition)
10	Unbalance Tone – 150 Hz high
11	Attenuate signal to Front antenna (2 dB attenuation)
12	Attenuate signal to Rear antenna (2 dB attenuation)
13	Park truck* in front of Front antenna - Position 1
	(see Figure 11–121)
14	Park truck in front of Rear antenna - Position 2
o o	(see Figure 11–121)
15	Move center of Rear antenna forward 6 inches
August 13, 1975	Simbleted barolania
16	Three wet cloths over center slots on Rear antenna (slots #48, 49, 50)
17	Three wet cloths over center slots on Front antenna (slots #44, 45, 46)
18	Drop center of reflector element over Front antenna
19	Drop center of reflector element over Rear antenna
20	Lower center of Rear antenna by removing two center support stands
21	Lower center of Front antenna by removing two center support stands
22	Move center of Front antenna forward 3 inches
23	Move center of Rear antenna forward 3 inches
24	Park truck in front of Rear antenna - Position 3
	(see Figure 11–121)
25	Park truck in front of Front antenna - Position 4
	(see Figure 11-121)
26	Park truck at distribution box - Position 5 (see Figure 11-121)
27	Park truck in front of Rear antenna - Position 6
	(see Figure 11–121)
28	One wet cloth over center slot of Rear antenna (slot #49)
29	One wet cloth over center slot of Front antenna (slot \$45)
30	Release air pressure from distribution lines

(4) Monitor Results. A total of 30 faults was introduced into the system and the corresponding monitor responses were recorded. The corresponding flight checks consisted of a level pass on centerline at an altitude of 1000 feet to check path angle and path width, and a perpendicular cut at a distance of 5.4 miles at an altitude of 1700 feet to check the path structure in azimuth. From this the approach path structure can be inferred.

^{*} The truck used for these tests was a 1972 Ford Club Wagon with the following external dimensions: Length - 14 feet, 9 inches; Height - 6 feet, 4 inches; Width - 6 feet, 2 inches.

Plan View: 1 inch = 50 ft.

*These Numbers Indicate Radiation Slots. HOW - MAN SOME STATE OF THE S

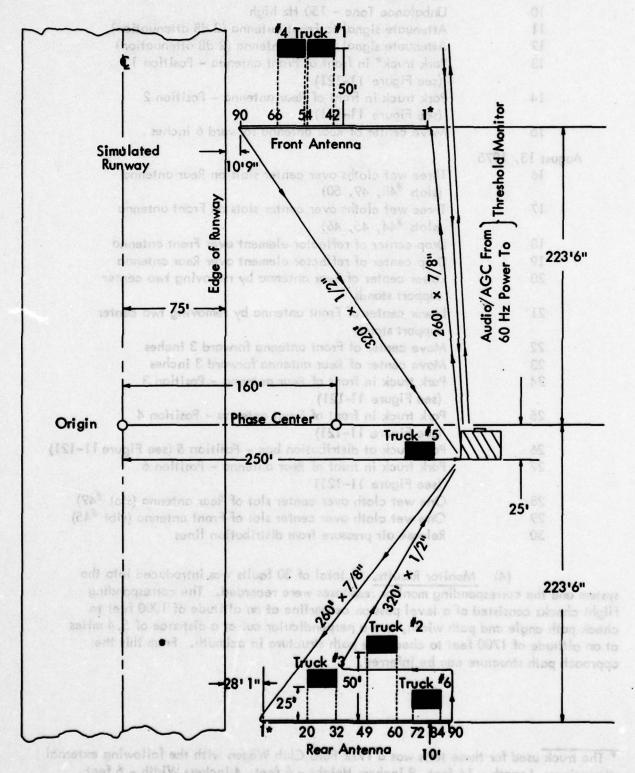


Figure 11-121. Truck Positions for Fault Tests Mark 2 System.

Table 11-5 summarizes the results of the tests, showing that for the 30 faults investigated, the monitor responses and the flight check results agree perfectly in 20 cases (both indicated 15 out-of-tolerance and 5 in-tolerance conditions) and disagreed in 10 cases. The monitors indicated 5 cases out-of-tolerance with the aircraft showing in-tolerance conditions and, unfortunately, the aircraft saw 5 out-of-tolerance conditions while the monitors were not in alarm (see Table 11-4).

		8888	MONIT	ORS	d die
		. In	C	out of Tolerance	8 2 2
		Tolerance	Integral	Far-Field	Alarm Conditions
RAFT	In Tolerance	5	(*10, *11, *12)	2 (*6, *22)	5
AIRCRAFT	Out of Tolerance	5 (*14, *25, *27, *28, *29)	6	14	TIS SE ANGLE

Table 11-4. Fault Events.

Table 11-5 lists the monitor responses and flight check data with the out-of-tolerance conditions underlined. Unfortunately, during the first set of tests from July 3, 1975, only the alarm conditions were recorded for the monitor responses in most cases and thus an entry in Table 11-5 of a double dash (--) indicates a non-alarm state of the monitor, but not necessarily a normal monitor condition.

(5) <u>Discussion of Results</u>. Following is a discussion of the 10 fault conditions for which the monitor responses and the aircraft flight check results were not in agreement.

Case I: Undesirable

(Monitor out-of-tolerance; aircraft recordings in-tolerance)

Fault 6 - Retard Sideband Phase

Far-Field Monitor *1 at alarm limit of 330 DDM

Flight check showed normal path angle, 3°, and width 0.69°, and good structure, 5.7% [2]

			The state of the s		200	MOINING RESPONSE	2			The state of the s				LEIGHT CHECK	-	100000000000000000000000000000000000000
		Integr	Integral Monitors	itors	4 (E.) 8 (1985)	9-1		Far-Field Monitors	Monitors			rtes witt		es III O nes	00 Vino 20 20 4	
Foult		diod-no	080	below-path	nul, o ta	edy			12		13	EA On .	Path	Path	Structure	Status
Set 1 - July 3, 1975	DDM	유 유	% Pou	RF % db mod	DDM	유명	% pom	MOD	RF % db mod	DDM	A 유	% w	(degrees)	A STATE OF THE PARTY OF THE PAR	(%)	
Normal	.002 150Hz	0	83	0 100	.410	0	86	u	n.a.*		n.a.*		3.01	99.0	di ga e zil sion	:
Alorn Limits	840		17.17		.330					25,		bit	2.80	0.50	i wej uosi mal	
8	2406	7	75	-1 75	07 (1.76	7.	75		A.		•	14.	9	do)	7.5%	1
Tolerance Limits	.052 150Hz		in e	nos	8.	00/2	45 Pes					For	3.20	0.00	(45)5, 1 che 1 54n	
1. Open front antenna	.018 150Hz	পা	in ion	-3.8	.018 150Hz	-5.5	vi ti			1	•		8	8	enti I Heath one o	<
2. Open rear antenna	.020 90Hz	91	G Just	- 7:5	.020 90Hz	7	oq ³			\$12	•	i ir	9.0	8	o alia odło umate	<
3. Short front antenna	.014 150Hz	-5.5	ion.	1	.012 150Hz	91	1		•3	11,	•	n 9.10	0.0	8	isar o ino as ilikolo	<
4. Short rear antenna	.028 90Hz	-5.8	1	3.7	.028 90Hz	7	1 =			01/0	•		0.00	8 W	ria ess renoqe o Hiso stude	∢
5. Decrease sb. power- broad alarm	1	1	ida-e	aless aless	.340	et Inc	1				. `		3.00	0.0	5.4%	۷
6. Retard sb. phase	1	:	1	1	.330	1	1	,8	20		•	501	3.00	69.0	5.7%	>
7. Advance sb. phase	1	1	4	1	.570	1	:	3	200			16.73	2.96	0.97	6.8%	4
8. Decrease % mod.	1	!	21	1	1	ni el	21	[05 [05]	har N		•	el al	3.00	19.0	8.2%	4
9. Unbalance - 90 Hz	946	1	1	1	.370	1 2	!						2.80	99.0	7.1%	<
			noil		endil e ad					STATE OF						

*n.a. - not applicable as only one far-field monitor was installed for the fault checks of Set 1.

Table 11-5. Monitor Responses and Flight Check Results for 30 Faults Introduced into the Watts Glide-Slope System.

Fourth Companies Four-Field Monitors Four-Field Four-Field Monitors Four-Field Four-Field Monitors Four-Field Monito			The second secon															
ODM RF % RF % DDM RF % DDM RF % DDM RF % Gegrees Geg	1540 340		Integr	al Mor	ritors				Fa	-Field M	onitors							
DDM RF % RF % DDM RF % DDM RF % ODDM RF % OD	Fault	1000	on-path		below-	hack		0	9	,			13	eg B	Path		Structure	Status
1024440440	John Ty, 201	97.0	동육	% pom	1000			The state of			90	-		% pow	(degree	(degrees)	(%)	c
		.054 150Hz		* I	67		a .	ps.	8	.n.a	38 OX	¥	n.a.*	8.8	3.19	79.0	4.8%	A D
	•	.1.	7	385 T 10		18	6	6		6		ş -			2.85	0.78	6.9%	5
22) 2.68 0.67 5.4% 1.504		044 50Hz	-1.25	81		Q.	0		<u>. </u>			g —			3.11	0.54	7.2%	5
22) 22) 22)	-		4.2	1					8 1	7.		9	•		2.78	29.0	5.4%	4
22) Reply 18 To the control of the c			4.2	1			8		9	i• 1			•		2.88	0.71	89	٥
### Figure 11-122) ###################################		2 100	1	1		2			<u>.</u>	9		N.	i i		2.68	0.93	18%	∢
Figure 13 FASC 25 0 ac offer to 20 25 1.03	6 inches (See Figure 1H22)			13.	. 7	×						A				8.0	18.5	
1904 1904	Alored Floring	1004										.Q.;			13.5	R a		
de de la	Normal In	100.		100		R						¥			1.03	8		
algoria es servicio de la filia de la servicio del servicio de la servicio del servicio de la servicio della servicio de la servicio della se						1 2			9.4			2	N SE	bent bent	(008.00)	6,000	(65)	
excitional distributed and another than the second	- Company		04-40												State of the last	A STATE	Servicina I	
									5.									

*n.a. - not applicable as only one far-field monitor was installed for the fault checks of Set 1.

Table 11-5. (Continued).

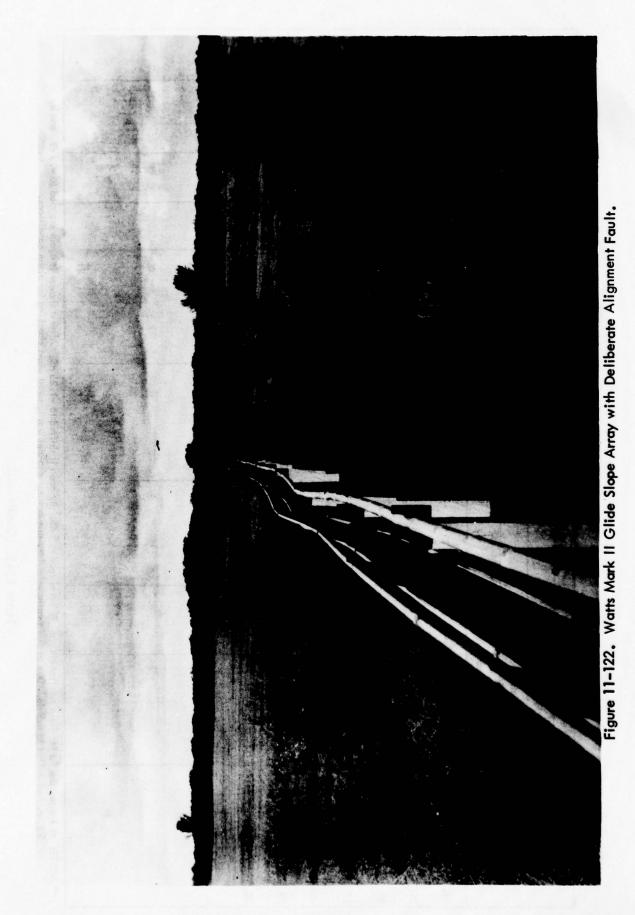
					×	DIINO	MONITOR RESPONSE	ONSE								FLIGHT CHECK	ECK	
		Integra	Integral Monitors	Itors	Limited.			Ţ	a -Field	Far-Field Monitors	£							
Foult		on-path		below-	-path		5			1,2			1,3		Path	Path Width	Structure	Status
Set 2 - August 13, 1975	MOO	de de	% Po	유명	% pour	DDM	₹ 4	% Pour	DDM	유유	% Po	DDM	유 유	% P	(degrees)	(degrees)	8	
Normal	.004 150Hz	0	26	0	%	44	0	16	.420	-,25	8	.410	5	82	3.01	8.		1
Alorn Limits or	.054 150Hz	7	25	7	. 25	. 595	7	22	.570	7	2	.560	7	22	3.20	0.0	7.5%	1
Tolerance Limits	.046 90Hz					365			.340			.330		٠	2.80	0.56		
16. Wet cloths-rear ant.	.042 40%	25	26	•	<u>ه</u>	340	75	8	.460	-1.75	8	18	71	22	3.48	0.91	8	<
17. Wet cloths-front ant.	.034 150Hz	20	8	1.5.	8	99	-2.3	RI	320	8.	8	.330	4:	8	2.85	0.69	23%	4
18. Reflector over front ant.	.012 150Hz	05	8	•	8	280	7:1	8	4.	1.8	8	.490	-2.4	82	2.94	0.67	8	<
19. Reflector over rear ant.	.00. 200. 240.	05	84	•	25	.340	•	8	320	£	46	.376	1.6	82	2.80	0.67	<u>%</u>	<
20. Lower center rear ant.	.012 90Hz	35	8	0	2	. 450	25	8	. 430	75	82	.460	1.3	8	3.09	0.53	ž	4
21. Lower center front ant.	.02040 150Hz	40	6	e	. 6	. 480	25	88	.430	70	8	.420	-	88	3.00	0.57	ž	<
22. Move center front ant. fwd.	.0103 150Hz	£3	4	5		. 530	.5	8	.540	1.8	1	.510	71	1	3.18	0.55	*	-
23. Move center rear ant. fwd.		35	4	2		.400	+.2	95.	.3%	25	8	.370	-1.2	&	2.87	0.54	Ł	₹
						OHE	3550	180							-	(CH)		

** NOTE: At 9 a.m. the *3 far-field monitor channel RF level read -.5 dB. By noon it shifted to -1.25 dB. After a shower it again dropped to -.5 dB, and by 5 p.m. had shifted to -.9 dB. Due to this erratic behavior, this monitor channel was ignored when checking for alarm conditions.

Table 11-5. (Continued).

				Section of the second	3	MONITOR RESPONSE	KESTO	35							ירופחו כחבכא	NO STATE OF THE PROPERTY OF TH	
		Integr	Integral Monitors	itors		e sak		For-F	For-Field Monitors	nitors							
Foult		on-path		below-path	ŧ	1			1,2			13		Path	Path Width	Structure	Status
	DDM	₩ 4	% Po €	RF % db mod	1995	DDM RF	% mod	WQQ P	A BB	% pow	ром	유 명	% pom	(degrees		(%)	
24. Truck-rear ant. position 3	•	0	88	+35 94	99	2075	.5 80	.410	-1.0	8	.426	71	85	3.21	0.49	%5.6	<
25. Truck-front ant. position 4	96. 24.0 24.0	+25	8	+.5 94	•	102	95	.360	•	&	.390	6:	8	3.00	0.55	<u>8</u>	٥
26. Truck-distribution box-position 5	96. 24.	+.2	8	+.3 %	34.	0 +.25	5 94	.384	•	٤	64.	75	&	2.92	0.51	ģ	<
27. Truck-rear ant. position 6	90. 24%	+.25	8	+.3 94	.380	30 +.25	8	64.	•	8	.420	7	8	2.86	0.65	<u>%</u>	•
28. One wet cloth rear ant.	.034 2406	•	8	+.5 92	2 .3%	9	44	6.	5.	&	3	5	8	3.16	0.52	<u>%</u>	۵
29. One wet cloth front ont.	•	•	8	+.35 95	2.480	3025	5 88	380	•	\$.370	7	8	2.87	0.59	<u>*</u>	٥
30. No air pressure	•	0	8	+,3 %5	\$. \$	0	76	\$.	2	8	3%	6:	8	2.91	0.56	*	<

** NOTE: at 9 a.m. the *3 far-field monitor channel RF level read -.5 dB. By noon it shifted to -1.25 dB. After a shower it again drapped to -.5 dB, and by 5 p.m. had shifted to -.9 dB. Due to this erratic behavior, this monitor channel was ignored when checking for alarm conditions.



11-158

Fault #10 - Tone Unbalance, 150 Hz High

Integral path monitor was at limit of .054 DDM (150Hz).

Flight check showed a path angle of 3.19° or 0.01° from the upper limit. The width, 0.67°, and structure, 4.8%, were good.

Fault #11 - Attenuate Signal to Front Antenna by 2 dB

Integral path monitor alarmed at -1.1 dB.

Flight check showed a lowered path angle, 2.85° increased width, 0.78°, and fair structure, 6.9%.

Fault #12 - Attenuate Signal to Rear Antenna by 2 dB

Integral path monitor alarmed at -1.25 dB.

Integral below path monitor alarmed at -1.3 dB.

Flight check showed a raised path angle, 3.11°, a narrow width, 0.54°, and the structure getting rough, 7.2%.

Fault #22 - Move Center of Front Antenna Forward

Far-Field Monitor *2 alarmed at -1.8 dB.

Flight check showed the path to be high, 3.18°, and narrow,

0.55°, but smooth in structure, 2%.

In a normally operating and properly adjusted system, the occurrence of conditions similar to faults \$6, 10, 11, 12, or 22 would indicate an abnormal change in the system and the alarm would tend to alert maintenance personnel to take the appropriate corrective measures.

Case II: Dangerous

(Monitors in-tolerance; flight check out-of-tolerance)

Fault #14 - Truck at Position #2 (see Figure 11-121).

Flight check showed a lowered path, 2.88°, and width, 0.71°, but a very rough structure, 16%.

Far-Field Monitor *1 was 80% into alarm at .500 DDM.

Fault #25 - Truck at Position #4

Flight check showed normal path angle, 3°, but narrow width, 0.55°, and rough structure, 10%.

Far-Field Monitor *2 was 75% into alarm at .360 DDM.

Fault #27 - Trück at Position #6.

Flight check showed a lowered path angle, 2.86°, and normal width, 0.65°, but rough structure, 12%.
Far-Field Monitor *1 was 75% into alarm at .380 DDM.

Fault #28 - One Wet Cloth Over the Center Slot of the Rear Antenna

Flight check showed a path angle, 3.16°, approaching the upper
limit and path width, 0.52°, approaching the narrow limit.

The structure was rough, 12%.

Far-Field Monitor #1 was 65% into alarm at .396 DDM.

Fault #29 - One Wet Cloth Over the Center Slot of the Front Antenna Flight check showed a lowered path angle, 2.87°, and narrow width, 0.59°, but a rough structure, 11%. Far-Field Monitor #2 was 80% into alarm at .360 DDM.

For faults #14, 25, and 27, the position of the truck in front of either the front or rear array element was carefully selected so that the monitors indicated a marginal in-tolerance condition. Movement of the truck a few feet in either direction along, and parallel to, the array would put one of the far-field monitors into alarm.

Faults #28 and 29, while physically unusual in that several thick layers of wet cloth were wrapped around an antenna radiation slot, point out the need to keep the antenna radiation slots clear of any possible obstructions.

(6) Effects of Transmitter Changeover. The Watts Mark 2 Array was tested over a period of 5-1/2 months from mid-June, 1975 to the end of November, 1975 and during that period the array was energized either by a Wilcox Mark 1-C solid state transmitter generating 4 watts of carrier power, or by a TU-4 tube type transmitter generating approximately 10-12 watts of carrier power. Although in a typical installation the antenna power distribution feed box would be located inside the glide slope hut, at Tamiami it was necessary to locate this distribution box in the field approximately 250 feet from the transmitter hut and, even though low-loss transmission lines were used, there resulted only 1.75 watts of carrier power into the distribution box when using the Wilcox transmitter. In order to insure adequate signal strength in space, the TU-4 transmitter which provided between 2.5 and 3 watts of carrier power into the distribution box was, therefore, used for some of the flight checks. Except for the large difference in power output, this use of two transmitters does in fact correspond to a possible situation at a commissioned facility where two transmitters would be used. The effects of changing from one transmitter to the other are shown in Table 11–6 which gives the monitor dial settings necessary to obtain a zero DDM indication on the monitor panel meters, and the path angle and width as measured by flight check, and in Figure 11-123a which shows the perpendicular glide path structure as measured at a distance of 5.4 miles fron the array. From Figure 11-123a, it can be seen that in the ±3 degree sector about the extended runway centerline, using the TU-4 transmitter, the glide path angle went from 2.87 degrees to 3.07 degrees for a change of 0.20 degree, with the corresponding values using the Wilcox transmitter being 2.94 degrees to 3.19 degrees for a change of 0.25 degree. Also, the perpendicular structures using the two transmitters both exhibit the same oscillation on

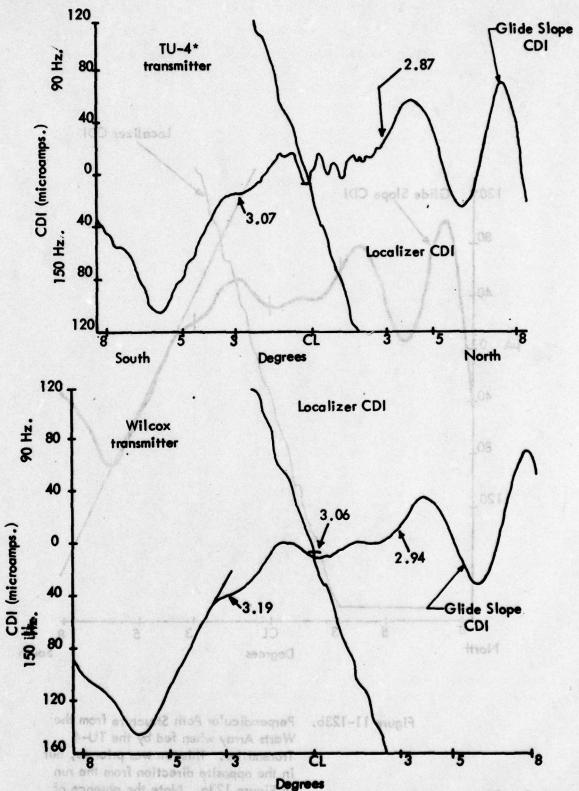


Figure 11–123a. Perpendicular Path Structure From the Watts Array When Fed by the TU-4 and Wilcox Transmitters.

Note: The ripple between centerline and 3° N on the TU-4 crossover was due to an aircraft overflight of the array (see Figure 11-123b).

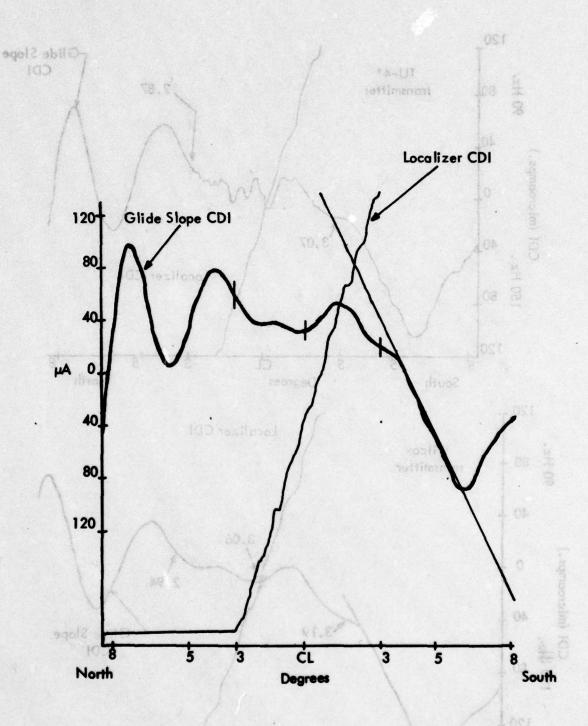


Figure 11-123b. Perpendicular Path Structure from the Watts Array when fed by the TU-4 Transmitter. This run was prior to, but in the opposite direction from the run in Figure 123a. Note the absence of ickne From the World Array When Fed aircraft overflight interence on this recording. there the right between centerline and 3" M on the TU-A crossover was due to on aircraft overflight of the array (see Figure 11-133b).

TRANSMITTER		RO DD		INGS TO	FLIGH	IT CHECK
	integral path	#1 fo	r-field #2	#3	path angle	path width
TU-4	.070 (90 Hz)	.330	.346	.390	2.94	0.62
Wilcox	.084 (90 Hz)	.313	.331	.369	2.98	0.70

Table 11-6. Effects of Changing Transmitters on the Watts System.

the north side of the centerline between 3 degrees and 8 degrees and the same large, 150 Hz, excursion at approximately 6 degrees on the south side of the centerline. A recording in the opposite direction for the TU-4 transmitter is shown in Figure 11-123b.

(7) Effects of Antenna Displacement. In a permanent installation, one parameter that must be maintained is antenna position or alignment. At some point in the latter half of the test period for the Watts system (i.e., sometime between the beginning of September, 1975 and the end of November, 1975) the end nearest the runway centerline of the rear antenna was inadvertently displaced approximately 3 inches forward, the most probable cause of the displacement being that the end antenna support was jarred by a piece of mowing equipment. The effects of this antenna misalignment are illustrated in Table 11-7 and in Figure 11-124.

CONDITION		OR DIAI		NGS TO TERS	FLIGH	T CHECK
	integral path	#1 fo	or-field #2	1 3	path angle	path width
array end displaced	.084 (90 Hz)	.313	.331	.369	2.98	0.70
array straightened	.086 (90 Hz)	.320	.336	.370	3.01	0.74

Table 11-7. Effects of Antenna Misalignment.

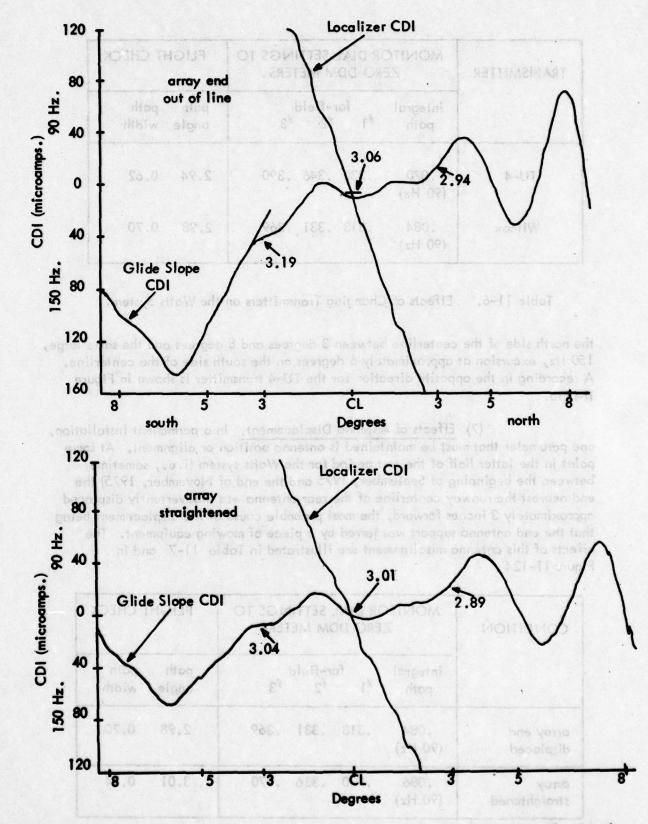


Figure 11-124. Perpendicular Path Structure From the Watts Array Showing the Effects of Antenna Misalignment. (Wilcox Transmitter)

While the results listed in Table 11-7 show almost negligible change resulting from straightening the end of the rear antenna, an examination of the perpendicular path structures as illustrated in Figure 11-124 shows that a definite improvement to the perpendicular path structure occurred after the array was straightened, especially to that portion of the path structure that existed in space on the south side of the extended runway centerline. Also, within the ±3 degree sector about the extended centerline, straightening the array resulted in improving the dispersion of the path angle from 0.25 regree (from 2.94 degrees to 3.19 degrees) to 0.15 degree (from 2.89 degrees to 3.04 vegrees).

(8) Faults. For the final series of tests on the Watts Mark 2 system, seven fault conditions were investigated, and the selection of these faults was predicated on the results of the initial fault tests which were performed in July and August of 1975. The results of those initial fault tests, which are summarized in Table 11-8, showed five fault conditions labeled as dangerous; that is, there were five fault conditions that did not give a monitor alarm but which were shown to be out-of-tolerance on the aircraft flight check results. Of the five conditions that exhibited this unsatisfactory monitor response, three were truck positions in front of the antennas, and two were foreign objects on the antenna.

In view of the above, the final fault tests concentrated on these two types of faults, namely vehicular presence around the antenna and foreign objects on the antennas. The faults introduced into the system were:

Numb (November 23		(c) a	
. 31	One layer of we between slots #3	t cloths spread out along 1 to [‡] 58.	the rear antenna
OZ.	Four wet cloths (#47, and #48 on	(one each) lumped over s the rear antenna.	lots #45, #46,
33	Truck position #3 between slots #4	7, 125 feet ahead of the and #13 (north end).	front antenna,
34	Truck position #8 between slots #4	B, 125 feet ahead of the 7 and #56 (center).	front antenna,
35	Truck position *9 between slots *8	9, 125 feet ahead of the 0 and #89 (south end).	front antenna,
36	in line with the	10, between the two ante phase center, with the tr isturbance of the far-fiel	ruck positioned

		мон	I T O R S
		In Tolerance	Out of Tolerance
RAFT	In	A (5) Letter the order of the little of the little of the little order of the little order of the little order of the little order	
AIRCRAFT	Out of Tolerance	D (5)	A (15)

and he regional representation of the rear selection are represented from the commence of the

on the south side of the extended runway centerline. Aids, within the \$3 degree

the dispersion of the party and is from 3, 25.1 spread from 2,004 at grees to 3,10 degrees)

Table 11-8. Fault Events. A comparison of Monitor Status and Aircraft Flight Check Results for the Fault Tests of July 3 and August 13, 1975. The three states illustrated by the matrix are defined as acceptable (A), undesirable (U), or dangerous (D).

Charles of Sell and TAN Hale reconstant

found would be med to be to the most obtained and the most written and the found to
Truck position ") 175 feet check of the front aptients,

Iruck position "10, between the two nategna elements,

for a maximum dissubbende of the for-field member DDM

Detween slots "III" in "III."

Two layers of semi-damp cloths spread out along the front antenna between slots #32 and #69.

37

Chart recordings were made of the far-field monitor responses that resulted from the presence of a van being driven parallel to the antenna elements at distances of 75 feet, 100 feet, and 125 feet ahead of the front antenna, and also between the antennas at the array phase center.

(9) Results. For each of the seven faults introduced into the system, the corresponding monitor responses were recorded, and the corresponding flight checks made. The flight checks consisted of a level pass at an altitude of 1000 feet to check path angle and path width, and a perpendicular cut at a distance of 5.4 miles and altitude of 1700 feet to check the path structure in azimuth. Table 11-9 summarizes the results of the seven fault tests, showing that the monitors' responses agreed with the flight check results in six of the seven cases, and disagreed in only one case. For the case where the disagreement occurred, the monitors indicated an alarm condition while the flight check results showed that the path angle had dropped 0.17 degrees out of the maximum permissible 0.20 degrees change.

Although this case would be considered as undesirable in that the monitor removed the facility from service prematurely, the data in Table 11-9 shows the monitor system to be only slightly conservative in nature. In fact, of the three far-field monitors in operation, unit #1 showed only a slight change in DDM value, unit #2 showed no change at all, and unit #3 alone registered an alarm condition.

The locations for the truck position faults were determined by first observing the far-field monitor responses while the truck was driven at a slow speed parallel to the antenna elements, first between the antenna elements on a line through the array phase center, and then ahead of the front antenna at distances of 75 feet, 100 feet, and 125 feet. At the same time, both the signal strength (RF level) and DDM indications for far-field monitor unit *1, and the DDM indication only for far-field monitor unit *2 were recorded, and these chart recordings are shown in Figure 11-125. An examination of Figure 11-125 shows that while only a 60% alarm condition was obtained with the truck between the antenna elements, alarm conditions were recorded with the truck at the 100 foot distance ahead of the front antenna. At the 125 foot distance, far-field monitor unit *1 reached only a 65% DDM alarm, but still exceeded momentarily the -1 dB RF level alarm limit.

(10) System Stability Monitoring for the Mark 2. The purpose of this section is to present the results of long-term monitor tests for the Watts Mark 2 Glide Slope Array. These tests were run continuously from September 13 through November 3, 1975, except for a two-week period between October 4 and October 21, 1975, during which time the system was shut down while the transmitter hut air-conditioner was being repaired.

The monitor distribution setup of the Watts Array is diagrammed in Figure 11-126. The transmitter but was located approximately 250 feet from the distribution box and the distribution box, which would normally be inside the but,

٦	i de				MON	TOR RE	MONITOR RESPONSE				81		823	FLIGHT CHECK	HECK	
de de	Integra	Integral Monitor	tor	FI.	pare		Far-Field Monitors	Monito	2	£		123	lo total		est. nors	nor!
Foult	8	on-path	D (e (fi Iftwe Lectur	-	dev	870	2	no i	900	3	os in		Path Width	Structure	Status
Set 3 - November 23, 1975	МОО	25 卷	% Pg	WQQ	# 8	% Po	DDM	₩ 89 ₩ 89	% pom	DDM	품 용	% Po	STATE OF THE PARTY.	(degrees)	8	Griedy
Normal	.084 90 Hz.	0	8	.340	0	8	.360	0	011	.390	25	55	3.01	0.74	4.0	100
Alam Limits	.034 90 Hz.	0 1	เกอร์เ	.260	ta tra	no d	.280	lo i	é., 110	.310	ยาม ละเอ	EQ.	2.80	0.50	391 580 51-0	bba
Tolerance Limits	13. 13.	7 ::	K	.490	- 100	K	.510	ogn T be	8	.540	ono.	K .	3.20	0.00	olin S'no Matr	ege 2
31. Wet cloths spread out-rear antenna	980	0	8	4.	25	8	.390	orto i	8	.480	ç	8	3.05	0.73	6. It o	Móla ≸n 3
32. Wet cloths lumped rear antenna	980.	25	8	64.	-1.25	8	.380	ngila ya∓an	91	.540	na grat oktano	8	3.37	29.0	16.8	sarab E < ≥va
33. Truck - front antenna position 7	.086 +.2	+.2	8	.350	0	26	380	•	202	.400	25	20	2.95	0.70	3.3	-Timez Is ≺ ree
34. Truck - front antenna position 8	.084 +.2	7	8	.310	÷.25	20	.400	5.	8	98.	+.25	115	2.94	0.73	de of	eis of Verv
35. Truck - front antenna position 9	.084 +.25	+.25	8	.350	•	8	.370	+.25	19	64.	v 2 00 J i lw	56	3.00	12.0	7 7 0 2 0 2 0 2 0 2 0 3	yol ay a≮afa
36. Truck - middle array position 10	.082 +.25	+.25	8	614 ,	25	8	.410	0	9	₹.	5,	8	3.08	29.0	w ton rev p bno undu	T ne ≪
37. Wet cloths - spread out front antenna	.100 +.20	+.20	8	370	25 fe	8	.360	4.20	801	980	£.3	112	2.84	0.67	ecordi ce 3.2 i set,	,
38. Normal	220.	+.65	100	.370	+.25	%	.390	+.20	104	.410	0	28	n ad tolo	1	n tho 1949 101	ı

Table 11-9. Monitor Response and Flight Check Results for Seven Faults Introduced into the Watts Glide-Slope System. Below-path integral monitor was not used in these tests.

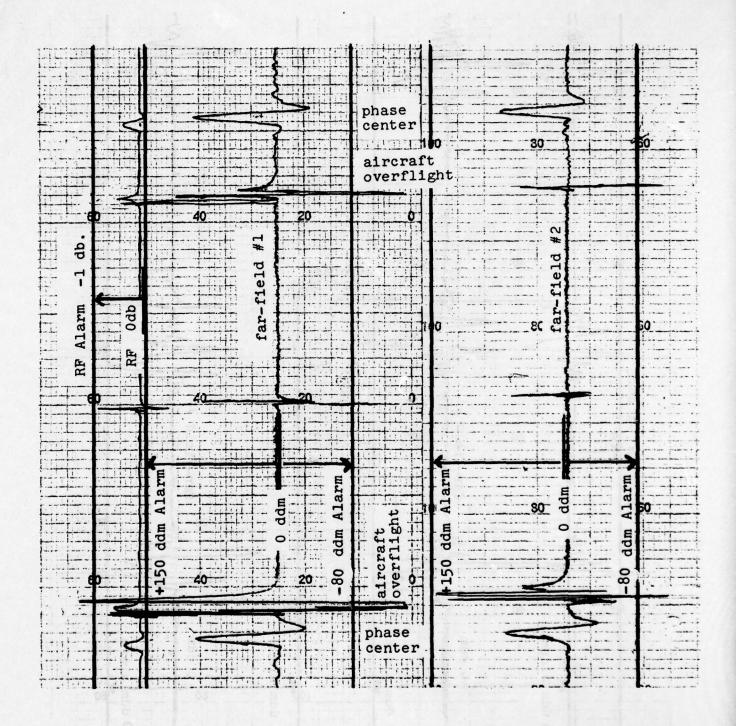


Figure 11–125. Far–Field Monitor #1 RF Level and DDM and Far–Field Monitor #2 DDM Responses to Vehicular Traffic Along the Phase Center and at 75, 100, and 125 Foot Distances Ahead of the Front Antenna.

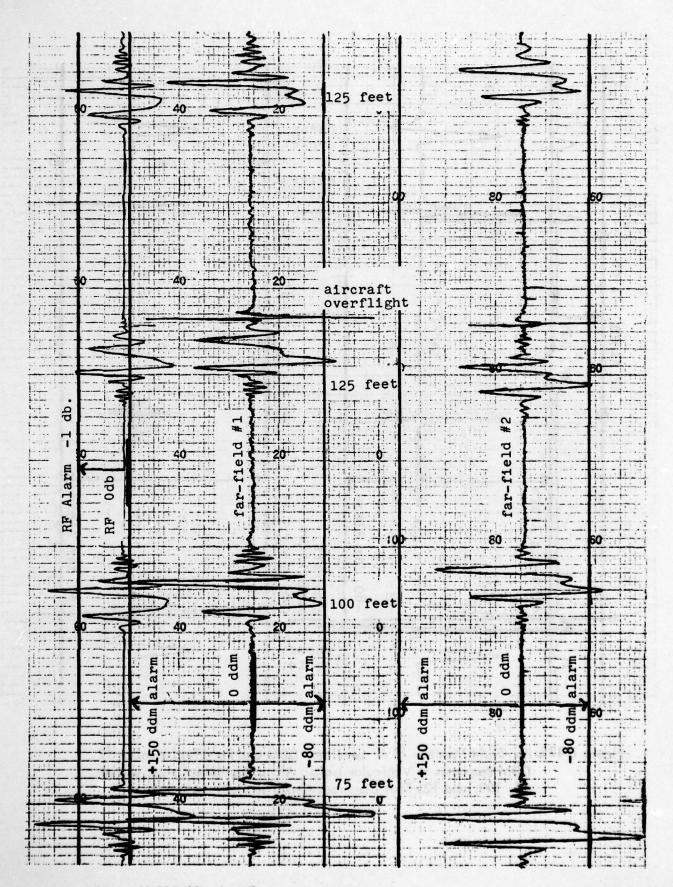


Figure 11-125. (Continued)

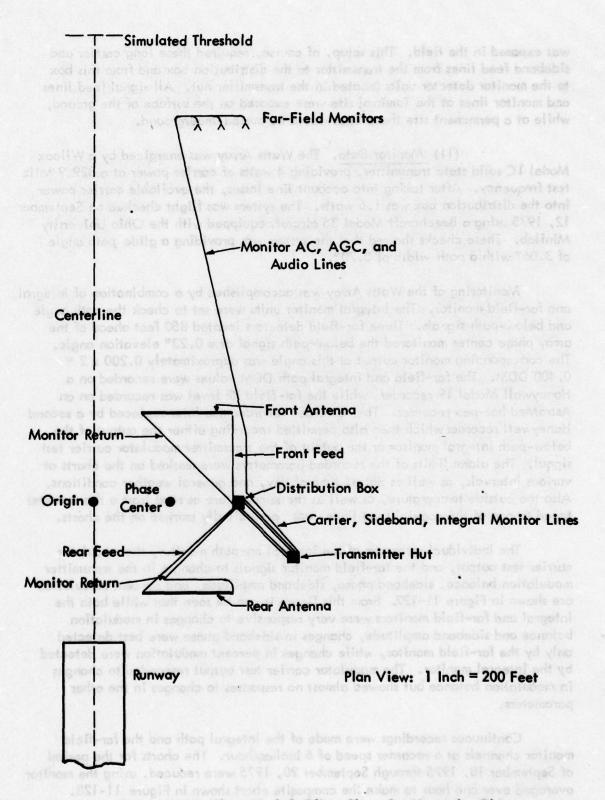


Figure 11–126.Watts Mark 2 Glide–Slope Set Up at the Ohio
University Test Site, Tamiami, Florida.

was exposed in the field. This setup, of course, required these long carrier and sideband feed lines from the transmitter to the distribution box and from this box to the monitor detector units located in the transmitter hut. All signal feed lines and monitor lines at the Tamiami site were exposed on the surface of the ground, while at a permanent site these lines would be buried underground.

(11) Monitor Data. The Watts Array was energized by a Wilcox Model 1C solid state transmitter, providing 4 watts of carrier power at a 329.9 MHz test frequency. After taking into account line losses, the available carrier power into the distribution box was 1.6 watts. The system was flight checked on September 12, 1975 using a Beechcraft Model 35 aircraft equipped with the Ohio University Minilab. These checks showed that the system was providing a glide path angle of 3.06° with a path width of 0.70°.

Monitoring of the Watts Array was accomplished by a combination of integral and far-field monitor. The integral monitor units were set to check the path angle and below-path signals. Three far-field detectors located 850 feet ahead of the array phase center monitored the below-path signal at a 0.23° elevation angle. The corresponding monitor output at this angle was approximately 0.200 x 2 = 0.400 DDM. The far-field and integral path DDM values were recorded on a Honeywell Model 19 recorder, while the far-field RF level was recorded on an AstroMed hot-pen recorder. The AstroMed recorder was later replaced by a second Honeywell recorder which then also permitted recording either the output of the below-path integral monitor or the output of the transmitter modulator carrier test signal. The alarm limits of the recorded parameters were marked on the charts at various intervals, as well as dates, time of day, and general weather conditions. Also the outside temperature, as well as the temperature as read from a thermometer taped to one of the coaxial feed lines, was periodically marked on the charts.

The individual responses of the integral on-path monitor, the modulator carrier test output, and the far-field monitor signals to changes in the transmitter modulation balance, sideband phase, sideband amplitude, and percent modulation are shown in Figure 11-127. From this figure it can be seen that while both the integral and far-field monitors were very responsive to changes in modulation balance and sideband amplitude, changes in sideband phase were best detected only by the far-field monitor, while changes in percent modulation were detected by the integral monitor. The modulator carrier test output responded to changes in modulation balance but showed almost no responses to changes in the other parameters.

Continuous recordings were made of the integral path and the far-field monitor channels at a recorder speed of 6 inches/hour. The charts for the period of September 18, 1975 through September 20, 1975 were reduced, using the monitor averaged over one hour to make the composite chart shown in Figure 11-128. As can be seen, the integral path monitor was very erratic, especially on September 18, and indicated an out-of-tolerance condition from 1400 hours to 1600 hours (Eastern Daylight Savings Time). Figures 11-129a,b,c are reproductions of the

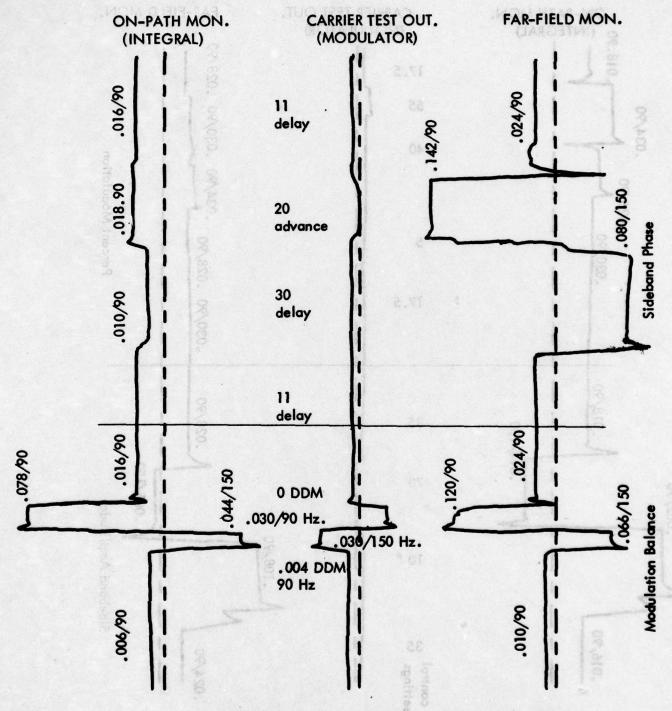
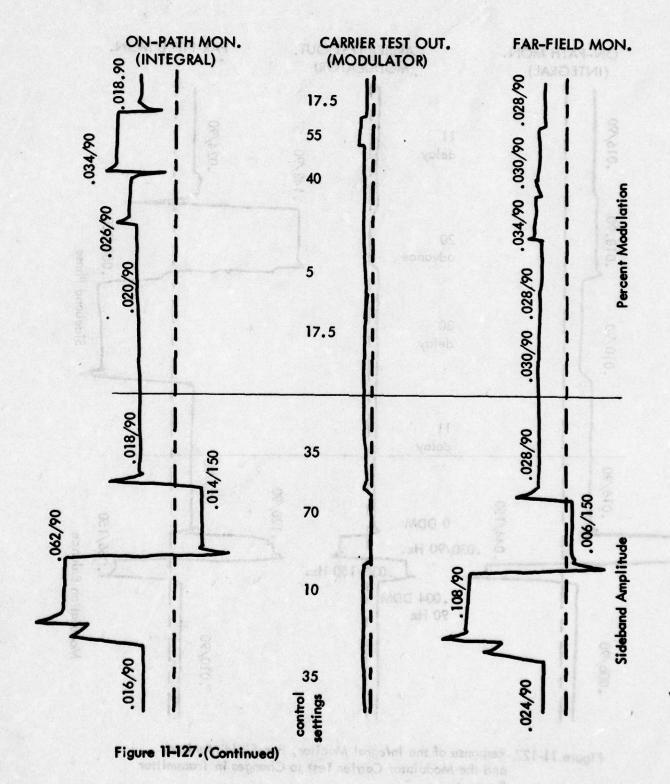


Figure 11-127. Response of the Integral Monitor, Far-Field Monitor, and the Modulator Carrier Test to Changes in Transmitter Parameters.



11-174

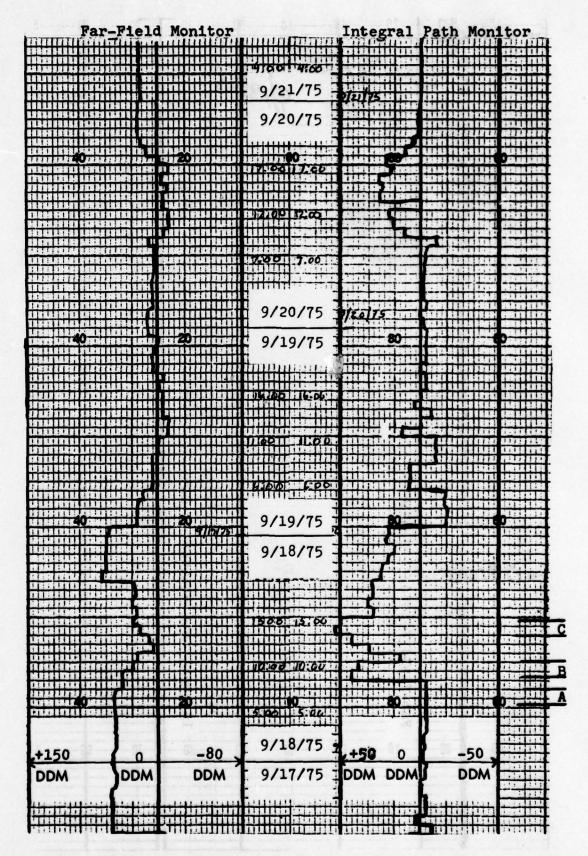


Figure 11-128. Monitor Response for the Period of September 18 to September 21, 1975.

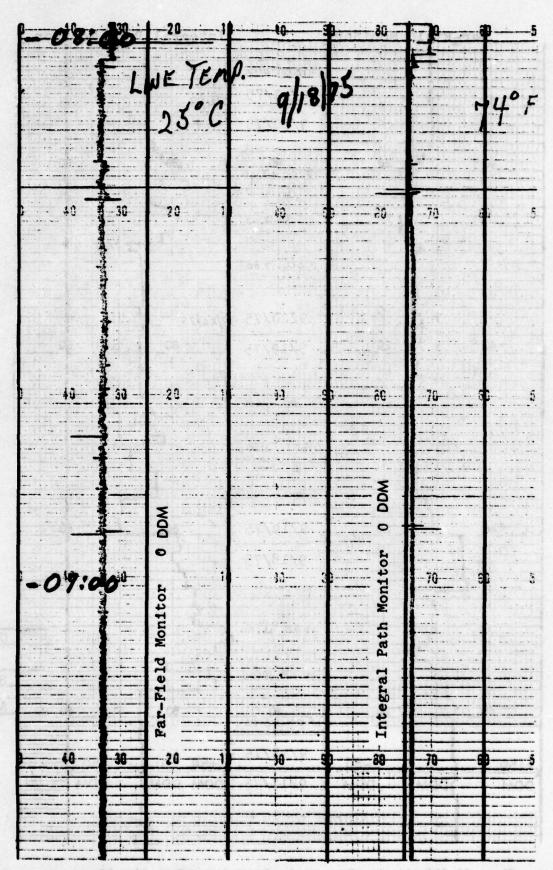


Figure 11–129a. Monitor Response, September 18, 1975, from 0630 hours to 0800 hours.

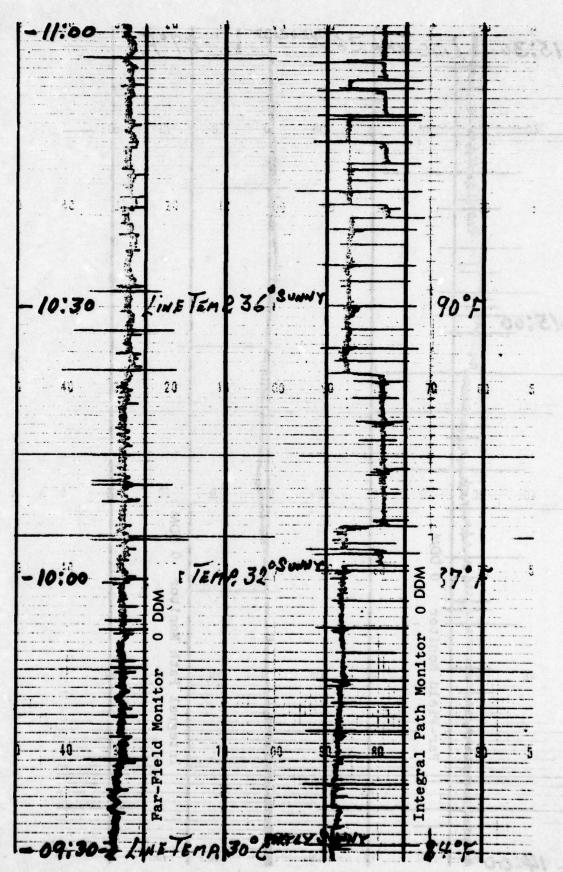


Figure 11-129b. Monitor Response, September 18, 1975, from 0930 hours to 1100 hours.

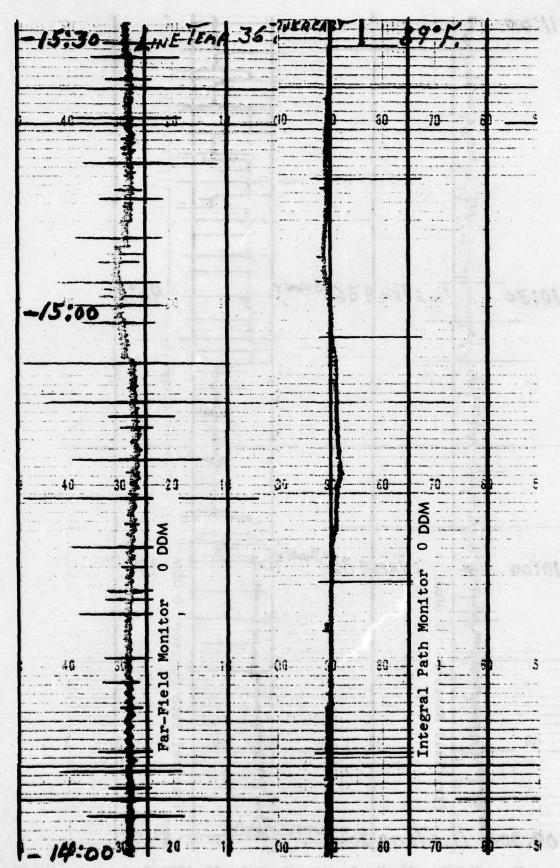


Figure 11-129c.

Monitor Response, September 19, 1975, from 1400 hours to 1530 hours.

actual chart recordings for the periods, marked A, B and C on Figure 11-128, from 0630 to 0800 hours, 0930 to 1100 hours, and 1400 to 1530 hours on September 18, 1975.

The far-field monitor was relatively stable over these periods, varying from a maximum of +0.060 DDM to a minimum of +0.012 DDM as measured from the far-field monitor 0 DDM reference line. In general, the far-field monitor did not exceed a 50% alarm condition.

The integral path monitor, while stable during the night and early morning hours, became very erratic during the daylight hours, exhibiting a series of random jumps as can be seen in Figure 11-129b. The monitor eventually drifted into the alarm condition as shown in Figure 11-129c. Also shown in Figures 11-129 a,b,c are random spikes on both the far-field and the integral path monitor channels. Some of the spikes in the far-field channel, and all of the spikes in the integral path channel, are due to the cycling on and off of a faulty transmitter hut airconditioner. The remaining spikes in the far-field channel were due to aircraft overflights of the glide-slope transmitting and the monitor receiving antennas.

Figure 11-130 is a reproduction of the far-field monitor RF level (Detector AGC Level) during the periods as indicated by A and C in Figure 11-128. As noted previously, the spikes are due to aircraft overflights and air-conditioner cycling. The stability exhibited in Figure 11-130 is typical of the stability exhibited in the RF channel over the entire monitoring period. The RF level consistently remained within ± 0.5 dB of the initial 0 dB reference setting.

Examination of the monitor charts from September 13 through October 3 indicated that a fault existed somewhere in the system that was causing the integral monitor to become erratic. It was clearly evident that the fault was temperature-induced since the integral monitor was stable during the cooler night hours and consistently became erratic around 0800 hours each morning when the equipment first received direct exposure from the sun. Thus, on October 4, 1975 the system was shut down so that the transmitter hut air-conditioner could be repaired. Due to a faulty motor, the unit was excessively loading the 60 Hz power line during compressor turn-on and turn-off. This loading was reflected through the power lines and the monitor power supply and showed up as spikes on the monitor recordings. Also, the air-conditioner was not providing a stable environment for the transmitting equipment. On October 21 the air-conditioner was returned to service and the monitoring resumed.

In order to isolate the fault, the below-path integral monitor, which is identical to the on-path integral monitor, was adjusted to provide a second on-path monitor channel which was then connected to the recording equipment. The transmitter carrier test output was also recorded as a check on the stability of the modulation balance. As illustrated in Figure 11–131, this second integral monitor exhibited jumps similar to those exhibited by the first monitor, except that the

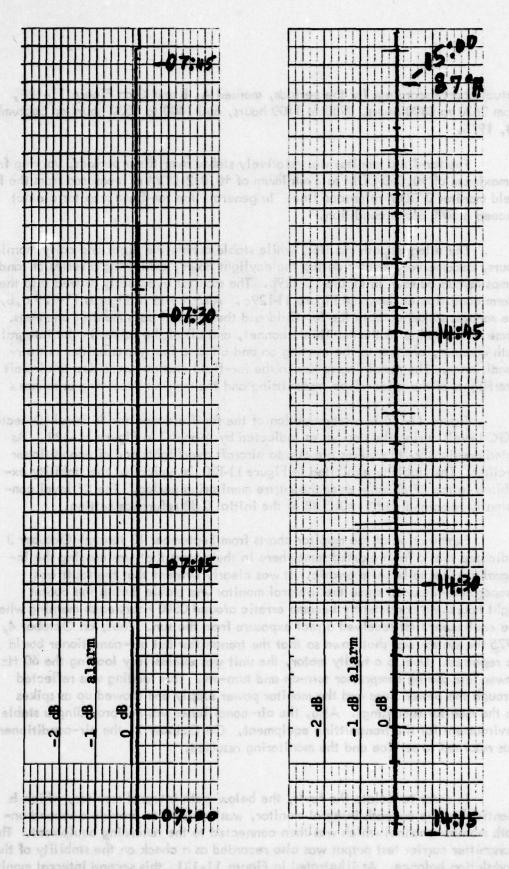


Figure 11-130. Far-Field Monitor RF Level, September 18, 1975.

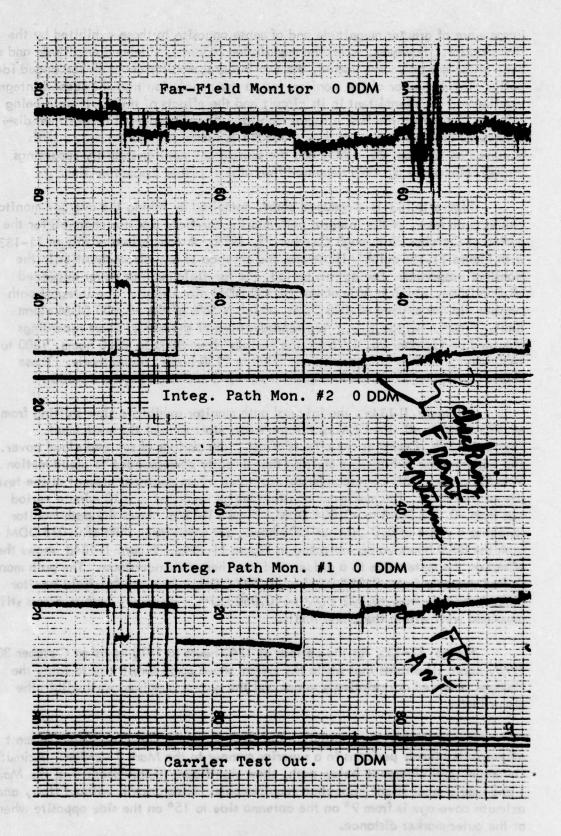


Figure 11-131. Effects Due to a Fault in the Monitor Circuit.

jumps were of greater magnitude and of sense opposite to those exhibited by the first monitor. However, when the modulation balance, sideband amplitude and sideband phase controls were varied, the two integral monitor channels responded identically. This behavior of the monitors led to the conclusion that the second integral monitor had an intermittent in its circuit and the effects of this fault were being reflected back into the first integral monitor. The second monitor was then disconnected and the feed ports dummy loaded as shown in Figure 11–132. This occurred on October 23, 1975, and the subsequent monitor stability recordings through November 3, 1975 remained free of any further discontinuities.

Figure 11-133 is a reduced chart, compiled by taking the average monitor values each hour, of the integral path and the far-field monitor channels for the period of October 26 through October 29, 1975. A comparison of Figure 11-133 with Figure 11-128 quickly illustrates the absence of any discontinuities in the monitors' responses. During this period, the far-field monitor never exceeded +0.055 DDM, which is 36% of the +0.150 DDM alarm limit. The integral path monitor did not exceed -0.028 DDM, which is 56% of the -0.050 DDM alarm limit. Figures 11-134a,b,c,d are reproductions of the actual chart recordings obtained on October 28, 1975 for the periods* from 0800 to 0930 hours, 1300 to 1430 hours, 1445 to 1615 hours, and 2000 to 2130 hours, respectively. These charts correspond to the periods marked A, B, C and D on Figure 11-133.

In Figure 11-134a, the integral path monitor exhibits a slow shifting from -0.023 DDM to -0.014 DDM as the sun's rays start to heat the equipment. Figure 11-134b illustrates the effects of alternate periods of sun and cloud cover. The path monitor exhibited a shifting that directly corresponded to cloud motion over the array. This correspondence was noted by an engineer present at the test site at that time. The maximum monitor change recorded in a 10 minute period was from -0.022 DDM to -0.004 DDM. Figure 11-134c shows the path monitor reaching a value of 0.0 DDM at 1500 hours, for a maximum shift of 0.025 DDM from the 0800 hours value indicated in Figure 11-134a. Figure 11-134d shows the effect on the system due to a sudden and very heavy thunderstorm. The path monitor shifted abruptly from -0.017 DDM to -0.027 DDM, while the far-field monitor shifted abruptly from +0.032 DDM to +0.060 DDM. However, both monitors still remained well within the alarm limits.

Figure 11-135, for the periods of 1240 hours to 1410 hours on October 30, 1975, again illustrates that while the system shows some sensitivity to rain, the changes observed are relatively minor and the system remained well within the alarm limits.

(12) Conclusions. The Mark 2, Watts End Fire System in most all respects clearly performs in a superior manner to the Mark 1 version. Azimuth coverage, and clearance below path, show significant improvement over the Mark 1 and would meet flight inspection requirements. Clearance is without flaw, and azimuth coverage is from 9° on the antenna side to 15° on the side opposite when at the outer marker distance.

^{*} Eastern Standard Daylight Savings Time.

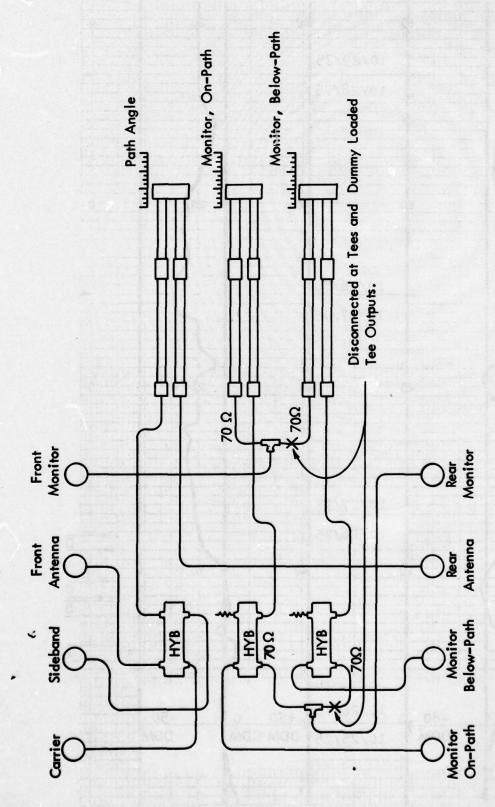


Figure 11–132. RF Cable Diagram for 2-Antenna End-Fire Glide Slope Junction Box Showing Where Faulty Below-Path Monitor is Disconnected.

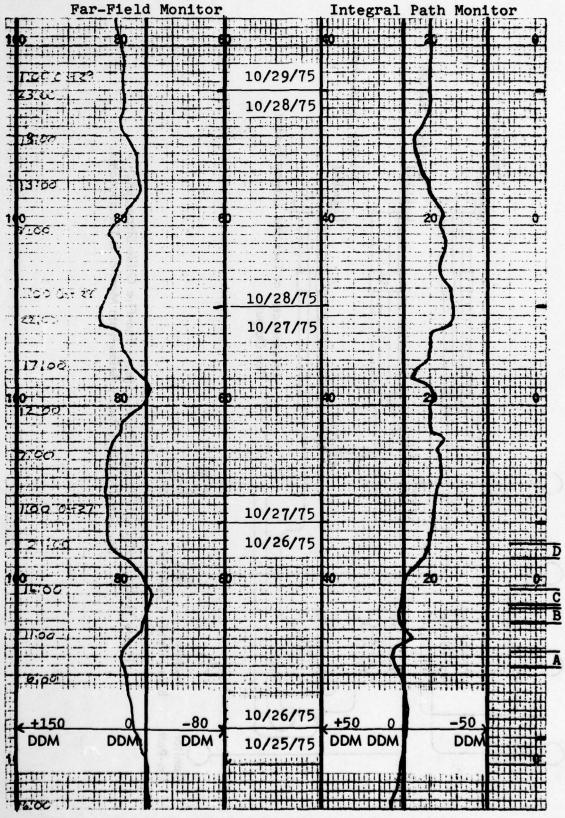


Figure 11-133. Monitor Response for the Period of September 26 to September 29, 1975.

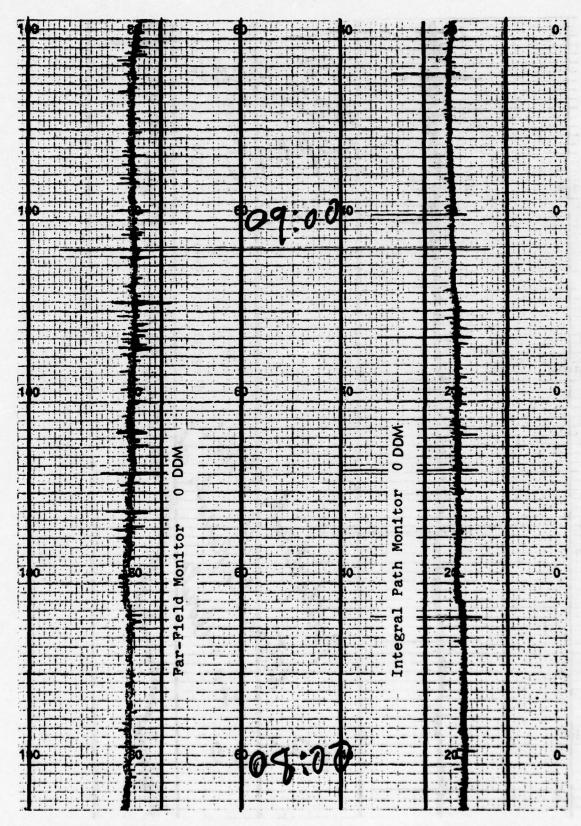


Figure 11-134a. Monitor Response, September 27, 1975, from 0800 hours to 0930 hours.

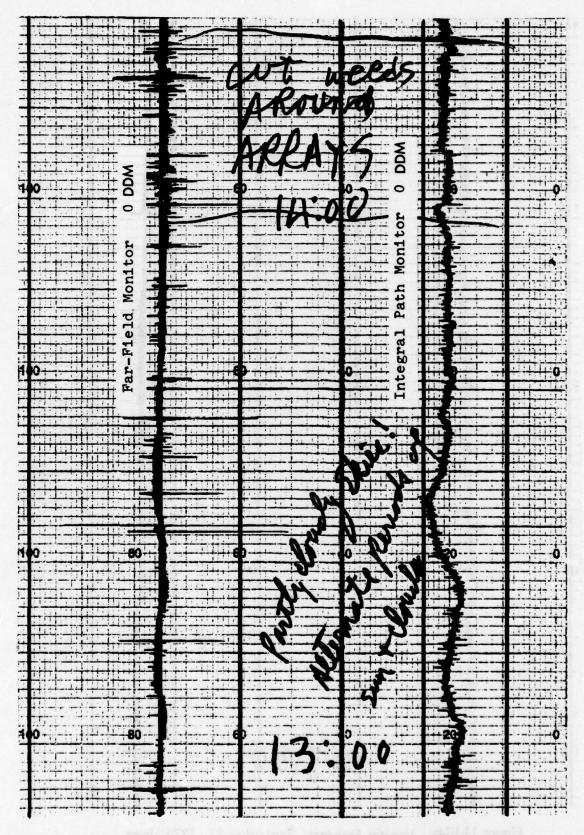


Figure 11–134b. Monitor Response, September 27, 1975, from 1300 hours to 1430 hours.

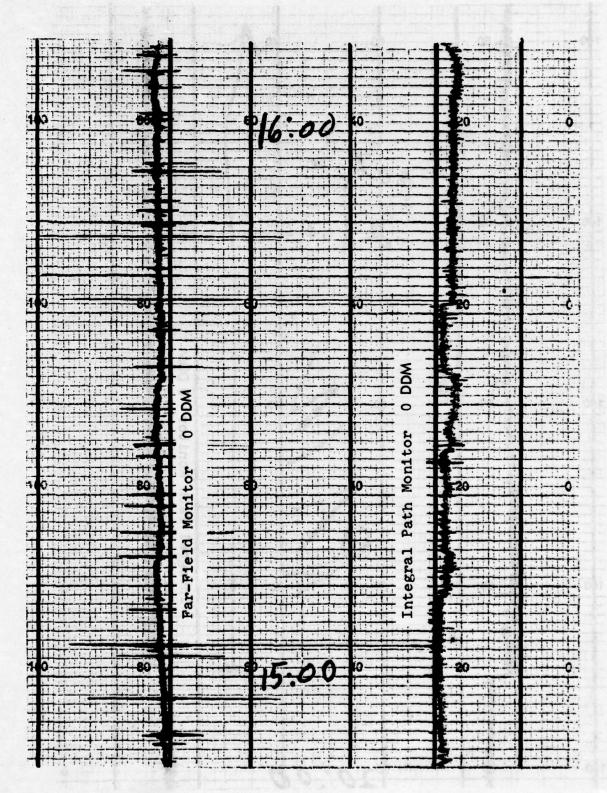


Figure 11-134c. Monitor Response, September 27, 1975, from 1445 hours to 1615 hours.

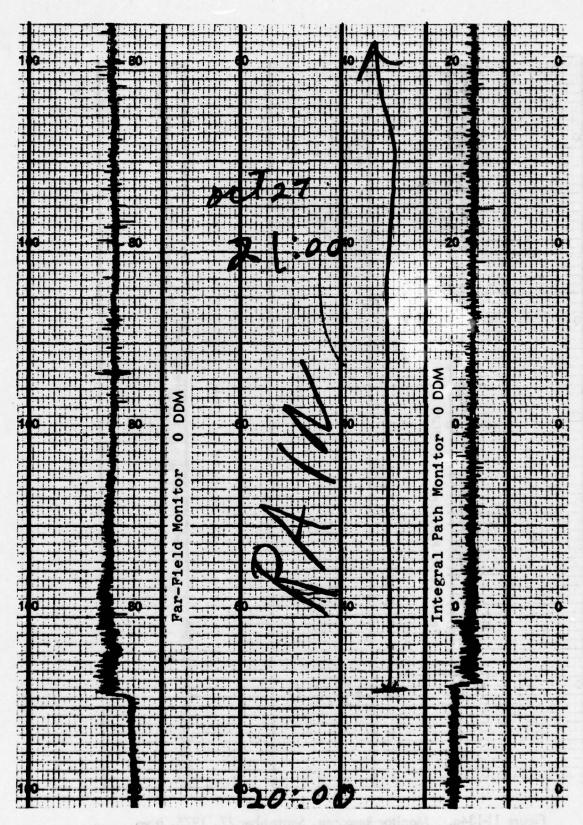


Figure 11-134d. Monitor Response, September 27, 1975, from 2000 hours to 2130 hours.

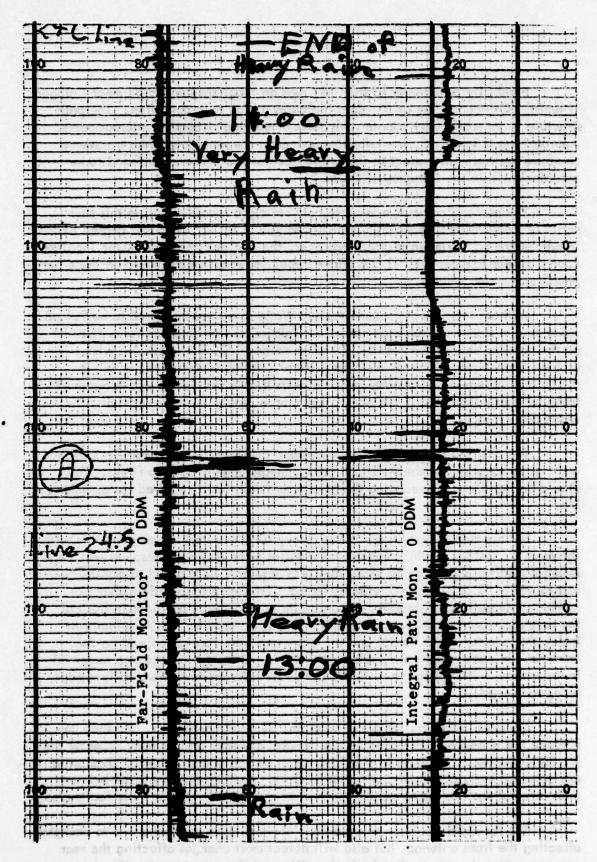


Figure 11–135. Monitor Response, September 30, 1975, During Varying Rain Conditions.

Flyability as determined from RTT runs on localizer centerline meet Category II limits. Off-centerline at 5° data indicates a high path condition. The path structure is generally very smooth with noise amounting to about 2 microamperes. Approaching ILS point C, irregularities appear in the path due to the transverse structure skewed with respect to the runway centerline. These are found to be contained within the Category II limits.

The perpendicular or transverse path structure recorded during this first series of measurements lacks high quality because of a .17° slope per degree azimuth in part of the $\pm 5^{\circ}$ azimuth sector. However, the angles either side of the localizer course appear to meet the 7-1/2% flight inspection requirement based on these perpendicular measurements.

Without the reflector elements, the Watts array was measured to be 9.6 dB lower than a sideband reference antenna. This value was obtained for a point 8° on the antenna side of the runway, 10 miles range, 1500 feet altitude, where usable distance measurements are most critical. An absolute value, which is difficult to determine accurately because of available standards, was determined to be 50 hard microvolts at this point, assuming a dipole in space receiving the Watts array signal.

The antenna system with linear antenna configuration is readily established and can be extensively checked with ground measurements prior to flight. This should be significant in reducing the number of flight hours required for commissioning.

For the first time with the Watts array, field monitoring was available with the Mark 2. Initial findings showed the monitor to be generally responsive. Two integral monitor channels plus three far-field detectors were found to monitor satisfactorily 32 of 37 fault conditions tested. Of the five conditions that exhibited an unsatisfactory monitor response, three were truck positions in front of the antennas carefully selected to exhibit a monitor response that remained just inside the monitor alarm limits, and the other two were foreign objects on the antenna. In each case, path angle and width in the far-field air space remained in-tolerance, with the structure limits and 7.5% tolerances at the localizer edge being exceeded.

Changes in transmitter signal strength, percent modulation, and tone unbalance are adequately detected by the integral monitors and in many cases by the far-field monitors. Changes in sideband power and sideband to carrier dephasing are detected best, at present, with the far-field monitors; however, the belowpath integral monitor set to monitor path width should then detect these faults also.

The far-field monitor, as expected, appears to be most sensitive to changes affecting the front antenna, but also will detect most changes affecting the rear antenna. Disturbances to the physical positions of the antennas, or reflectors, as might be expected are detected only by the far-field monitors.

The integral monitors are sensitive only to changes in the transmitted signal and could be eliminated if the glide slope transmitter has self-monitoring capabilities. However, in this Mark 2 design the integral monitor is needed.

From the results of faults \$28 and 29, it is imperative that the area around the arrays be kept clear of obstructions such as high weeds, attention be given both to the possibility of a flock of birds roosting on an antenna element similar to that seen quite frequently on telephone and power lines, and to the effects of ice accumulating on the antennas. Vehicular traffic around the array must be controlled. If access to the glide slope transmitter hut must be made from the runway, then the best place for the access road would be from the runway, behind the rear antenna, and then to the side of the transmitter hut away from the runway. The shortest route is along a line from the runway to the transmitter hut that goes through the array phase center. This route will cause some disturbance to the signal in space, but this disturbance is well within tolerance limits. However, no vehicle should be cleared to use this route if an aircraft is on final approach. Finally, any access route that may be placed ahead of the front antenna must be at least 125 feet forward of the front antenna. From the results shown in Table 11-9 and in Figure 11-125 no vehicles must be permitted within the area extending from the antenna out to a distance of 125 feet forward of the antenna. Vehicle presence in this area, as well as in the area between the two antennas, must be met with appropriate restrictions on the use of the glide slope.

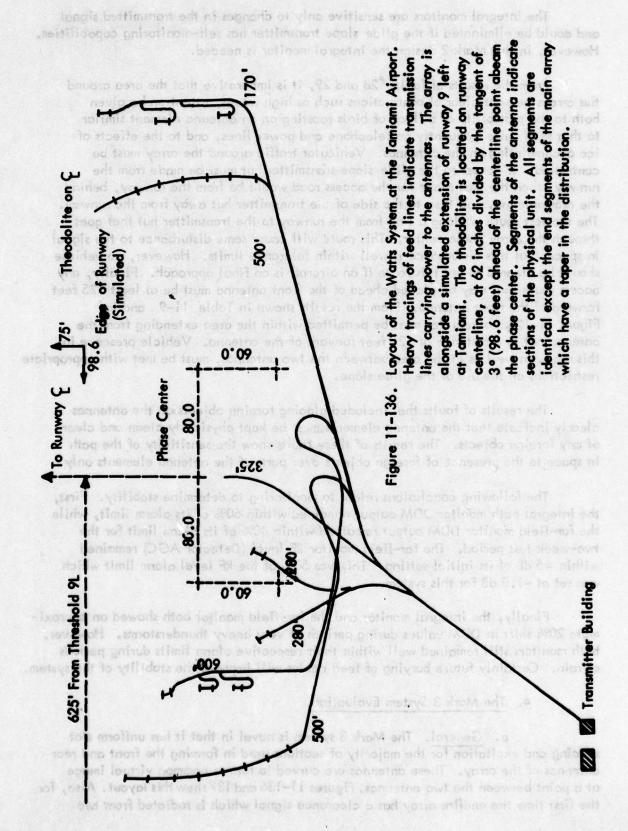
The results of faults that included placing foreign objects on the antennas clearly indicate that the antenna elements must be kept physically clean and clear of any foreign objects. The results of these faults show the sensitivity of the path in space to the presence of foreign objects over parts of the antenna elements only.

The following conclusions relate to monitoring to determine stability. First, the integral path monitor DDM output remained within 60% of its alarm limit, while the far-field monitor DDM output remained within 40% of its alarm limit for the two-week test period. The far-field monitor RF level (Detector AGC) remained within ± 5 dB of its initial setting. This was 50% of the RF level alarm limit which was set at ± 1.0 dB for this system.

Finally, the integral monitor and the far-field monitor both showed an approximate 20% shift in DDM values during periods of very heavy thunderstorms. However, both monitors still remained well within their respective alarm limits during periods of rain. Certainly future burying of feed cables will improve the stability of the system.

4. The Mark 3 System Evaluation.

a. General. The Mark 3 system is novel in that it has uniform slot spacing and excitation for the majority of sections used in forming the front and rear antennas of the array. These antennas are curved to form a common virtual image at a point between the two antennas. Figures 11-136 and 137 shew this layout. Also, for the first time the endfire array has a clearance signal which is radiated from two



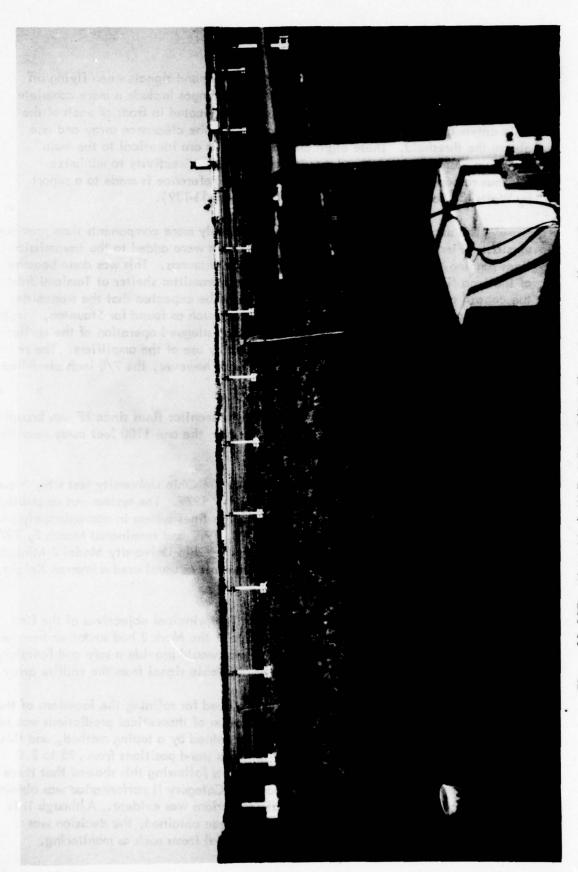


Figure 11-137. Watts Mark III End-Fire Glide Slope Array Installed at Tamiami.

separate slotted cable elements to give fly-up command signals when flying off localizer centerline more than 8°. Additional changes include a more complete monitor system using three slotted-cable sections located in front of each of the main antennas (see Figure 11-138), one in front of the clearance array and one abeam the threshold. These eight antenna sections are identical to the main radiating element sections and provide considerable directivity to minimize spurious responses to causes such as overflights. Reference is made to a report by Watts [3] for details of the monitor (see Figure 11-139).

The experimental system contains noticeably more components than previous versions. First, in-line amplifiers with 18 dB gain were added to the transmission lines running to each of the main and clearance antennas. This was done because of the long line (200 feet) needed to reach the transmitter shelter at Tamiami from the central part of the array. Normally it would be expected that the transmitter building would be near the midpoint of the array such as found for Staunton, Virginia tests in 1974. Since marginal signal strength had plagued operation of the earlier arrays, Watts decided to eliminate this problem by use of the amplifiers. The reflectors added to the Mark 2 continue to be used; however, the 7/8 inch air-filled feed lines were replaced with 1/2 inch lines.

Amplifiers with 34 dB were placed in the monitor lines since RF was brought back to the shelter from each of the pickups, even the one 1100 feet away near the threshold.

The complete system arrived by truck at the Ohio University test site, New Tamiami Airport, Miami, Florida on February 14, 1977. The system was assembled and installed with the monitoring and transmission lines system in approximately one week. Flight measurements began February 23, 1977 and terminated March 2, 1977. A Beechcraft Model 35 aircraft was used with the Ohio University Model 2 Minilab to collect some 92 flight records. All measurements as usual used a Warren Knight WK 83 theodolite, RTT reference.

b. <u>Discussion of Experiments</u>. The principal objectives of the first series of flight measurements were to determine if the Mark 3 had smoother transverse course structures and whether a clearance signal would provide a safe and functional means of effectively widening the sector of available signal from the endfire array.

The first set of measurements showed a need for refining the locations of the transmitting antenna inasmuch as good duplication of theoretical predictions was not evident. The original locations had been determined by a taping method, and this was rechecked resulting in adjustment of antenna stand positions from .75 to 2.0 inches throughout the array. Flight measurements following this showed that there was significant improvement such that marginal Category II performance was obtained and reasonable duplication of theoretical predictions was evident. Although it is believed that further improvement could have been obtained, the decision was made that time could be best spent on more crucial items such as monitoring.

antenna array incidental to the experiments is seen in the background. (Photo by C. Watts) Figure 11–138. Shown in the Foreground Are Three Slotted-Cable Monitor Antennas Serving the Rear Antenna Which Is Partially Evident. A capture effect

Figure 11-139. Watts Mark III Glide Slope Array.

The first measurements were run with the monitor pickup antennas placed on the ground to avoid any possible contamination of far-field patterns. Following these tests the monitor antennas were mounted on stands identical to those for the array and the far-field was again checked. No measureable effects were found, except the field strength observed with the threshold pickup was reduced by 1 dB.

Other experiments included variation of the phase in the main antenna line and change of the sideband power. These permitted calibration of the monitor system in terms of far-field path angle and width changes.

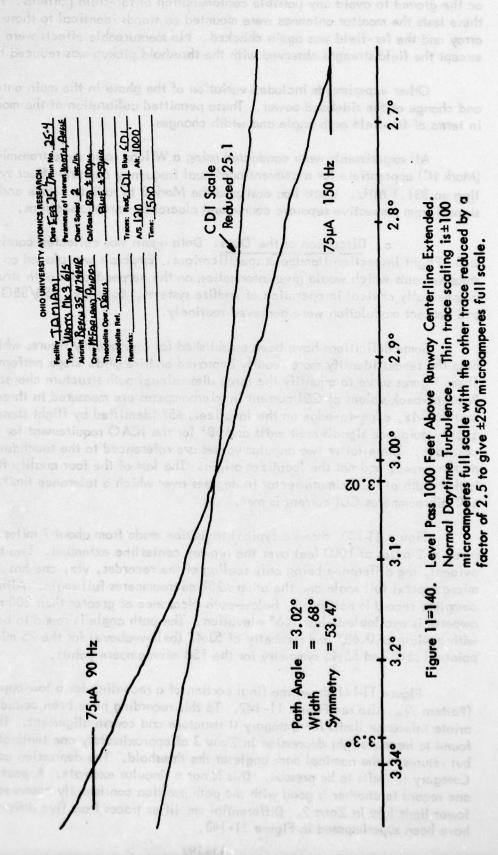
All experiments were conducted using a Wilcox solid state transmitter system (Mark IC) appropriate for a conventional dual frequency capture-effect system operating on 331.1 MHz. Watts had designed the Mark 3 to radiate course and clearance signals from respective separate course and clearance antenna sections.

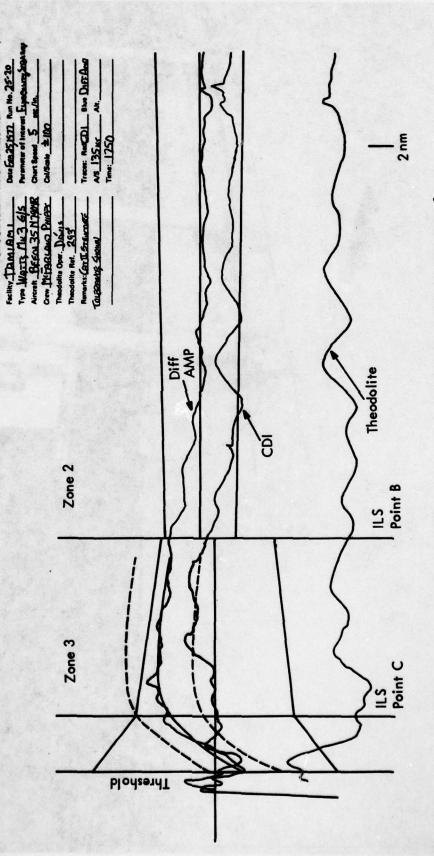
c. Discussion of the Data. Data again was collected consistent with U.S. Flight Inspection Handbook specifications. Emphasis was placed on additional measurements which would give information on the perpendicular path structure which is especially critical in operation of endfire systems. Equality, CSB/SBO phasing, and percent modulation were achieved routinely.

Some definitions have been established for four quality figures which may help the reader identify more readily improved endfire glide slope performance. These figures serve to quantify the three dimensional path structure characteristics. Peak-to-peak values of CDI current in microamperes are measured in three azimuth sectors, viz, edge-to-edge on the localizer, $\pm 5^{\circ}$ identified by flight standards where quality guidance signals must exist and $\pm 8^{\circ}$ for the ICAO requirement for path coverage. These latter two angular values are referenced to the touchdown point on the runway and not the localizer origin. The last of the four quality figures is the width of the azimuth sector in degrees over which a tolerance limit of ± 30 microamperes CDI current is met.

Figure 11–140 shows a typical transition made from about 7 miles from the array to 2 miles at 1000 feet over the runway centerline extended. Two traces are evident, the difference being only scaling of the recorder, viz, one has ± 100 microamperes full scale and the other ± 250 microamperes full scale. Although the complete record is not shown, below-path clearance of greater than 200 microamperes is available below 1.6° elevation. The path angle is found to be 3.02° with a width of 0.68° and symmetry of 53:47 (below-above) for the 75 microampere points; 1.51° and 55:45 symmetry for the 150 microampere points.

Figure 11-141 shows the final portion of a recording for a low approach (Pattern A). Also see Figure 11-142. To this recording have been added the appropriate tolerance limits for Category II structure and course alignment. The path is found to have a slight depression in Zone 3 of approximately one tenth of one degree but returns to the nominal path angle at the threshold. The depression causes the Category II limits to be pressed. This is not a singular example. Repeatability from one record to another is good with the path position consistently observed near the lower limit late in Zone 2. Differential amplifier traces from five different runs have been superimposed in Figure 11-143.





OHIO UNIVERSITY AVIONICS RESEARCH

Figure 11–141. CDI, Theodolite, and Differential Amplifier Recordings from Run 25–20. From the tolerance limits shown it is evident that Category II tolerances are met for these parameters.

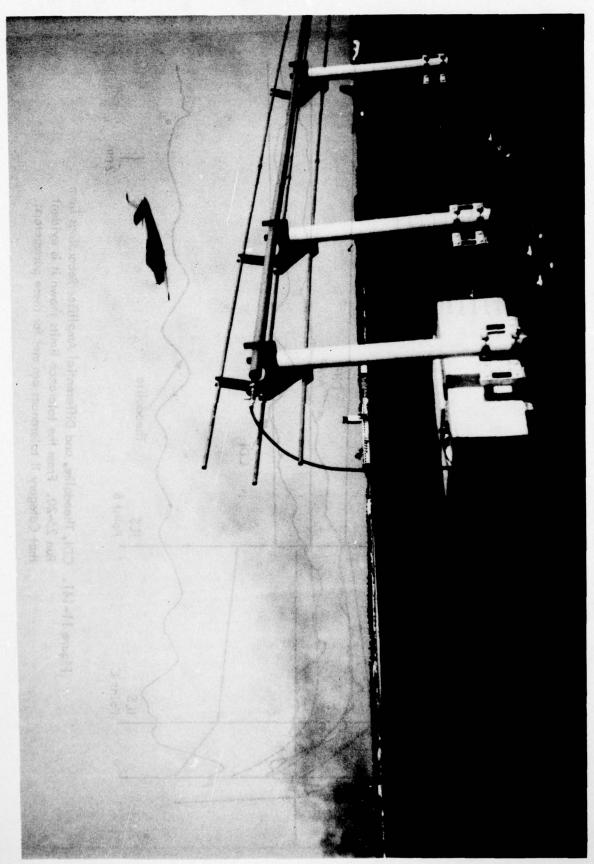


Figure 11-142. Completion of a Pattern A Run With the Bonanza 35 Aircraft During Watts Mark III Testing at Tamiami.

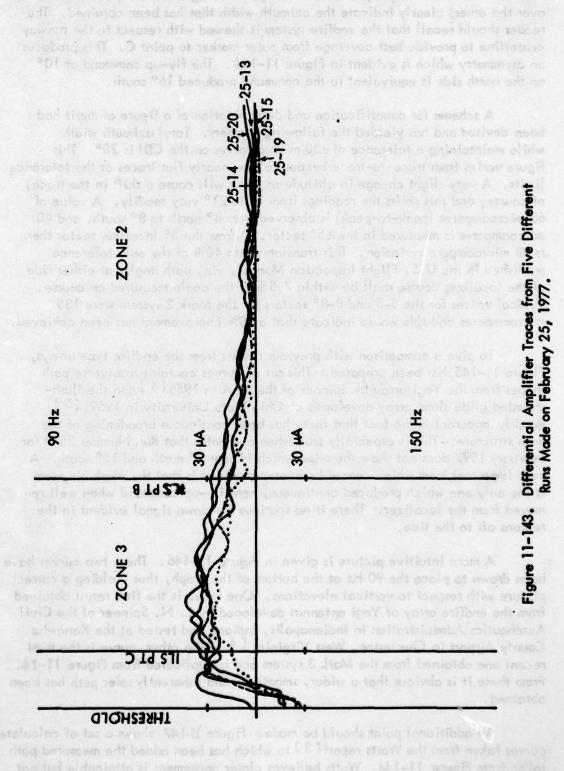


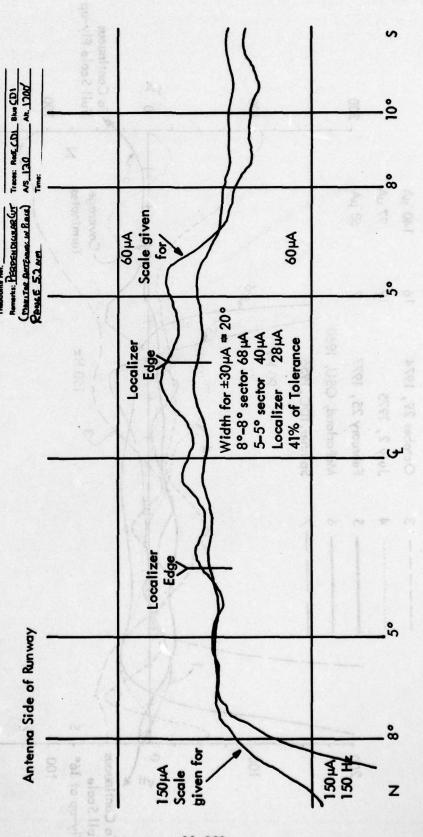
Figure 11-144 reveals the principal improvement that has been obtained with the Mark 3. These very repeatable traces (one having a scale expansion of 2.5:1 over the other) clearly indicate the azimuth width that has been obtained. The reader should recall that the endfire system is skewed with respect to the runway centerline to provide best coverage from outer marker to point C. This produces an asymmetry which is evident in Figure 11-144. The fly-up command at 10° on the north side is equivalent to the command produced 16° south.

A scheme for quantification and determination of a figure of merit had been devised and has yielded the following numbers. Total azimuth width while maintaining a tolerance of ± 30 microamperes on the CDI is 20° . This figure varies from trace-to-trace because of the nearly flat traces at the tolerance limits. A very slight change in altitude or track will cause a shift in the trace, of course, and this shifts the readings from 16 to 21° very readily. A value of 68 microamperes (peak-to-peak) is observed from 8° north to 8° south, and 40 microamperes is measured in the $\pm 5^\circ$ sector. Across the 5° localizer sector there is 28 microampere variation. This translates into 40% of the only tolerance published in the U.S. Flight Inspection Manual, viz, path angles at either side of the localizer course shall be within 7.5% of the angle measured on course. Typical values for the 5-5 and $8-8^\circ$ sectors for the Mark 2 system were 135 microamperes and this would indicate that a 50% improvement has been achieved.

To give a comparison with previous results from the endfire type arrays, Figure 11–145 has been prepared. This set of curves contains transverse path shapes from the Yagi array by Spinner of the CAA in 1956 [4] and the flush-mounted glide slope array developed at Ohio State University in 1959. [5] Readily apparent is the fact that there has been continuous broadening of the path structure. This is especially true when one notes that Run Number 25–9 for February 1977 does not show the edge which is near 9° north and 15° south. A very important item which cannot be overemphasized is that the Mark 3 system is the only one which produced continuous, hard fly-up command when well removed from the localizer. There is no spurious fly-down signal evident in the regions off to the side.

A more intuitive picture is given in Figure 11–146. These two curves have been drawn to place the 90 Hz at the bottom of the graph, thus yielding a correct picture with respect to vertical elevations. One curve is the first result obtained from the endfire array of Yagi antennas developed by L. N. Spinner of the Civil Aeronautics Administration in Indianapolis, Indiana and tested at the Kanawha County Airport in Charleston, West Virginia. [4] The other curve is the most recent one obtained from the Mark 3 system and is duplicated from Figure 11–144. From these it is obvious that a wider, smoother, and inherently safer path has been obtained.

An additional point should be made. Figure 11–147 shows a set of calculated curves taken from the Watts report [3] to which has been added the measured path taken from Figure 11–144. Watts believes closer agreement is attainable but not easily so when the antenna supports must be placed directly on irregular sod surfaces.



Deto EES S 1977 Run No. 25-9

OHIO UNIVERSITY AVIONICS RESEARCH

Chart Speed sec./in.

Nicoral BEELU 35 N 7904R

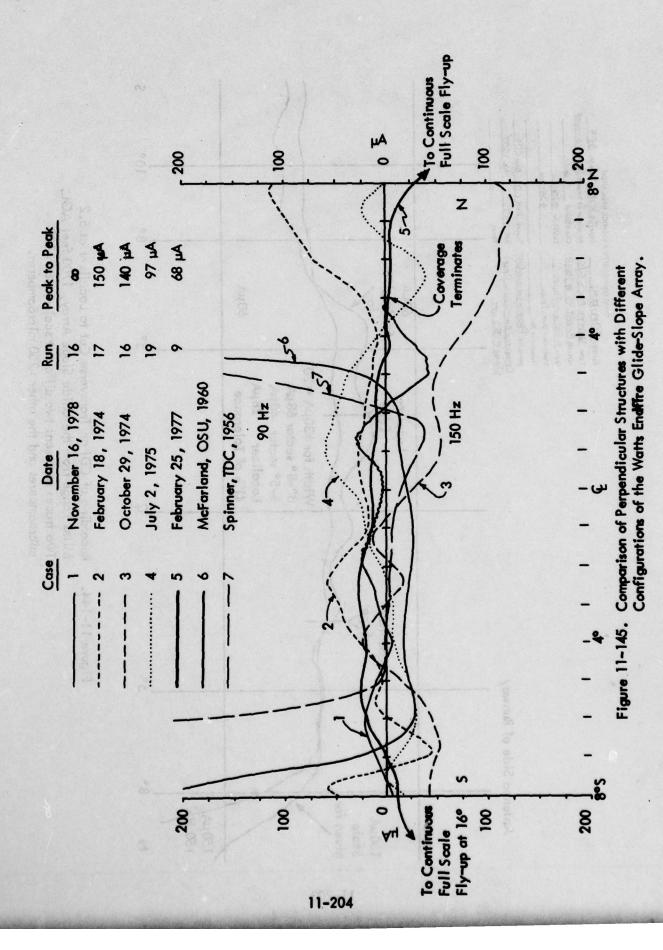
Com Pringuenn Pulps

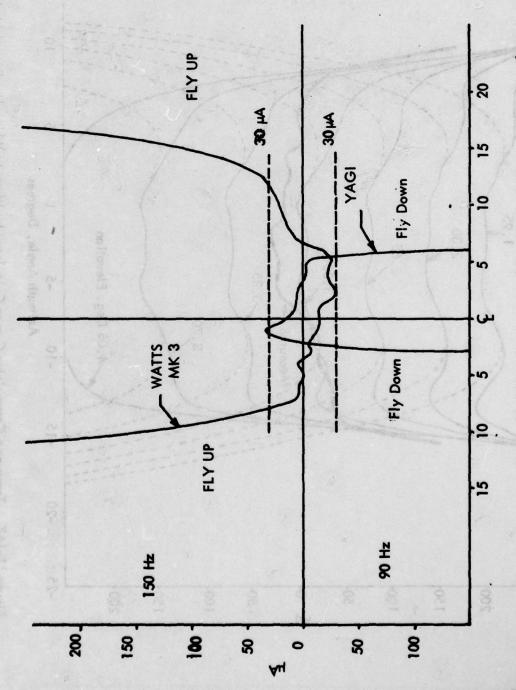
Theodolite Oper. Days

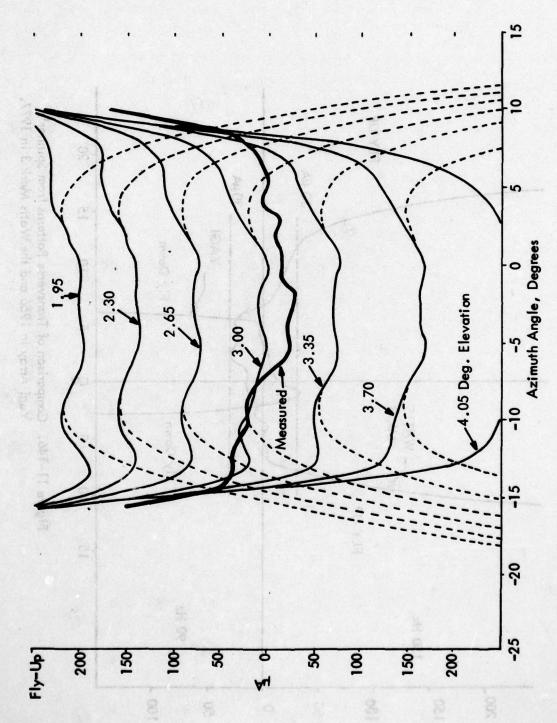
Tree WASTS PK36/5

Caiscale \$100,000

Figure 11-144. Recording of CDI on Transverse Cut to Localizer at 5.2 Miles Range from the Glide Slope Array, 1700 feet AGL. Two traces represent two different scales, one ±100 microamperes and the other ±250 microamperes.







Transverse Crosspointer Curves Calculated by Watts to Which Has Been Added the Measured CDI Values During a Perpendicular Cut, Run 25-9. All are for a distance of the outer marker. Figure 11-147.

Field strength (usable distance) is more than adequate. Measurements showed that the Minilab system reached threshold of signal operation at 10 miles, 1500 feet with 25 dB of attenuation which indicates that the signal level is better than 7 dB above FAA minimum requirements of 15 microvolts. No current standard was available on site for reference.

Below-path clearance measurements indicate that a minimum of 205 microamperes of 150 Hz signal exists at 1° elevation from 6 miles to the threshold.

d. Monitor Investigation for the Mark 3. The emphasis was placed on determining and, when necessary, improving the performance of the monitoring system. This was done by monitoring the stability of the system and observing response of the monitor to deliberate and accidental faults in the system. Two principal items of concern are, therefore, stability and representativeness.

During the period from March 14 to May 12, 1977, additional measurements were made on the Watts slotted-cable endfire Mark 3 glide slope system. The major objective of this work was to examine the operation of the endfire system with respect to monitoring capability and effectiveness. In the process several specific deficiencies were identified and corrective measures were implemented by the Watts Company to overcome these. A Wilcox Mark I transmitter was used at a frequency of 331.1 MHz. As before, the airborne measurements were made using a Beechcraft Model 35 with the Ohio University Minilab II. Calibrations were performed with standards on hand at the Ohio University FAA-Approved Repair Station.

The investigation naturally became involved with stability of the system including component performance and faults over time periods amounting to nearly two months. All of the effort was directed towards evaluating the system as it would eventually operate in a practical environment.

The monitor investigation began by first establishing alarm limits on path angle and width through the straightforward use of changes in the feed line length and changes in sideband power respectively. Once these limits were established, specific faults were introduced in the antennas and the environment until a monitor showed a near-alarm condition. Flight measurements were then made to determine whether flight inspection tolerances had been exceeded.

e. Monitor Investigation. First, it was clear very early in March that the stability of the glide slope system was not satisfactory. Both the path conditions and the monitor were suffering from the fact that the unusually long, exposed feed lines from the transmitter building connecting to the antennas and the monitor antennas were producing serious problems in maintaining the system. Immediate action was taken by the Watts Prototype Company to alleviate the problem by (1) installing the monitor combiner in the field near the geometrical center thus reducing the lengths of three pairs of phase sensitive monitor cables from 720 feet

to 310 feet, and (2) replacing the foam-filled cable with the more phase-stable Spiroline. This stabilized the monitors which allowed a better tracking of the path angle over a period of time.

Unfortunately the sensitivity of the path angle to temperature change of the transmission lines was not eliminated. These lines rested on top of the ground and experienced a change estimated to be at least 50°F between the early morning hours and the bright noon sun. On days when it was cloudy, changes of less than 0.05° were observed.

Indications were that the path plus monitor drift would amount to approximately 300% of alarm limit, whereas after the modifications were made to the monitor lines, the observed drift was principally path, with typical diurnal excursions up to 90% of alarm limits.

Second, a series of approximately 28 discrete faults were introduced sequentially in the transmitting system. These included transmitter changes, foreign objects on the antenna and a truck parked at various locations in front of the antennas. The attempt was made to bring the system just to alarm* and then measure the far-field angle and width plus the perpendicular structure.

Monitor alarm limits were set by adjustment of path angle to $\pm 0.2^{\circ}$ with the line phaser and a broadening of 0.2° with sideband power reduction. There was insufficient sideband power at the transmitter to give a 0.5° width so that the monitor was merely set to a symmetrical sharp value.

The fault testing took place over a period of 3 days during which time a temperature difference of 30°F was experienced and this caused the reference path position to drift as much as 0.3°. This was taken into account in reducing the data shown in Table 11-10.

The foreign object positions and the truck positions are defined relative to the transmitting and monitor antennas in Figure 11-148. The truck is a Dodge Van 16.2 feet long and 6.7 feet high. The foreign objects consisted of several layers of wet cloth draped over the antenna at the positions designated in Figure 11-148. The layers were made sufficient in number to cause the monitor to approach the alarm limit. In certain cases the alarm limit was exceeded accidentally.

The absence of the clearance transmitter allows the hard fly-down to be observed beyond 7° on the north side and beyond 15° on the south and produces an alarm, of course. This is shown in Figure 11–149. The significance of adding the clearance signal can be observed by comparing this figure with Figure 11–150. Although the structure near the localizer is not affected, it is believed important from a safety consideration that fly-up command in regions away from the approach

^{*} The path alarm limit was set by moving the line phaser to the front antenna until the aircraft measured a change of 0.20° in path angle, and the width alarm was set by changing the sideband power until a 0.20° change in path width was observed.

Fault	Run .	Angle	Width	Structure	% Mon. Path Aperture	Mon. Width (Thresh.)	Remarks on Perpendicular Structure
Nominal	26-13	2.97	69.	42%	0	0	
Feed Line Phase +	26-7	2.81	.75	•	100	29	
Feed Line Phase -	26-8	- 3.19	.63	19	100	29	
SBO Power Decrease	26-5	3.02	8.	•	•	100	
Tone Unbal	12-29	3.17	89.	•	100	40	
Tage Unbal	12-30	2.80	.73	- 68	-100	53	Salar section to the section of the
SBO/CSB Phasing +	12-31	3.01	87.	100	-18	100	
SBO/CSB	12-32	2.93	22.		5	-100	
Clearance Power - dB	12-20	×	×	%69	×	×	AP theid allegeded gio
Clearance Power +1 dB	12-16	×	×	21%	×	×	ricProteIG solo
Power +3dB	26-15	2.96	17.	26%	ω	0	7 U U U U U U U U U U U U U U U U U U U
Poeign 1*	26-17	3.04	.73	100%	+116**	-127	Osci Ilatory South Side
2	26-19	3.06	92.	44%	+138	-120	Good
3	26-21	2.65	.82	81%	88	95	Oscillatory North Side. Although
	29-50	10.50	P	96890	100	80.7	path angle appears to be out-of- tolerance, the monitor indicated a
6	56-53	2 22	åV.	35.05	8	1 8	2.85° value at this time. Final flight check value was 2.71° due to drift.
4 6 10916	26-23	2.79	.79	%95	φ	4	Small Oscillations N

*See Figure 11-148 for location of specific fault. **|

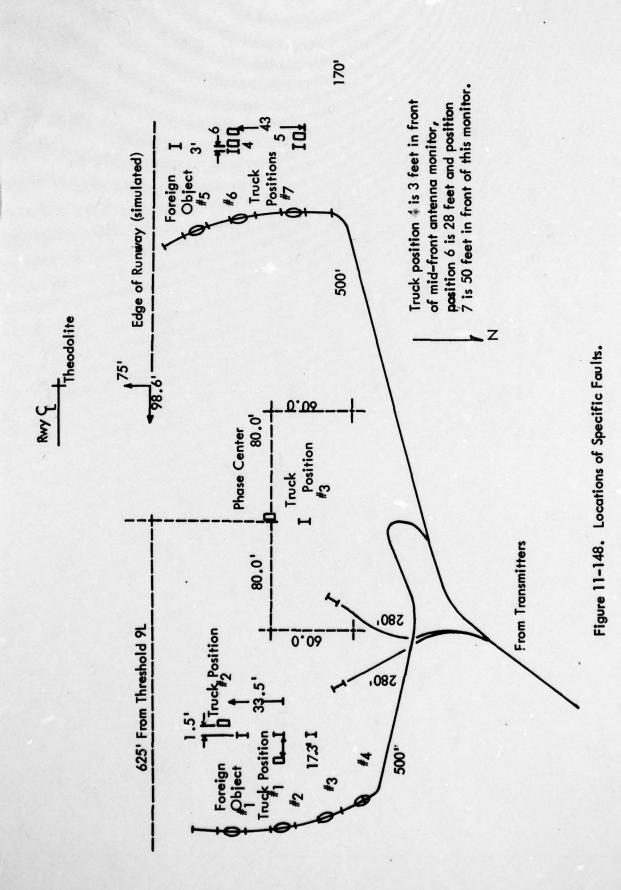
**Note monitor % has been nominalized to a no-fault condition to eliminate path drift effect.

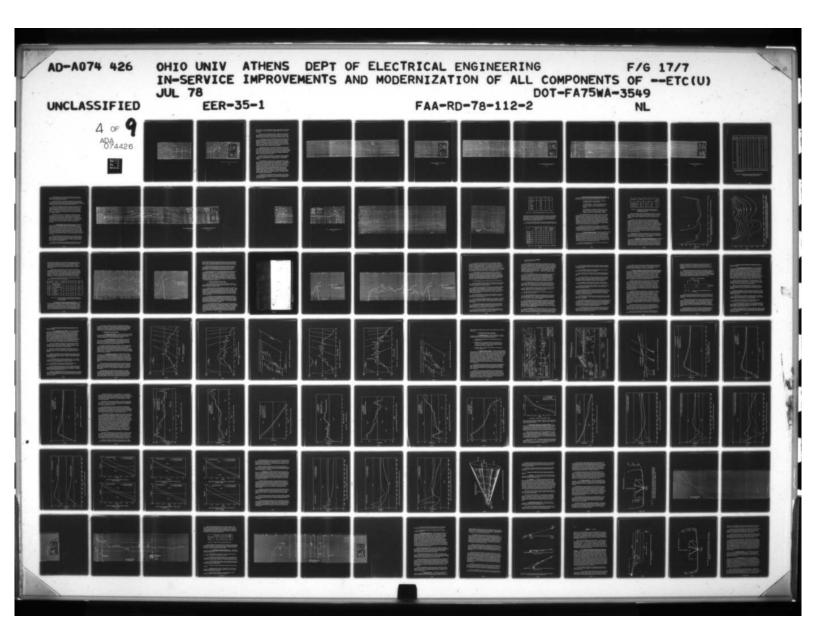
Table 11-10. Responses to System Faults.

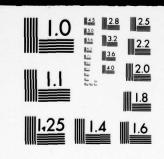
Fault	Run	Angle	Width	Structure	% Mon. Path Aperture	Mon. Width (Thresh.)	-2.3
Object 5	26-25	2.88	٤.	85%	-188	164	Oscillatory South
9	26-27	2.73	.76	48%	-25	20	Essentially Nominal
7	26-29	2.84	22.	%69	146	108	Oscillatory North
Truck Position 1*	28-6	3.25	99.	86%	. 46	100	3 Large Oscillations
	28-8	3.02	г.	39%	4	3	Minimal Effect
6	28-10	3.17	99.	25%	4	8	No Effect
* The second	28-12	3.18	59.	107%	8	9	Major Distortion
5	28-14	3.03	79.	%62	0	9	Major Deformation North Side
9	12-22	10.8	99	%88		100	Moderate Oscillations Over Entire Azimuth Sector
Tage Inde	12-28	3.00	.73	%68	100	33	Moderate Oscillations Over Entire Azimuth Sector (Little Change from 6)
Rear Ant Atten 4dB	12-35	3.02	.74		18	-100	
Rear Ant Displacement	26-11	3.08	29.	38%	73	80	
High angle with phasor and broad with low SBO No. 1 12–33	n phasor and SBO No. 1 12-33	3.14	.84	45.00	100	33	
High angle with phasor and broad with low SBO No. 2 12–34	h phasor and SBO No. 2 12-34	3.12	1.00	sighour 12	45	100	ОТ

*See Figure 11-148 for location of specific fault.

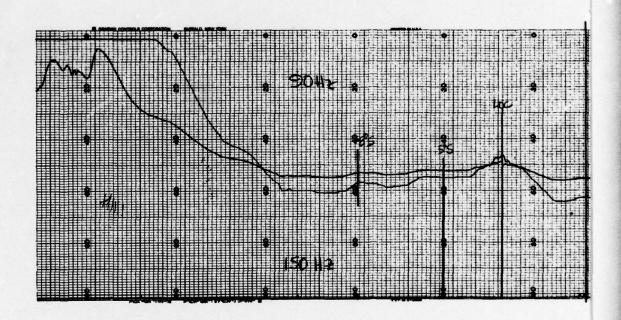
Table 11-10, Responses to System Faults (Continued).







MICROCOPY RESOLUTION TEST CHART



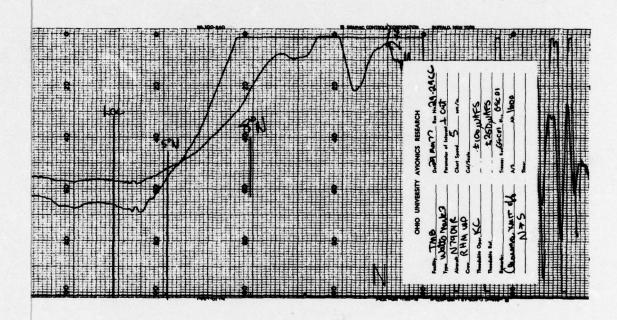


Figure 11-149. Transverse Path Structure in the Absence of the Clearance Transmitter

11-213/11-214

path is desired. If one were considering a design of a glide slope with no restrictions as to form, the fly-up off-localizer course command might very well be a design requirement.

The record made for the absence of the main transmitter but with clearance signal radiating is as one intuitively would expect. There are full-scale 150 Hz regions either side of the approach region where flag appears due to lack of signal. As will be recalled, the clearance array produces a null near the localizer course.

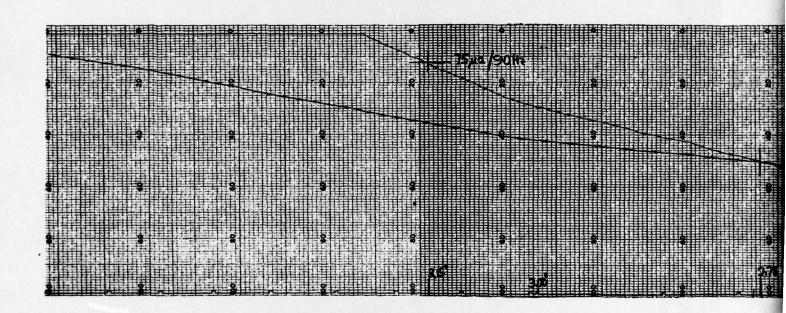
A re-evaluation was made of the desirability and need for the in-line power amplifiers used to compensate for the cable losses produced by the extraordinary long sections of feed line. The long lines were necessary because the transmitter building at Tamiami was not relocated to the appropriate place near the midline of the array. The amplifiers were removed giving slightly less than minimum field strength requirements; however, measurements were accomplished without difficulty because of adequately sensitive airborne receiving equipment.

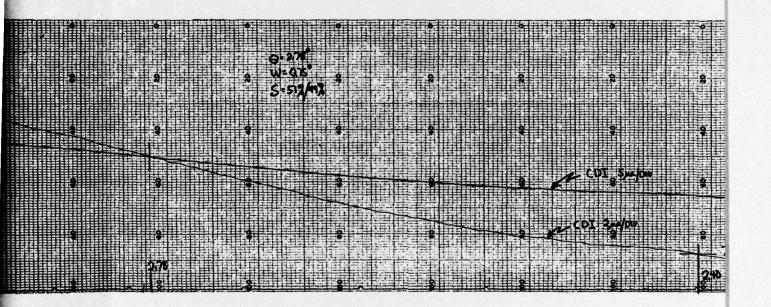
Improvements in the system were obtained by replacement of monitor cables with a more phase-stable type, by replacement of original antenna reflectors with copper element sections soldered to insure electrical continuity, and by modification of the monitor sequencing to dwell on any segment when an out-of-tolerance condition exists. This last allows the monitor scanning system to sample more rapidly and yet permit the monitor to enter the alarm condition after the standard 5-second delay when an out-of-tolerance sequel is received.

Figures 11–150,151 and 152 show the three patterns which are considered normal and which are used for standard, baseline conditions. These represent the conditions for an unperturbed array with copper reflectors on all slotted-cable elements.

The perpendicular or transverse structures of endfire glide slopes is always the most critical in obtaining an operationally acceptable path. In an attempt to obtain a figure of merit for the quality of the transverse structure, the classification scheme previously mentioned has been used to aid the reviewer in assessing the superiority of certain path conditions. Table 11–11 shows the numbers for 19 runs made under nominal conditions. The numbers for the 8°, -8°, 5°, -5°, and Loc columns are the microampere values representing the peak-to-peak excursion throughout the respective azimuth sectors. The $\pm 30\,\mu$ A column contains the number of degrees in azimuth surrounding the localizer on-course which allows a ± 30 microampere tolerance to be achieved. In contrast to the situation where a smaller number for peak excursions means higher quality, a larger number for the $\pm 30\,\mu$ A identifies the better condition.

The reader should note that the flight tracks are performed with reference to pressure altimeter and a roadway below. Deviations from the reference altitude and track introduce errors and certainly account for much of the dispersions seen in the nominal values.





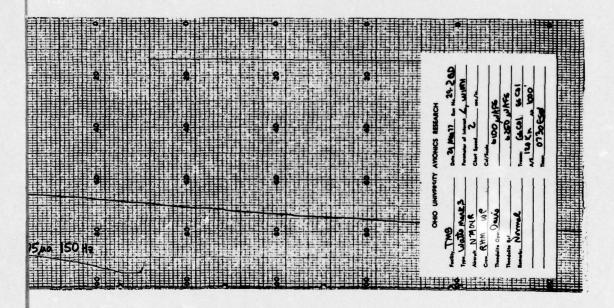
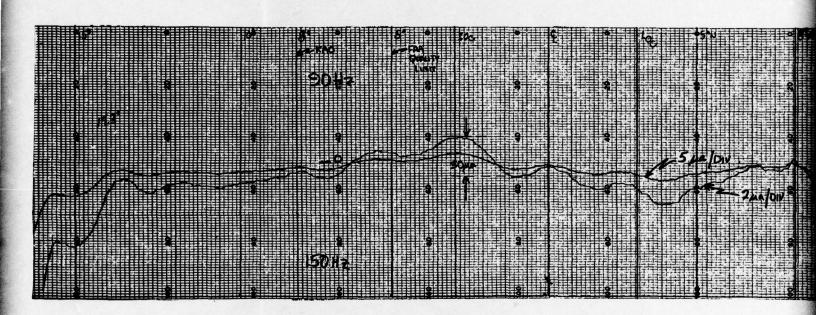


Figure 11-150. Recording of Gilde-Slope CDI During Level Flight Along Localizer Course, 1000 Feet Altitude.

11-217/11-218



.

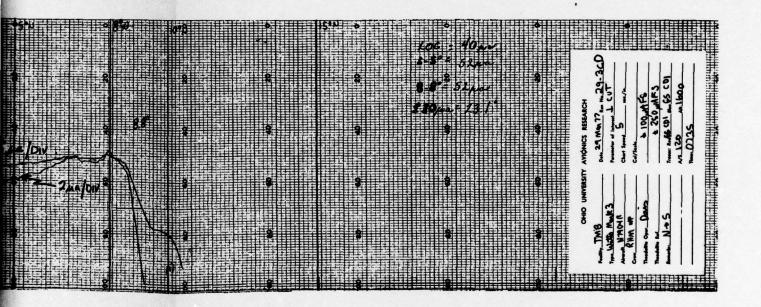
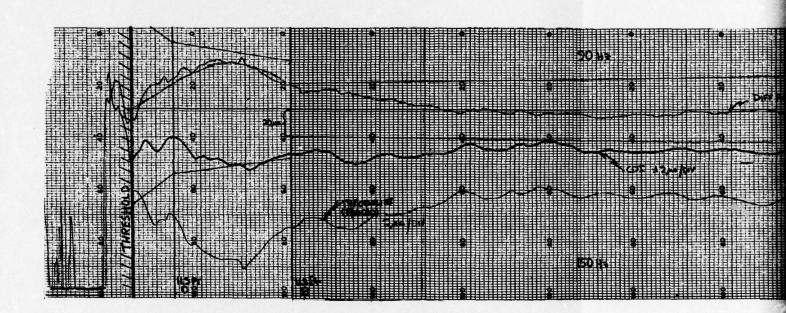


Figure 11-151. Recording of Gilde-Slope CDI During Level Flight Perpendicular to Localizer, 5.4 Miles From Runway, 1600 Feet Altitude.

11-219/11-220



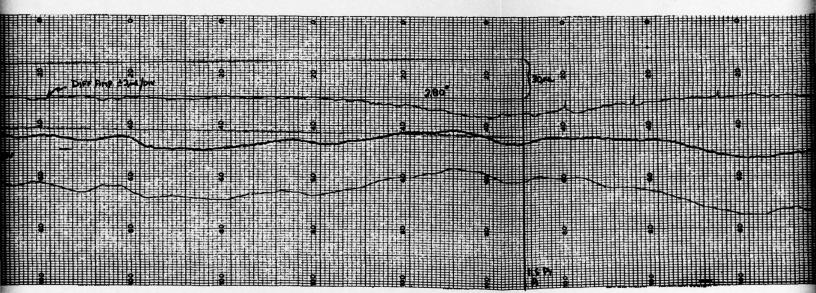


Figure 11-152.

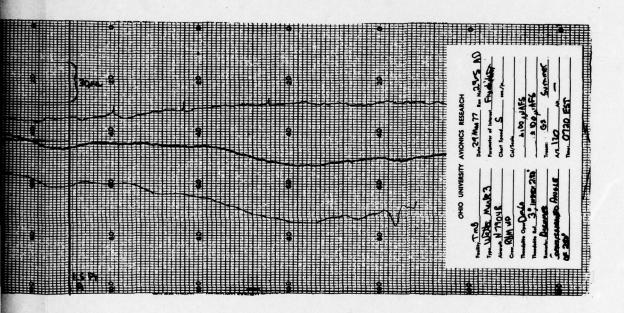


Figure 11-152. Recordings of CDI and Differential Amplifier Output During Lov Approach. Theodolite trace is also included.

11-221/11-222

7

3

Run Nui	mber	Loc µA	5-5° μΑ	8-8° μA	±30 μA °	Direction
March	17-18	40	45	55	18.3°	N-S
	17-19	34	42	79	21.9°	S-N
	26-4	38	42	42	21.6°	N-S
stont be adi . an	26-10	40	46	46	23.2°	N-S
oneins :	26-14	40	60	60	22.5°	N-S
graining to a col	28-3	42	58	58	23.4°	N-S
refaeller	28-4	32	32	48	18.6°	S-N
	28-17	54	64	64	18.0°	-
botwaer	28-23	38	55	55	23.5°	N-S
ed) to q arealitar	29-3	40	52	52	23.1°	N-S
dw yHsi	29-4	49	60	60	22.7°	S-N
buo uai	29-16	54	69	85	21.4°	N-S
al to	29-19	50	65	65	17.6°	S-N
	29-27	42	55	62.6	19.4°	N-S
	29-28	62	71	71	5.8°*	S-N
May	12-12	37	44	117.5	17.1°	N-S
	12-13	48	50	50	20.2°	S-N
	12-14	27	40	49	19.6°	N-S
	12-15	34	44	45	18.5°	S-N

^{*}Track 100° high in south section. This offers a correction of 37µA which will broaden the azimuth coverage to 23°.

Table 11-11. Nominal Values for Transverse Path Structure Seen at 5.4 Nautical Mile Range, 1600 Feet Altitude.

The dispersions evident are useful to have identified when evaluating the significance of recordings made with deliberate faults in the system as is the case when monitor performance is being checked.

A partial flight check by the FAA with a Saberliner aircraft was performed. Figure 11–153 shows a plot of a hand calculation of the difference between the CDI recording taken by the FAA Saberliner and the telemetry provided by a radio telemetering theodolite transmitting signals to a ground-based receiver/recorder unit.

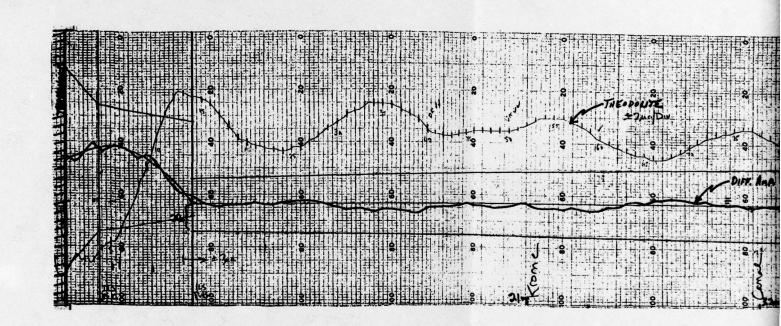
When the first measurements of this series were made, it was noted that the transverse structure had changed noticeably from the previous observations. The subsequent investigation revealed the defect in the reflector for the rear antenna, and this prompted removal of the reflectors from both front and rear transmitting antennas. The measurements which followed reveal the effects of change of gain due to removal of reflectors from the main antennas while retaining the reflectors on the clearance antennas.

This observation pointed to the significance of the relative gain between the clearance array and the main array. Although the initial Watts setup of the system placed the ratio near optimum, subsequent changes in the line amplifiers and reflectors pointed to the importance of maintaining this ratio, especially when considering monitoring and the maintaining of the facility. It was deemed important to look at the effect of changes in the relative amplitudes of the clearance and main arrays. Figure 11-154 shows parametric changes in clearance power in 1.5 dB steps.

f. Off-Centerline Path Characteristics for the Mark 3. Although recordings made flying perpendicular to the runway centerline reveal the character of path off-centerline, it is nevertheless desirable to have recordings indicating the angle and width of the path structure either side of centerline. Also, it is believed desirable to have some flyability recordings revealing the structure the pilot would encounter when flying other than the localizer on-course. Table 11-12 lists angle and width values taken from level flights at 1000-foot altitude. The azimuth angle was controlled by the pilot flying telemetry information coming from the azimuth portion of the radio telemetering theodolite located on runway centerline opposite the phase of the array.

The recordings for the structure were made using voice call-outs to provide azimuth guidance since the telemetry channel was being used for conventional RTT operation. Figure 11-155 shows a composite of 7 recordings of the different amplifier trace. In general no particular problem is evident. There is a change in average path angle amounting to approximately 0.3°.

There is an item that should be noted when reviewing this type of data. The theodolite reference is a conical surface elevated above the horizontal by 3.00°.



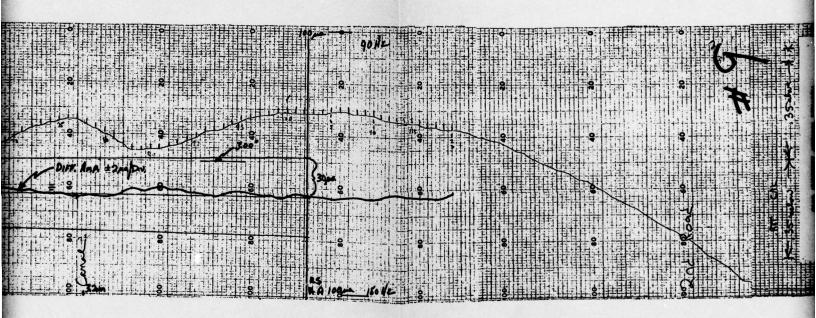


Figure 11-153, Recording of Theodolite Trace for I Hand-Calculated Differential Tree

11-225/11-226

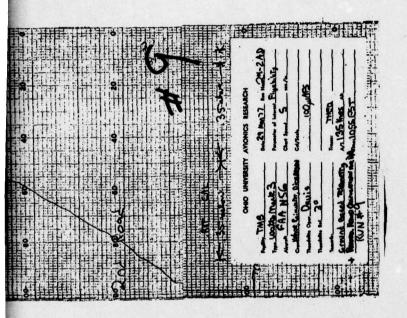
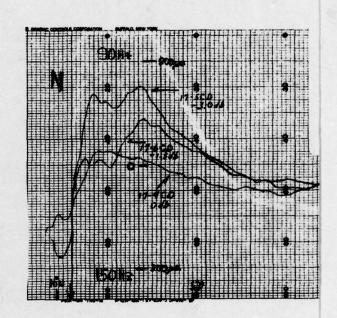


Figure 11-153, Recording of Theodolite Trace for FAA Scherliner Flight with a Hand-Calculated Differential Trace Added.

11-225/11-226



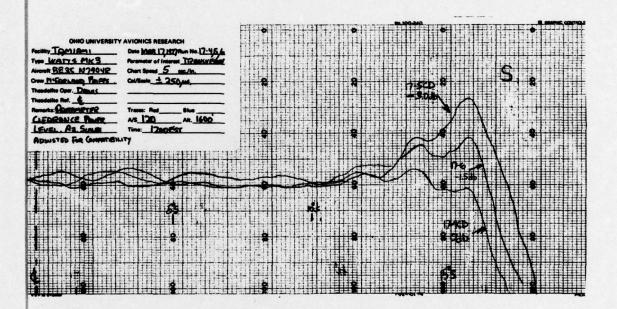
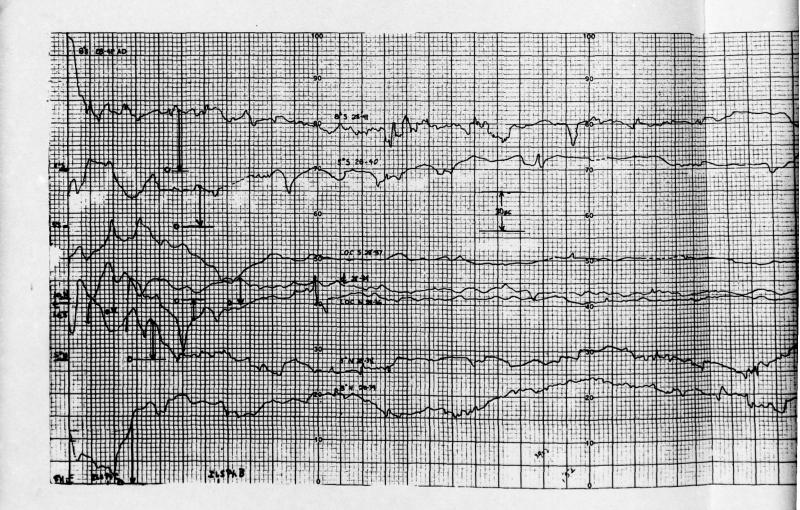
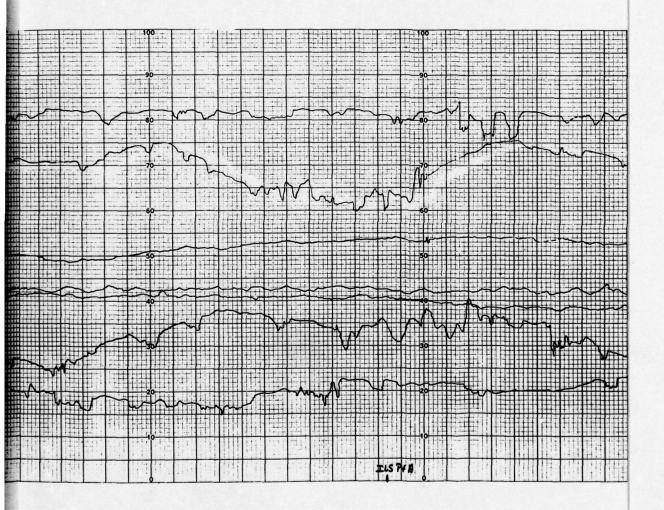


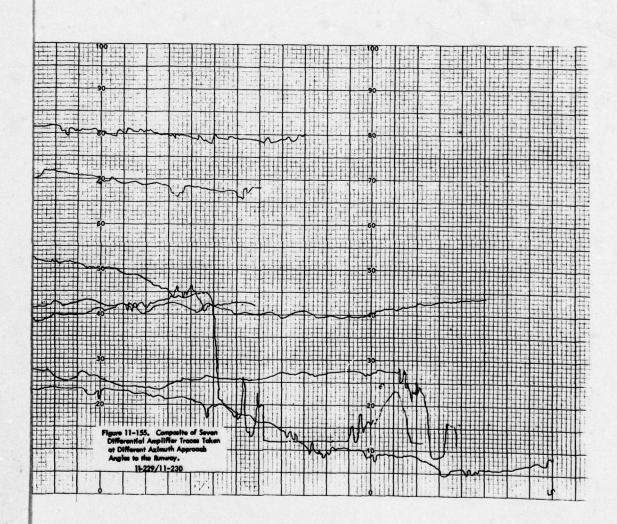
Figure 11-154. Effects of Clearance Transmitter Power Level on Perpendicular Structure as Seen at 5.4 Miles, 1600 Feet.

11-227/11-228

7







Azimuth	Angle and the	Width
Normal ©	3.09	.67
Loc N	3.20	.58
Loc S	2.98	.74
5° North	3.19	.65
5° South	3.02	.66
8° North	3.01	.97
8° South	3.03	.68

Table 11-12. Path Angle and Width Values as a Function of Azimuth.

The glide slope surface from the Watts Mark 3 system is ideally on an inclined plane meaning that at ILS point C an ideal path measured at 8° azimuth will be shown as a low path by only .03°, 6 microamperes; however, when tracking the localizer edge at ILS point C, this difference is 13 microamperes and at the threshold this becomes a flare downward of 33 microamperes.

It is instructive to observe the quality values for the perpendicular structure of the path during several fault conditions. Some of these are listed in Table 11–13.

Fault	Localizer Sector µA	5°-5° Sector µA	8°-8° Sector µA	±30µA Azi- muth Sector Degrees
Nominal		binox 44) enti	45	18.5
Clr. Pwr.	60	76	76	16.0
Clr. Pwr. +1 dB	62	78		11.0
Clr. Pwr. +3 dB	60	88	140	9.0
No. 6 Truck Position	84	106	106	8.0
No. 7 Truck Position	elliy 88 ve ve	90	90	8.0

Table 11-13. Listing of Quality Figures for Several Fault Conditions.

- g. Special Tests to Examine Special Characteristics of the Array. The final phase of the work at Tamiami with the Watts Mark 3 system was directed at three particular areas of interest concerning the system performance. These were:
 - (1) Identifying available increase of azimuth coverage by increasing the length of the slotted cables.
 - (2) Ascertaining the incorpendence of the system performance with respect to location of particular cable sections in the array; i.e., determining that the cable sections are true duplicates.
 - (3) Investigating the independence of the path in space with respect to elevation of the slotted cable element sections above ground; i.e., determine if the path in space is affected by drainage ditches or terrain irregularies below the elements.

At certain possible locations it may be necessary to locate the array farther from the runway centerline than is expected at typical locations and that which is simulated at Tamiami. At Tamiami the runway width is 150 feet. This permits placement of the near end of the front antenna element at 85 feet from the runway centerline. If the airport were assumed to have a 200-foot wide runway, then this distance would increase to 135 feet thus making it impossible to provide the desired coverage (±8°) on the opposite side of the runway at threshold while maintaining coverage 5 to 10 miles out on the side of the localizer towards the antenna array. The objective with the larger aperture or slotted cable length is to provide adequate azimuth coverage to meet the wide-runway requirements.

Calculations involving the geometries of a standard array whose phase center is positioned 160 feet from centerline and an expanded aperture version with its center located 205 feet from centerline reveals that approximately 18° of coverage is needed for the standard case and 21.8° for the wide runway case. These conditions were those selected for measurements at Tamiami.

(1) Effects of the Expanded Aperture. The conversion from the standard array to the expanded aperture took less than 2 days. Flight measurements made of the transverse structure revealed that indeed the azimuth was approximately 60% greater with no deterioration of the quality of the on-course surface. At first this might seem startling if one considers that the increase in the aperture sections went only from 7 to 9; however, a more correct intuitive picture can be obtained by considering that the increase of the main antenna sections went from 3 to 5 for both the front and rear elements. The main sections contribute most of the energy to form the path with the taper sections controlling side lobes in effect.

Table 11-14 indicates typical quality figure values for the standard array along with those of the expanded aperture.

Run Number	Localizer	5° - 5°	8° - 8°	±30 µA Sector
Standard 12-14	27 μΑ	40 µA	49 μΑ	19.6°
Expanded 24-23	38 µA	38 µA	54 µA	32.7°
Expanded 25-2	40 µA	44 µA	54 µA	32.5°

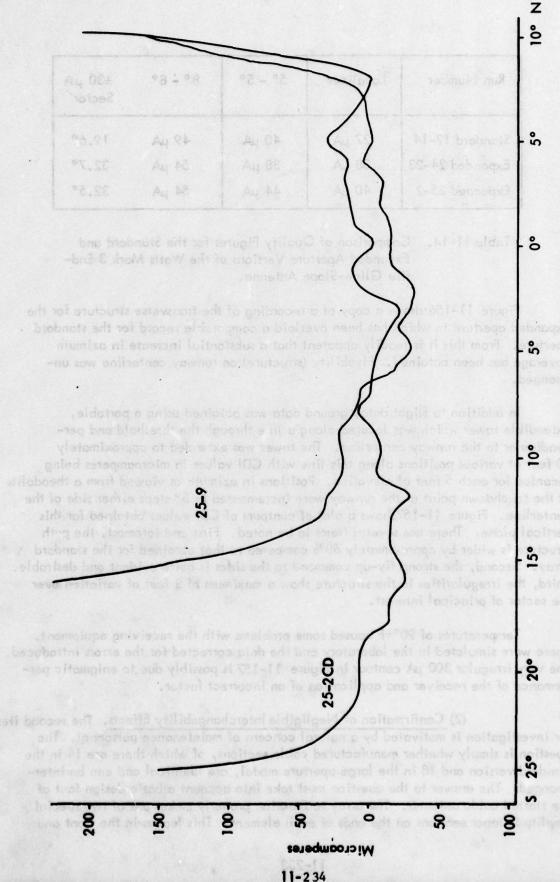
Table 11–14. Comparison of Quality Figures for the Standard and Expanded Aperture Versions of the Watts Mark 3 Endfire Glide–Slope Antenna.

Figure 11-156 shows a copy of a recording of the transverse structure for the expanded aperture to which has been overlaid a comparable record for the standard aperture. From this it is readily apparent that a substantial increase in azimuth coverage has been obtained. Flyability (structure) on runway centerline was unchanged.

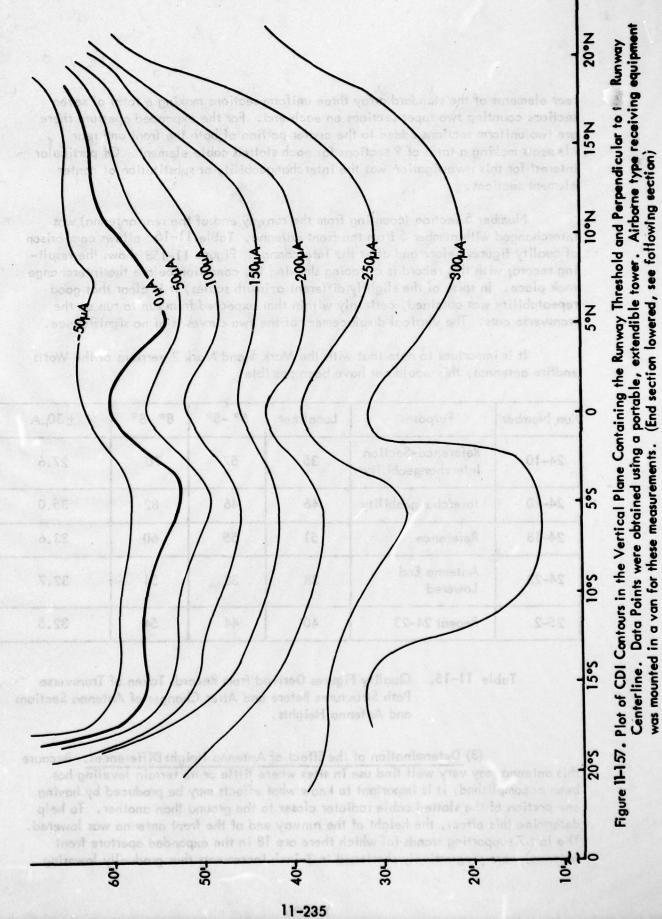
In addition to flight data, ground data was obtained using a portable, extendible tower which was located along a line through the threshold and perpendicular to the runway centerline. The tower was extended to approximately 60 feet at various positions along this line with CDI values in microamperes being recorded for each 5 feet of elevation. Positions in azimuth as viewed from a theodolite at the touchdown point of the runway were incremented in 5° steps either side of the centerline. Figure 11–157shows a plot of contours of CDI values obtained for this vertical plane. There are several items to be noted. First and foremost, the path structure is wider by approximately 60% compared to that obtained for the standard array. Second, the strong fly-up command to the sides is quite evident and desirable. Third, the irregularities in the structure show a maximum of 8 feet of variation over the sector of principal interest.

Temperatures of 90°+F caused some problems with the receiving equipment. These were simulated in the laboratory and the data corrected for the errors introduced. The very irregular 300 µA contour in Figure 11-157 is possibly due to enigmatic performance of the receiver and application of an incorrect factor.

(2) Confirmation of Negligible Interchangability Effects. The second item for investigation is motivated by a natural concern of maintenance personnel. The question is simply whether manufactured cable sections, of which there are 14 in the standard version and 18 in the large aperture model, are identical and can be interchanged. The answer to the question must take into account a basic design fact of the slotted cable antenna. The array to function properly makes use of two special amplitude taper sections on the ends of each element. This leaves in the front and



Tracings of the Flight Records of Transverse Structure for the Standard and Expanded Aperture for the Watts Mark 3 Endfire Glide-Slope Array. Figure 11-15&



rear elements of the standard array three uniform sections making a total of seven sections counting two taper sections on each end. For the expanded aperture there are two uniform sections added to the center portion of both the front and rear elements making a total of 9 sections for each slotted cable element. Of particular interest for this investigation was the interchangeability or substitution of center element sections.

Number 5 section (counting from the runway end of the rear antenna) was interchanged with number 5 from the front antenna. Table 11-15 allows comparison of quality figures before and after the interchange. Figure 11-158 shows the resulting record; with this record is a tracing showing the condition before the interchange took place. In spite of the slightly different azimuth scales, it is clear that good repeatability was obtained, certainly within that expected from run to run on the transverse cuts. The vertical displacement of the two curves is of no significance.

It is important to note that with the Mark 1 and Mark 2 versions of the Watts endfire antennas, this would not have been possible.

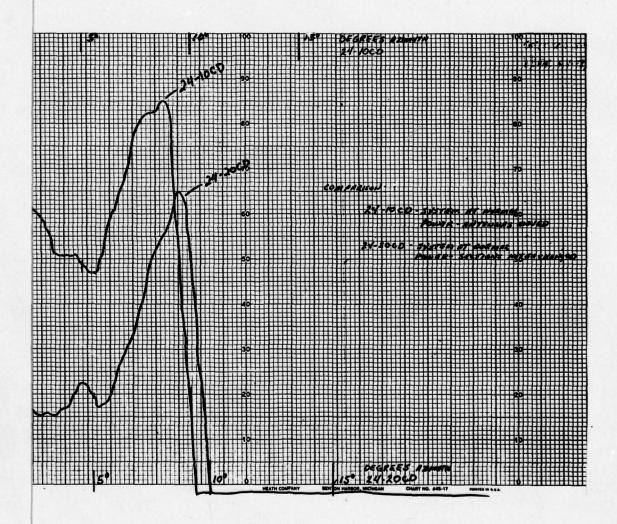
Run Number	Purpose	Localizer	5° -5°	8° -8°	±30µA
24-10	Reference-Section Interchangeability	35	57	70	27.6
24-20	Interchangeability	46	46	82	35.0
24-18	Reference	51	55	60	33.6
24-23	Antenna End Lowered	38	38	54	32.7
25-2	Repeat 24-23	40	44	54	32.5

Table 11-15. Quality Figures Derived from Records Taken of Transverse Path Structures Before and After Changes of Antenna Sections and Antenna Heights.

(3) Determination of the Effect of Antenna Height Differences. Because this antenna may very well find use in sites where little or no terrain leveling has been accomplished, it is important to know what effects may be produced by having one portion of the slotted cable radiator closer to the ground than another. To help determine this effect, the height of the runway end of the front antenna was lowered. The last 7 supporting stands (of which there are 18 in the expanded aperture front antenna) were progressively shortened in 3-inch increments thus gradually lowering



Figure 11-158. Comparison of Transverse Structures Before and After the Interchange of Single Sections of the Front and Rear Antennas.



the last 60 feet of the front antenna from 42 inches above ground to approximately 21 inches. Figure 11–159 shows a photograph of the results of this antenna modification. This also could be a modification used to reduce obstruction heights near the runway.

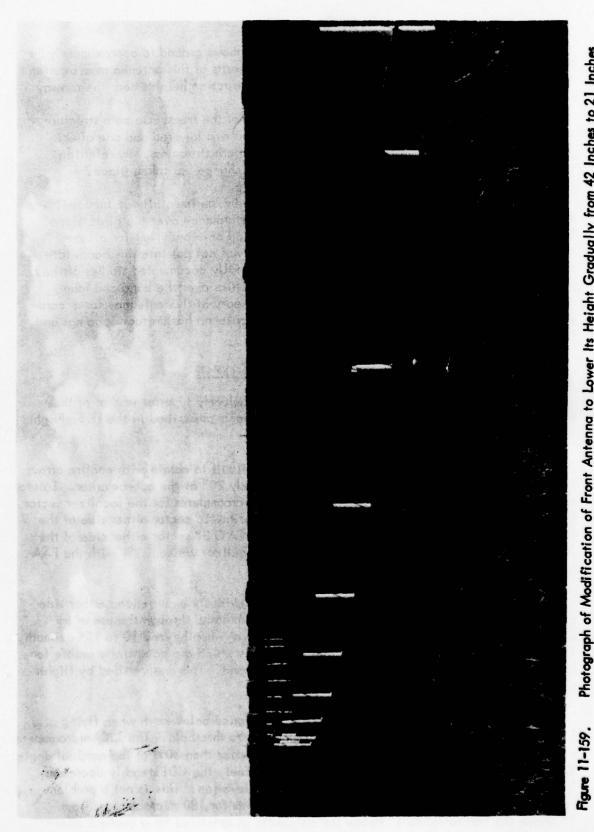
Figure 11-160 shows tracings of two records of the transverse path structure, one taken before the end portion of the front antenna was lowered and one after. There appears to be no significant difference in the path structures. By referring again to Table 11-15, it is evident that no major change has taken place.

One item originally planned, but not pursued experimentally at Tamiami, was the bandwidth characteristics, i.e., operational performance over the glide slope band of 329.3 to 335.0 MHz. The array was operated only on 331.1 for all the experiments conducted since February 1977. Effort was not put into this bandwidth experiment because the Watts Company had run carefully documented studies of the slotted cable section amplitude and phase characteristics over the band and found essentially no change. This is consistent with the theory of this antenna, for according to Watts, unlike the Mark 1 and 2 versions, this antenna has uniform spacings and is not critically dependent on frequency.

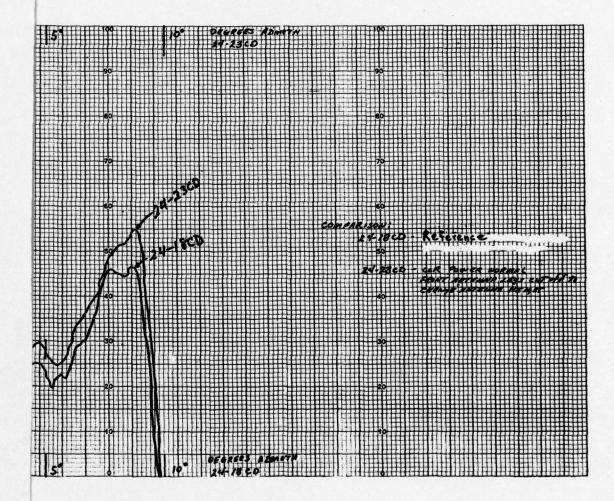
h. Conclusions Concerning the Mark 3 System.

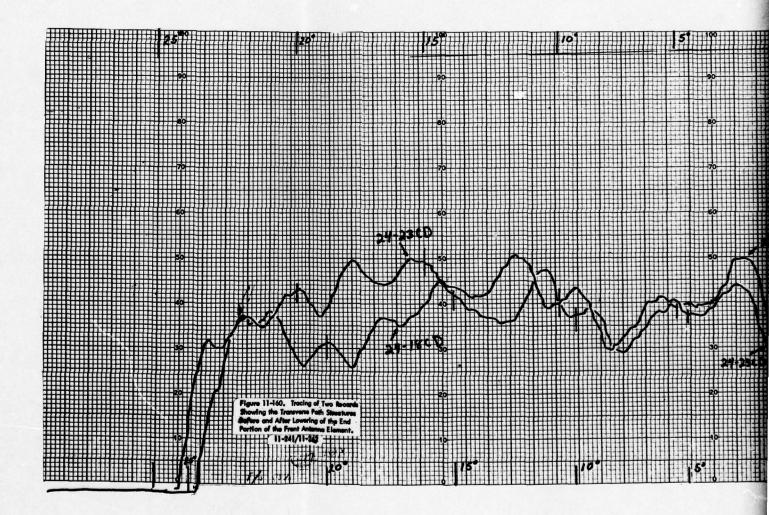
- 1. The performance of the Mark 3 system is clearly superior to that of the previous models, and at Tamiami will meet requirements prescribed in the U.S. Flight Inspection Handbook for Category II quality.
- 2. Azimuth coverage, most critical and difficult to obtain with endfire arrays, has been improved to achieve a total of approximately 20° at the outer marker. Lateral roughness has been reduced to approximately ± 15 microamperes for the localizer sector (measured at the outer marker); ± 20 microamperes for the 5° sector either side of the localizer on-course; and ± 35 microamperes for the ICAO 8° sector either side of the localizer. Path angle from centerline to edge of localizer varies 3.2% with the FAA tolerance being 7.5%.
- 3. All areas of fly-down command signal previously experienced either side of the main course region have been successfully eliminated through the use of an auxiliary clearance signal which captures the receiver when beyond 10 to 15° azimuth. This provides a major improvement in that all regions which are potentially unsafe for flight contain strong 150 Hz signals for fly-up command. This was verified by flights below and to either side of the on-course region.
- 4. The structure below path is good. Clearance below path when flying at a 1° approach angle is better than 200 microamperes to threshold. The 190-microampere value is reached consistently above 1.9° which is better than 30% of the nominal angle. When flying at a constant altitude of one thousand feet, the CDI steadily decreases from 250 microamperes to 175 microamperes at 2° elevation. This is not a problem but one should note that it does not meet requirements for 180 microamperes from 1° above the horizontal to 1° below the on-course as specified for a capture effect system.

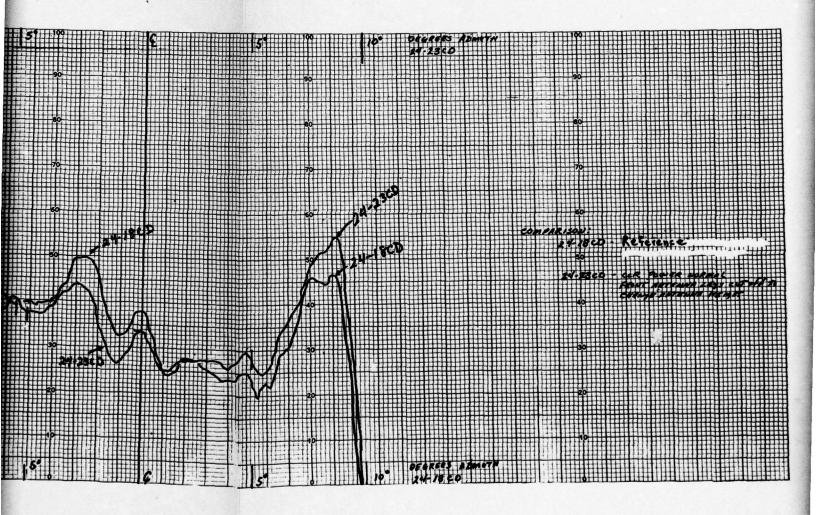
11-239



Photograph of Modification of Front Antenna to Lower Its Height Gradually from 42 Inches to 21 Inches at the Runway End.







5. Structure of the path as determined from radio telemetering theodolite recordings is good and will marginally meet Category II requirements. Generally the path is extremely smooth and easy to fly. For example, structure tolerances from the radio telemetering theodolite reference and differential amplifier indicate roughness of ±7 microamperes in ILS Zone 2. A slight dip amounting to 0.20° exists in Zone 3 but this is smooth and a complete flight run from the outermarker to the threshold can be made with CDI variations no greater than ±10 microamperes. The level transition flown through the vertical path structure indicates a near-perfect condition.

6. Signal strength, of concern when operating with extra-long cable runs but primarily limited by the low antenna elevation, was increased using special amplifiers so that margins better than 7 dB above FAA requirements are available at 10 nautical miles at the intercept altitude of 1500 feet. Indications are that typical placement of the transmitter building for commissioned operation would yield adequate signal levels without transmitter amplifiers provided the 7/8 inch air-filled coaxial

EGRAQUERATE ELEGAND TOLS EL MON ELIM

7. Coupled approaches can be successfully flown to the runway threshold.

cables are used to feed the antennas with reflectors currently being used.

- 8. The system requires close tolerances of 1/2 inch or better for antenna placement. This dictates a careful survey and installation, in particular, for the slotted cables which are placed in a curvilinear formation.
- 9. The Mark 3 antennas except for the end sections are comprised of segments which are identical and interchangeable. This permits an increase of the aperture without redesign to achieve greater azimuth coverage for cases where the array is displaced distances greater than 100 feet from runway centerline. The Watts Company reports that manufacturing and testing requirements are much more easily attained with this antenna uniformity.
- 10. The characteristics of this system are such that ground measurements can be used for all aspects of the setup. The potential exists, therefore, to commission the system with a minimum of flight time.
- 11. The measured results compare reasonably well with theoretical calculations. Closer results are conceivably possible by refining the antenna positions. Since path values were within tolerances, the unknown areas of monitoring were stressed in the time available.
- 12. Monitor stability appears adequate; however, the path angle stability must be reassessed after the transmitter is relocated to the midline of the array and cable runs are buried. At this time indications are that these changes will provide adequate stability for practical operations at any potential site.
- 13. The Ohio University measurement of signal strength at 1500 feet, 10 nautical miles with no in-line amplifiers in the system, was 23 dB above the airborne receiver threshold or 14 hard microvolts at the receiver terminals.

- 14. The monitors, which include three pairs of aperture monitors combined to give readings of angle and width, provided readings which allowed no out-of-tolerance condition in the far field without a monitor alarm condition for a series of 27 discrete faults. Path angle drift of .3° due to temperature change on the cables complicated this data reduction. One case was particularly affected when wet cloths were placed over a section of the rear antenna giving a 2.65° rath angle with 88% of alarm value indicated, referenced to a nominal monitor path angle of 2.85° for that time. Path angle drift was significant during the time of its subservation. Flight check showed 2.71° at the end of the series.
- 15. A van positioned at various locations in front of the antenna (both front and rear) and the wet cloths on the element in general disturbed the transverse structures very noticeably but did not place them outside of published flight inspection tolerance limits. It should be noted that the flight inspection tolerances are not written to stress scrutiny of the transverse structure; hence, substantial aberations may exist but no published tolerances are exceeded. The van and wet cloths do not affect angle and width parameters without affecting the monitors.
- 16. Truck positions just in front of the monitors for the front antenna did not, of course, disturb the aperture monitors and did not affect path angle and width in the far field. The transverse structures were very definitely affected. This indicates a sterile area of at least 100 feet in front of the array should be specified.
- 17. The van positioned at the phase center of the array did not affect system operation. Apparently this result is obtained because the obstruction was too far from the monitors and at too low of an angle for the far field.
- 18. Experiments with clearance power levels indicate that a maximum of ± 1 dB of change be allowed as a limit.
- 19. Loss of clearance power is evident most dramatically by the strong areas of fly-up command beginning at 9° azimuth on the antenna side of the runway and 15° on the side opposite. There is a slight narrowing of the good central transverse area but the path structure is not altered fundamentally.
- 20. The aperture width channel appeared to track with the width information obtained from the threshold monitor for system stability considerations; however, this has not been proved for the case of discrete width fault conditions. Experiments have shown that the path angle is independent of width but width does change when the path angle changes. An approximate mathematical relation is: PW = 2.1/PA where PW is the path width in degrees and PA is the path angle in degrees. Thus, as the path angle rises, the path width gets sharper.
- 21. The combination of a low, broad path is protected by the aperture monitors. The combination of a low path angle with a sharp width is protected only by the aperture monitor. A high, out-of-tolerance broad path is not observed by the monitors but is not deemed to be a dangerous condition because below-path clearance remains unchanged.

- 22. Results of fault conditions consisting of feed line length change (phase shift to one of the transmitting antennas) and tone unbalance conditions are found to be essentially the same.
- 23. An electrically-discontinuous reflecting element for the transmitting antennas produces a fault condition which is detectable.
- 24. An open circuit at the load end of the transmitting antennas produces oscillations in the transverse path structure amounting to 144 microamperes peak-to-peak.
- 25. In-line amplifiers are a troublesome item in the system and should be avoided when possible. Interactive items such as changing the input level changes not only the output but the percentage modulation on the output signal as well, complicates the operation and affects the stability of the system operation.
- 26. Path angle and width measurements were made at altitudes of 1000, 1500, 2000 feet, and there were no significant differences in the values obtained.
- 27. There is no usable back-course information. First, the RF level is down 36 dB and second, the focusing of the energy from the slotted cables precludes formation of a semblance of a path.
- 28. An increase in the length of the slotted cable elements serving as the front and rear transmitting antennas of the endfire array increases the azimuth coverage of the system by approximately 60%. The number of sections of each antenna was increased from 7 to 9 with the additional sections being inserted in the midportion between the end amplitude taper sections.
- 29. Interchanging mid sections of the front and rear antennas has no significant effect on the array performance. This indicates that manufacturing tolerances for this Mark 3 array are adequate.
- 30. Lowering of the last 60 feet of the runway end of the front antenna gradually in a uniform decrease of height from 42 to 21 inches produced no measurable change in the path in space. This information indicates that there is a reasonable independence of the path structure with respect to antenna height above ground. This suggests that the antenna would be able to span across drainage ditches and other irregularities in the earth's surface available for installation of the system.
- 31. The transverse path structure in space will show effects of fore-aft movement of sections of the antenna but will not show effects of vertical displacements. Experience with the aperture monitors shows that the monitor will detect the foreaft type of movement (parallel to the array axis).

- 32. Nearly four months of extensive data collection involving the Watts Mark 3 endfire glide slope system have been completed. All indications are that the system is ready for testing at a problem site. More work on the system stability cannot be done effectively until the installation involves shorter, buried cables.
- 5. Prediction of Performance of the Watts Mark 1 Endfire Glide Slope System. The intent of this section is to present a technique which has been developed to predict the performance characteristics of the Watts endfire glide slope system when operating in the presence of irregular terrain in the approach region. For the past 12 years engineers on the Avionics Engineering Staff at Ohio University have been working on the development of mathematical models which would take into account multipath and permit calculation of DDM values in space for both localizer and glide slope. This work draws on much of the previous Ohio work for background and yields prediction capability for this special non-image glide slope system.

Although the Watts system does not use the image to form the path in space, it is nevertheless susceptible to multipath coming from terrain which may be illuminated in the aircraft approach region. The vertical lobe structure of the Watts antennas is such that one would, in general, expect performance in the presence of upslopes to be somewhat better than the null reference system and not as good as the capture effect type. It is interesting to note that the Watts company has been giving consideration to the development of a version of the endfire system that would provide modification of the vertical pattern much the same as the present capture effect system does.

A capability to predict is a valuable asset for the engineer who is responsible for making the selection of the glide slope type to be installed at a particular site. The expense of installing and flight checking an inappropriate type can hopefully be avoided by proper application of prediction models such as given in this report for the Watts system. In such applications accuracy is of considerable importance. Fortunately two rather complete sets of experimental data were on hand from Tamiami and Staunton, Virginia to allow an opportunity to compare the theory with practice. This text reports the results of the direct comparisons for a near ideal site and one where a significant upslope is present that makes performance of null reference and sideband reference systems unacceptable. An attempt has been made to quantify statistical parameters which will give some index of the prediction capability.

The mathematical model has shown instances of good approximation with mean error of 6 μA and on occasion some relatively poor approximations with mean error with 24.58 μA . This error is believed to be due to a lack of capability to determine precisely the ground contour and to the fact that the terrain beyond 200 feet left and right of the runway extended centerline is not known.

All in all, this is a major first step in gaining an improved capability in glide path siting with the Watts system. The next step will be to implement this

procedure, predict performance at a virgin site, and assess final accuracy. Some refinements are possible and may ultimately be desirable; however, the basic capability, which is good, now exists and can be derived from this section. Considerable detail is presented including the computer programs for mechanizing the calculations.

The basic elements comprising the Watts Mark 1 endfire glide slope array are a two slotted-cable antenna array, each cable having an aperture of approximately 130 feet. The wide apertures of the antennas are to provide for broadening of the cone, produced by the endfire array, to give satisfactory coverage for flights deviating from the localizer centerline (azimuth deviations). Each antenna is fed by the standard carrier and sideband signals through a hybrid as shown in Figure 11-161.

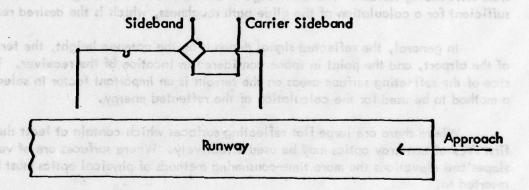


Figure 11-161. Diagram of Carrier and Sideband Being Fed into the Antenna.

There are 99 slots in the rear antenna and 81 slots in the front antenna. The gap spacing is not constant throughout the length of the antenna, as this parameter is used by the Watts Prototype Company to control the phase distributions of the gap excitations.

Although the Watts glide slope does not require the ground plane to form the pattern, a ground plane indeed exists, and it can cause unwanted reflection of the signals from the ground to the aircraft. In some airports there even exist hills and valleys in the direct approach region of the runway. The irregular ground plane, hills and valleys will contribute to irregularities to the glide path. This problem has been studied by D. A. Hill and R. H. McFarland [6] for the image glide slope systems.

The primary objective of this study is to derive a mathematical model which will help predict the effects of existence of irregular terrain on the Watts glide slope system performance and to show how accurately the mathematical model performs by comparing the theoretical predictions with the experimental results.

a. Theory and Analysis of the Effects of Irregular Terrain on Watts Endfire Glide Slope.

(1) General Discussion of the Problem. The on-course position of the endfire glide slope is determined by the lobe structure of the two antennas and the array pattern defined by the antenna spacing. The vertical radiation pattern of the system is formed by the sum of all the electromagnetic energy transmitted directly from the slots of the antennas and that which is reflected from the ground plane. The relative magnitude and phase excitations of each slot or source can be easily measured experimentally with a dipole antenna probe and vector voltmeter. The glide path, therefore, depends on the locations of the antennas, the relative magnitude and phase of the slot excitations and reflected energy components from surrounding terrain. The knowledge of direct and reflected signal will be sufficient for a calculation of the glide path roughness, which is the desired result.

In general, the reflected signal depends on the antenna height, the terrain of the airport, and the point in space considered as location of the receiver. The size of the reflecting surface areas on the terrain is an important factor in selecting a method to be used for the calculation of the reflected energy.

Where there are large flat reflecting surfaces which contain at least the first Fresnel zone, ray optics may be used effectively. Where surfaces are of various slopes and elevations the more time-consuming methods of physical optics must be resorted to.

A program was developed at the Avionics Engineering Center which combines these methods taking advantage of the speed of ray optics where applicable but using the physical optics technique where required. The model as used for the Watts Mark 1 endfire array assumes:

- 1. Uniform terrain slope is assumed at an elevation angle. This is defined to mean the area of hillside whose contours are straight lines over the area of interest and these contour lines are perpendicular to the runway centerline.
- 2. The radiation is nearly uniform in the vertical direction and has a horizontal pattern which can be approximately represented by $\cos \theta$.
- 3. For cases where the terrain is known to vary in a direction perpendicular to runway centerline, divide the area for integration into discrete sections so that each section considered will be essentially uniform in slope and orientation. The maximum number of sections considered in this work is two.

The direct and reflected fields for each of the 180 slots is calculated as a complex phasor and summed over appropriate slots to give CSB and SBO fields at each chosen point in space. From these DDM and CDI can be calculated and the various properties of the space pattern predicted.

a. Theory and Analysis of the Effects of Irregular Terrain on Watts Endfire Glide Slope.

(1) General Discussion of the Problem. The on-course position of the endfire glide slope is determined by the lobe structure of the two antennas and the array pattern defined by the antenna spacing. The vertical radiation pattern of the system is formed by the sum of all the electromagnetic energy transmitted directly from the slots of the antennas and that which is reflected from the ground plane. The relative magnitude and phase excitations of each slot or source can be easily measured experimentally with a dipole antenna probe and vector voltmeter. The glide path, therefore, depends on the locations of the antennas, the relative magnitude and phase of the slot excitations and reflected energy components from surrounding terrain. The knowledge of direct and reflected signal will be sufficient for a calculation of the glide path roughness, which is the desired result.

In general, the reflected signal depends on the antenna height, the terrain of the airport, and the point in space considered as location of the receiver. The size of the reflecting surface areas on the terrain is an important factor in selecting a method to be used for the calculation of the reflected energy.

Where there are large flat reflecting surfaces which contain at least the first Fresnel zone, ray optics may be used effectively. Where surfaces are of various slopes and elevations the more time-consuming methods of physical optics must be resorted to.

A program was developed at the Avionics Engineering Center which combines these methods taking advantage of the speed of ray optics where applicable but using the physical optics technique where required. The model as used for the Watts Mark 1 endfire array assumes:

- 1. Uniform terrain slope is assumed at an elevation angle. This is defined to mean the area of hillside whose contours are straight lines over the area of interest and these contour lines are perpendicular to the runway centerline.
- 2. The radiation is nearly uniform in the vertical direction and has a horizontal pattern which can be approximately represented by $\cos \theta$.
- 3. For cases where the terrain is known to vary in a direction perpendicular to runway centerline, divide the area for integration into discrete sections so that each section considered will be essentially uniform in slope and orientation. The maximum number of sections considered in this work is two.

The direct and reflected fields for each of the 180 slots is calculated as a complex phasor and summed over appropriate slots to give CSB and SBO fields at each chosen point in space. From these DDM and CDI can be calculated and the various properties of the space pattern predicted.

Since a method is available to theoretically calculate DDM or glide-path flyability, it is appropriate to proceed to compare experimental results with theoretical predictions in the next section. Calculations and measurements have been made for the Tamiami site in Florida representing an ideal location and for Shenandoah Valley Airport, Virginia, where a significant upslope exists in front of the antennas.

b. Experimental and Theoretical Results.

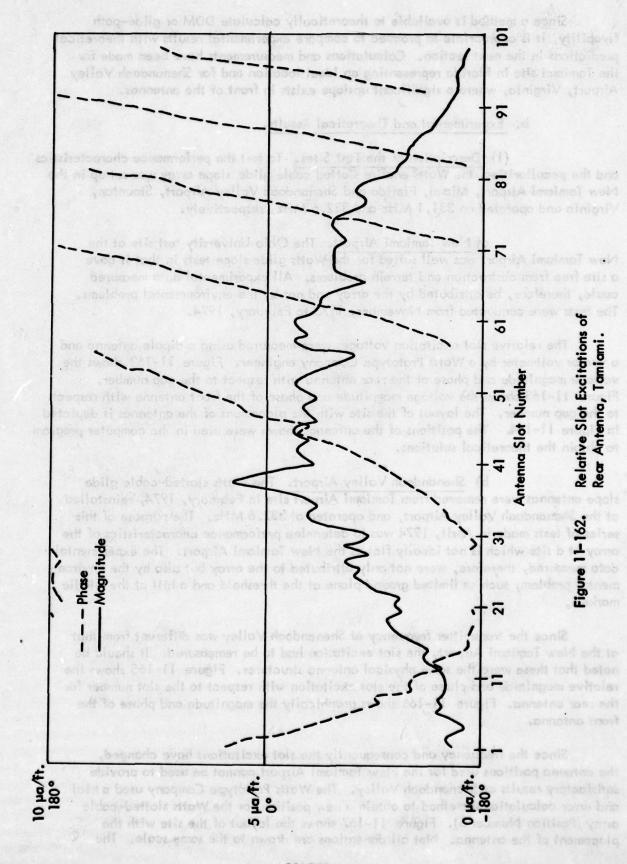
- (1) <u>Description of the Test Sites</u>. To test the performance characteristics and the peculiarities, the Watts endfire slotted cable glide slope array was set up in the New Tamiami Airport, Miami, Florida and Shenandoah Valley Airport, Staunton, Virginia and operated on 331.1 MHz and 332.6 MHz, respectively.
- a) New Tamiami Airport. The Ohio University test site at the New Tamiami Airport was well suited for the Watts glide slope tests in that it gave a site free from obstruction and terrain problems. All experimental data measured could, therefore, be attributed by the array and not by the environmental problems. The tests were conducted from November, 1973 to February, 1974.

The relative slot excitation voltages were measured using a dipole antenna and a vector voltmeter by a Watts Prototype Company engineer. Figure 11-162 shows the voltage magnitude and phase of the rear antenna with respect to the gap number. Figure 11-163 shows the voltage magnitude and phase of the front antenna with respect to the gap number. The layout of the site with the placement of the antennas is depicted in Figure 11-164. The positions of the antennas shown were used in the computer program to obtain the theoretical solutions.

b) Shenandoah Valley Airport. The Watts slotted-cable glide slope antennas were removed from Tamiami Airport site in February, 1974, reinstalled at the Shenandoah Valley Airport, and operated at 332.6 MHz. The purpose of this series of tests made in April, 1974 was to determine performance characteristics of the array at a site which is not ideally flat as the New Tamiami Airport. The experimental data measured, therefore, were not only attributed to the array but also by the environmental problem, such as limited ground plane at the threshold and a hill at the middle marker.

Since the transmitter frequency at Shenandoah Valley was different from that at the New Tamiami Airport, the slot excitation had to be remeasured. It should be noted that these were the same physical antenna structures. Figure 11-165 shows the relative magnitude and phase of the slot excitation with respect to the slot number for the rear antenna. Figure 11-166 shows graphically the magnitude and phase of the front antenna.

Since the frequency and consequently the slot excitations have changed, the antenna positions used for the New Tamiami Airport cannot be used to provide satisfactory results at Shenandoah Valley. The Watts Prototype Company used a trial and error calculational method to obtain a new position for the Watts slotted-cable array (Position Number 6). Figure 11-167 shows the layout of the site with the placement of the antenna. Not all dimensions are drawn to the same scale. The



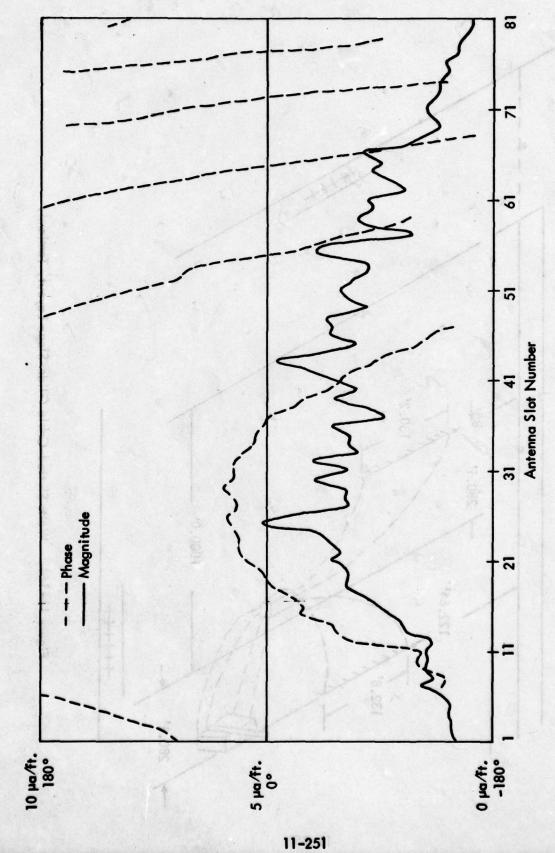


Figure 11–163. Relative Slot Excitations of Front Antenna, Tamiami.

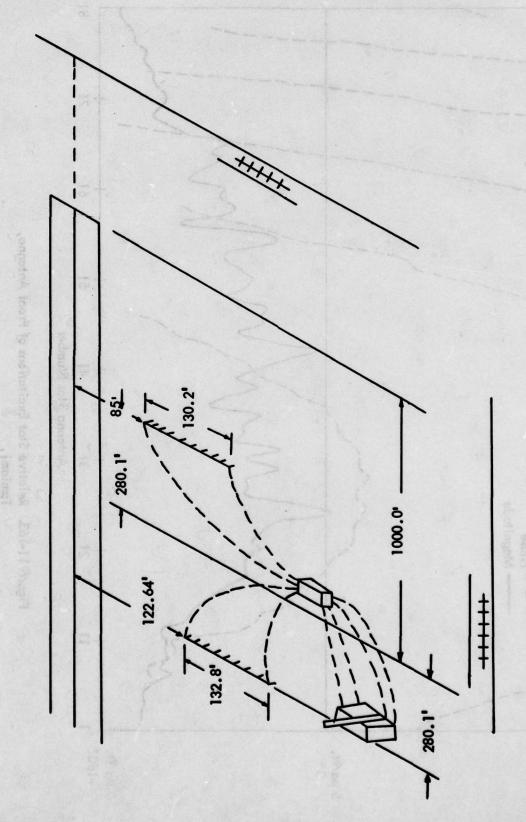


Figure 11-164. Watts Slotted-Cable Glide-Slope Layout, Tamiami.

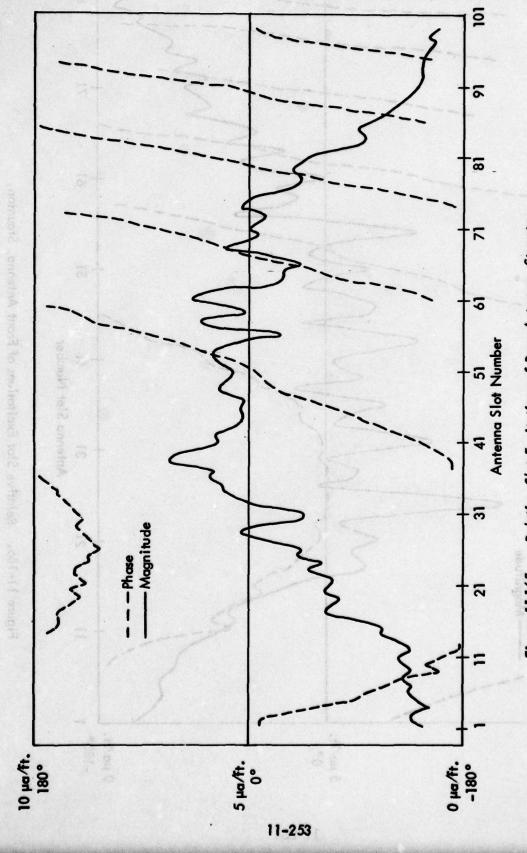


Figure 11-165. Relative Slot Excitations of Rear Antenna, Staunton.

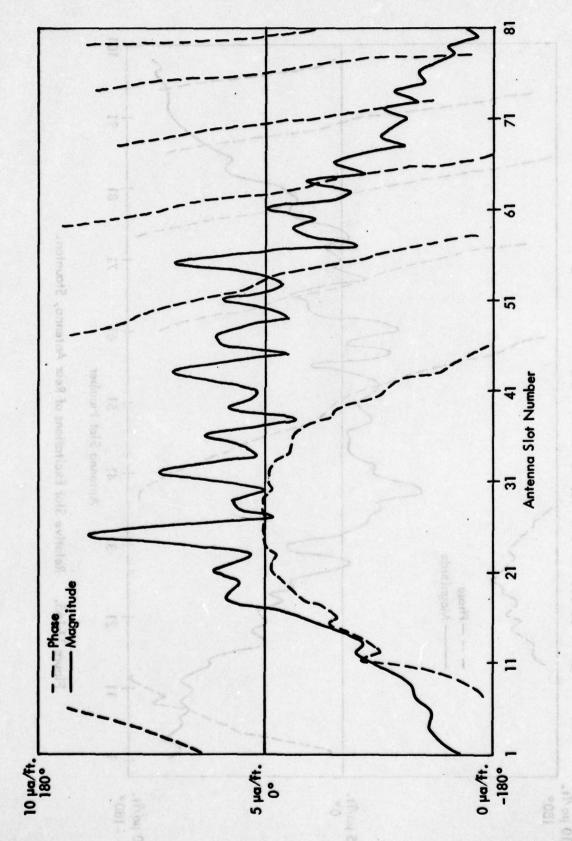
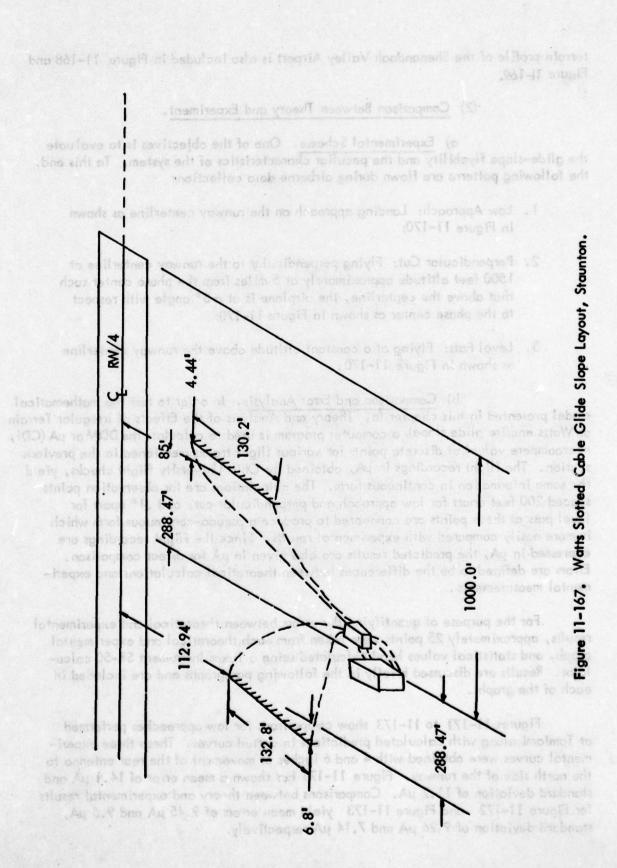


Figure 11-166. Relative Slot Excitations of Front Antenna, Staunton.



terrain profile of the Shenandoah Valley Airport is also included in Figure 11–168 and Figure 11–169.

(2) Comparison Between Theory and Experiment.

- a) Experimental Scheme. One of the objectives is to evaluate the glide-slope flyability and the peculiar characteristics of the system. To this end, the following patterns are flown during airborne data collection:
 - 1. Low Approach: Landing approach on the runway centerline as shown in Figure 11–170;
 - 2. Perpendicular Cut: Flying perpendicular to the runway centerline at 1500 feet altitude approximately at 5 miles from the phase center such that above the centerline, the airplane is at a 3° angle with respect to the phase center as shown in Figure 11–170;
 - 3. Level Pass: Flying at a constant altitude above the runway centerline as shown in Figure 11-170.
- b) Comparison and Error Analysis. In order to test the mathematical model presented in this chapter (a. Theory and Analysis of the Effects of Irregular Terrain on Watts endfire glide slope), a computer program is used to calculate the DDM or μ A (CDI, microampere value) at discrete points for various flight tracks mentioned in the previous section. The flight recordings in μ A, obtained by Ohio University flight checks, yield the same information in continuous form. The calculations are for observation points spaced 200 feet apart for low approach and perpendicular cut, and .1° apart for level pass as these points are connected to produce a pseudo-continuous form which is more easily compared with experimental results. Since the flight recordings are expressed in μ A, the predicted results are also given in μ A for direct comparison. Errors are defined to be the differences between theoretical calculations and experimental measurements.

For the purpose of quantifying the errors between theoretical and experimental results, approximately 25 points were taken from each theoretical and experimental graph, and statistical values hand calculated using a Texas Instrument SR-50 calculator. Results are discussed briefly in the following paragraphs and are included in each of the graphs.

Figures 11–171 to 11–173 show comparisons for low approaches performed at Tamiami along with calculated predictions in dotted curves. These three experimental curves were obtained with 4 and 6 inches of movement of the rear antenna to the north side of the runway. Figure 11–171 has shown a mean error of 14.1 μ A and standard deviation of 11.2 μ A. Comparisons between theory and experimental results for Figure 11–172 and Figure 11–173 yield mean errors of 9.45 μ A and 9.5 μ A, standard deviation of 9.26 μ A and 7.14 μ A respectively.

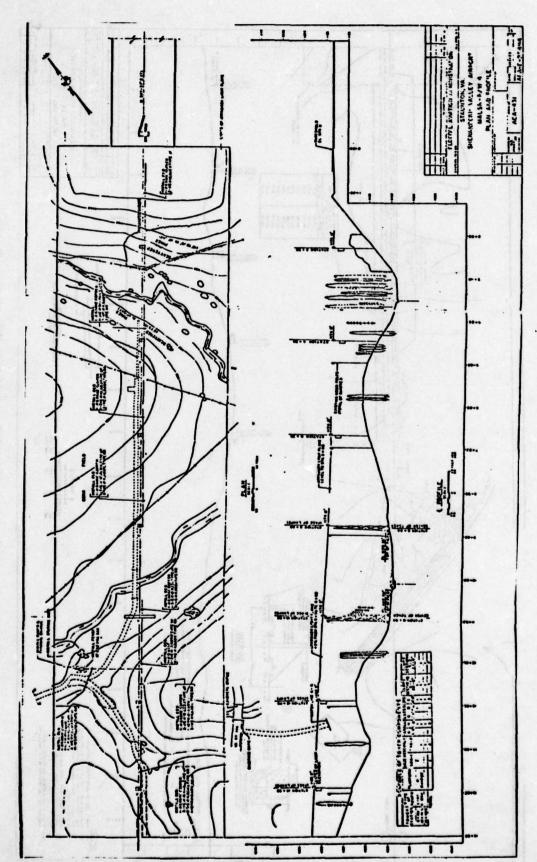


Figure 11-168. Terrain Profile of Shenandoah Valley Airport, Staunton.

THIS PAGE IS BEST QUALITY PRACTICABLE.
FROM GOFY PURAISHED TO DDG

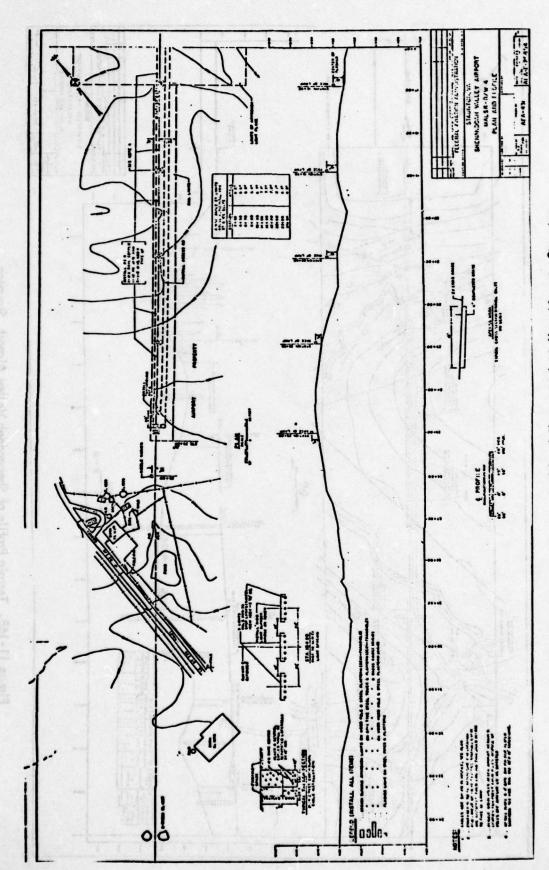


Figure 11-169. Extended Terrain Profile of Shenandoah Valley Airport, Staunton.

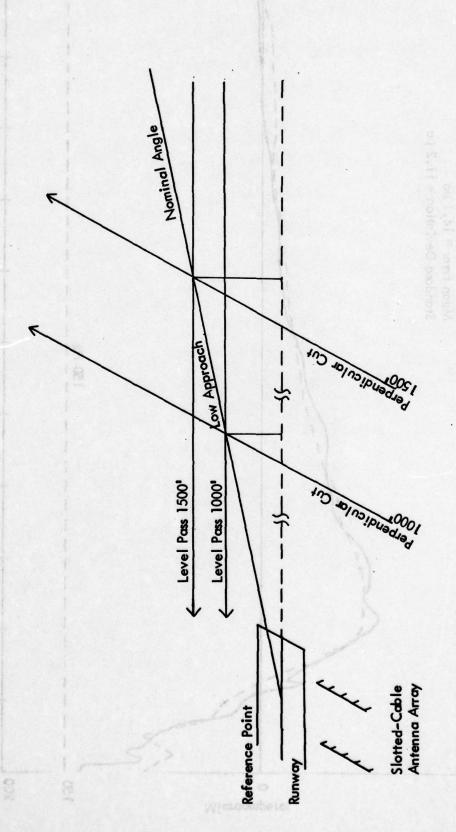
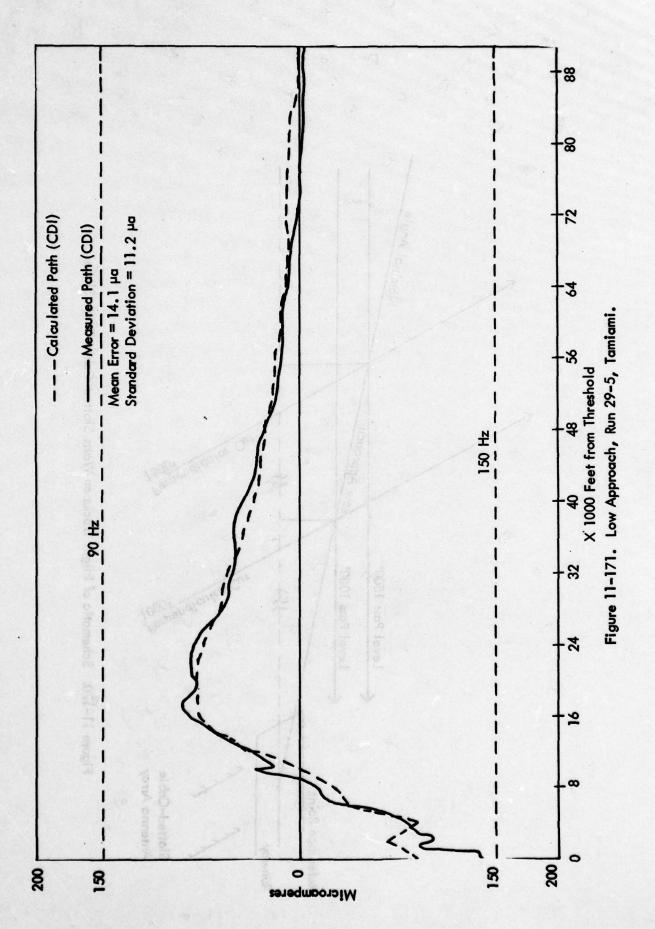


Figure 11-170. Schematic of Flight Tracks on Watts Slotted-Cable Glide Slope.



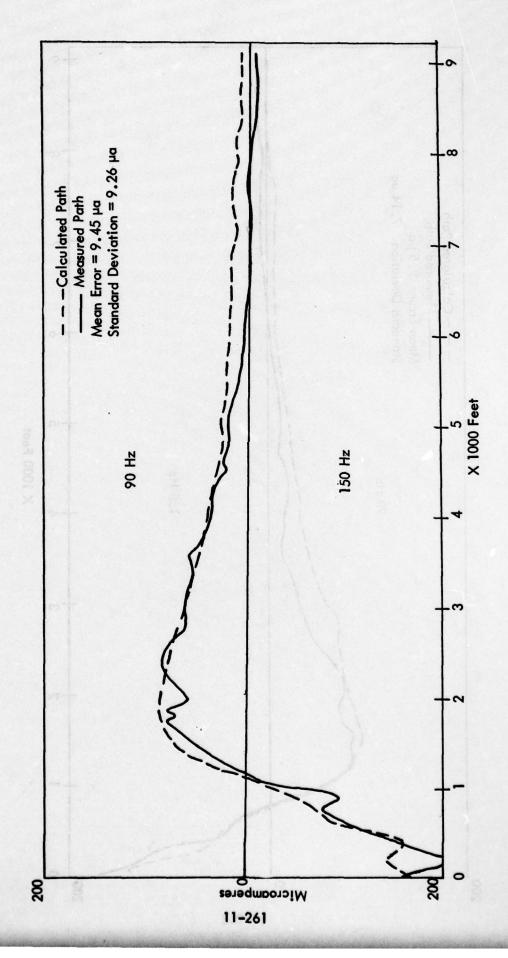


Figure 11-172. Low Approach, Run 29-6, Tamiami.

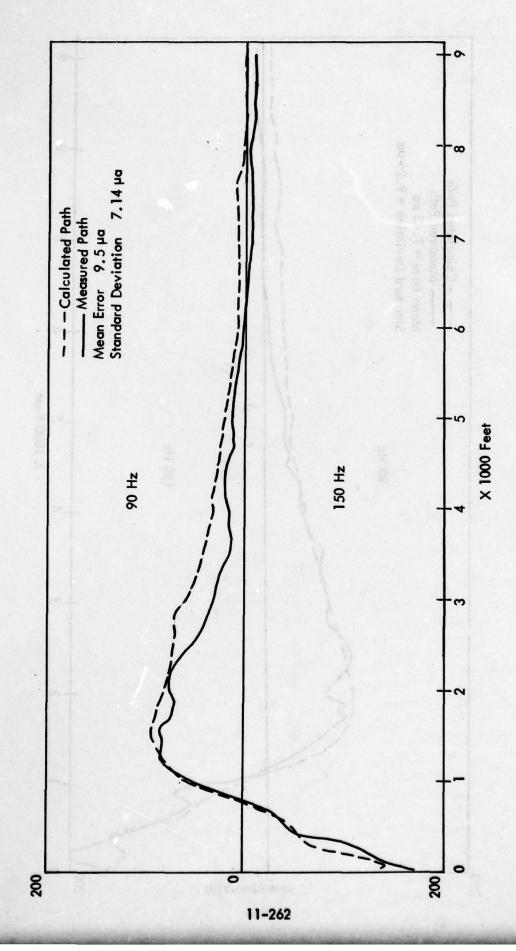


Figure 11-173. Low Approach, Run 29-8, Tamiami.

To determine the azimuthal coverage, perpendicular cuts were performed at altitudes of 1600 feet and 1700 feet at a range of 5.78 and 6.14 nm, respectively. Experimental results are shown along with predictions in Figure 11–174 and Figure 11–175 The predicted paths follow the experimental paths with a maximum error of $40\,\mu\text{A}$. The mean errors are 24.58 μA and 19.91 μA ; the standard deviations are 16.68 μA and 17.05 μA respectively.

Prediction for level pass at altitude 1000 feet is compared with experimental results in Figure 11-176. The calculated zero crossing is close to the experimental zero crossing. The maximum error is 12 µA at one end of the curve. Mean error is 6.49 µA and standard deviation is 3.58 µA.

It is important to point out in the previous theoretical and experimental graphical data that the glide-slope three dimensional on-course surface produced by the Watts endfire array is irregular even at a flat site such as the Tamiami Airport. The irregularity is due to imperfections in the antenna slot excitations. With irregular terrain, the glide path will have further irregularities as will be demonstrated in the discussion of the Watts array operation at a site with irregular terrain.

At the Shenandoah Valley Airport, the glide path is, as expected, rough due to the effect of the terrain; the predicted calculation for flyability is a better approximation at 9000 feet than at 1000 feet from the threshold as shown in Figure 11-177. The maximum error is 30 µA at near field and 11 µA at far field. One notes that in Figure 11-177 the greatest deviation between calculated and measured curves occurs approximately 700 feet from the threshold. At this point in the flight track the rough terrain is either below or behind the aircraft and the terrain should have essentially no effect on the measured path. It is known from calculations made by the Watts Prototype Company and from extensive measurements by Ohio University that the path structure in space is critically dependent on the physical positioning of the antennas. Moves of only a few inches are significant. It is probable that the location of the antennas for the measurements was not precisely that specified in the calculations. The region in space for the effect of this discrepancy to be most evident is that near the 700-foot point in Figure 11-177; hence, it is reasonable to conclude that the discrepancy observed in Figure 11-177 and other low approach profiles can be attributed to antenna positioning accuracy rather than the mathematical method.

Experiments for perpendicular cuts at altitude 1300 feet from South to North are shown in Figure 11–178, and 1500 feet from North to South in Figures 11–179 and 11–180, along with the theoretical calculations. Maximum errors are 57 $\mu\text{A}, 44~\mu\text{A},$ and 41 μA respectively; standard deviations are 14.04 $\mu\text{A},$ 14.75 $\mu\text{A},$ and 11.83 μA respectively. The errors are understandably large here because the terrain beyond 200 feet on either side of the runway extended centerline is not known.

Level pass at an altitude of 1000 feet is shown in Figure 11–181 with the calculated results. The mean error is $13.26\,\mu\text{A}$ and standard deviation is $8.89\,\mu\text{A}$.

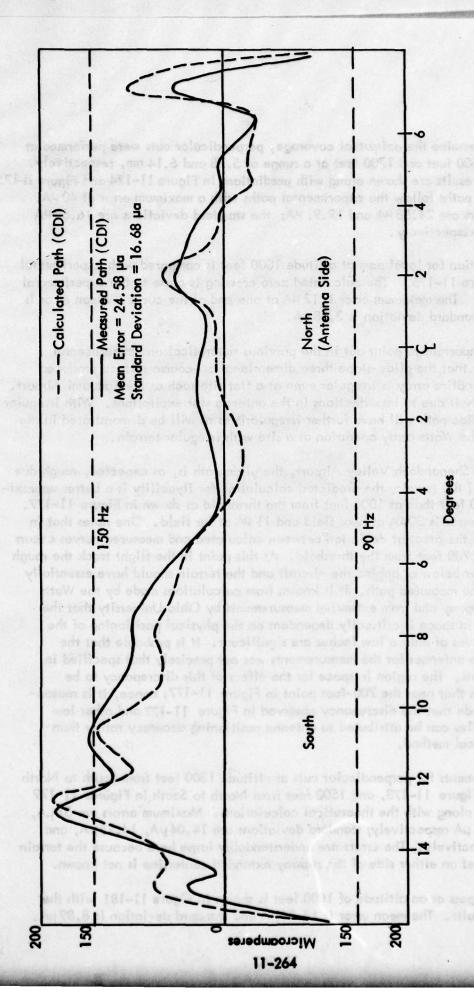
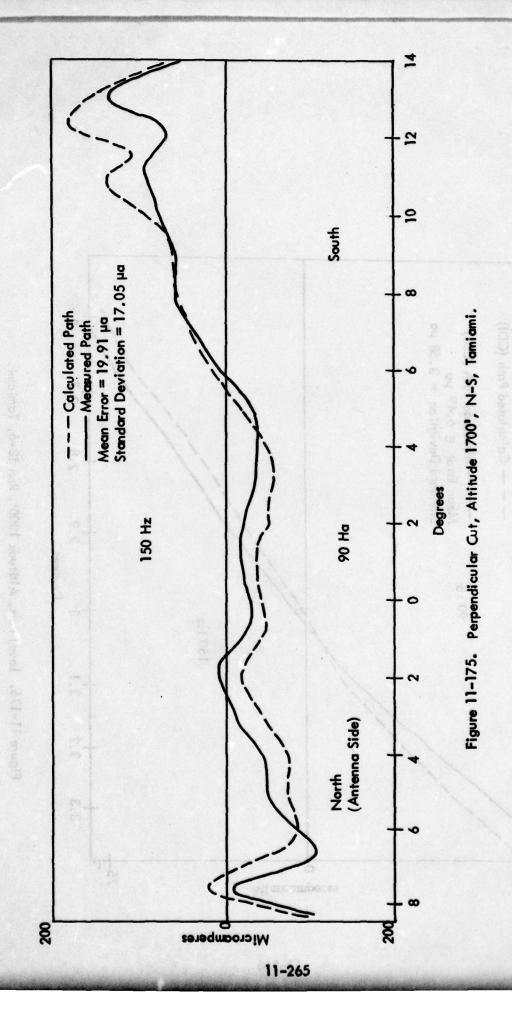


Figure 11-174. Perpendicular Cut, Altitude 1600', Run 18-17, Tamiami.



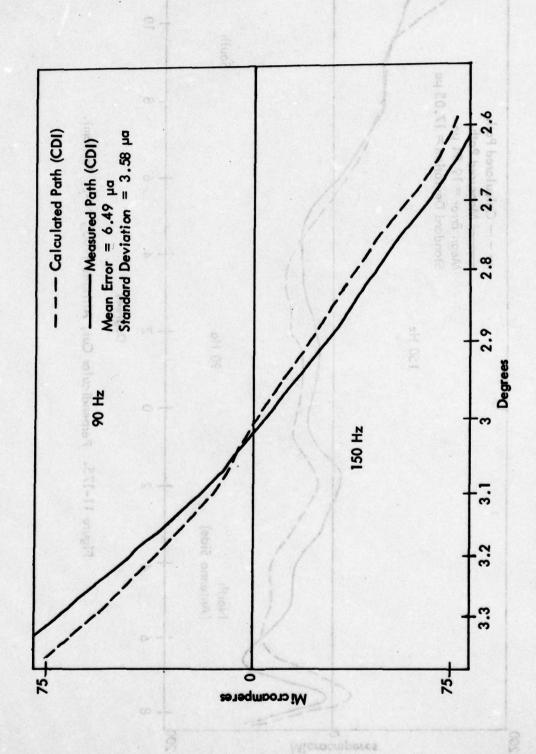
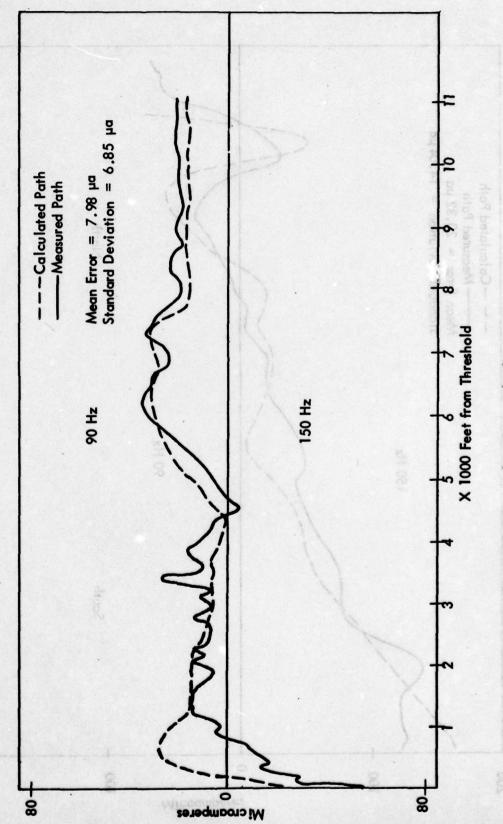
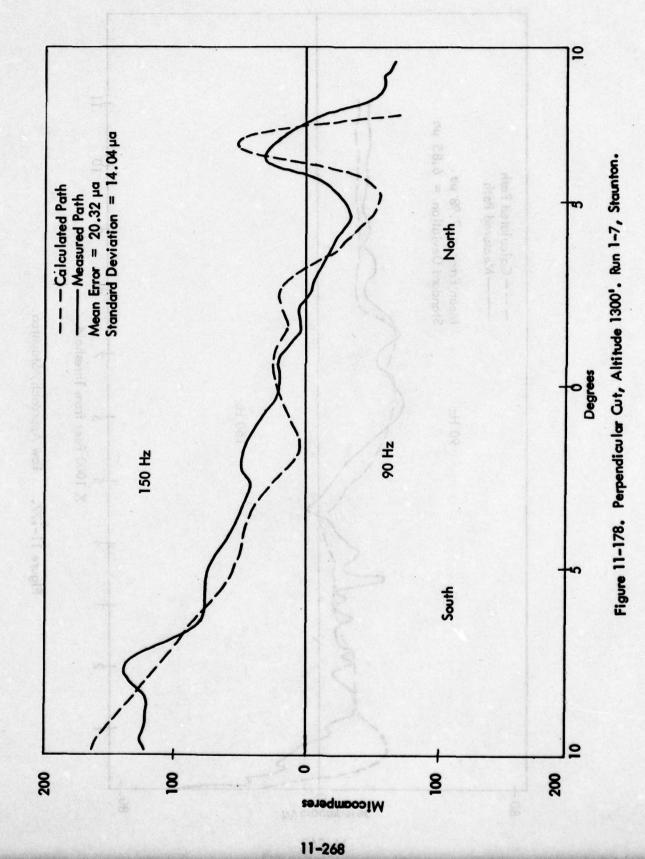


Figure 11-176. Level Pass, Altitude 1000', Run 18-6, Tamiami.



Perpendicular Cut, Allflude 13001, Pup 1-7, Stauman.

Figure 11-177. Low Approach, Staunton.



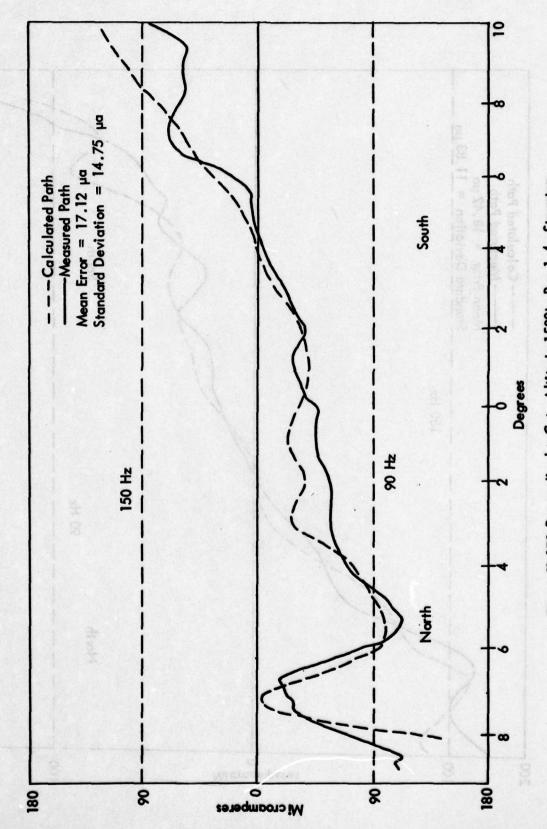
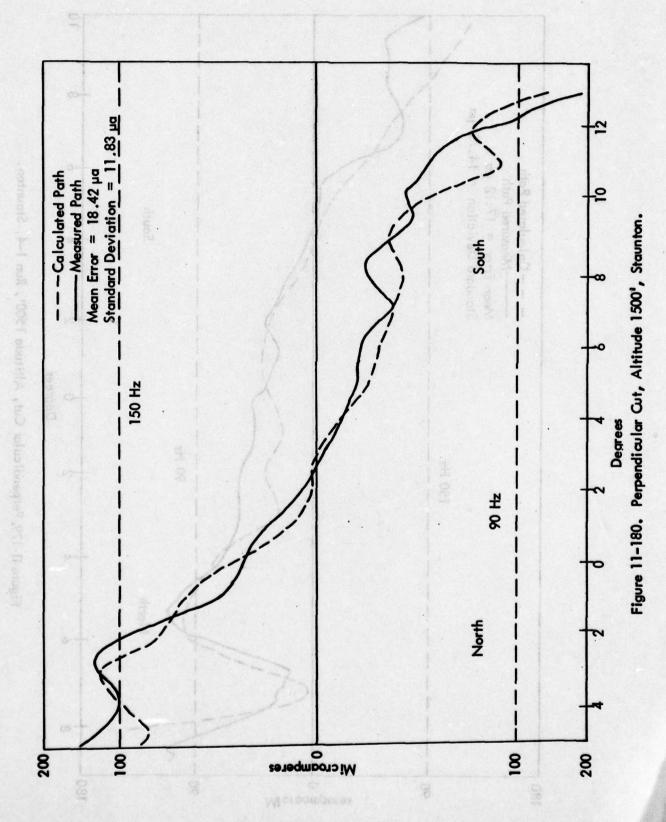


Figure 11-179, Perpendicular Cut, Altitude 15001, Run 1-4, Staunton.



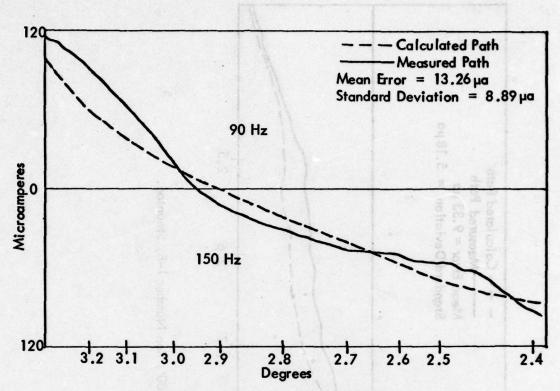


Figure 11-181. Level Run, Altitude 1000', Staunton.

Figure 11–182 shows a level pass at 1500 feet on centerline. Again the mean error is $9.33\,\mu\text{A}$; the standard deviation is $5.18\,\mu\text{A}$. Note that a flat spot is apparent on Figure 11–182 from 2.5° to 2.7° .

c. Characteristics of Off-Centerline Theoretical Prediction. As is shown in the previous section, the glide slope is irregular on the runway extended centerline and the cone produced by the endfire array has been flattened to cover approximately 24° in azimuth (8° North and 16° South of centerline). The theoretical predictions are made for either side of the centerline to show how much symmetry exists and to aid the reader in visualizing the three-dimensional structure.

With the frequency transmitter at 331.1 MHz, Figures 11–183 to 11–185 show the theoretical calculated glide paths for low approaches with 4° North and South, 6° North and South, and 8° North and South respectively. These curves show some peculiar characteristics of the array if we make a low approach off the runway centerline at a given angle in azimuth. Figure 11–186 shows the theoretical .35° above and below path approaches.

Figures 11–187 to 11–192 are theoretical calculations for level passes off the centerline at 3° , 4° , 5° , 6° , 7° and 8° North and South at an altitude of 1000 feet. Note that the zero crossings for 5° N and 5° S are very close to each other. This is confirmed by Figure 11–174, run number 18–17.

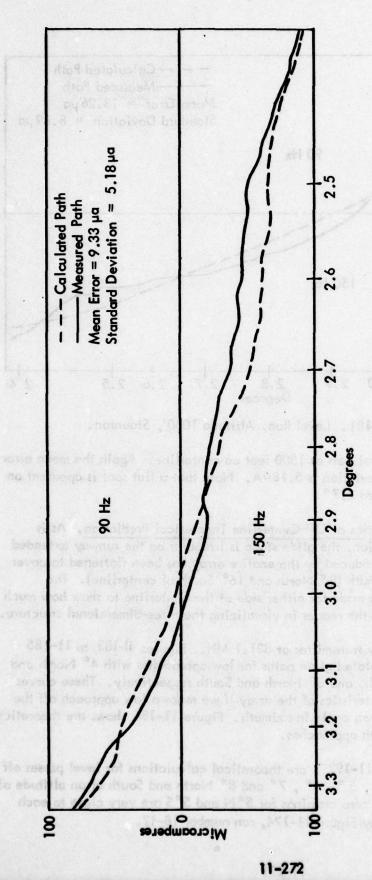
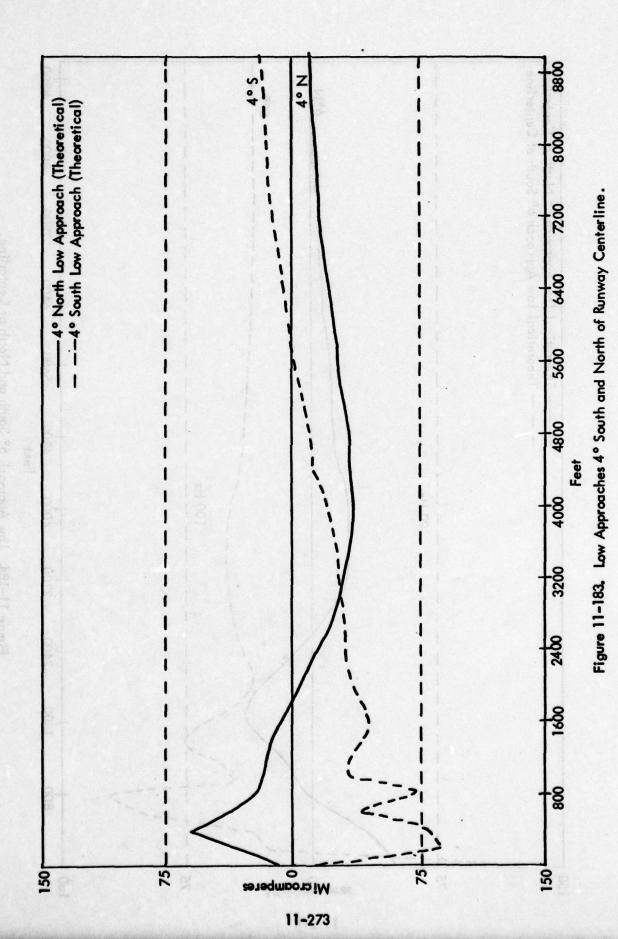
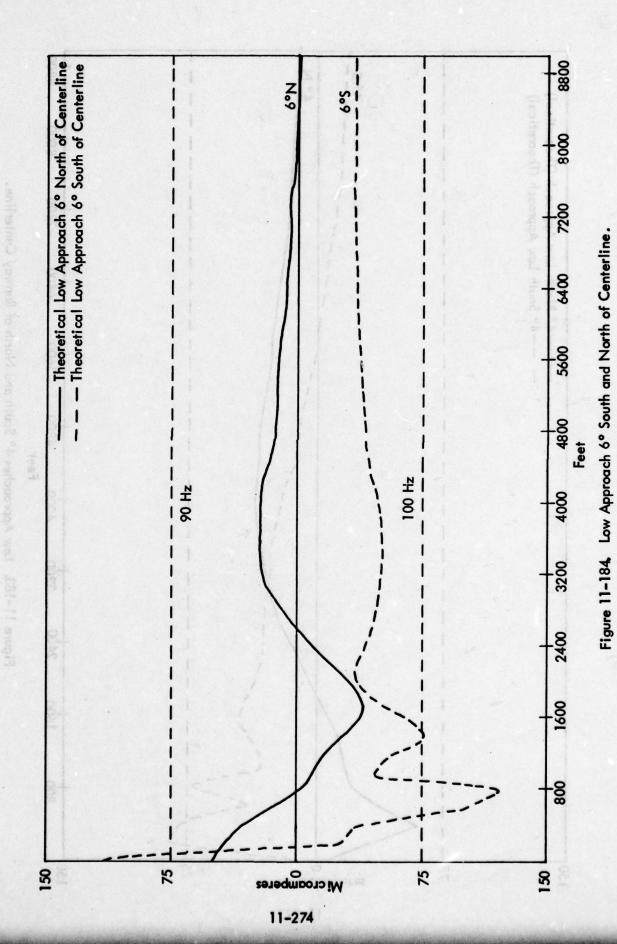


Figure 11-182. Level Run, Altitude 1500', Run Number 1-8, Staunton.





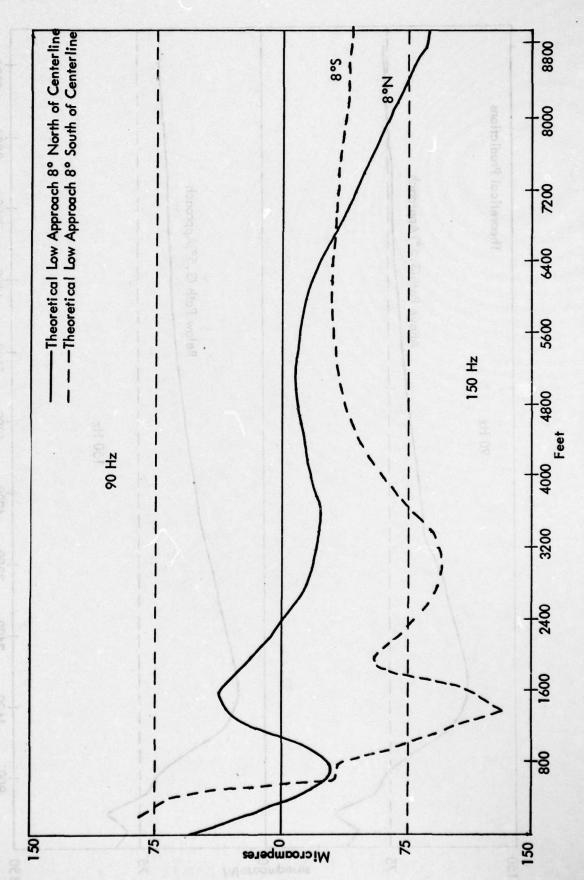


Figure 11-185. Low Approach 8° South and North of Centerline, Tamiami.

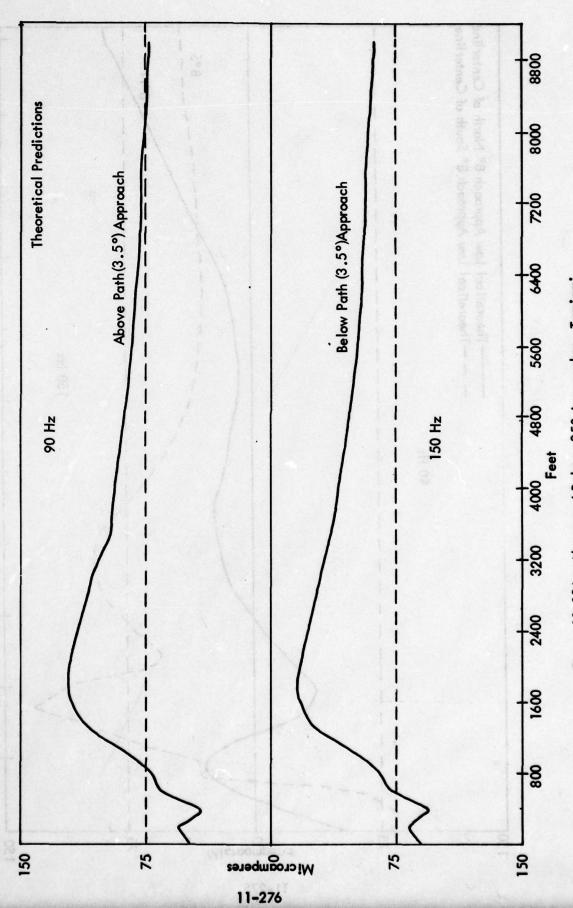


Figure 11-186. Above and Below .35° Approaches, Tamiami.

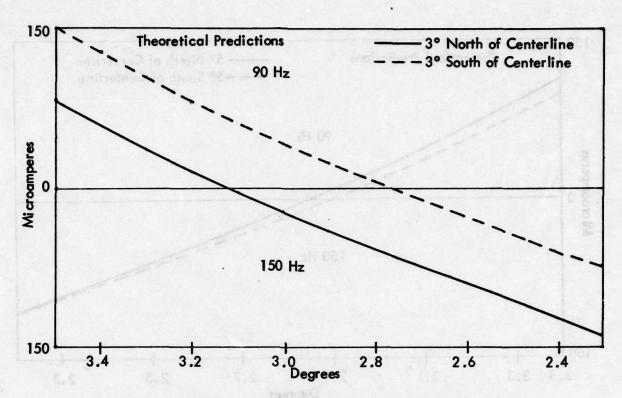


Figure 11–187. Level Pass, Altitude 1000', 3° North and South of Centerline.

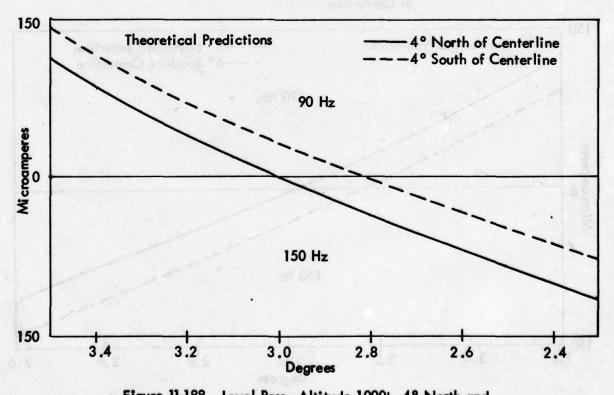


Figure 11–188. Level Pass, Altitude 1000', 4° North and South of Centerline.

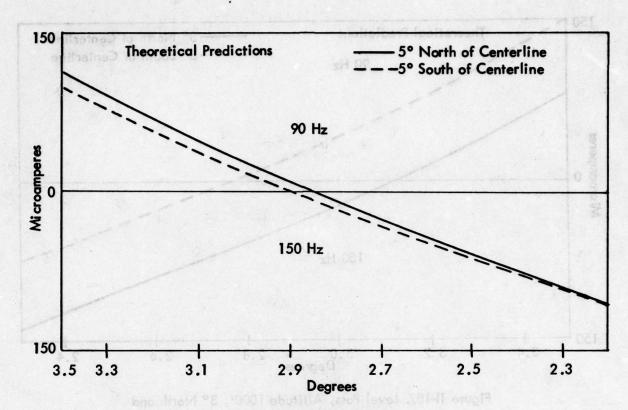


Figure 11–189. Level Pass, Altitude 1000', 5° North and South of Centerline.

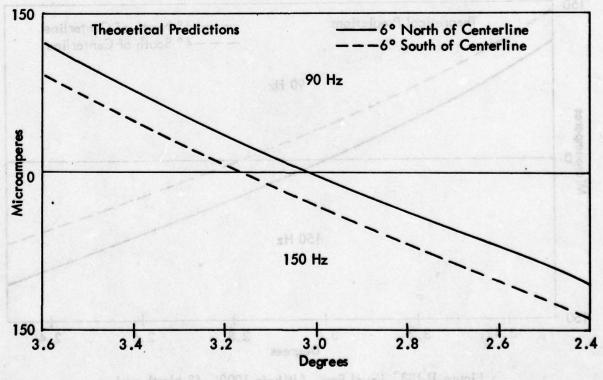


Figure 11–190. Level Pass, Altitude 1000', 6° North and South of Centerline.

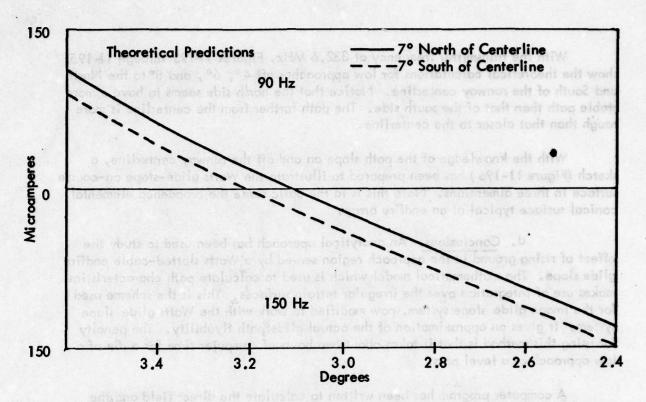


Figure 11–191. Level Pass, Altitude 1000', 7° North and South of Centerline, Tamiami.

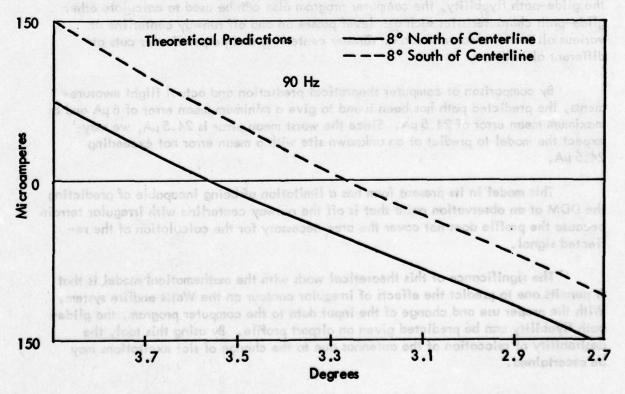


Figure 11–192. Level Pass, Altitude 1000', 8° North and South of Centerline, Tamiami.

With the transmitter frequency at 332.6 MHz, Figures 11–193 through 11–195 show the theoretical calculations for low approaches off 4°, 6°, and 8° to the North and South of the runway centerline. Notice that the north side seems to have a more stable path than that of the south side. The path farther from the centerline is more rough than that closer to the centerline.

With the knowledge of the path slope on and off the runway centerline, a sketch (Figure 11–196) has been prepared to illustrate the Watts glide-slope on-course surface in three dimensions. Note this is in the basic sense the broadened elemental conical surface typical of an endfire array.

d. Conclusions. An analytical approach has been used to study the effect of rising ground in the approach region served by a Watts slotted-cable endfire glide slope. The mathematical model which is used to calculate path characteristics makes use of integration over the irregular terrain surfaces. This is the scheme used for the image glide slope system, now modified to work with the Watts glide slope system. It gives an approximation of the actual glide path flyability. The penalty for using this method is that it takes about two hours of computer time for a run of a low approach or a level pass.

A computer program has been written to calculate the direct field and the reflected field by the ray-optic technique as well as the integration technique. It provides the resultant glide path in DDM or CDI deflection. As well as predicting the glide-path flyability, the computer program also can be used to calculate other glide-path characteristics such as: level passes on and off runway centerline at various altitudes; clearance run on runway centerline and perpendicular cuts at different altitudes.

By comparison of computer theoretical prediction and actual flight measurements, the predicted path has been found to give a minimum mean error of $6\,\mu\text{A}$ and a maximum mean error of $24.5\,\mu\text{A}$. Since the worst mean error is $24.5\,\mu\text{A}$, we may expect the model to predict at an unknown site with a mean error not exceeding $24.5\,\mu\text{A}$.

This model in its present form has a limitation of being incapable of predicting the DDM at an observation point that is off the runway centerline with irregular terrain because the profile does not cover the area necessary for the calculation of the reflected signal.

The significance of this theoretical work with the mathematical model, is that it permits one to predict the effects of irregular contour on the Watts endfire system. With the proper use and change of the input data to the computer program, the glidepath flyability can be predicted given an airport profile. By using this tool, the desirability of relocation of the antennas due to the change of slot excitations may be ascertained.

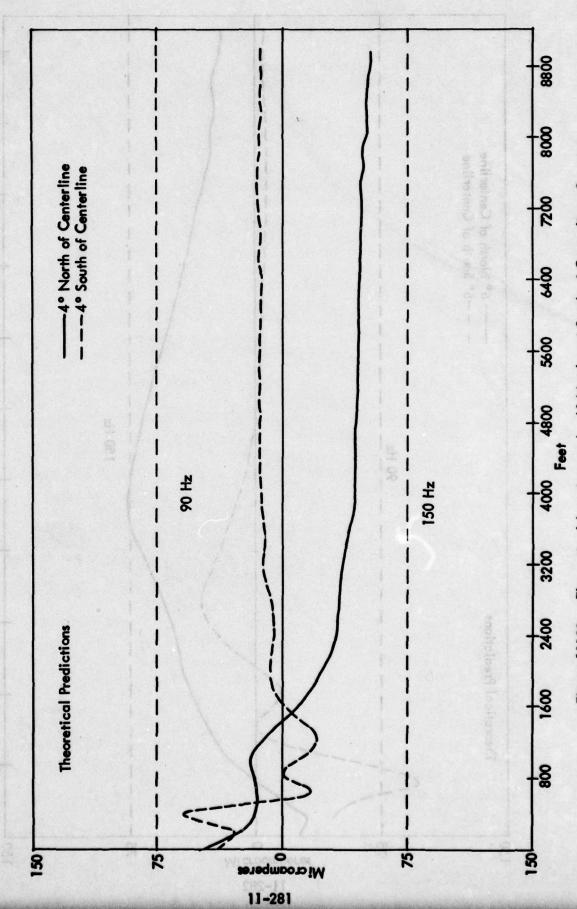


Figure 1 H93. Theoretical Low Approach, 4° North and South of Centerline, Staunton.

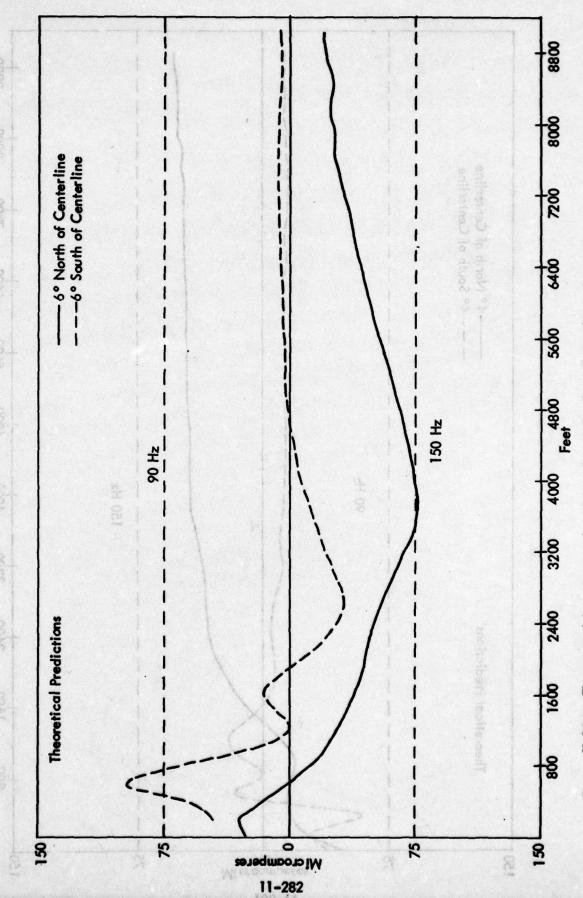
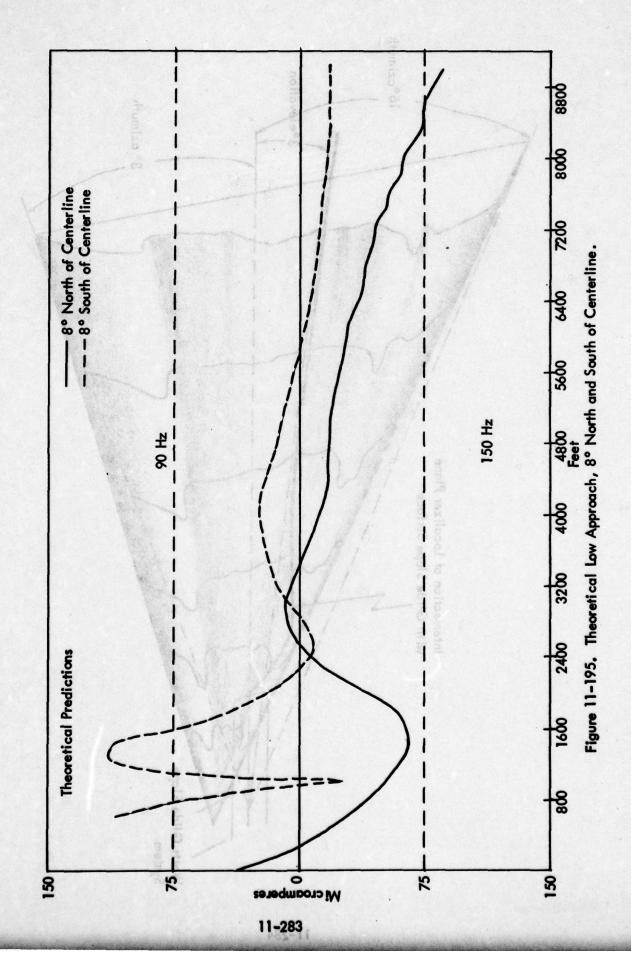


Figure 19193, Theoretical Low Approach, 4° North and South of Centerline, Security,

Figure 11-194. Theoretical Low Approach, 6° North and South of Centerline, Staunton.



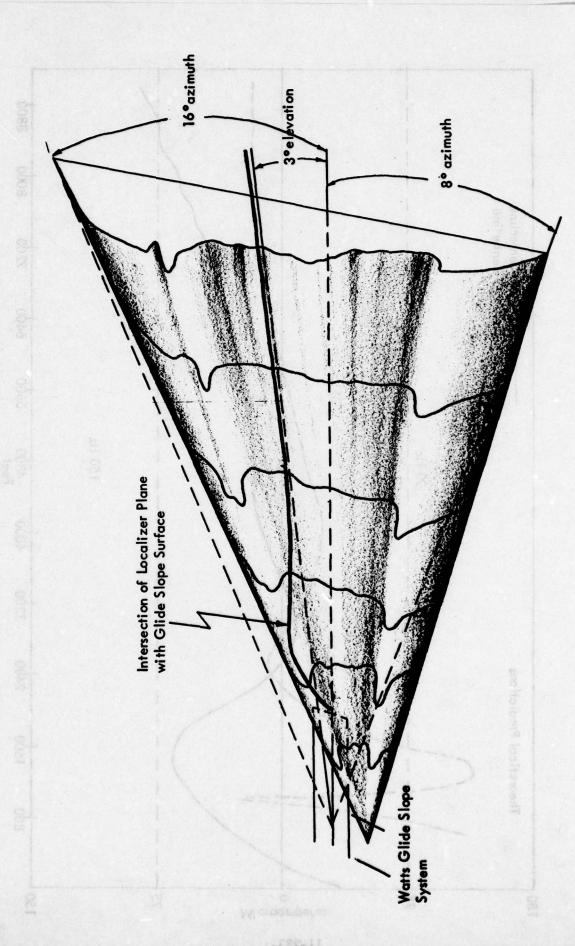


Figure 11-196. Diagram to Show the Conical Structure of the Watts Array.

The classical method of ray-optics technique is also used in cases where the first Freenel zones are smaller than the flat terrain of the airport. This will help to reduce the long computing time caused by the large number of Huygen's sources with the integration technique.

Improvements in the model can be obtained by incorporating the diffraction effects from hill tops or edges of flat terrain areas which suddenly drop off into valley areas.

- 6. Evaluation of the Watts Mark 3 Endfire Glide Slope at Rock Springs, Wyoming.
- a. <u>Introduction</u>. Two flight evaluations of the Watts Mark 3 glide slope system were performed November, 1977 and May, 1978. This section presents results and conclusions from these evaluations.
- b. <u>Background</u>. The Rock Springs (Sweetwater County), Wyoming Airport is situated on top of a mesa at an altitude of 6747 feet MSL and is located in southwest Wyoming. A new runway (9/27) is presently under construction that offers a limited ground plane that would prohibit operation of an image-type system. Consequently, a Watts Mark 3 endfire (non-image) glide slope system, using standard length slotted-cable antennas has been selected and installed on Runway 27 now under construction. This system has been set up before runway completion in order to permit evaluation of monitoring and performance stability, factors heretofore studied only with temporary experimental site conditions as described earlier in this report. This is the first example of a Watts system being installed as a permanent facility.

This section contains the results of airborne evaluations of the Watts system performed in November, 1977 and May, 1978, by members of the FAA, Ohio University, and the Watts Prototype Company.

The aircraft used for the November, 1977 measurements was a Beechcraft Bonanza A-36 equipped with the Ohio University Mark 3 Minilab data collection package. A Bonanza V-35, similarly equipped, was used in May, 1978. Because no localizer was available for Runway 27, azimuth guidance for the aircraft was provided by Warren Knight Model WK 83 theodolite through a second telemetry channel.

c. <u>Flight Evaluation</u>, <u>November 1977</u>. The theodolite, which provided both azimuth and elevation references, was located on runway centerline 62 inches high, 98 feet in front of the touchdown point.

The weather for the testing period involved temperatures ranging from 0° in the morning to 20° F in the afternoon and moderate gusting winds at times; on several occasions, snow showers restricted visibility and halted flight checking.

At the time of these tests, commercial power was not yet available at the glide slope site; therefore, an FAA-furnished emergency generator was used. The use of a mobile power source rather than commercial power did not in any way appear to degrade system performance. The slotted-cable antennas are presently positioned for a runway that is 5 feet lower than the existing runway. A fly-down signal, referencing the runway, is then produced when approaching close to the threshold. This along with the path angle depression exhibited in the previous Tamiami tests yields an undesirable composite which will necessarily be modified.

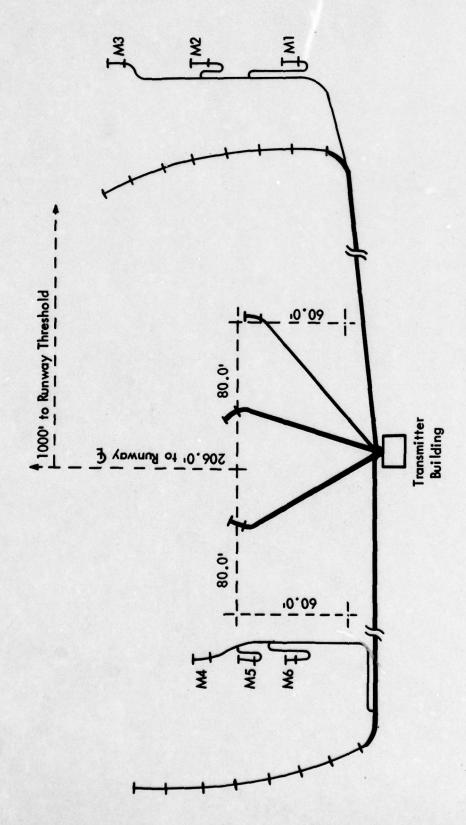
The transmitter and monitor used with the Watts antenna are part of the standard Wilcox Mark I D two-frequency system. Three monitor channels are provided. Transmitting and monitoring antenna positioning for this system are shown in Figure 11-197. The position of the antennas with respect to each other is the same as they were in the Tamiami installation discussed earlier; however, the phase center is displaced an additional 40 feet from the runway center and the antenna system is canted by one more degree (a total of 4.5 degrees) towards the runway.

(1) <u>Discussion of the Data</u>. Data-taking at Rock Springs was performed in a manner consistent with U.S. Flight Inspection Handbook specifications. In addition, emphasis was placed on measurements that would provide special information on perpendicular path structure, a component that is crucial to proper endfire operation.

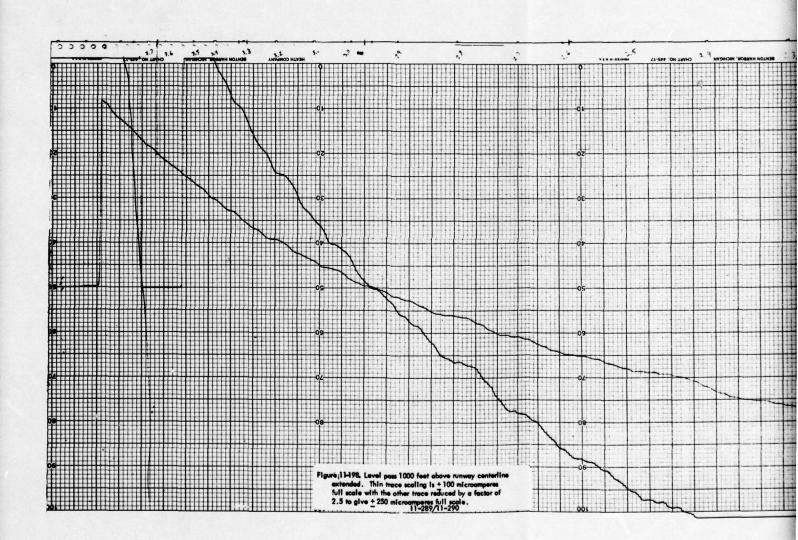
Figure 11-198 shows a typical transition made from 7 miles from the array to 2 miles at 1000 feet over the extended centerline. The two traces on this recording represent the same information only at different scale factors, one with \pm 100 microamperes full scale, and the other at \pm 250 microamperes full scale. Although not shown in Figure 11-198, below path clearance is greater than 200 microamperes below 2.07°. The path angle is measured at 2.97°, the width at .70°, with a symmetry of 50:50 for the \pm 75 microampere points; 1.42° total width angle with a symmetry of 48:52 (above/below) for the 150 microampere points. A very good, nearly linear vertical path structure is evident.

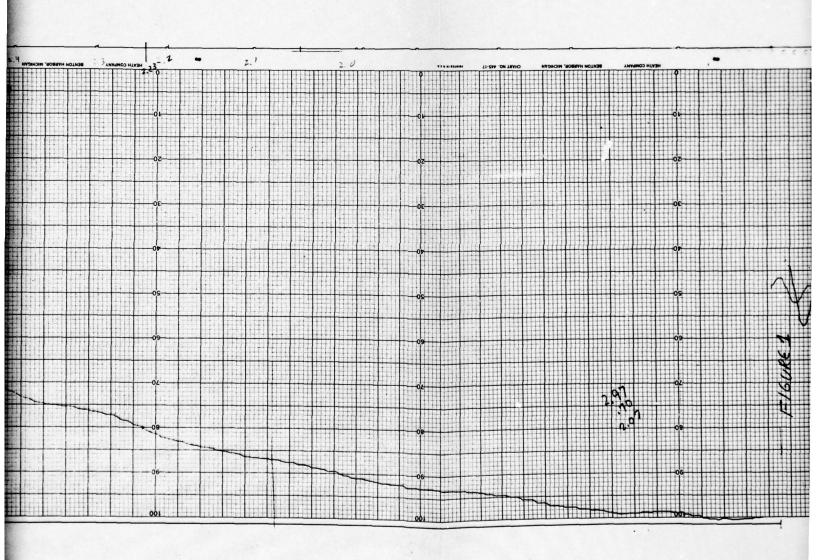
Figure 11-199 shows the final portion of a low approach (Pattern A). Tolerance limits for Category I structure and course alignment have been added to this figure; scale factor for both the difference amplifier and CDI trace is \pm 100 microamperes full scale. As seen in Figure 11-199, the path dips downward beyond tolerance limits near runway threshold.

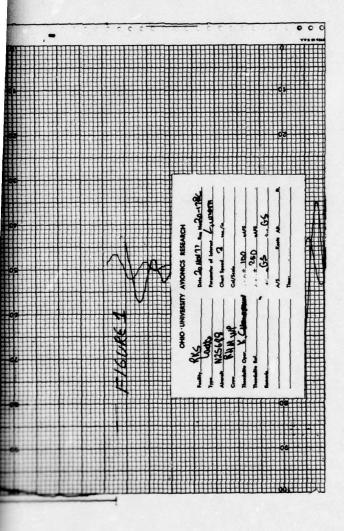
Calculations show that a 5-foot height differential between the reference and a low path indicate a 0.29° depression at the threshold. Flight checks on this Watts Mark 3 array at a level Tamiami site revealed a smaller (40 microampere) dip in the path structure with a reversal 500 feet before the threshold. Means for modifying this depression is now under investigation by Watts.

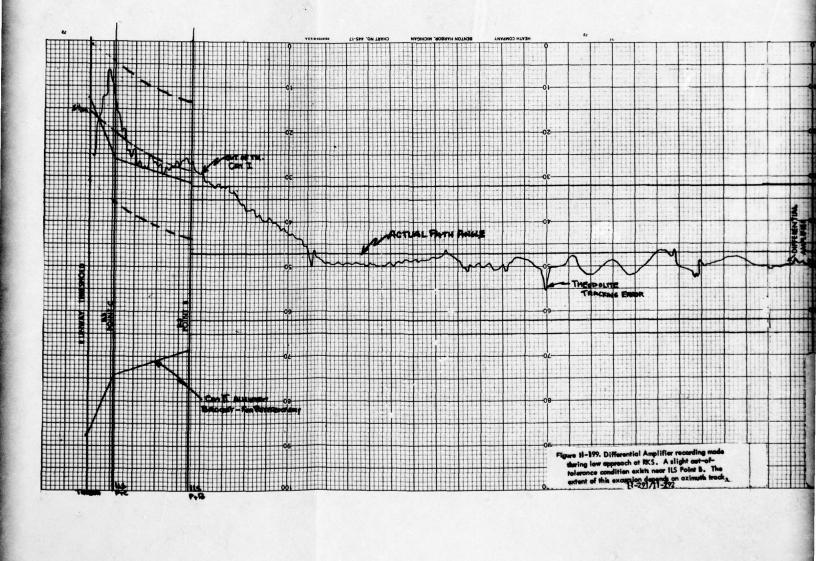


Layout of the Watts System at Rock Springs Airport. Heavy tracings of feed lines indicate transmission lines carrying power to the antennas. The theodolite is located on runway centerline at 62" divided by the tangent of 3° (98.6') ahead of the centerline point abeam the phase center. (September, 1977) Figure 11-197.









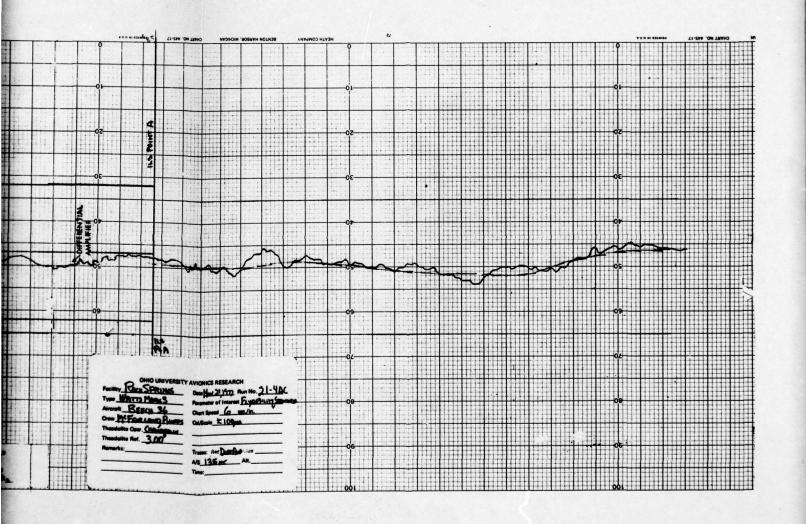


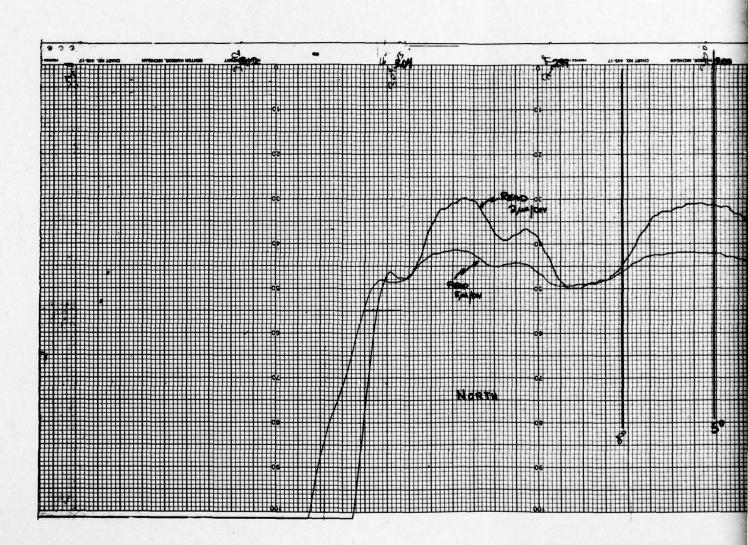
Figure 11-200 reveals the path structure as a function of azimuth. As with Figure 11-198, both traces represent CDI, only with varying scale factors (2.5:1). As can be seen the azimuth coverage is skewed with respect to runway centerline to provide best possible path structure from the outer marker to point C. Figures of merit for the perpendicular structure can be determined by the difference in CDI values between specific azimuth angles (see Table 11-16).

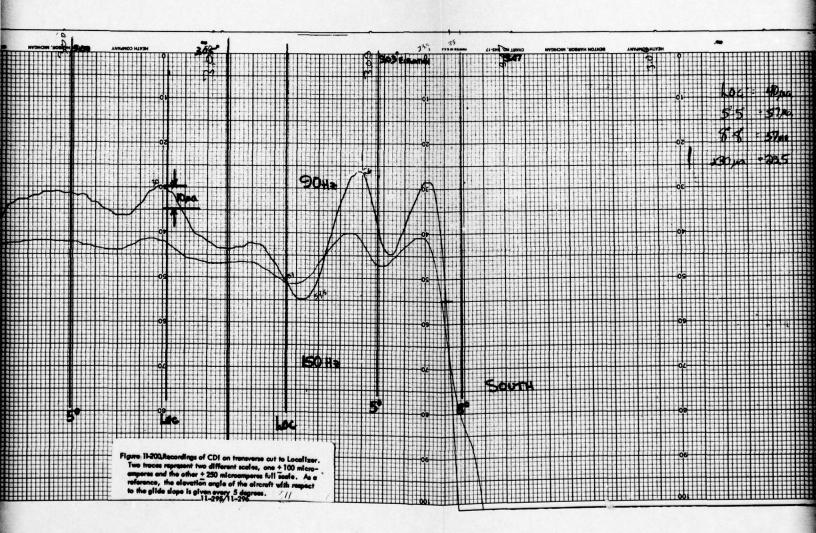
	Localizer	5°-5°	8°-8°	±30 μA Sector
Rock Springs	40 هـ 40	57 µA	57 µA	23.5°
Tamiami	27 µA	40 µA	49 µA	19.6°

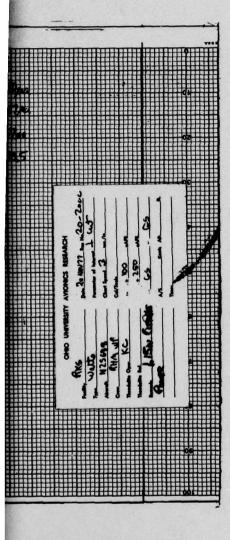
Table 11-16. Figures of Merit for Perpendicular Structure.

Monitor alarm limits for the path angle were set by adjusting tone balance and checked by line dephasing. Path width alarm limits were set by adjusting the sideband power level and checked by sideband-to-carrier dephasing. Weather conditions prevented more extensive checking during this series of tests.

- (2) <u>Conclusions November, 1977 Test Series</u>. The following conclusions are based on data obtained from flight measurements made at Rock Springs, Wyoming, November, 1977.
- 1. Data obtained on the characteristics of the Watts system operating at Rock Springs are consistent with those obtained at Tamiami.
- 2. Differential in runway height and effective antenna array height results in a decrease of the path angle, observed approaching the runway threshold, when referencing the touchdown point on the runway. This condition needs to be corrected.
- 3. Azimuth coverage appears adequate. The increased displacement of the array from the runway centerline compared to the Tamiami installation has resulted in a less desirable azimuth coverage pattern.
- 4. Clearance below path and smoothness of the general path structure are excellent.
- 5. Recordings of the level transition through the vertical path structure indicate very little influence of the irregular terrain near the site. A very nearly perfect linear vertical structure is present.
- 6. The Mark I D serves adequately as a transmitter; however, signal strength available at 10 miles is at minimum allowable levels.







- 7. Clearance power level should be monitored with a ± 1 dB tolerance. Main transmitter power level should also be maintained within this tolerance.
- 8. The two-frequency operation is considered essential for adequate coverage and performance.
- d. Flight Evaluation, May, 1978. This section presents data on the performance of the Watts Mark 3 endfire glide slope array installed on Runway 27 at Rock Springs, Wyoming, as measured in May, 1978. Following the November, 1977 flight checks discussed in the previous pages, Watts determined new antenna positions necessary to compensate for the dip noted in the path as the aircraft approached the threshold. It was decided, however, that the antennas not be moved to the new positions until a second series of flight measurements were made. The motive was to allow determination of stability and the effects of other system changes. Three known changes had occurred, viz, (1) removal of approximately one foot of earth from the runway surface, (2) relocation of the monitor pickup probes from approximately 50 feet in front of the antennas to a position a few inches to the rear of the transmitting slotted cable, and (3) replacing the plastic antenna pedestals with fiberglass pedestals for improved rigidity.

Results of the changes given above were seen as an increase in path angle and width and the lateral tilting of the on-course surface. Indications are that changes associated with installation of the new pedestals are responsible because the other system changes are known to be incapable of altering the path characteristics as observed between the November and May flight evaluations.

Antenna phasing and sideband power were adjusted so as to provide a path angle and width of 3.00 and 0.70, respectively. This action did bring about Category I performance although the transverse slope in the course structure remained. The antenna positions were then changed resulting in minimization of that tilt.

The monitor pickup probes had been moved from their position of approximately fifty feet in front of the antennas to several inches behind the antennas to minimize the effect of changes in the ground plane on the monitor readings. Sizable snow drifts between the antenna and the pickup probes had caused large fluctuations in the monitor during the winter. The new pickup probe positions did make the monitor less susceptible to ground plane variations, but unfortunately desensitized the monitor to some fault conditions.

Delays in acquiring data were caused by heavy snow, dust storms, and high gusting winds (up to 50 MPH). Temperatures ranged from 25°F in the mornings to the low 50's in the afternoon. Once weather conditions improved, 136 flight runs were made over a four-day period.

(1) Theodolite Placement. The position of the theodolite is, of course, most important to the apparent course structure recorded near threshold. Because the endfire system is an entirely different physical configuration of radiating

elements forming the glide slope, the instructions provided in the Flight Inspection Handbook 8200.1 for theodolite placement are not applicable. The basic philosophy still applies, viz, that the reference system should provide for an ideal reference path leading to the touchdown portion of the runway.

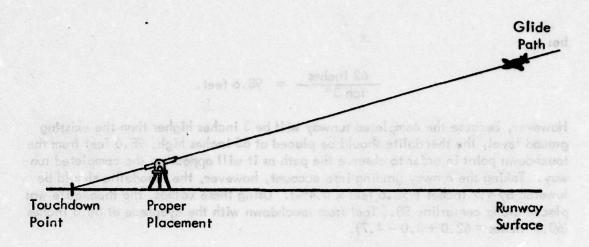
Two theodolite locations were used for the measurement made at Rock Springs. The theodolite was located on the planar surface rising at a 3-degree elevation angle from the touchdown point on the runway. The first location was on the centerline of the runway in order to provide convenience in referencing the mathematical predictions. Because of anticipated problems of locating on the runway for practical, routine flight checking, the theodolite was relocated on the reference 3-degree plane but at the edge of the runway. A comparison shows that no significant difference in observed values is produced.

Concern with theodolite placement was heightened because of the earth movement associated with construction of this new Runway 27. Upon arrival at Rock Springs it was learned that the earth surface representing Runway 27 was now one foot lower than it had been in November. Earlier complications had occurred when a 3-degree lateral slope was graded and the antenna array necessarily had to be placed on this slope.

Figure 11-201 indicates the nature of measurement errors that can occur with improper theodolite placement. If properly placed, the theodolite will not have to deviate from the actual glide path angle as the aircraft moves in toward the theodolite. For a theodolite positioned above the actual path angle, an apparent dip in the path will occur as the aircraft nears threshold; conversely, a theodolite positioned below the path angle will see an apparent rise in the path near threshold (a report presenting a detailed analysis of measurement errors introduced by theodolite placement has been written [17]). Obviously, the eyepiece of the theodolite should be positioned along the glide path to measure accurately and directly the structure of the radiated glide slope signal.

On Runway 27, the touchdown point on the runway is where a perpendicular to the runway centerline intersects the phase center of the antenna array. The runway slopes upward toward threshold at a 0.4% grade; the completed runway surface will be 3 inches higher than the ground level at the time the flight evaluations were run.

To position a theodolite on a level runway surace at a 3° path angle with the eyepiece at the nominal 62 inch height, the distance from the touchdown point would



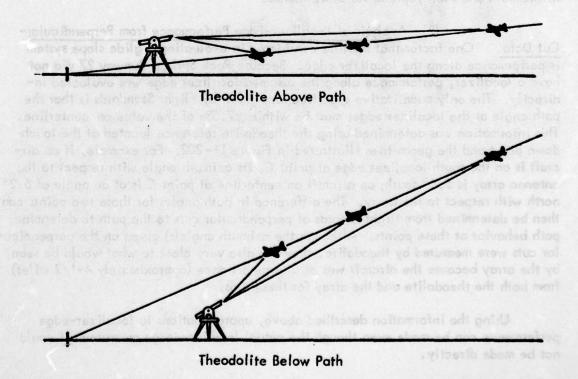


Figure 11-201. Conceptual Drawing Depicting the Effect of Theodolite Placement on the Measured Path Structure Near Threshold.

be:

However, because the completed runway will be 3 inches higher than the existing ground level, the theodolite should be placed at 65 inches high, 98.6 feet from the touchdown point in order to observe the path as it will appear on the completed runway. Taking the runway grading into account, however, the theodolite should be lowered by 4.7 inches (=98.6 feet \times 0.4%). Using these values, the theodolite was placed along centerline 98.6 feet from touchdown with the eyepiece at 60.3 inches (60.3 inches = 62.0 + 3.0 - 4.7).

When selecting the theodolite position off-centerline, it is assumed that the glide path forms a plane consisting of points that are at a 3° angle with respect to the runway touchdown point. Any position near the runway where the eyepiece of the theodolite intersects that plane is correct. The phase center is four feet below the runway centerline elevation on Runway 27. Human factors, however, dictate that the theodolite be positioned at close to 62 inches. In order to achieve that, the theodolite was moved 15 feet from the phase center towards the far side of the runway at threshold and the eyepiece set at 62 inches.

(2) Analysis of Localizer-Edge Performance from Perpendicular-One factor that must be considered in evaluating a glide slope system is performance along the localizer edge. Because Rock Springs Runway 27 did not have a localizer, performance along the assumed localizer edge was evaluated indirectly. The only quantitative specifications given by Flight Standards is that the path angle at the localizer edges must be within ±7.5% of the value on centerline. This information was determined using the theodolite reference located at the touchdown point and the geometries illustrated in Figure 11-202. For example, if an aircraft is on the south localizer edge at point C, its azimuth angle with respect to the antenna array is 5.3° south; an aircraft on centerline at point C is at an angle of 6.2° north with respect to the array. The difference in path angles for those two points can then be determined from flight records of perpendicular cuts to the path to determine path behavior at these points. Although the azimuth angle(s) given on the perpendicular cuts were measured by theodolite, they are also very close to what would be seen by the array because the aircraft was at a large distance (approximately 4-1/2 miles) from both the theodolite and the array for these runs.

Using the information described above, approximations to localizer-edge performance can be made even though the actual localizer-edge measurement could not be made directly.

(3) The monitor pickup probes had been moved since the November flight evaluation to positions shown in Figure 11-203. The former probe locations had proven effective in Tamiami, Florida; however, sizable snow drifts encountered in Rock Springs resulted in unacceptable monitor response. The probes were moved to a

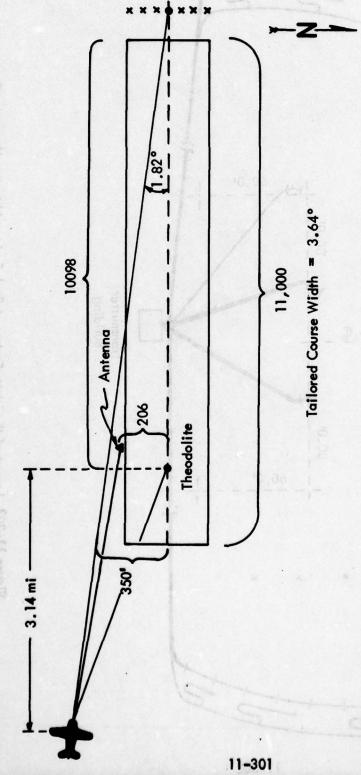


Figure 11-202, Pertinent Dimensions for Determining and Measuring the Localizer Edge. (Mot to scale)

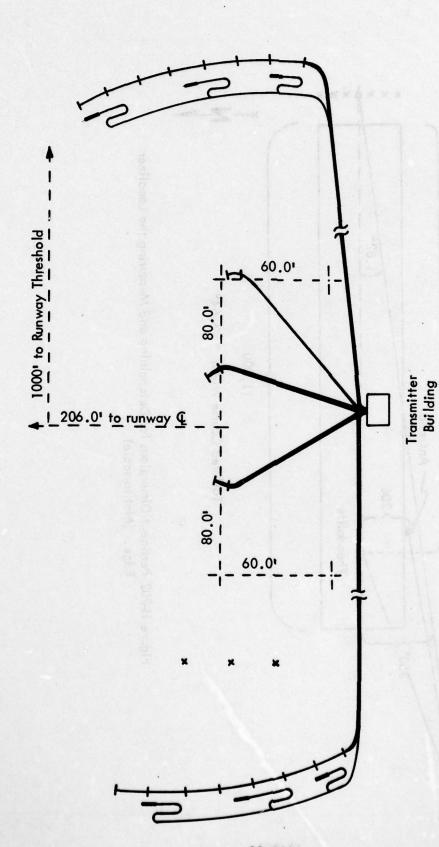


Figure 11–203. Layout of the Watts System at Rock Springs Airport. Heavy tracings of feed lines indicate transmission lines carryina power to the antennas. (May, 1978)

position a few inches behind the slotted-cable transmitting antennas and just behind the reflectors. This minimized effects caused by such local ground plane changes.

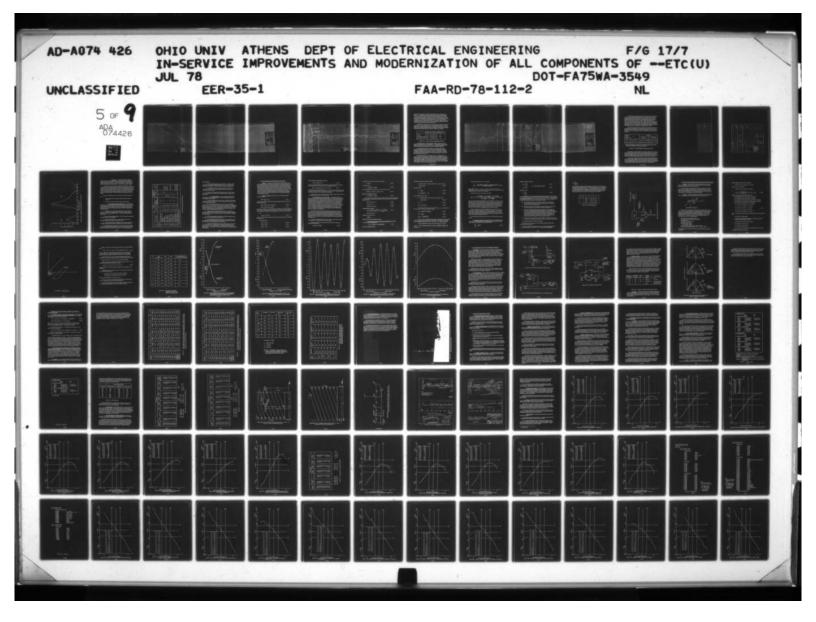
Movement of the monitor probes did result in stable monitor operation; however, the monitor was no longer capable of responding properly to faults located on the slotted cable between the monitor sampling elements. Modifications to the pickup probes are planned by Watts to bring about proper monitor operation.

At one point in the test sequence, the monitor probes were removed from their present position to determine what, if any, effect they had on the radiated glide path. Flight checks performed with the probes removed revealed no significant change in path characteristics with respect to data taken with the probes in place.

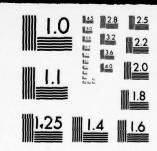
The Mark I D monitor system requires two "path" inputs in order to perform properly. When operating with a capture-effect system, these inputs are provided by the integral path detector and the 360° proximity point detector. As configured with the Watts system, one of these path signals comes from the integral monitor, and the other is sampled from a point in the antenna distribution network where the sideband and carrier signals add in quadrature. This auxiliary monitor responds to changes in carrier-to-sideband phasing and, as will be shown in the section on fault testing, will alarm well before any degradation is observed in the far-field signal. Relaxation of the alarm limits for this monitor, however, are not considered necessary due to the stability that is typically realized in carrier-to-sideband phasing with the Mark I D transmitting system.

- (4) <u>Discussion of the Data</u>. As in November, 1977, this May, 1978 data collection at Rock Springs was accomplished in a manner generally consistent with U.S. Flight Inspection Handbook specifications. Special emphasis as usual with the Watts array was placed on measurements providing information on the perpendicular path structure.
- a) Normal Operation. Figure 11-204 shows a typical transition (Pattern B) made from 7 miles from the array to 2 miles at 1000 feet over the extended runway centerline. The two traces on this recording represent the same information only at different scale factors, one with ±100 microamperes full scale, and the other at ±250 microamperes full scale. As seen in Figure 11-204, below path clearance is greater than 200 microamperes below 2 20°. The path angle is measured at 3.00°, the width at 0.68°, with a symmetry of 48:52 (above/below); 1.24° total width angle with a symmetry of 47:53 (above/below) for the 150 microampere points. As with the level transmission data taken in November, a very good, nearly linear vertical path structure is evident.

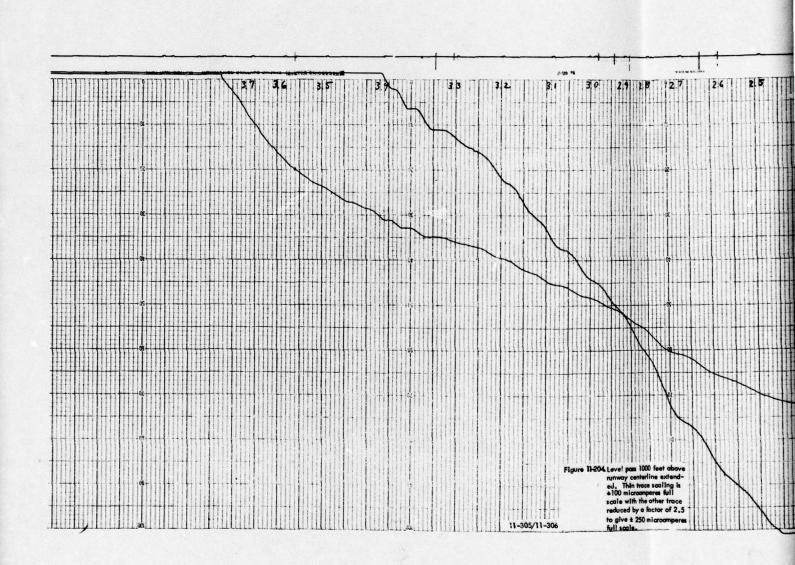
Figure 11-205 presents several low approaches (Pattern A). Tolerance limits for Category I structure and course alignment have been added to this figure; scale factor for these traces is ±100 microamperes full scale. As can be seen in Figure 11-205, path structure meets Category I specifications for path structure. However, a depression in the path is still evident inside ILS point C which may, due to measurement

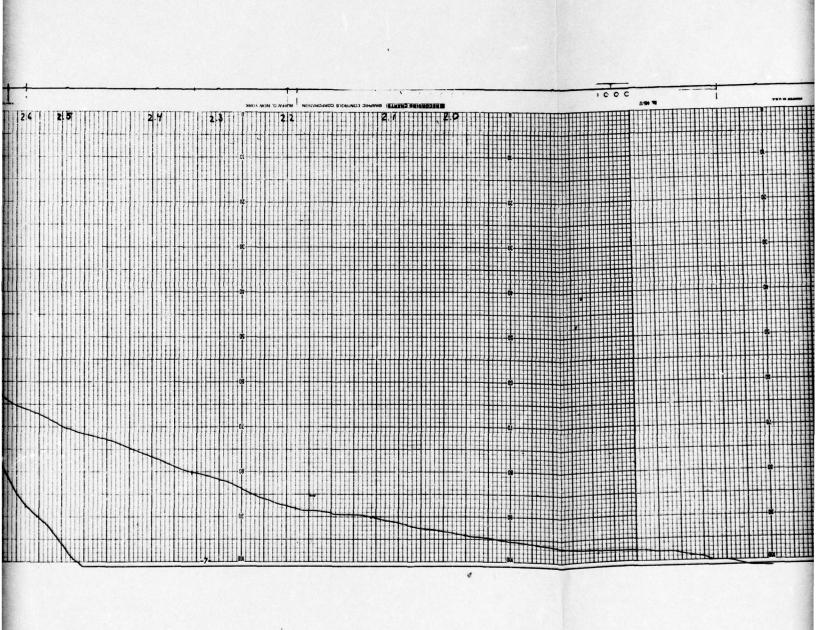


5 OF SADA 426



MICROCOPY RESOLUTION TEST CHART



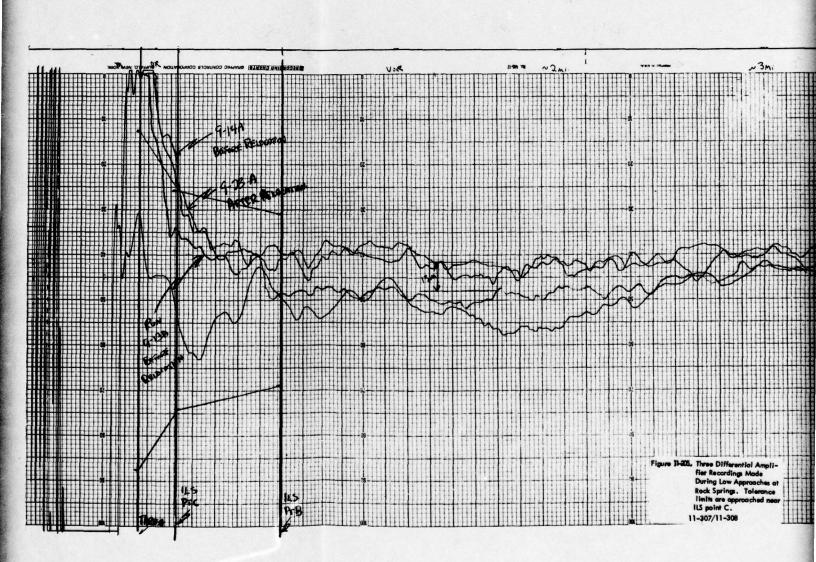


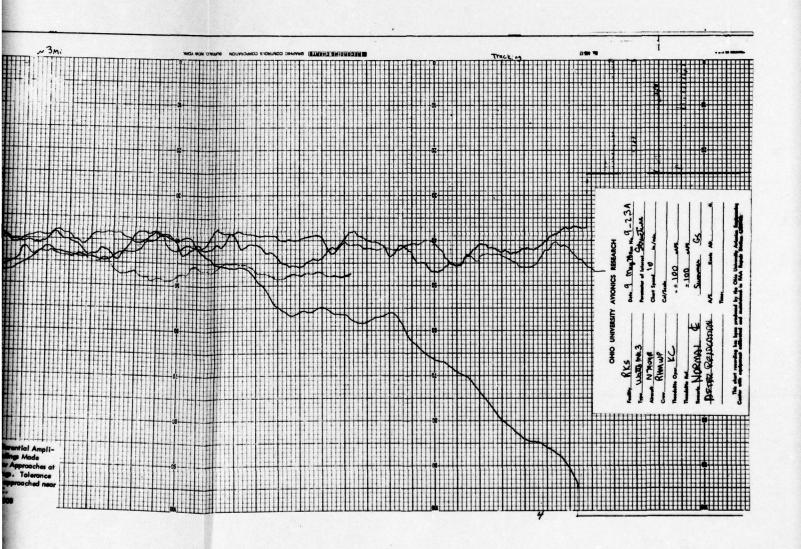
OND UNIVERSITY AND WEST BEAUCH

WIND MA 3

W

7





error or due to fluctuations in the path, cause the path structure to appear out-of-tolerance. It is suggested that consideration be given to raising the path angle to a 3.10° value at point A so that the path structure approaching ILS point C threshold will not be marginal with respect to tolerance limits. Of the three records, two were performed with the theodolite on centerline and the other with the theodolite positioned off-centerline. The similarity of these records provides good evidence that the theodolite position may be moved off-centerline. Also evident in Figure 11-205 is the smoothness of the path outside of point B; some of the apparent roughness after point B was due to tracking and aircraft motion from turbulance.

Degradation in the lateral path structure has occurred, probably due to antenna repositioning. A typical perpendicular cut to the path (Pattern C) is shown in Figure 11–206. Figures of merit previously defined for the endfire array identify the maximum difference in CDI values between specific azimuth angles. Values observed at Tamiami, Florida and Rock Springs in November are given in addition as a reference:

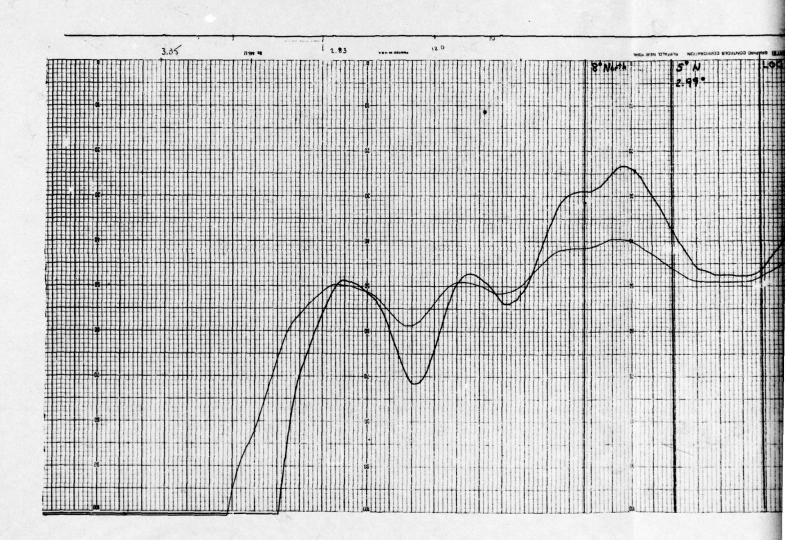
	Localizer	5°-5°	8°-8°	±30µA Sector
Tamiami	27 μΑ	40 µA	49 µA	19.6°
Rock Springs (11/77)	40 µA	57 µA	57 µA	23.5°
Rock Springs (5/78)	54 µA	70 µA	90 µA	8.3°

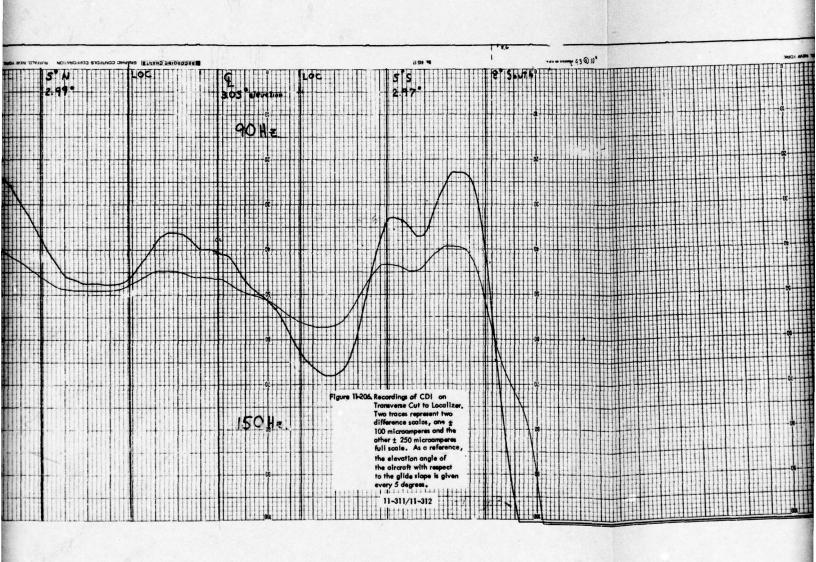
Table 11-17. Figures of Merit for Perpendicular Cut Data.

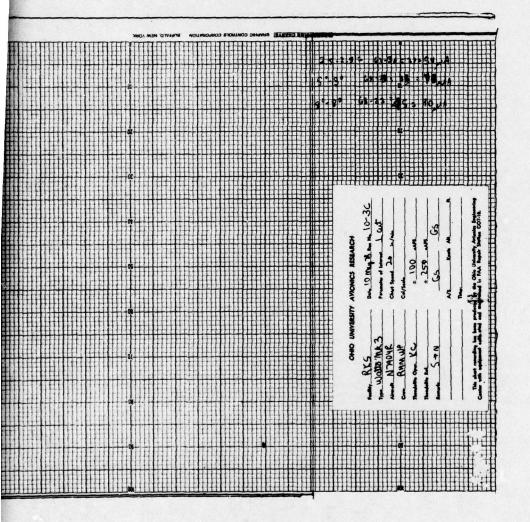
As mentioned earlier, the data presented in Figure 11–205 can be used to determine performance along the localizer edges. This measurement is assumed to be made on a level flight run along the localizer edges. Localizer-edge Pattern B runs at Rock Springs showed path angles within 7.5% of the angle at centerline.

Low approaches (Pattern A's) were flown with an RTT providing azimuth guidance for 5-degree azimuth tracks. The path structures observed on the south side exhibit a smooth but low (2.74°) up to 2.5 miles. Then it begins a .05 degree per thousand feet increase which continues for almost 1 1/2 miles with a reversal to give a decreasing trend to the threshold. The maximum path angle is 3.18° and the minimum to ILS point C is 2.83° .

On the north side the actual path angle in zone 2 is approximately 2.74° with a lowering to 2.65° into zone 3. The path character was generally very smooth. It should be noted that the flight inspection manual does not call out any specifications for these regions as measured. The only values for the off-centerline measurements are the maximum allowable ± 7 1/2 percent path angle changes to the localizer edges. These tolerances were met with Pattern C observations, viz, 2.88° on the south edge of the localizer; 3.05° on the north edge of the localizer.







To elaborate further concerning behavior off-centerline, principally because of the crucial nature of endfire operation, Table 11–18 is given below. This lists calculated azimuth angles (with respect to the antenna array) and measured CDI readings corresponding to those angles for aircraft positions along centerline and both sides of the localizer course at 4.5 nautical miles from threshold and at point C. The results presented in Table 11–18, which were derived from perpendiclar-cut flight records, compare closely with other flight records at positions where comparisons can be made. For example, a 50 microampere fly-down indication was measured at point C, on-centerline on low approaches which compares well with the 51 microampere indication calculated from the perpendicular-cut data.

The pertinent information that can be derived from this table is that the path along both localizer edges are well within tolerance when the aircraft is far from threshold; the south localizer edge is within 18 microamperes of the centerline path angle at point C, and a strong fly-up signal is seen along the north localizer edge at point C.

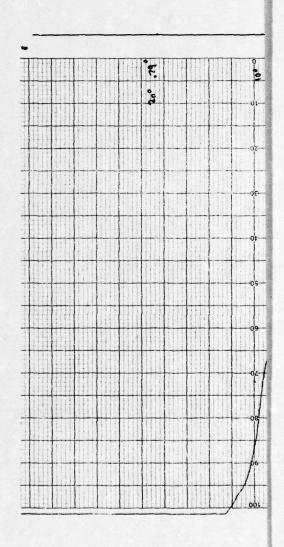
Distance	c	Loca	alizer o
from Threshold	*	South Edge	North Edge
4.5 NM ILS Point C	19µA/90 Hz (0°)* 51µA/90 Hz (6.2°N)		22µA/90 Hz (1.82°N) 170µA/150 Hz (17°N

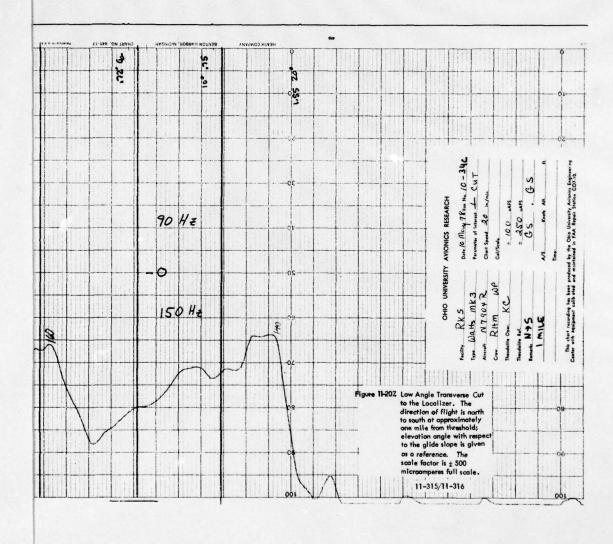
^{*}Numbers in parentheses are azimuth values referencing the phase center of the array which is 206 feet south of the runway centerline.

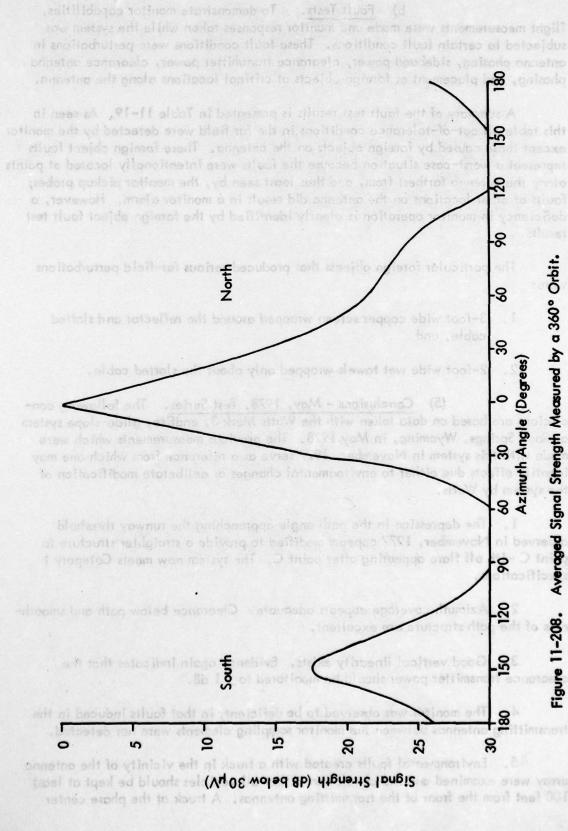
Table 11-18. Calculated Performance Along Localizer Edge.

Figure 11-207 is a flight recording of a low-angle, perpendicular cut to the path to evaluate clearance below path. Note that the scale factor for this recording is 500 microamperes full scale. The azimuth and elevation angles are also given. The pertinent information derived from this record is that there is a hard fly-up signal (full-scale on CDI) everywhere below path for greater than $\pm 20^{\circ}$ off centerline.

A 360° orbit was flown around the antenna system with approximately 4 miles radius to measure signal strength as a function of azimuth; the result of this measurement is plotted in Figure 11–208. The values were derived from the AGC voltage of a receiver calibrated with respect to known input signals. The information presented in Figure 11–208 is consistent with theory and reveals no anomalous behavior.







b) Fault Tests. To demonstrate monitor capabilities, flight measurements were made and monitor responses taken while the system was subjected to certain fault conditions. These fault conditions were perturbations in antenna phasing, sideband power, clearance transmitter power, clearance antenna phasing, and placement of foreign objects at critical locations along the antenna.

A summary of the fault test results is presented in Table 11-19. As seen in this table all out-of-tolerance conditions in the far field were detected by the monitor except those caused by foreign objects on the antenna. These foreign object faults represent a worst-case situation because the faults were intentionally located at points along the antenna farthest from, and thus least seen by, the monitor pickup probes; faults at other locations on the antenna did result in a monitor alarm. However, a deficiency in monitor operation is clearly identified by the foreign object fault test results.

The particular foreign objects that produced serious far-field perturbations were:

- 1. 3-foot wide copper screen wrapped around the reflector and slotted cable, and
- 2. 2-foot wide wet towels wrapped only about the slotted cable.
- (5) Conclusions May, 1978, Test Series. The following conclusions are based on data taken with the Watts Mark 3, endfire, glide-slope system at Rock Springs, Wyoming, in May, 1978. The previous measurements which were made with this system in November, 1977 serve as a reference from which one may identify effects due either to environmental changes or deliberate modification of the system by Watts.
- 1. The depression in the path angle approaching the runway threshold observed in November, 1977 appears modified to provide a straighter structure to point C with all flare appearing after point C. The system now meets Category I specifications.
- 2. Azimuth coverage appears adequate. Clearance below path and smoothness of the path structure are excellent.
- 3. Good vertical linearity exists. Evidence again indicates that the clearance transmitter power should be monitored to ± 1 dB.
- 4. The monitor was observed to be deficient, in that faults induced in the transmitting antennas between the monitor sampling elements were not detected.
- 5. Environmental faults created with a truck in the vicinity of the antenna array were examined and the conclusion is that all vehicles should be kept at least 100 feet from the front of the transmitting antennas. A truck at the phase center

	nach Mari	S.	Far Field	elija Ti	wow	Monitor Kesponse % Alarm	56
Run	Fault Condition	Angle	Width	# 35 A Azimuth Sector Width	Path	Width	Remarks
Normal	ing ing i ing ing	910		eki 1 56	ino it	nont do o	gra geo
10-13	Truck at Phase Center	3.02	۲.	8.5°	0	0	relo orli : ,4:01
10-14	Truck 50' in front of Antenna	2.96	4.	8.3	0	10 10 10 10 10 10 10 10 10 10 10 10 10 1	sei vi strate viur p
9-28	SBO decrease	2.97	%	o and leter	57 1	9	Alarm Set
9-30	Mod. Unbalance	3.20	8.	Sen	100	1	Alarm Set
9-31	Mod. Unbalance	2.77	89.	(*) (*)	92	e Pé	Alarm Set
9-34	Dephase Antenna	2.71	2.	ele qu	<u>8</u>	nijs dos	ele l eole las e
10-10	Decrease CI. Power	•	it a ni P	7.9	100	Till Nor	CL RF Alarm
10-28	Wire mesh on Ant.	2.55	જુ	ah ilho ido	95	edi edi	only only only
10-30	Wet Towel on Ant.	2.71	.74	7.5	95	o c it	arls entr
10-11	CSB /SBO Dephasing +	2.97	٤.	oel oli oli i pa		14 e	Quad. Alarm
10-12	CSB/SBO Dephasing -	3.01	8.	ada gra grig	(1)	io iti nti :	Quad. Alarm

Table 11-19. Summary of Fault Test Results.

posed no problem. 6. Signal strength measurements using an IFR 401 L calibration standard indicate that at intercept altitude (9100 feet MSL), there is a 5 dB margin over FAA minimum requirements. The field elevation is 6747 feet above sea level. 7. Measurements show that relocating the reference theodolite to the runway edge, but still on the 3-degree reference planar surface, provides an acceptable, practical location. Relocation of the monitor sampling elements from in front of the transmitting antennas to the rear of the reflector elements produced no change in the path in space. These recommendations are offered Recommendations. with the objective of producing an optimum Watts endfire glide slope facility at Rock Springs and other locations. The array configuration should be modified to recognize the difference in effective array height, the height of the reference which serves the runway, and the runway threshold crossing height. The antenna array should be kept as close to the runway as possible. Eighty five feet, i.e., ten feet from the front antenna to the edge of a 150 foot wide runway, would seem most desirable. Should a 50 inch high obstruction be objectionable at locations where there is no deep snow expected, the end of the antenna could be lowered. If displacements from centerline greater than 125 feet are necessary, then the longer version of the slotted cables should be used. 3. Additional monitor checks should be made, first, to insure that the limits are adequately tight to produce alarms when far-field tolerances are exceeded, and second, to insure that on a long-term basis that the far-field path characteristics have not changed. 4. The manitoring deficiency noted for faults between sampling points must be corrected and a new series of fault tests executed. 5. Additional flight measurements should be made to acquire airborne data for determination of the degree of far-field path stability. Measurements should be made to acquire data during temperature extreme conditions. 6. Consideration should be given to raising the path angle by at least 0.05° as seen on Pattern B runs. The purpose of this is to provide an improved close-in path characteristic. The overall tendency is for the path angle to decrease as the range increases. Since the Pattern B values are obtained far out, they should be biased on the high side. 11-320

D. ILS Glide Slope Set-Up Measurements Using Thruline Meters.

- 1. General. In setting up the ILS glide slope it is highly desirable to be able to achieve as nearly as possible complete adjustment through ground measurements before making flight checks. This section discusses the use of Thruline meters in adjusting the relative power fed to the various antennas to achieve the proper relation—ships among the various components of antenna currents. These currents are related to power through the impedances seen looking from the meters into the antenna cables. If all the antenna systems are identical, as they are intended to be, then the currents can be assumed to be proportional to the square roots of the powers at the meter locations. If there are unavoidable differences in the antenna and cabling systems, then correction factors may be calculated with the aid of impedance measurements and a transmission line chart.
- 2. Theory The A-Ratio. Consider first a null reference glide slope. The DDM is given by

$$DDM = M_{150} - M_{90}$$
 (11.9)

where M_{150} and M_{90} are the depths of modulation (modulation indices) for the 150 Hz and 90 Hz respectively.

$$M_{150} = (E_{ss}_{150} \cos \gamma_{150} + E_{cs}_{150})/E_{c}$$
 (11.10)

$$M_{90} = (E_{ss}90 \cos \gamma 90 + E_{cs}90)/E_{c}$$
 (11.11)

where E_{ss150} and E_{cs90} are the field strengths of the sideband only sidebands (suppressed carrier) and E_{cs150} and E_{cs90} are field strengths of the sidebands of the modulated carrier. γ_{150} and γ_{90} are the angles between these sidebands. E_c is the carrier field strength.

Now

$$E_{cs}150 = E_{cs}90 = mE_{c}$$
 (11.12)

where m is the coefficient of modulation for each modulating frequency for the amplitude modulated carrier.

With proper balance

$$E_{ss}150 = E_{ss}90 {(11.14)}$$

$$\gamma_{150}^{+\pi} = \gamma_{90}$$
 (11.15)

Substituting (11.10) through (11.15) in (11.9) gives

$$DDM = 2m(E_{ss}/E_{cs})\cos\delta \tag{11.16}$$

here E_{ss} , E_{cs} and δ are functions of position and thus functions of the elevation angle α measured from the base of the antenna tower. (11,16) may be rewritten as

$$DDM = 2m(I_{ss}f_1(\alpha)/I_{cs}f_2(\alpha)) \cos \delta(\alpha) = 2mAF(\alpha)$$
 (11.17)

From (11.17) it is obvious that increasing either m or A will increase the magnitude of the DDM everywhere without changing the zero DDM locus in space. Thus if m is held constant, A controls the path width and is an important set-up parameter.

A similar analysis can be carried through for the sideband reference system and for the capture-effect system leading to the same conclusion.

3. Power Measurement - The Thruline Meter. The Bird Model 43 Thruline Meter consists of a section of 50 ohm airline into which is inserted an especially designed dual pickup probe. Pickup is both inductive and capacitive. Currents produced by the inductive coupling will have components produced by the forward traveling wave 180° out-of-phase with those produced by the backward traveling wave. The capacitively-coupled currents will be proportional to the sum of the forward and reverse traveling waves and, therefore, independent of the wave direction. By careful adjustment the reverse wave inductive current is just nulled by the capacitive current due to the reverse wave, leaving only an indication proportional to the forward wave current. This RF current is rectified and filtered (envelope detected) and fed to an averaging type dc meter. The indication is converted to a power reading by making the scale read proportional to the square of the deflection.

The Thruline thus responds to the average instantaneous peak value of the RF. In other words, the envelope is detected by the diode and associated filter and this AF is applied to the meter movement which responds by averaging over the audio cycle. In the case of carrier and sidebands the detected audio consists of 90 Hz and 150 Hz sine waves plus the dc average which is just the peak of the RF carrier. For an AM signal modulated 100% or less with zero average AF components the Thruline meter will read carrier power only.

In the case of the suppressed carrier, however, there is no carrier power and the audio envelope is not simply two sine waves of zero average.

With proper adjustment of the audio amplitude and phase the envelope after detection will have the form

$$|\sin 2\pi 150t - \sin 2\pi 90t|$$
 (11.18)

To simplify the math this will be written as a function of

$$\theta = 2\pi 30t$$
 (11.19)

Its average is then

$$2\pi$$
 (1/2 π) $\int |\sin 5\theta - \sin 3\theta| d\theta$ (11.20)

Since the magnitude of an odd function is an even function and since

$$\left|\sin 5(\pi - \theta) - \sin 3(\pi - \theta)\right| = \left|\sin 5\theta - \sin 3\theta\right| \tag{11.21}$$

(11.20) may be reduced by symmetry to

$$(2/\pi) \int_{0}^{\pi/2} |\sin 5\theta - \sin 3\theta| d\theta$$
 (11.22)

When, and only when, $\sin 5\theta = \sin 3\theta$ the integrand goes to zero and may change sign. Thus it is sufficient to integrate between adjacent zeros and add the magnitudes of these integrals. Since

$$\sin \phi = \sin((2n+1)\pi - \phi)$$
 (11.23)

$$5\theta = (2n+1)\pi - 3\theta$$
 (11.24)

whence
$$\theta = \pi/8$$
 or $3\pi/8$ (11/25)

consequently (11,22) becomes

$$(2/\pi) \left\{ \left| \int_{0}^{\pi/8} F(\theta) d\theta \right| + \left| \int_{\pi/8}^{3\pi/8} F(\theta) d\theta \right| + \left| \int_{3\pi/8}^{\pi/2} F(\theta) d\theta \right| \right\}$$
(11.26)

$$F(\theta) = \sin 5\theta - \sin 3\theta$$

(11.26) has the numerical value

0.80235

which will be called 0.8 for practical purposes.

4. Using the Thruline Meter to Set-Up Antenna Current Ratios. Consider now the amplitude modulated carrier.

$$I = I_0(1 + m\sin 2\pi 150t + m\sin 2\pi 90t)\cos 2\pi ft$$
 (11.27)

where f is the carrier frequency.

Expanded by trigonometric identities this yields as a still would be still with the still will be still be stil

$$\frac{1}{0}\left(\cos 2\pi ft + \frac{1}{2}m\sin 2\pi (f + 150)t + \frac{1}{2}m\sin 2\pi (f + 90)t - \frac{1}{2}m\sin 2\pi (f - 150)t - \frac{1}{2}m\sin 2\pi (f - 90)t\right)$$
(11.28)

The power will be

r will be
$$P_{c} = \frac{1}{2}I_{o}^{2} Z_{o}$$

$$P_{sb} = 2I_{o}^{2} (m/2)^{2} Z_{o} = m^{2} P_{c}$$
(11.30)

$$P_{sb} = 2I_{o}^{2}(m/2)^{2}Z_{o} = m^{2}P_{c}$$
 (11.30)

For the suppressed carrier we have

$$I = I_0 A(m/2) (\sin 2\pi (f + 150)t - \sin 2\pi (f + 90)t - \sin 2\pi (f - 150)t + \sin 2\pi (f - 90)t)$$
(11.31)

$$P = 0$$
 (11.32)

$$P_{\rm sb} = \frac{1}{2} A^2 \, {\rm m}^2 \, {\rm I}^2 \, {\rm Z} \tag{11.33}$$

In order to set up the antenna current ratio so that $I_{ss} = AI_{sc}$, one must know the proper ratio of thruline power indications P_{ss}^{i}/P_{c}^{i}

$$P_{ss}^{i} = (0.80235)^{2} A_{m}^{2} (I_{c}^{2}/2) Z_{0}$$
 (11.34)

$$P_c^i = (I_c^2/2)Z_c$$
 (11.35)

$$P_{s}^{i}/P_{c}^{i} = (0.80235)^{2}A^{2}m^{2}$$
 (11.36)

Thus, if 1 watt of amplitude modulated carrier is indicated by the thruline meter in the lower antenna line of a null reference glide slope and the DDM is to be 0.0875 (75 μ a) 0.35 degrees above and below the 3° path with m = 0.4, the far field equation

DDM = 2Am(sin(180° (sin a/sin3°))/sin (180° (sina/sin6°)) (11.37)

yields A = 0.300, and P_{ex}^{i} read by the thruline should be $(0.80235)^{2}$ $(0.300)^{2}$ $(0.4)^{2}$ = 0.00922 watts.

For the sideband reference with a 3° path angle

$$DDM = \frac{2mA(\sin(180^{\circ} (\sin\alpha/\sin12^{\circ})) - \sin(180^{\circ} (\sin\alpha/\sin4^{\circ})))}{\sin(180^{\circ} (\sin\alpha/\sin12^{\circ}))} (11.38)$$

Setting DDM = 0.0875, m = 0.4 and $\alpha = 2.65^{\circ}$ or 3.35° yields A = 0.302. As indicated before, 1 watt of carrier power (indicated) requires 9.22 milliwatts of indicated sideband only power into each of the two antennas.

The capture effect system is somewhat more complex.

DDM = 2mA
$$\frac{\sin(180^{\circ} \frac{\sin \alpha}{\sin 3^{\circ}}) - 0.5\sin(180^{\circ} \frac{\sin \alpha}{\sin 2^{\circ}}) - 0.5\sin(180^{\circ} \frac{\sin \alpha}{\sin 6^{\circ}})}{\sin(180^{\circ} \frac{\sin \alpha}{\sin 6^{\circ}}) - 0.5\sin(180^{\circ} \frac{\sin \alpha}{\sin 3^{\circ}})}$$
 (11.39)

Again substituting 0.0875 (75 μ a) for DDM, 0.4 for m and 2.65° or 3.35° for a, gives A = 0.301. Thus, if the thruline for the lower antenna indicates I watt of carrier, the middle thruline should read 250 milliwatts. With the carrier off and the sideband only fed to the APCU, the upper and lower antenna thrulines should read 9.22/4 milliwatts while the middle antenna thruline should read 9.22 milliwatts. These calculations neglect the clearance signal since the ratio of clearance carrier to course carrier will be less than 0.1 which will have negligible effect on path width or angle.

To set the clearance carrier level with respect to the course carrier level, it is only necessary to compare the square roots of the indicated powers. If it is desired to have the ratio of clearance sideband currents to carrier sideband current in the lower antenna equal to some value, R, then the thruline indication for 1 watt carrier power on the lower antenna should read (RM/mc)² where M is the main modulation index (0.4) and mc is the clearance modulation index (0.9).

The foregoing comments apply also to the HP Vector Voltmeter and a directional coupler.

5. Experimental Verification of K Equal to 0.80. Equation (11.40) gives the ratio of the indicated (indicated on an average responding instrument) SBO (sideband only) power to the indicated Carrier plus sidebands power.

$$\frac{P_{ss}^{i}}{P_{c}} = K^{2}A^{2}m^{2}$$
 (11.40)

Defining the indicated voltages as:

$$v_{ss}^{i} = \sqrt{p_{ss}^{i} R_{o}}$$
 (11.41)

$$V_c^i = \sqrt{P_c^i R_c^i}$$
 R_o = system impedance (resistive) (11.42)

Solving for K gives:

$$K = \frac{V_{ss}^{i}}{V_{c}^{i} Am}$$
 (11.43)

Figure 11-209 shows a test set-up for measuring the indicated voltages. If port A of the hybrid is dummied, the vector voltmeter probe for channel B will measure the carrier component of the <u>carrier plus sidebands</u> signal. If pure carrier is then applied to port A of the proper phase and amplitude to cancel the carrier component from port B at port C, only the sidebands will remain to be measured by channel B. The procedure is as follows:

- (a) With the 608 unmodulated, adjust the phaser and the output attenuator until the signal measured by channel B is minimum (should be at least -40 dB from the amplitude with port B disconnected).
- (b) Dummy port A and set for 40% modulation with one tone present. The channel B IF may be observed on an oscilloscope in making this determination.
- (c) With carrier modulated by both tones measure channel B. This voltage is V_C^i . Note: the two tones must have a phase relationship for this test different from that for the normal amplitude modulated carrier signal. Normally at a simultaneous zero crossing both tone waveforms have first derivatives of the same sign. To display the SBO envelope, the first derivatives must have opposite signals at the point where both have a simultaneous zero crossing. In other words, one tone must be 180° out-of-phase from its normal phase relationship.
- (d) Reconnect port A and measure the channel B voltage. This voltage is V_{ss}^{i} and will be lower than that measured in (c) because the carrier component has been canceled.
- (e) Repeat (a) through (d) to check for consistency.

For better resolution on the vector voltmeter reading, a digital voltmeter may be connected to the recorder output.

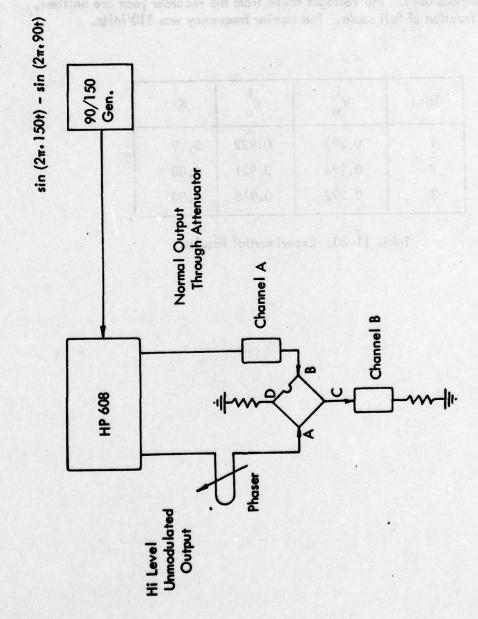
The level of sidebands in (c) and (d) is the same, so for this set of measurements A = 1.0. The modulation was set at 40%, so m = 0.4. Equation (11.43) then becames

$$K = \frac{V_{ss}^{i}}{(0.4) V_{c}^{i}}$$

Table 11-20 below indicates the measured values for V_{ss}^i and V_{cs}^i and the values of K calculated from the equation above. The results are sufficiently close to the theoretical value of 0.80 to make this value usable. The calculation here is only as accurate as the measurement of the percent modulation which can be made to about two places, at best, by the methods used. The voltages taken from the recorder jack are unitless, representing a fraction of full scale. The carrier frequency was 110 MHz.

Trial	v ⁱ ss	v ⁱ _c	к
1	0.293	0.922	0.79
2	0.294	0.921	0.80
3	0.292	0.918	0.80

Table 11-20. Experimental Results.



Trute 11 20 beton tedicous the measured values for V and V and the values of 10 calculation the values of 10 calculated from the exception cover. The results one sufficiently first to the the theoretical value of 0.30 to make this value weaks. The calculation here is only as occurate as the exception of the percent modulation while, can be made to about two places, at the exceptions of the percent modulation while, can be made to about two places, at

Figure 11-209. Test Set-Up for Verifying K.

E. Monitoring Tilt of a Null-Reference Glide Slope Mast with Near Field Detectors.

1. General. This section presents a mathematical analysis of the antenna mast of a null-reference ILS glide slope. The tilt considered is in the vertical planes parallel and perpendicular to the runway centerline.

It is concluded that the far-field angle is not greatly affected by this tilt but that path width is significantly changed by tilts of as little as one degree. Monitoring of this change is accomplished at the 180 degree proximity point only by detectors above (or below) the course angle. Tilt in the plane parallel to the runway centerline is most critical; tilt in the perpendicular plane is non-critical.

2. Analysis. If one assumes a perfectly-conducting infinite horizontal ground plane, the DDM of a null-reference glide slope may be developed as follows.

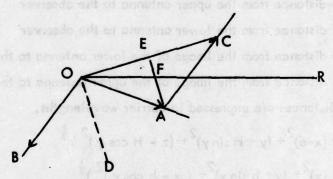


Figure 11-210. Phasor Diagram.

Figure 11-210 is a phasor diagram of the signals from the upper antenna and its image. OR is an arbitrary reference. OA is the phasor representing the direct signal arriving at the point of observation delayed by the distance δ_1 . OB is the phasor representing the signal from the image delayed by the distance δ_4 . Since the reflection coefficient is assumed to be -1, OB is subtracted from OA to give the resultant signal. The phasor AC is parallel to OB but oppositely directed. The sum of OA and AC, OC, is the resultant phasor.

The triangle OAC is isosceles since OA = AC.

The angle AOB = OAC since OB is parallel to AC.

Let AE bisect OAC.

Then OE = EC = OAsin(OAC/2).

Let OD be parallel to EA.

Angle ROD = ROA + AOB/2

ROD = ROB - AOB/2.

Adding and dividing by 2 gives ROD = (ROA + ROB)/2.

From the right triangle FEO the angle ROC = (π - (ROA + ROB))/2.

Now the angle ROA is $2\pi\delta_1$ and ROB is $2\pi\delta_4$ where these distances are measured in wavelengths.

Thus the composite signal from the upper antenna is

OAsin
$$\pi (\delta_4 - \delta_1)$$
 at an angle $\pi/2 - \pi (\delta_1 + \delta_4)$

Similarly, for the lower antenna

Ksin
$$\pi$$
 ($\delta_3 - \delta_2$) at an angle $\pi/2 - 3$ ($\delta_2 + \delta_3$)

DDM =
$$2mA \frac{\sin \pi (\delta_4 - \delta_1)}{\sin \pi (\delta_3 - \delta_2)} \cos \pi (\delta_4 + \delta_1 - \delta_3 - \delta_2)$$
 (11.44)

Where 2mA is adjusted to give the desired path width

 δ_1 is the distance from the upper antenna to the observer

8, is the distance from the lower antenna to the observer

 \mathcal{E}_3 is the distance from the image of the lower antenna to the observer

 δ_4 is the distance from the image of the upper antenna to the observer and all distances are expressed in carrier wavelengths.

$$\delta_{1} = ((x-e)^{2} + (y + H \sin \gamma)^{2} + (z - H \cos \gamma)^{2})^{\frac{1}{2}}$$

$$\delta_{2} = ((x)^{2} + (y + h \sin \gamma)^{2} + (z - h \cos \gamma)^{2})^{\frac{1}{2}}$$

$$\delta_{3} = ((x)^{2} + (y + h \sin \gamma)^{2} + (z + h \cos \gamma)^{2})^{\frac{1}{2}}$$

$$\delta_{4} = ((x-e)^{2} + (y + H \sin \gamma)^{2} + (z + H \cos \gamma)^{2})^{\frac{1}{2}}$$
(11.45)

where x is the perpendicular distance from the antenna pole base to the runway center-line.

e is the offset of the upper antenna

y is the distance measured along the centerline (extended) from the point opposite the antenna pole to the observer

z is the height of the observers above the ground

H is the height of the upper antenna

h is the height of the lower antenna

y is the angle of tilt of the antenna pole counterclockwise in the y-z plane.

Figure 11-211 illustrates these coordinates.

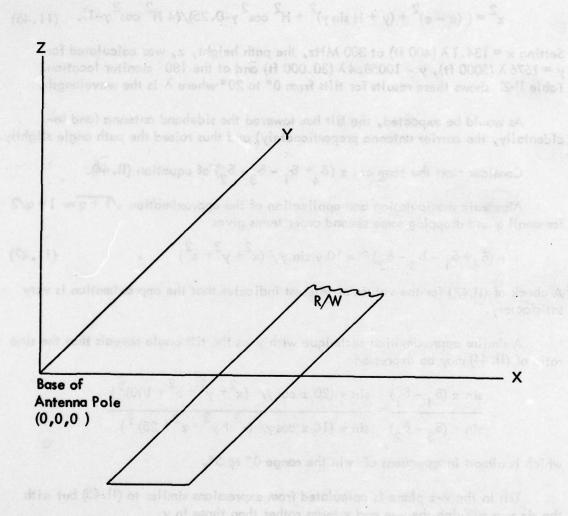


Figure 11-211. Coordinate System.

values used in playing the curves of Figures U-IX through il-216 were obtained

Algebraic manipulation of equation (11.44) and insertion of the quantities (11.45) yields

$$z^2 = ((x - e)^2 + (y + H \sin y)^2 + H^2 \cos^2 \gamma - 0.25)/(4 H^2 \cos^2 \gamma - 1).$$
 (11.46)

Setting $x = 134.1 \lambda$ (400 ft) at 300 MHz, the path height, z, was calculated for $y = 1676 \lambda$ (5000 ft), $y = 10058.4 \lambda$ (30,000 ft) and at the 180° monitor location. Table 11-21 shows these results for tilts from 0° to 20° where λ is the wavelength.

As would be expected, the tilt has lowered the sideband antenna (and incidentally, the carrier antenna proportionately) and thus raised the path angle slightly.

Consider next the term $\cos \pi (\delta_4 + \delta_1 - \delta_3 - \delta_2)$ of equation (11.44).

Algebraic manipulation and application of the approximation $\sqrt{1+q}\approx 1+q/2$ for small q and dropping some second order terms gives

$$\pi (\delta_4 + \delta_1 - \delta_3 - \delta_2) \approx \pi 10 \text{ y sin } \gamma / (x^2 + y^2 + z^2)$$
 (11.47)

A check of (11.47) for the values of interest indicates that the approximation is very satisfactory.

A similar approximation technique with γ as the tilt angle reveals that the sine ratio of (11.44) may be expressed

$$\frac{\sin \pi (\delta_4 - \delta_1)}{\sin \pi (\delta_3 - \delta_2)} = \frac{\sin \pi (20 z \cos \gamma / (x^2 + y^2 + z^2 + 100)^{\frac{1}{2}})}{\sin \pi (10 z \cos \gamma / (x^2 + y^2 + z^2 + 25)^{\frac{1}{2}})}$$

which is almost independent of yin the range 0° to 5°.

Tilt in the x-z plane is calculated from expressions similar to (11.45) but with the sin γ modifying the x-e and x terms rather than those in γ .

Values used in plotting the curves of Figures 11-212 through 11-216 were obtained from a computer program using the exact formulas, (11.44) and (11.45).

TILT	180° MONÍTOR	5,000	30,000	DISPLACEMENT OF TOP OF POLE IN INCHES
00	2.8916	2.8752	2.8662	0.00
Jo.	2.8921	2.8756	2.8667	6.24
2°	2.8934	2.8769	2.8680	12.5
3•	2.8955	2.8791	2.8702	18.7
4°	2.8986	2.8822	2.8732	25.0
5°	2.9025 .	2.8862	2.8772	31.2
10°	2.9355	2.9196	2.9105	62.4
15°	2.9919	2.9767	2.9674	92.5
20°	3.0742	3.0599	3.0504	122.3

Table 11-21. Path Angle for Zero DDM in Degrees for Indicated Tilt and Displacement of Upper Antenna.

too to Most I'll in the Plane Parellel to Barway Centrelians

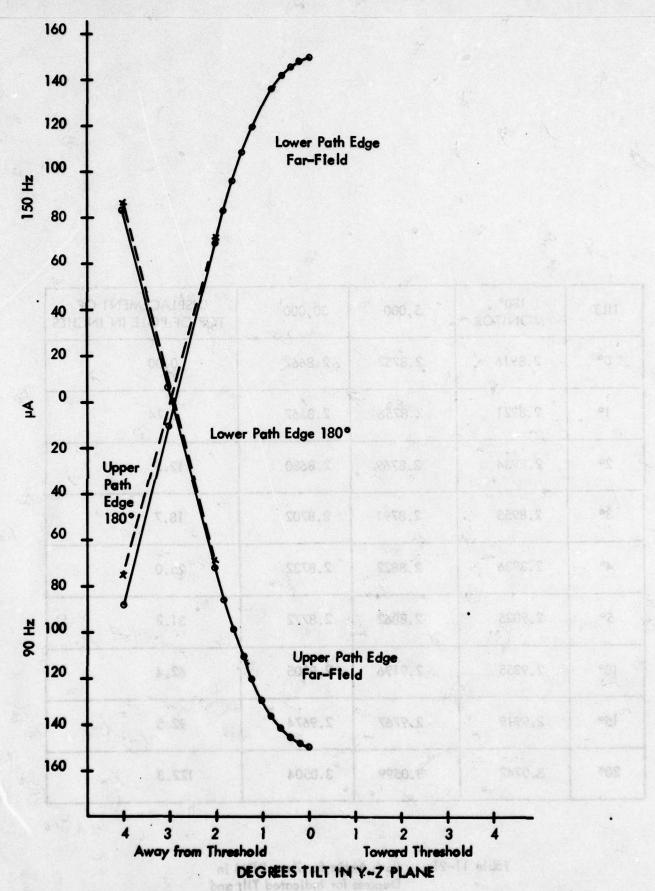


Figure 11-212. Plots of Path-Width Changes Seen in the Far-Field (30,000 ft.)

Due to Mast Filt in the Plane Parallel to Runway Centerline.

Near-Field response is shown by the dashed curves.

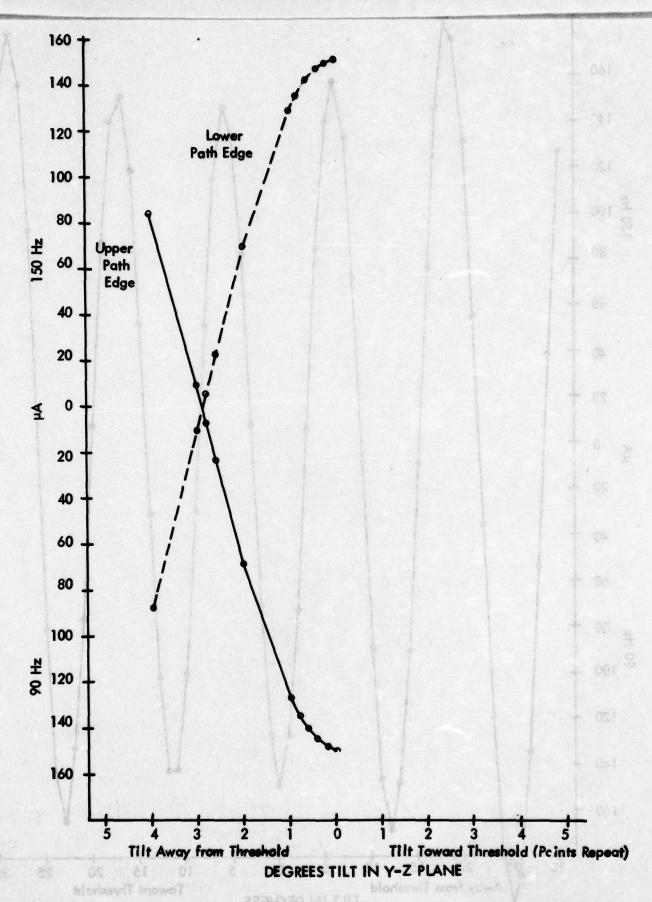


Figure 11-213, Plots of Path-Width Changes Seen at 5,000 ft. Due to Mast Tilt in the Plane Parallel to Runway Centerline.

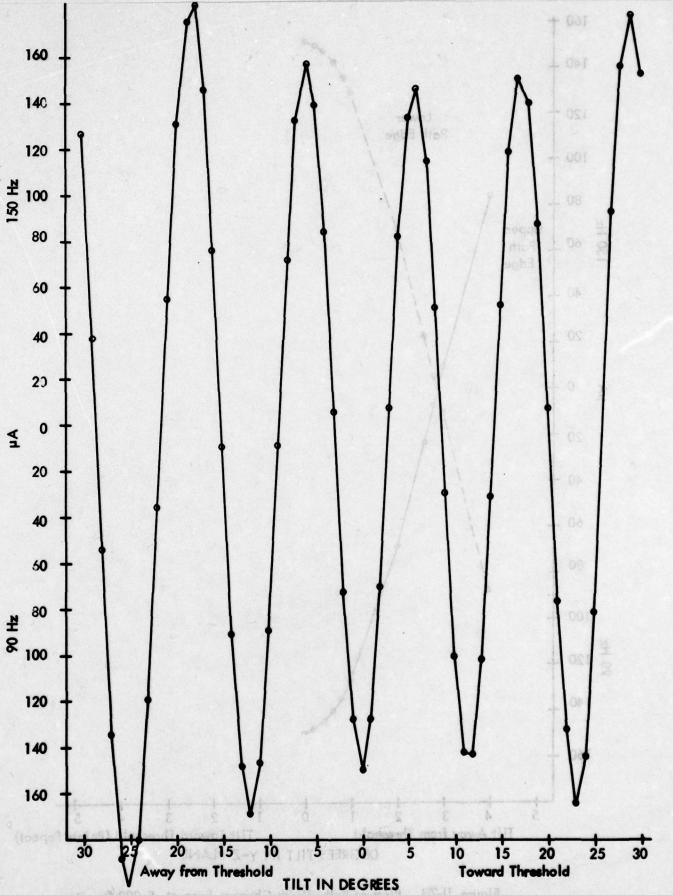


Figure 11-214. Plots of Changes Seen at 0.7° Below Path at the 180° Proximity Point Due to Mast Tilt in the Plane Parallel to the Runway.

11-336

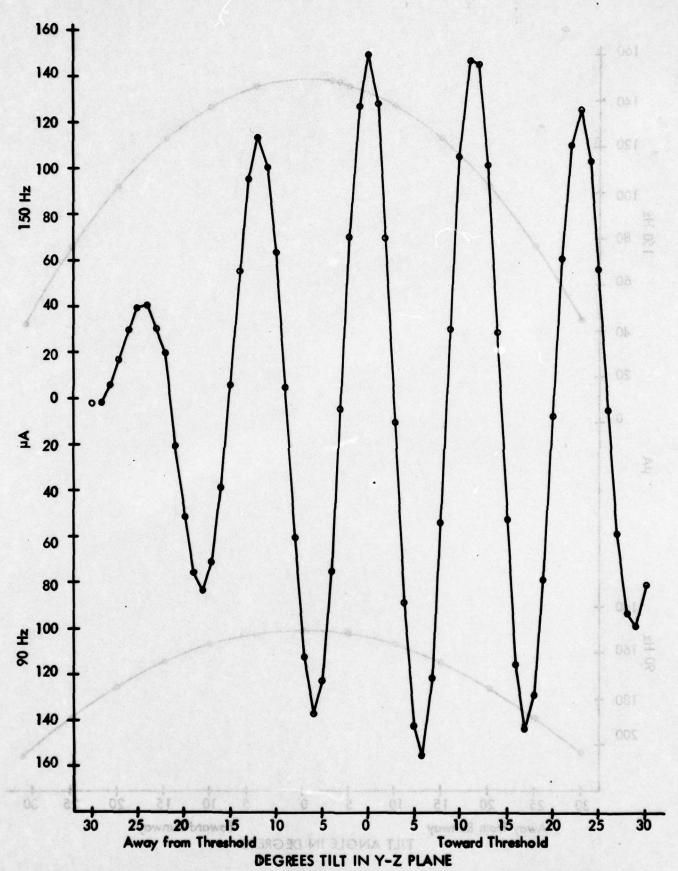


Figure 11-215. Plot of Changes Seen at 0.7° Above Path at the 180° Proximity Point Due to Mast Tilt in the Plane Parallel to the Runway.

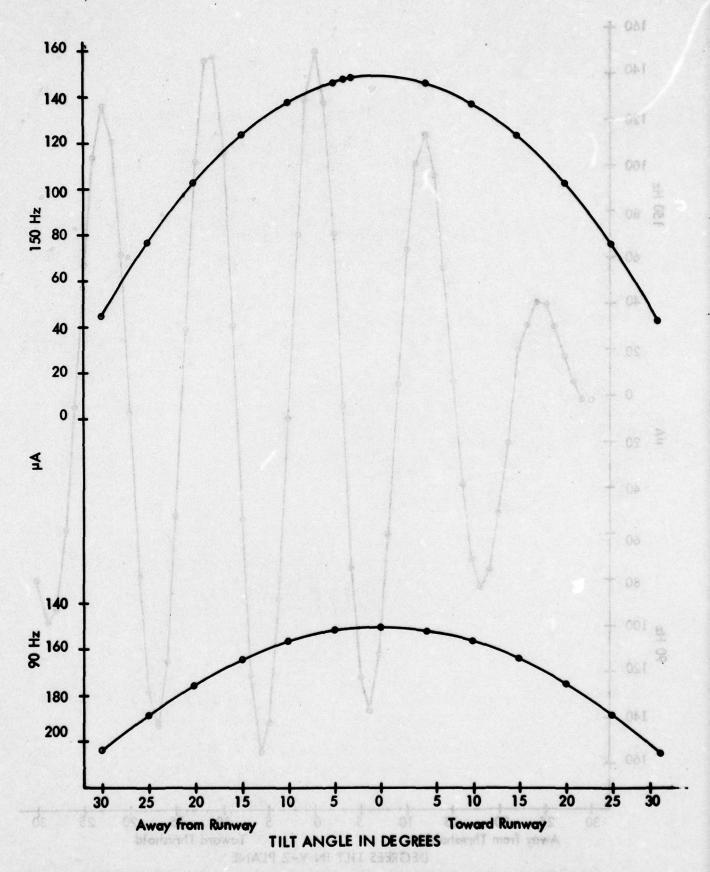


Figure 11–216. Plot of Near Field Responses at $^\pm$ 0.7° to Mast Tilt in the Plane Perpendicular to Runway.

F. Integral Path Monitor Test Circuit for Null-Reference Glide Slope.

1. Introduction. The current concept for monitoring a null-reference glide slope is to use a combination of integral width and near-field (180° point) path monitors as is diagrammed in Figure 11-217. As the path angle of a properly adjusted null-reference system is determined principally by the height of the sideband antenna, a simple integral path monitor can be made by sampling the signal from the carrier antenna to detect any changes in the 90 Hz/150 Hz equality (see Figure 11-218). A tilt monitor, and/or other mechanical types of devices, can be used to insure the physical integrity of the tower and antenna system.

With the use of an executive-action, path monitor, a method of testing the course alarm limits is needed; viz, a simple method of simulating a 0.2° (0.050 DDM) change in path angle. On the newer solid state transmitters, this can be done by upsetting the modulation balance, but on some of the older, tube-type transmitters, the front panel controls may not have enough range to reach a 0.2° change in path angle. Also, it would be more desirable to have a precise, two position (normal/alarm) control when shifting the path angle rather than having to make adjustments on the transmitter modulation balance to check monitor action.

Described below is a simple circuit similar to that used in a sideband reference type glide slope system that will provide a precise shift in path angle without upsetting the normal operation of the null-reference glide slope.

2. Circuit Description. The null-reference path monitor test unit was connected into the carrier and sideband antenna feed lines of a null-reference glide slope system as shown in Figure 11-219. The hybrid in the SO antenna line splits the sideband power sending half the power to the sideband antenna and half the power to the monitor test unit. The hybrid in the CS antenna line splits the carrier power with half the power going to the carrier antenna and half the power going into the RF load. Also, a predetermined amount of sideband power from the monitor test unit is sent to the carrier antenna via this hybrid.

With RF switch #1 set to the "normal" position, the signal power diverted from the sideband antenna feed line is dissipated in the RF load and the system operates in the normal null-reference configuration.

With RF switch #1 set to the "test" position, and RF switch #2 set to the "monitor" position, the sideband signal is combined in a hybrid with a sample of the carrier signal obtained from the monitor pickup loop located at the carrier antenna. When properly phased and attenuated, the resultant signal presented to the detector and monitor should cause an alarm indication on the path monitor. This configuration will provide a simple test of the path monitor alarm without disturbing the glide path in space.

With RF switch *1 set to the "test" position and RF switch *2 set to the "flight" position, the sideband signal power diverted from the sideband antenna feed line is combined, after phasing and attenuation, with the carrier signal power in a hybrid.

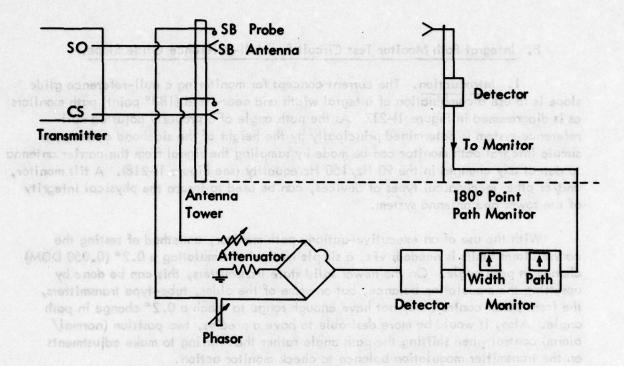


Figure 11-217. Conventional Null-Reference Monitor System.

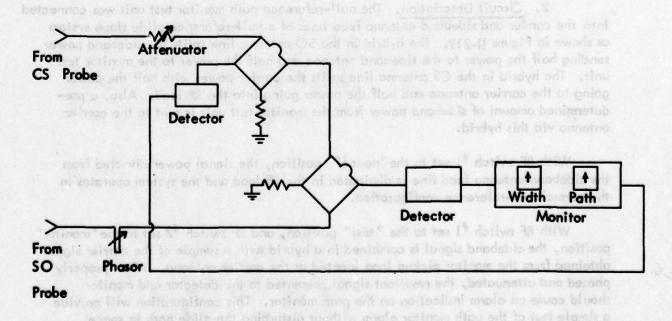


Figure 11-218. Integral Path and Width Monitor for a Null-Reference System.

Sideband Antenna Carrier Antenna SO W with Pickup Monitor Loop 4 Watts CS 2 Watts Transmitter is obtained from the filterty-couck aircraft and from **Attenuators** Normal Detector Test Path Monitor **RF** Switches

ing on the phating of the monitor test unit, this combined signal with this the pilde path in space either up or down by an amount determined by the strength of sideband signal unjected into the comics line, In this most the operation of the office sings system is

3. Experiment and Results. The circuit shown in Figure 11-218 was februared

Figure 11-219, Null-Reference Monitor Test Unit.

The combined carrier and sideband signals are then sent to the carrier antenna. Depending on the phasing of the monitor test unit, this combined signal will shift the glide path in space either up or down by an amount determined by the strength of sideband signal injected into the carrier line. In this mode the operation of the glide slope system is identical to that of a sideband-reference glide slope system using a 2 to 1 antenna height ratio (see Figure 11-220.)

3. Experiment and Results. The circuit shown in Figure 11-219 was fabricated and tested at the Ohio University Tamiami Test Site on January 27 and 28, 1976. A nominal 3° path angle was set up using a Wilcox Mark 1-C solid state transmitter, providing 4 watts of carrier power as a signal source. The glide slope was then checked by use of an aircraft and the path angle and width were measured as 2.95° and 0.77° respectively. The Ohio University Mini-Lab with theodolite reference was used. The integral path monitor was set at 0 DDM. The monitor test unit was then set to the "test" mode and the unit was phased using the standard quadrature phasing techniques. Next the amplitude controls were adjusted for a 0.050 DDM alarm condition and the path angle and path width were rechecked. Finally, the monitor test unit was returned to the "normal" mode and a final check of the path angle and path width was made.

Table 11-22 lists the results as obtained from the flight-check aircraft and from the integral path monitor. As can be seen, the path angle shifted upwards exactly 0.2° when the integral path monitor indicated 0.050 DDM. The higher path angle also agrees with the 150 Hz sensing of the path monitor.

Path Angle By Aircraft	Path Width By Aircraft	Path Shift	Monitor Indication	Test Condition
2.95°	0.77°	■■orthook	0 DDM	Normal
3.12°	0.82°	0.17°	0.042/150 Hz	"Test" Mode
3.15°	0.82°	0.20°	0.050/150 Hz	Adjust Attenuators for Monitor Alarm
2.95°	0.76°	-	0 DDM	"Normal" Mode

Table 11-22. Comparison of Flight Test Data and Monitor Results.

4. Conclusions. The circuit described above accomplishes the objective of shifting the path angle of a null-reference glide slope by a precise, predetermined amount, and allows for precise resetting of the system normal. The only setup task that is required is a flight check to phase the system properly and verify the amount of path angle shift.

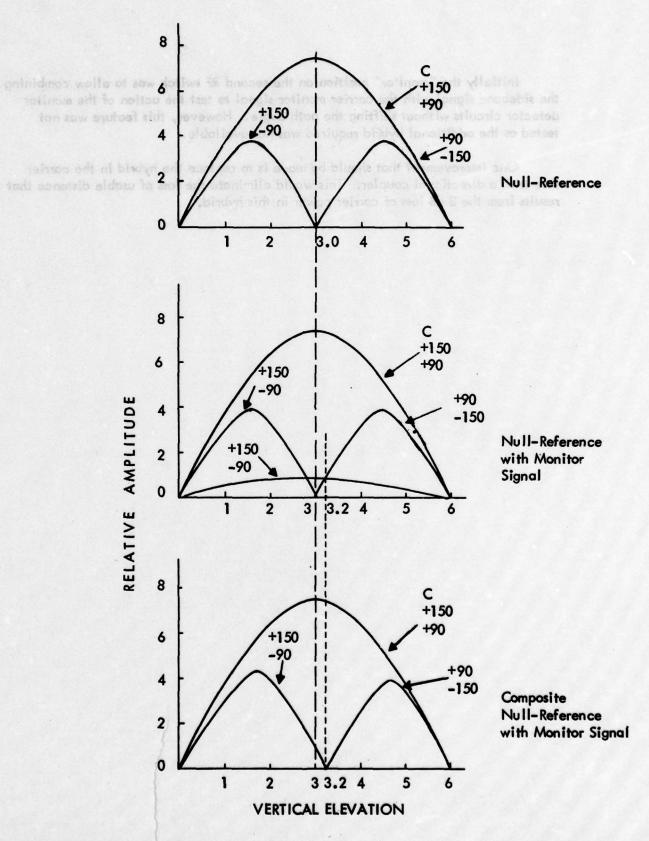


Figure 11-220. Vertical Lobe Structures for Null-Reference and Perturbed Null-Reference Glide Slope.

Initially the "monitor" position on the second RF switch was to allow combining the sideband signal with the carrier monitor signal to test the action of the monitor detector circuits without shifting the path angle. However, this feature was not tested as the additional hybrid required was not available.

One improvement that should be made is to replace the hybrid in the carrier line with a directional coupler. This would eliminate the loss of usable distance that results from the 3 dB loss of carrier power in this hybrid.

- G. Effects of Carrier Sideband Leakage into Sideband Only Signal on ILS Glide Slope Performance.
- 1. Frequency Components in Detected SBO + CSB Signals. The ILS transmitter and modulator produce two signals, a carrier and sideband (CSB) signal and a sideband only (SBO) signal. The two can be expressed as:

$$CSB = C_{\alpha}[\cos(\omega_{c}t) + m\sin(\omega_{1}t)\cos(\omega_{c}t) + m\sin(\omega_{2}t)\cos(\omega_{c}t)]$$
 (11.48)

SBO = A[m
$$\sin(\omega_2 t)\cos(\omega_c t) - m \sin(\omega_1 t)\cos(\omega_c t)$$
] (11.49)

where $\omega_1 = 2\pi \cdot 90$, $\omega_2 = 2\pi \cdot 150$, ω_c is carrier frequency, and where we have assumed that the relative phase between the two signals is a multiple of π radians (i.e., C_a might be negative). If $C_a = 1$, then A is the usual A ratio.

If we combine the two signals, i.e., if CSB leaks into the SBO port, then the resulting sum can be expressed as:

SBO + CSB =
$$cos(\omega_c t)[C_a + m(C_a + A)sin(\omega_2 t) + m(C_a - A)sin(\omega_1 t)]$$
 (11.50)

If the above combined signal were processed by a linear detector, the resulting detected signal could be expressed as:

Detected(SBO+CSB) =
$$\left[C_a + m(C_a + A)\sin(\omega_2 t) + m(C_a - A)\sin(\omega_1 t)\right]$$
 (11.51)

where the vertical bars indicate absolute value. The ratio of the sideband amplitude due to the presence of CSB signal to the sideband amplitude of the SBO signal is given by C_a/A . If a Fourier spectrum analysis is performed on the detected (SBO+CSB) signal, the relative magnitudes of the various frequency components as a function of the C_a/A ratio are given in Table 11-23 for the two signals in phase, and in Table 11-24 for the two signals 180° out-of-phase, i.e., $C_a < 0$. The 90 and 150 Hz components are also expressed as a percentage of either the 60 Hz or 240 Hz component, whichever is larger. Note that for no CSB signal present, the 90 and 150 Hz amplitudes are zero, and that these amplitudes increase as the amount of CSB signal present increases.

- 2. Effect of CSB Leakage into SBO Signal on Null Reference and Capture-Effect Path Width and Symmetry. Effects of CSB leakage into the SBO signal on the path angle, width, and symmetry produced by null reference and capture-effect glide slope systems operating above flat terrain were calculated using the OUGS glide slope model. The usual CSB signal was assumed to be nominal, i.e., as described by equation (11.48) with $C_a = 1$. The combined SBO and CSB signal of equation (11.50) was used in place of the nominal SBO signal with various C_a/A ratios. The A value was held at 0.3, and the antenna heights adjusted to produce a 3.0 degree path. As is evident from Tables 11-25 and 11-26, the effect of this CSB leakage is quite minimal.
- 3. Conclusions. It is evident from inspection of the data contained in this section that no significant changes in path angle, width, or symmetry for null reference

and capture-effect glide slopes take place until the $C_{\rm cl}/A$ ratio is greater than 0.01, i.e., until the 90 or 150 Hz components of the detected SBO and CSB signal are greater than 5% of the 60 Hz component. Even for a $C_{\rm cl}/A$ ratio of .316, i.e., the CSB signal only 10 dB below the SBO signal, the path width and symmetry are affected less than 0.02 degrees. This level of carrier corresponds to a 90 or 150 Hz component greater than 200% of the 60 Hz component in the detected SBO + CSB signal.

where wy = 2x - 90, ag = 2x - 150, wy is corrier frequency, and where we have

commed that the relative plants returned the two signals is a multiple of a radiant (i.e., C might be negative). If C = 1, then A is the usual A ratio.

if we combine the two signals, i.e., if C55 (eaks into the 580 port, then the .

G. Effects of Carrier Sideband Leakage into Standard Only Stand on ItS

Effect Path Width and symmetry. Here's of Cod (nokoga late the Shi signal on the

by equation (11.48) with C. = 1. The combined 580 and CSB signal of equation (11.50) was used in pince of the norther 500 ligned with various Cy/A cultar. The

Frequency	C = 0	$\frac{C_{o}}{A} = 0.001$ $(-60dB)$	C_=0.00316 A=0.00316 (-50dB)	$\frac{C}{A} = 0.01$ (40dB)	$\frac{C_{q}}{A} = 0.0316$ (-30dB)	$C_{\frac{\alpha}{A}} = 0.1$ (-20dB)	$\frac{C}{A} = 0.316$ (-10dB)
OH2	.321	.321	.321	.322	.323	.338	.429
30Hz	0	0	1.7 × 10 ⁻⁴	5.3 × 10 ⁻⁴	1.68 × 10 ⁻³	.0082	.013
zH09	.225	.224	.224	.223	.219	.204	.126
2H06	0	6.6 × 10 ⁻⁴	2.1 × 10 ⁻³	6.65 × 10 ⁻³	.021	950.	911.
120Hz	.059	.059	850.	.058	.054	<u>1</u> 8.	200.
150Hz	0	9.4 × 10 ⁻⁴	2.97×10 ⁻³	9.40 × 10 ⁻³	.030	101.	.337
180Hz	160.	160.	060.	880.	.082	.062	.028
210Hz	0	4.3 × 10 ⁻⁴	1.36 × 10 ⁻³	4.29 × 10 ⁻³	.013	980.	.065
240Hz	.205	.205	.205	.205	.206	.195	.127
270Hz	0	2.4 × 10 ⁻⁴	7.6 × 10 ⁻⁴	2.39 × 10 ⁻³	.0075	.023	610.
300Hz	820	620.	620.	180.	780.	.103	.106
90 60 or 240 %	% 0	0.29%	.94%	2.98%	9.59%	27.61%	93.8%
150 60 or 240%	%0	0.42%	1.33%	4.22%	13.56%	49.84%	265.3%

Relative. Amplitudes of Frequency Components in Detected SBO + CSB Signal as Function of $C_{\rm a}/A$ Ratio. Also indicated are 90 and 150 Hz amplitudes expressed as a percentage of the larger of the 60 or 240 Hz components. Table 11-23.

Relative Amplitudes of Frequency Components in Detected SBO + CSB Signal as Function of C $_{\rm a}/{\rm A}$ Ratio where C $_{\rm a}<0$. Also indicated are 90 and 150Hz amplitudes expressed as a percentage of the larger of the 60 or 240Hz components. Table 11-24.

Ca	Path Angle	Path Width	$\frac{\text{Ca}}{\text{A}} > 0$	Path Symmetry $\frac{C_a}{A} < 0$
0	3.00	.701	.500	.500
.001	3.00	.701	.500	.500
.00316	3.00 /	.701	.500	.500
.01	3.00	.701	.500	.501
.0316	3.00	. 701 §	.498	.502
Sign and	3.00	.701	.495	.506
.316	3.00	.702	.483	.518

Path Symmetry =
$$\frac{\alpha_0 - \alpha_p}{\alpha_w}$$

α_U = Upper 75μA Angle

a = Path Angle

a = Path Width

Table 11-25. Null Reference. Path angle, width, and symmetry as calculated by simulating a 1000' level run for a null reference system with SBO + CSB fed into the upper antenna as a function of the C_a/A ratio.

è		90°		10%		.04	5
Path Symmetry Ca < 0	.500	.500	.500	.500	.501	.503	.509
Path Symmetry $\frac{C_{\mathbf{G}}}{A} > 0$	005*	.500	.500	.500	.499	.497	.492
Path Width Ca < 0	.701	.701	.700	.701	.700	.702	.704
Path Width Ga > 0	102.	102.	.700	.701	.701	.700	669.
Path Angle	3.00	3.00	3.00	3.00	3.00	3.00	3.00
<u>C</u> ₀	0	100.	.00316	.01	.0316	.1	.316

Table 11-26. Capture Effect. Path angle, width, and symmetry as calculated by simulating a 1000' level run for a capture effect system with CSB leakage into the SBO signal as a function of the C_AA ratio.

H. Mobile Glide Slope Facility. Figure 11-221 shows a general view of Ohio University's Mobile Glide Slope Facility made available for FAA use in this program. The unit, developed at no cost to the FAA, contains dual TUS glide slope transmitters, antenna phasing units, monitor hardware and communications transceiver. Work areas and standard test equipment are available for use in field work.

The antenna tower, with capability to extend to 55 feet, has fully adjustable mountings for three antennas and integral monitor ports. A clearance transmitter amplitude and phase control unit plus sideband reference distribution components are available. All equipment can be transported in the truck shown in the figure.

The Mobile Glide Slope Facility has been made available by Ohio University to meet the requirements of the contract, viz, evaluation of glide slopes at problem sites. This is in conjunction with the ILS mathematical modeling capabilities described elsewhere in this report and gave complete capability for site analysis. In addition, predictions were available for minimal earth-moving requirements through computer modeling, followed up, if necessary, by these field measurements.

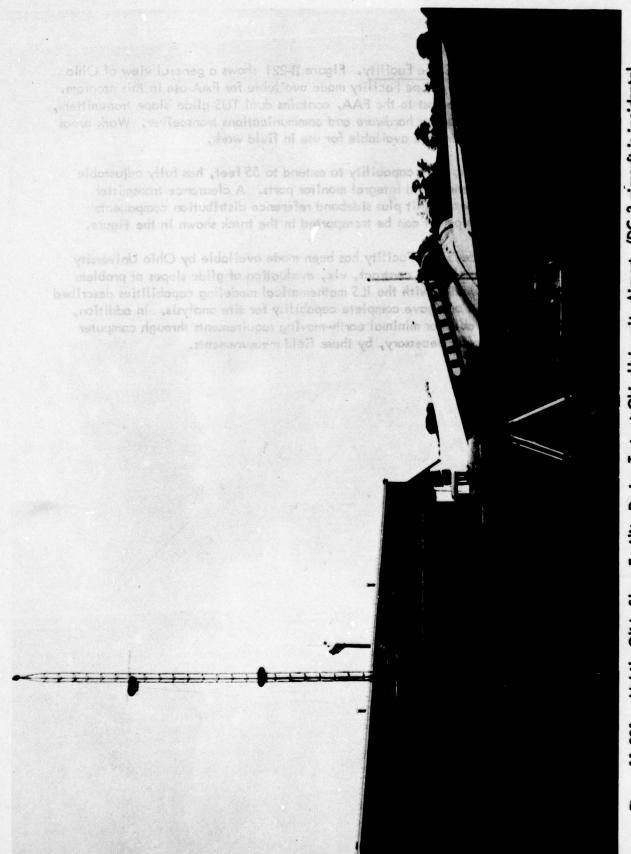


Figure 11-221. Mobile Glide Slope Facility During Tests at Ohio University Airport. (DC-3 aircraft is incidental to the truck-mounted mobile facility)

1. On-Site Glide Slope Evaluation Activities.

1. Westinghouse Broadside Glide Slope Array Tests. Five series of flights were made at the Lynchburg, Virginia, Airport for the purpose of obtaining engineering data to aid Westinghouse engineers in finalizing development of their broadside, non-image glide slope array. Ohio University provided the flight crew and one man to handle theodolite tracking responsibilities on the ground.

Consistent with the basic purpose of providing engineering support in contrast to performing an independent evaluation, all records were provided to Westinghouse engineers for their analysis and use.

a. Mission 1: August 4-6, 1976. Approximately ten hours of flight with the Beechcraft Model 35 aircraft equipped to measure and record CDI, flag and signal strength was accomplished.

Observations of interest were:

- 1) In spite of moderately rough air, RTT runs showed good flyability.
- 2) Very smooth level crossovers were obtained.
- 3) Sideband power had to be reduced approximately 75% from that predicted to give a nominal course width of 0.70°.
- 4) Relative radiation pattern peaks at 5° elevation were found to be CSB/SBO: 4 dR.
- 5) Signal strength in the far-field appeared low. A comparison using 2 watts out of the transmitter showed the broadside array to be 33 dB below a commissioned null-reference with bent dipoles fed from a TV-4. Measurements were made at 10 nm, 1500 feet. No absolute reference was available.
- 6) With a course near 3° peak value of DDM (150) occurs at 0.9°, with a false, inverted course at 0.6°.

Copies of flight data logs together with some 50 analog strip chart recordings were given to Westinghouse engineers with verbal comments concerning the seriousness of items 5 and 6.

b. <u>Mission 2: August 12-13, 1976</u>. A second series of measurements was made on the Westinghouse broadside array following replacement of a feed unit which had been damaged in shipment. A total of 52 runs was made.

Difficulties in airborne phasing were encountered. Three rather distinct readings of first 90 Hz, then 150 Hz, followed by 90 Hz again over a four mile path were found with the system in quadrature. The phasing runs were attempted at below-path angle to stay out of the SBO null which defined the on-course.

Another problem area was the lack of full scale fly down indications above path. At the request of the Westinghouse engineers three series of level runs were made with variations in CSB/SBO phasing with a family defined by SBO power level. After selecting the best settings evidenced from the recordings, three low approaches were recorded for structure made in line with the edge of the runway closest to the antenna and three low approaches over centerline. These different tracks were used to check the effects of array focusing.

Usable distance checks were made after a 10 dB pad was removed from the CSB circuit in the transmitting antenna. Calibration against a glide slope standard (military version of the Boonton 232 signal generator) showed that a 6 dB margin existed over the FAA minimum specifications for 1500 feet elevation, 10 miles range.

c. Mission 3: August 19-20, 1976. The third series of flight tests was made on the Westinghouse broadside glide slope array using the Ohio University DC-3 containing specially-installed Mini-Lab equipment from the Beechcraft.

The DC-3 was used for this series of measurements for several reasons. Among these are that it permitted an extra person to be available to analyze records during the flight, it allowed signal generators to be carried on board the flight to make signal strength and DDM calibations, it permitted a larger target and lights to permit optical tracking during conditions of haze and reduced visibility, and it permitted two sets of dual equipment for cross-checking the data from the measurements.

Substantial improvement was found immediately when phasing the CSB and SBO energies. Responses were as would be expected from theory and the system was quickly set for optimum conditions. Clearances above and below-path were adequate but not strong and this raises some questions because theory would predict DDM values almost twice those which were measured.

Because of these relatively low clearance values the clearance runs made at 1 degree elevation (theodolite controlled) yielded oscillatory traces which averaged at or slightly below tolerance values.

Approximately 10 normal approaches were run which showed good flyability on centerline, 75 feet to the right of centerline (approximate line of focus for the array) and 8 degrees either side of centerline. An apparent slope of the glide slope on-course plane exists with 0.2 degrees change observed from centerline to 8 degrees right. A significant change of vertical thickness also is evident, but Westinghouse reported this was very likely due to an abnormal site condition.

It appeared that the below-path clearance area is in need of improvement. DDM values were minimal in some of the below-path regions, and there was a small area or lobe between the middle marker and threshold where zero DDM was observed when flying below 1 degree elevation. Lateral tilt of the on-course plane was observed to be near maximum allowable, and change in vertical path widths with azimuth was observed. Flyability and vertical structure above 1 degree were good. No monitoring had been installed and hence no checks were made. Approximately 50 flight records were made.

11-354

d. Mission 4: September 29, 1976. These measurements were accomplished subsequent to those made by FAA NAFEC in which problems were uncovered due to water entering connectors. The connectors were replaced and these measurements reflect the results of that change. A Beechcraft model 35 aircraft was used for the tests.

Initially difficulty was experienced in sharpening the path width to a nominal 0.7° value and this was found to be due to the improved performance of the CSB system. It became evident that the 10 dB pad present in the original installation is necessary (the pad was removed during the second series to improve usable distance). Insertion of the pad allowed a proper ratio of CSB and SBO energies and a 0.7° width was obtained. Path angle was high indicating 3.30°.

Smooth transitions were obtained showing virtually no effects due to multipath. As would be expected, flyability was excellent with \pm 20 microamperes roughness to inside point C.

Clearance was deficient with a false (zero DDM) area at 1.4° elevation. Westinghouse engineers believed that decreasing the path angle by moving the antenna would improve this clearance area. Due to the lowering of ceilings to 400 feet and forecasts for no significant improvement, this measurement series was terminated.

e. Mission 5: October 12, 1976. The fifth series of tests on the Broadside array was motivated by need to ascertain precisely the effects of changing the tilt of the antenna to lower the path angle. Considerable rain had fallen during the time period between the fourth and fifth series. A DC-3 was used for this flight check due to mechanical problems with the Beechcraft.

During initial check of the CSB/SBO phasing it was found that optimum phasing fell 20 degrees retarded from that previously set. Phasing runs showed much more roughness in the CDI than previously observed. Level transition runs on the path revealed that the on-course was nearly 2.8 degrees which was almost 0.5 degrees less than previously observed but the antenna tilt change was only 0.125 degrees.

A major defect appeared in the transition records, that being a very soft region in the 150 Hz near 75 microamperes. The records would hover at that value for nearly 0.8 degrees of elevation change and made path width determination meaningless. Restoring the phase to the value used for the fourth series produced no significant improvement. Increasing the SBO power produced an apparently narrower path as would be calculated but did not cure the problem of a very soft region between 150 and 75 microamperes in the 150 Hz region.

The antenna tilt was then returned to its value used in the fourth series and a path angle of 2.98 degrees was measured. Thus the fourth series parameter values were duplicated but a very different vertical path structure was observed. This held true in particular for the below path clearance where now an inverted false course was observed with hard fly down below it. These occurred at and below one degree elevation. Flag was observed at points below the path angle and this is undoubtedly due to nulls existing in the CSB pattern.

The measurements were terminated pending an investigation and correction of obvious faults which had developed in the array. Water in the transmission system is again suspected because of the heavy rain period just prior to this series of tests.

- 2. Documentary Flight Data for a Capture-Effect Glide Slope System Operating at a Typical Upslope Site.
- a. <u>Introduction</u>. This section presents the results of an extensive series of systematic measurements on a capture-effect glide slope system operated with specific faults in the transmission lines, distribution elements, and transmitter components of the system. The Lawton, Oklahoma site was used for the tests made in November 1976, since it represented a rather typical capture-effect site with a slight dropoff and prominent upslope in the approach region inside two miles.

The capture effect system is the most complex of the contemporary, commissioned systems and it is important to recognize the far-field DDM signal response to system parameters which are set at non-optimum values. Documentation of this type is also important in establishing tolerance limits on parameter values, in determining the appropriateness of monitor responses, and in aiding the technician when setting up and maintaining the system.

This section is, in effect, a sequel to Chapter XI-B, which presented much of the same type of data but for a capture effect system operating at the ideal (Tamiami) site. The irregular terrain at the Lawton site makes these data different.

The glide slope data were collected in three groups of measurements. The first group measured the system as it existed. These measurements are referred to as the commissioned values. The second group of measurements was made with the phase and amplitude of the antenna currents set to the theoretically correct values. The third group of measurements was made with the middle antenna delayed 10 degrees. This experimental phasing produced optimum conditions as measured by the aircraft.

In-flight measurements were made using Ohio University's Mark II Minilab which was fitted into a Beechcraft Model V35A Bonanza. These are presented in Table 11-32 and in Figures 11-241 to 11-337. Calibration of the Mark II Minilab was performed on site using a bench standard transported from Ohio University.

A Warren-Knight Model 83 theodolite was used for reference for all recorded data. The radio telemetering theodolite method was used to measure the path structure. The theodolite position was surveyed and in order to comply with Paragraph 217.32 of the Flight Inspection Manual, a base was constructed to provide the theodolite operator with a convenient height. This base was left at Lawton for future use.

During the investigation the faults introduced into the system were: antenna current phase delays and advances, feedline attenuation, APCU maladjustments, CSB to SBO phasing, and change of course to clearance power ratio. Principal instrumentation for reference purposes was a vector voltmeter.

b. Glide Slope System Parameters. The glide slope at Lawton is located 400 feet from the runway centerline and 1100 feet back from the threshold. The antenna heights were measured to be 12.79, 25.33 and 37.25 feet above the base of the tower. The ratio of the middle and upper antenna height to the lower are respectively 1.91:1 and 2.91:1. The assigned frequency for the glide slope was 331.4 MHz.

The system is excited with a TU4 Transmitter and an FAA type 8954 Clearance Transmitter. The current distribution to the antenna system is provided by an FAA 8989 type APCU. Three element colinear arrays (APC antennas) are used as antennas. Clearance power to the upper antenna was measured at 90 mw with the carrier power to the middle at 500 mw.

The on-path detector is located 211.66 feet from the base of the tower and 402.73 feet from the runway centerline. Near-field data was collected with a PIR and portable mast at a point 212.833 feet in front of the tower and 410.76 feet east of the runway centerline. The theodolite was placed 28 inches east and 2 inches south from a point directly below the middle antenna. The center of the theodolite eyepiece to the ground was 67.87 inches, the elevation of the runway opposite the mast.

c. Antenna Current Measurements. The relative phase and amplitude of the antenna currents were measured using a handheld probe and a Hewlett-Packard 8405A Vector Voltmeter. The procedure used is described below.

With the sideband only (SBO) to the APCU dummied, the carrier sideband (CSB) energy was fed to the SBO input to the APCU. The clearance transmitter was denergized and the CSB input to the APCU dummied. This radiated CSB to all the elements to provide means to measure the antenna current phase.

To minimize the effect of temperature on the readings, two identical RG-214 cables were run out to the tower. The cable used to provide the vector voltmeter reference was connected to the monitor output on the middle antenna. The second cable used to sample the RF field produced by the antenna was connected to the handheld probe. Both cables were exposed to nearly the same environmental conditions to maintain a constant phase differential. The probe was placed in close proximity to the center element of the middle antenna, and the vector voltmeter adjusted for a zero reference. The probe was then moved to the upper antenna and the relative phase measured. To insure the stability of the setup, the probe was again placed on the middle antenna and the zero reference checked. The probe was then moved to the lower antenna and the measurements repeated.

The relative phase and amplitude of each of the antenna currents are shown in Table 11-27. All measurements are referenced to the middle antenna. CSB energy placed into the SBO input of the APCU provides the excitation for the measurements. The readings tabulated were made before the introduction of the faults.

d. Faults. A calibration test was made of the antenna phasors. This test was conducted using the previously described method with one exception. Zero

November 17,	1976	
	SBO*	CSB*
COMMISSION	ED SETTINGS	
Lower Middle Upper	-12.6 dB, Φ=186° -7.4 dB, Φ=0° -11.2 dB, Φ=168°	-7.0 dB, Φ=4° -12.4 dB, Φ=180°
THEORETICAL	SETTINGS	a Three element of
Lower Middle Upper	-12.6 dB, Φ=180° -7.4 dB, Φ=0° -11.2 dB, Φ=180°	-7.4 dB, Φ=4° -12.4 dB, Φ=180°
RETURN TO CO	OMMISSIONED	the ronway carterline
Lower Middle Upper	-12.6 dB, Φ=186° -7.4 dB, Φ=0° -11.2 dB, Φ=168°	-7.0 dB, Φ=4° -12.4 dB, Φ=180°
November 18,	1976	nts) anteraA
	SBO*	CSB*
THEORETICAL S	SETTINGS	
Lower Middle Upper	-12.6 dB, Φ=180° -6.5 dB, Φ=0° -12.8 dB, Φ=180°	-7.0 dB, Φ=0 -12.4 dB, Φ=180°
EXPERIMENTA	L SETTINGS	
Lower Middle Upper	-12.5 dB, Φ=197° -7.2 dB, Φ=0° -11.0 dB, Φ=179°	-7.0 dB, Φ=10° -12.4 dB, Φ=197°
RETURN TO CO	OMMISSIONED	
Lower Middle Upper	-12.5 dB, Φ=187° -7.2 dB, Φ=0° -11.0 dB, Φ=-169°	-7.0 dB, Φ=0° -12.4 dB, Φ=169°

^{*} All amplitudes with respect to arbitrary vector voltmeter reference.

Commissioned - Antenna current values as found.

Theoretical - Antenna currents set to near theoretically correct values as specified in texts.

Experimental - Experimentally determined value which produced optimum path conditions.

Table 11-27. Antenna Currents.

November 19, 1976 CSB* SBO* THEORETICAL SETTINGS -7.0 dB, Φ=1° -12.6 dB, Φ=180° Lower -6.5 dB, $\Phi=1^{\circ}$ -12.4 dB, Φ=180° Middle -12.8 dB, Φ =180° Upper RETURN TO COMMISSIONED SETTING -12.5 dB, Φ=187° -7.0 dB, Φ=0° Lower -7.2 dB, Φ=0° $-12.4 \text{ dB, } \Phi = -187^{\circ}$ Middle -11.0 dB, Φ=169° Upper

*cf. previous page

phase on the vector voltmeter was set with the probe monitoring the upper antenna current and the antenna phasor set to zero. The results of this calibration are shown in Table 11-28. With the use of the calibration data, antenna phasing faults were introduced by adjusting the APCU antenna phasers.

9 7 = 4	Vec	tor Voltmeter Reading	
Dial Setting	Upper Antenna	Middle Antenna	Lower Antenno
-80	441 001	d3⊭0-127 MO	54
-60	351/2	-138	44
-40	$23\frac{1}{2}$	-151	32
-20	12	-165	20
0	0	-178	61/2
20	-11	168	$-6\frac{1}{2}$
40	$-22\frac{1}{2}$ $-32\frac{1}{2}$	155	-18
60	$-32\frac{1}{2}$	145	-28
80	$-40\frac{1}{2}$	137	-36

Table 11-28. APCU Calibration.

Antenna amplitude faults were introduced into the system by placing a continuously variable attenuator into the antenna feeds. As before, a calibration of the attenuator was made using the vector voltmeter.

- e. <u>Terrain Features</u>. Included in this report is an account of the terrain features present at Lawton. Figures 11-222 and 11-223 portray the land features in the vicinity of the glide slope station. On this profile map, taken from the grading plan, is the location of the glide slope tower, the on-path detector and the near-field monitoring location. Figure 11-224 is the profile of the terrain along a straight line from the tower base to the middle marker. Figure 11-225 provides additional detail for the terrain profile in the approach zone for Runway 35.
- f. Ground Measurements at the 360° Monitor Point. Ground data were taken for various fault conditions at a 360° monitor point; this data is presented in Tables 11–29 and 11–30 and in Figures 11–226 to 11–241.

The location of the existing on-path detector and the near-field probe used for these ground tests is shown in Figure 11-222. The on-path detector is positioned at the 360° monitor point directly in front of the antenna mast along a line parallel with the runway centerline. The near-field probe was located 8.1 feet from the on-path detector along an arc which describes a locus of 360° phase proximity points (see "Installation Instructions for the ILS Glide Slope", FAA Manual 6750.6A,

				Faul	Fault Applied	derived a second			
Elevation	Normal	CI Off	A2-10 CI On	A2-10 CI Off	A2+10 CI Off	A2+10 CI On	2dB A2 CI On	6dB A3	A2-10 348 A1 CI On
ANGLE	103	CDI	CDI	CDI	CDI	10 3	CDI	CDI	CDI
1.62	-291.	-266.	-274.	-300.	-291.	-274.	-266.	-274.	-306
1.89	-223.	-249.	-240.	-249.	-240.	-231.	-214.	-240.	-266
2.15	-189.	-189.	-197.	-189.	-189.	-180.	-171.	-206.	-223
2.42	-129.	-129.	-130.	-137.	-137.	-120.	-120.	-154.	-141
2.69	-77-	-88-	-81.	-86.	-69-	-69-	-69-	-120.	69-
2.96	-27.	-26.	-27.	-26.	-25.	-30.	-26.	-86.	M
3.22	22.	21.	21.	24.	17.	17.	14.	-39.	98
3.49	34.	34.	51.	47.	27.	23.	36.	.0	129
3.76	34.	34.	.69	.69	10.	14.	51.	24.	120.
4.03	ò	-2.	.09	.09	-51.	-36.	26.	37.	43
4.30	-51.	-98-	34.	-12.	-120.	-86.	•	36.	-77-
4.57	-64.	-150.	43.	-77.	-171.	-103.	••	38.	69-
4.84	-69-	-249.	77.	-189.	-274.	-120.	15.	19.	6-
5.10	-43.	-326.	86.	-306.	-343.	-137.	26.	-39.	-29

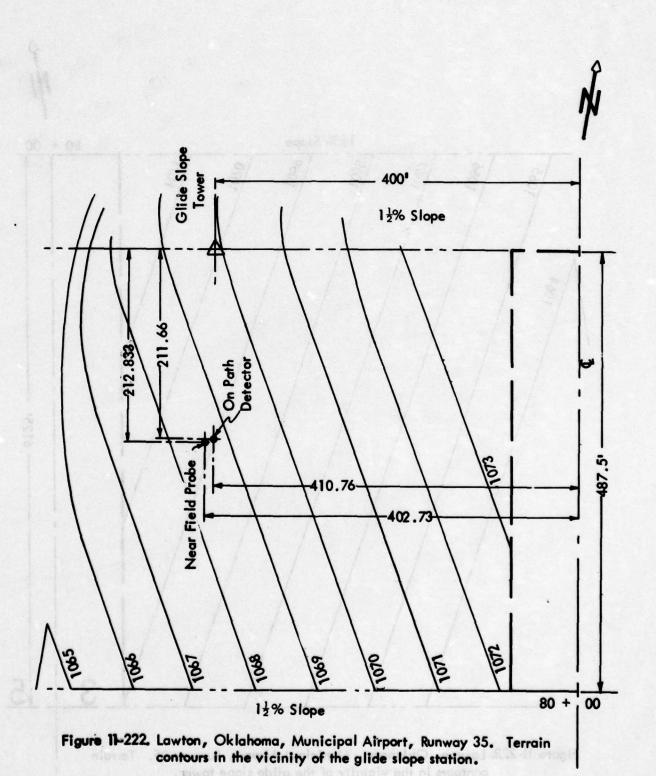
8	:	-12.4 dB, $\Phi = 180^{\circ}$	-7.0 dB, $\Phi = 4^{\circ}$
80	-11.2 dB, $\Phi = -168.0^{\circ}$	$-7.4 dB, \Phi = 0.0^{\circ}$	-12.6 dB, $\Phi = -186.5^{\circ}$
	(A3) Upper Antenna	(A2) Middle Antenna	(A1) Lower Antenna
	(A3)	(₹3	(A)

Table 11-29. Ground Monitor Data Site as Commissioned.

				Faul	Fault Applied				
Elevation Angle	Normal	CI Off	A2-10 CI On	A2-10 CI Off	A2+10 CI Off	A2+10 Cl On	2dB A2 CI On	6dB A3 CI On	A2-10 3dB A1 CI On
	0		100	100	1 1 1 1 1 1 1 1 1 1 1 1 1 1 1 1 1 1 1	· 设计	4 6 6 6 6 6 6 6 6 6 6 6 6 6 6 6 6 6 6 6	in the second	M G P M
L	Tub	coi	CDI	CDI	CnT	CDI	CDI	CDI	CDI
15	-201	-266.	-274.	-300	1001	-274.	-266.	-274.	-308.
100	-202	-249.	-240.	-249.	-240.	-231	-214.	-240.	-266.
, L	-180	-189	-197.	-189.	-180.	-180.	-171.	-206.	-223.
0 0	-120.	-129.	-130.	-137.	-177.	-120.	-120.	-154.	-141.
40,	-77.	-86.	-81.	-86.	-69-	-69-	-69-	-120.	-69-
70	-27.	-26.	-27.	-26.	105	-30.	-26.	-86.	See . 3.
20	22.	21.	21.	24.	17.	17.	14.	-39.	86.
104	34.	34.	51.	47.	27.	23.	36.	•	129.
76	34.	34.	69	69.	10.	14.	51.	24.	120.
03	.0	-2.	.09	.09	100	-36.	26.	37.	43.
30	-51.	-98-	34.	-12.	-120.	-86.	•	36.	-77.
57	-64.	-150.	43.	-77.	-171.	-103.	0	28.	-69-
84	-69-	-249.	77.	-189.	-274.	-120.	15.	19.	-6-
10	-43.	-326.	86.	-309.	-343.	-137.	26.	-36.	-29.

(A2) Upper Antenna -11.2 dB, Φ = -168.0° (A2) Middle Antenna -7.4 dB, Φ = 0.0° -12.4 dB, Φ = 180° (A1) Lower Antenna -12.6 dB, Φ = -186.5° -7.0 dB, Φ = 4°				3 1
$-7.4 dB, \Phi = 0.0^{\circ}$ - $-12.6 dB, \Phi = -186.5^{\circ}$	(A3)	Upper Antenna	-11.2 dB, Φ=-168.0°	;
	(A2)	Middle Antenna	-7.4 dB, $\Phi = 0.0^{\circ}$	-12.4 dB, $\Phi = 180^{\circ}$
	(A)	Lower Antenna	-12.6 dB, $\Phi = -186.5^{\circ}$	-7.0 dB, Φ= 4°

Table 11-30. Ground Monitor Data Site as Commissioned.



11-363

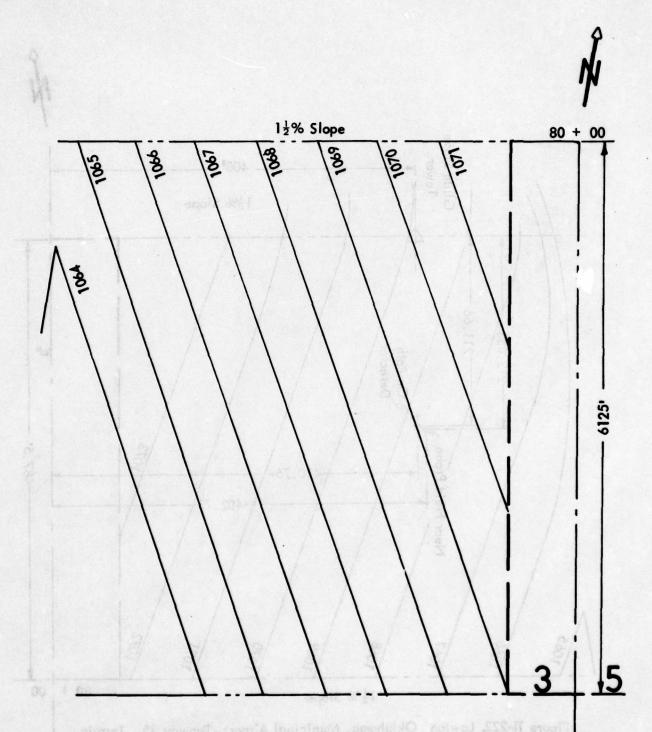


Figure 11-223. Lawton, Oklahoma, Municipal Airport, Runway 35. Terrain contours in the vicinity of the glide slope tower.

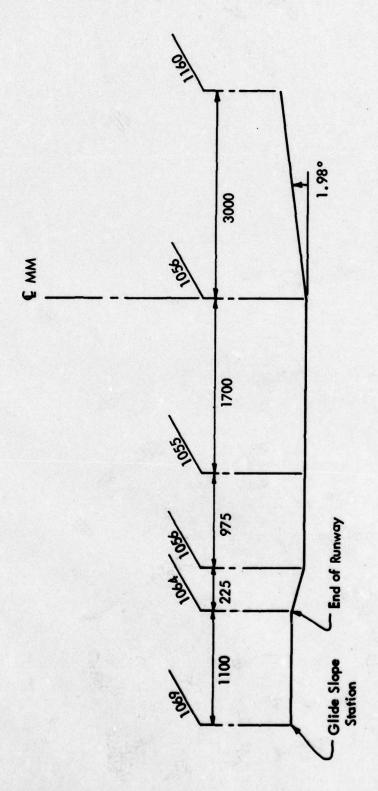


Figure 1424 Profile of the Terrain Along a Straight Line Down from the Tower Base to the Middle Marker (Lawton, Oklahoma, Municipal Airport).

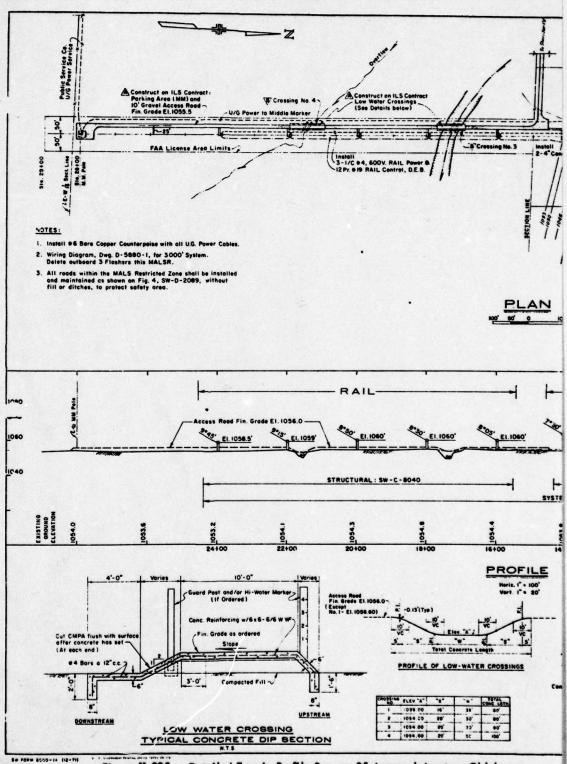
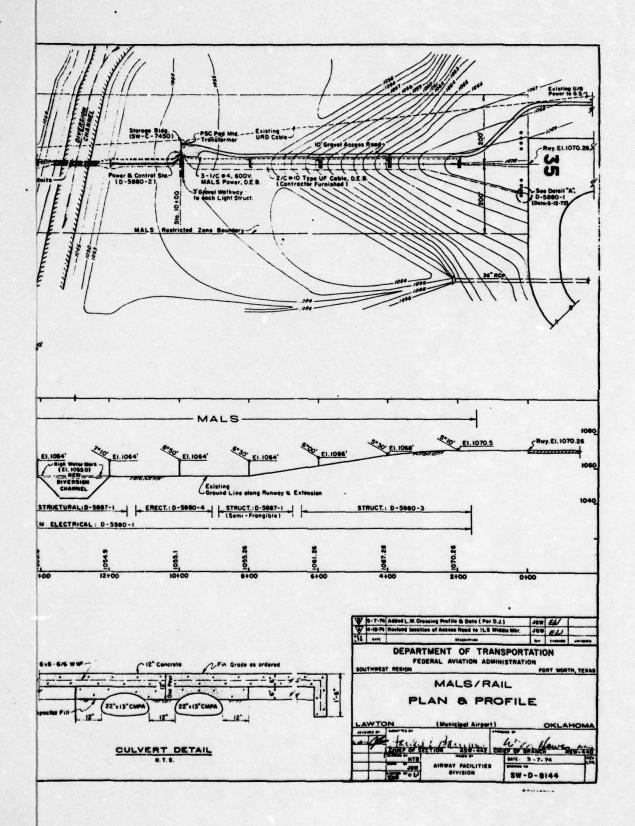


Figure 11-225. Detailed Terrain Profile Runway 35 Approach Lawton, Oklahoma. 11-867/11-368



page 90). It should be noted that identical data can be collected from any 360° phase proximity point when taken with respect to elevation angle. Interaction between the on-path detector and the near-field probe has been assumed to be negligible for these tests.

As seen in the ground data, the sensitivity to perturbations in the middle antenna is small. This phenomenon is due to the fact that the 360° monitor point is, by definition, located at the null of the middle antenna.

g. Graphical Data Presentation. The plots presented in the data section of this report were generated on a Hewlett-Packard 7203A graphic plotter which was controlled by the Ohio University IBM Model 370 computer system. The data was input to the computer from flight recordings via a device designed and built at Ohio University* that converts graphical data to digital data that is compatible with the Ohio University computer system.

Calibration information from the minilab was input to the computer so that the graphs presented in this report are free from errors due to non-linearities in the measurement equipment.

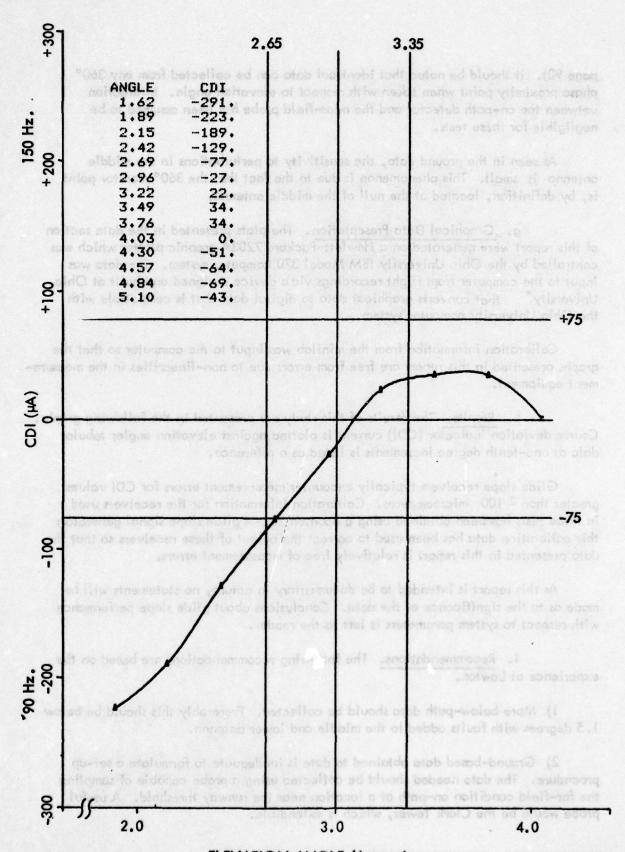
h. Results. The results of this study are presented in the following graphs. Course deviation indicator (CDI) current is plotted against elevation angle; tabular data at one-tenth degree increments is listed as a reference.

Glide slope receivers typically encounter measurement errors for CDI values greater than $\frac{1}{2}$ 100 microamperes. Calibration information for the receivers used in these tests has been obtained using a Boonton 232-A glide slope signal generator; this calibration data has been used to correct the output of these receivers so that the data presented in this report is relatively free of measurement errors.

As this report is intended to be documentary in nature, no statements will be made as to the significance of the data. Conclusions about glide slope performance with respect to system parameters is left to the reader.

- i. Recommendations. The following recommendations are based on the experience at Lawton.
- 1) More below-path data should be collected. Preferably this should be below 1.5 degrees with faults added to the middle and lower antenna.
- 2) Ground-based data obtained to date is inadequate to formulate a set-up procedure. The data needed should be collected using a probe capable of sampling the far-field condition on-path at a location near the runway threshold. A useful probe would be the Clark Tower, which is extendible.

^{*} See Section IV.B



ELEVATION ANGLE (degrees)
Figure 11-226. Ground Data (Commissioned) - Clearance On.

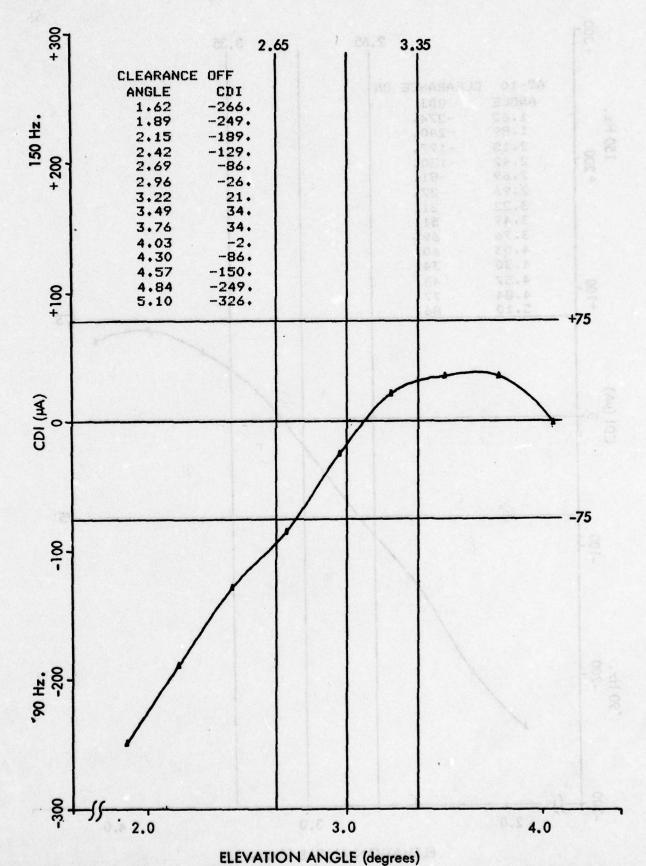


Figure 11-227. Ground Data (Commissioned) - Clearance Off.

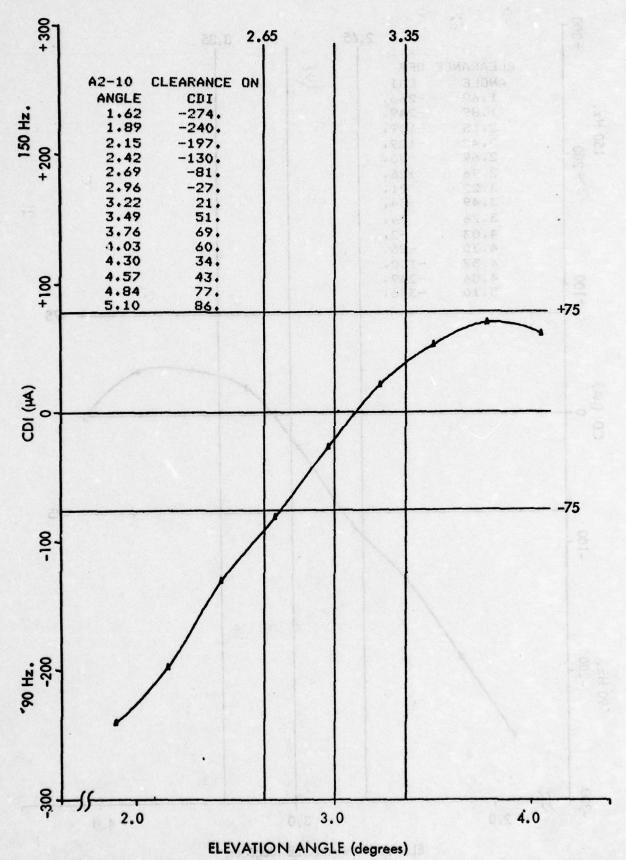


Figure 11–228. Ground Data (Commissioned)–10° Delay in Middle Antenna, Clearance On .
11–372

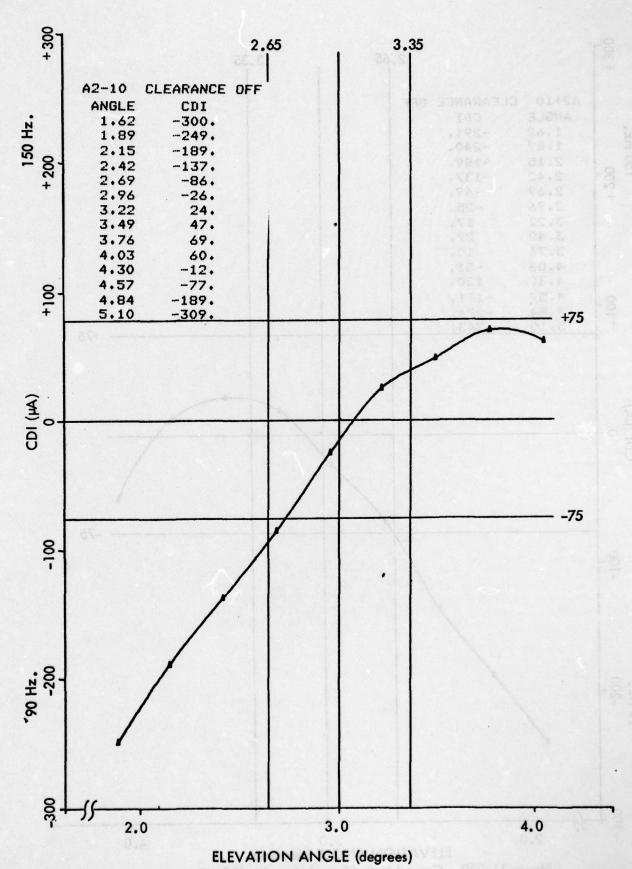
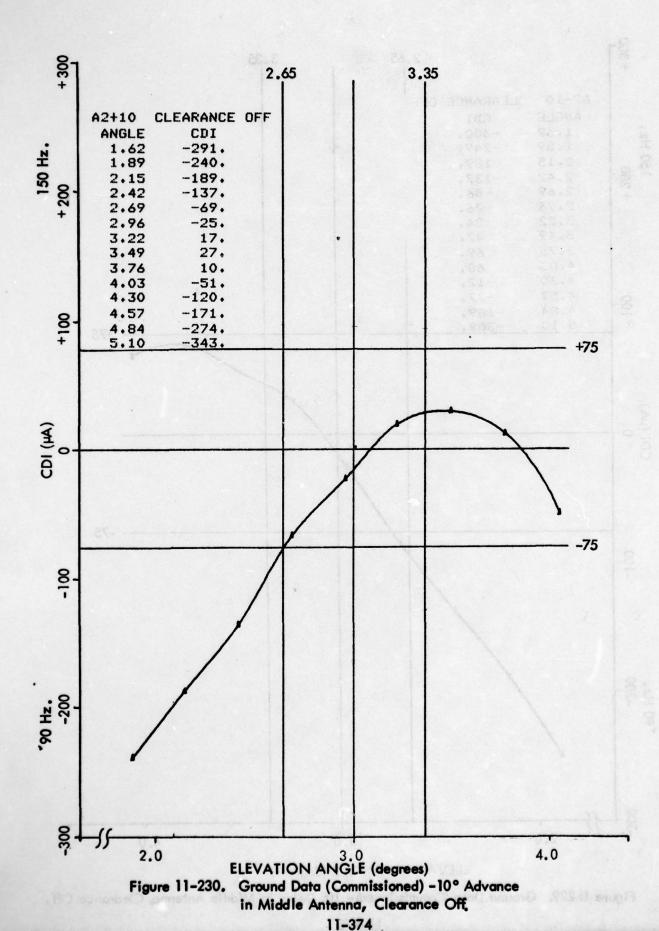
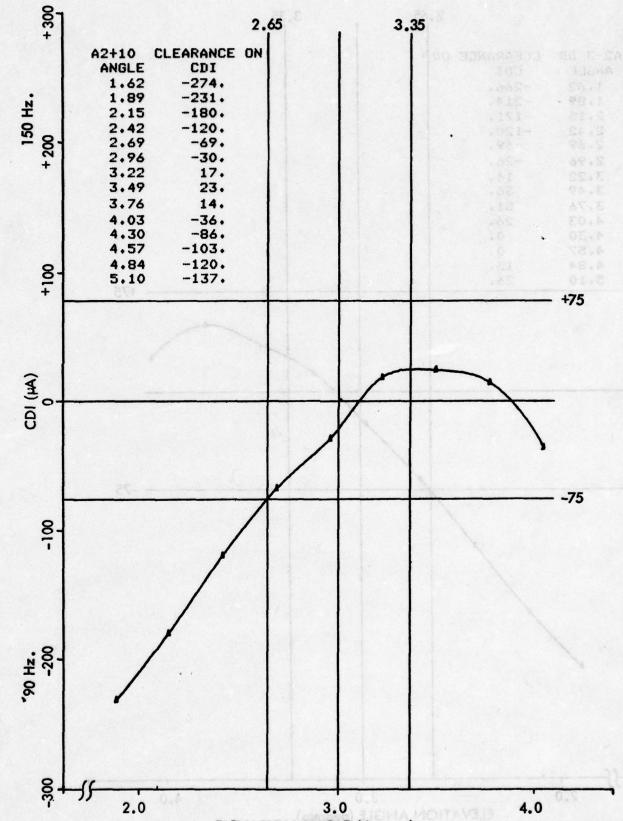


Figure 11-229. Ground Data (Commissioned) - 10° Delay in Middle Antenna, Clearance Off.
11-373





ELEVATION ANGLE (degrees)
Figure 11–231. Ground Data (Commissioned) – 10° Advance in Middle Antenna, Clearance On.

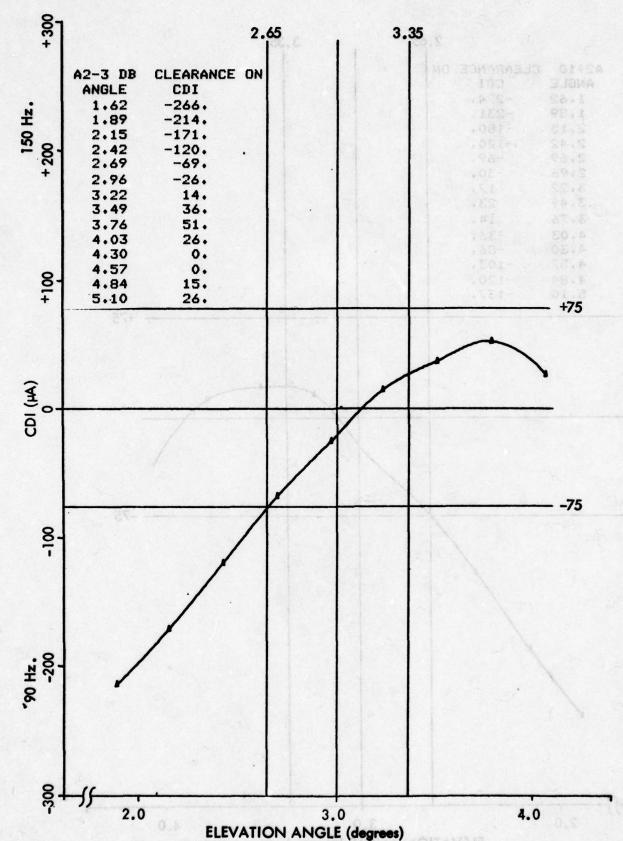
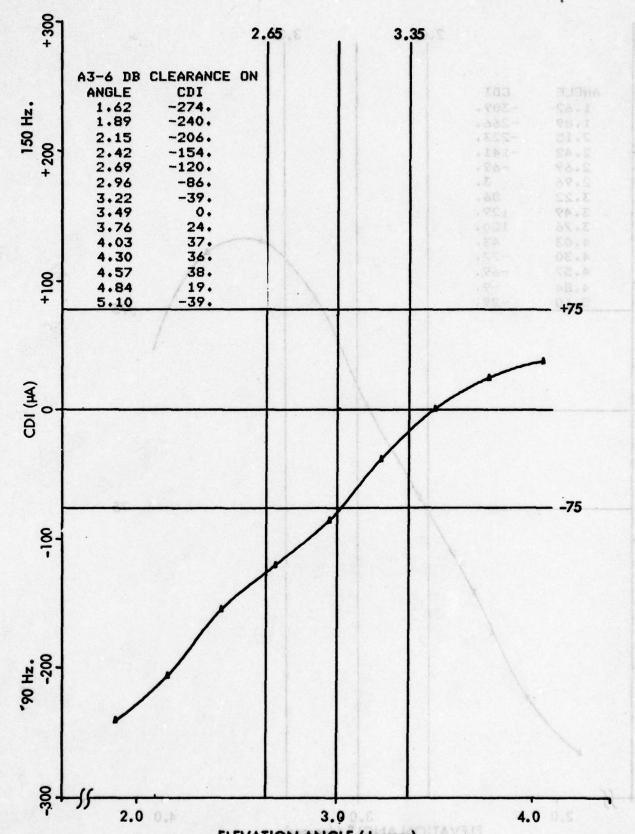


Figure 11-232. Ground Data (Commissioned) -2dB Attenuation in Middle Antenna, Clearance On.



ELEVATION ANGLE (degrees)
Figure 11–233. Ground Data (Commissioned) – 6 dB Attenuation in Upper Antenna, Clearance On.

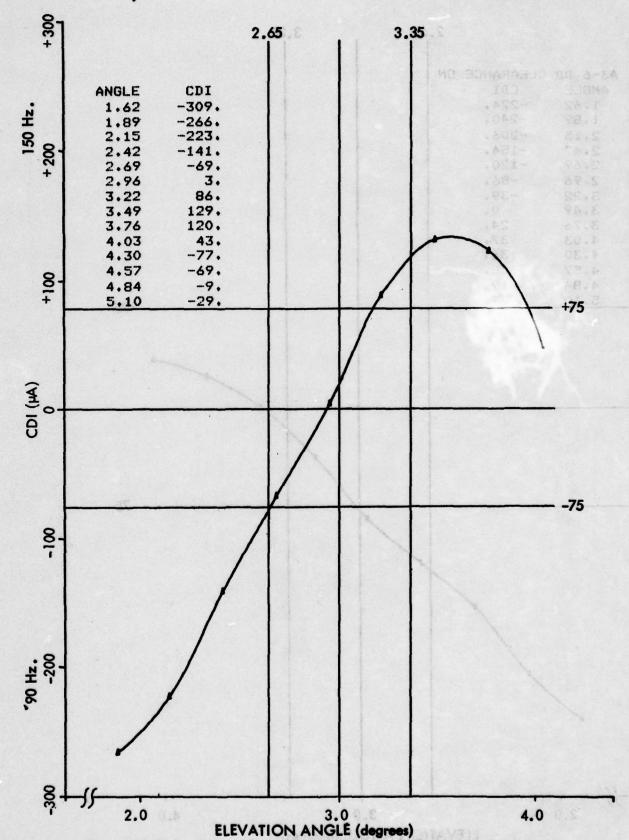
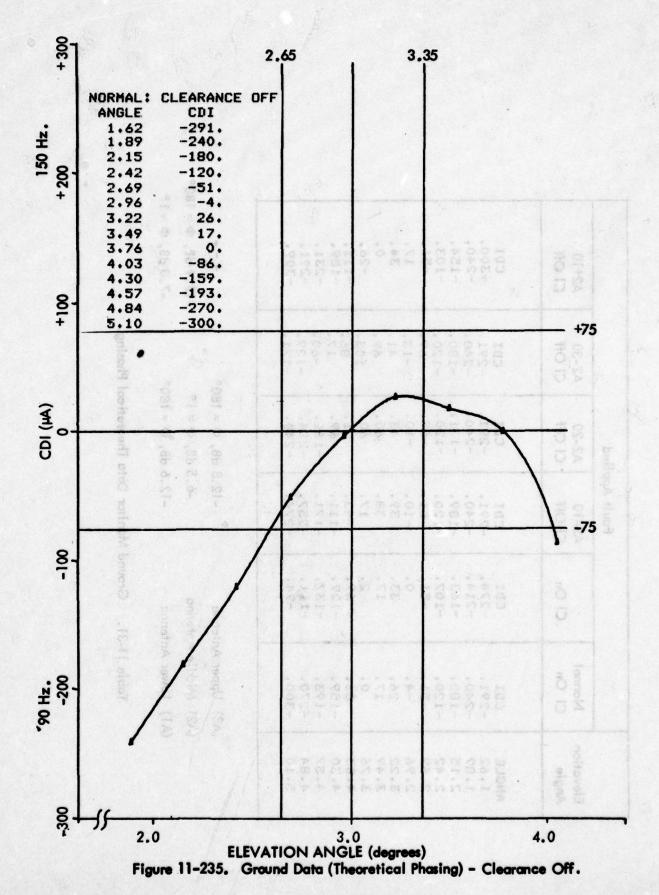


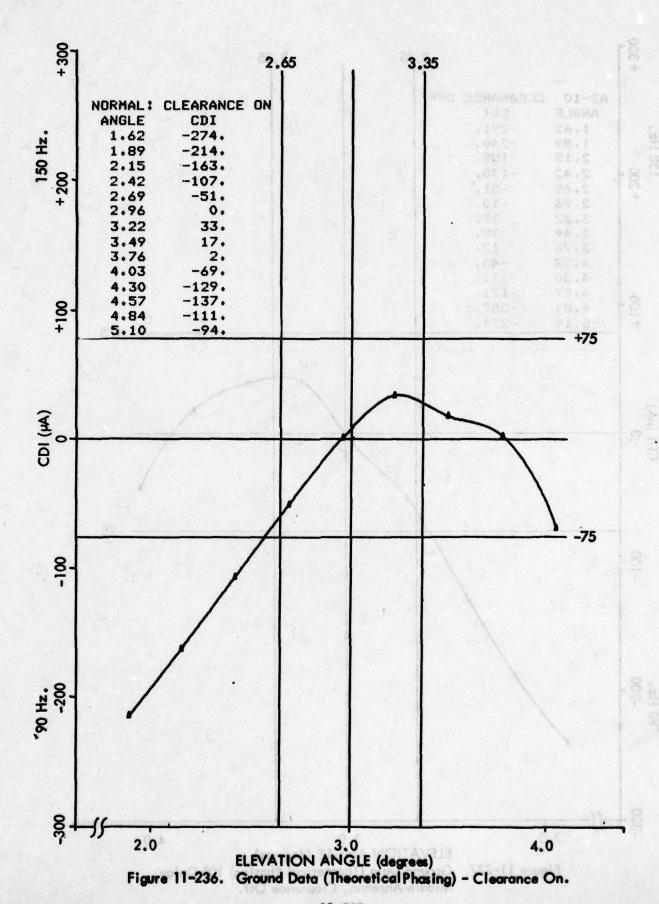
Figure 11-234. Ground Data (Commissioned) - 3 dB Attenuation in Lower Antenna - 10° Retard in Middle Antenna, Clearance On.

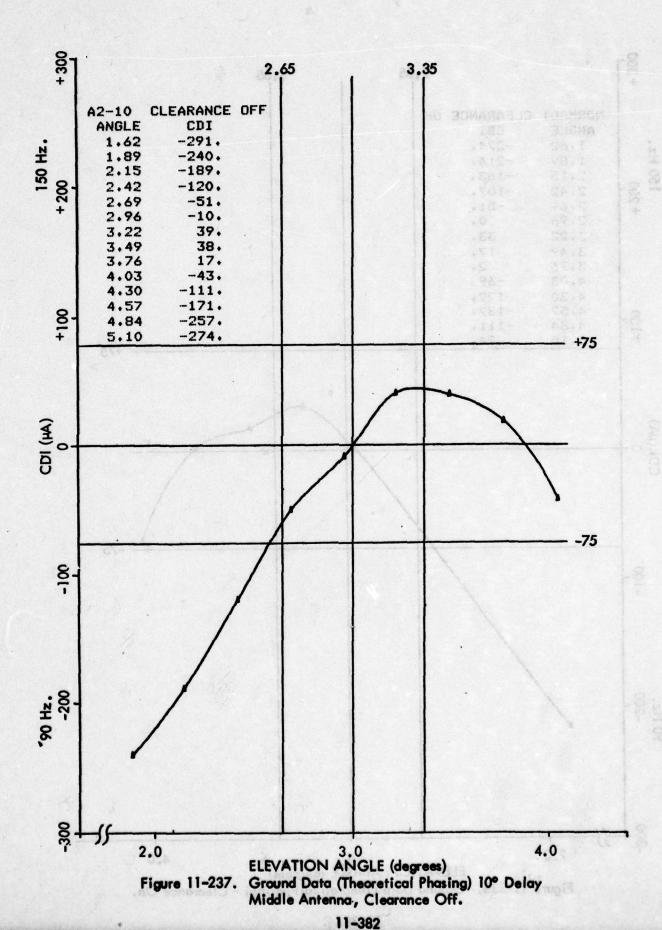
			Fault Applied	plied		
Elevation Angle	Normal CI On	ار ان ان	A2-10 CI Off	A2-20 CI Off	A2-30 CI Off	A2+10 CI Off
ANGLE	CDI		CDI	7		CDI
1.62	-291.	-274.	-291.	-291.	-291.	-300.
1.89	-240.	-214.	-240.	-240.	-240.	-240.
2.15	-180.	-163.	-189.	-171.	-180.	-154.
2.42	-120.	-107.	-120.	-120.	-120.	-103.
2.69	-51.	-51.	-51.	-69-	-69-	-51.
2.96	-4.	•	-10.	-10.	-13.	17.
3.22	26.	33.	39.	43.	41.	34.
3.49	17.	17.	38.	.09	.69	•
3.76	ò	5	17.	.09	103.	-26.
4.03	-86.	-69-	-43.	51.	. 84.	-111.
4.30	-159.	-129.	-111.	-69-	17.	-189.
4.57	-193.	-137.	-171.	-111.	-09-	-231.
4.84	-270.	-111.	-257.	-214.	-129.	-291.
5.10	-300.	-94.	-274.	-240.	-171.	-309.

0.0000000000000000000000000000000000000	-12.4 dB, $\Phi = 180^{\circ}$	$-7.0 dB, \Phi = 1^{\circ}$
-12.8 dB, $\Phi = 180^{\circ}$	$-6.5 dB, \Phi = 1^{\circ}$	-12.6 dB, $\Phi = 180^{\circ}$
(A3) Upper Antenna	(A2) Middle Antenna	(A1) Lower Antenna

Table 11-31. Ground Manitor Data Theoretical Phasing.







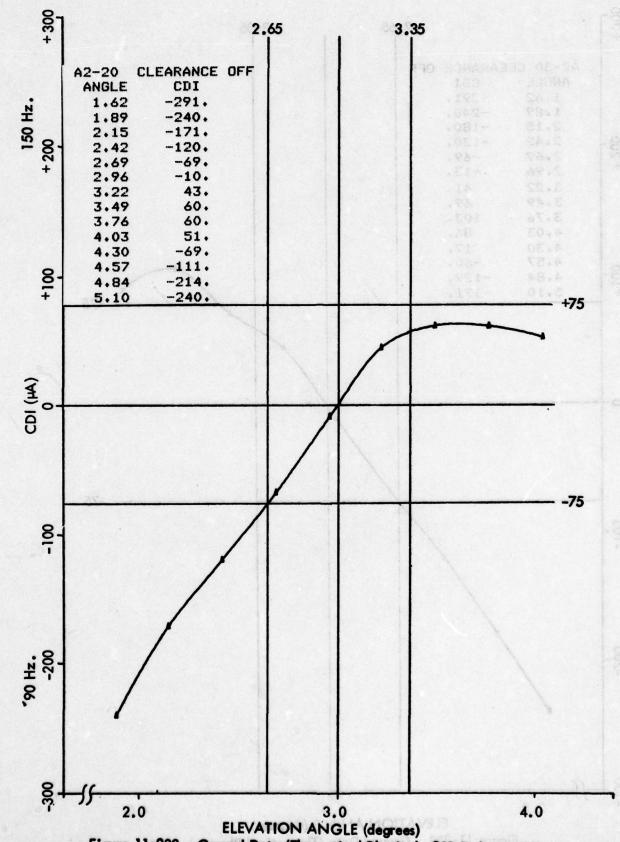
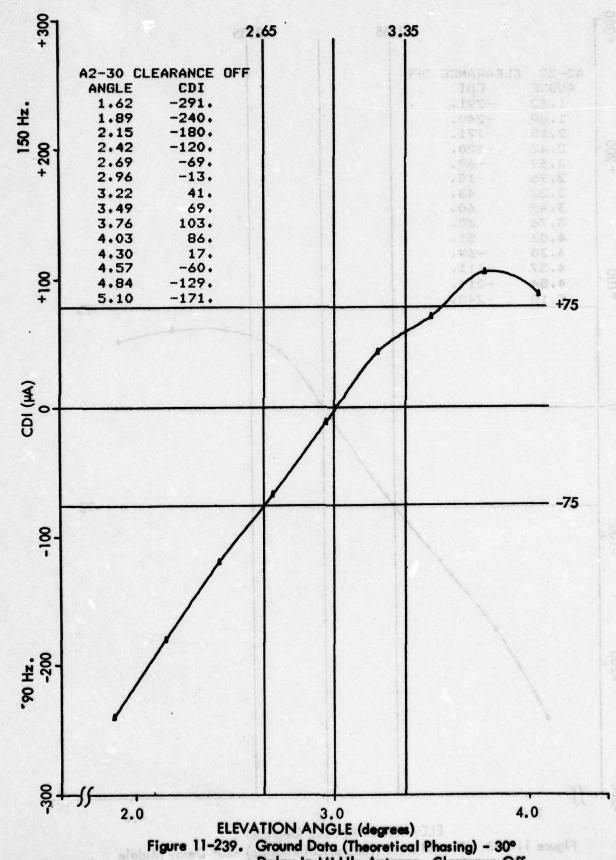


Figure 11-238. Ground Data (Theoretical Phasing) -20° Delay Middle Antenna, Clearance Off.

11-383



Delay in Middle Antenna, Clearance Off-

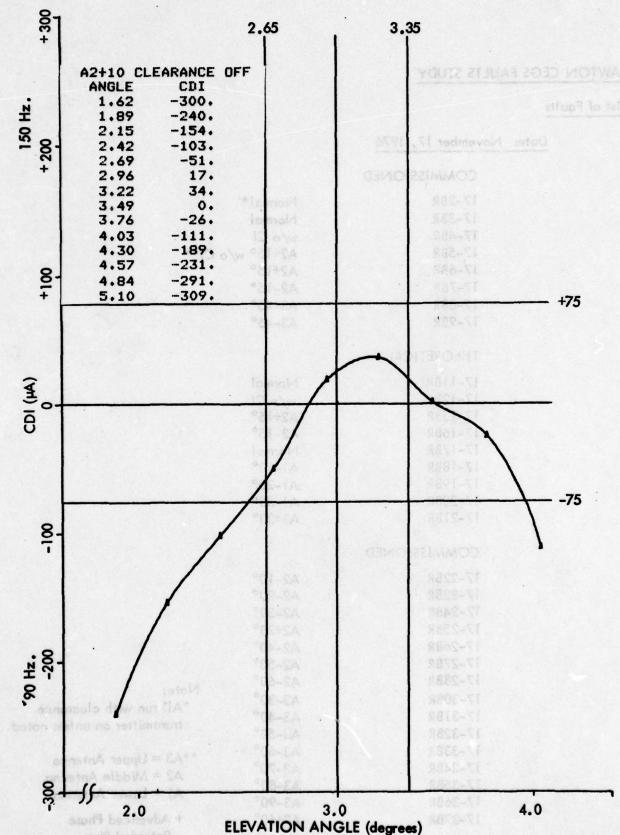


Figure 11-240. Ground Data (Theoretical Phasing) - 10° Advance in Middle Antenna.

LAWTON CEGS FAULTS STUDY

List of Faults

Date: November 17, 1976

17_2RP

co		166	VIEU
CO	IAMAI	133	NED

17-2DK	INORMAL
17-3BR	Normal
17-4BR	w/o CI
17-5BR	A2+15° w/o Cl*
17-6BR	A2+15°
17-7BR	A2-15°
17-8BR	A3+45°
17-9BR	A3-45°

THEORETICAL

17-11BR	Normal
17-12BR	w/o CI
17-15BR	A2+15°
17-16BR	A2-15°
17-17BR	Normal
17-18BR	A1-10°
17-19BR	A1-20°
17-20BR	A1-30°
17-21BR	A1+20°

COMMISSIONED

17-22BR	A2-10°
17-23BR	A2-20°
17-24BR	A2-30°
17-25BR	A2+20°
17-26BR	A2-40°
17-27BR	A2-50°
17-28BR	A2-60°
17-30BR	A3-30°
17-31BR	A3-40°
17-32BR	A3-50°
17-33BR	A3-60°
17-34BR	A3-70°
17-35BR	A3-80°
17-36BR	A3-90°
17-37BR	A3+60°

Table 11-32. Airborne Data.

Note:

- *All run with clearance transmitter on unless noted.
- **A3 = Upper Antenna A2 = Middle Antenna
 - A1 = Lower Antenna
 - + Advanced Phase
 - Retarded Phase

Date: November 18, 1976

	THEORETICAL	
	18-1BR	Normal*
	18-2BR	A2+10**
. ab 0 =	18-3BR	A2+20
	18-4BR	A2+20
	18-5BR	A2-10
	18-6BR	A2-20
	18-7BR	Normal
	18-8BR	A2-30
	· 18-9BR	A2-20
	18-10BR	보다 하는데 집에 가장하면 하면요? 하는데 보다를 보다 하는데 하면요? 그리고 하는데
	10-TUDK	
	EVDEDIALENITAL	
	EXPERIMENTAL	18-535R 18-548R
	18-11BR	Normal
	18-12BR	Normal after Mod equality set (2/90) 3.07
	18-13BR	Normal
	18-14BR	A2 10
	18-15BR	A2-10 A2-20
	18-16BR	A2-30
	18-17BR	A2+10
	18-18BR	A3+40
	18-19BR	A3-40
	18-20BR	Al-1dB
	18-21BR	A1-3dB
		71. GGB
		AT SHOTTED
	18-25BR	A2-1dB
	18-26BR	A2-2dB
	18-27BR	A2-4dB
	18-28BR	A2 shorted
	18-29BR	A2 open
ote:	18-30BR	A3-3dB
'All run with clearance	18-31BR	A3-6dB
transmitter on unless	18-32BR	A3-10dB
noted.	18-33BR	A3 shorted
A3 = Upper Antenna	18-34BR	A3 opened
A2 = Middle Antenna	18-36BR	Normal
A1 = Lower Antenna	18-37BR	20 SBO dephase
AI - LOWER Antenna	18-38BR	30 SBO dephase
+Advanced Phase	18-39BR	50 SBO dephase
-Retarded Phase	18-40BR	CI-3dB 9 watts Normal
	18-41BR	CI-6dB
	18-42BR	Cl+3dB
	Table 11-32 (C	
	10010 1153/ /(

Date: November 18, 1976

EXPERIMENTAL (Continued)

18-43BR	C = +5.2 dB
18-44BR	Cl Mod at Alarm Cl = 0 dB
18-45BR	Pwr Div A CW
18-46BR	Pwr Div A CCW
18-47BR	Pwr Div B CW
18-48BR	Pwr Div B CCW
18-49BR	Carr Div CW
18-50BR	Carr Div CCW
18-51BR	Z8 CW
18-52BR	Z8 CCW
18-53BR	Normal
18-54BR	Normal 8 degree W

Nati-Bi

Date: November 19, 1976

THEORETICAL

19-1BR	Normal
19-3BR	Normal
19-4BR	CI Off
19-5BR	CI Off
19-6BR	No Cl
19-7BR	No Cl
19-8BR	A2-10
19-9BR	A2-20
19-10BR	A2-30
19-11BR	A2-40
19-23BR	CI Off
19-24BR	CI On

Table 11-32. (Continued)

Lambert Steve & Sixt-13

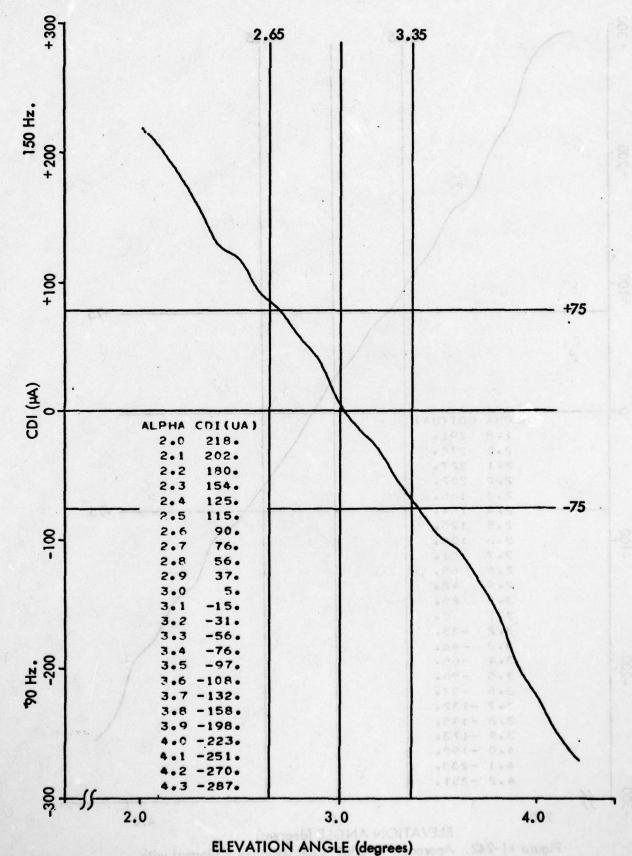
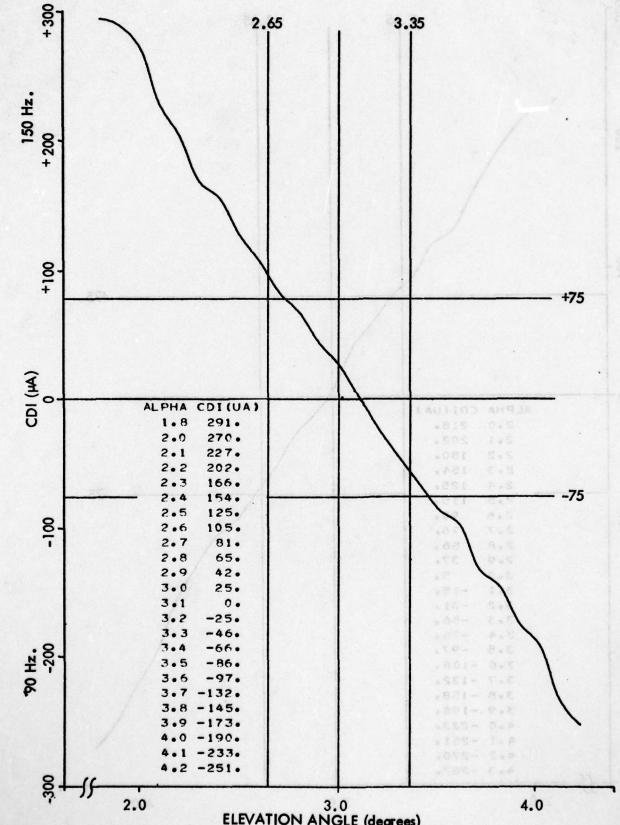


Figure 11-241. Approach 17-02 BR Commissioned - Normal with Clearance.



2.0
3.0
4.0
ELEVATION ANGLE (degrees)
Figure 11-242. Approach 17-03BR Commissioned - Normal with Clearance - (Repeat 17-02BR).

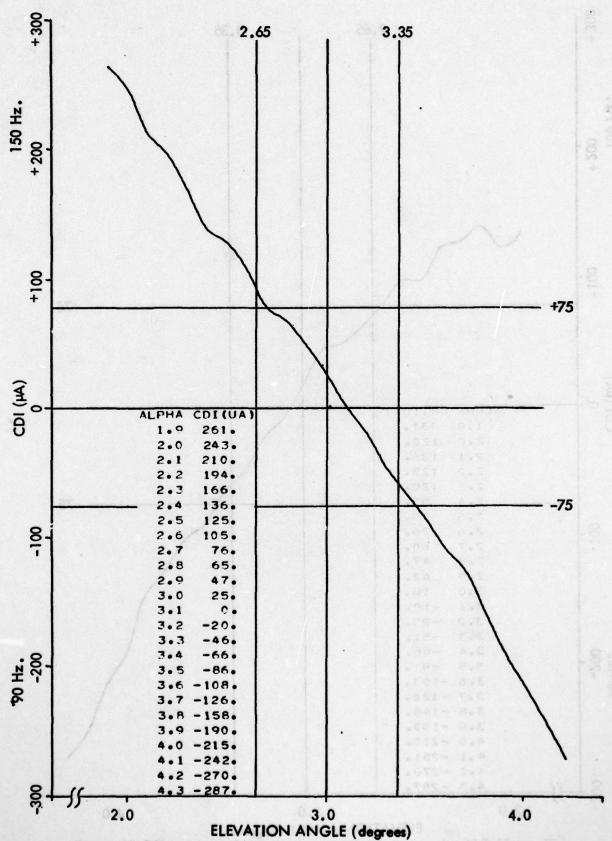


Figure 11-243. Approach 17-04 Commissioned - Normal without Clearance.

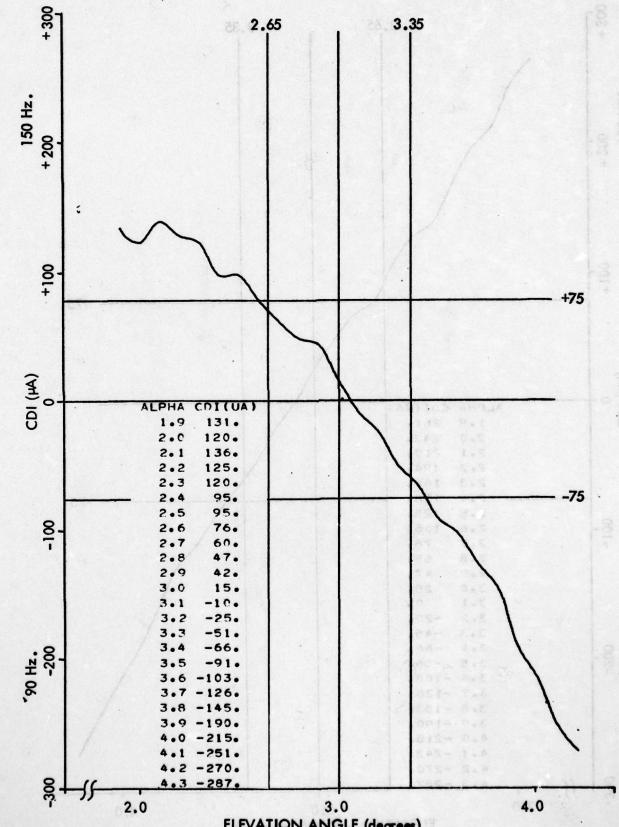
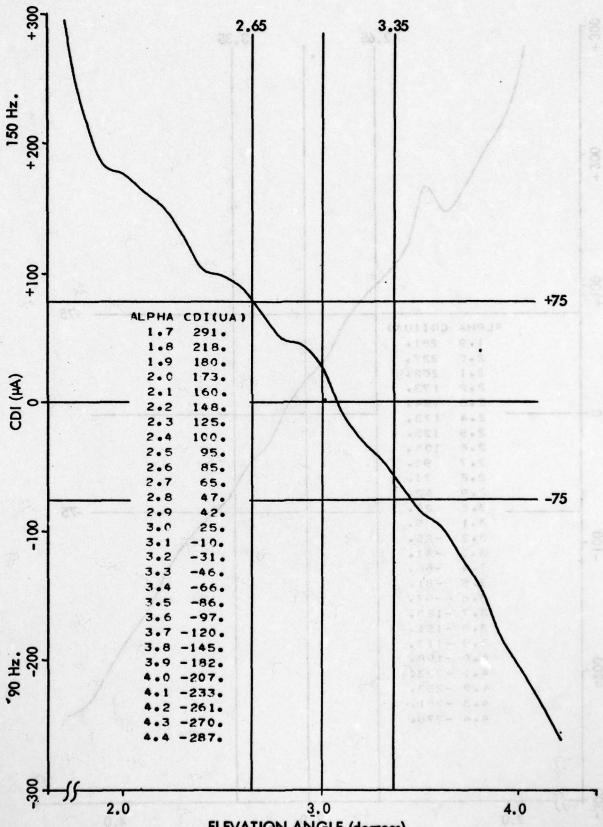
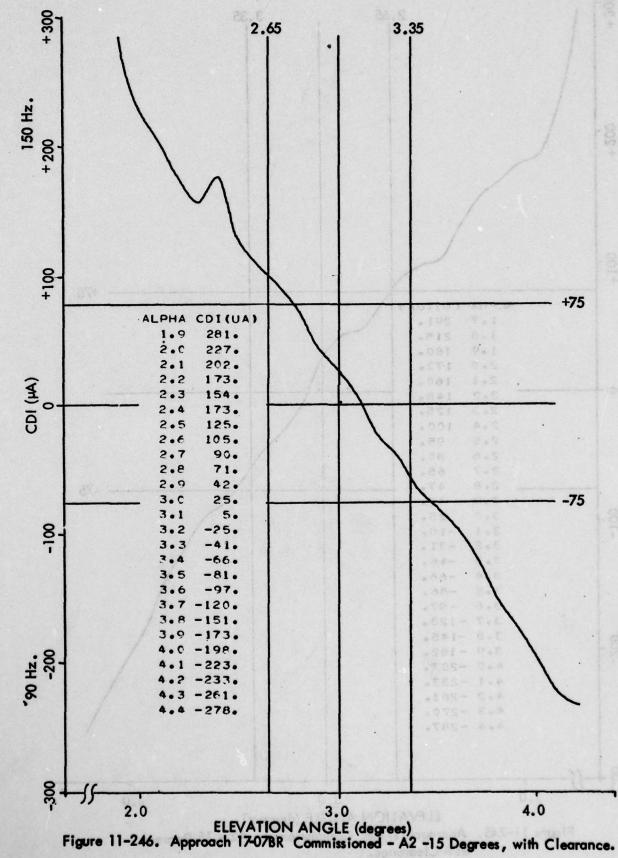


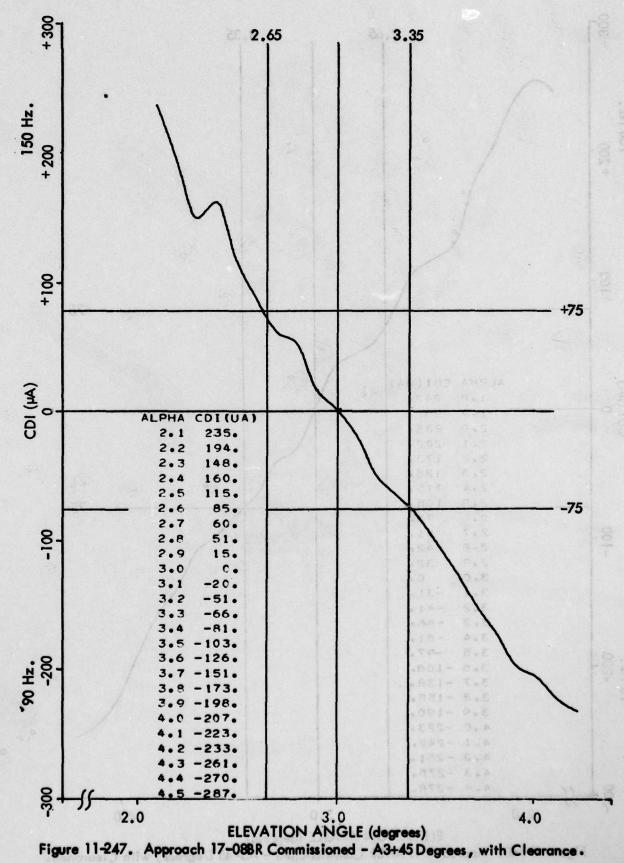
Figure 11-244. Approach 17-05BR Commissioned - A2+15 Degrees,
Clearance Off-

11-392



ELEVATION ANGLE (degrees)
Figure 11-245. Approach 17-06 Commissioned - A2 + 15 Degrees, with Clearance.





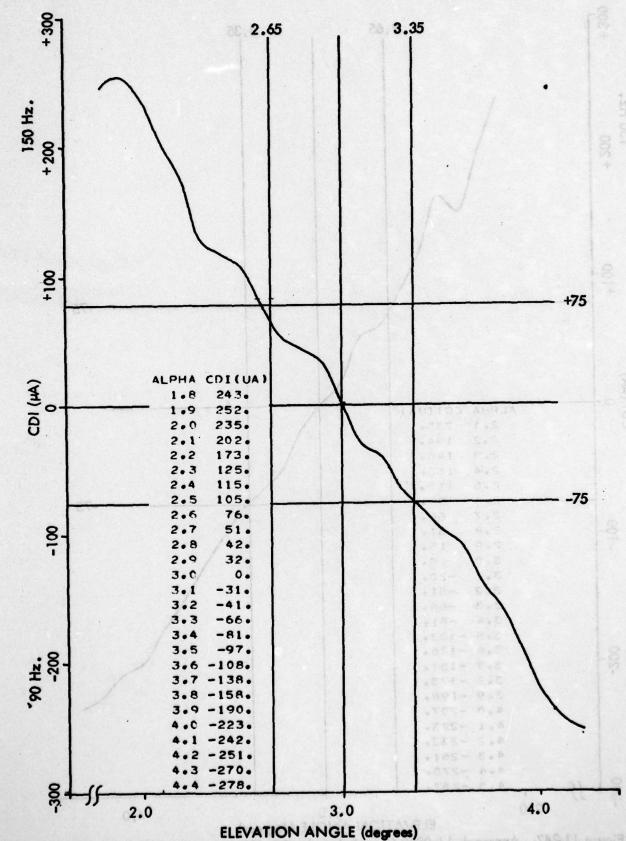
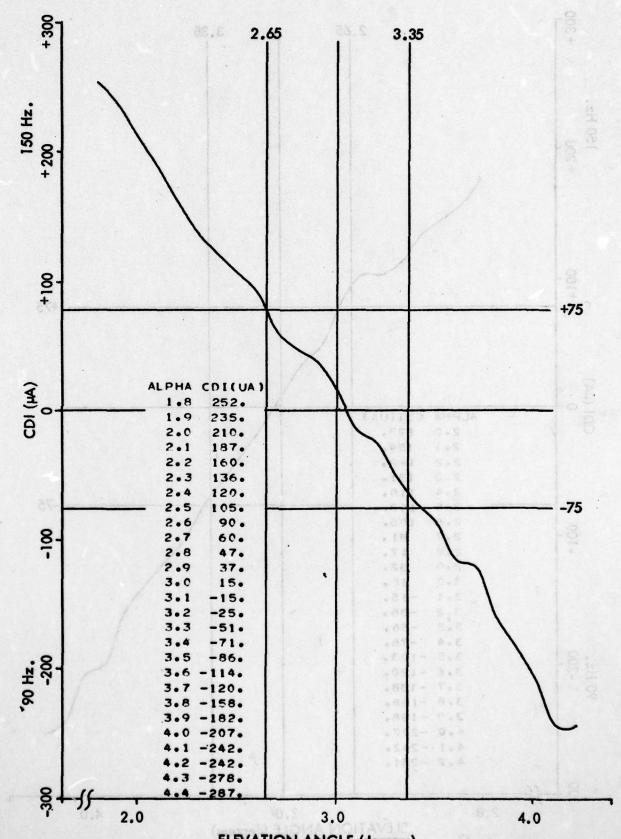
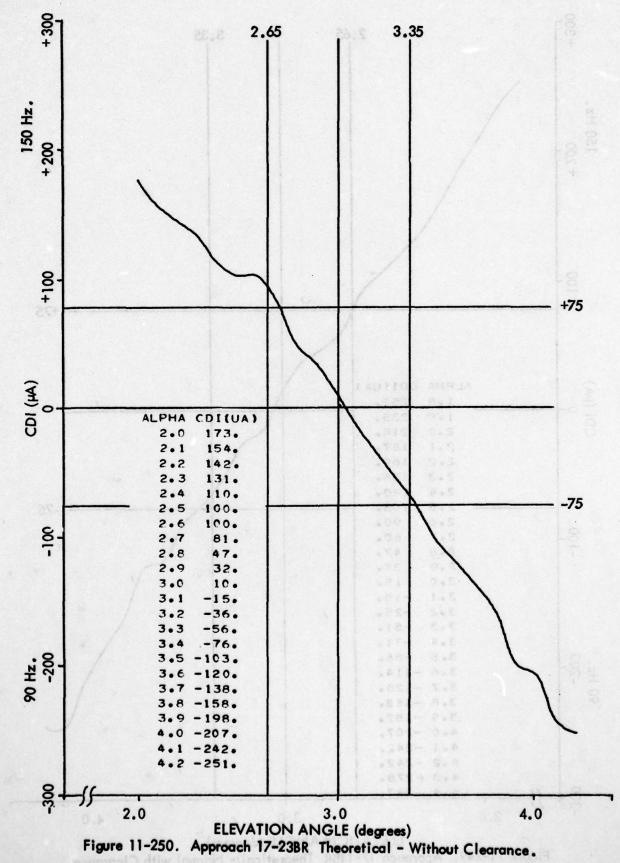


Figure 11-248. Approach 17-09BR Commissioned - A3-45 Degrees, with Clearance.



ELEVATION ANGLE (degrees)
Figure 11-249. Approach 17-11BR Theoretical - Normal with Clearance.



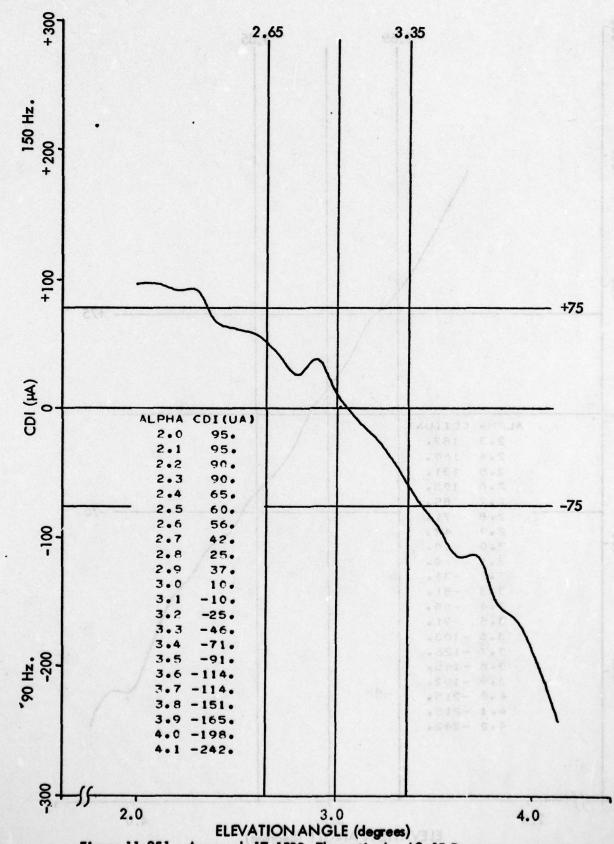
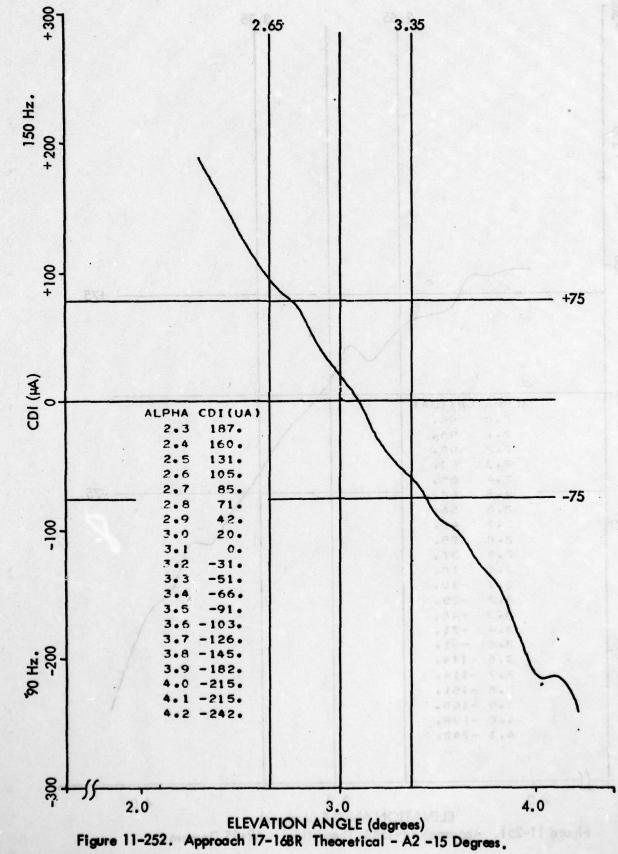
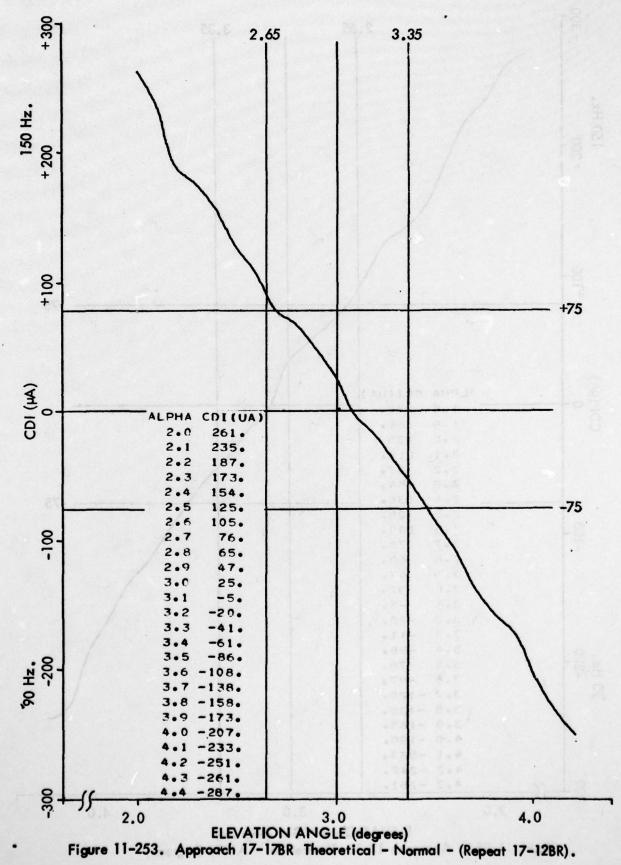
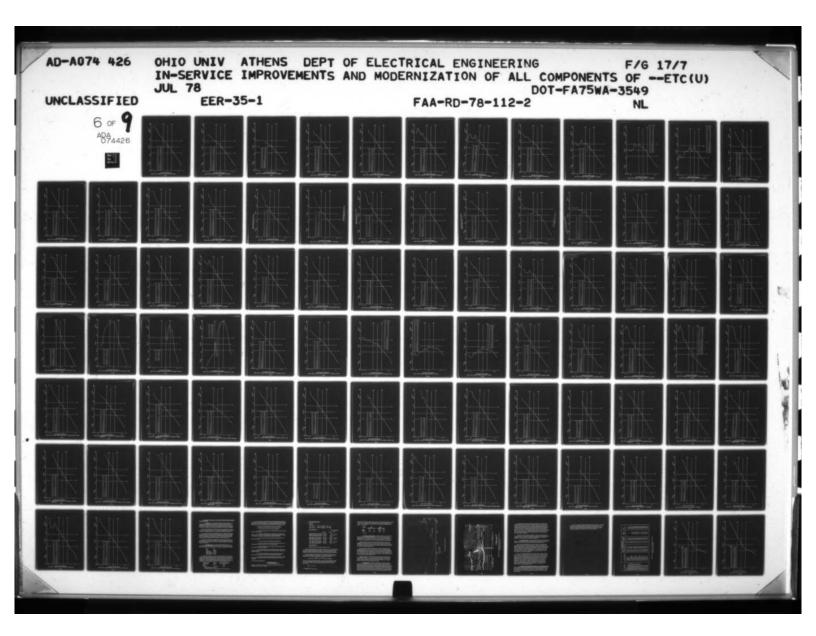


Figure 11-251. Approach 17-15BR Theoretical - A2+15 Degrees.



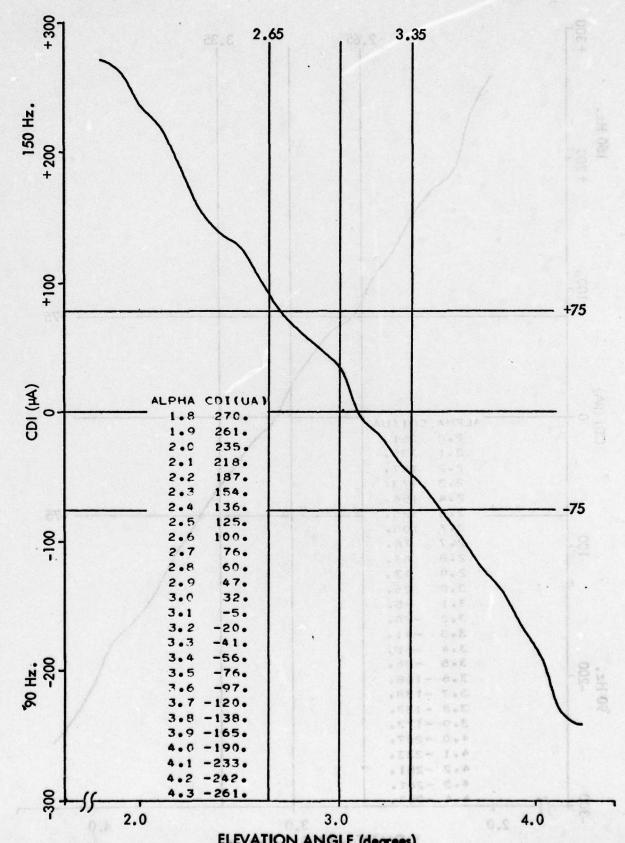




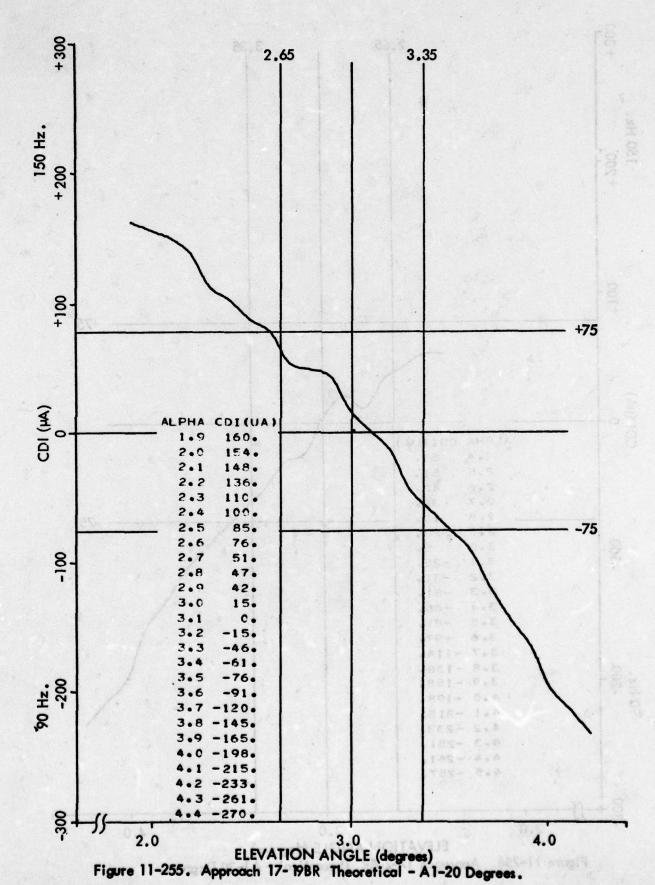
G OF ADA ADA 426



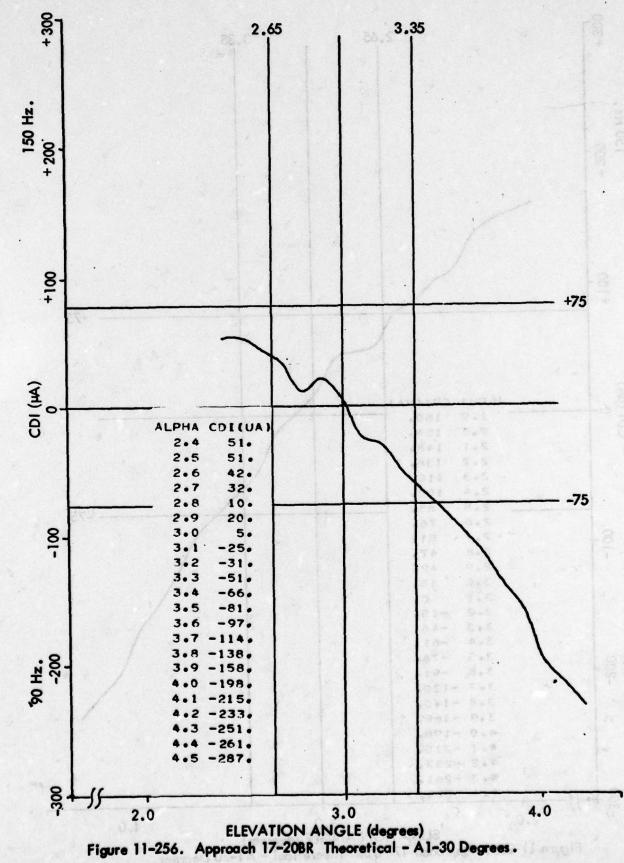
MICROCOPY RESOLUTION TEST CHART

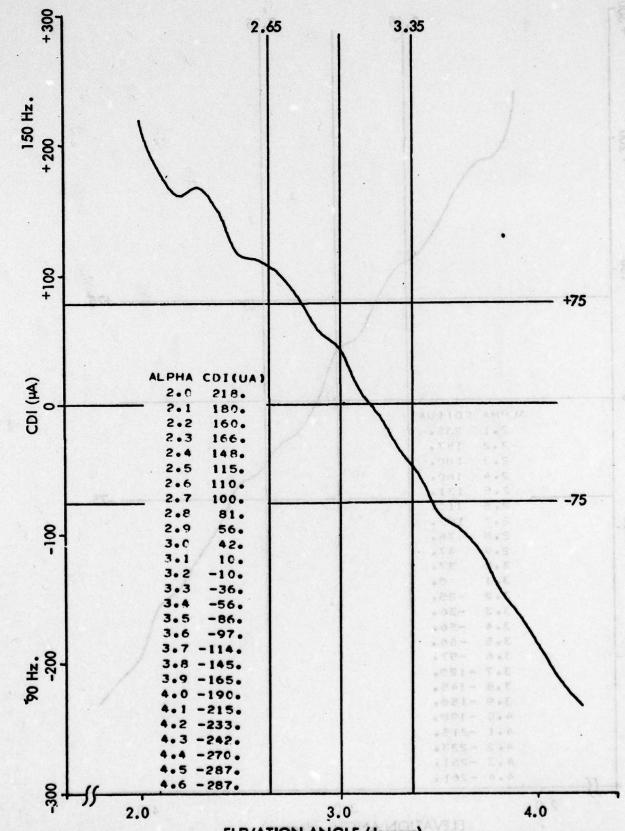


ELEVATION ANGLE (degrees)
Figure 11-254. Approach 17-18 Theoretical - A1-10 Degrees.

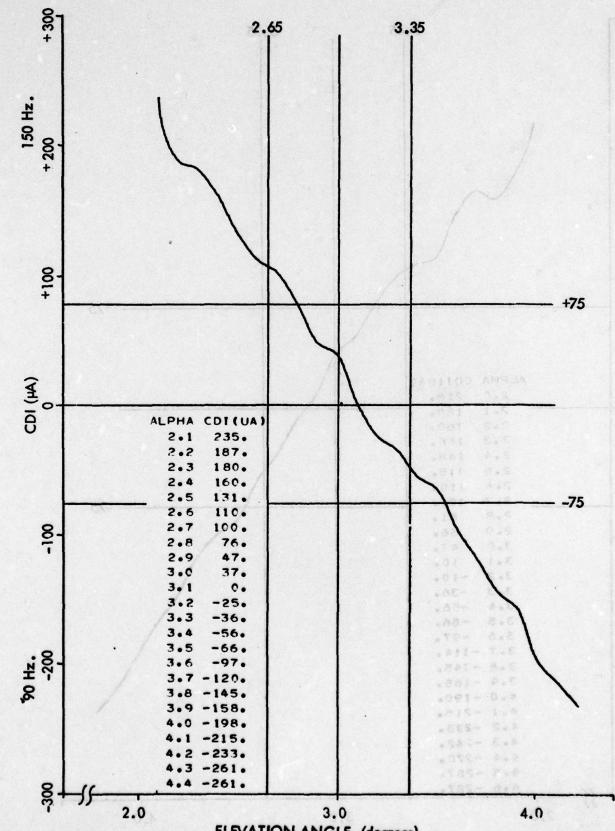


11-403

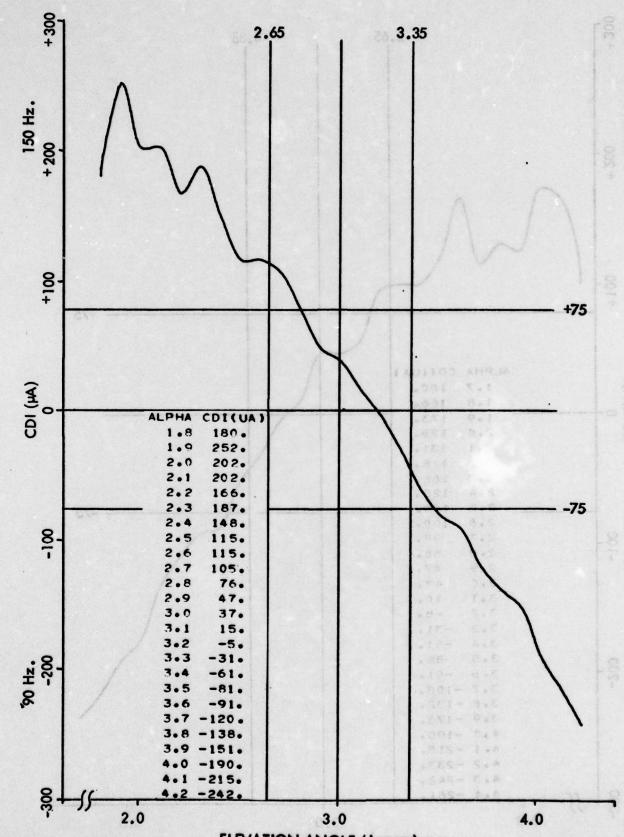




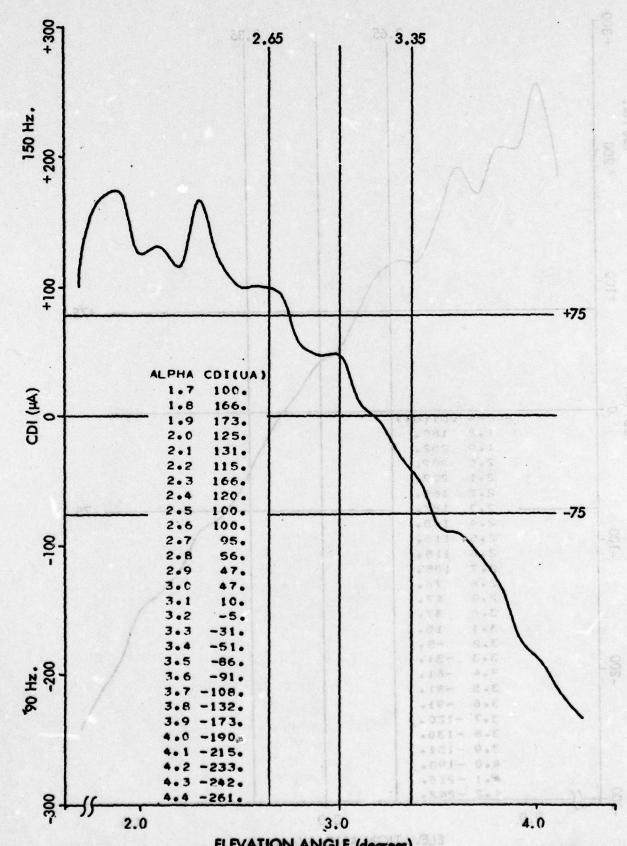
ELEVATION ANGLE (degrees)
Figure 11-257. Approach 17-21BR Theoretical - A1 +20 Degrees.



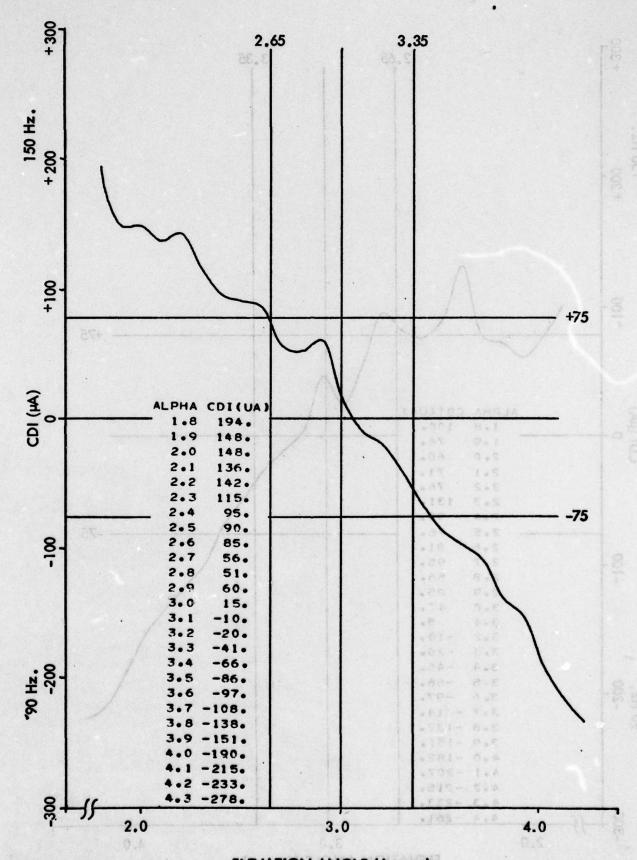
ELEVATION ANGLE (degrees)
Figure 11-258. Approach 17-22BR Commissioned - A2-10 Degrees.



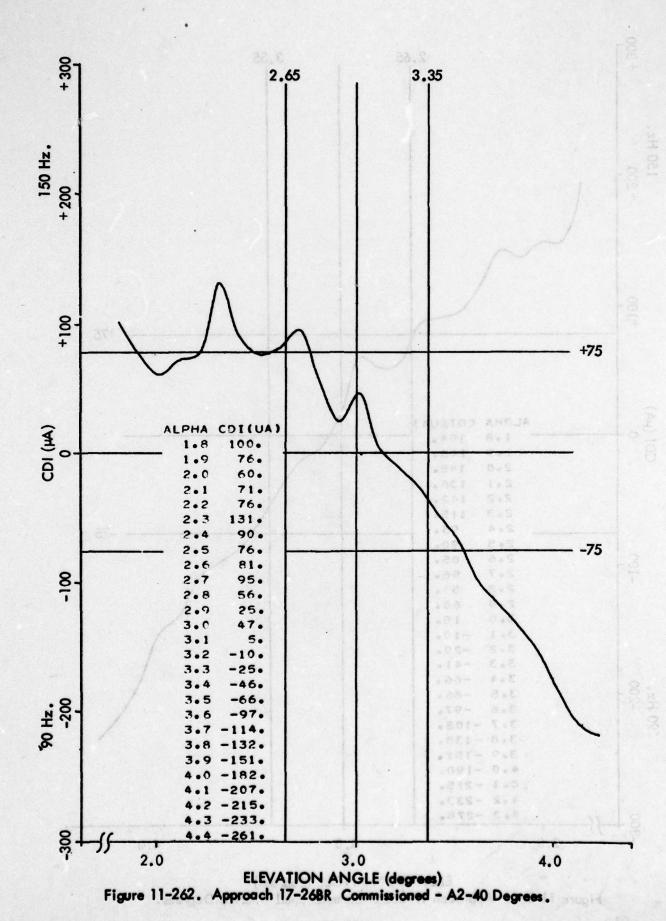
ELEVATION ANGLE (degrees)
Figure 11-259. Approach 17-23BR Commissioned - A2-20 Degrees.



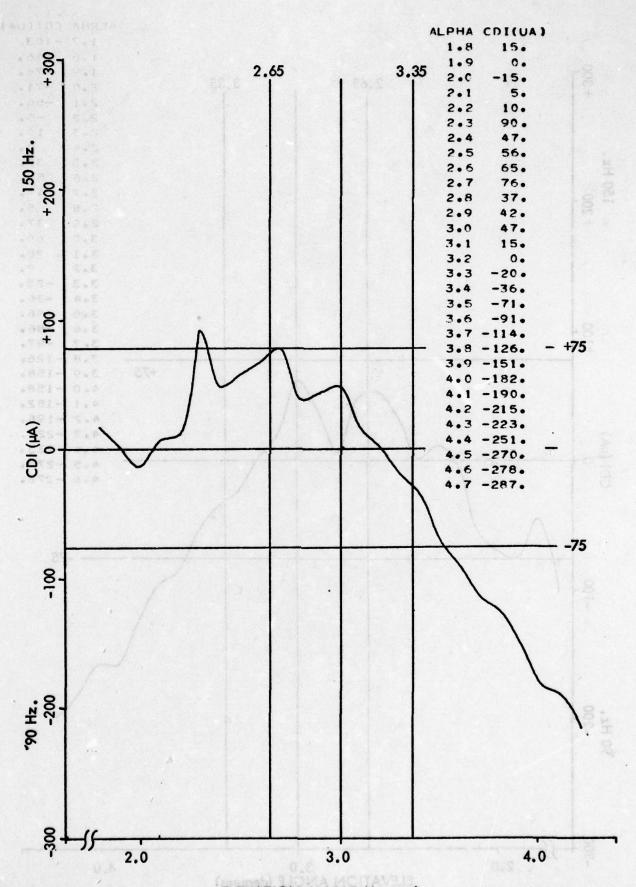
ELEVATION ANGLE (degrees)
Figure 11-260. Approach 17-24 Commissioned - A2-30 Degrees.



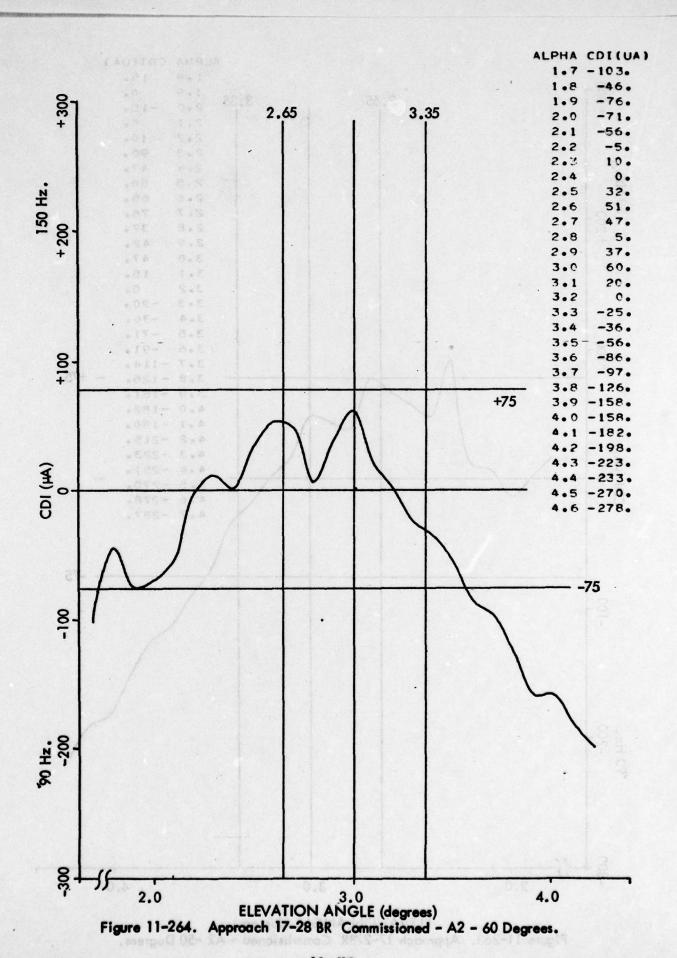
ELEVATION ANGLE (degrees)
Figure 11-261. Approach 17-25BR Commissioned - A2+20 Degrees.

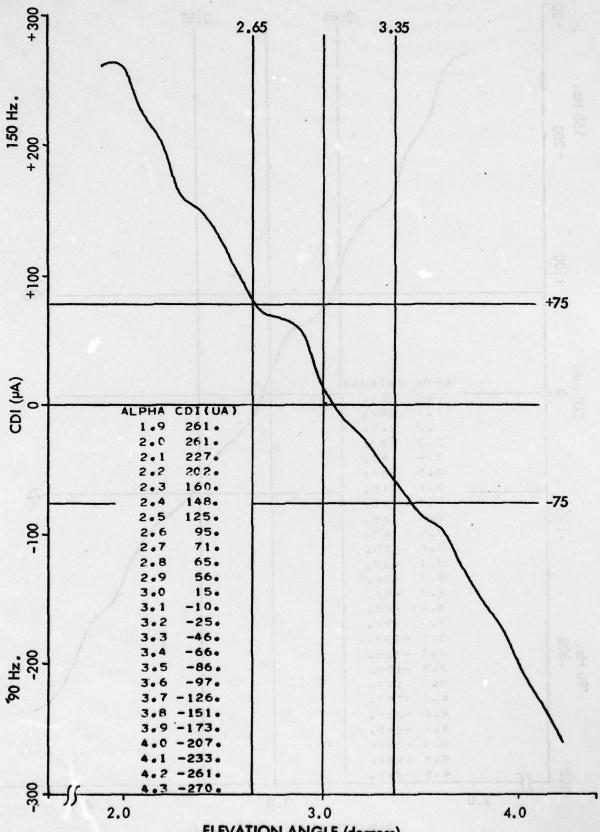


11-410

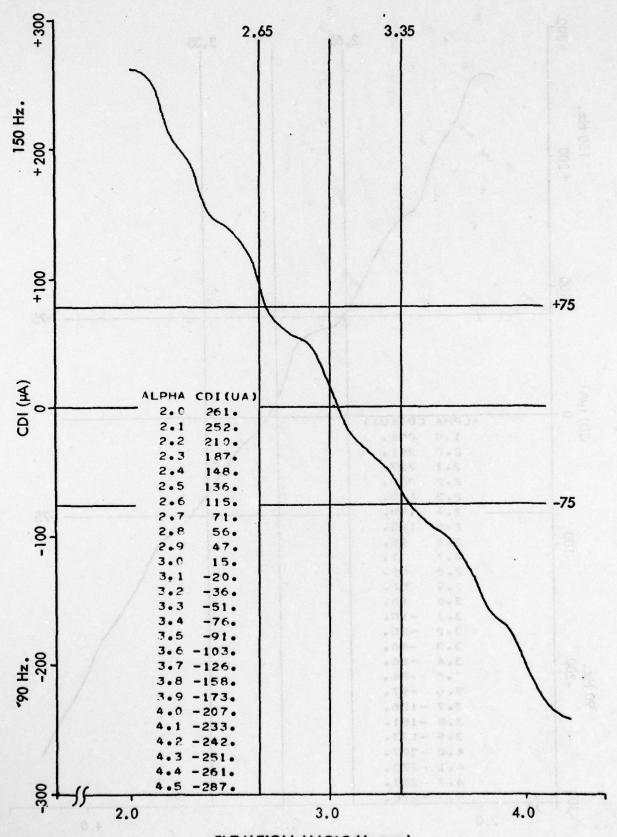


ELEVATION ANGLE (degrees)
Figure 11-263. Approach 17-27BR Commissioned - A2 -50 Degrees.

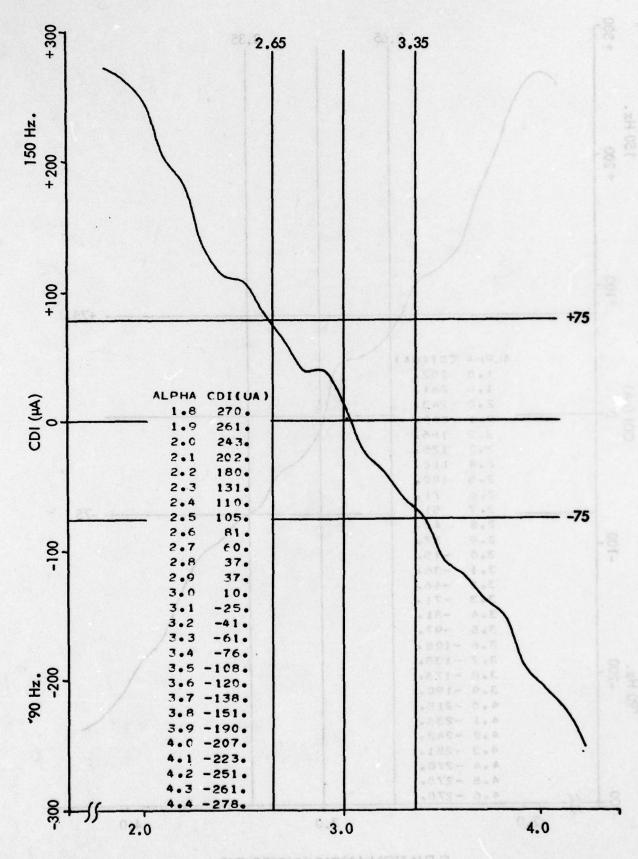




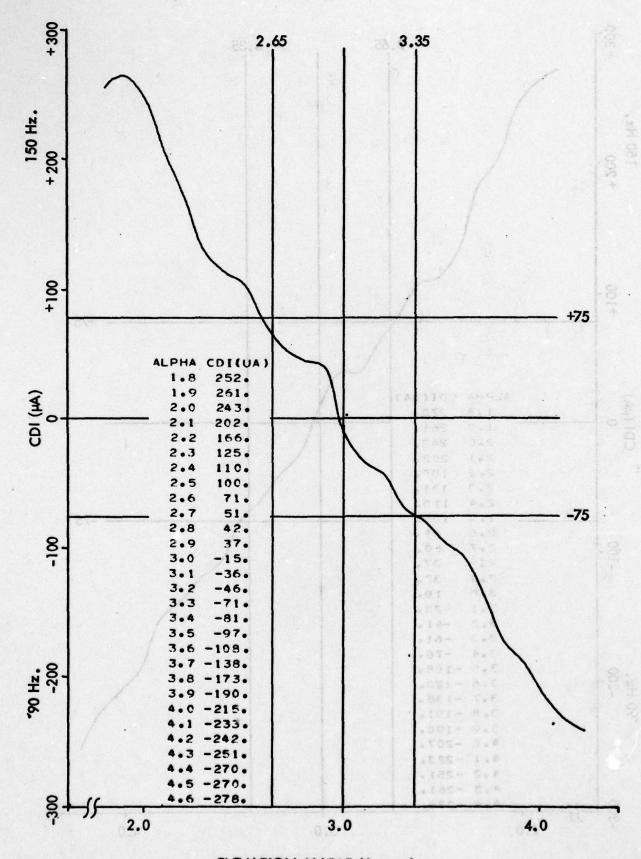
ELEVATION ANGLE (degrees)
Figure 11-265. Approach 17-30BR Commissioned - A3 -30 Degrees.



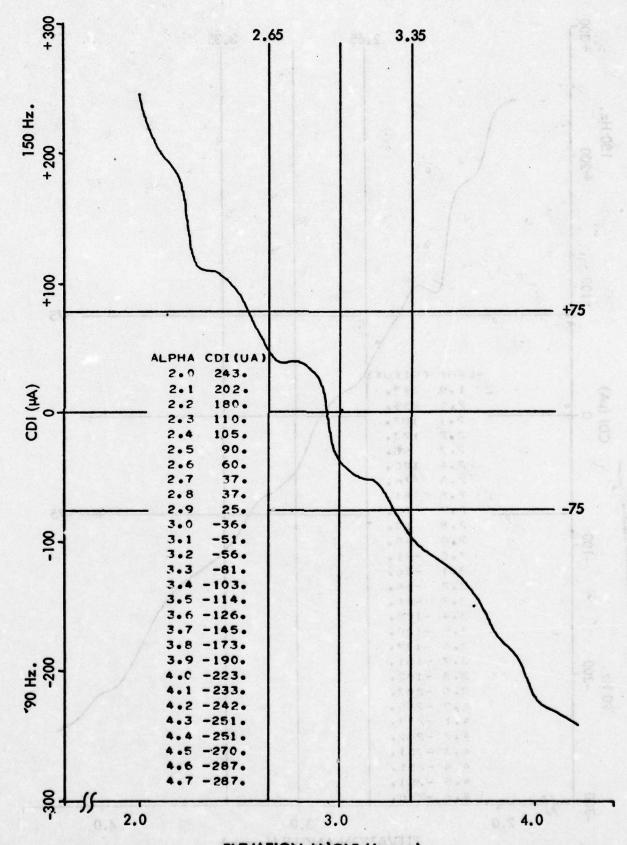
ELEVATION ANGLE (degrees)
Figure 11-266. Approach 17-31BR Commissioned - A3 -40 Degrees.



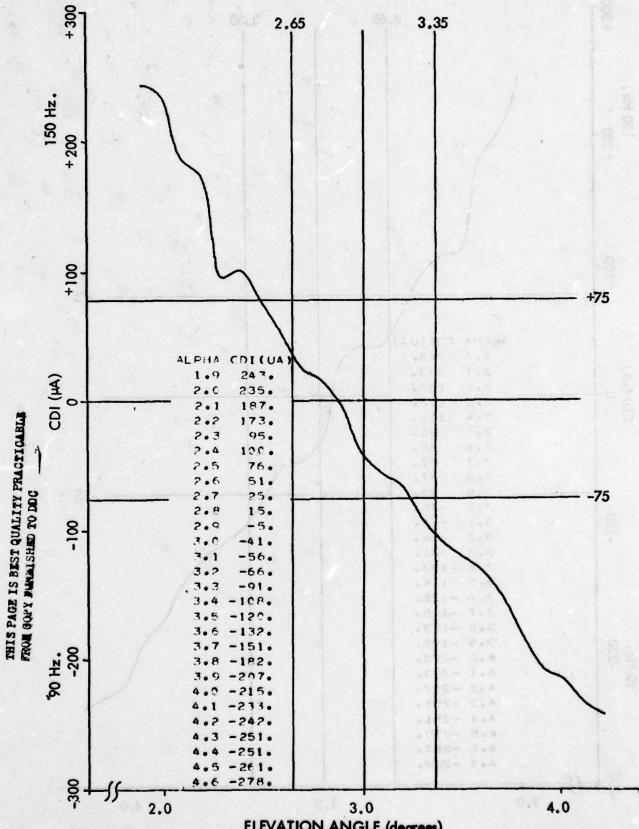
ELEVATION ANGLE (degrees)
Figure 11-267. Approach 17-32BR Commissioned - A3 - 50 Degrees.



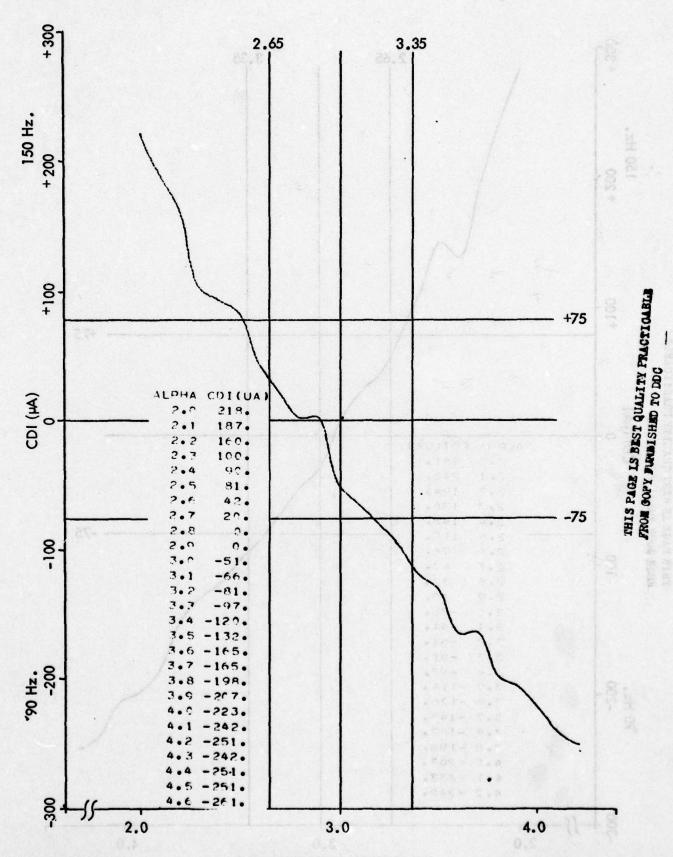
ELEVATION ANGLE (degrees)
Figure 11-268. Approach 17-338R Commissioned - A3 -60 Degrees.



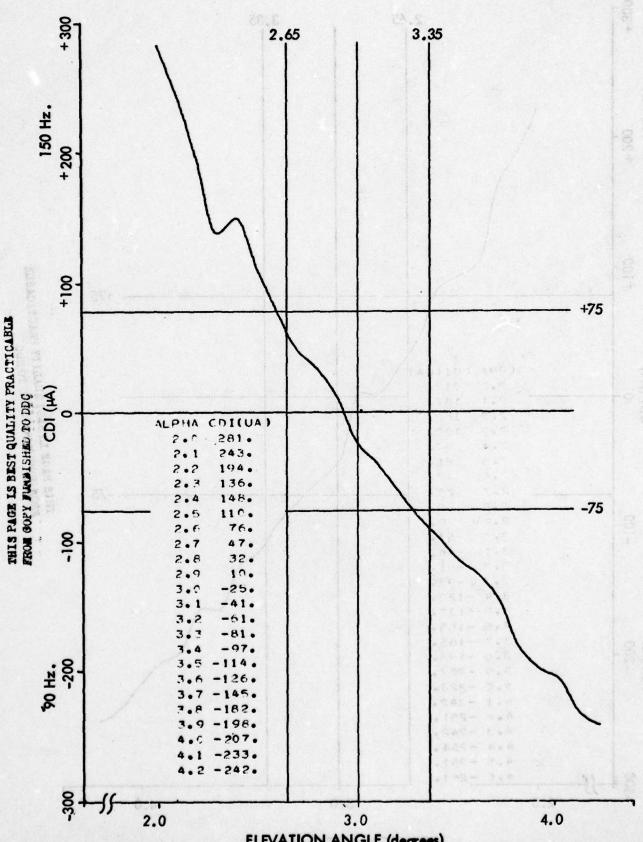
ELEVATION ANGLE (degrees)
Figure 11-269. Approach 17-34BR Commissioned - A3 -70 Degrees.



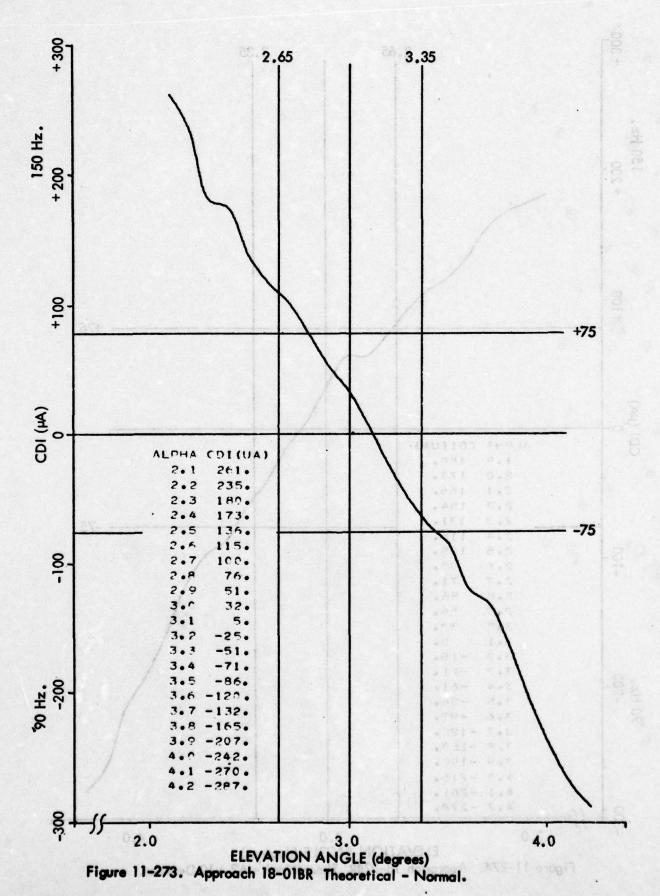
ELEVATION ANGLE (degrees)
Figure 11-270. Approach 17-35BR Commissioned - A3 -80 Degrees.

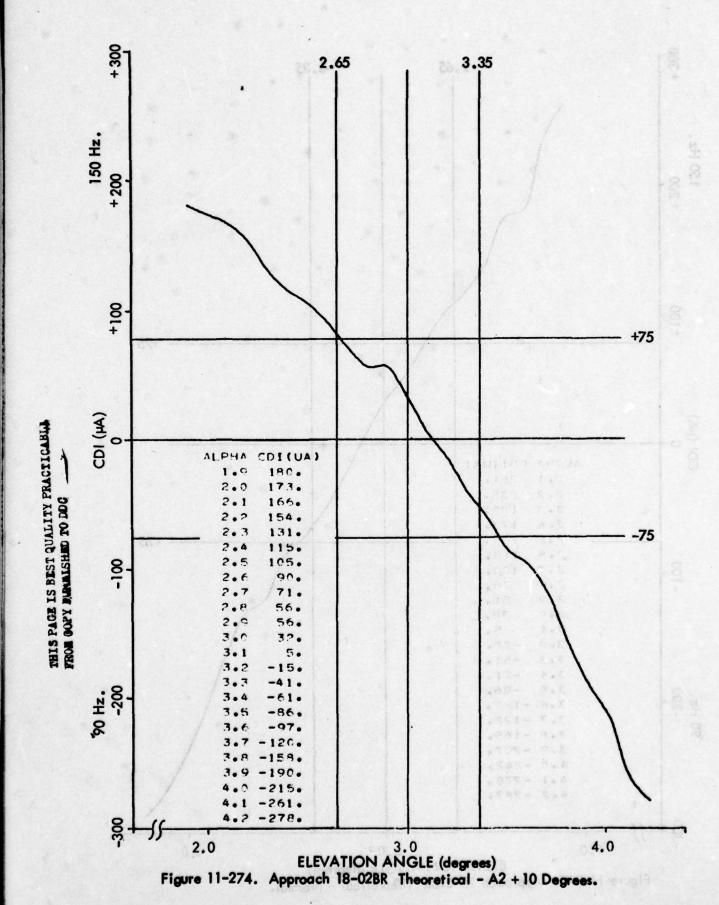


ELEVATION ANGLE (degrees)
Figure 11-271. Approach 17-36 BR Commissioned - A3 -90 Degrees.
11-419

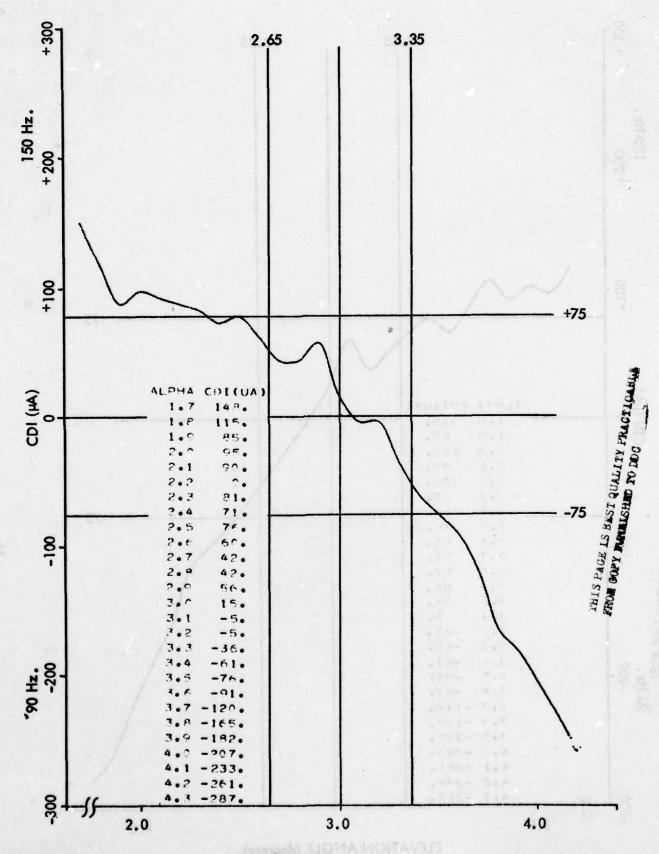


ELEVATION ANGLE (degrees)
Figure 11-272. Approach 17-37BR Commissioned - A3 + 60 Degrees.

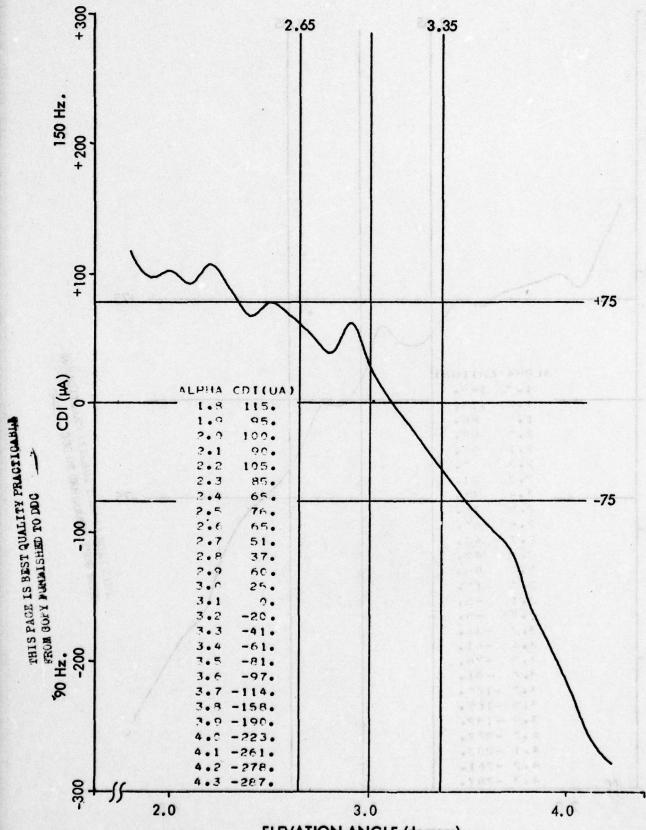




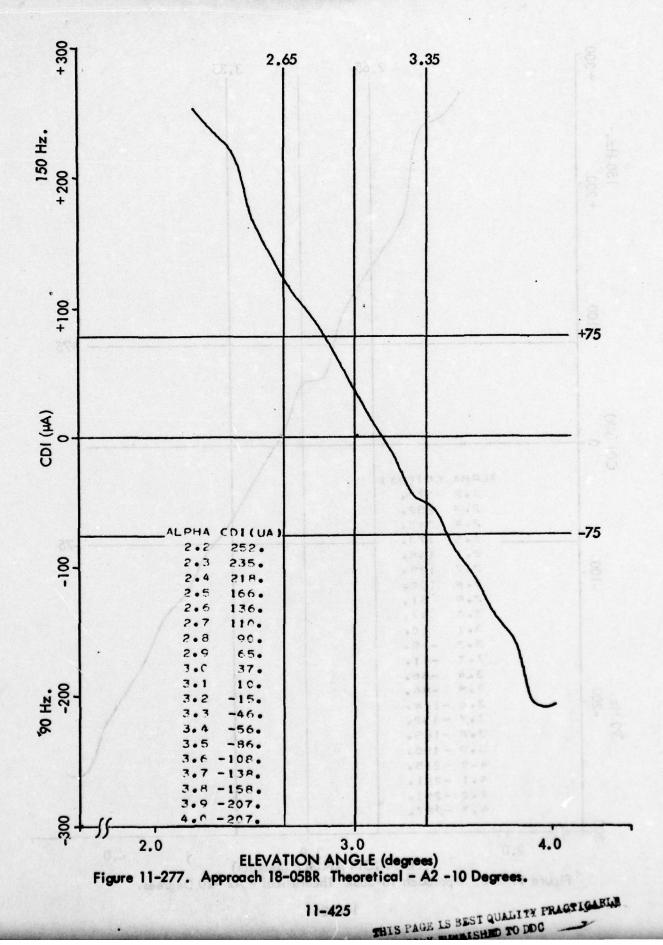
11-422



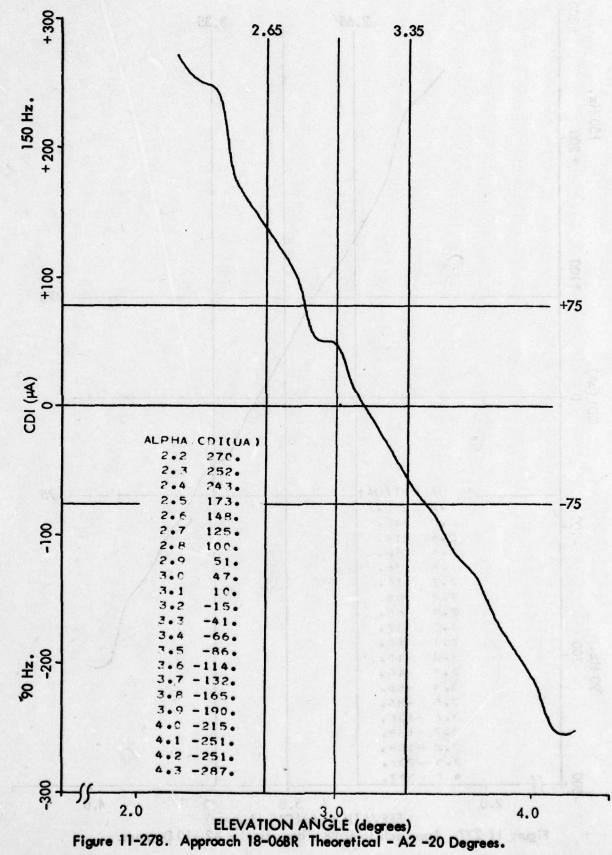
ELEVATION ANGLE (degrees)
Figure 11-275. Approach 18-03BR Theoretical - A2 +20 Degrees.

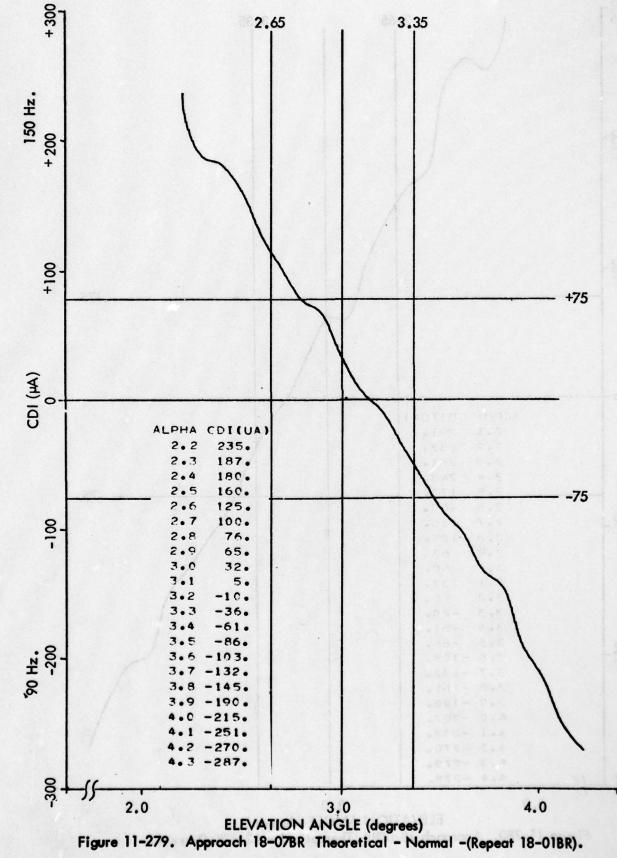


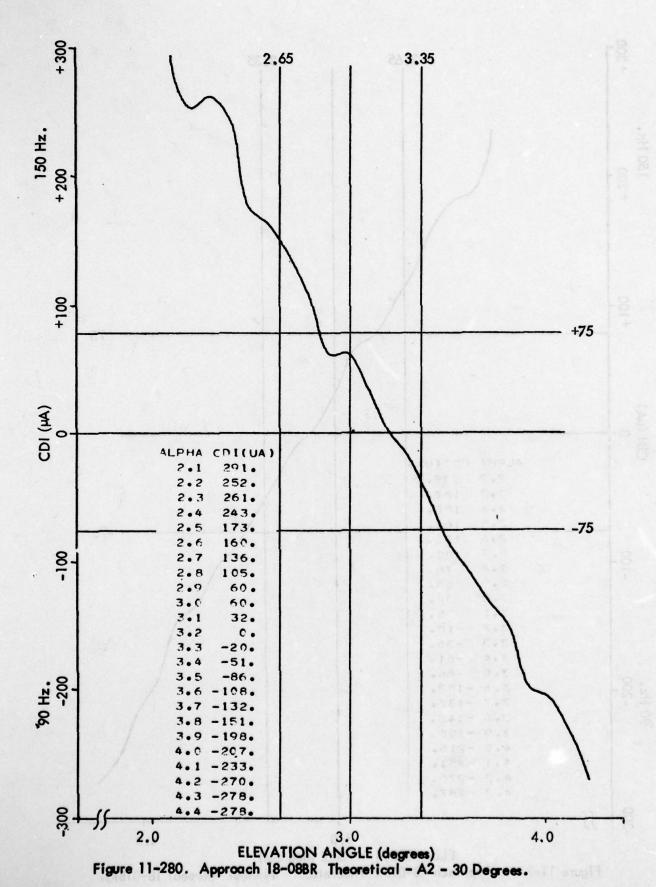
ELEVATION ANGLE (degrees)
Figure 11-276. Approach 18-04BR Theoretical - A2 + 20 Degrees (Repeat 18-03 BR).



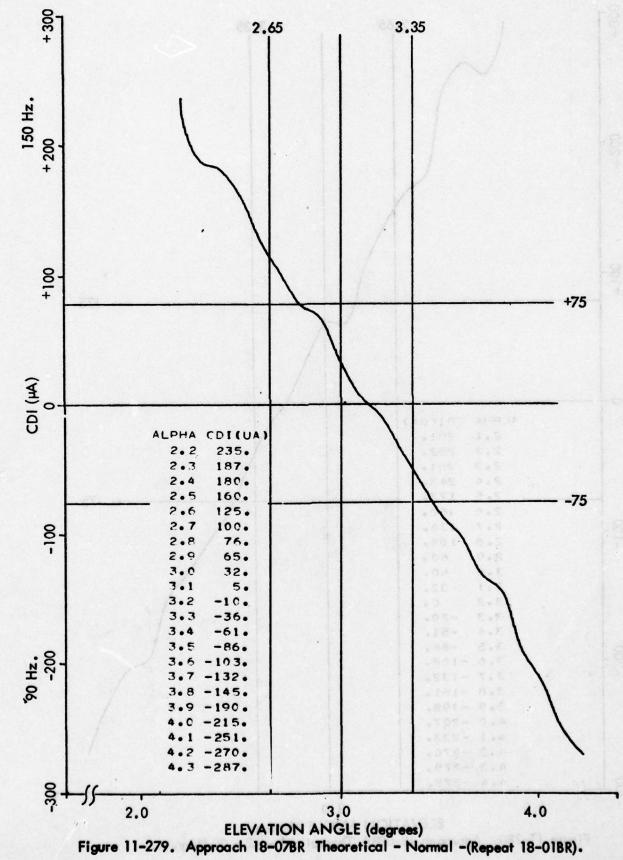
11-425

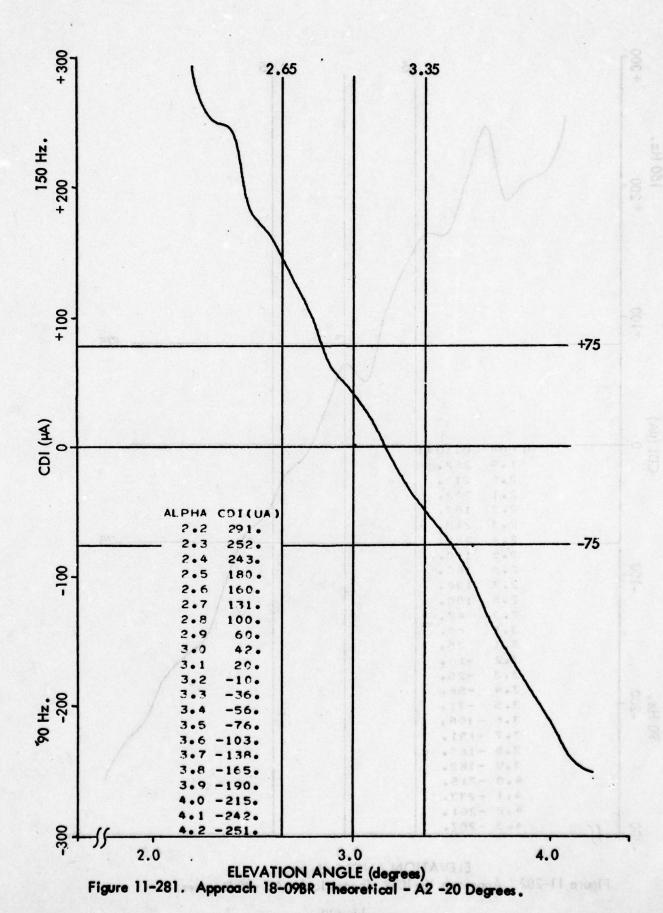


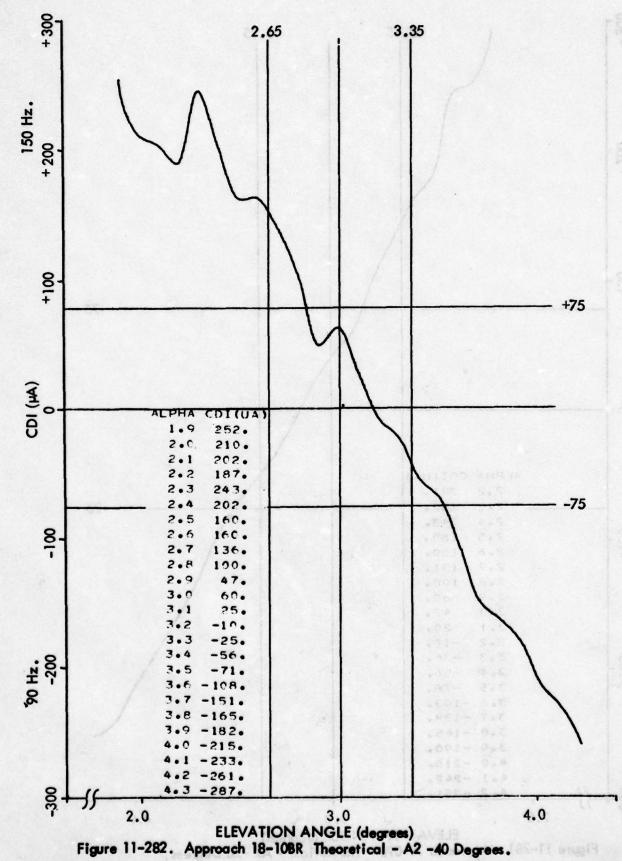


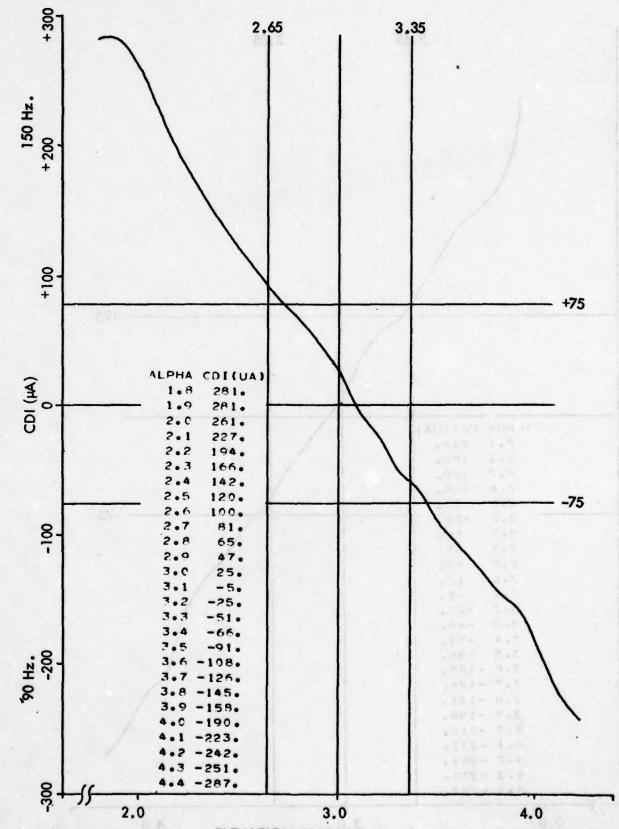


11-428

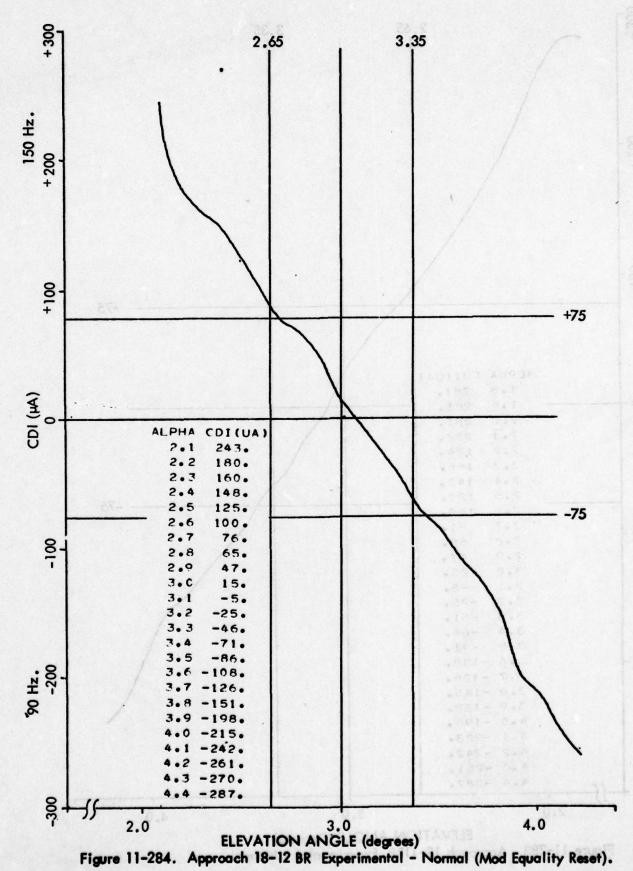


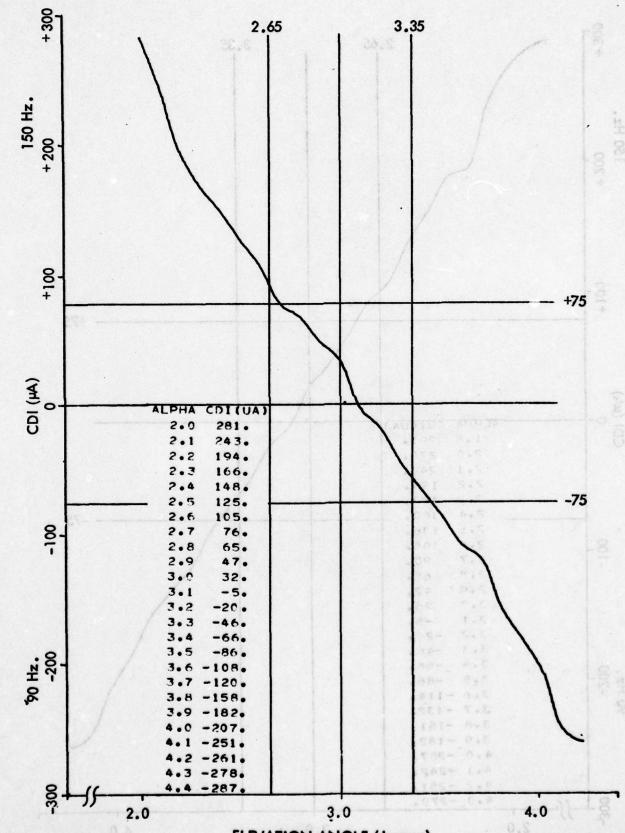




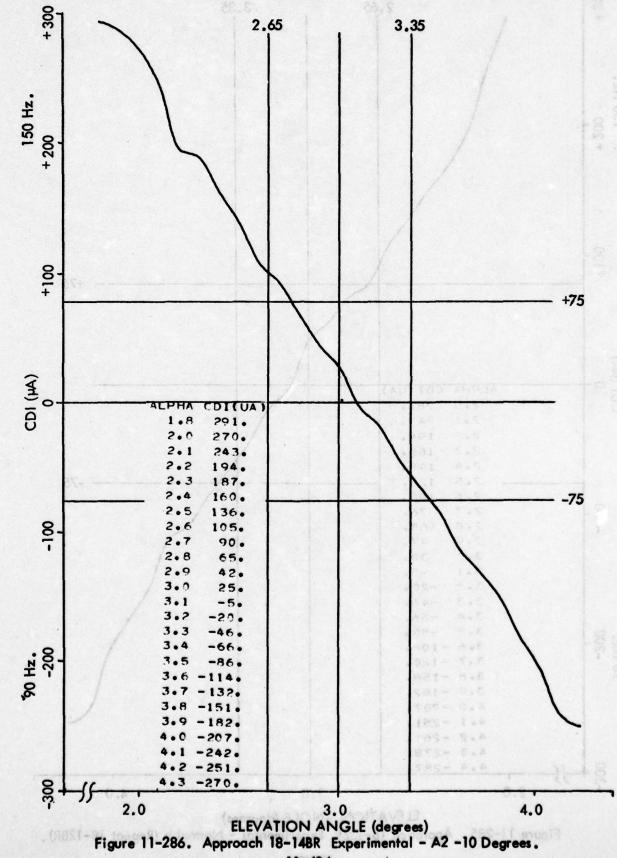


ELEVATION ANGLE (Degrees)
Figure 11-283. Approach 18-11BR Experimental - Normal.

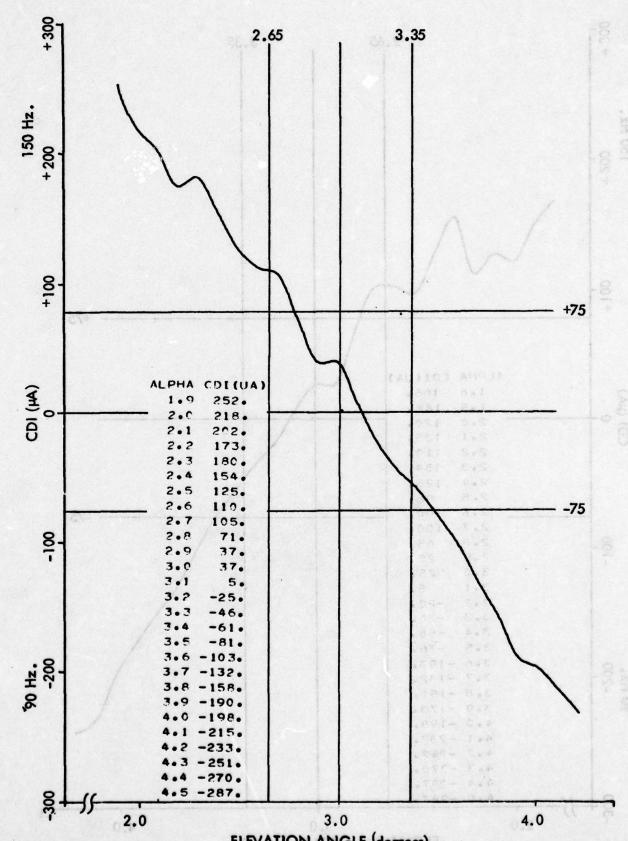




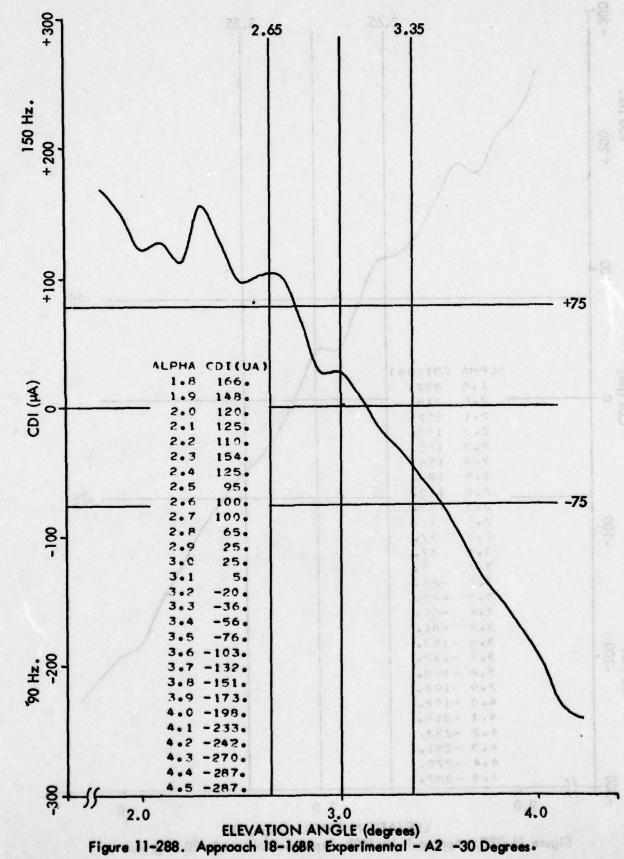
ELEVATION ANGLE (degrees)
Figure 11-285. Approach 18-13BR Experimental - Normal - (Repeat 18-12BR).

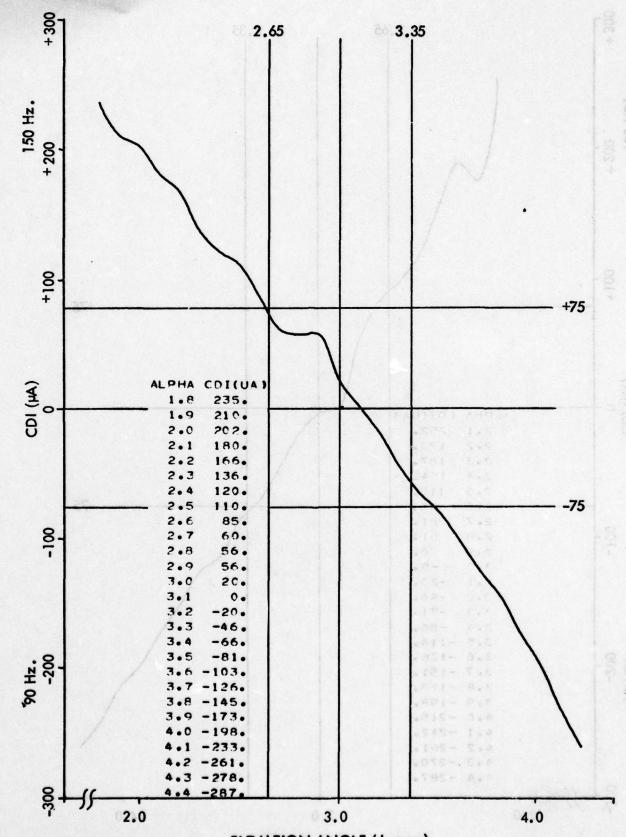


11-434

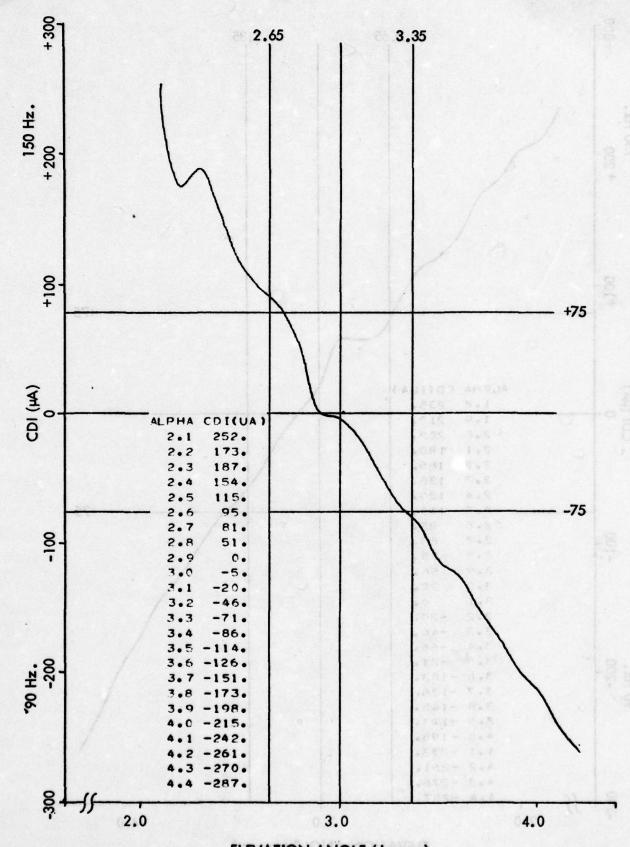


ELEVATION ANGLE (degrees)
Figure 11-287. Approach 18-15BR Experimental - A2 -20 Degrees.

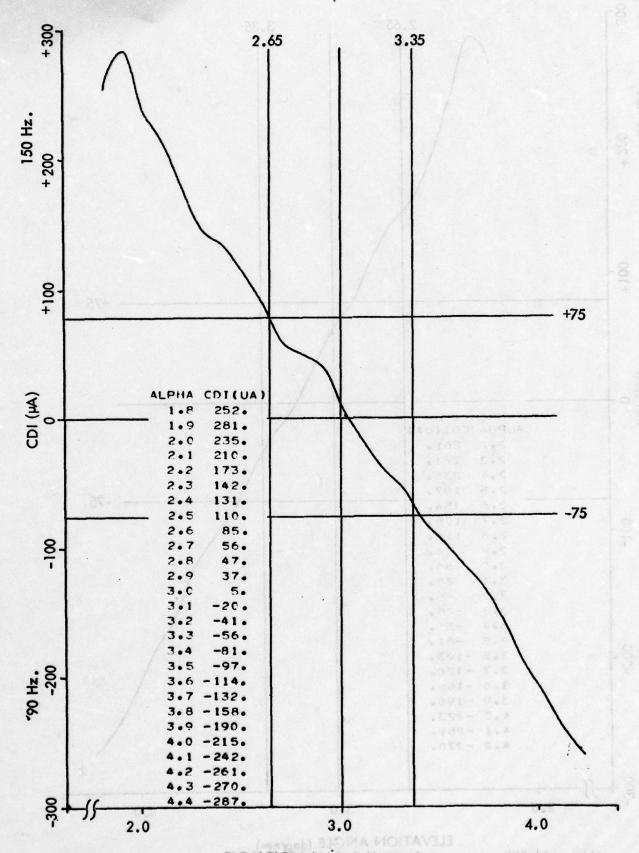




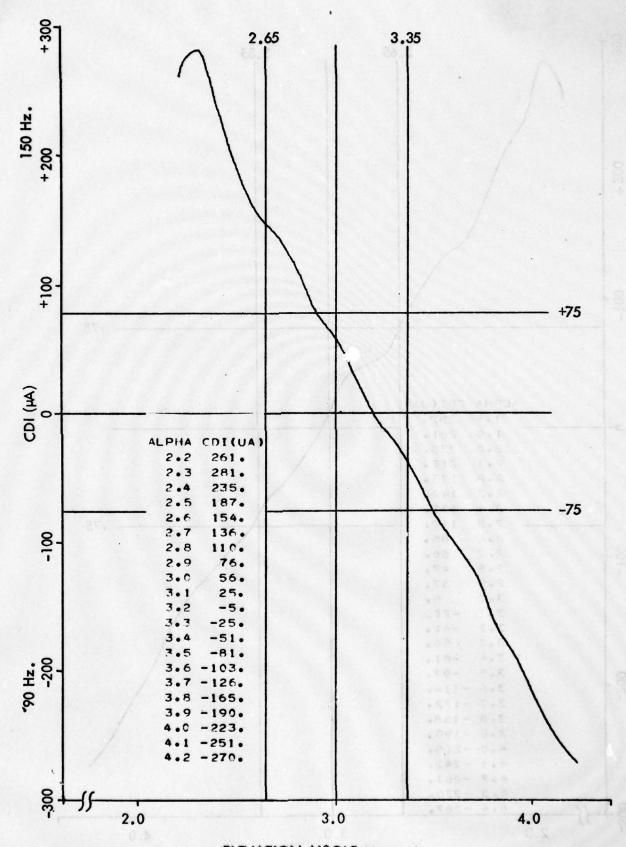
ELEVATION ANGLE (degrees)
Figure 11-289. Approach 18-17BR Experimental - A2 + 10 Degrees.



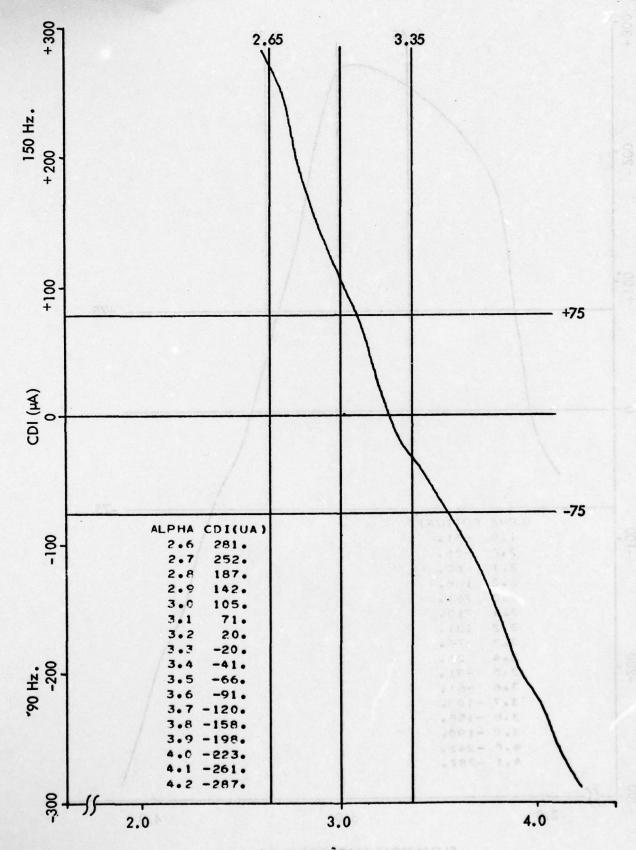
ELEVATION ANGLE (degrees)
Figure 11-290. Approach 18-18BR Experimental - A3 + 40 Degrees.



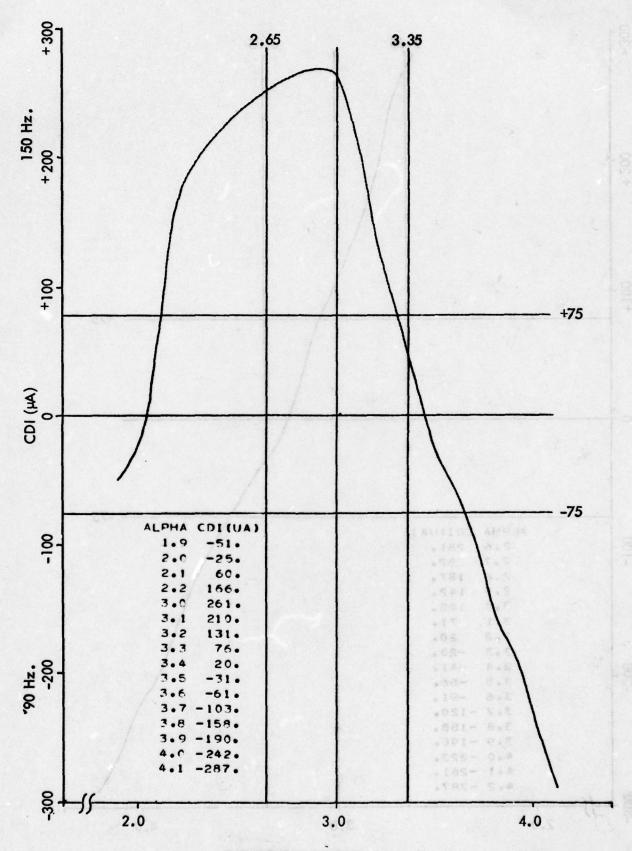
ELEVATION ANGLE (degrees)
Figure 11-291. Approach 18-19BR Experimental - A3 -40 Degrees.
11-439



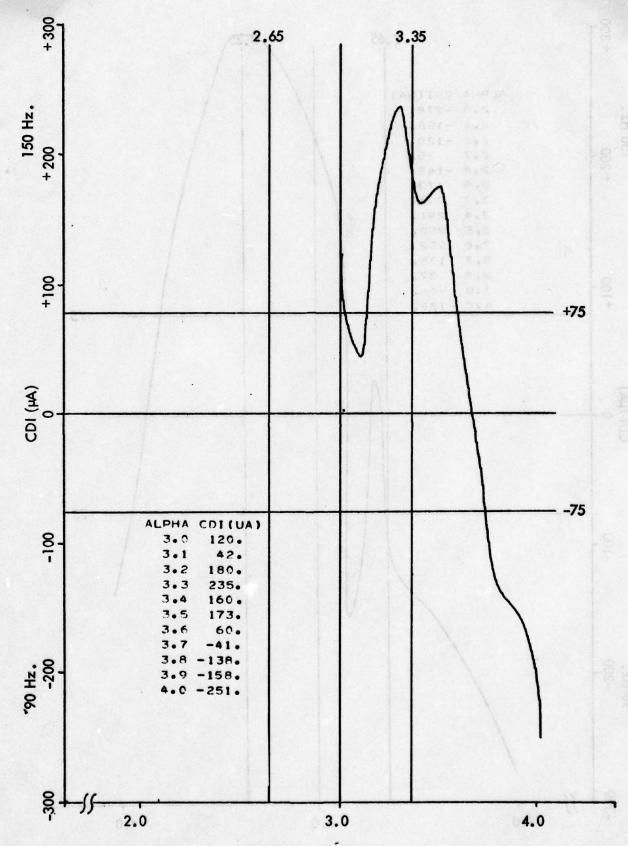
ELEVATION ANGLE (degrees)
Figure 11-292. Approach 18-20BR Experimental - A2 -10 Degrees, A1-1 dB.



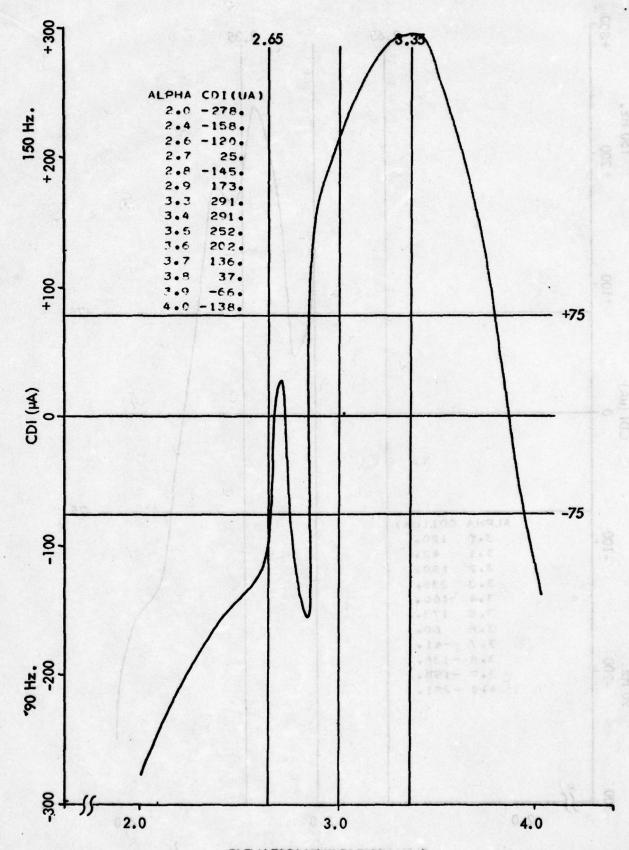
ELEVATION ANGLE (degrees)
Figure 11-293. Approach 18-21BR Experimental - A2 -10 Degrees, A1-3 dB.



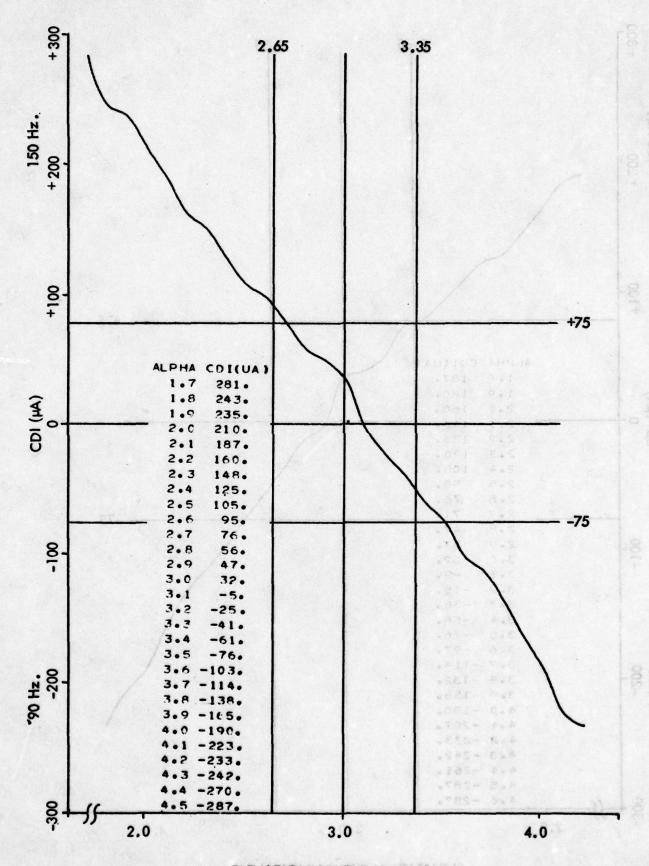
ELEVATION ANGLE (degrees)
Figure 11-294. Approach 18-22 BR Experimental - A2 -10 Degrees, A1 -7 dB.



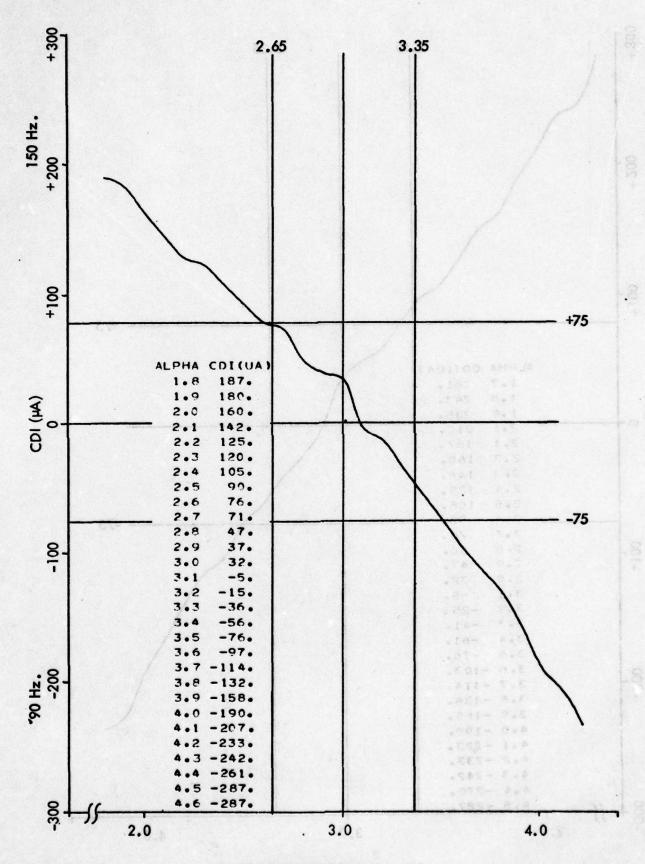
ELEVATION ANGLE (degrees)
Figure 11-295. Approach 18-23 BR Experimental - A2-10 Degrees, A1 Shorted.



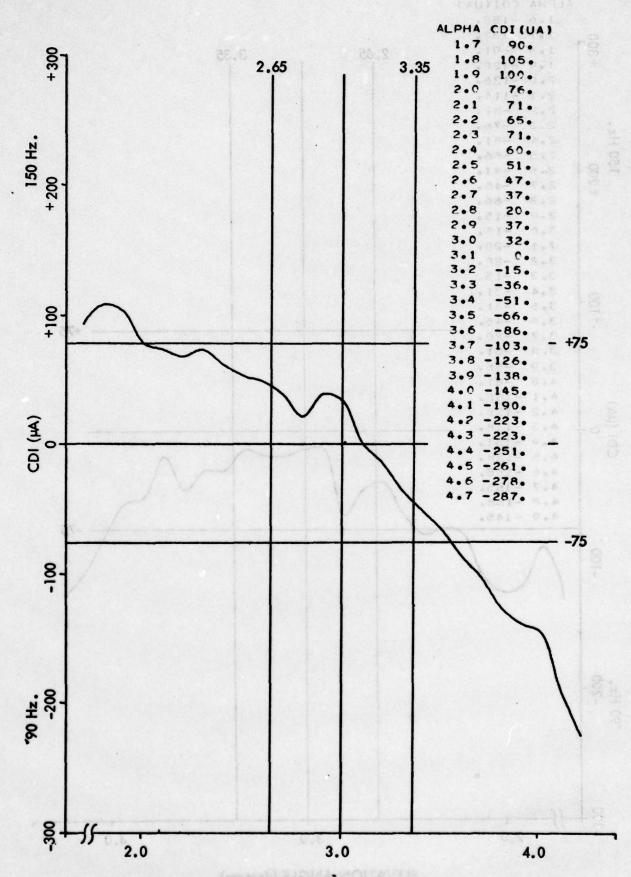
ELEVATION ANGLE (degrees)
Figure 11-296. Approach 18-24BR Experimental - A2-10 Degrees, A1 Open.



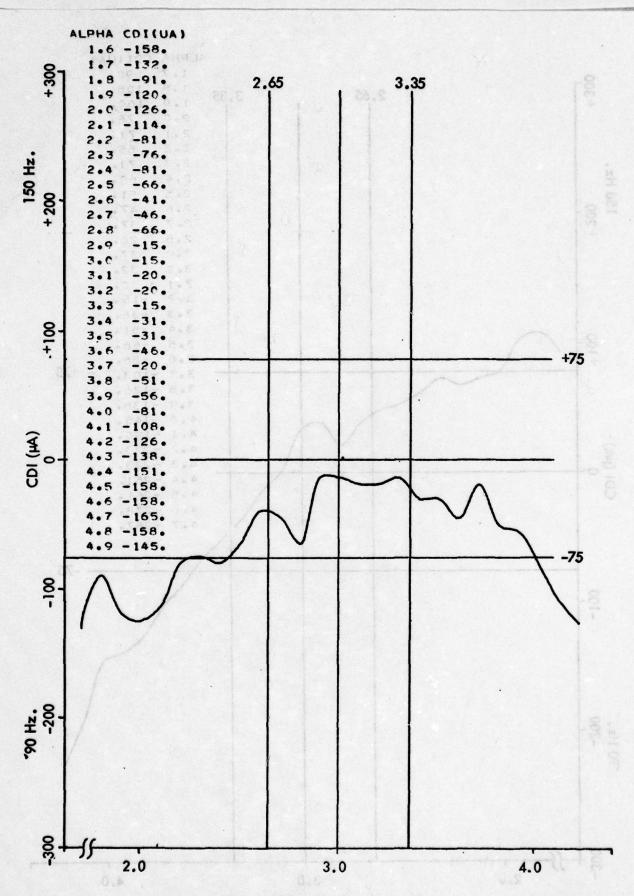
ELEVATION ANGLE (degrees)
Figure 11-297. Approach 18-25BR Experimental - A2 -10 Degrees, A2-1 dB.



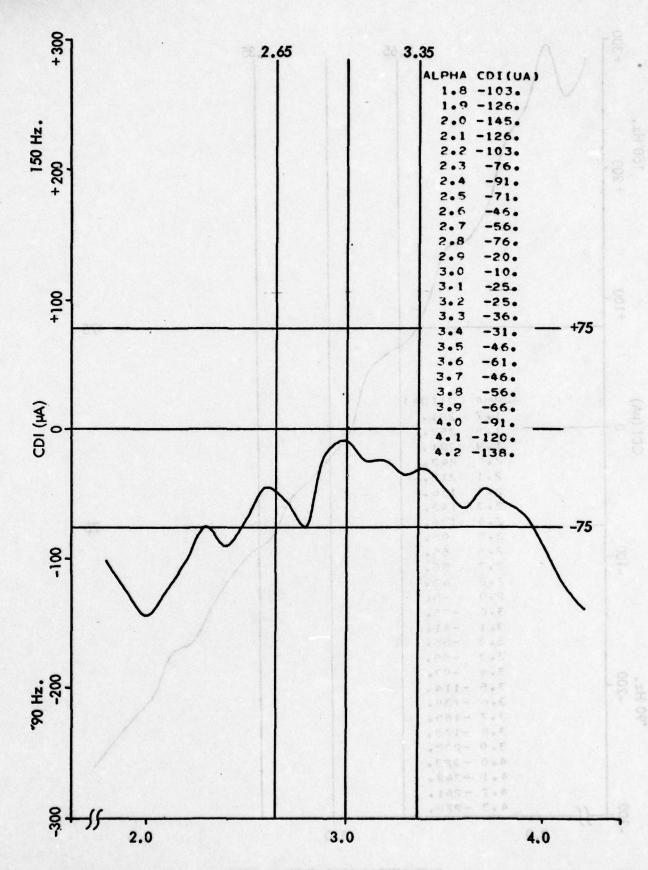
ELEVATION ANGLE (degrees)
Figure 11-298. Approach 18-268R Experimental - A2 -10 Degrees, A2-2 dB.



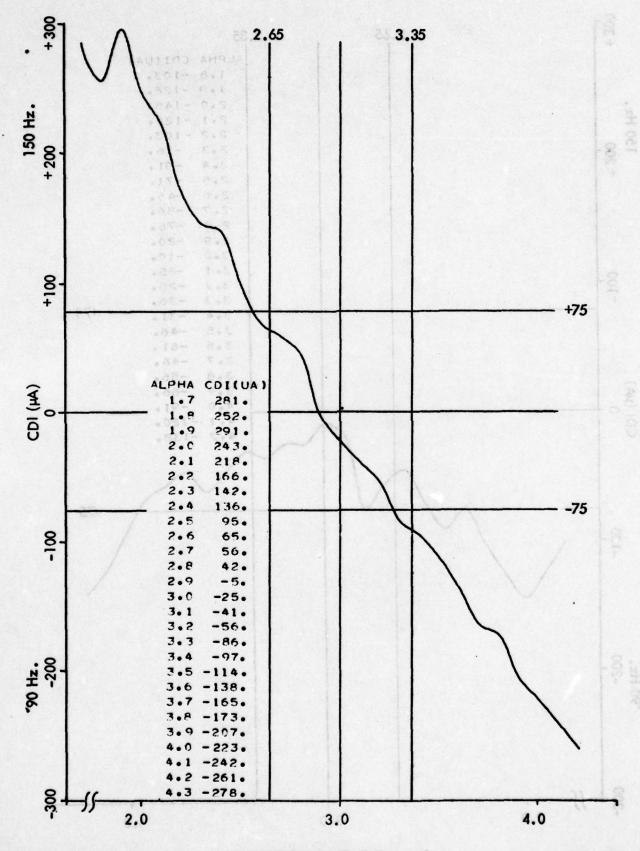
ELEVATION ANGLE (degrees)
Figure 11-299. Approach 18-27BR Experimental - A2-10 Degrees, A2-4 dB.



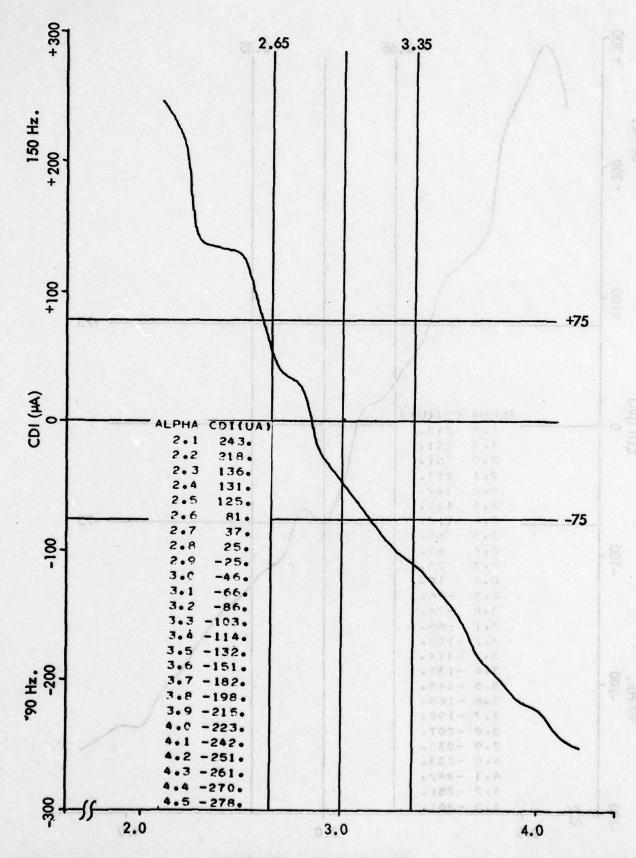
ELEVATION ANGLE (degrees)
Figure 11-300. Approach 18-28BR Experimental - A2 Shorted.



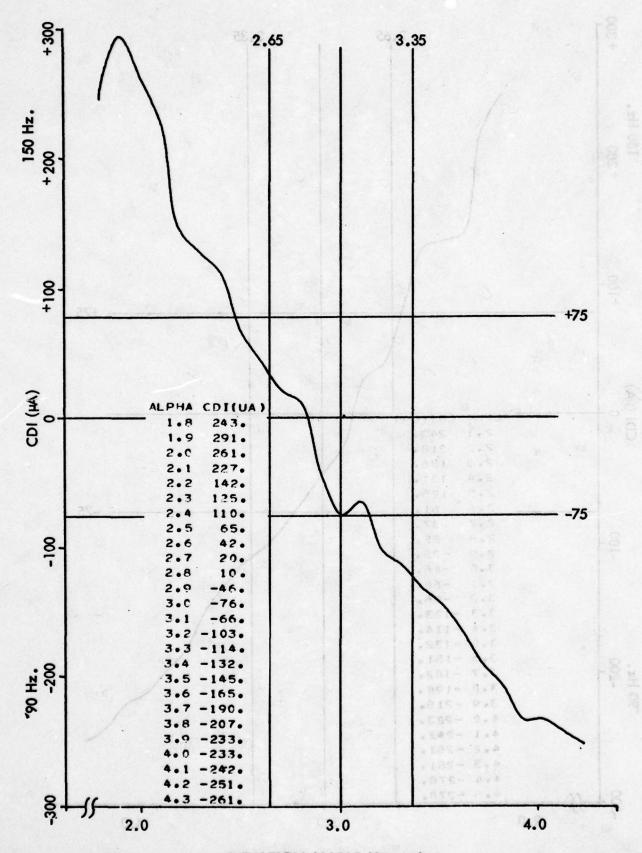
ELEVATION ANGLE (degrees)
Figure 11-301. Approach 18-29BR Experimental - A2 Open.



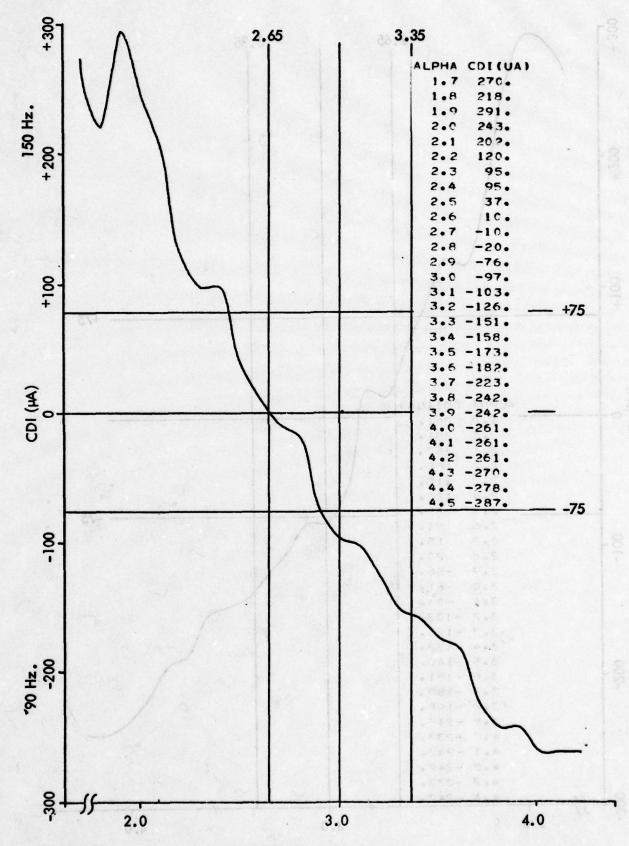
ELEVATION ANGLE (degrees)
Figure 11-302. Approach 18-30BR Experimental - A2 -10 Degrees, A3-3dB.



ELEVATION ANGLE (degrees)
Figure 11-303. Approach 18-31 BR Experimental - A2 -10 Degrees, A3-6 dB.



ELEVATION ANGLE (degrees)
Figure 11-304. Approach 18-32BR Experimental - A2-10 Degrees, A3-10 dB.



ELEVATION ANGLE (degrees)
Figure 11-305. Approach 18-33BR Experimental - A2 -10 Degrees, A3 Shorted.

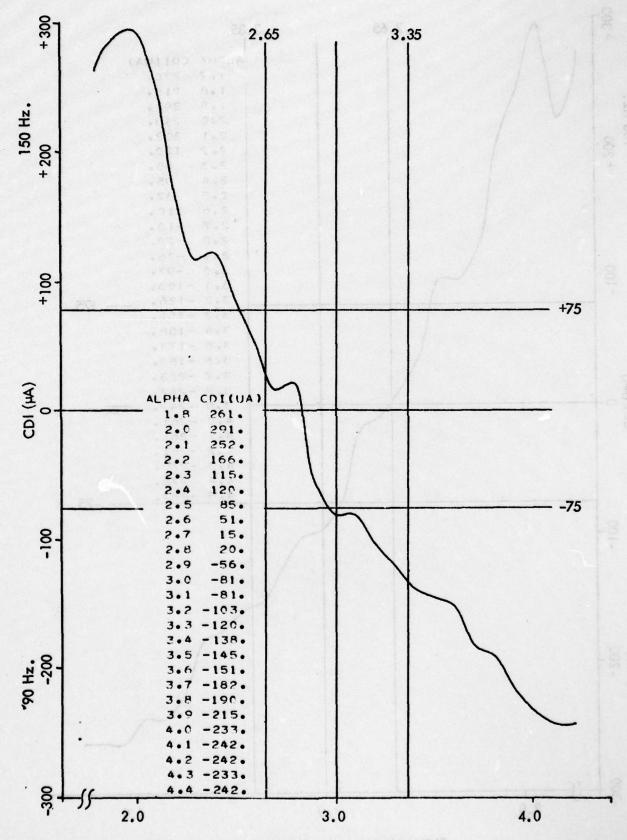


Figure 11-306. Approach 18-34BR Experimental - A2-10 Degrees, A3 Open.

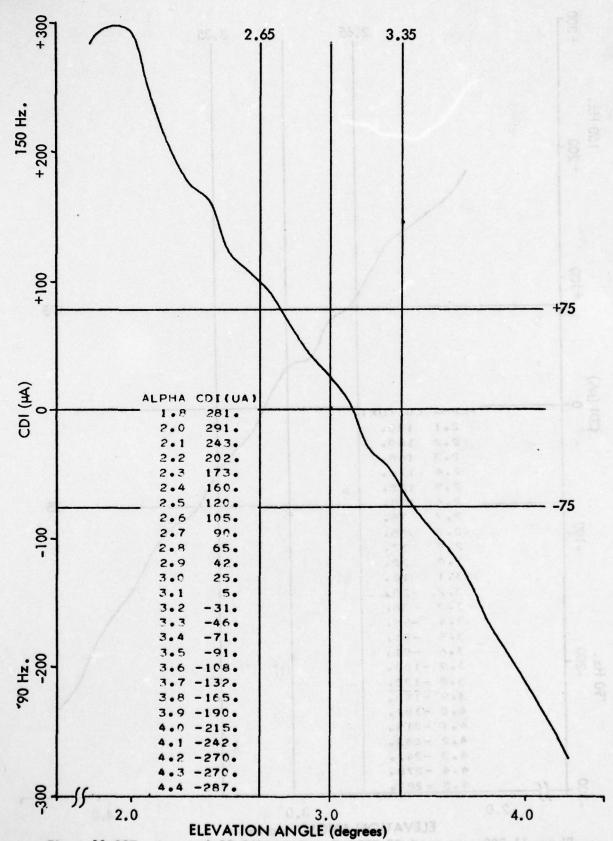


Figure 11-307. Approach 18-36BR Experimental - A2-10 Degrees (Repeat 18-14BR).

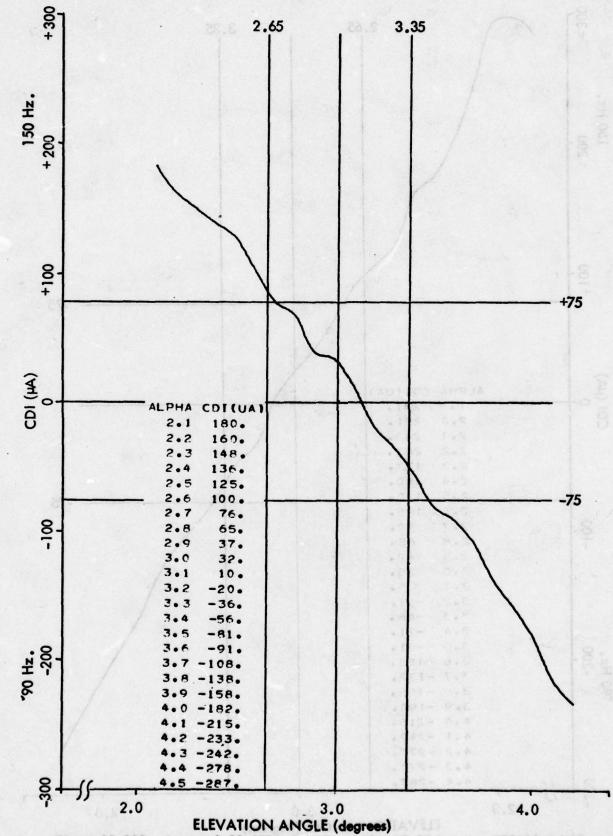


Figure 11-308. Approach 18-37BR Experimental - A2-10 Degrees, 20 Degrees SBO Dephase.

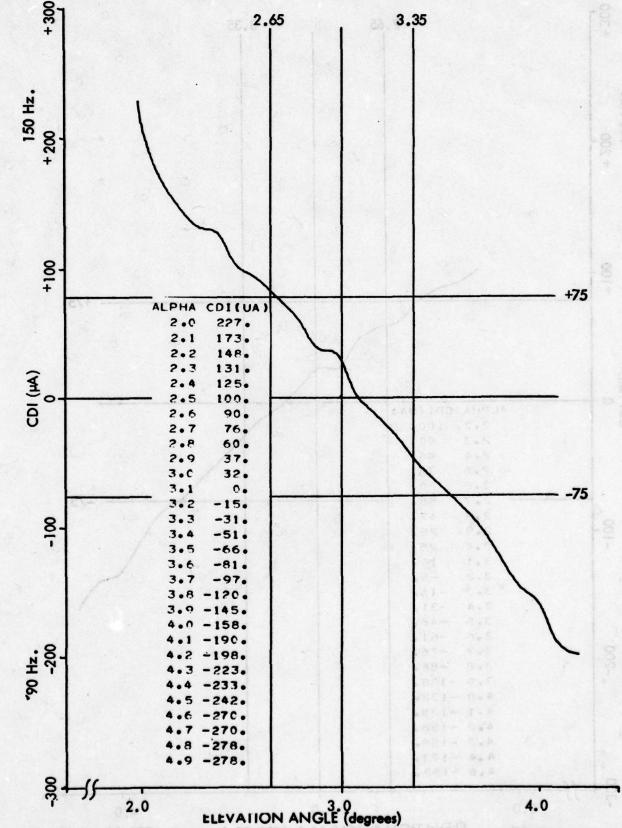
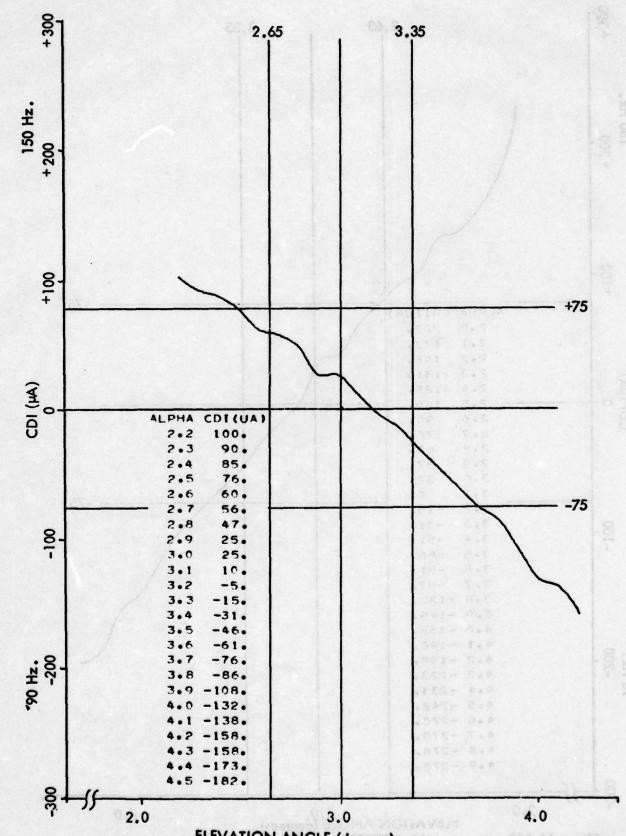


Figure 11-309. Approach 18-38BR Experimental - A2 -10 Degrees, 30-Degree SBO Dephase.



ELEVATION ANGLE (degrees)
Figure 11-310. Approach 18-39BR Experimental - A2-10 Degrees, 50 Degree SBO Dephase.

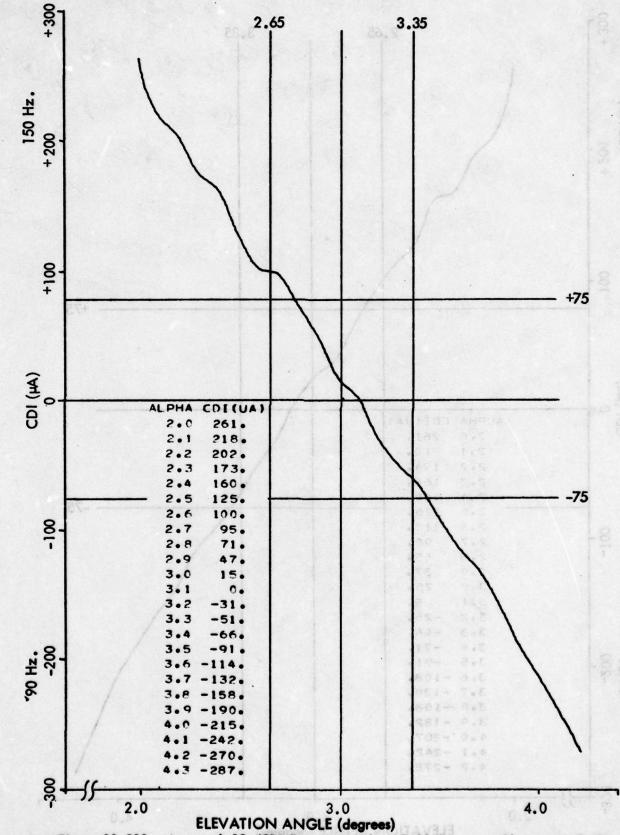
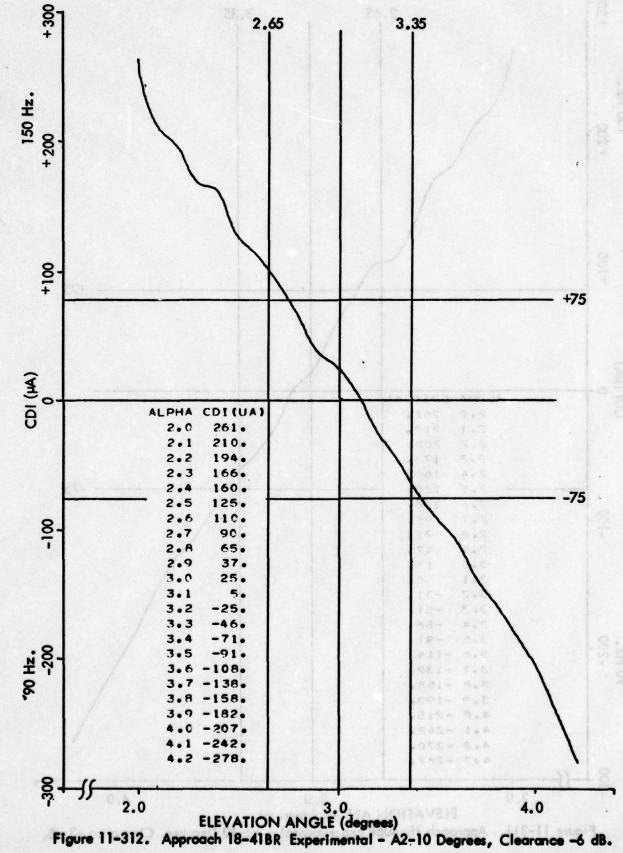
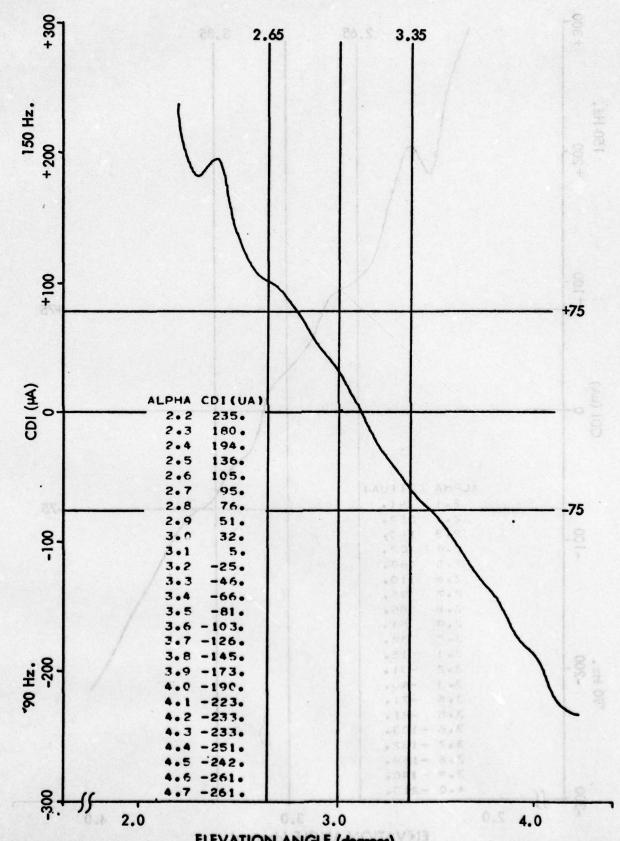
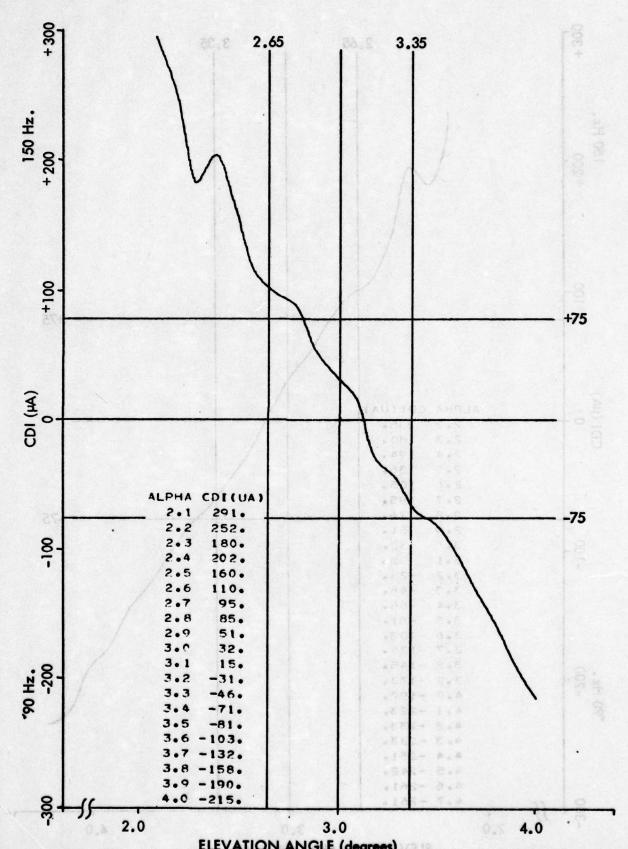


Figure 11-311. Approach 18-40BR Experimental - A2-10 Degrees, Clearance -3 dB.





ELEVATION ANGLE (degrees)
Figure 11-313. Approach 18-42BR Experimental - A2-10 Degrees, Clearance +3 dB.



ELEVATION ANGLE (degrees)
Figure 11-314. Approach 18-43BR Experimental - A2-10 Degrees, Clearance =+5.2dB.

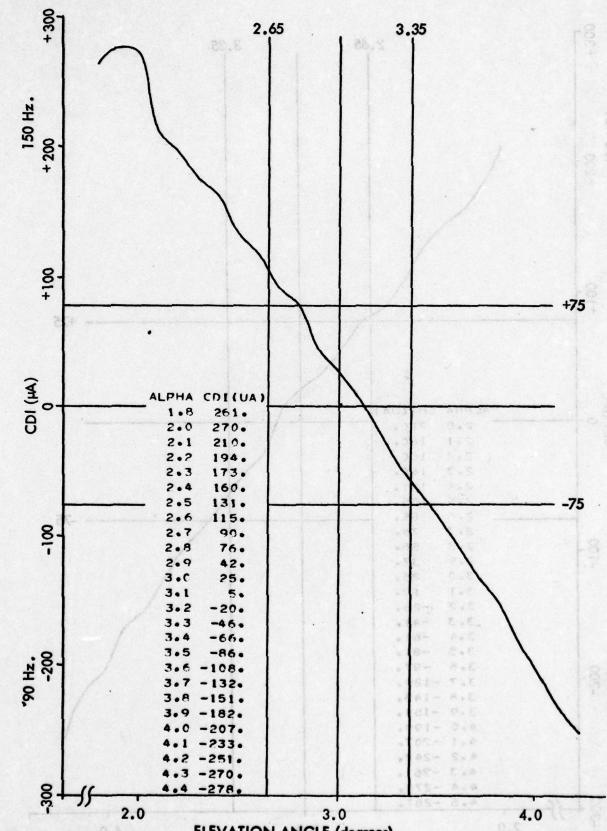
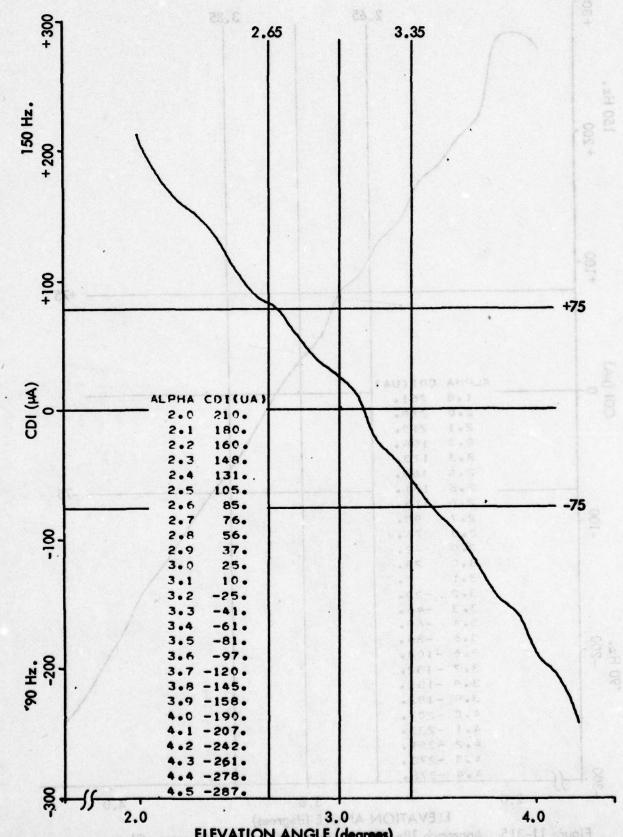


Figure 11-315. Approach 18-44BR Experimental - A2-10 Degrees, Clearance Mod at Alarm CI - 0 dB.



ELEVATION ANGLE (degrees)

Figure 11-316. Approach 18-45BR Experimental - A2-10 Degrees, PWR Divider A Clockwise.

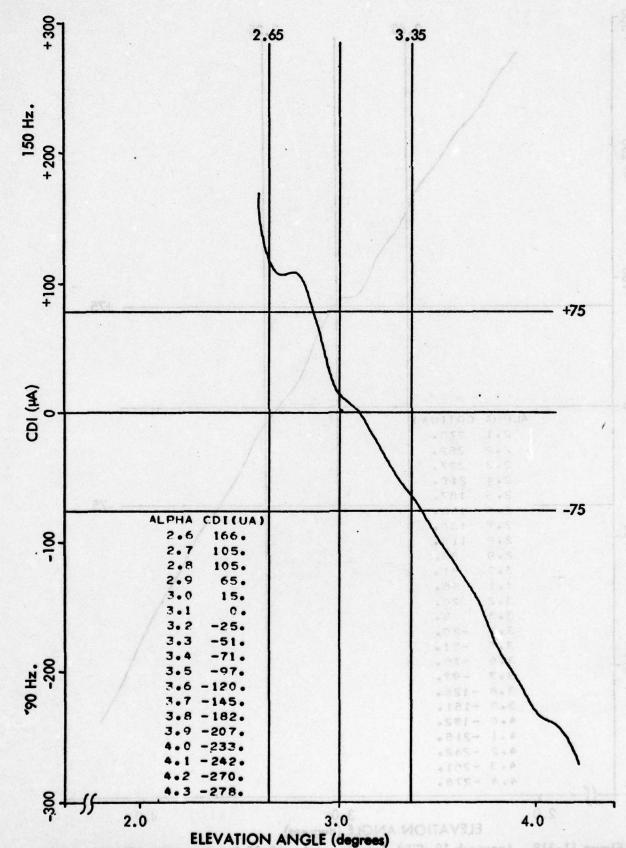


Figure 11-317. Approach 18-46BR Experimental - A2-10 Degrees, PWR Divider A CCW.

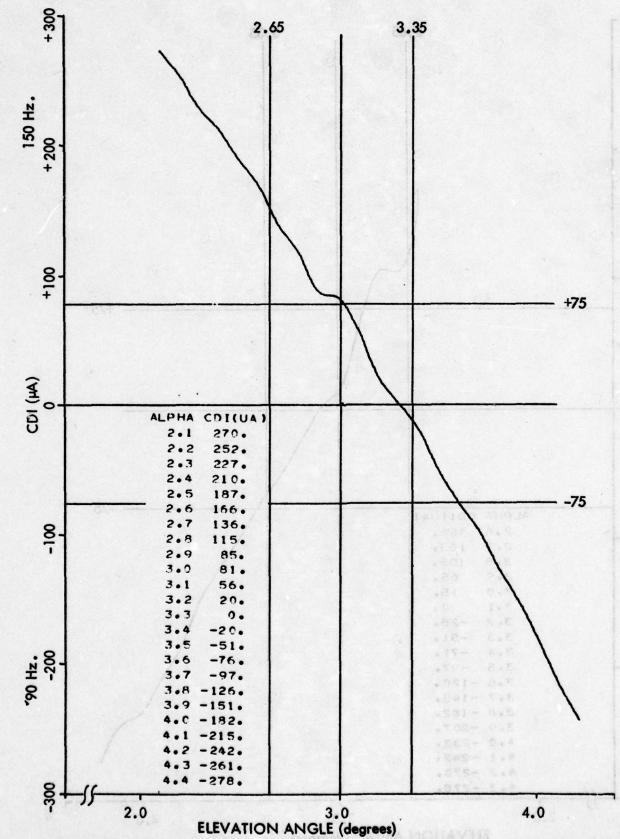


Figure 11-318. Approach 18-47BR Experimental - A2-10 Degrees, PWR Divider B Clockwise.

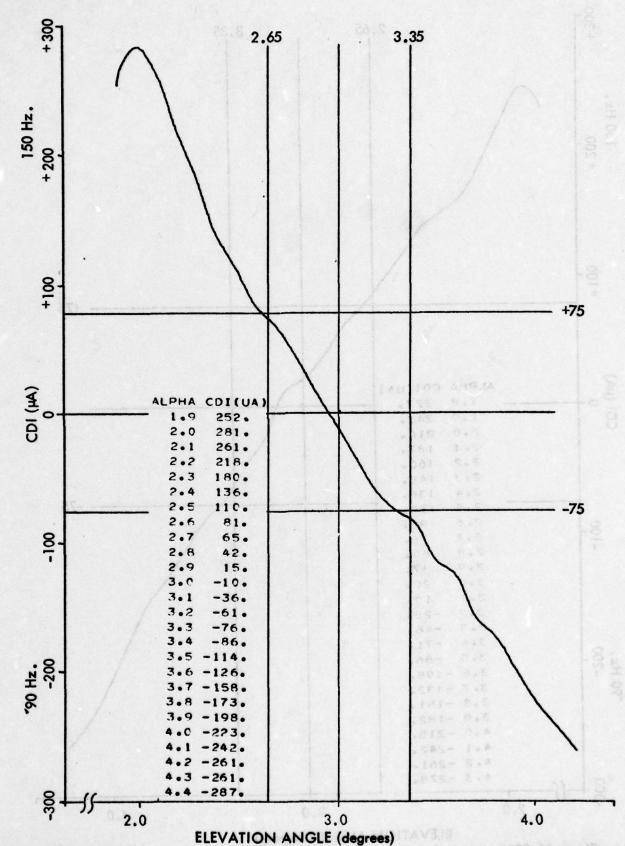


Figure 11-319. Approach 18-48BR Experimental - A2-10 Degrees, PWR Divider B CCW.

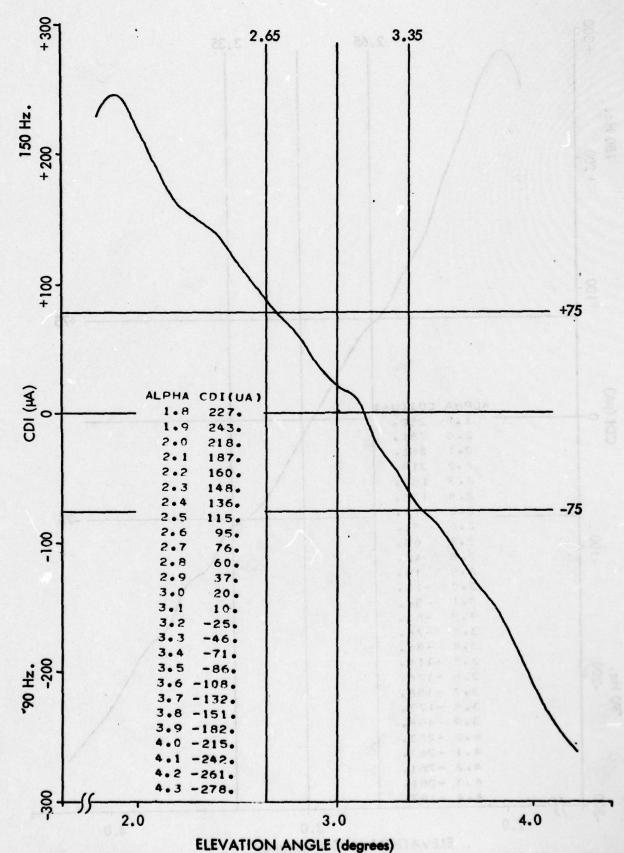


Figure 11-320. Approach 18-49BR Experimental - A2-10 Degrees, Carrier PWR Divider Clockwise.

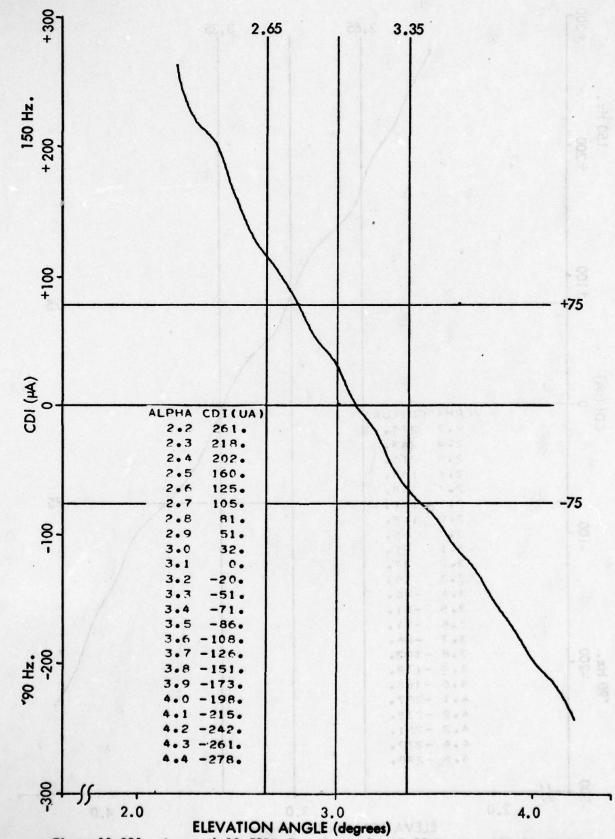


Figure 11-321. Approach 18-50BR Experimental - A2-10 Degrees, Carrier PWR Divider CCW.

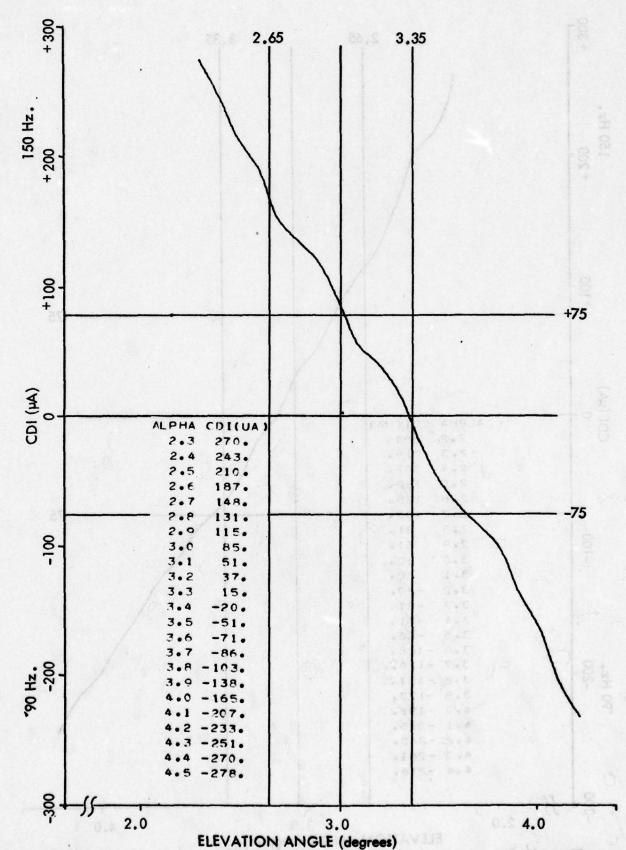
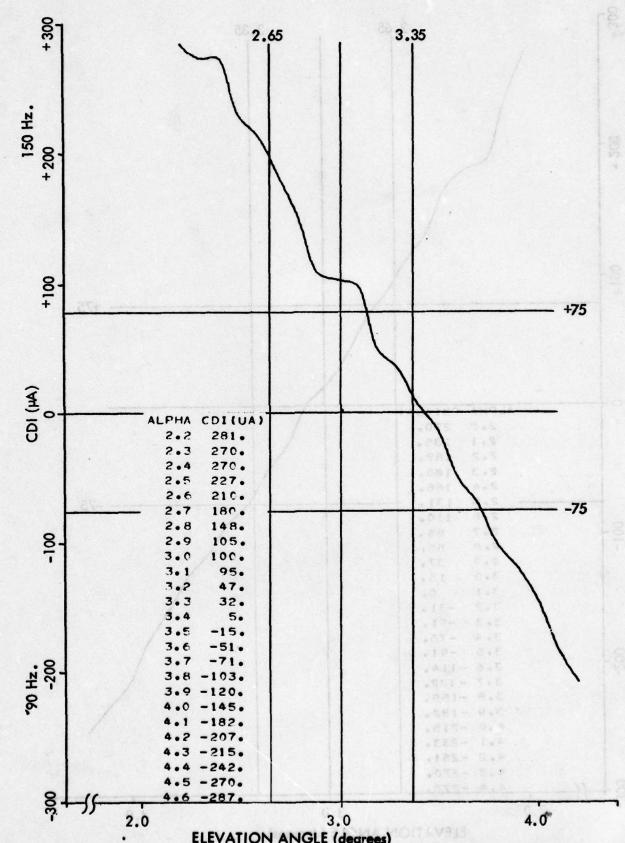


Figure 11-322. Approach 18-51BR Experimental - A2-10 Degrees, Control Z8 Clockwise.



ELEVATION ANGLE (degrees)
Figure 11-323. Approach 18-52BR Experimental - A2-10 Degrees, Control Z8 CCW.

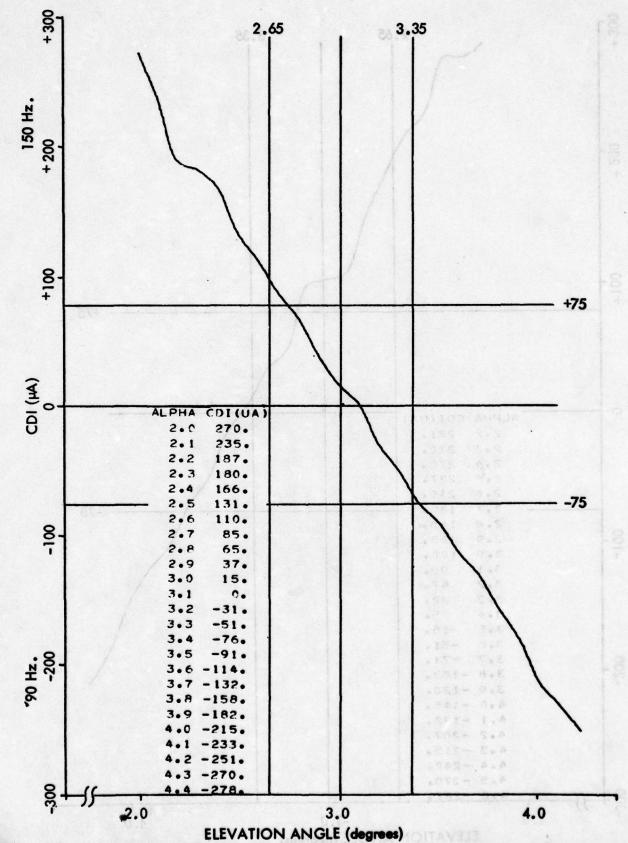


Figure 11-324. Approach 18-53BR Experimental - A2-10 Degrees, Normal (Repeat 18-36BR).

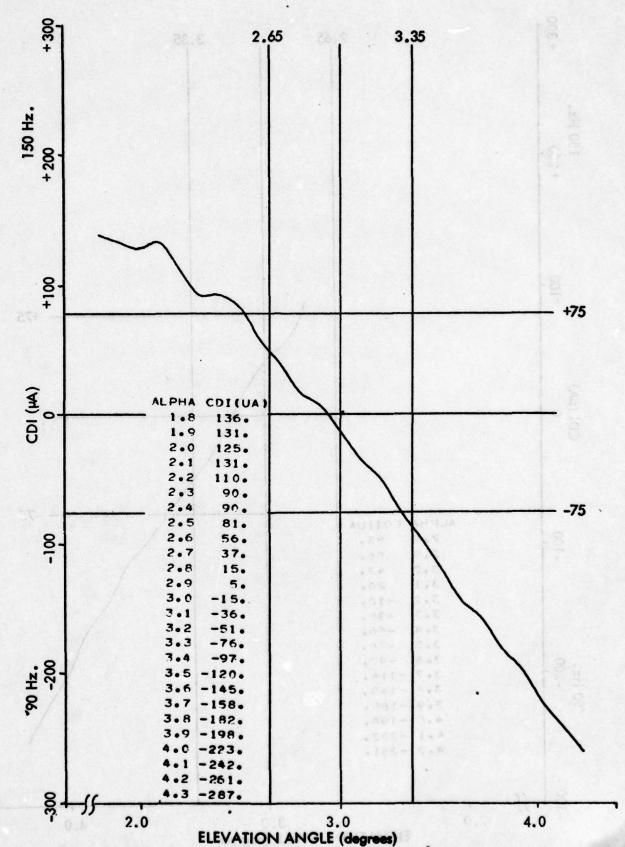
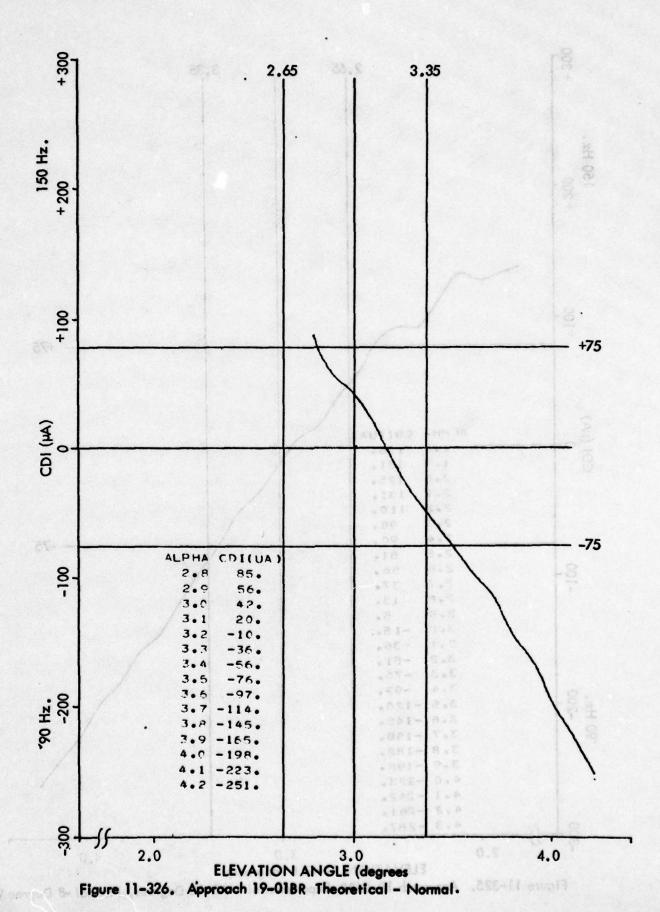
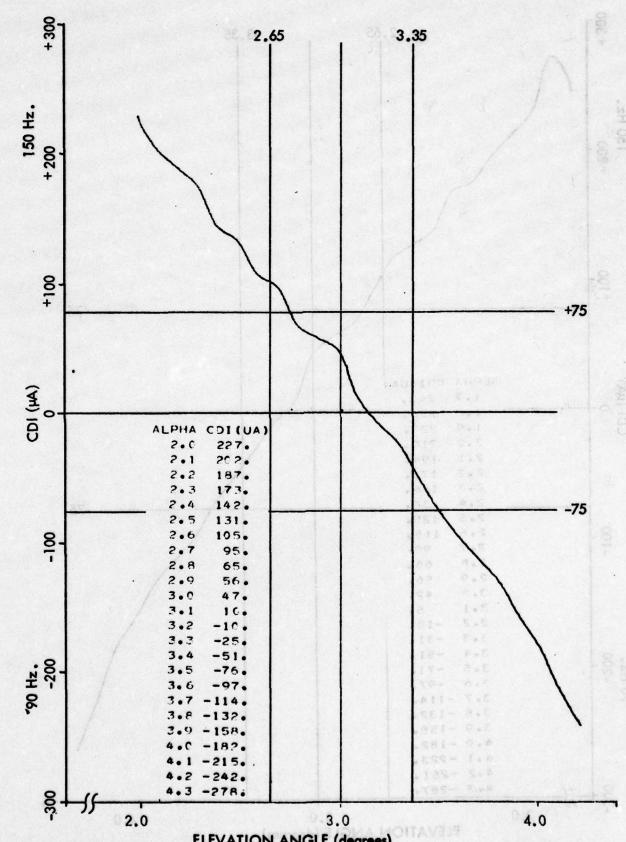


Figure 11-325. Approach 18-54BR Experimental - A2-10 Degrees, Normal -8 Degree W.



11-474



ELEVATION ANGLE (degrees)
Figure 11–327. Approach 19–03BR Theoretical – Normal (Repeat 19–01BR).

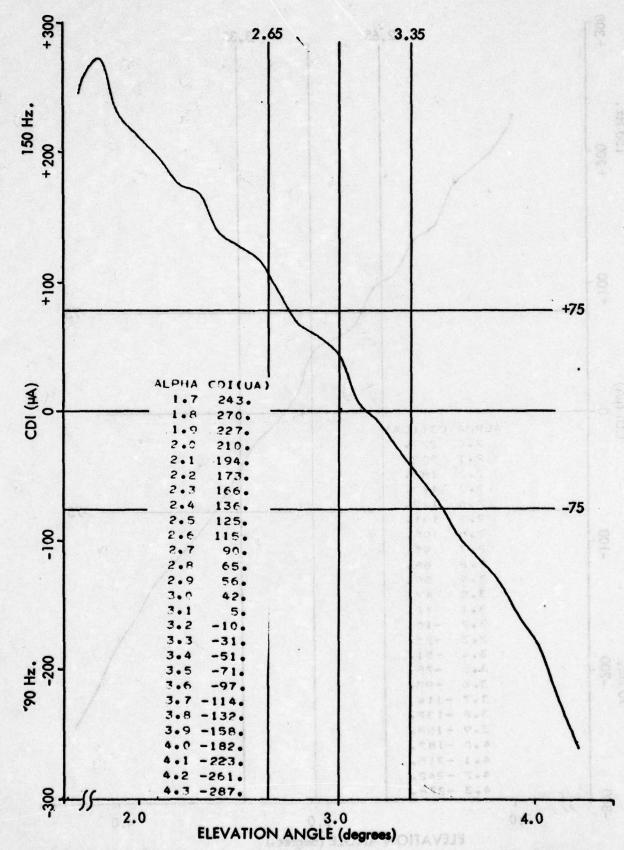
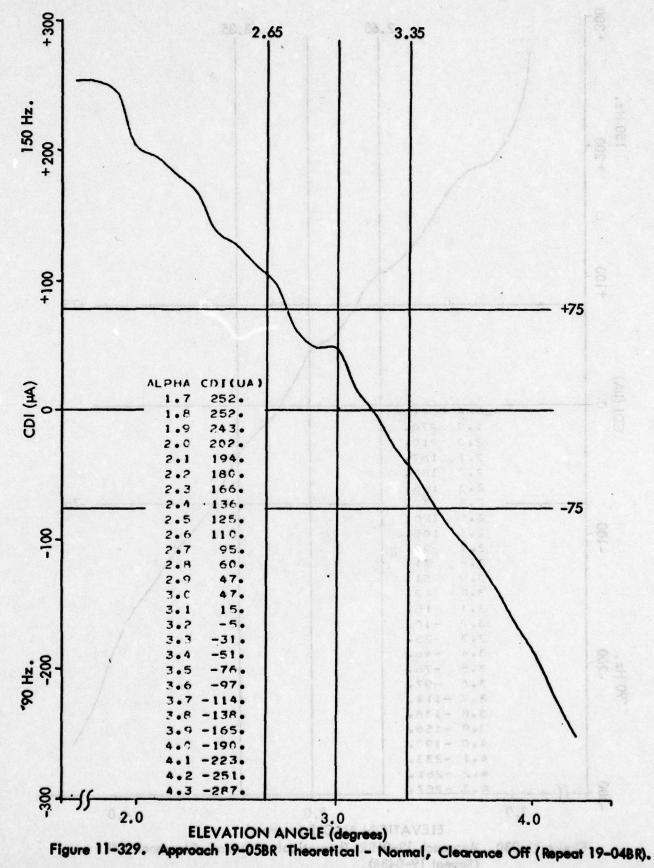


Figure 11-328. Approach 19-04BR Theoretical - Normal, Clearance Off.



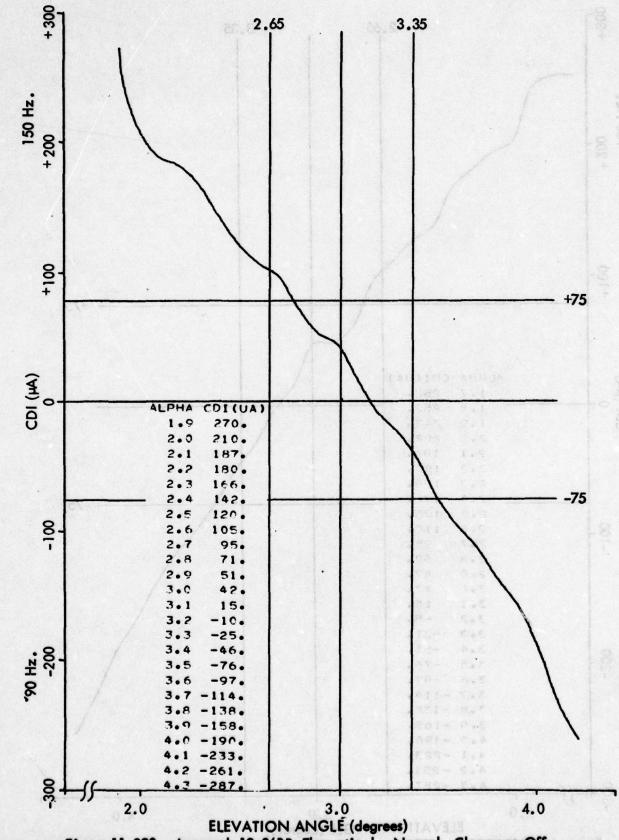
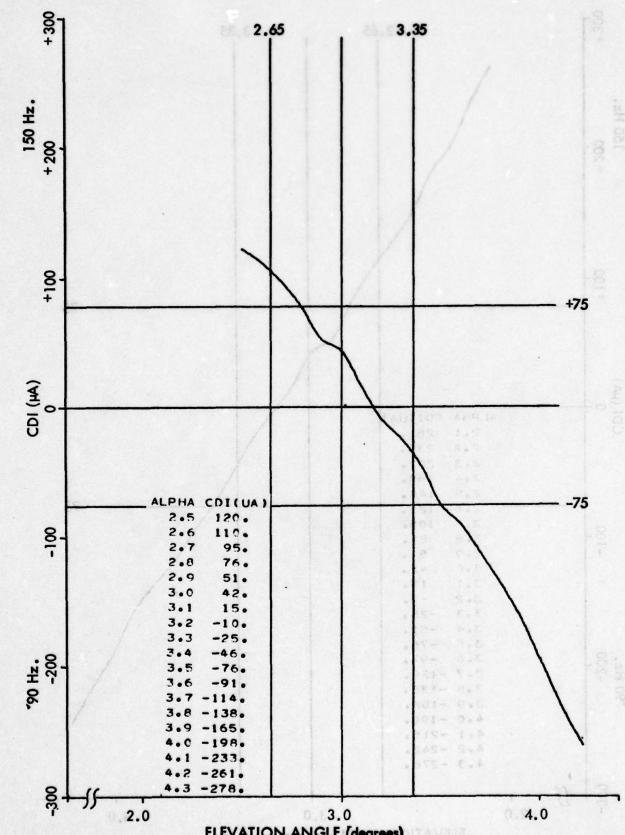
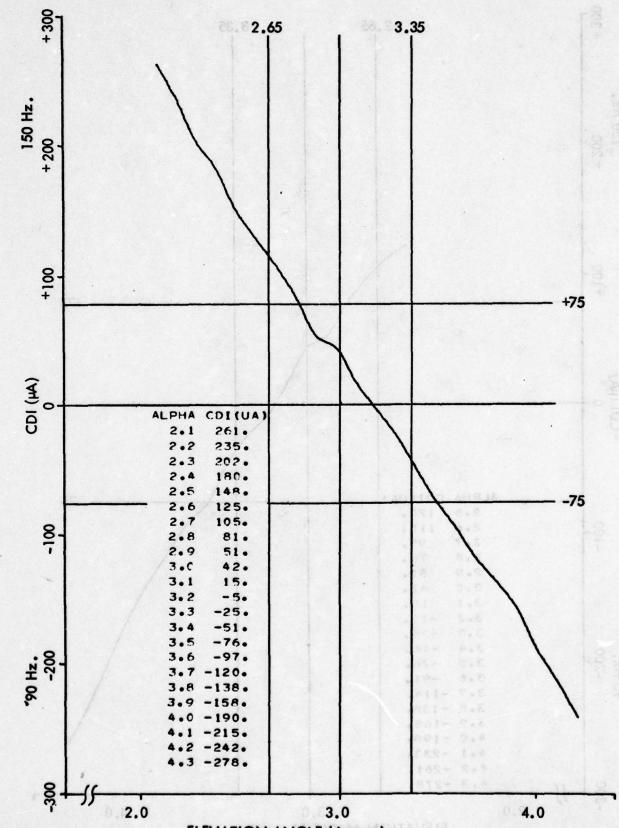


Figure 11-330. Approach 19-06BR Theoretical - Normal, Clearance Off (Repeat 19-04BR).



ELEVATION ANGLE (degrees)
Figure 11-331. Approach 19-07BR Theoretical - Normal, Clearance Off (Repeat 19-04BR).



ELEVATION ANGLE (degrees)
Figure 11-332. Approach 19-08BR Theoretical - A2 -10 Degrees.

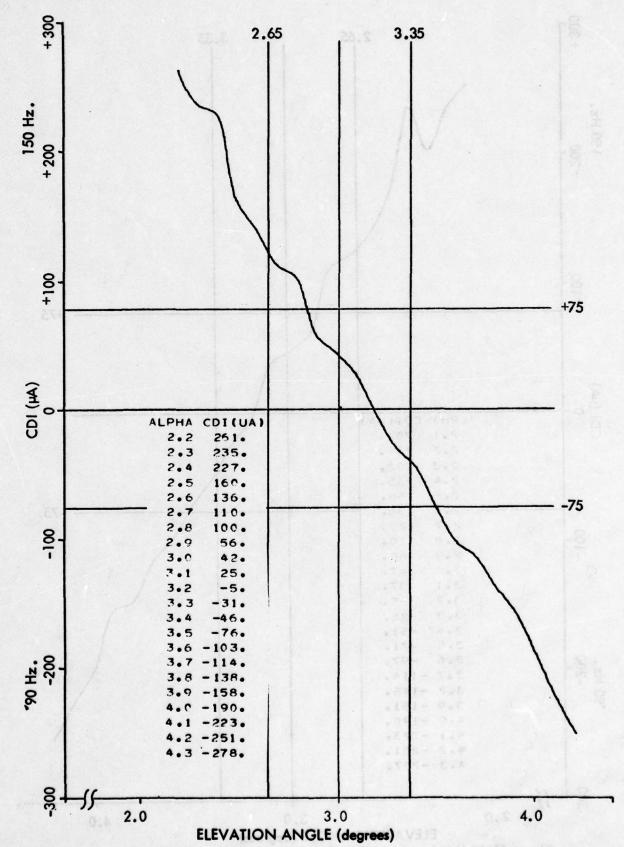
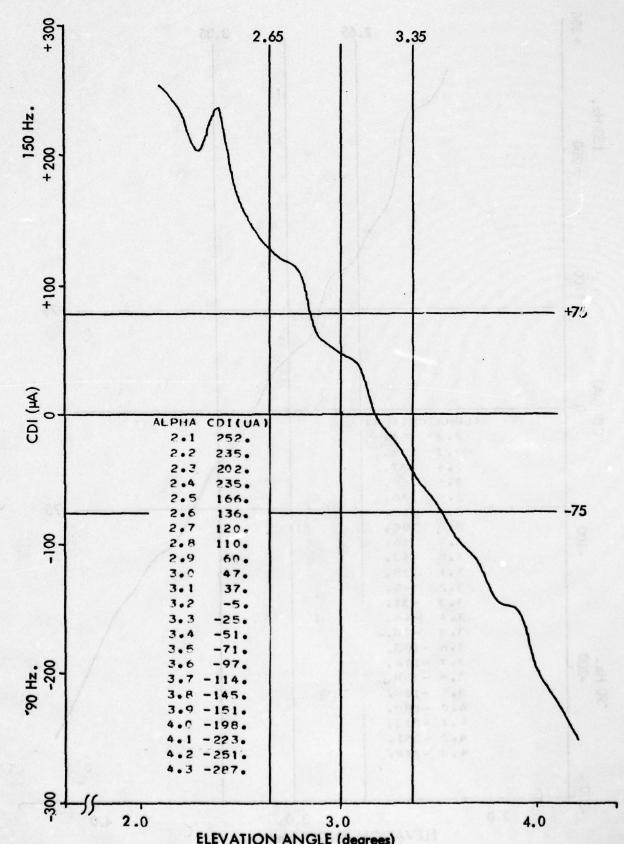
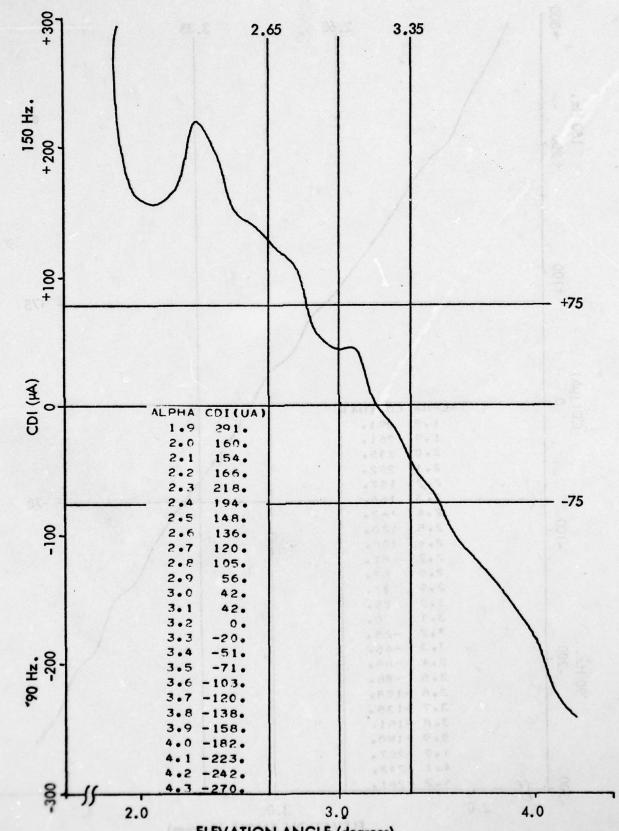


Figure 11-333. Approach 19-09BR Theoretical - A2-20 Degrees.

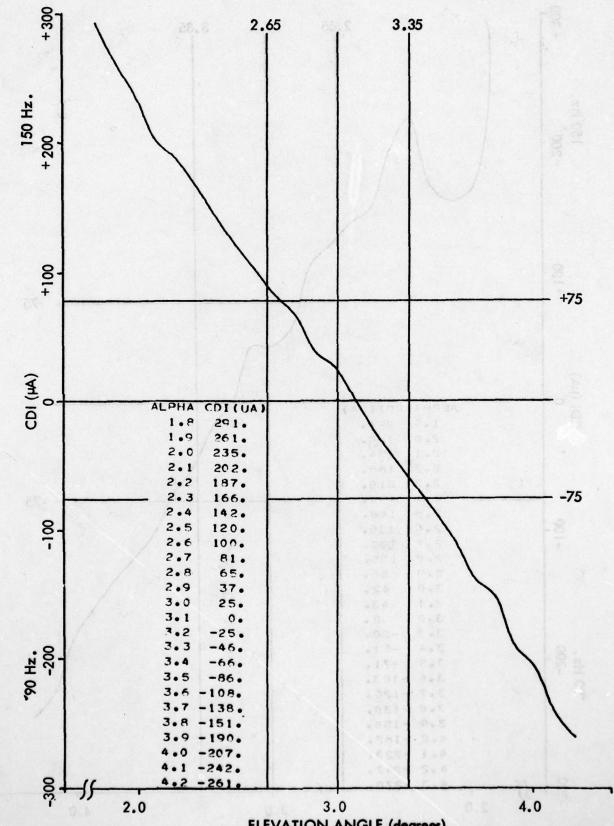


1

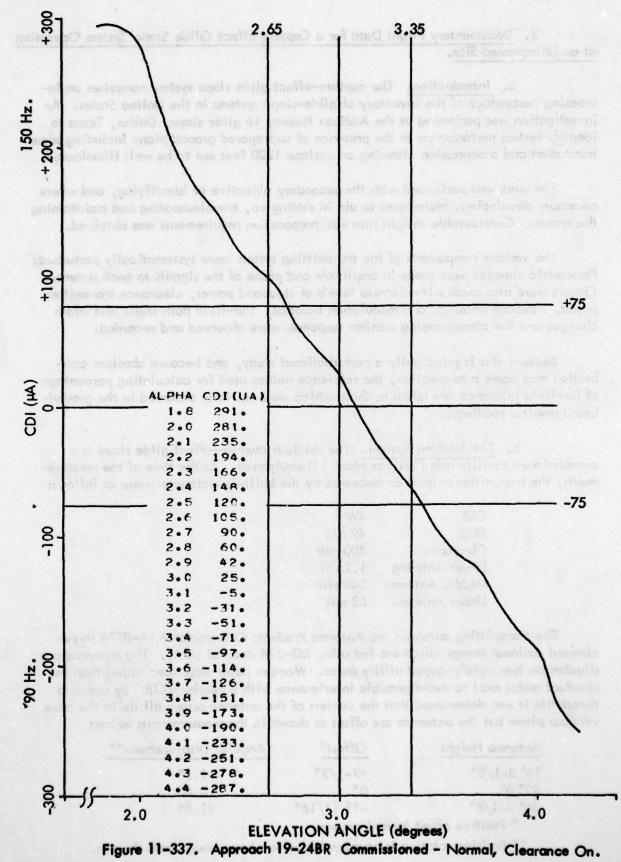
ELEVATION ANGLE (degrees)
Figure 11-334. Approach 19-10BR Theoretical - A2-30 Degrees.



ELEVATION ANGLE (degrees)
Figure 11-335. Approach 19-11BR Theoretical - A2-40 Degrees.



ELEVATION ANGLE (degrees)
Figure 11-336. Approach 19-23BR Commissioned - Normal, Clearance Off.



- 3. <u>Documentary Flight Data for a Capture Effect Glide Slope System Operating</u> at an Unimproved Site.
- a. <u>Introduction</u>. The capture-effect glide slope system comprises an increasing percentage of the inventory of glide-slope systems in the United States. An investigation was performed at the Addison Runway 16 glide slope, Dallas, Texas to identify system performance in the presence of unprepared ground plane including some truncation and a depression allowing an upslope 1200 feet out to be well illuminated.

The work was performed with the secondary objective of identifying, and where necessary developing, techniques to aid in setting up, troubleshooting and maintaining the system. Considerable insight into site preparation requirements was obtained.

The various components of the transmitting system were systematically perturbed. Parametric changes were made in amplitude and phase of the signals to each antenna. Checks were also made with discrete levels of sideband power, clearance transmitter power, sideband phasing, and modulation balance. Far-field path angle and width changes and the corresponding monitor responses were observed and recorded.

Because this is principally a perturbational study, and because absolute calibration may come into question, the reference values used for calculating percentage of far-field tolerance are taken as those which were initially observed in the ground-based monitor readings.

b. The Addison System. The Addison capture-effect glide slope is a commissioned facility using Wilcox Mark I D equipment. At the time of the measurements, the transmitter outputs as measured by the built-in wattmeter were as follows:

CSB	4W
SBO	49 mW
Clearance	400 mW
Lower Antenna	1.25 W
Middle Antenna	340 mW
Upper Antenna	62 mW

The transmitting antennas are Antenna Products Corporation FAA-8976 three-element colinear arrays which are fed using RG-214 coaxial cable. The antennas are situated on two rigidly-guyed utility poles. Wooden poles were used rather than the standard metal mast to avoid possible interference with a nearby VOR. By use of a theodolite it was determined that the centers of the antenna arrays all lie in the same vertical plane but the antennas are offset as shown in the measurements below:

Antenna Height	Offset*	Angular Displacement**
13' 8-1/8"	+7-1/2"	-1.2°
27' 0"	0"	0.00
40' 4-1/8"	-11 11/16"	+1.5°

^{*} Positive offset toward runway.

^{**} Positive rotation is counterclockwise when viewed from the top.

In order to determine the magnitude and phase of the signals being radiated from each antenna, probe measurements were taken with a jig-mounted probe and a Hewlett-Packard vector voltmeter Model 8405A. The detailed procedure followed when making these measurements is given in the following sections along with the measured values.

- c. Procedures for Probe Measurement Taking on CEGS Systems.
 - 1. Turn off clearance transmitter and dummy sidebands.
- Connect the vector volt meter (VVM) reference input to the monitor port of the middle antenna.
- 3. Attach the probe jig (which is connected to the "B" input of the VVM) to the center element of the middle antenna; note the amplitudes of the reference and "B" signals set phase to zero by adjusting the trombone phase shifter.
- 4. Move the probe to the lower antenna, center element, and note phase and amplitude.
 - 5. At the APCU, insert the CSB signal into the SBO input.
- 6. Place the probe on the center element of the middle antenna, note the amplitude of the reference and "B" inputs, and zero the phase.
- 7. Measure both center and outer elements of all other antennas and note the measured phase and amplitude.
- 8. Move the reference input from the middle antenna monitor port to the upper antenna monitor port: probe the center element of the upper antenna noting phase and amplitude.
- 9. Connect the reference input to the lower antenna monitor port: probe the center element of the lower antenna noting phase and amplitudes.
- 10. Dummy the carrier and connect the SBO to the SBO input. Measure the amplitude of the center element of the middle antenna (the phase need not be measured).

The A ratio can be determined by:

$$A = \frac{SBO \text{ (middle antenna)}}{CSB \text{ (lower antenna)} \times .8 \times M}$$

where M is .4 typically and .8 is a correction factor that is used when measuring a sideband signal with a vector voltmeter.

d. Probe Measurement Results

CSB Only

Middle antenna	amplitude	-23.5 dB,	phase	00
Lower antenna	amplitude	-18.5 dB,	phase	140°

CSB into SBO Input

Effective Excitation

			Wilein
	Amplitude	Phase	
Middle antenna (center element) Middle antenna (runway element Middle antenna (outer element)		0° 34° 20°	-15.4 dB 18°
Upper antenna (center element) Upper antenna (runway element) Upper antenna (outer element)	-29.5 dB -31.0 dB -29.8 dB	+158° -132° -146°	-21.8 dB -160°
Lower antenna (middle element) Lower antenna (runway element) Lower antenna (outer element)	-30.5 dB -29.2 dB -29.5 dB	-154° -185° -184°	-20.3 dB 169°

SBO into SBO Input

Middle antenna, center element amplitude -38.5 dB

The values presented above give complete information as to what signals were being radiated at the time the measurements were taken. The pertinent data is contained in the individual element measurements; the monitor port readings were taken in order to establish a relationship between the actual radiated signal and the monitor port output.

The need to measure all three elements of the FA-8976 antenna is due to the fact that the radiated signal from the antenna is a composite of the signals from each of the elements. The equation describing this relationship is as follows:

$$F(\theta) = [I_2 + I_1 e^{j\beta d\sin\theta} + I_3 e^{-j\beta \sin\theta}] \cos(\pi/2 \sin\theta)/\cos\theta$$

where l_1 , l_2 , and l_3 are the complex element currents, β is the propagation constant, d is the element separation and θ the angle of propagation (zero on centerline. For this study, the excitation currents along centerline are the parameters of interest (i.e., $\theta = 0$):

^{*} Phasor sum of element currents.

The radiated signal along centerline is given by the sum of the individual element currents. This sum has been computed on the previous page and is denoted as the effective excitation current. Taking this into consideration, the system output relationship can be given by the following:

Antenna	CSB		SBO	•
	Magnitude	Phase	Magnitude	Phase
Upper	0		.48A	-178°
Middle	1.0	0.	1.00A	0°
Lower	0.57	140°	0.57A	141°
A = 0.31				

e. Terrain and Site Peculiarities. The terrain profile on a line parallel to the runway centerline through the antenna most (shown in Figure 11-338) reveals a depression beginning from 300 to 800 feet in front of the most and then sloping upwards abeam threshold. The depression and upslope are extremely critical in this location since they are in the first Fresnel zone [8] for aircraft just beyond the middle marker.

The pertinent terrain for forming and operating the glide slope is shown in the topographical map of Figure 11–339. The reader should note that the antenna site is 1090 feet back from the physical threshold, thus requiring a displaced runway threshold. The Addison site appears to be a good example of getting maximum utilization of a poor site without any terrain modification cost.

The existing terrain certainly encourages the use of the capture-effect system particularly because of the short ground plane and the upslope. Detailed predictions of glide-path performance have not yet been made using the sophisticated mathematical model dictated by the complex topography. Necessary information for modeling, however, is available in case an analysis is desired in the future. Future consideration and use of this information should recognize that the airport plans call for filling some of the low areas in front of the antennas before 1979.

Fortunately, there are no structures in the vicinity of the antennas that would cause multipath interference. It is noteworthy that a VOR station is located approximately 200 feet to the side of the directional glide slope antennas. It is this VOR, of course, which necessitated earlier conversion of the glide slope from the common steel tower structure to that using wooden utility poles.

f. Data Processing. Initial flight recordings were produced on analog strip charts and labeled as to run number, trace identification, and chart scale factors. Upon return to the Avionics Center, each chart was converted to digital format and recorded on magnetic tape. Using Avionics Engineering remote access computer facilities, the data was placed in formatted disk files and reviewed for reasonableness (placement of event marks, presence of communications radio interference, etc.). Each data point was then scaled to microamperes of CDI current corrected by the computer with receiver calibration data to take out any nonlinearities in receiver output at higher CDI values.

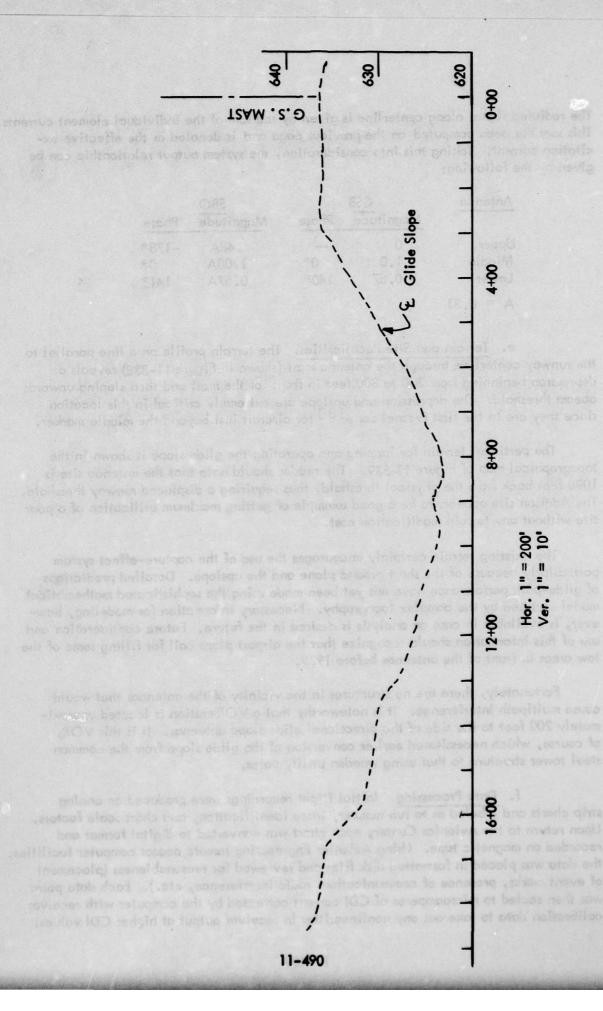


Figure 11-338. Centerline Profile.

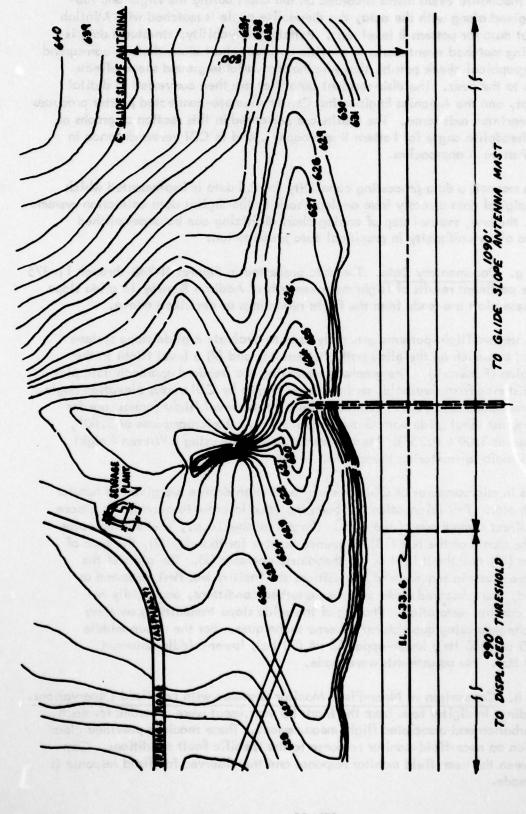


Figure 11-339. Topographical Map Indicating Terrain Around Glide Slope Reflecting Area.

Using theodolite event marks recorded on the chart during the flight and subsequently digized along with the data, the theodolite angle is matched with Minilab analog output data for pattern B level runs. Pattern A (flyability, structure) data is processed using matched event marks to provide constant chart dimensions to correspond to fixed geographical check points, thus eliminating variable ground speed effects from one run to the next. The disk-resident data files are then converted to digital plotter format, and the Avionics Engineering Center's remote-connected plotter produces graphs on preprinted axis forms. The results are presented in this section as graphs of CDI versus theodolite angle for Pattern B approaches, and as CDI versus distance in the case of Pattern A approaches.

In this manner, a data processing capability for ILS data is implemented which will accept digital data directly from analog charts or the digital data collection system. Fortunately, the one, manual step of analog chart digitizing can be accomplished efficiently to allow uniformity in graphical data presentation.

g. Documentary Data. The data presented in Figures 11-340 through 11-375 represent the pertinent results of flight measurements of Addison Runway 16 glide slope facility. These plots are made from the flight recordings as described above.

There are two flight patterns generally used to evaluate a glide slope system: (1) a standard approach on the glide path (Pattern A), and (2) a level flight in the approach region (Pattern B). The graphs representing the standard approach data plot CDI versus distance from threshold, and the level flights by CDI versus elevation angle. The ± 75 microamperes and $\pm 0.35^{\circ}$ reference lines on the level flight formats are for comparing against ideal glide path characteristics (i.e., 0 microamperes at 3.00°, ± 75 microamps at 3.00 \pm 0.35°). Measurements were made using a Warren Knight Model WK83 radio telemetering theodolite.

Values in microamperes of CDI for every one-tenth degree are given in tabular form on each plot. This information has been included in order to provide for a more convenient direct comparison of the data. The run number (e.g., 18-2BR) indicates the day of the month of the test (18), sequence number for that day (2), the type of flight pattern (B), and the initial of the theodolite operator (R). The plots of the flight data are given in sequence of acquisition; the facility was first measured as commissioned, then observed under various perturbed conditions, and finally remeasured to confirm restoration. Phasing of the glide slope transmitting antenna system was checked using quadrature/airborne techniques. For the upper-middle antennas, $40~\mu A$ (150 Hz); lower-upper 55 μA (90 Hz); lower-middle antennas 380 μA (150 Hz). No adjustments were made.

h. Comparison of Near-Field Monitor Response with Far-Field Observations. Monitor readings in digital form from the Mark ID equipment were recorded for each system perturbation and associated flight measurement. These readings provided clear documentation on near-field monitor response to the specific fault conditions. Comparison between the near-field monitor response and the observed far-field response is thus easily made.

Table 11-33 presents the observed response to the fault conditions. In general, doubling the fault condition doubles the detected fault, and phase advances and retardations of the same amount cause similar responses. Table 11-33 also reveals that the near-field monitor tends to be conservative in that it indicates an alarm condition well before an alarm condition in the far field is detected.

			Far-Field Response	Response			8
		Path	% Alarm	Width	% Alarm	Structure	B
Fault Condition	Monitor Response	Angle	Angle		Width	Angle	o
							0 0
Normal	No Alarm	3.07	%	8.	%	1	n Pite D
SBO decreased	Alarm (w)	3.06	2%	86.	%06	1	18-8
Middle phase +15°	Alarm (w)	3.04	15%	۲.	45%	1	18-3
Middle phase -14°	Alarm (w)	3.09	10%	98.	30%	ŀ	18-15
Middle phase +28°	x Alarm	3.01	30%	49.	%08	1	18-17
Middle phase -28°	2 x Alarm (w)	3.20	%59	8.	%05	1,61°	18-19
Upper phase +22°	larm (P)	3.07	%	.84	20%	2.20°	18-22
Upper phase -22°	Alarm (P)	2.99	40%	%:	%08	2.30°	18-24
Upper phase +44°	x Alarm	3.02	25%	98.	30%	2.13°	18-26
Upper phase -44°	2 × Alarm (P)	2.95	%09	%.	%02	2.30	18-28
Lower phase +15°	larm (w)	3.11	20%	.92	%09	2.25°	18-30
Lower phase -10°	Alarm (w)	3.06	2%	89.	. %09	1.80	18-32
Lower phase +30°	2 × Alarm (w)	3.13	30%	-:	150%	1.75°	18-34
Lower phase -20°	x Alarm	3.05	%01	69.	25%	1	18-36
Middle -1 dB	larm (w)	3.11	20%	16.	25%	2.25°	18-44
Middle -2 dB	2 × Alarm (w)	3.11	20%	16.	25%	2.01°	18-46
Upper -2 dB	larm (P)	3.00	35%	.92	%09	2,34°	18-48
Upper -4 dB	2 × Alarm (P)	2.89	%06	.75	25%	2.27°	18-50
Lower -1 dB	larm (w)	3.08	2%	.72	40%	2.48°	18-52
Lower -2 dB	2 × Alarm (w)	3.14°	35%	.63	85%	2.48°	18-54
SBO increased	larm (w)	3.10	15%	۲.	45%	2.41°	18-58

Table 11–33. Comparison of Near-Field/Far-Field Results for Various Fault Conditions.

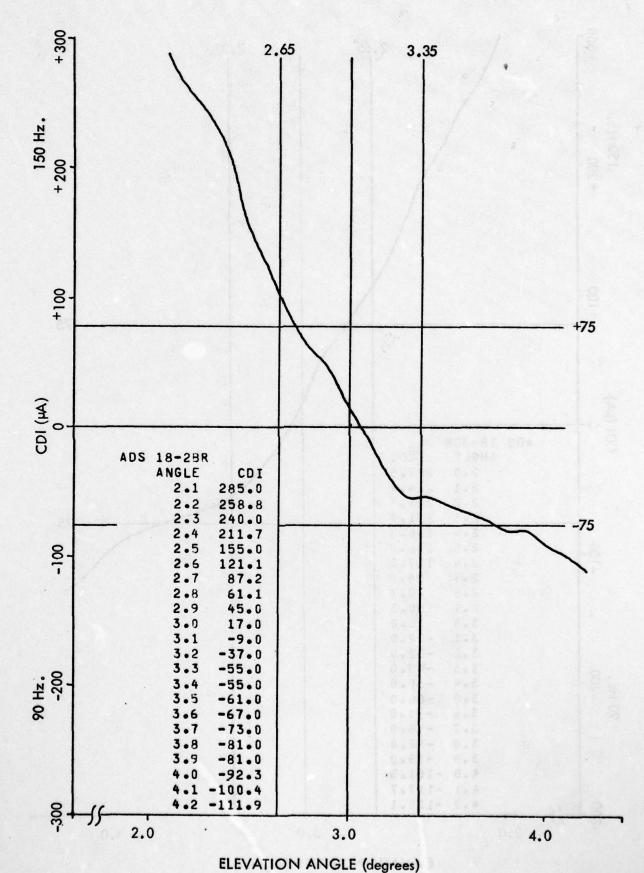


Figure 11-340. Approach 18-2 BR, Normal.

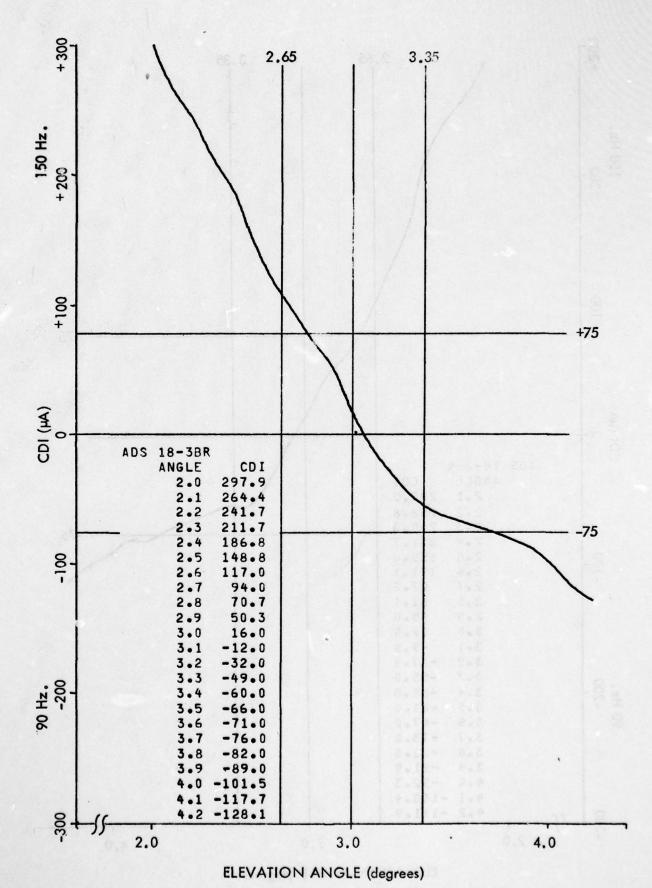
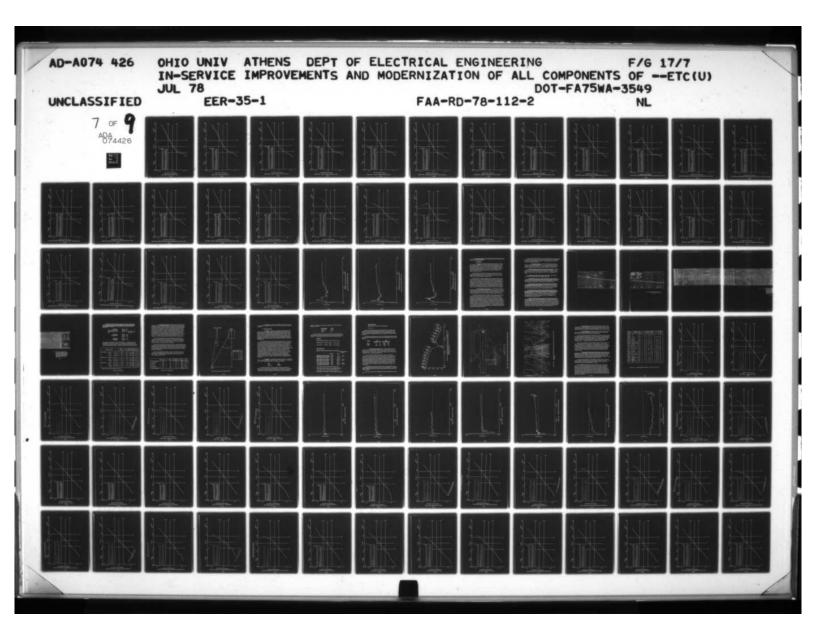


Figure 11-341. Approach 18-3BR, Normal.



OF ADA 074426



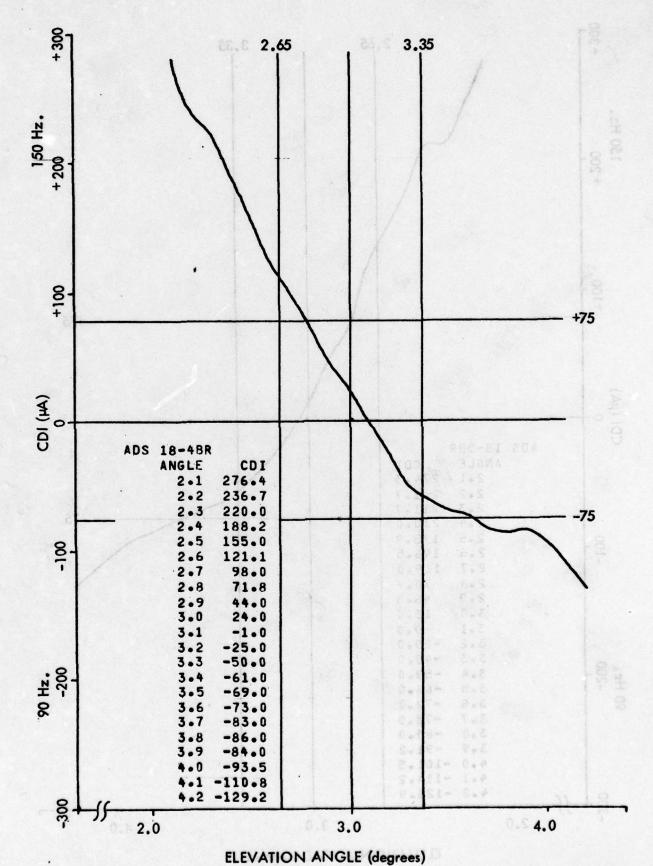
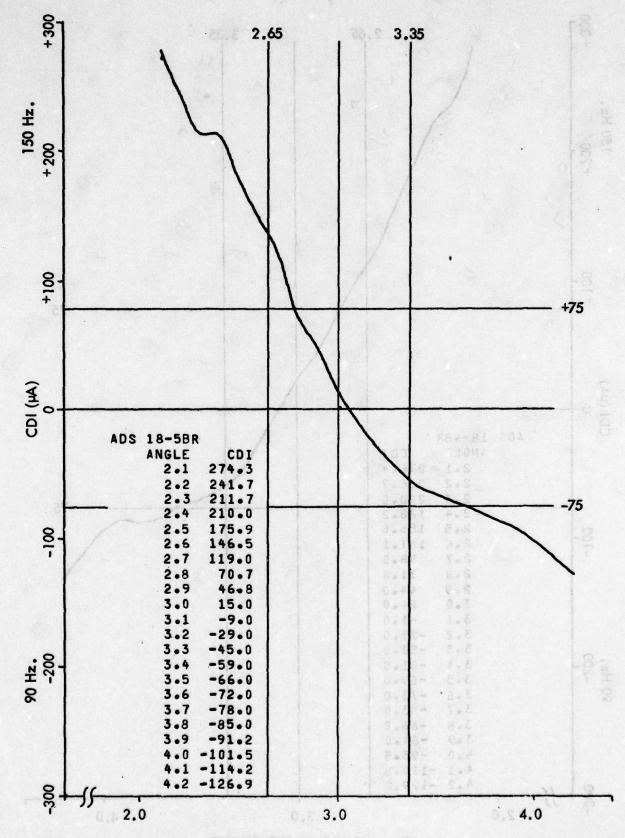


Figure 11-342, Approach 18-4BR, Normal.

11-497



ELEVATION ANGLE (degrees)

Figure 11-343. Approach 18-5BR, Normal.

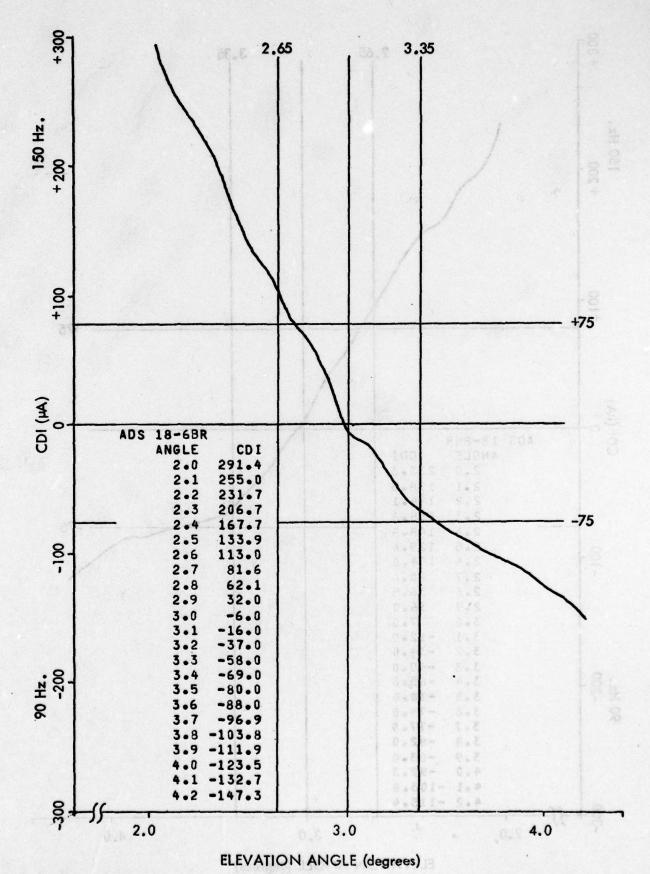


Figure 11-344. Approach 18-6BR, Normal, No Clearance.

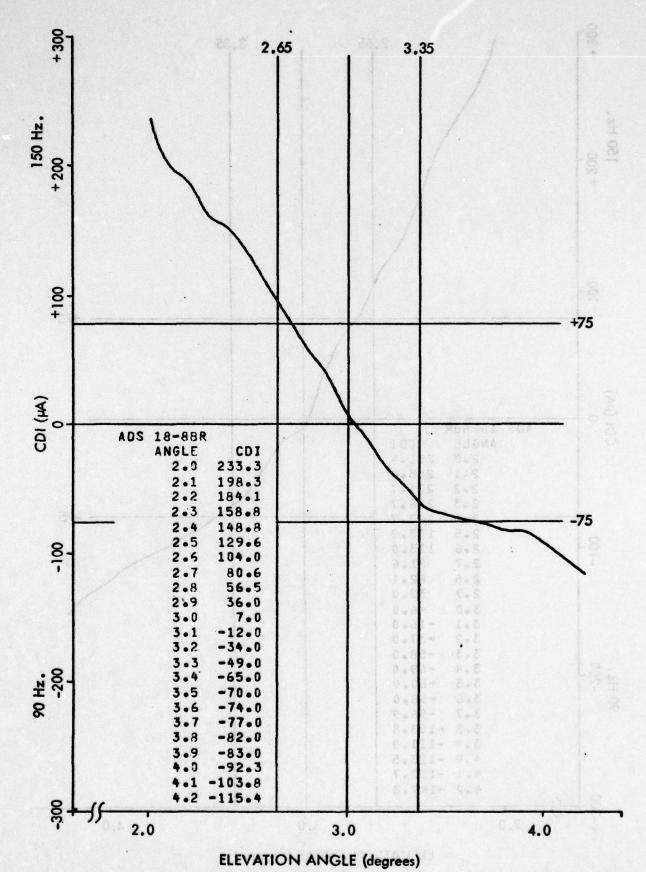


Figure 11-345. Approach 18-8BR, SBO Reduced to Alarm.

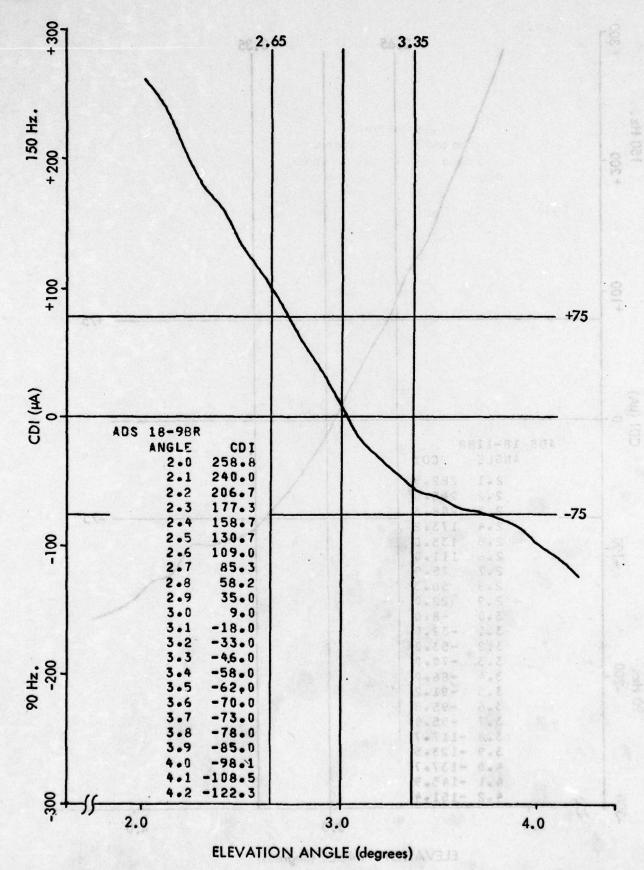


Figure 11-346. Approach 18-9BR, SBO Reduced to Alarm.

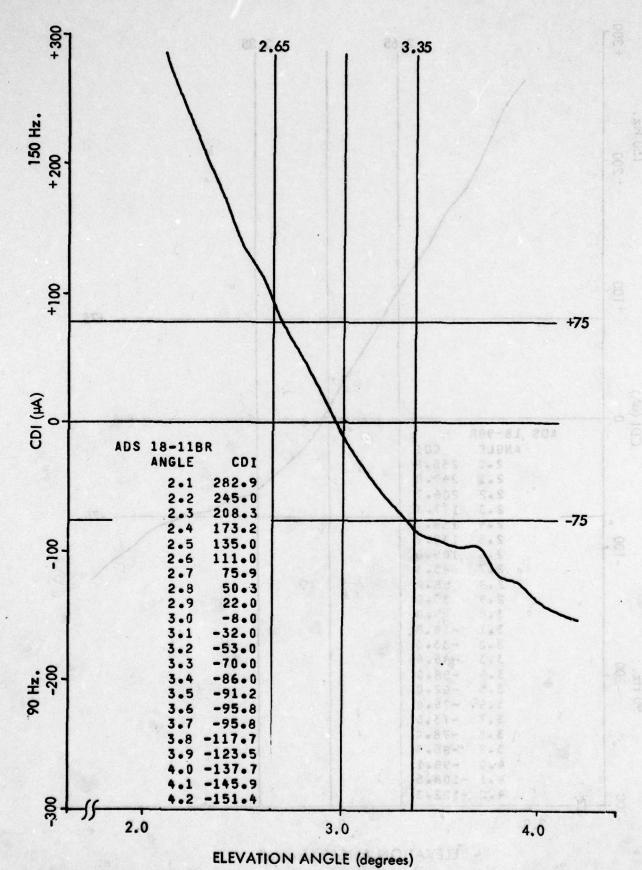


Figure 11-347. Approach 18-11BR, Normal, 8° West of Centerline.

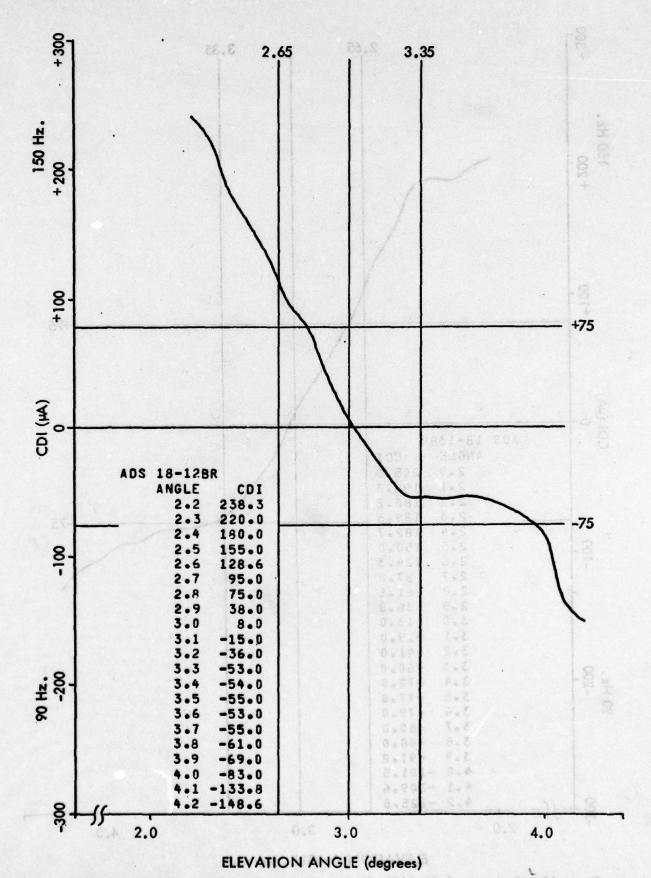


Figure 1.1-348. Approach 18-12BR, Normal, 8° East of Centerline.

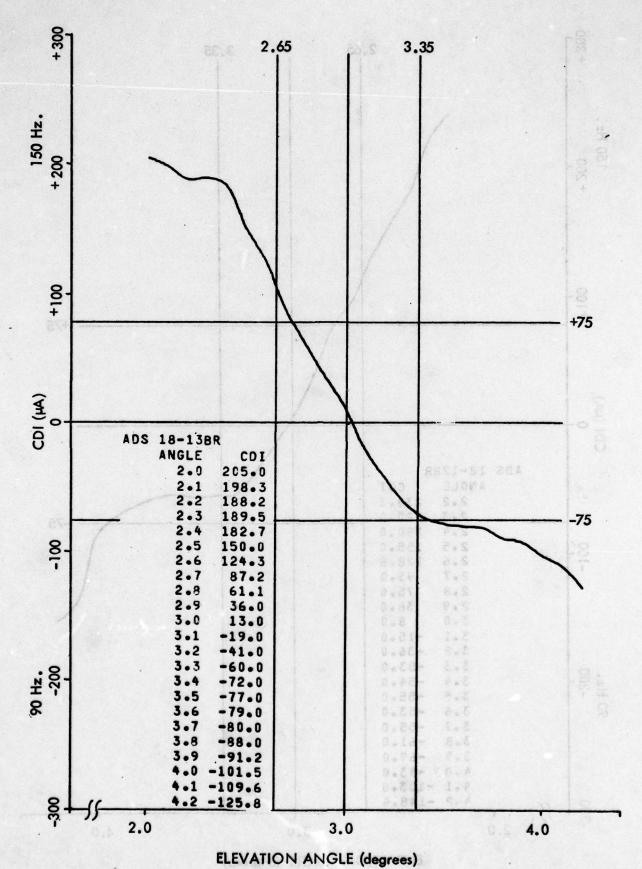


Figure 11-349. Approach 18-13BR, Middle Antenna Phase Advanced 15° to Alarm.

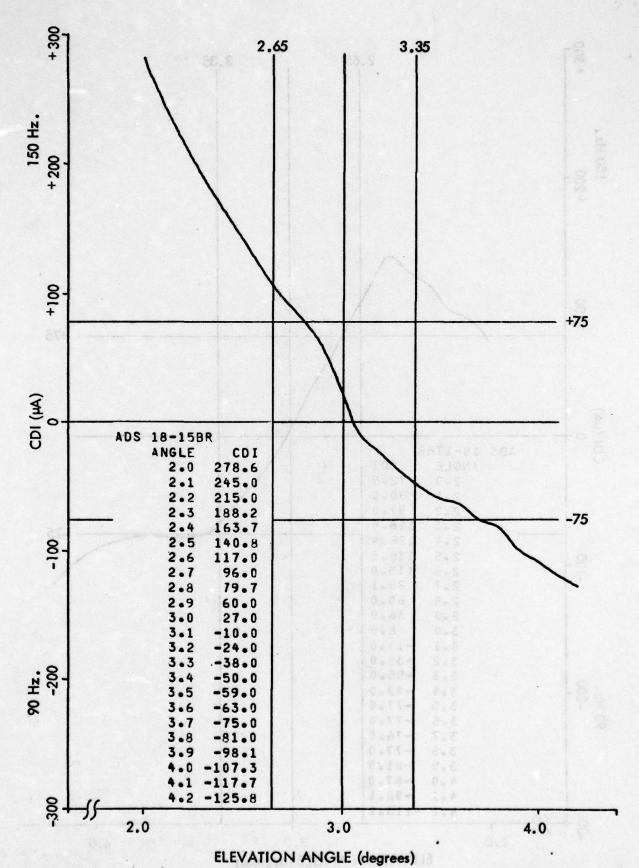


Figure 11-350. Approach 18-15BR, Middle Antenna Phase Retarded 14° to Alarm.

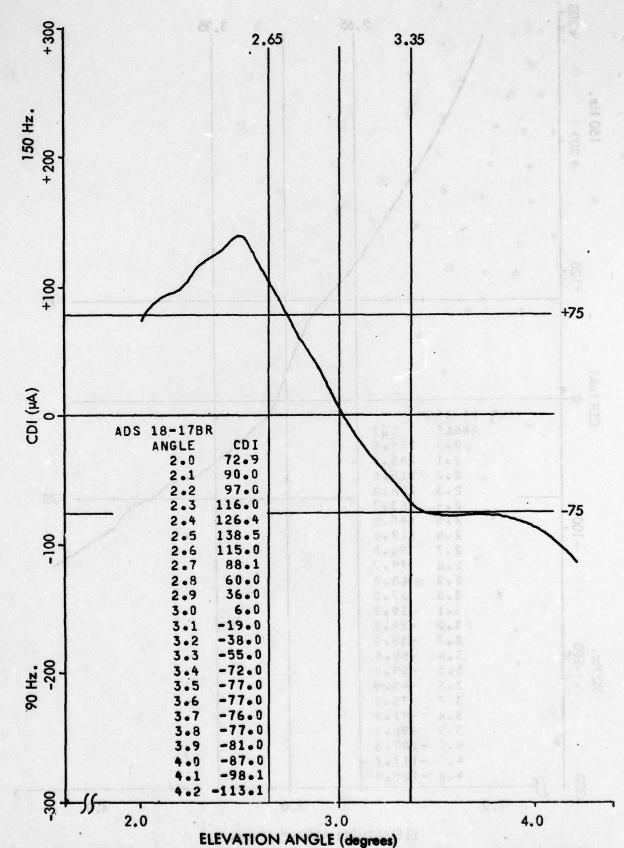


Figure 11-351. Approach 18-17BR, Middle Antenna Phase Advanced 28° to Twice Alarm.

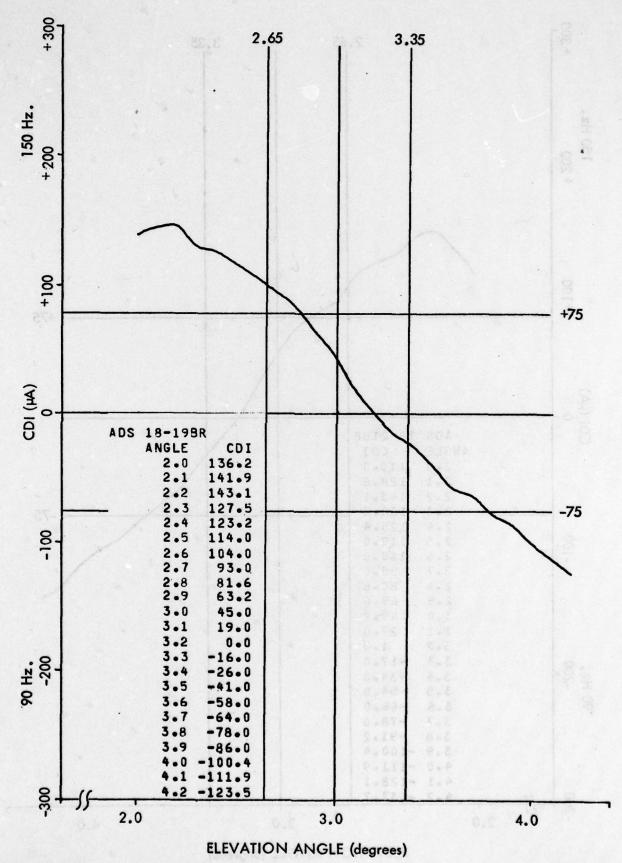


Figure 11-352. Approach 18-19BR, Middle Antenna Phase Retarded 28° to Twice Alarm.

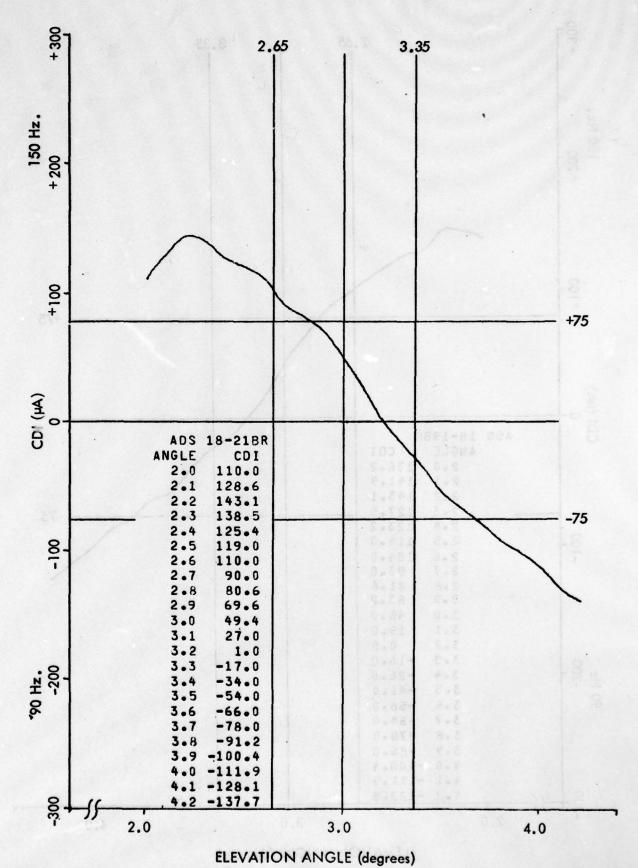


Figure 11-353. Approach 18-21 BR, Middle Antenna Phase Advanced 28° to Twice Alarm, No Clearance.

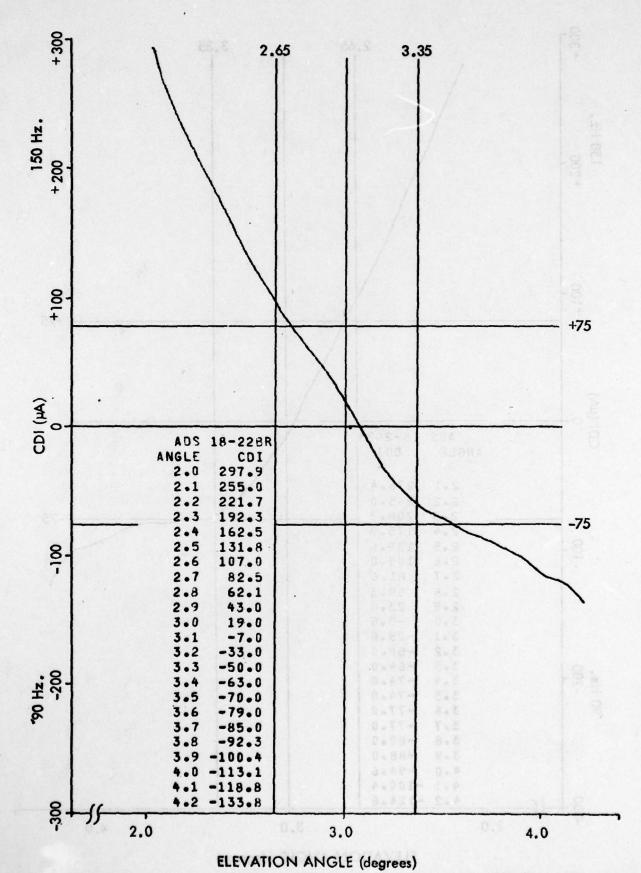


Figure 11-354. Approach 18-22BR, Upper Antenna Phase Advanced 22° to Alarm.

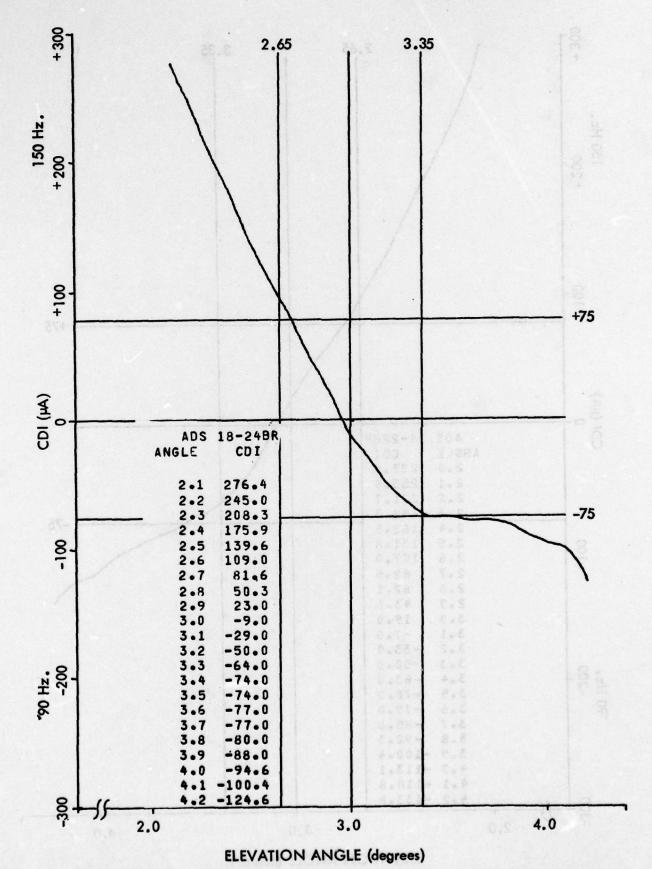


Figure 11-355. Approach 18-24BR, Upper Antenna Phase Retarded 22° to Alarm.

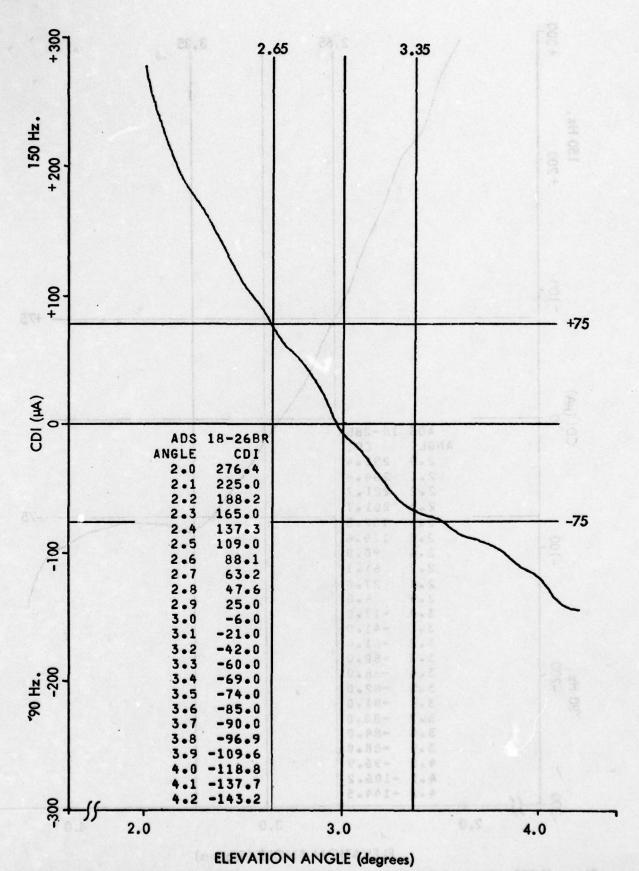


Figure 11-356. Approach 18-26BR, Upper Antenna Phase Advanced 44° to Twice Alarm.

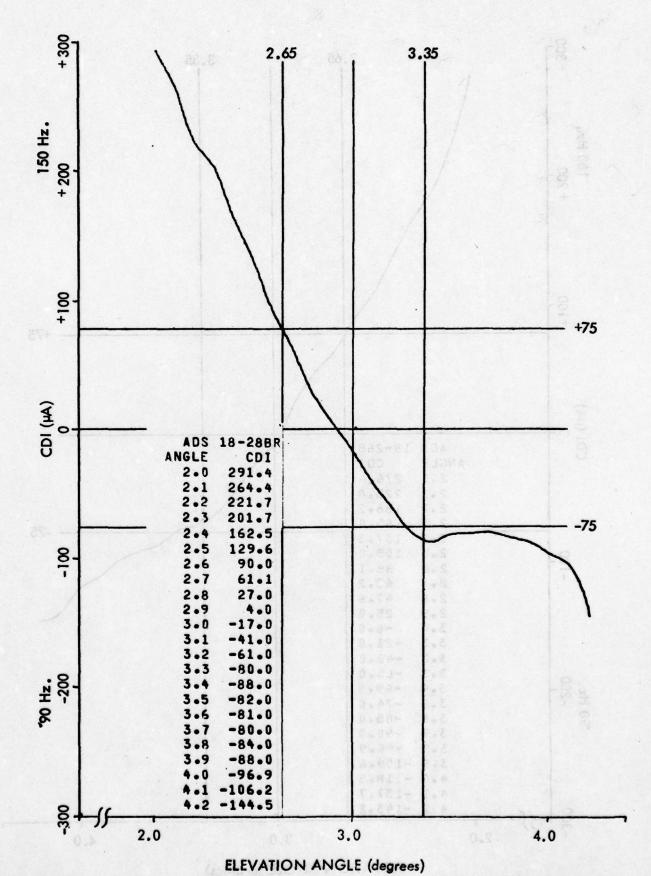


Figure 11-357. Approach 18-28BR, Upper Antenna Phase Retarded 44° to Twice Alarm.

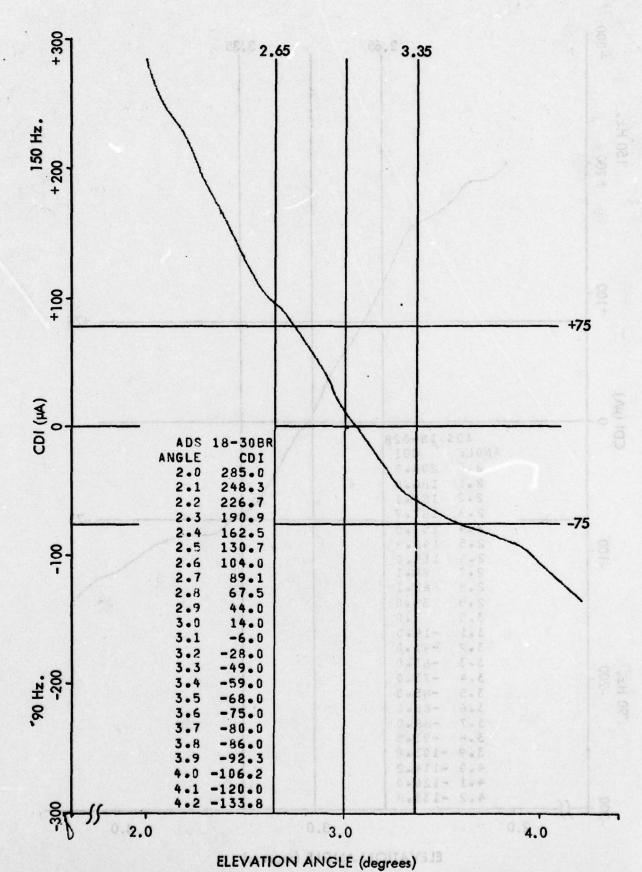


Figure 11-358. Approach 18-30BR, Lower Antenna Phase Advanced 15° to Alarm.

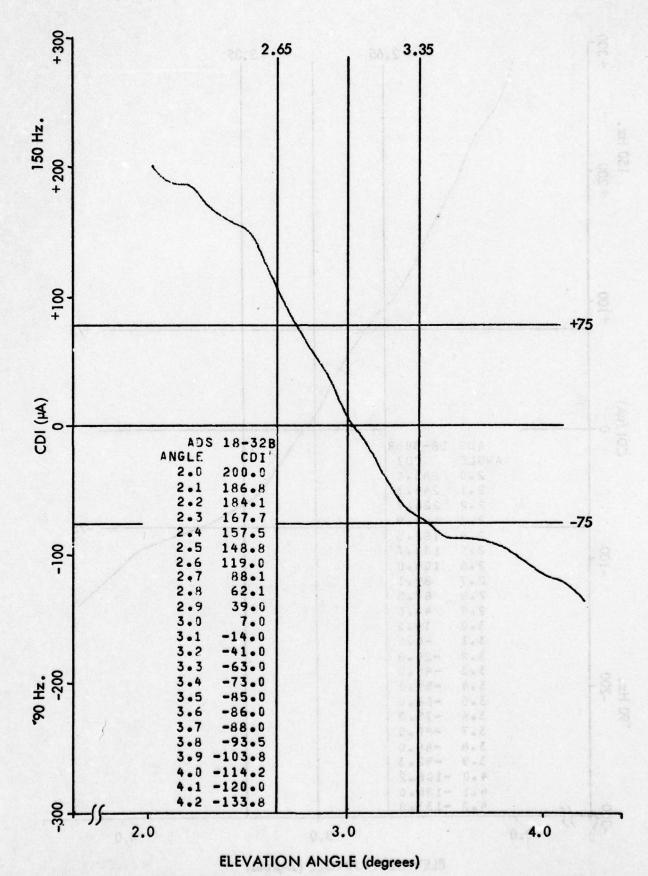


Figure 11-359. Approach 18-32BR, Lower Antenna Phase Retarded 10° to Alarm.

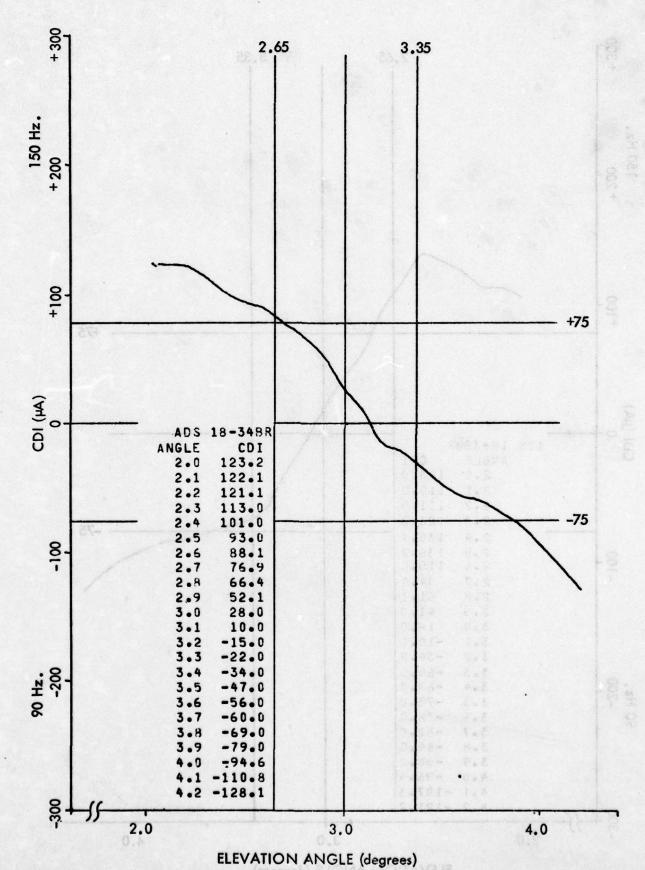


Figure 11-360. Approach 18-34BR, Lower Antenna Phase Advanced 30° to Twice Alarm.

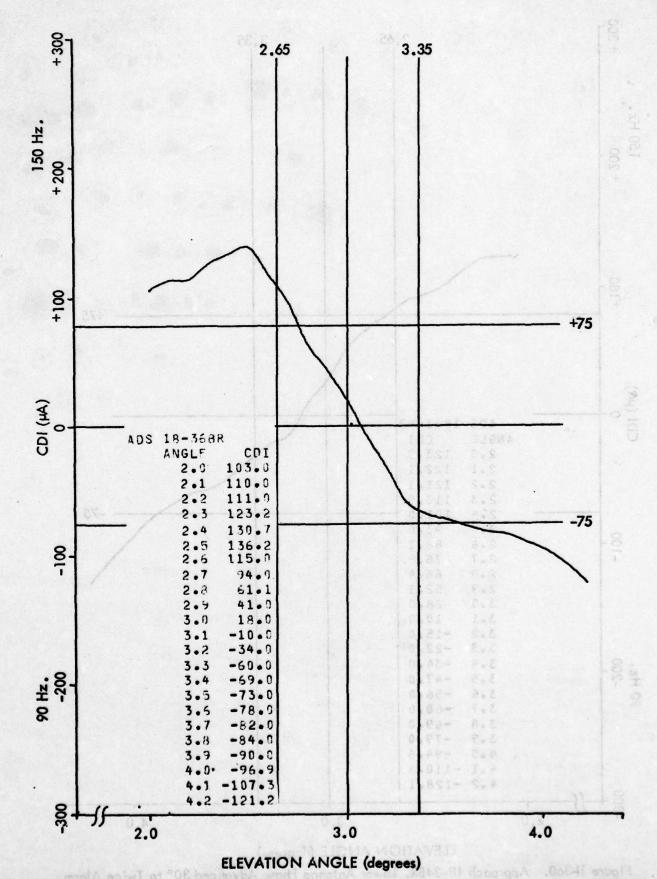


Figure 11-361. Approach 18-36BR, Lower Antenna Phase Retarded 20° to Twice Alarm.

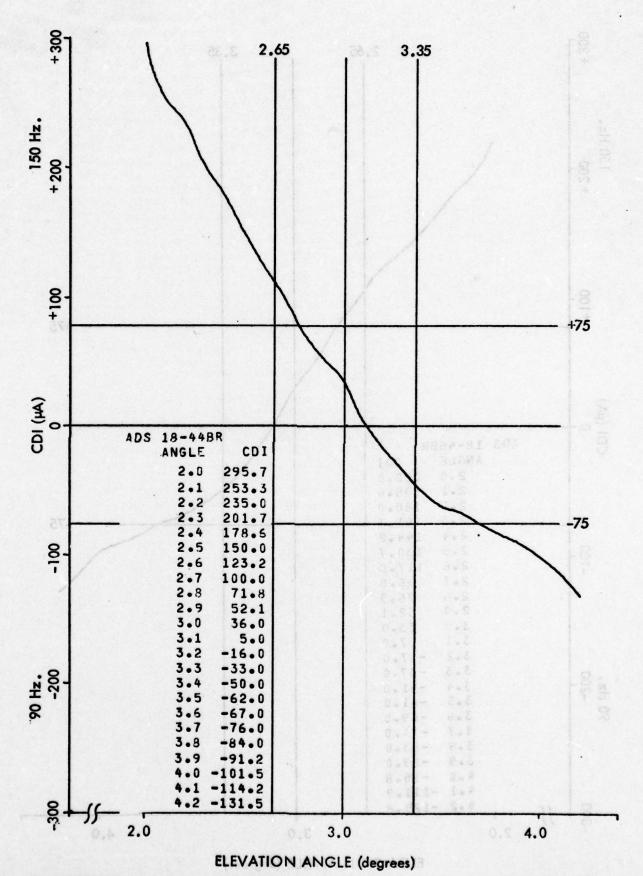


Figure 11-362. Approach 18-44BR, Middle Antenna Attenuated 1 dB to Alarm.

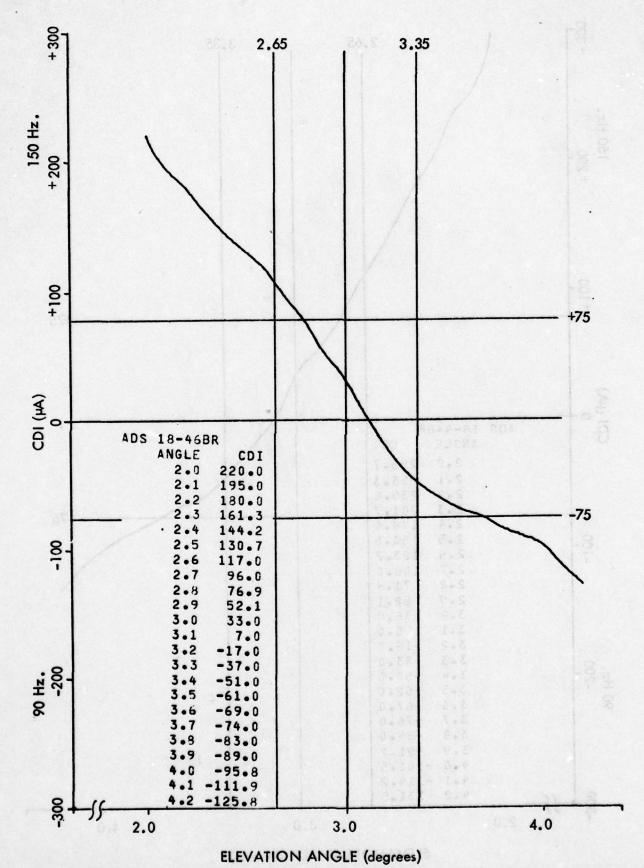


Figure 11-363. Approach 18-46BR, Middle Antenna Attenuated 2 dB to Twice Alarm.

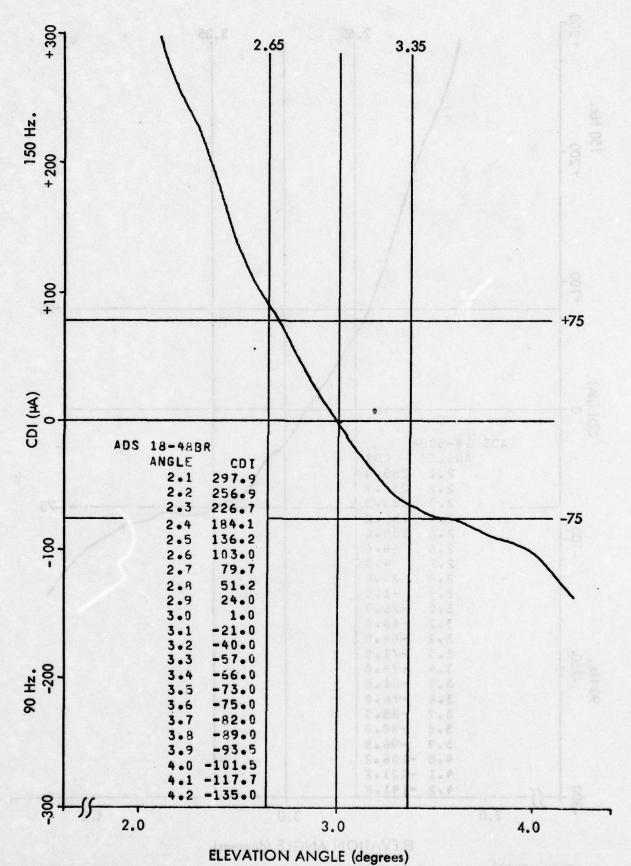


Figure 11–364. Approach 18–48BR, Upper Antenna Attenuated 2 dB to Alarm.

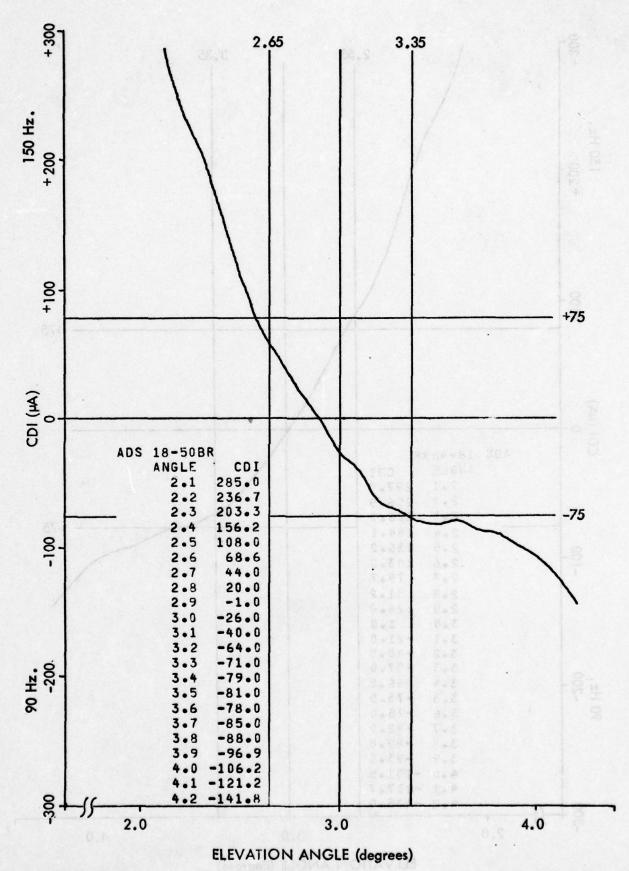


Figure 11-365. Approach 18-50BR, Upper Antenna Attenuated 4 dB to Twice Alarm.

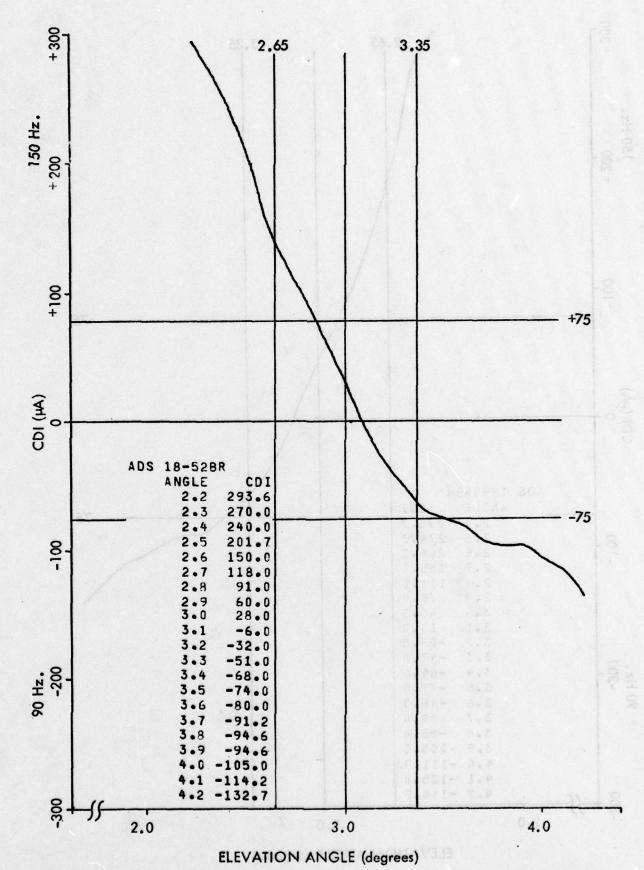


Figure 11-366. Approach 18-52BR, Lower Antenna Attenuated 1 dB to Alarm.

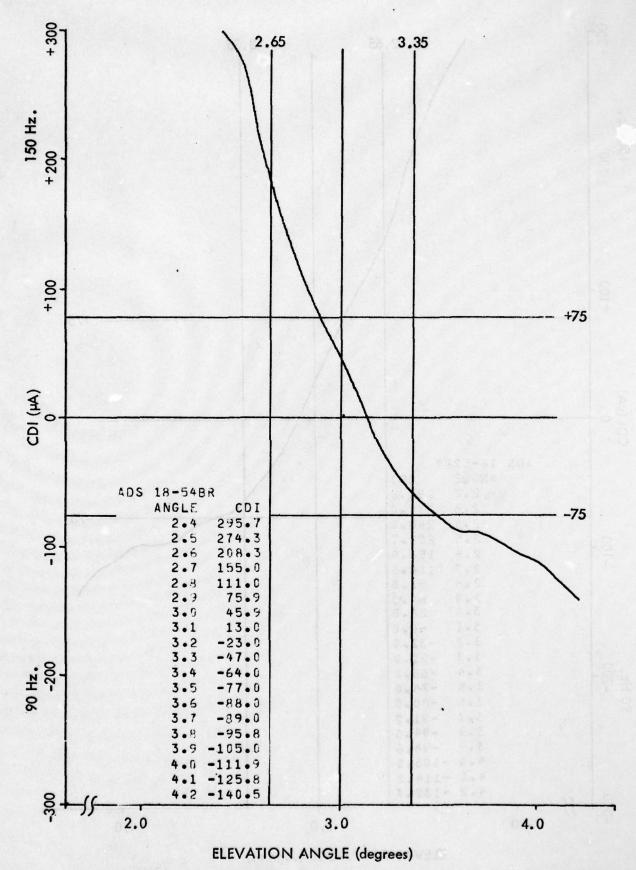


Figure 11-367. Approach 18-54BR, Lower Antenna Attenuated 2 dB to Twice Alarm.

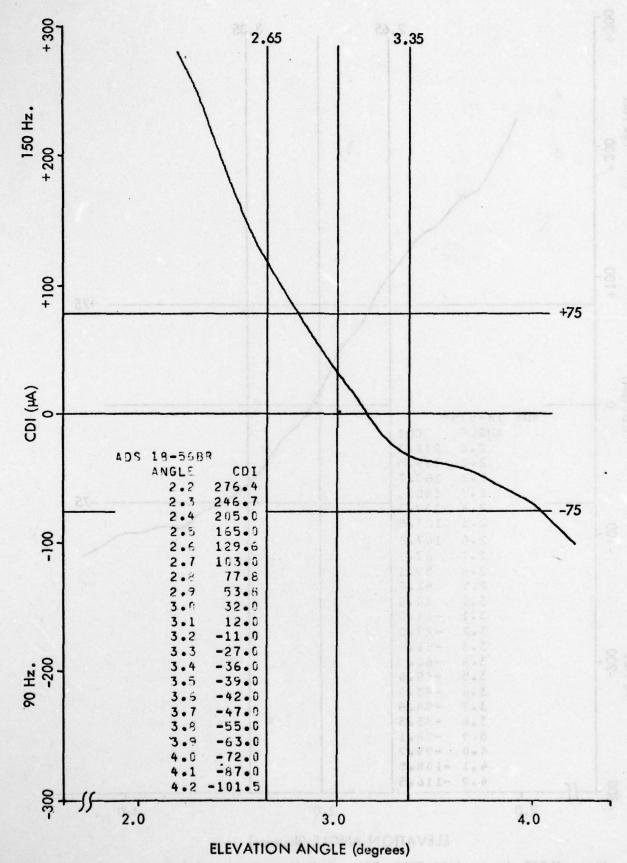


Figure 11-368. Approach 18-56BR, CSB to SBO Phase Shifted 30° to Alarm.

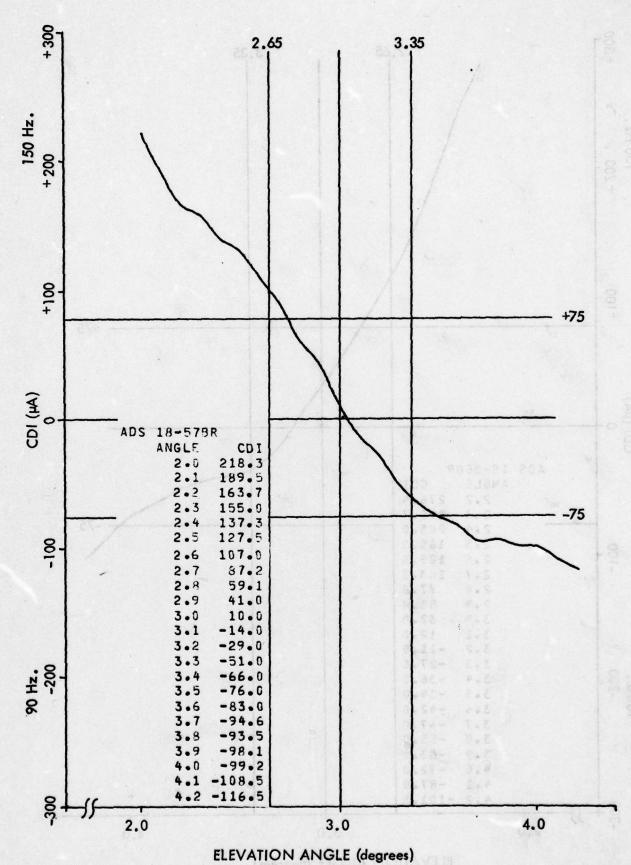


Figure 11-369. Approach 18-57BR, CSB to SBO Phase Shifted 30° to Alarm (Advance).

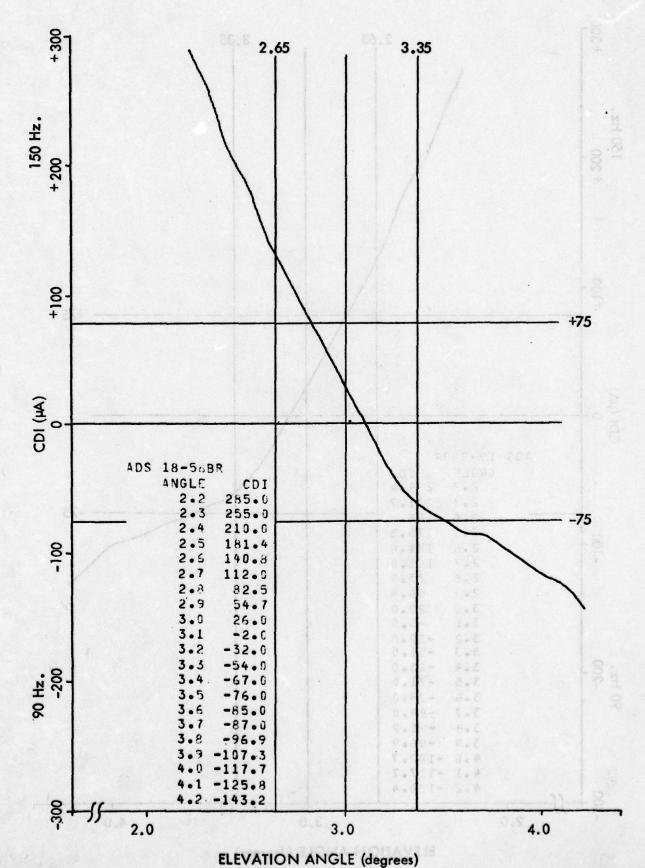


Figure 11-370, Approach 18-58BR, SBO Power Increased to Sharp Alarm.

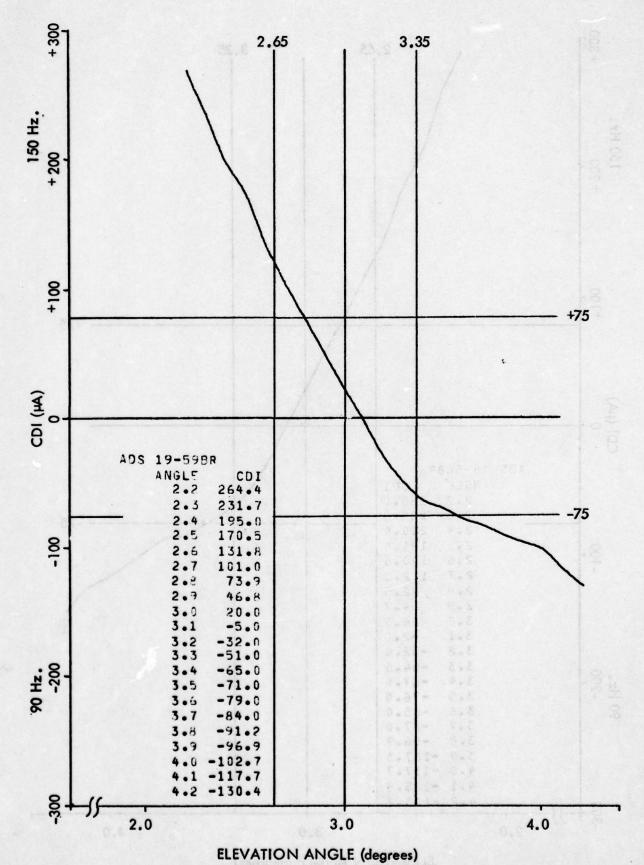


Figure 11-371. Approach 19-59BR, Normal.

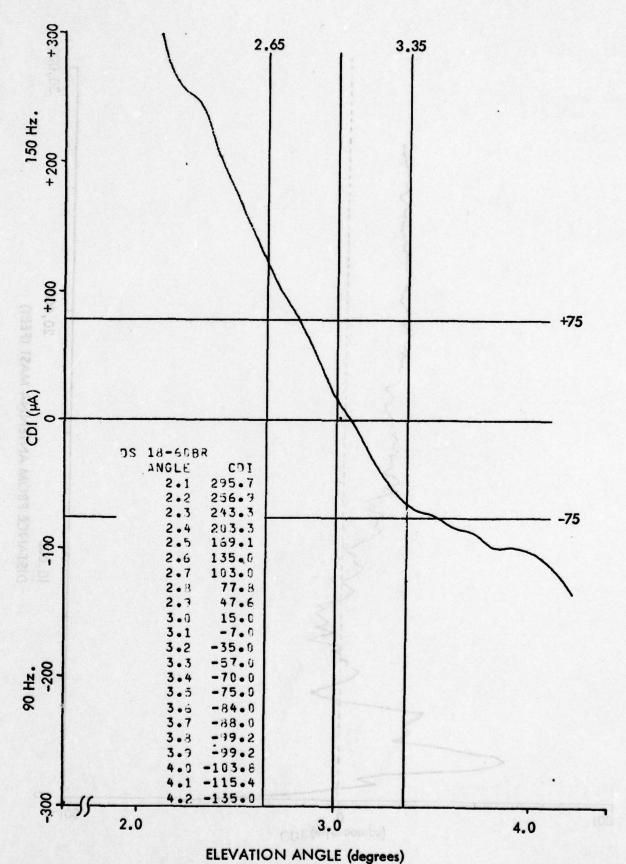
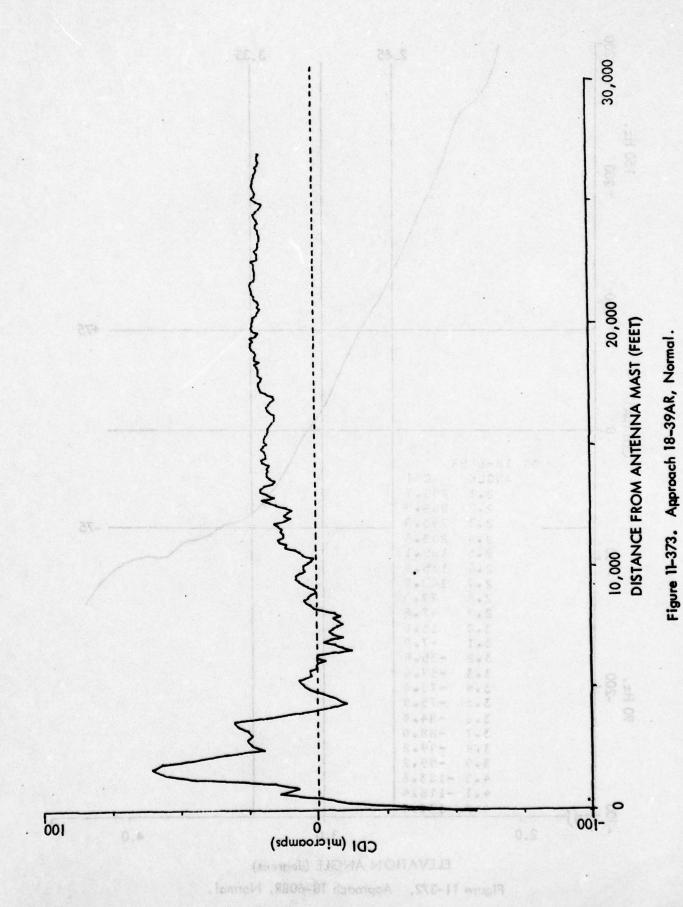


Figure 11-372. Approach 18-60BR, Normal.



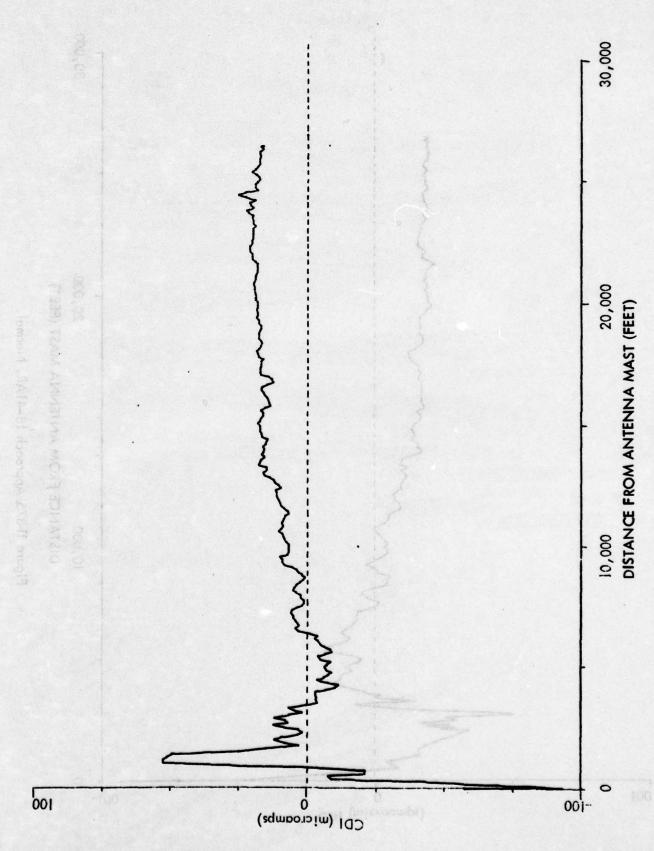
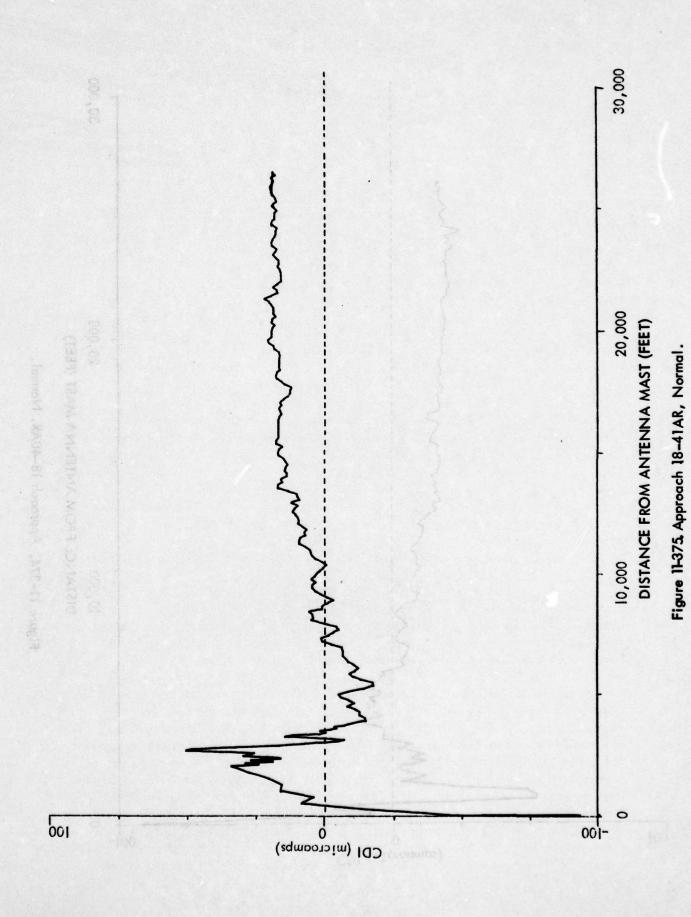


Figure 11-374. Approach 18-40AR, Normal.



4. Documentary Flight Data for a Capture Effect Glide Slope System Operating with a Truncated Ground Plane.

a. Optimization.

(1) General. The purpose of this section is to document the results of an optimization program conducted with the glide slope serving Runway 31 at the Reabird Airport, Dallas, Texas. The ground plane serving the image capture-effect glide slope at Redbird is far from ideal. Basically it is short (1000 feet), slopes downward away from the antennas at .39°, and on the side opposite from the runway the ground plane drops abruptly more than 10 feet. These complications clearly require that parameters of the system, phasing in particular, be adjusted to compensate for the non-ideal site.

The basic objective of the work was to document facility performance and insure a glide slope which will meet the requirements set forth in the U.S. Flight Inspection Handbook OAP 8200.1. This was achieved, and key documentation to support this is contained in Figures 11–376 and 11–377.

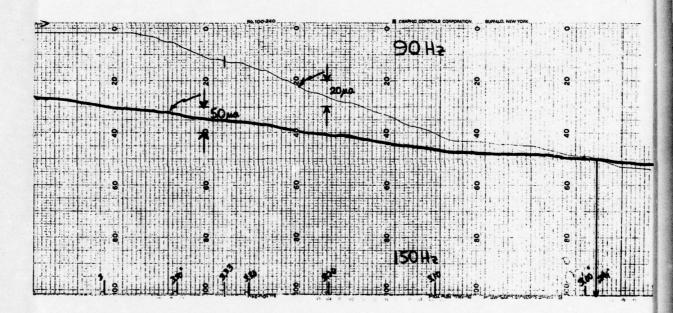
Initially the system was found configured as the Wilcox Corporation had left it several weeks earlier. Careful documentation data were taken on the ground and in the air so that, if desired, the facility could be returned to this configuration. Flight data indicated that the system was operating such as to meet 82.001 Handbook requirements with the exception of the below-path structure (maximum fly-up 60 microamperes at 2.2° elevation) and low path angle (2.63°) at 8° on the southwest side of the runway centerline extended. Although the specifications are not well defined by the handbook for this 8° region, it is believed that some flight inspectors, at least, would on a judgmental basis regard this type of condition as unacceptable.

(2) Instrumentation for Data Collection. The Ohio University Mark 2 Minilab was used for all airborne data collection. This was mounted in a Beechcraft Model 35 Bonanza which carried a complement of usual IFR avionics equipment (King Silver Crown) augmented with necessary items for Category II certification. This operational equipment was used to cross-check the values recorded in the Minilab.

The Mini lab consisted of three Narco UGR-2 receivers for processing the glide slope and telemetry information from the theodolite. A GS-2/GRM-4 (military equivalent of the Boonton 232A) was transported to the Redbird site and used for calibration and standardization of the Mini lab receivers. This generator, originally calibrated at the FAA Aeronautical Center, is currently maintained as a laboratory transfer standard at the FAA-approved repair station operated by the Avionics Engineering Center at Ohio University. This standard is traceable to the National Bureau of Standards in Boulder. Two Honeywell Electronik 19 strip chart recorders were used to record the data with a total of four analog channels and two binary which were used for event marking. Voltage supplies were regulated. A solid state differential amplifier was part of the laboratory thus allowing direct readout of the difference between the glide slope CDI and theodolite position.

A Warren Knight Model WK-83 radio telemetering theodolite was used for tracking the aircraft, and this was electrically connected to a Reaction Instrument Model 6050 telemetry transmitter operating on 329.0 MHz. Theodolite placement was surveyed according to Handbook OAP 8200.1.

- (3) <u>Parameters of Interest</u>. The U.S. Flight Inspection Handbook calls out the following parameters which are to be measured and compared to certain Category I tolerances for acceptability. These are identified in the following paragraphs and supporting flight records are contained in Figures 11-376 and 11-377.
- (a) Modulation Equality and Phasing (Tolerance ±5 microamperes). The facility was found to give zero microamperes initially for equality, and subsequent checks showed maximum indication of 2 microamperes into the 90 Hz. Sideband-to-carrier phasing was found to give 2 microamperes into the 150 Hz. No adjustments were made.
- (b) Modulation of 90 and 150 Hz (Tolerance 75% 85%). The modulation percentage was found to be 78%. No adjustments were made.
- (c) Angle and Width (Tolerance: Nominal angle $3.00^{\circ} \pm 0.05^{\circ}$ and nominal width of $0.70^{\circ} \pm 0.20^{\circ}$, symmetry of 40 60% or 60 40% maximum). The path angle was found to be 2.99° with a width of 0.74° and a symmetry of 54% to 46% (belowabove) established with adjustment of sideband power. See Figure 11-376.
- (d) Clearance (Below-Path Clearance 180 Microamperes Normal Width; 150 Microamperes with Path Lowered and Broad). Clearance was found to be at least 165 microamperes when flying below 1.8° or less on an approach to the airport from a distance of five miles to the threshold with broad alarm due to reduced sideband power and clearance transmitter at alarm for low percentage modulation.
- (e) Structure (Tolerance is ±30 microamperes throughout zones 1,2, and 3, referencing the graphical average path, the average path, and the graphic average path respectively). The structure (flyability) was found to be exceedingly good. The average path angle was 3.01° with ±8 microamperes roughness in zone two. Site-caused roughness was almost all within the noise of the measurements: Z1-12 microamperes/4.9 nm; Z2-8 microamperes/3 nm; Z3-8 microamperes/.3 nm (reference 13-35 AR, Figure 11-377).
- (f) Usable Distance (Minimum acceptable level is 15 hard microvolts at the antenna terminals). By using a variable attenuator and the threshold of the glide slope receiver calibrated against a standard signal generator, a signal level of 15.3 hard microvolts was found at intercept altitude (2200 feet MLSO 10 miles from the threshold. This provides no margin over minimum requirements; however, these measurements were made with the main transmitter reduced to 3 dB alarm and clearance transmitter powers reduced to the alarm limit (1 dB). It should be noted that the field strength measurement tolerance is such that no significant deficiency is deemed to exist.



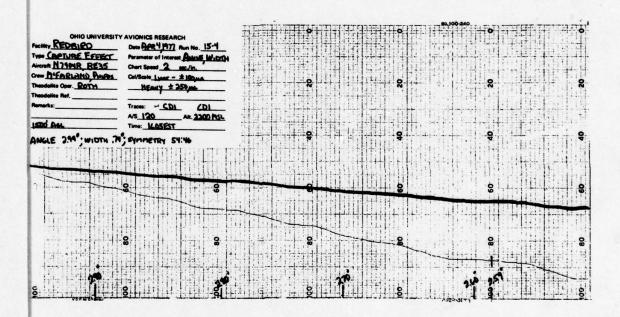
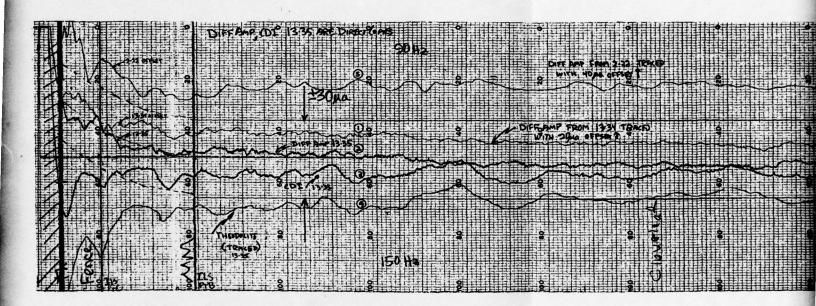


Figure 11–376. Dual Recording of CDI Made With Different Scales on a Flight on the Localizer Centerline 1600 Feet Above the Site Elevation.

11-533/11-534



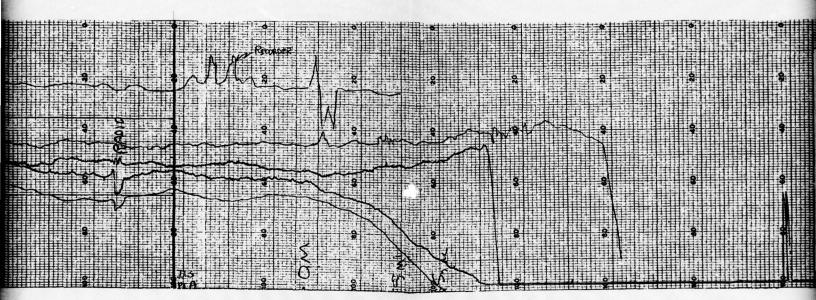


Figure 11-377 . Redbird Airport CDI and Different NOTE: This chart is a direct remade of the CDI and differential 13-35, and these are shown a godifferential amplifier record for a 20-microampere offset into the parison of repeatability. Trace for the 13-35 run. The CDI Inflat differential amplifier trace came receiver. The Category I toleran applied to trace Q .

11-535/11-536

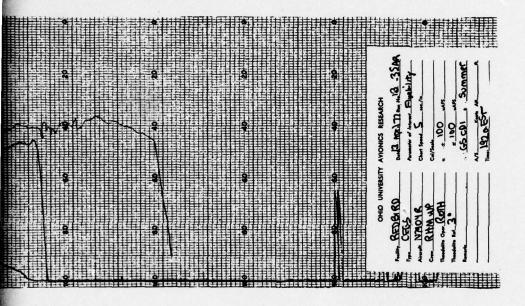


Figure 11-377. Redbird Airport CDI and Differential Amplifier Traces.

NOTE: This chart is a direct reproduction of the recordings made of the CDI and differential amplifier traces for Run No. 13-35, and these are shown as ② and ③. Trace ① is the differential amplifier record for Run No. 13-34 traced with a 20-microampere offset into the 90 Hz to allow a ready comparison of repeatability. Trace ④ is the theodolite record for the 13-35 run. The CDI information for the 13-35 differential amplifier trace came from the No. 2 glide slope receiver. The Category I tolerance brackets should be applied to trace ②.

11-535/11-536

7

3

(g) Monitors (Alarm limits shall be no greater than 7.5% for the path angle, limits no greater than 0.5 and 0.9° for the width; 0.9° path width maximum for a carrier-to-sideband dephasing). Monitor alarm limits were checked and found to be as follows:

Path Angle (No path angle, control, advanced of upper antenna	Normal 2.99° Upper
40°)	Lower 2.81° (Hard Alarm, Twice Alarm Limit)
Path Width	Normal .74°
(Sideband Power)	Broad .84°
	Sharp .63°
SBO/CSB 30°	Advance .94°
Dephasing	Retard .79°

These responses are satisfactory and will meet requirements. In addition each antenna was dephased, both advance and retard, to alarm limits and resulting path angle and width values were measured in space. Also, each antenna feed was attenuated to alarm and flight measurements were made. Following in Table 11–34 are the tabulated results:

Adjusted to Alarm		Path Angle	Width	Structure Angle°/ Max. Fly-UpinµA	Run No.	
Lower Antenna	Advance	15° (2-16)	3.08°	.65°	2.17°/>236µA	2-16
	Retard	6° (2-17)	3.00°	.80°	1.84°/>235µA	2-17
	Attenuate	1.5dB (2-19)	3.09°	.68°	1.95°/>233μA	2-19
Middle Antenna	Advance	+12° (2-11)	3.06°	.81°	1.77°/>234µA	2-11
	Retard	9.6° (2-12)	3.08°	.64°	2.21°/>235µA	2-12
	Attenuate	.5dB (2-18)	3.06°	.77°	1.93°/>238μA	2-18
Upper Antenna	Advance	20° (14-22)	2.88°	.73°	2.05°/>230µA	14-22
	Retard	27° (14-24)	2.94°	.71°	1.96°/>195µA	14-24
	Attenuate	1dB (15-18)	2.92°	.71°	1.95°/>245μA	15-18

These all indicate safe and satisfactory conditions.

Table 11-34. Fault Data.

(4) Additional Considerations. Although the U.S. Flight Inspection Handbook does not give quantitative tolerances for path characteristics off localizer centerline, except for the 1/2% allowable angle change, the ±8° sector designated by ICAO was carefully scrutinized. Results of the optimization permitted good path characteristics to be obtained in spite of the terrain drop-off existing on the west edge of the reflecting plane. It should be emphasized that satisfactory conditions were obtained only to 8° west in azimuth. At 9° unsatisfactory conditions existed, particularly in below-path. Continuous azimuth reference with telemetry was accomplished with the theodolite located at the point designated in Manual 8200.1. This is not the runway centerline reference specified by ICAO; however, it is a conservative value because the critical side is on the same side of the runway as the theodolite. A correction table is provided in Figure 11-378 for detailed analysis.

The flight checks showed also that the 190 microampere fly-up indication occurred at an angle greater than 1° elevation, and this is greater than 30% of the nominal path angle. On a level run 1000 feet above the elevation of the approach end of the runway from 10 miles inward, 1° elevation to 1° below the glide path angle, the clearance was not less than 180 microamperes.

In the process of obtaining the usual data to certify a capture-effect glide slope, additional data were obtained to insure quality performance and provide documentation of responses to certain fault conditions. Path angle, width, and structure angle measurements were made on faults of twice alarm limits produced by advancing and retarding the phases of the signals to each antenna and attenuating each to give twice an alarm value. See Table 11-35.

Also, a spot measurement below path at a point 4 miles from the runway 1.2° elevation was accomplished with and without clearance transmitter for most of the fault conditions. All conditions observed showed the system to be operating in an optimum condition based on theory.

Audiocytis s	Path Angle	Width	Structure Angle 190µA	Max Clearance	Run No.
8° East (Theodolite)	2.86°	.97°	1.54°	>250µA	15-28
Loc Edge East	3.03°	.63°	2.20°	250μΑ	12-8
Centerline	3.03°	.65°	2.10°	230µA	12-7
Loc Edge West	2.99°	.68°	1.40	195µA	12-9
8° West (Theodolite)	2.77°	.89°	1.49°	>240µA	15-27

Table 11-35. Azimuthal Data.

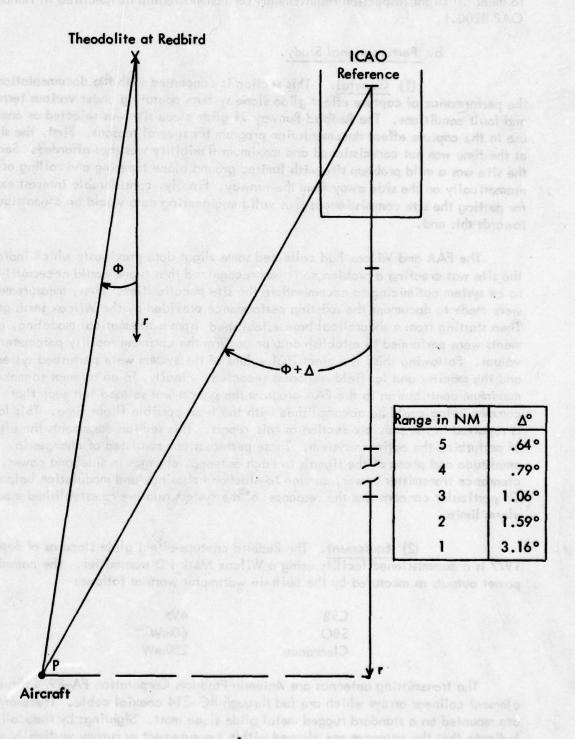


Figure 11-378. Geometry for Angle Correction.

(5) Conclusions. The glide slope at Redbird when optimized was found to meet all flight inspection requirements for commissioning as specified in Handbook OAP 8200.1.

b. Perturbational Study.

(1) General. This section is concerned with the documentation of the performance of capture effect glide slope systems operating under various terrain and fault conditions. The Redbird Runway 31 glide slope site was selected as one for use in the capture effect documentation program for several reasons. First, the site at the time was not commissioned and maximum flexibility was thus afforded. Second, the site was a mild problem site with limited ground plane tapering and rolling off dramatically on the side away from the runway. Finally, considerable interest existed for getting the site commissioned; thus valid engineering data would be a contribution towards this end.

The FAA and Wilcox had collected some flight data previously which indicated the site was creating a problem, so it was recognized that there would necessarily have to be system optimizing to accommodate the site peculiarities. First, measurements were made to document the existing performance provided by the Wilcox settings. Then starting from a theoretical base established from mathematical modeling, experiments were performed to establish and/or confirm the optimum facility parameter values. Following this, the electrical values of the system were perturbed systematically and the monitor and far field responses recorded. Finally, in an attempt to make a maximum contribution to the FAA program the system was set and left such that commissioning could be accomplished with the least possible flight time. This last is reported in the previous section of this report. This section documents the effects of perturbing the optimum system. These perturbations consisted of changes in amplitude and phase of the signals to each antenna, changes in sideband power, clearance transmitter power, carrier-to-sideband phasing, and modulation balance. Of particular concern was the response of the system relative to established monitor alarm limits.

(2) Equipment. The Redbird capture-effect glide slope as of September 1977 is a commissioned facility using a Wilcox Mark I D transmitter. The commissioned power outputs as measured by the built-in wattmeter were as follows:

CSB 4W SBO 60mW Clearance 250mW

The transmitting antennas are Antenna Products Corporation FA-8976 three-element colinear arrays which are fed through RG-214 coaxial cable. These antennas are mounted on a standard rugged metal glide slope mast. Sightings by theodolite indicate that the antennas are aligned within measurement accuracy vertically and

angularly. The heights of the antennas as measured from the cement base of the mast are given below:

Antenna Height	Offset
12.25 feet	8 inches
24.25	0
36.4	18

being radiated at the time the

In order to determine the signals being radiated from each antenna, probe measurements were taken using a jig-mounted probe and a Hewlett-Packard vector voltmeter. The data obtained is given below along with the measured values.

CSB ONLY

Reference amplitued (middle antenna monitor port)						
Middle antenna	amplitude	-27.8	_,	phase_	0°	
Lower antenna	amplitude	-20	4.	phase	168°	

CSB into SBO Input

Reference amplitude (middle anten	na monitor p		ective Excitation Current
A	mplitude	Phase	
Middle antenna (center element) Middle antenna (runway element) Middle antenna (outer element)	-22.0 -23.2 -22.7	0° 27° 20.5°	-13.3 15°
Upper antenna (center element) Upper antenna (runway element) Upper antenna (outer element)	-29.0 -30.5 -28.8	181°] 146.5° 148°]	-18.4 163°
Lower antenna (middle element) Lower antenna (runway element) Lower antenna (outer element)	-30.0 -31.8 -28.2	174° 181.5° 185°	-20.4 180.5°

Upper antenna monitor port (reference) amplitude <u>+3.0</u>

Center element, upper antenna – amplitude <u>-28.1</u>, phase <u>8°</u>

Lower antenna monitor port (reference) amplitude <u>+4.5</u>

Center element, lower antenna – amplitude <u>-29.0</u>, phase <u>1.0°</u>

SBO into SBO Input

Middle antenna, center element amplitude -37.5

A ratio = .42

The values presented above give complete information as to what signals were being radiated at the time the measurements were taken. The pertinent data is contained in the individual element measurements; the monitor port readings were taken in order to establish a relationship between the actual radiated signal and the monitor port output.

The radiated signal along centerline is the sum of the individual element currents. Taking the above into consideration, the system output relationships can be given by the following:

Antenna	CSB		SBO		
	Magnitude	Phase	Magnitude	Phase	
Upper	0.	1in	.55A	148°	
Middle	.44	0°	1.00A	0°	
Lower	1.00	165°	.44A	165°	

(3) Terrain and Site Peculiarities. The terrain profile along centerline for runway is shown in Figure 11-379. As seen in Figure 11-379, the terrain slopes downward for 1600 feet with its slope increasing with increasing distance from the antenna mast. The terrain then rises about 7 feet before continuing its downward slope which ends at a commercial shopping center.

In order to describe the effects of this terrain on glide slope performance, reference will be made to the first Fresnel [8] zone location. As is commonly understood, the center of the elliptical Fresnel zone moves closer to the antenna and its size continually decreases as the aircraft approaches the threshold. For aircraft positions greater than 20,000 feet from threshold, the Fresnel zone center is approximately 1000 feet from the antenna mast and is 1,500 feet long. As seen in Figure 11-379, the terrain 1000 feet in front of the antenna mast, it can be expected that this downslope will affect the glide slope for aircraft beyond the outer marker. As the aircraft moves closer to threshold, the Fresnel zone moves up the slope and its area decreases.

The topographical map of Figures 11-380 and 381 show that the terrain drops off more quickly to the west of the runway than the area along centerline. This quicker dropoff causes the Fresnel zone to be along a steeper slope for aircraft positions to the west of centerline.

There were no structures within 2,000 feet that would have interfered with these tests.

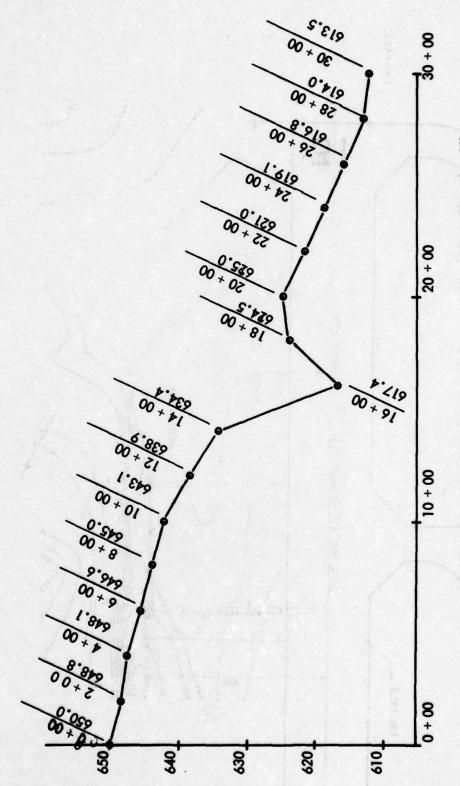


Figure 11–379. Redbird Profile Starting at Center of Tower Base (Sta. 0 + 00) Running Parallel with Runway at Distance of 3,000 Ft. in Southeasterly Direction.

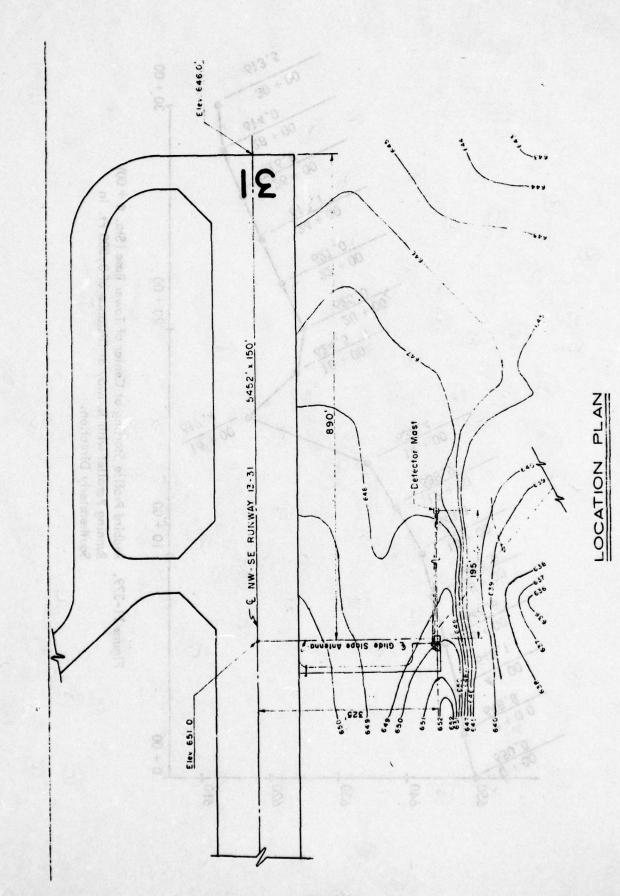
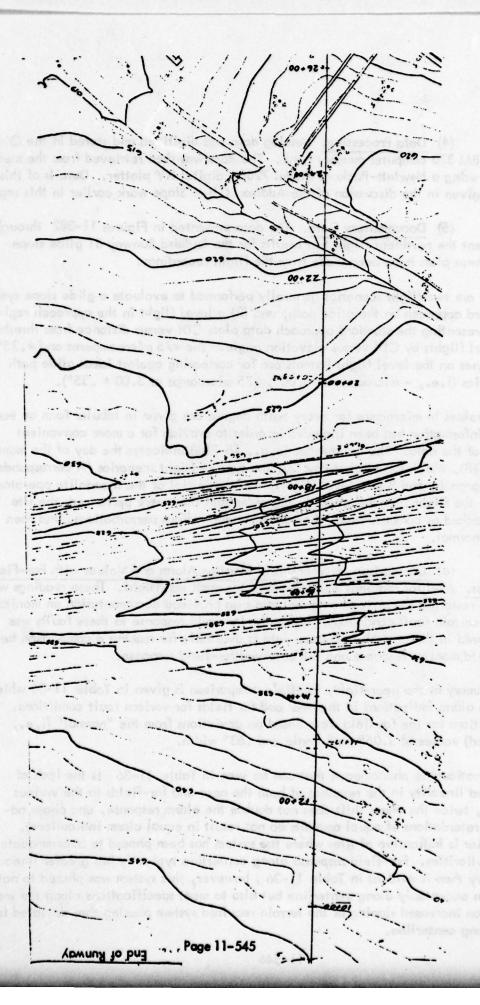


Figure 11-380. Topographical Map of Area Around Glide Slope Antennas at Redbird Airport.

100, 20, 0



Continuation of Topographical Map Showing Region in Front of Antennas Parallel to Centerline. Figure 11-381.

(4) <u>Data Processing</u>. Analog data was digitized and stored in the Ohio University IBM 370 computer memory bank. The data was then retrieved from the memory and plotted using a Hewlett-Packard Model 7203A digital XY plotter. Details of this process are given in the discussion of the Addison Glide Slope work earlier in this report.

(5) Documentary Data. The data presented in Figures 11-382 through 11-466 represent the pertinent flight test results for the Redbird Runway 31 glide slope facility. These plots have been made from the flight recordings.

There are two flight scenarios generally performed to evaluate a glide slope system: (1) a standard approach on the glide path, and (2) a level flight in the approach region. The graph presenting the standard approach data plots CDI versus distance from threshold, and the level flights by CDI versus elevation angle. The ± 75 microamperes and $\pm .35^{\circ}$ reference lines on the level flight formats are for comparing against ideal glide path characteristics (i.e., - microamps at 3.00°, ± 75 microamps at 3.00 $\pm .35^{\circ}$).

CDI values in microamps for every tenth degree are given in tabular form on each plot. This information has been included in order to provide for a more convenient comparison of the data. The run number (e.g., 18-2BR) indicates the day of the month of the test (18), which run on that day (2), the type of flight scenarios (A corresponds to a normal approach, and B to a level flight), and the initial of the theodolite operator. The plots of the flight tests are given in the order that they were performed; the site was first checked as commissioned, then tested under various perturbations, and then returned to normal.

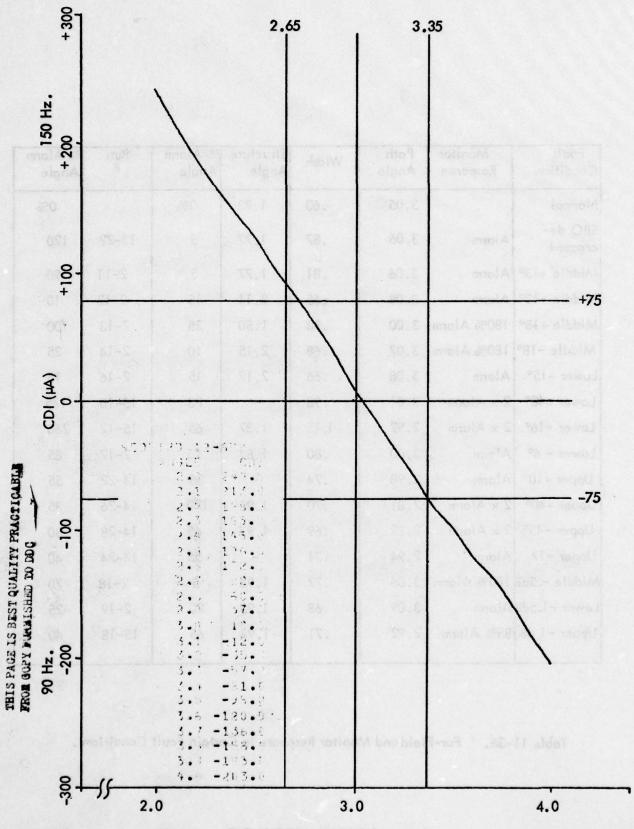
(6) Comparison of Near-Field Monitor Alarm and Values with Far-Field Observations. Monitor readings were recorded for each test flight. These readings were useful when restoring the system to normal and also provided documentation on monitor response to certain fault conditions. Since the far-field response to these faults was being measured in the air, all necessary data is available for making a comparison between the near-field monitor response and the observed far-field response.

A summary of the near-field, far-field comparison is given in Table 11-36 which presents the alarm indications in the near and far fields for various fault conditions. The alarm conditions for the far field were based on deviations from the "normal" (i.e., commissioned) values of 3.05° path angle and .63° width.

One noticeable phenomenon that can be seen in Table 11-36 is the lack of symmetry and linearity in the response of both the near and far-fields to the various faults (i.e., twice the phase shift does not double the alarm response, and phase advances and retardations of equal amounts do not result in equal alarm indications). Such behavior is indicative of sites where the system has been phased to accommodate terrain peculiarities. Far-field response along centerline typically has greater linearity and symmetry than is evident in Table 11-36; however, this system was phased to not only perform acceptably along centerline but also to meet specifications along the west side where an increased sloping of the terrain required system phasing that deviated from optimum along centerline.

Fault Condition	Monitor Response	Path Angle	Width	Structure Angle	% Alarm Angle	Run #	% Alarm Angle
Normal		3.05	.63	1.93	0%		0%
SBO de- creased	Alarm	3.06	.87	1.77	5	13-22	120
Middle +13°	Alarm	3.06	.81	1.77	5	2-11	90
Middle -13°	Alarm	3.08	.65	2.11	15	2-12	10
Middle +18°	180% Alarm	3.00	.93	1.50	25	2-13	100
Middle -18°	180% Alarm	3.07	.68	2.15	10	2-14	25
Lower +15°	Alarm	3.08	.66	2.17	15	2-16	15
Lower +40°	2 x Alarm	3.01	.98	-	20	15-10	175
Lower -16°	2 x Alarm	2.92	1.15	1.37	65	15-12	260
Lower - 6°	Alarm	3.00	.80	1.84	25	2-17	85
Upper +10°	Alarm	2.98	.74	-	35	14-22	55
Upper +40°	2 x Alarm	2.81	.70	1.95	120	14-26	35
Upper -45°	2 x Alarm	2.92	.69	1.97	65	14-28	30
Upper -17	Alarm '	2.94	.71	-	55	14-24	40
Middle5dB	180% Alarm	3.06	.77	1.93	5	2-18	70
Lower -1.5dB	Alarm	3.09	.68	1.95	20	2-19	25
Upper -1 dB	85% Alarm	2.92	.71	1.94	65	15-18	40

Table 11-36. Far-Field and Monitor Response to Certain Fault Conditions.



ELEVATION ANGLE (degrees)
Figure 11–382. Approach 12–6, Normal.

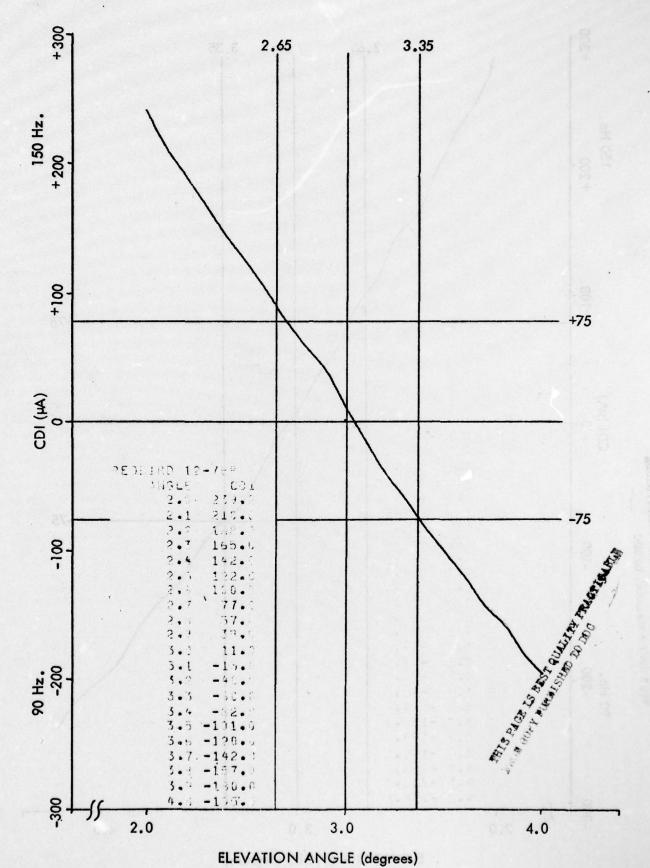


Figure 11-383. Approach 12-7, Normal.

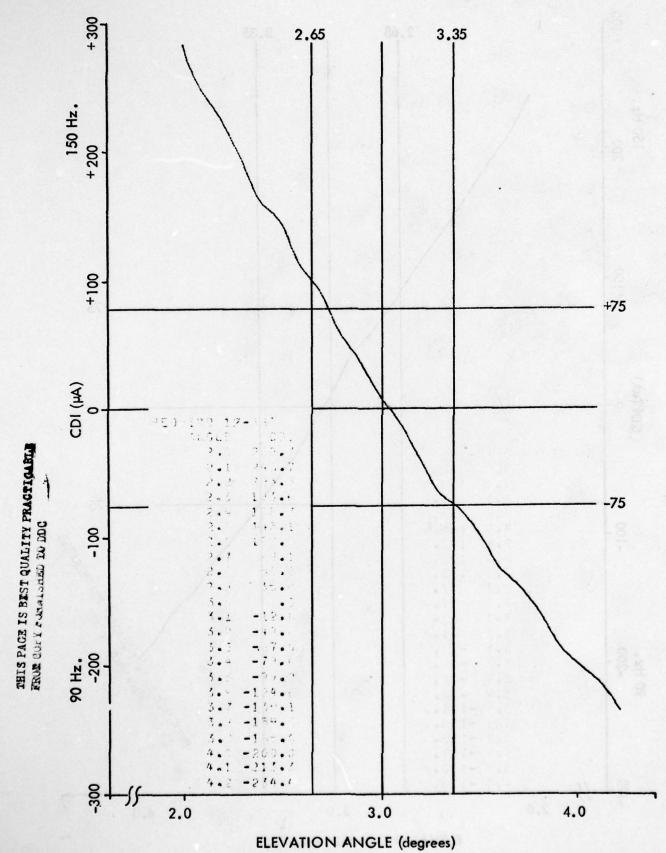


Figure 11-384. Approach 12-8, East Localizer Edge.

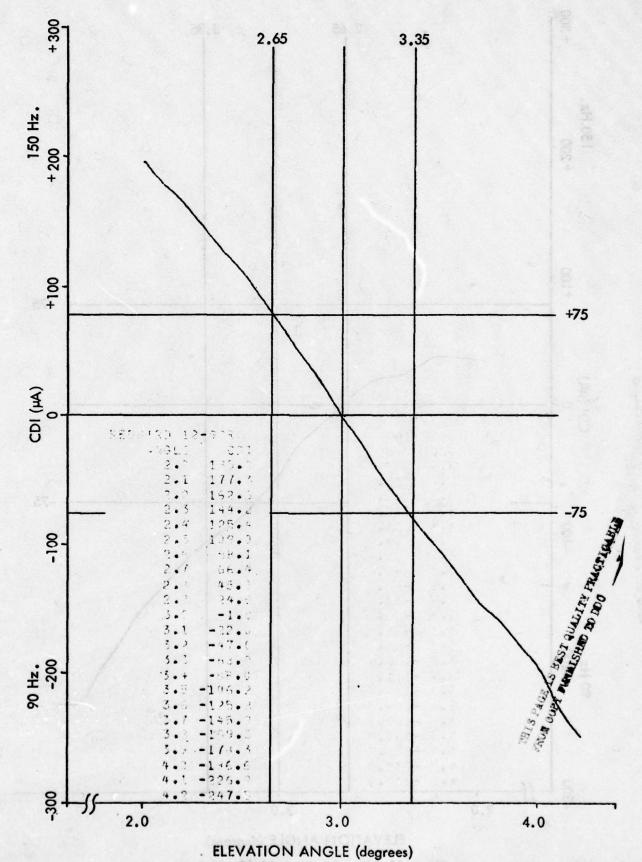


Figure 11-385. Approach 12-9, West Localizer Edge.

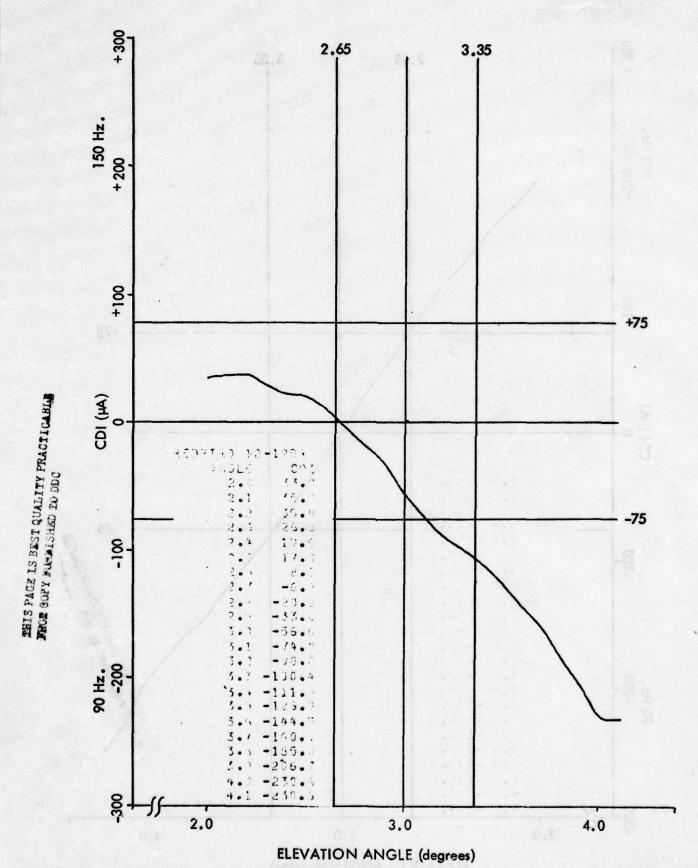


Figure 11-386. Approach 12-12, 8° East.

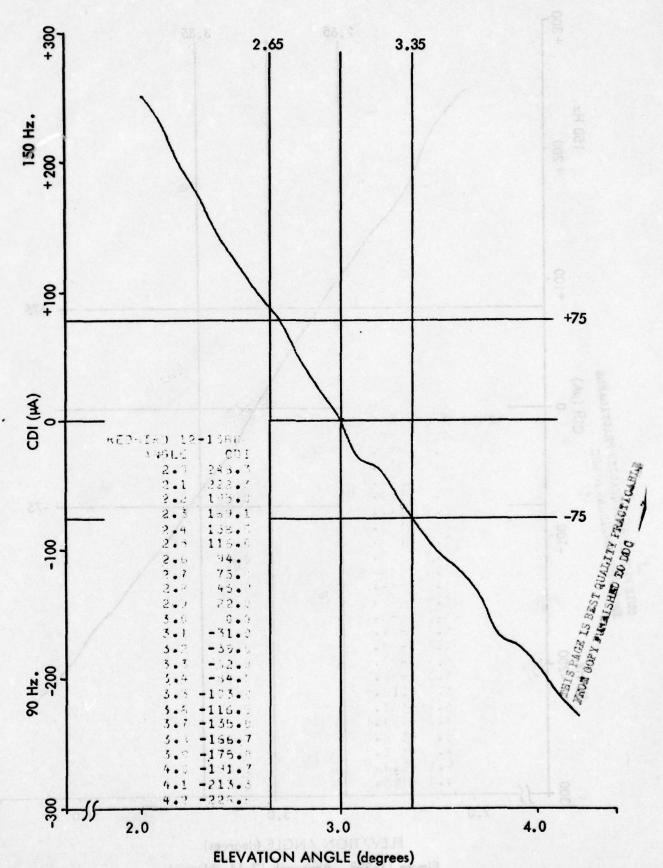


Figure 11-387. Approach 12-13, 8° West. 11-553

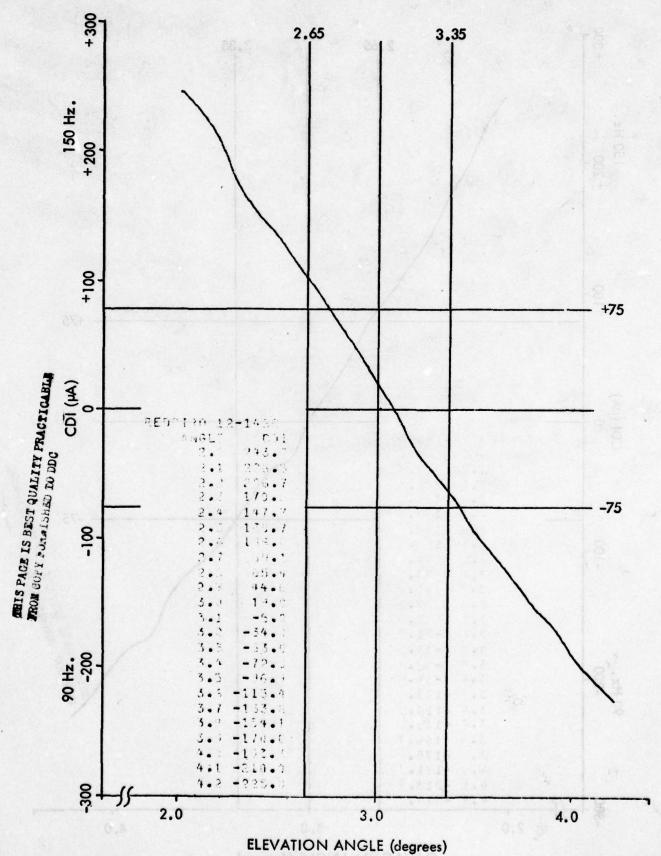
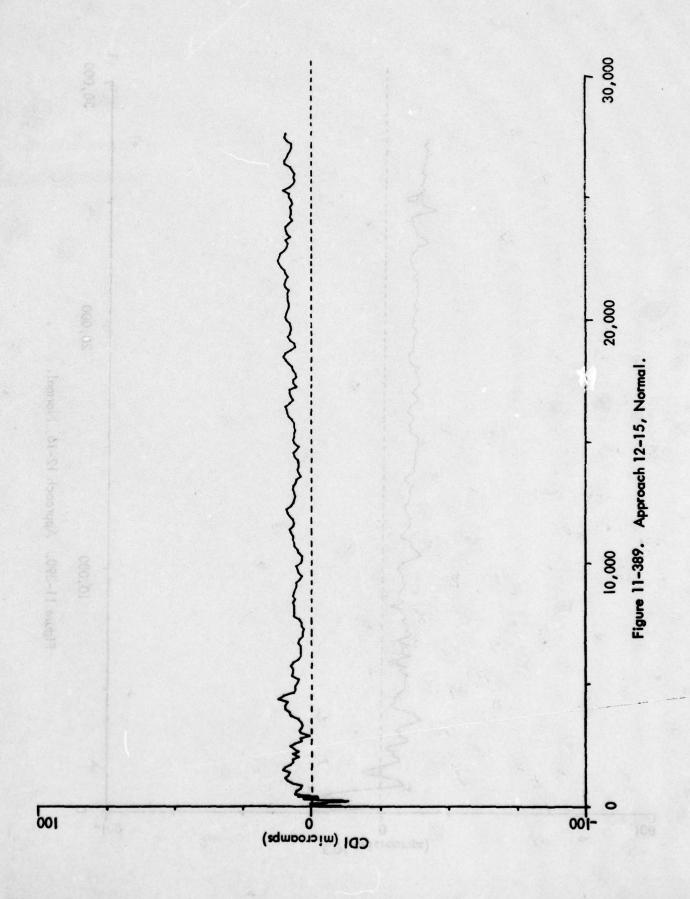
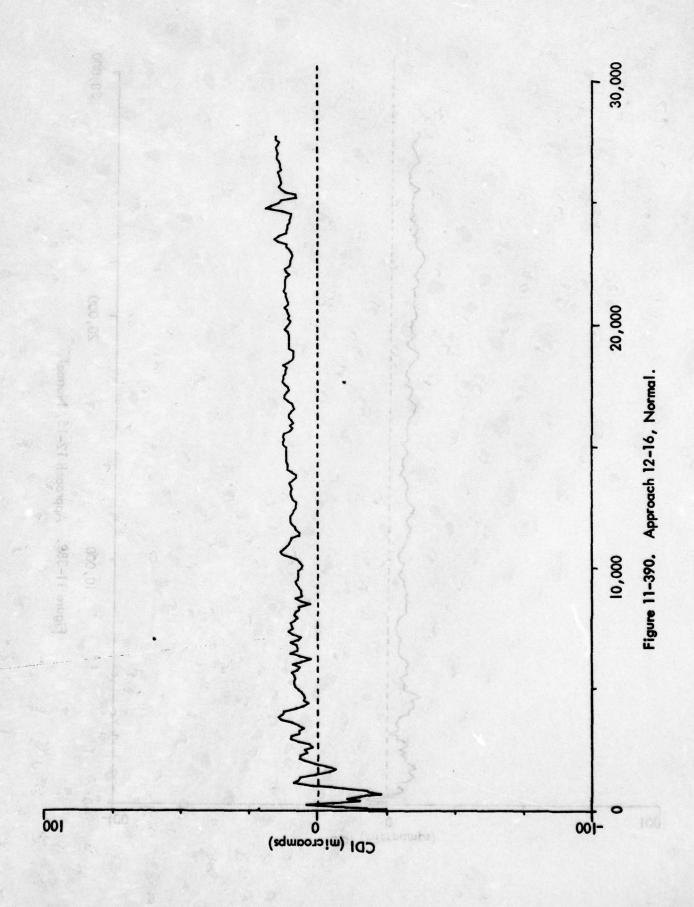
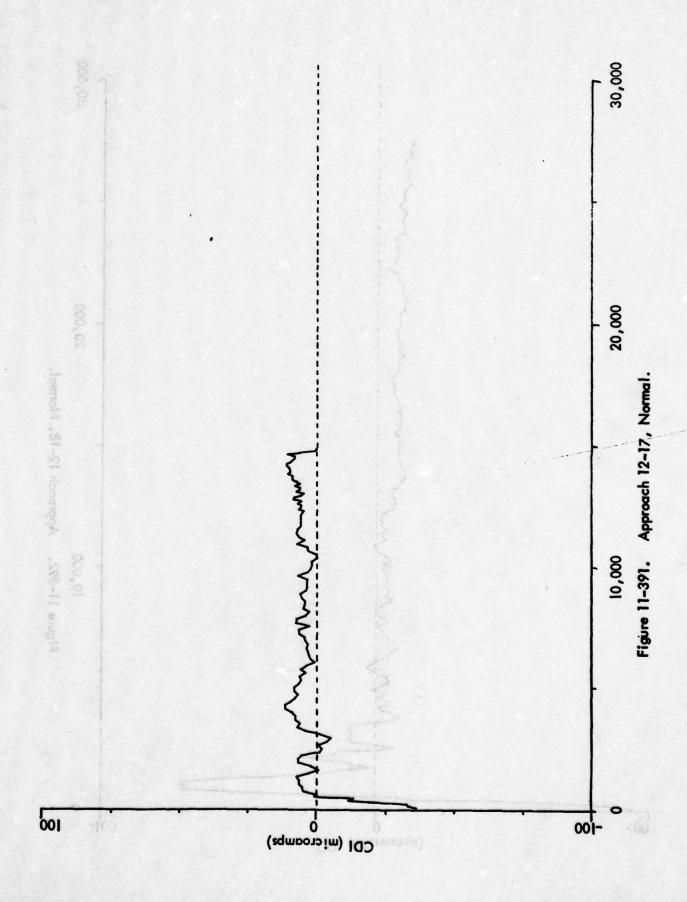
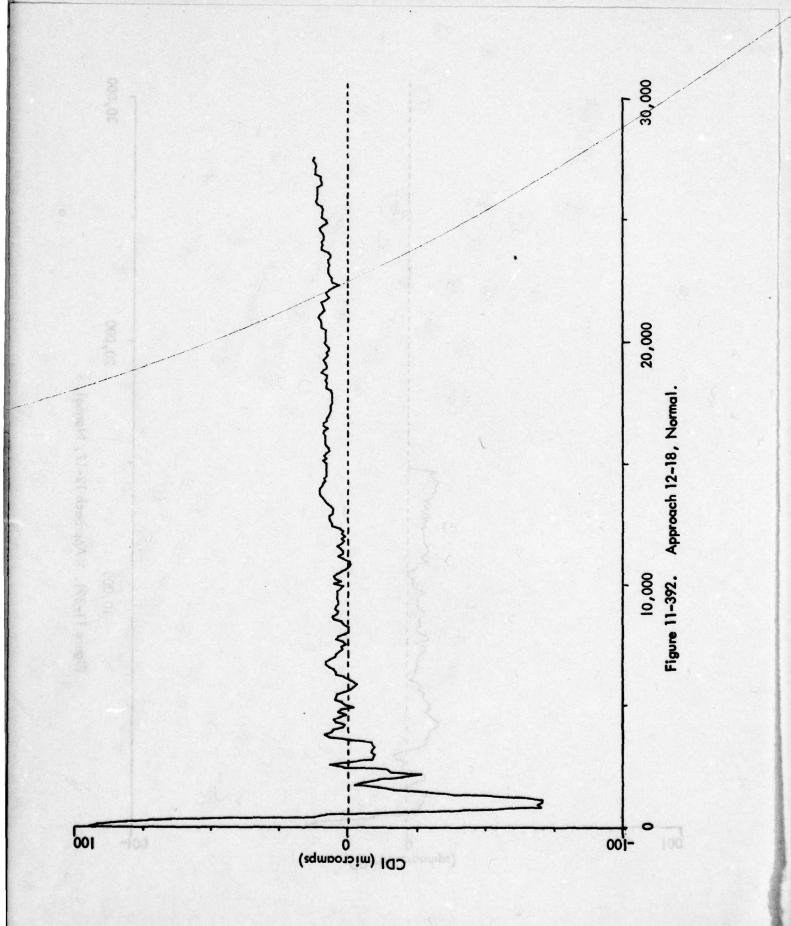


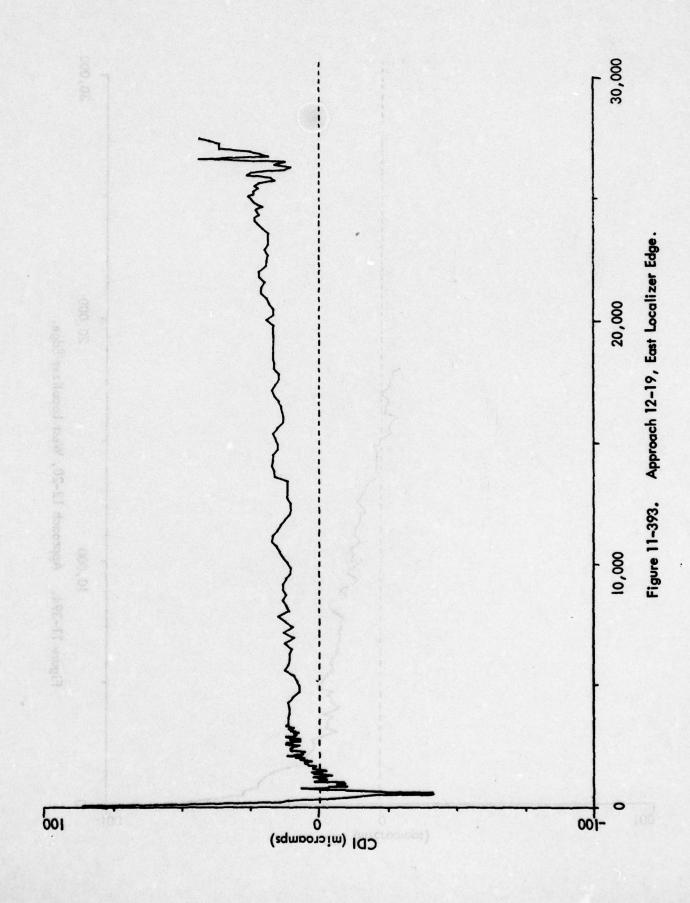
Figure 11-388. Approach 12-14, Normal.

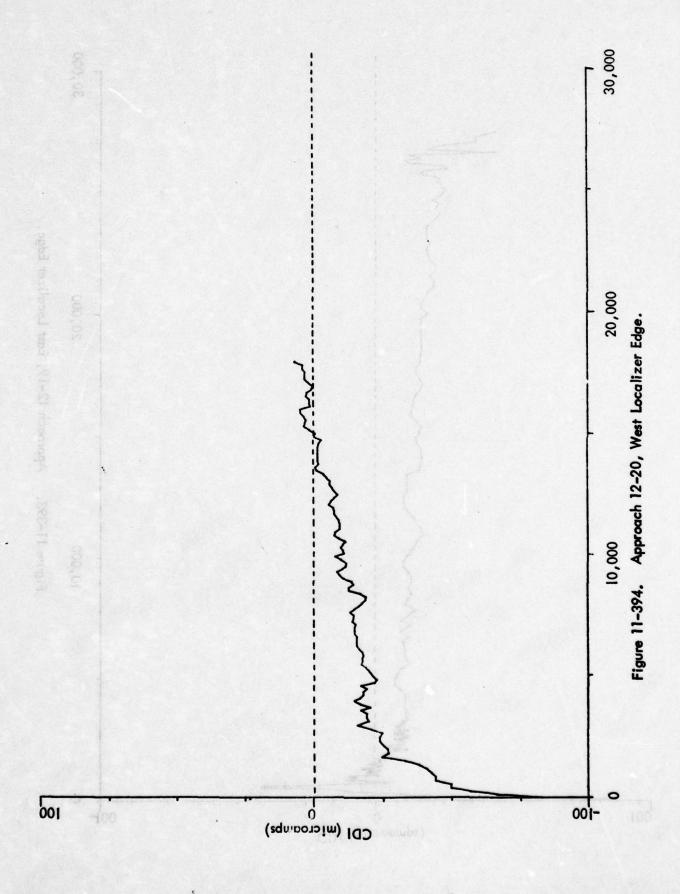


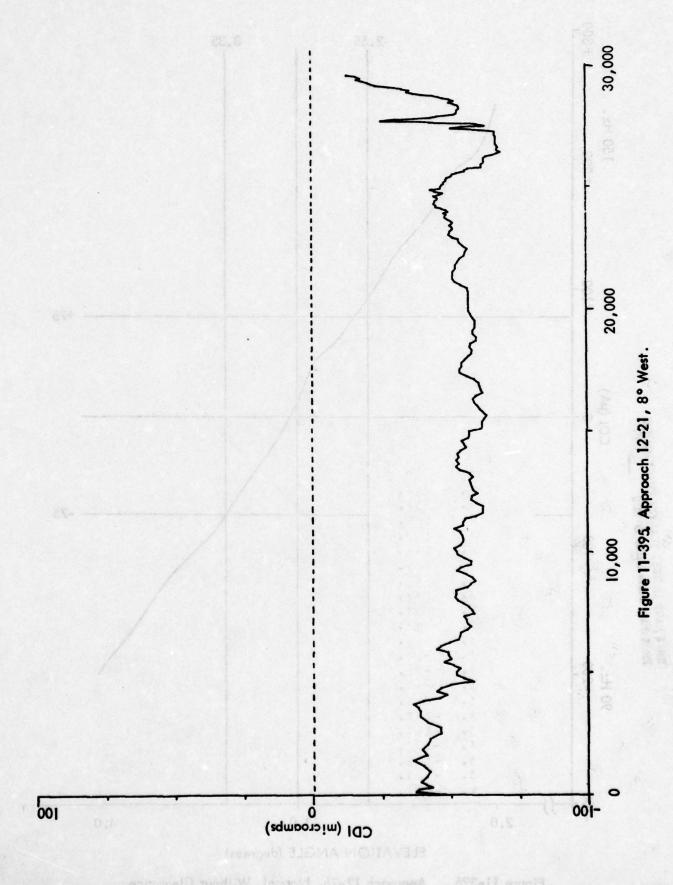












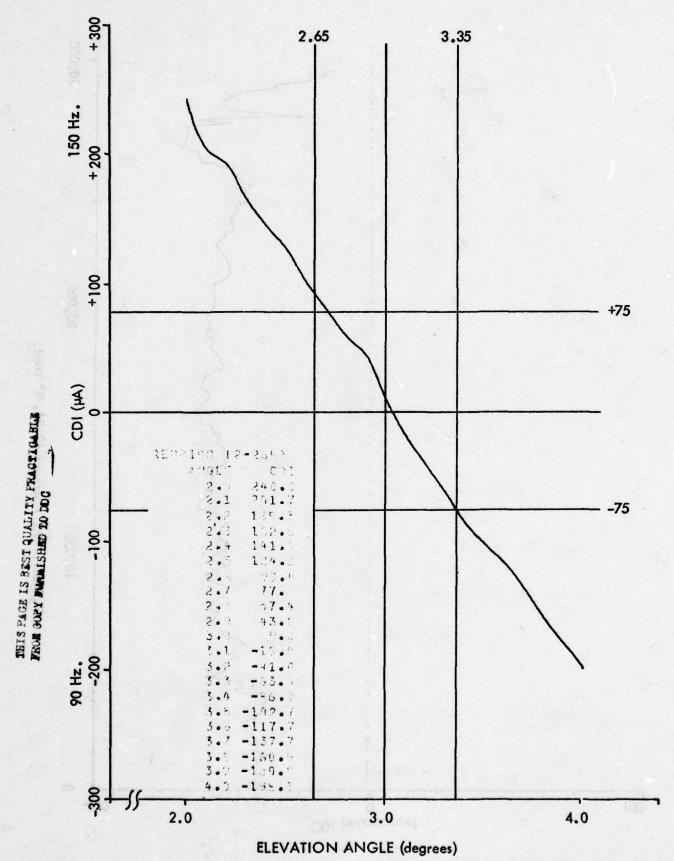
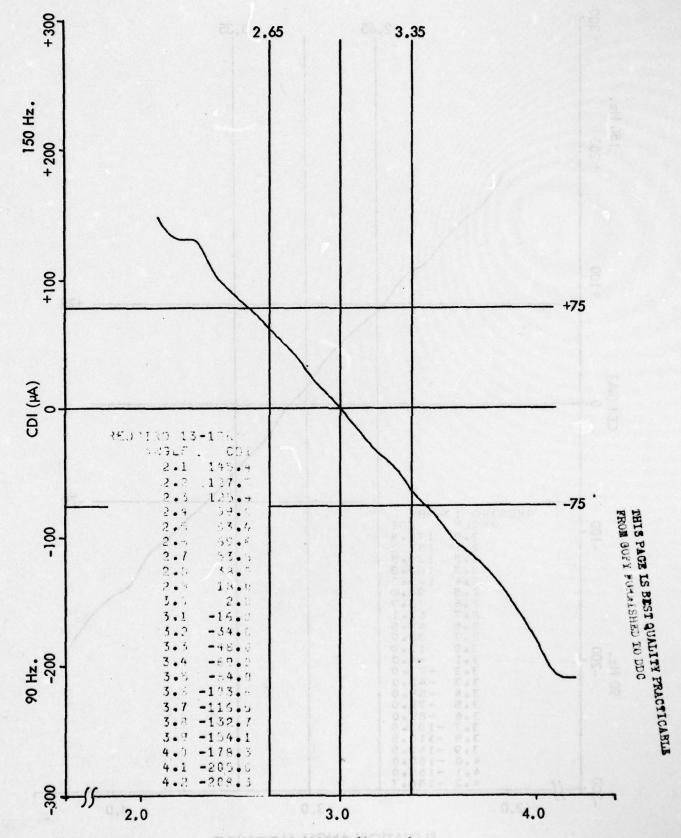


Figure 11-396. Approach 12-26, Normal, Without Clearance. 11-562



ELEVATION ANGLE (degrees)
Figure 11-397. Approach 13-1, Normal.

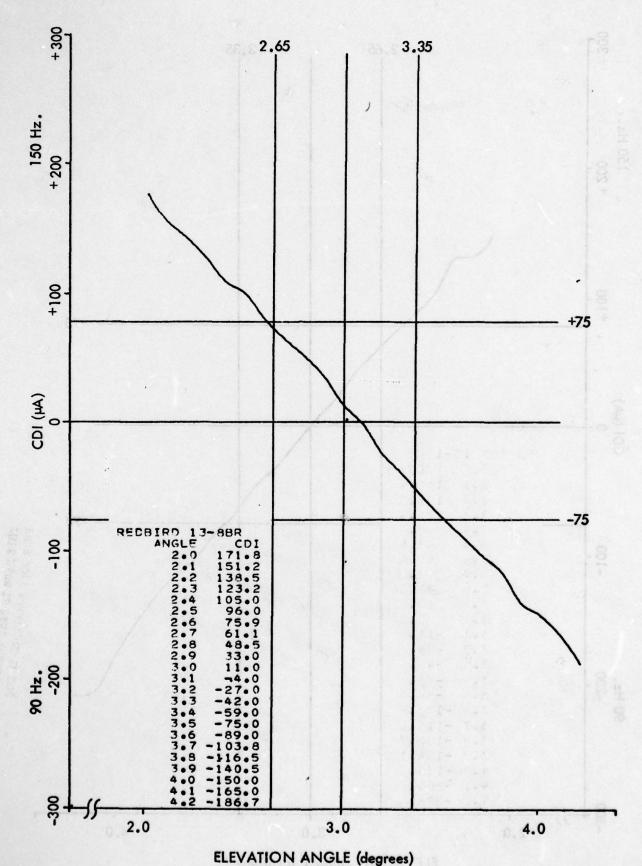
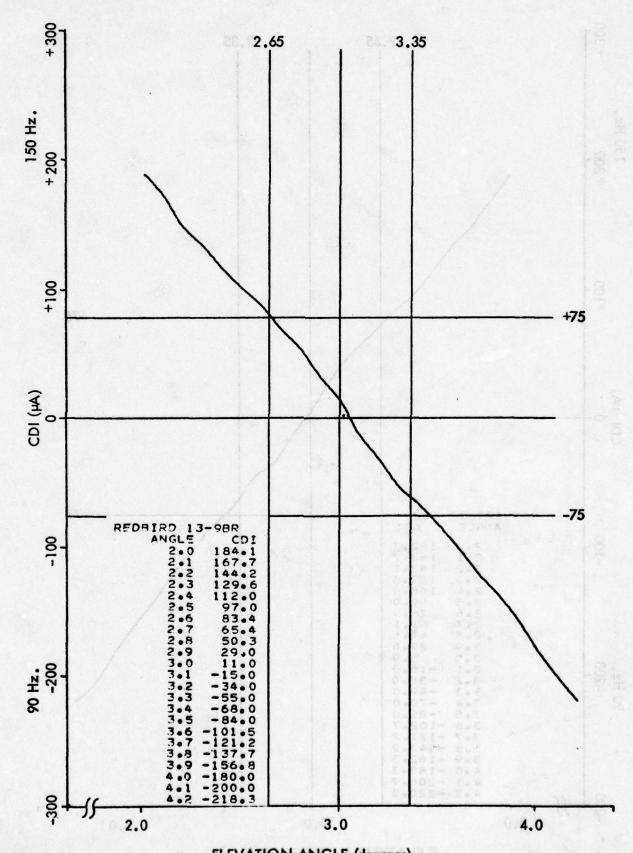


Figure 11-398, Approach 13-8, Normal.



ELEVATION ANGLE (degrees)
Figure 11-399. Approach 13-9, Increasing SBO.

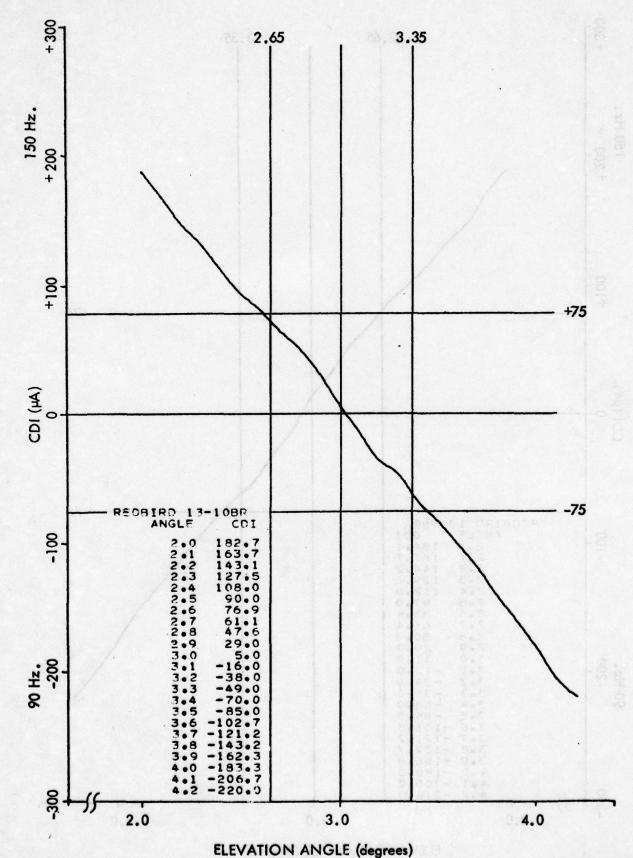
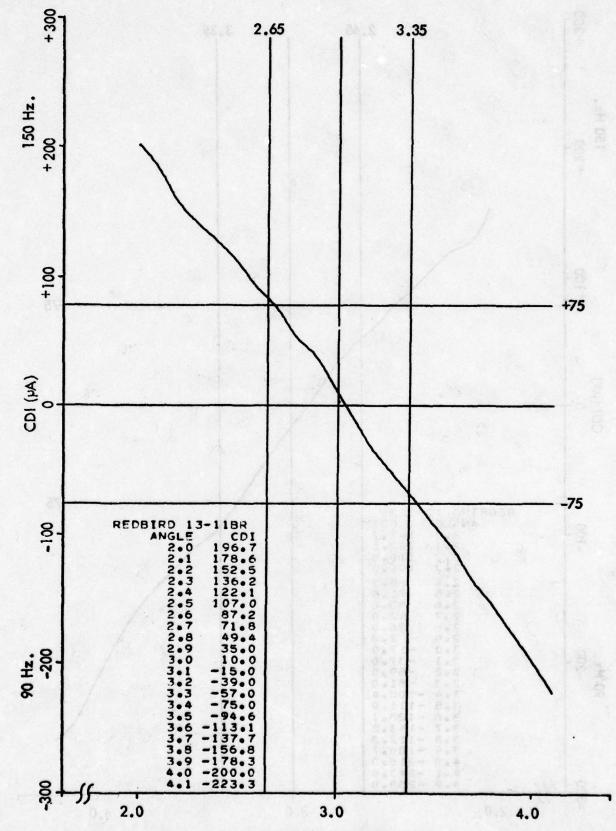
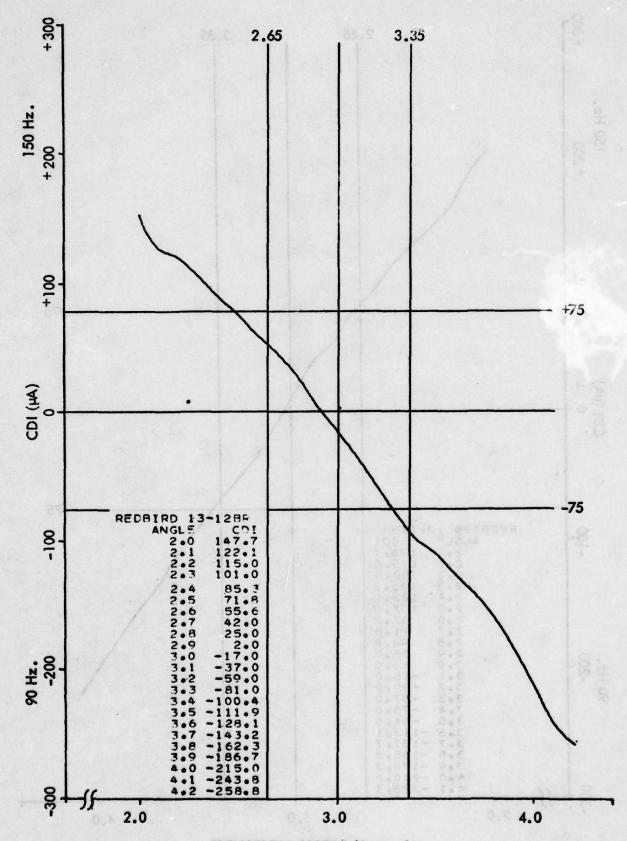


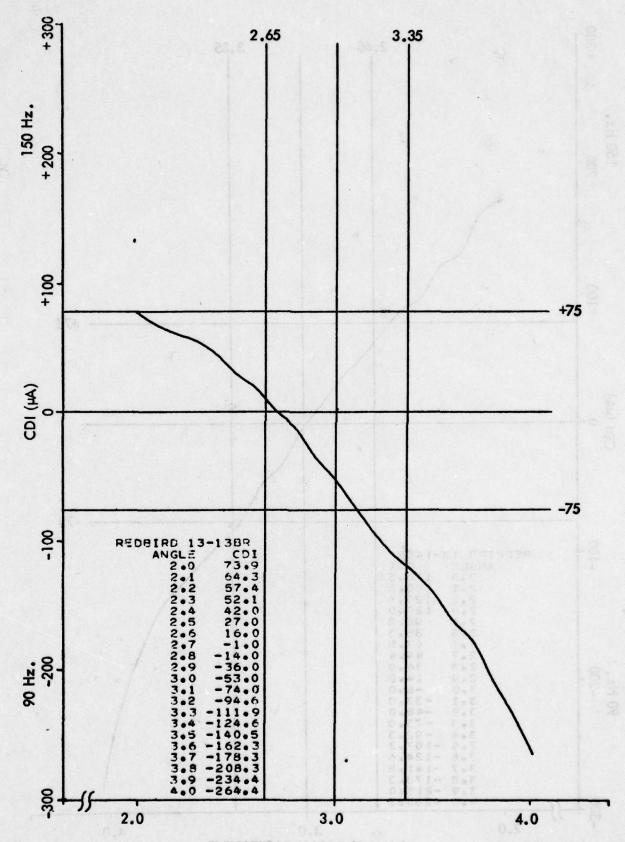
Figure 11-400, Approach 13-10, Increasing SBO. 11-566



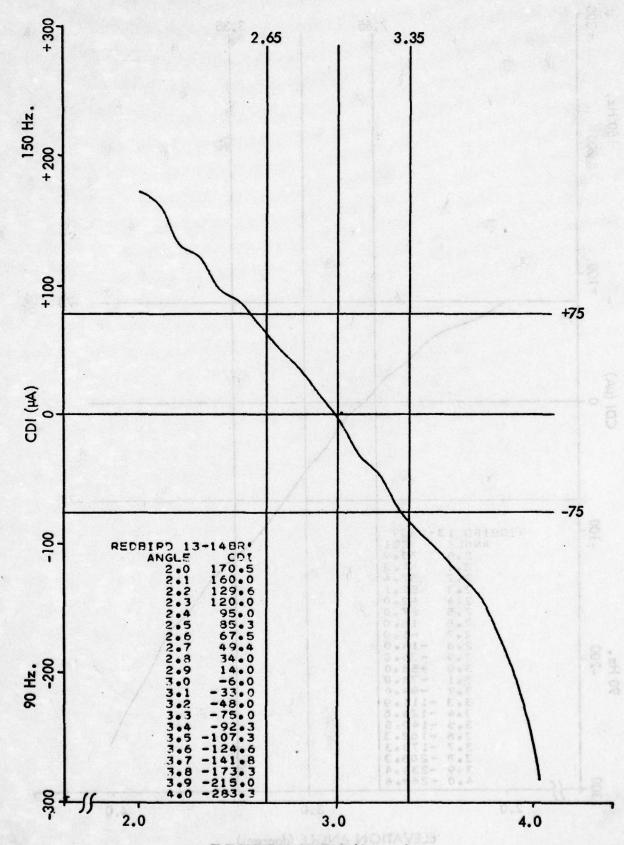
ELEVATION ANGLE (degrees)
Figure 11-401. Approach 13-11, Increasing SBO.
11-567



ELEVATION ANGLE (degrees)
Figure 11-402. Approach 13-12, 8° West.



ELEVATION ANGLE (degrees)
Figure 11–403. Approach 13–13, 8° West.



ELEVATION ANGLE (degrees)
Figure 11-404. Approach 13-14, 8° West.

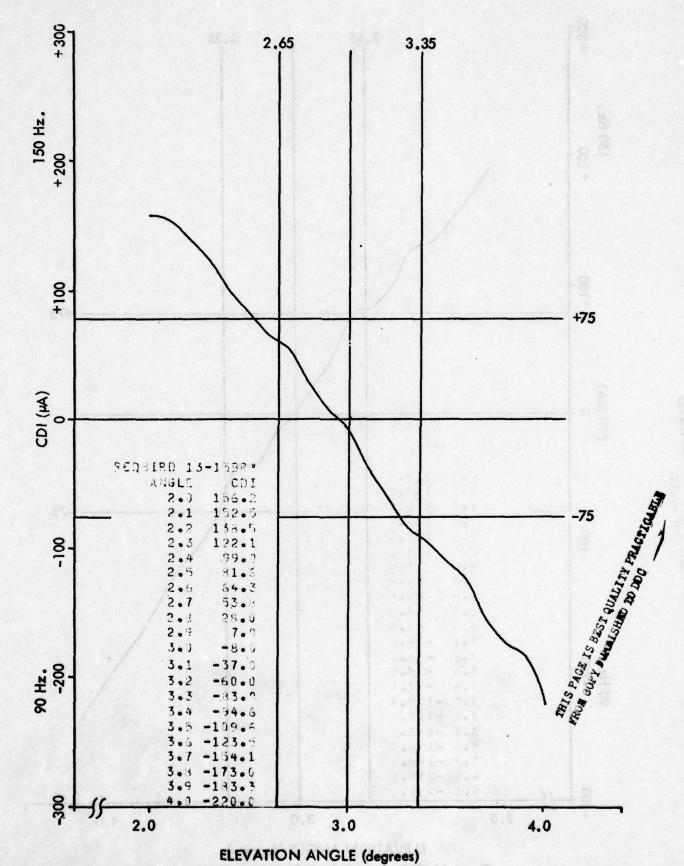
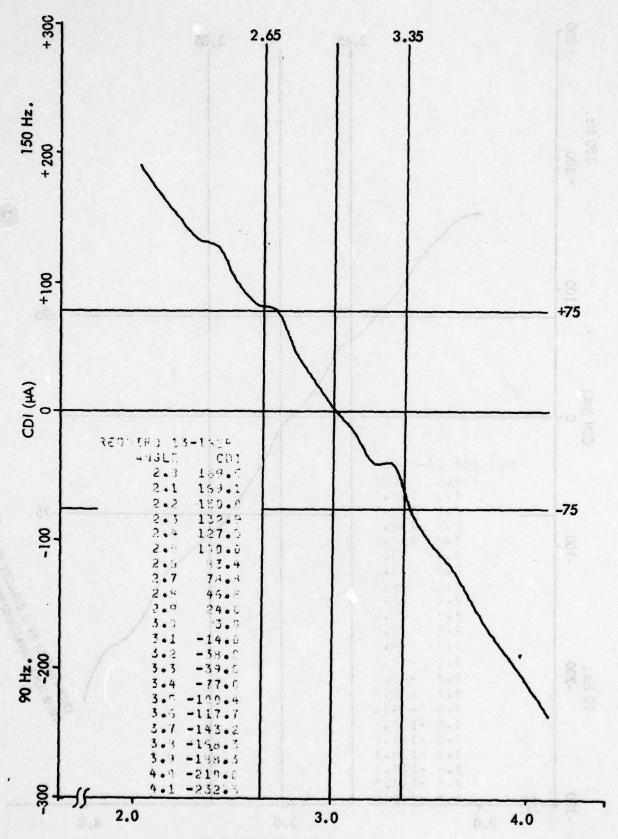
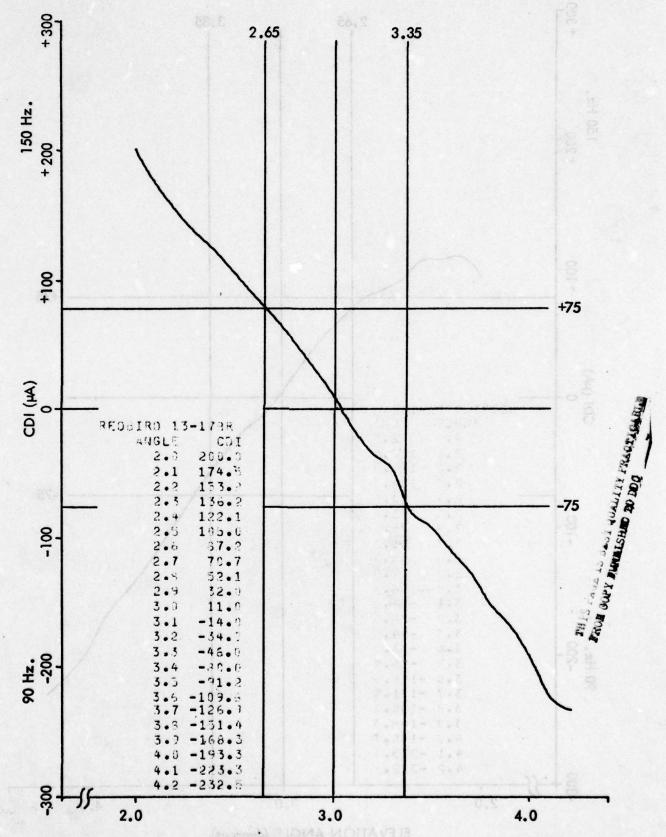


Figure 11-405. Approach 13-15, 8° West. 11-571



ELEVATION ANGLE (degrees)
Figure 11-406. Approach 13-16, Normal, Without Clearance.



ELEVATION ANGLE (degrees)
Figure 11-407. Approach 13-17, Normal.
11-573

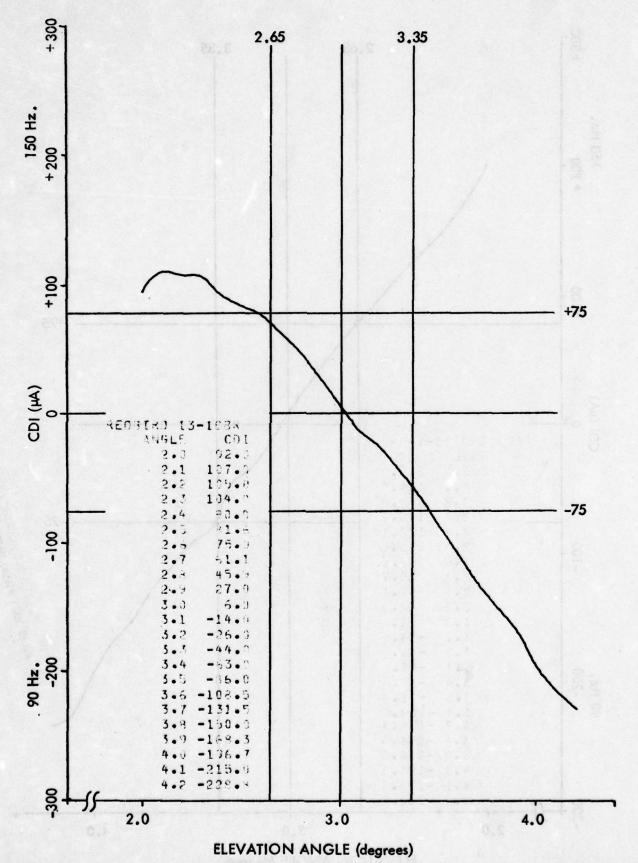
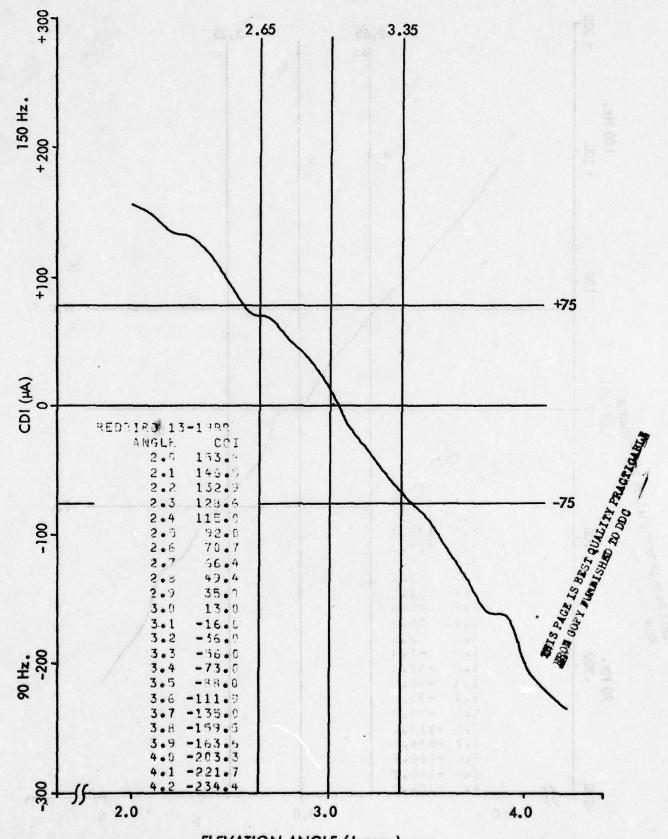
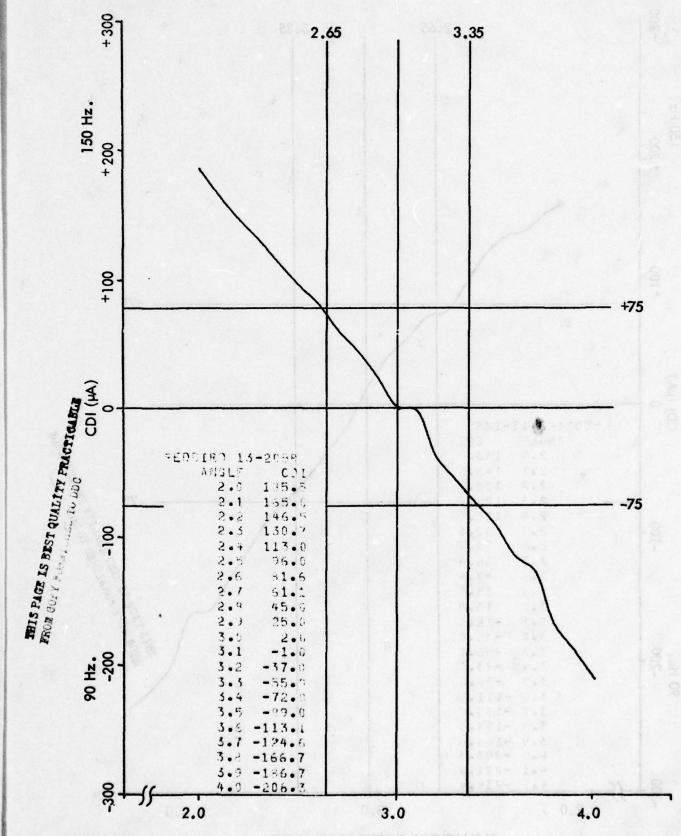


Figure 11–408. Approach 13–18, Middle Antenna Phase Retarded 15°. 11–574



ELEVATION ANGLE (degrees)
Figure 11-409. Approach 13-19, Middle Antenna Phase Retarded 12°.



ELEVATION ANGLE (degrees)
Figure 11-410. Approach 13-20, Normal.
11-576

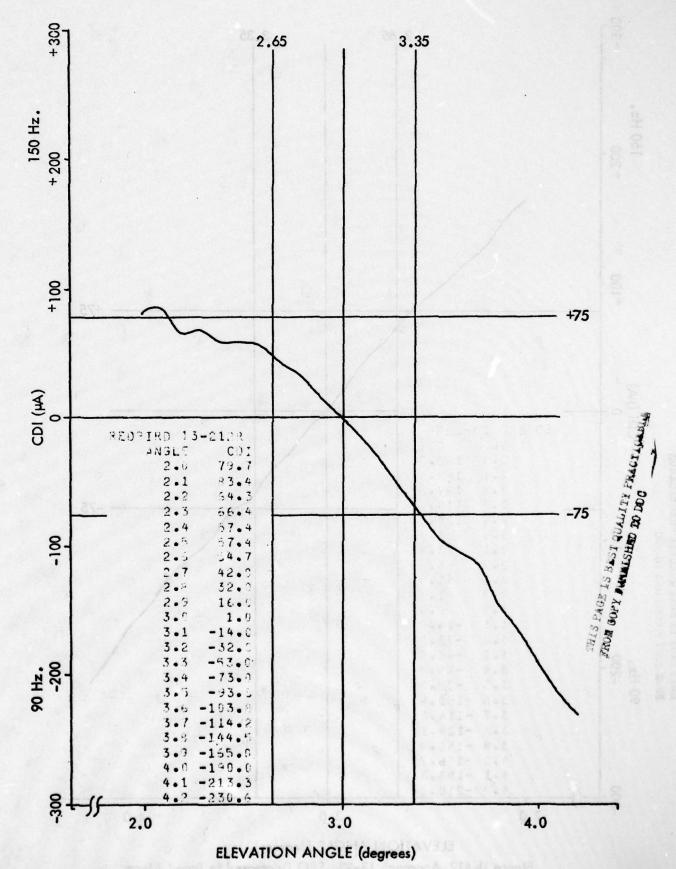
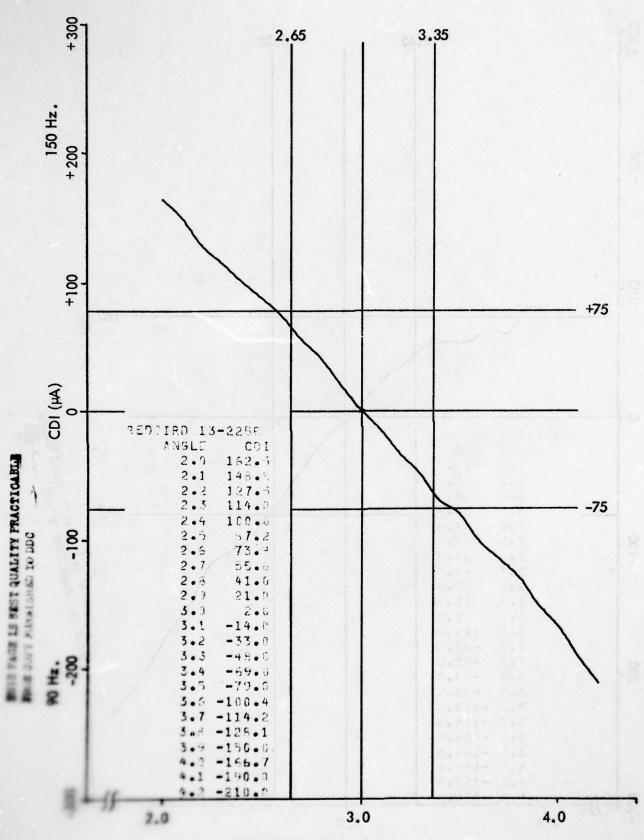


Figure 11-411. Approach 13-21, Middle Antenna Phase Advanced 12°. 11-577



ELEVATION ANGLE (degrees)

Marie 11-412 Approach 13-22, SBO Decreased to Broad Alarm.

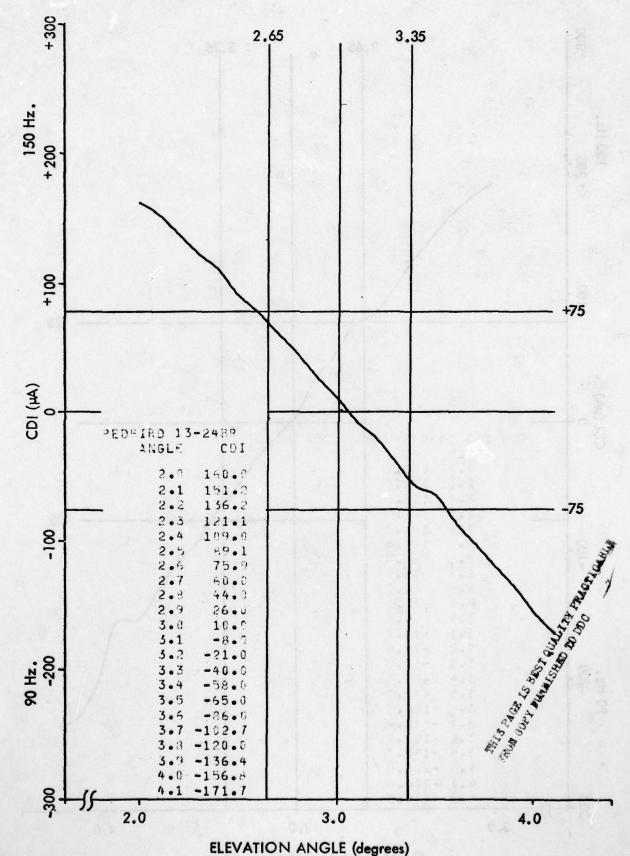
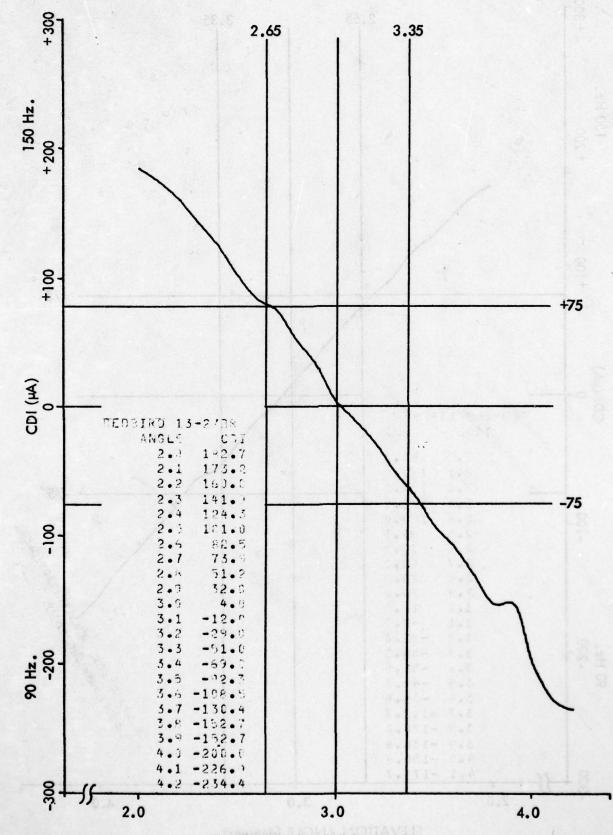
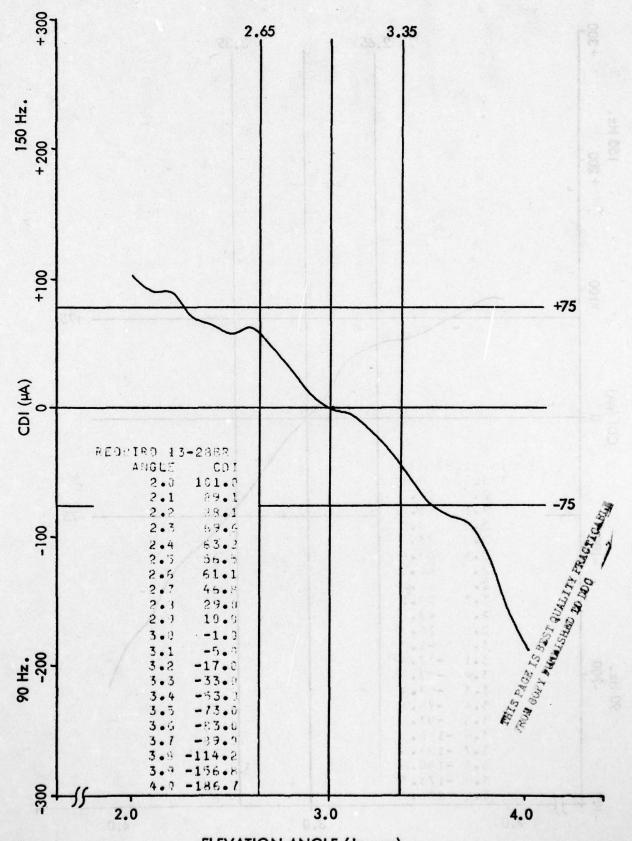


Figure 11-413. Approach 13-24, SBO Decreased to Broad Alarm.
11-579

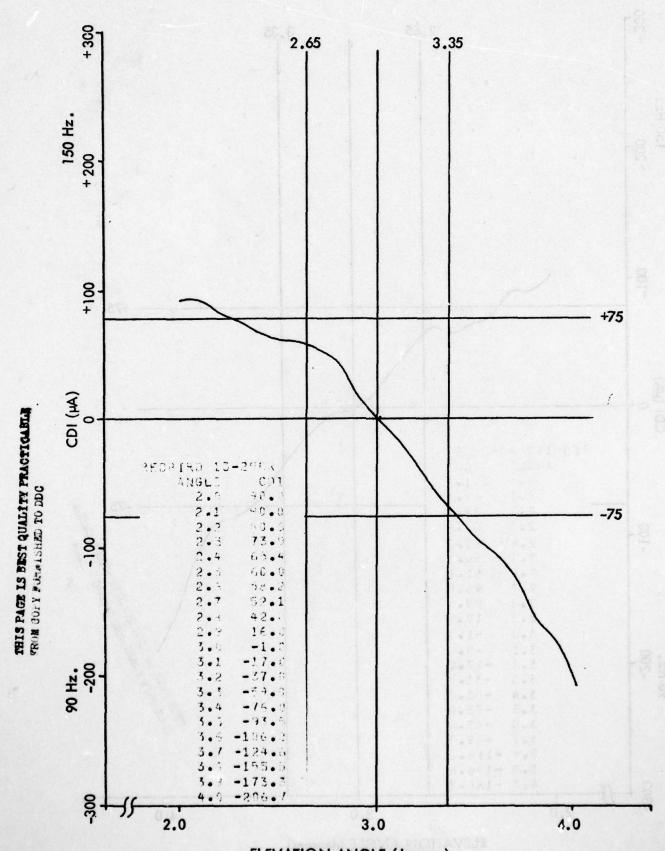


THIS PAGE IS BEST QUALITY PRACTICABLE FROM GOFY FURMISHED TO DDG

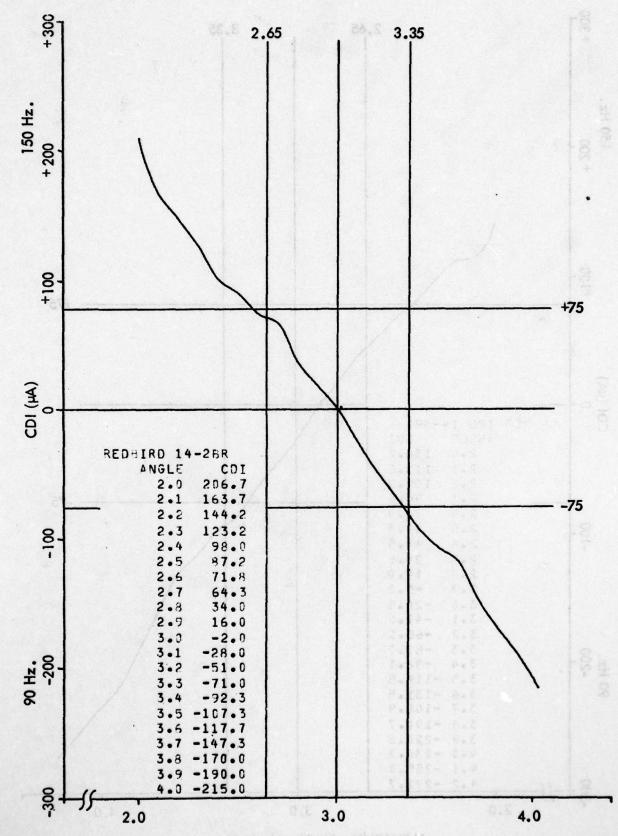
ELEVATION ANGLE (degrees)
Figure 11-414, Approach 13-27, Middle Antenna Phase Retarded 11°.



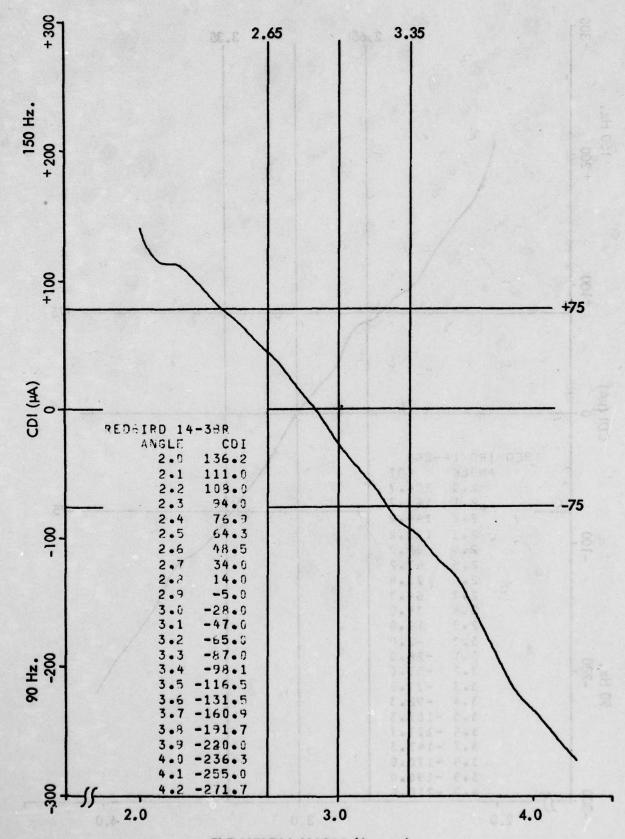
ELEVATION ANGLE (degrees)
Figure 11–415. Approach 13–28, Middle Antenna Phase Advanced 9°.



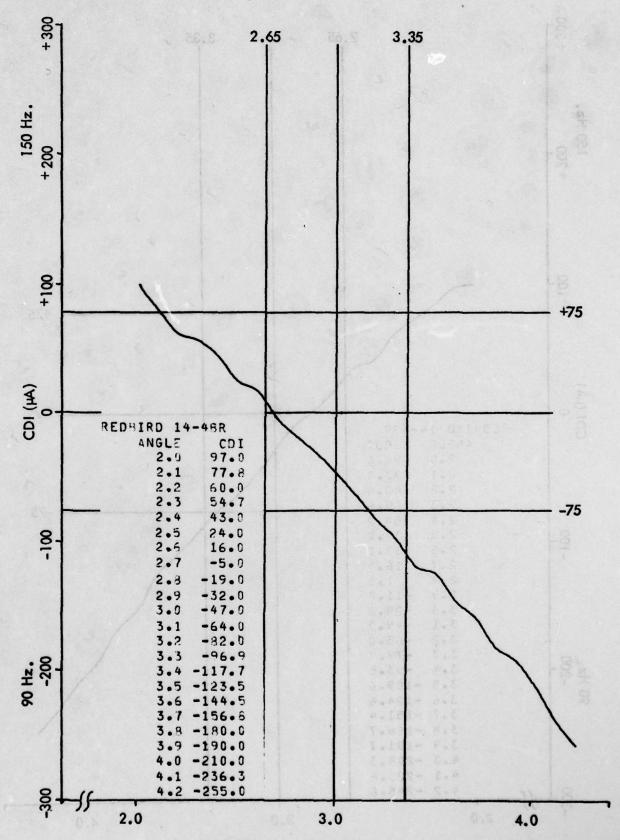
ELEVATION ANGLE (degrees)
Figure 11–416. Approach 13–29, Middle Antenna Phase Advanced 7°.



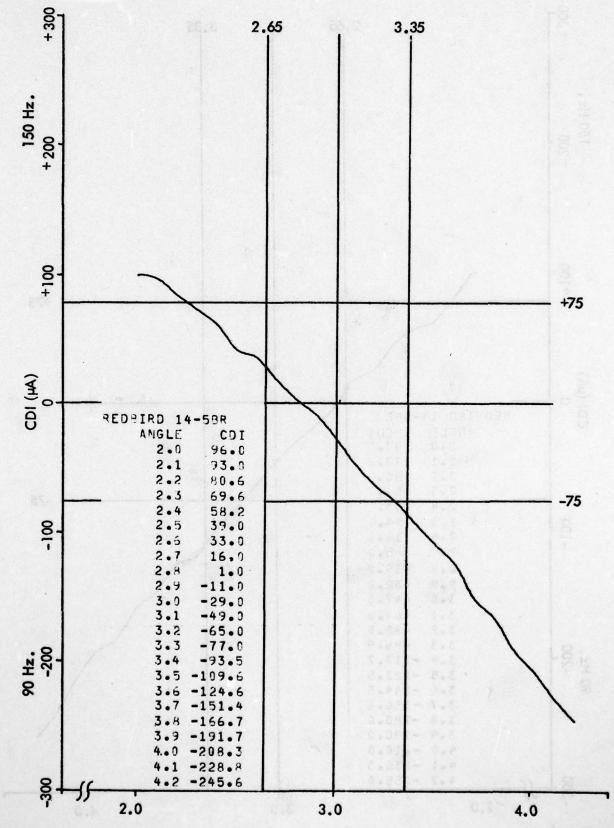
ELEVATION ANGLE (degrees)
Figure 11-417. Approach 14-2, Normal.



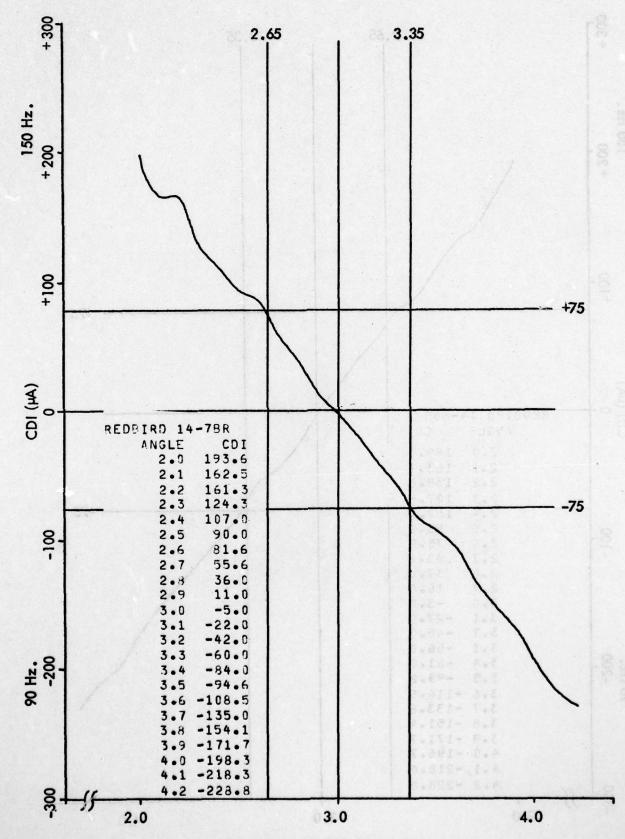
ELEVATION ANGLE (degrees)
Figure 11-418. Approach 14-3, 8° West.
11-584



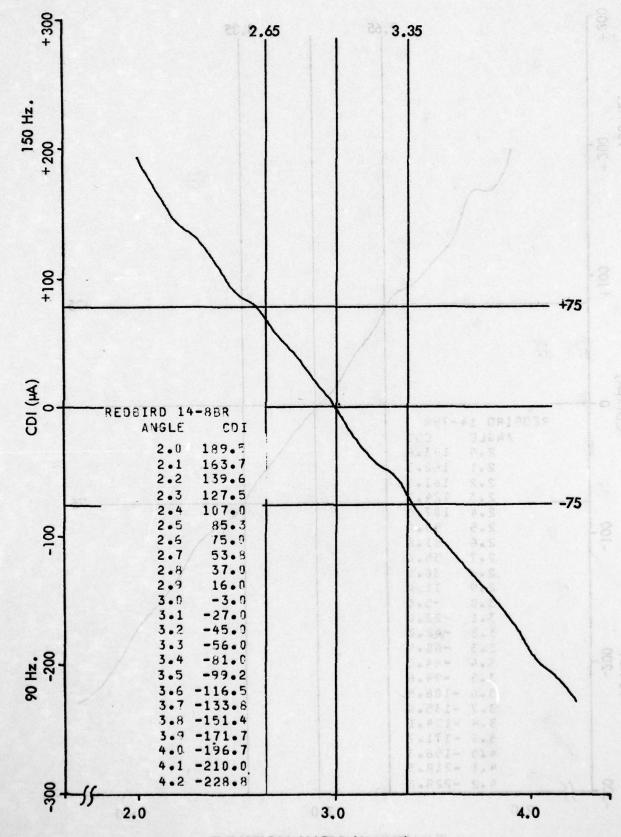
ELEVATION ANGLE (degrees)
Figure 11-419. Approach 14-4, 8° East.



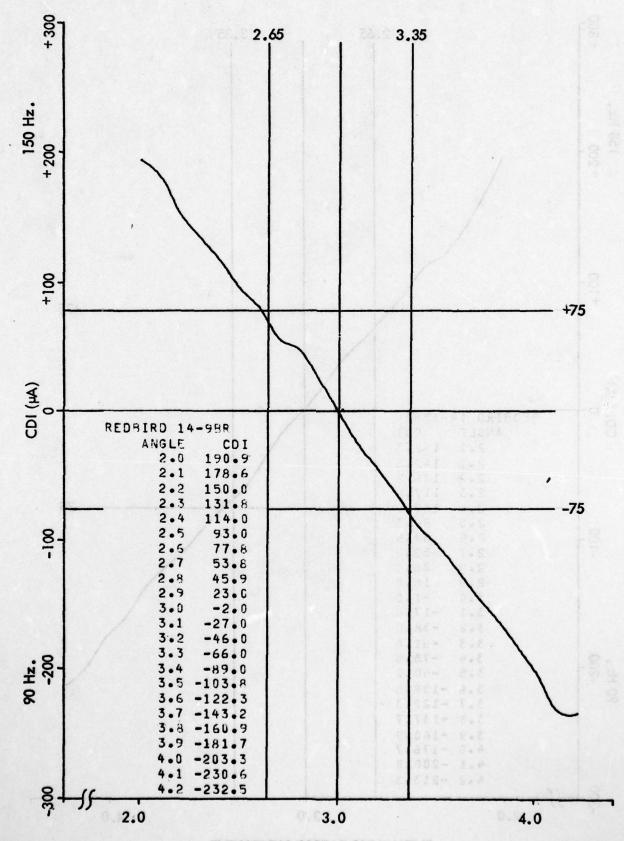
ELEVATION ANGLE (degrees)
Figure 11-420. Approach 14-5, 8° East.
11-586



ELEVATION ANGLE (degrees)
Figure 11-421. Approach 14-7, SBO Decreased to Broad Alarm.
11-587

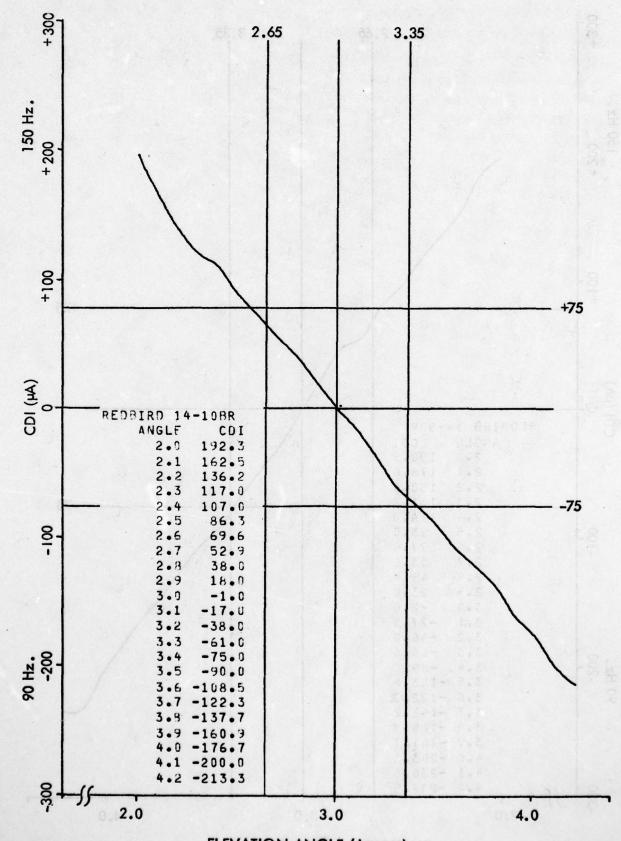


ELEVATION ANGLE (degrees)
Figure 11–422, Approach 14–8, SBO Decreased to Broad Alarm.

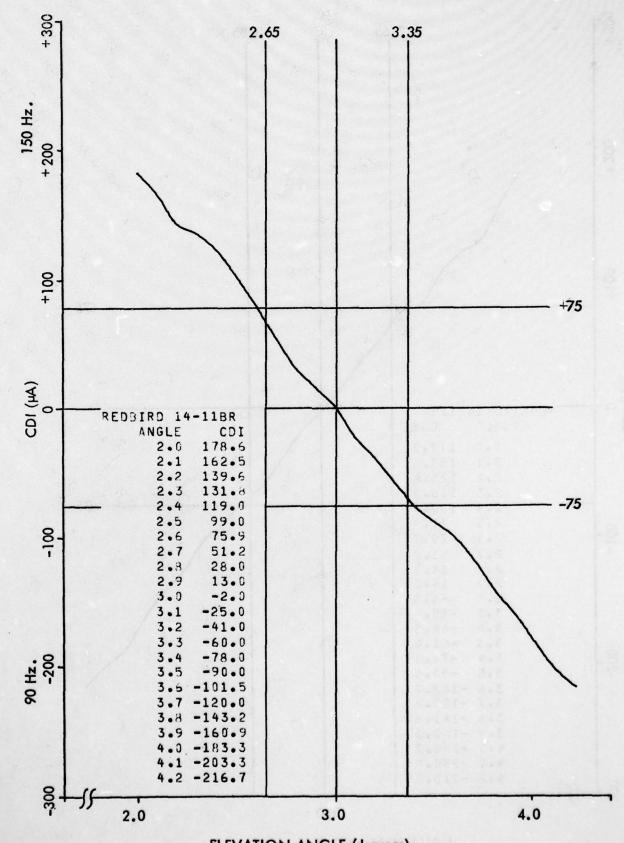


ELEVATION ANGLE (degrees)
Figure 11–423, Approach 14–9, Normal.

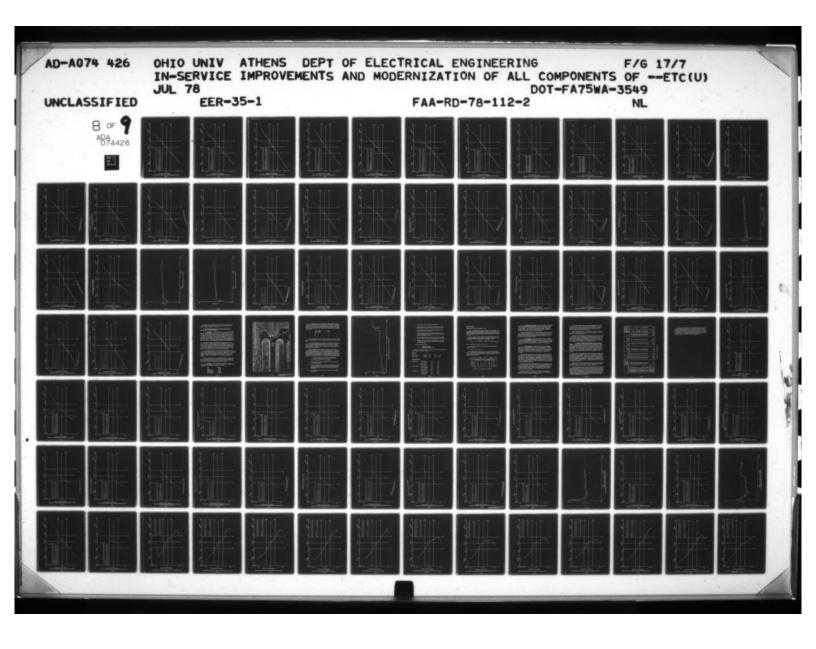
11–589



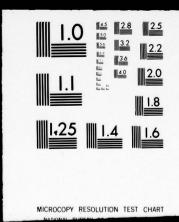
ELEVATION ANGLE (degrees)
Figure 11–424. Approach 14–10, SBO Decreased to Broad Alarm.

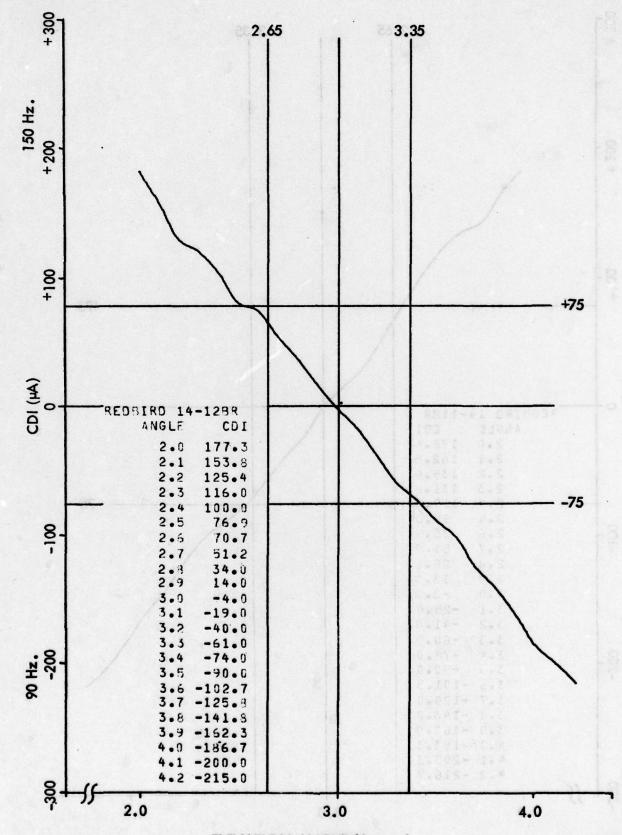


ELEVATION ANGLE (degrees)
Figure 11-425. Approach 14-11. SBO Decreased to Broad Alarm.

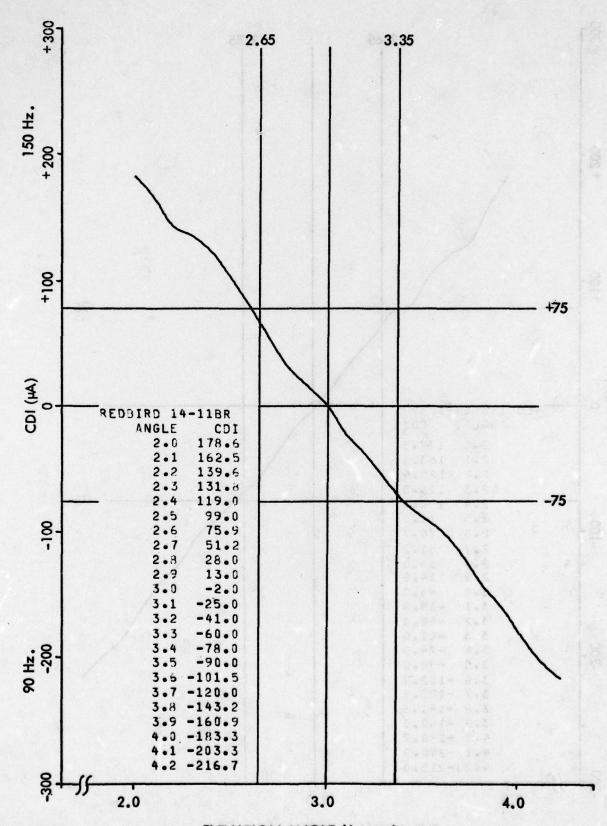


8 OF ADA ADA 6





ELEVATION ANGLE (degrees)
Figure 11-426. Approach 14-12, SBO Decreased to Broad Alarm.



ELEVATION ANGLE (degrees)
Figure 11-425. Approach 14-11. SBO Decreased to Broad Alarm.

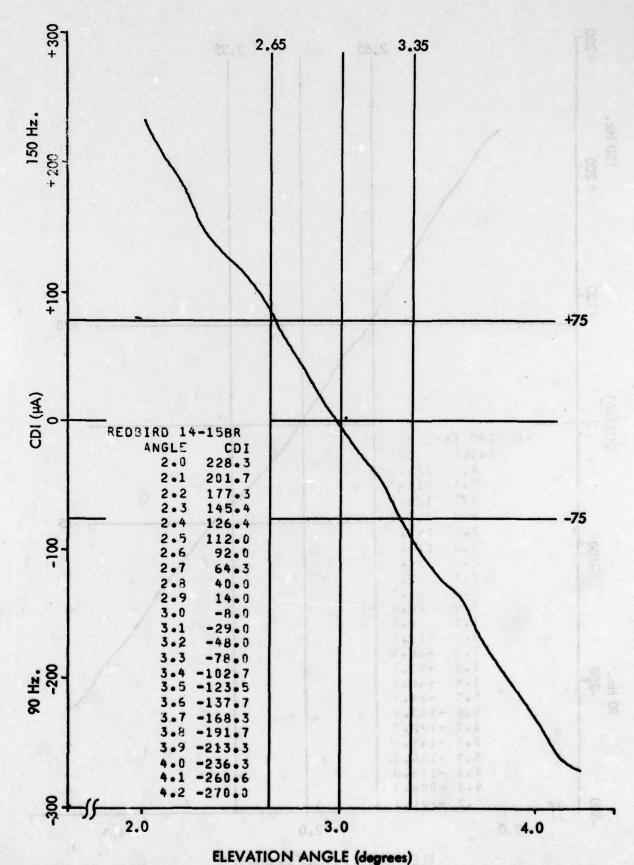


Figure 11-427. Approach 14-15, SBO Increased to Sharp Alarm.

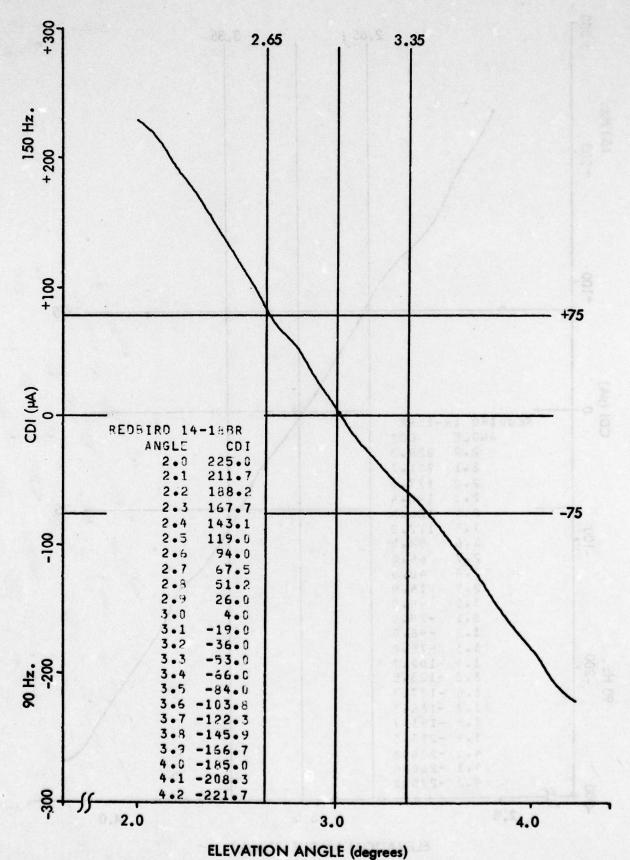
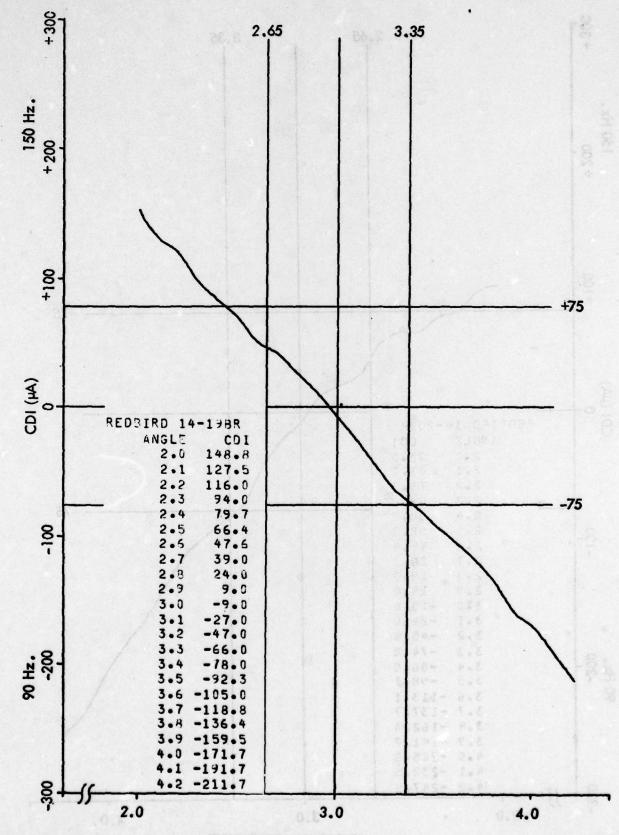
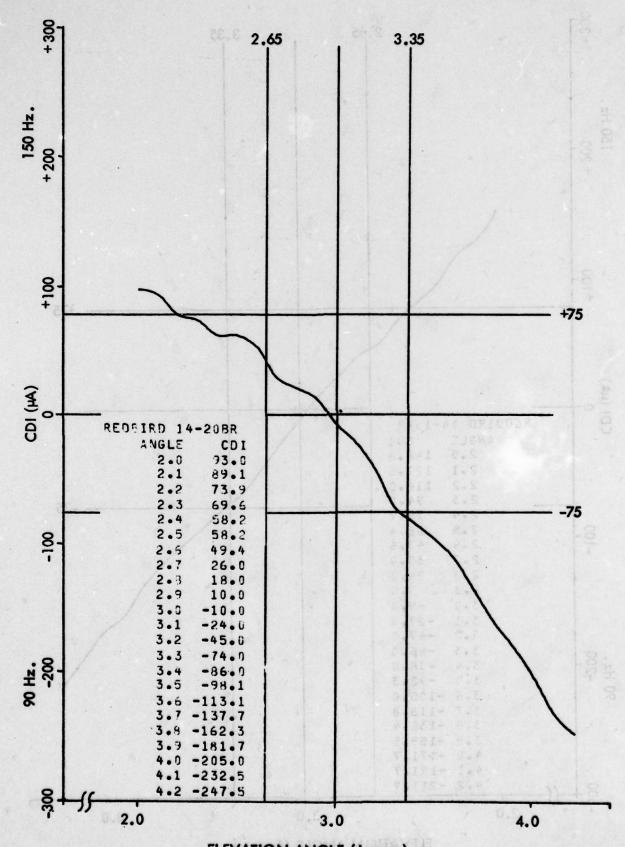


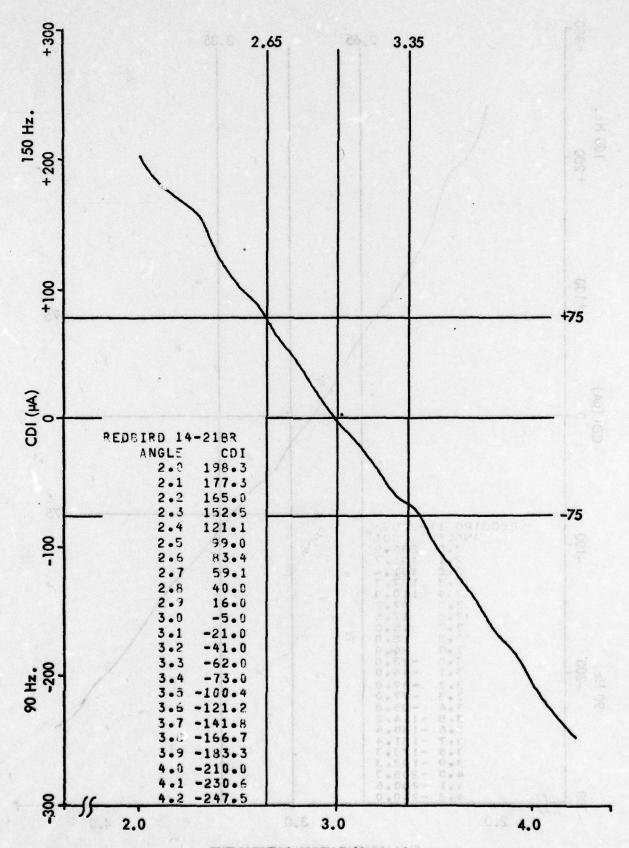
Figure 11-428. Approach 14-18, SBO Phase Retarded 30°.



ELEVATION ANGLE (degrees)
Figure 11-429. Approach 14-19, SBO Phase Advanced 30°.



ELEVATION ANGLE (degrees)
Figure 11-430. Approach 14-20, Middle Antenna Phase Advanced 8°.
11-596



ELEVATION ANGLE (degrees)
Figure 11–431. Approach 14–21, Middle Antenna Phase Retarded 8°.

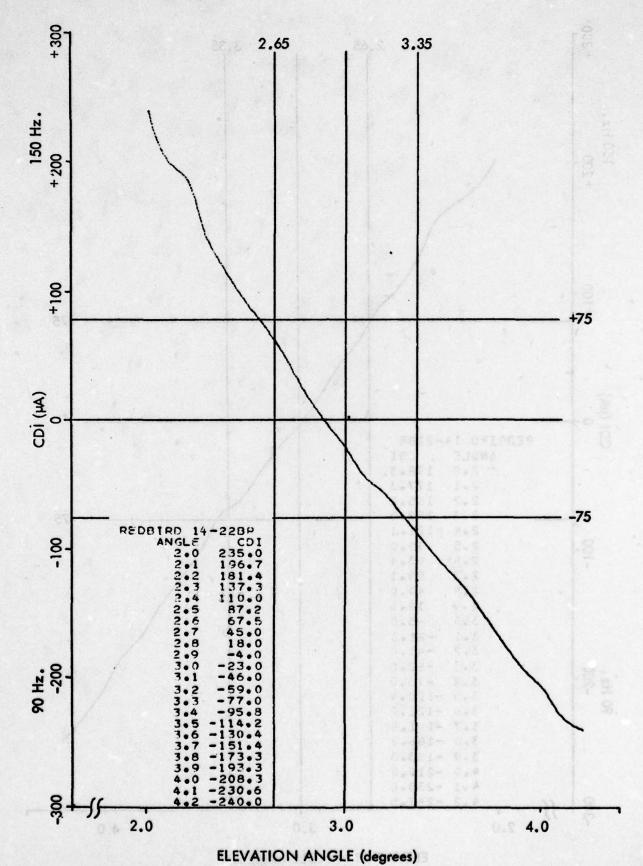


Figure 11-432. Approach 14-22, Upper Antenna Phase Advanced 10°. 11-598

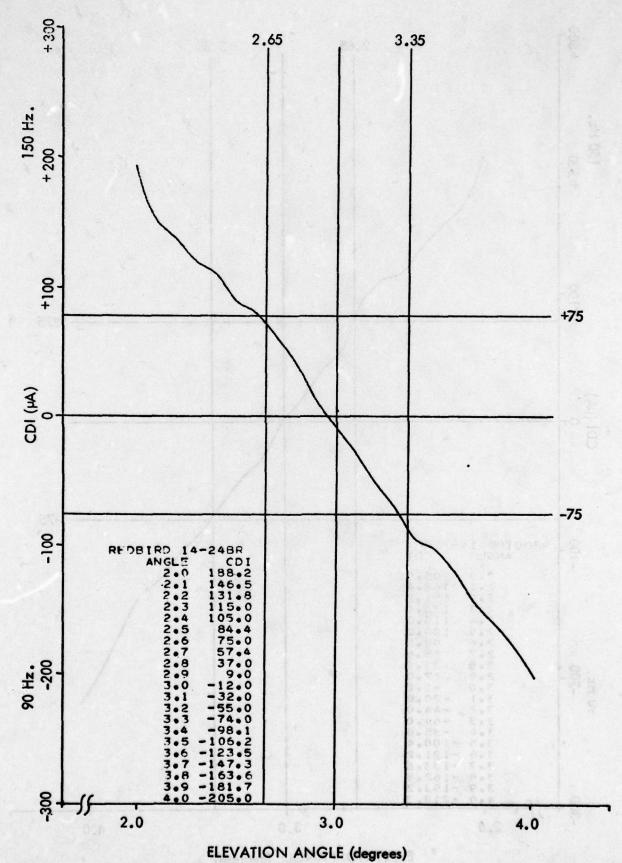
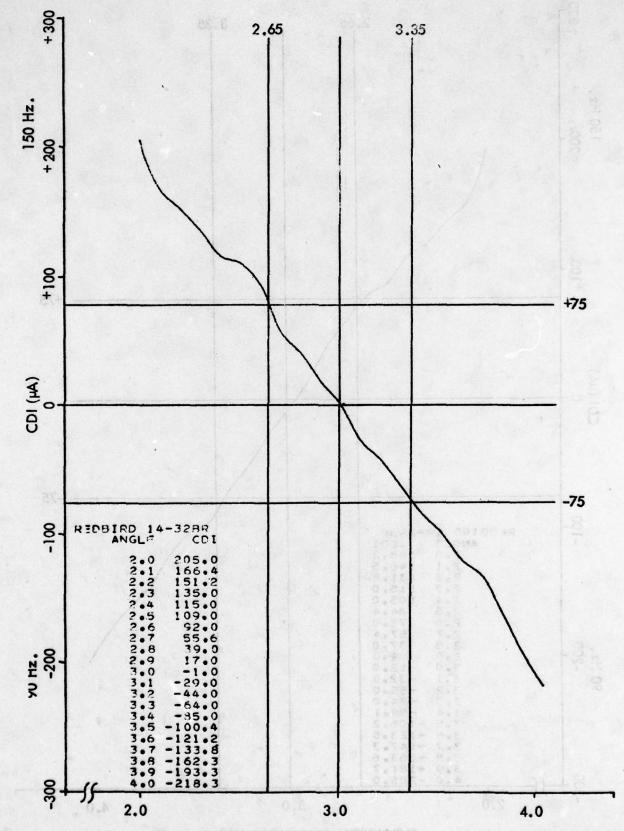


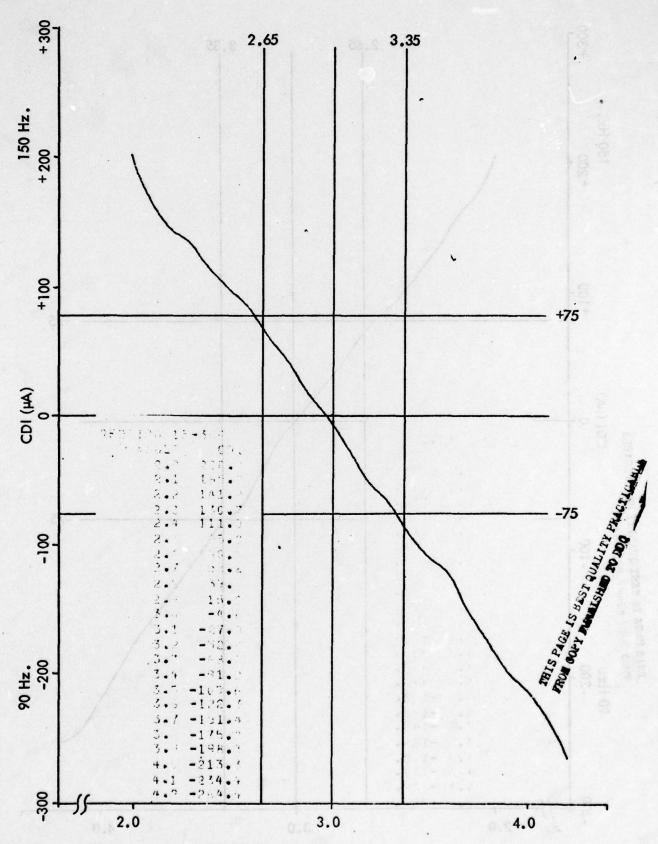
Figure 11-433. Approach 14-24, Upper Antenna Phase Retarded 17°.
11-599



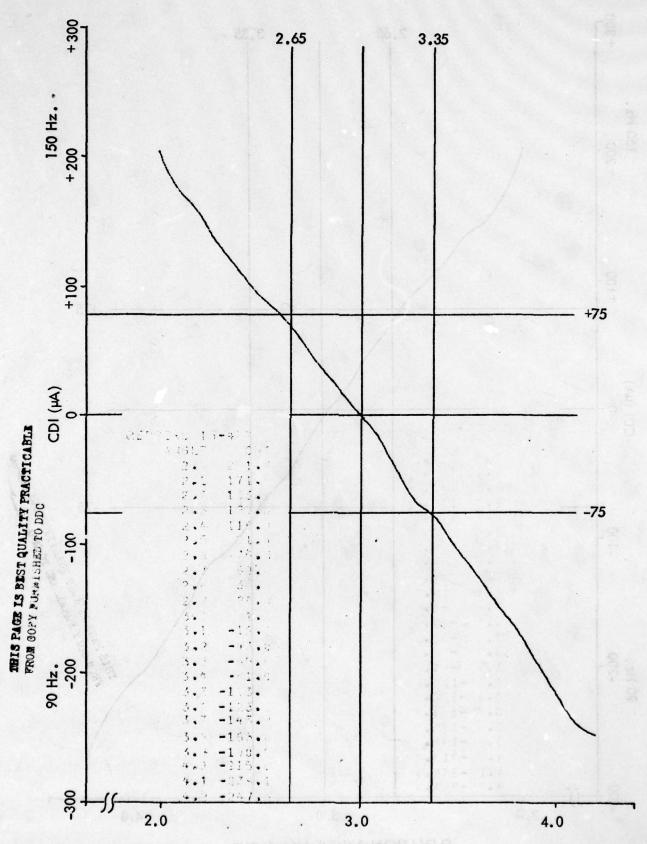
ELEVATION ANGLE (degrees)

Figure 11-434, Approach 14-32, Normal.

11-600



ELEVATION ANGLE (degrees)
Figure 11-435. Approach 15-3, Normal.



ELEVATION ANGLE (degrees)
Figure 11-436. Approach 15-4, Normal.

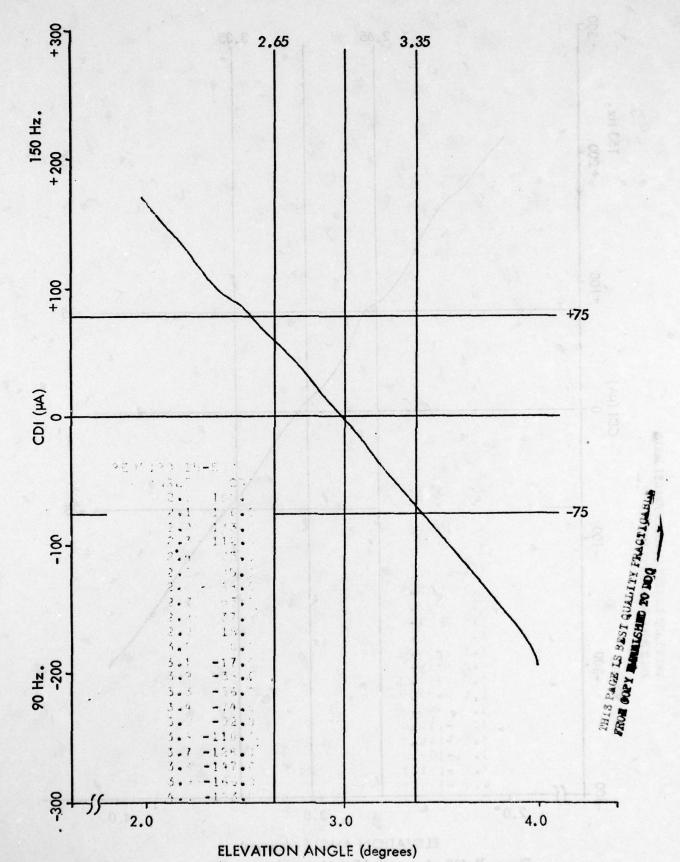
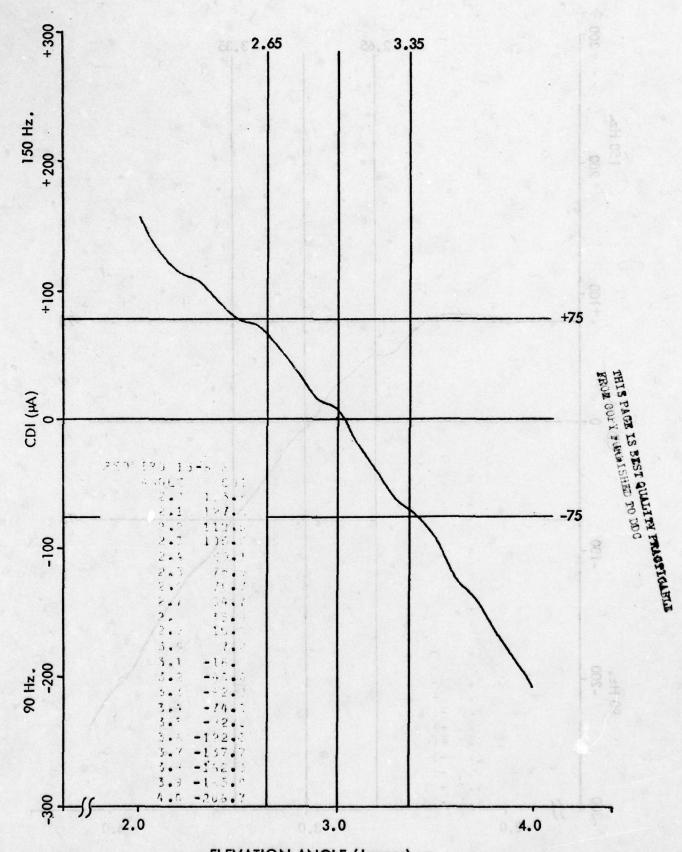


Figure 11-437. Approach 15-5, SBO Decreased to Broad Alarm.

Figure 11-438. Approach 15-6, Lower Antenna Phase Advanced 20°.



ELEVATION ANGLE (degrees)
Figure 11-439. Approach 15-8, Lower Antenna Phase Retarded 8°.



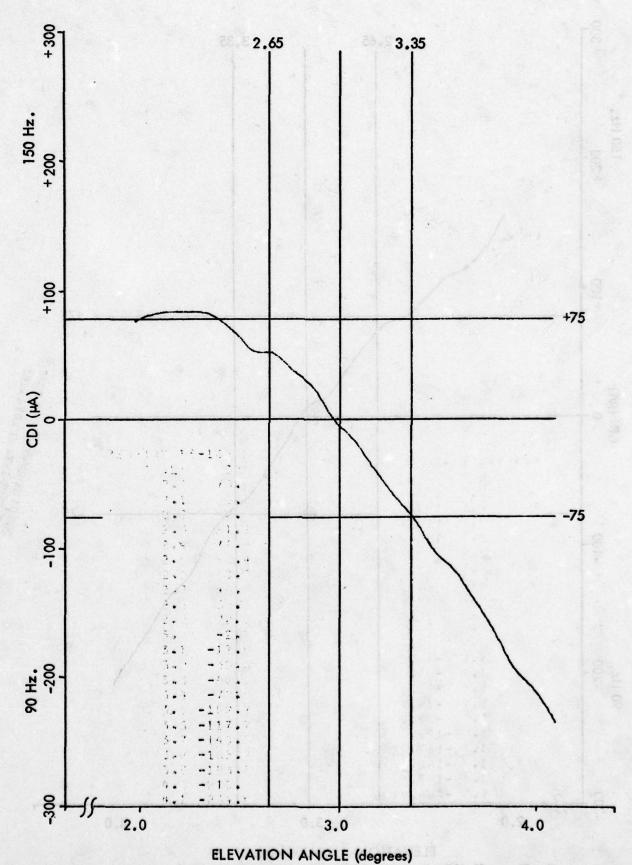


Figure 11-440. Approach 15-10, Lower Antenna Phase Advanced 40°.

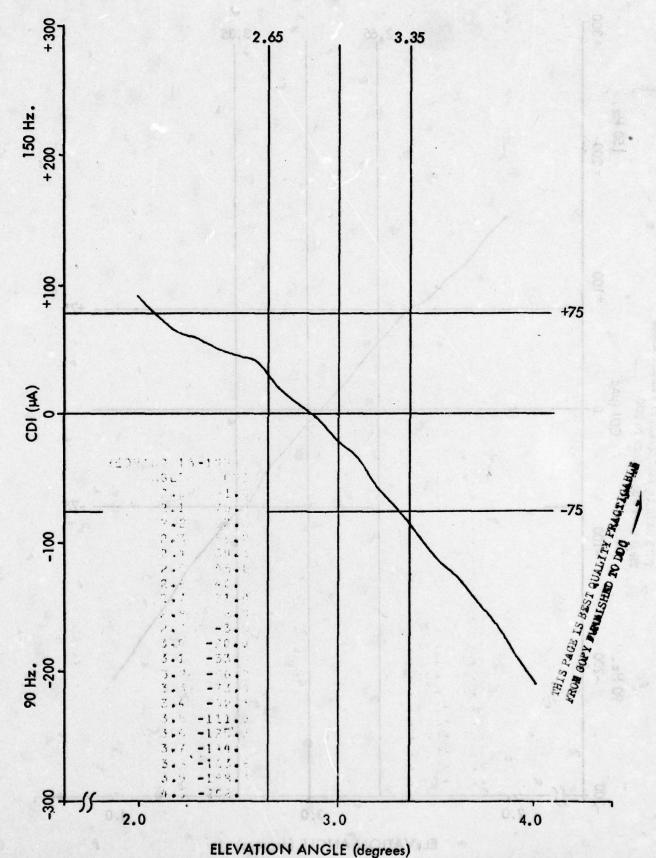


Figure 11-441. Approach 15-12, Lower Antenna Phase Retarded 16°.

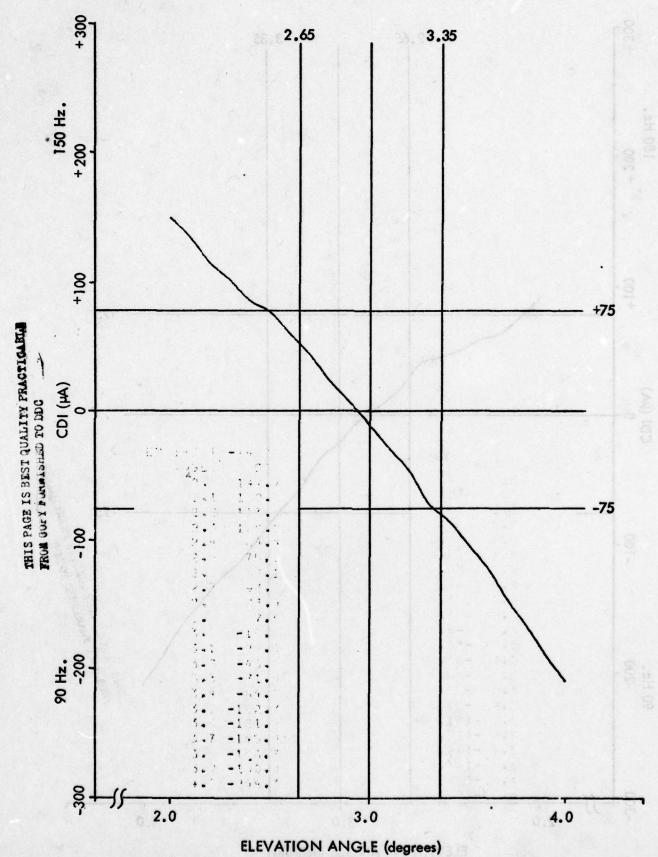


Figure 11-442. Approach 15-14, Middle Antenna Attenuated 1 dB.
11-608

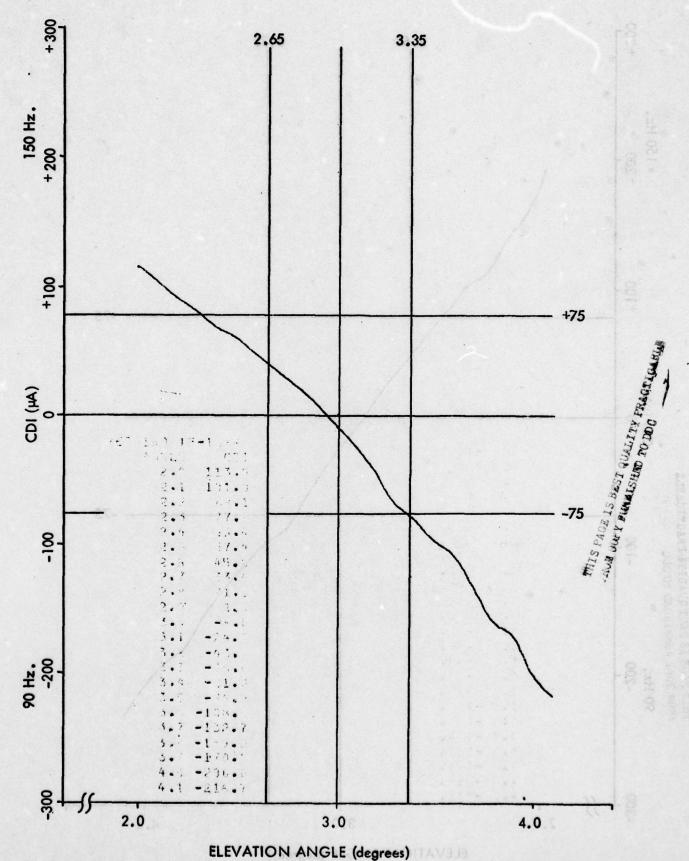
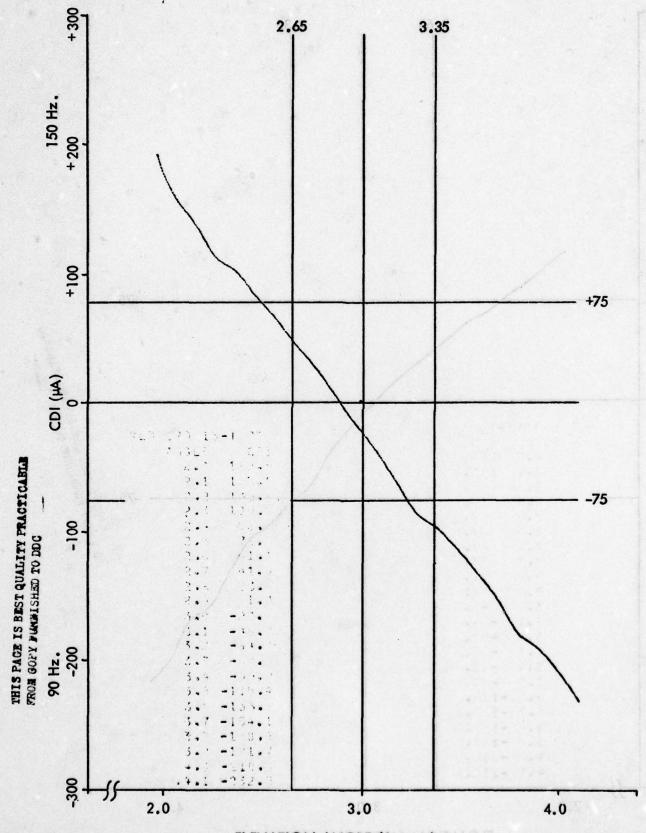


Figure 11–443. Approach 15–16, Middle Antenna Attenuated 2 dB.



ELEVATION ANGLE (degrees)
Figure 11–444. Approach 15–18, Upper Antenna Attenuated 1 dB.

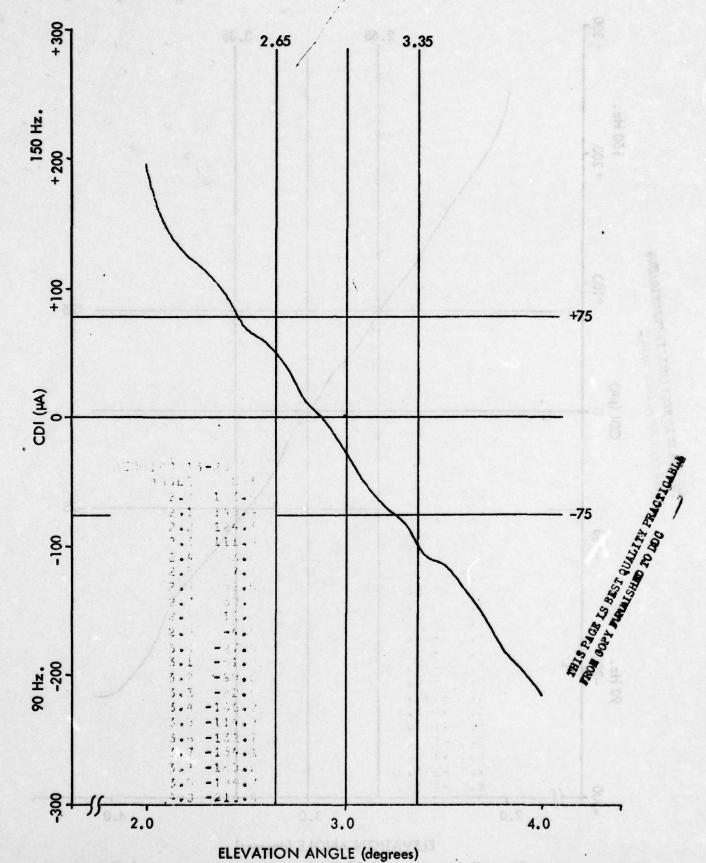


Figure 11-445. Approach 15-20, Upper Antenna Attenuated 2 dB.
11-611

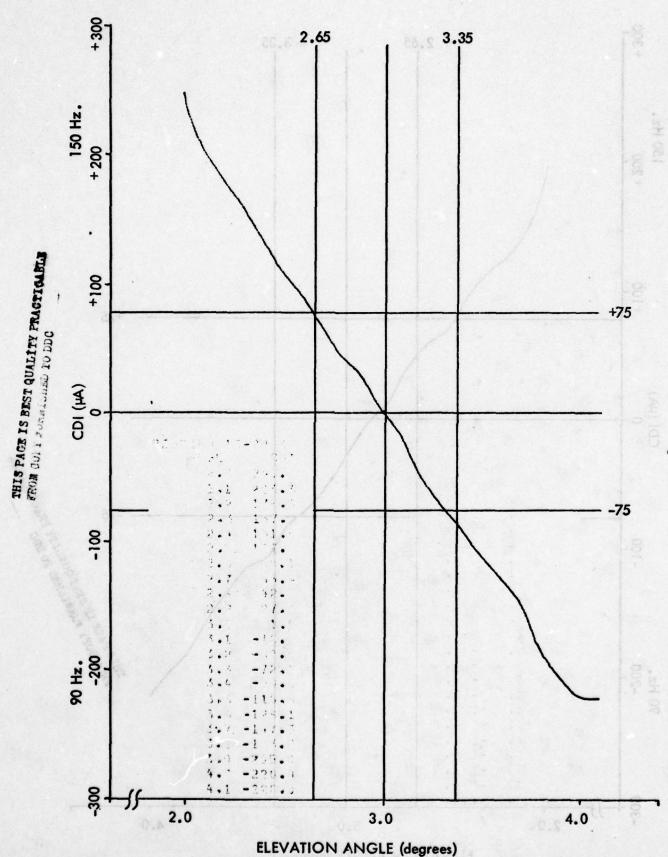


Figure 11-446. Approach 15-22, Lower Antenna Attenuated 1 dB.

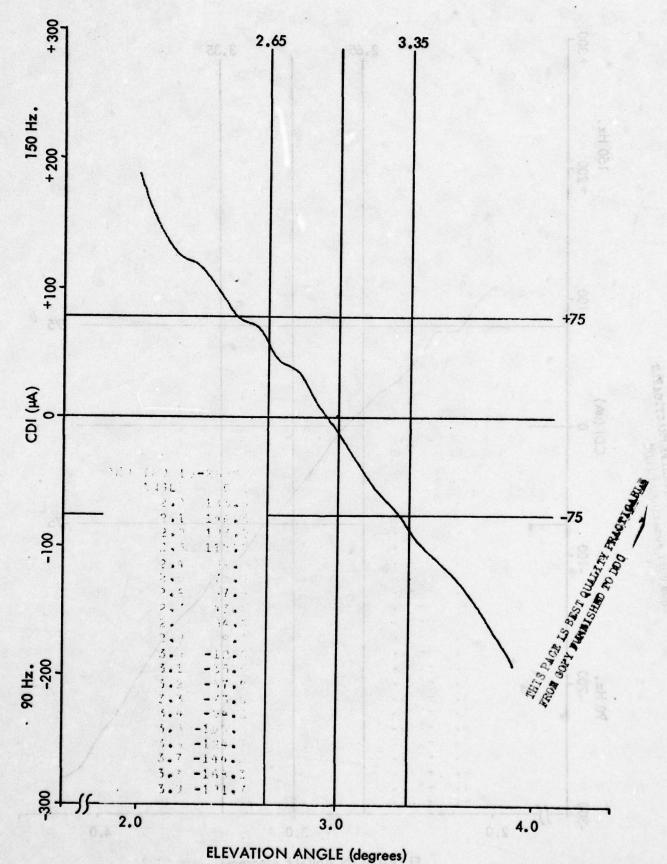
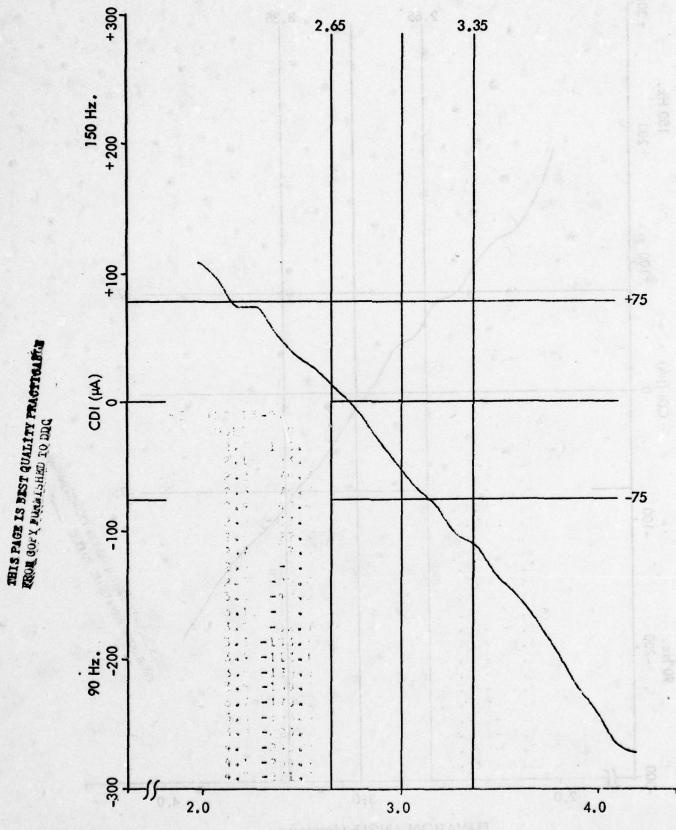
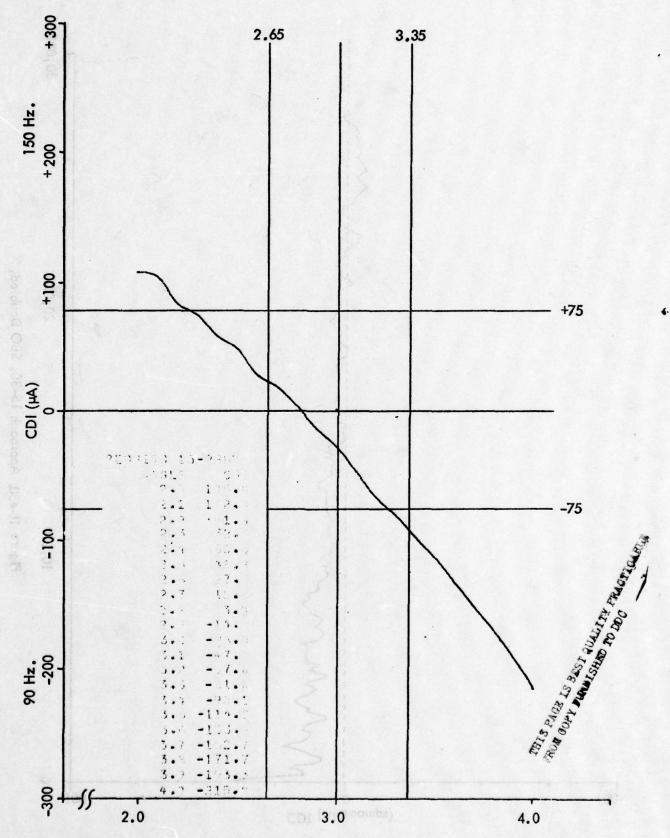


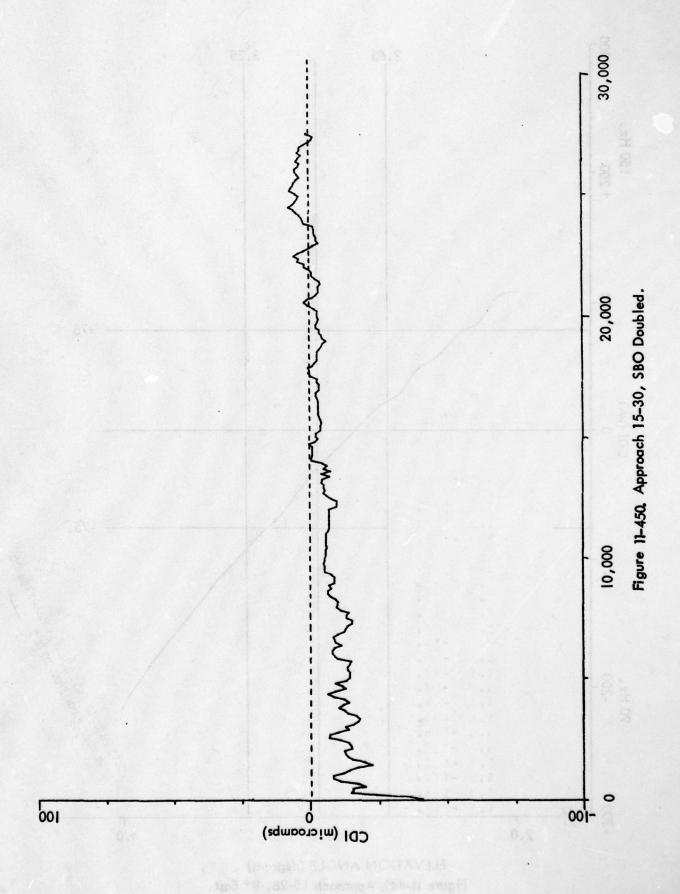
Figure 11-447. Approach 15-26, Normal.

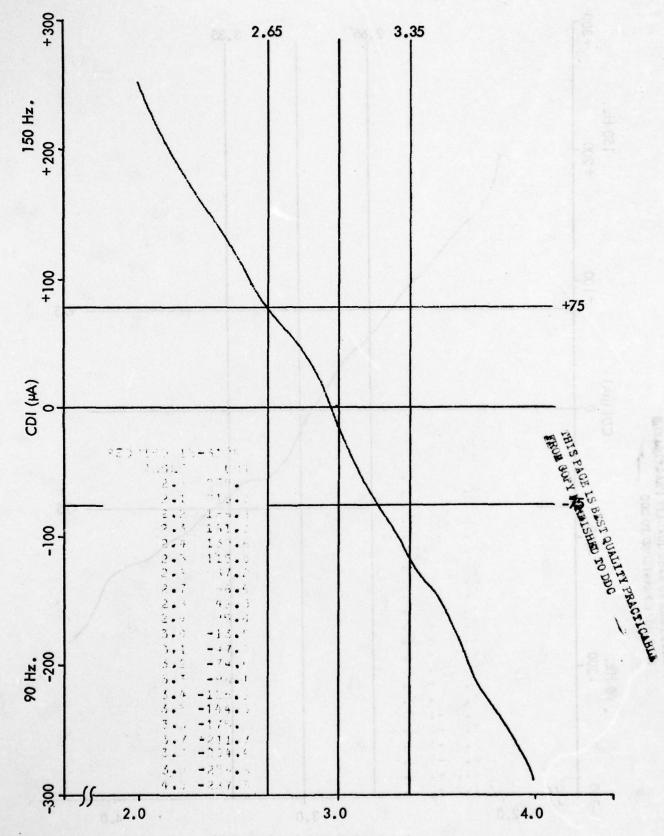


ELEVATION ANGLE (degrees)
Figure 11-448. Approach 15-27, 8° West.

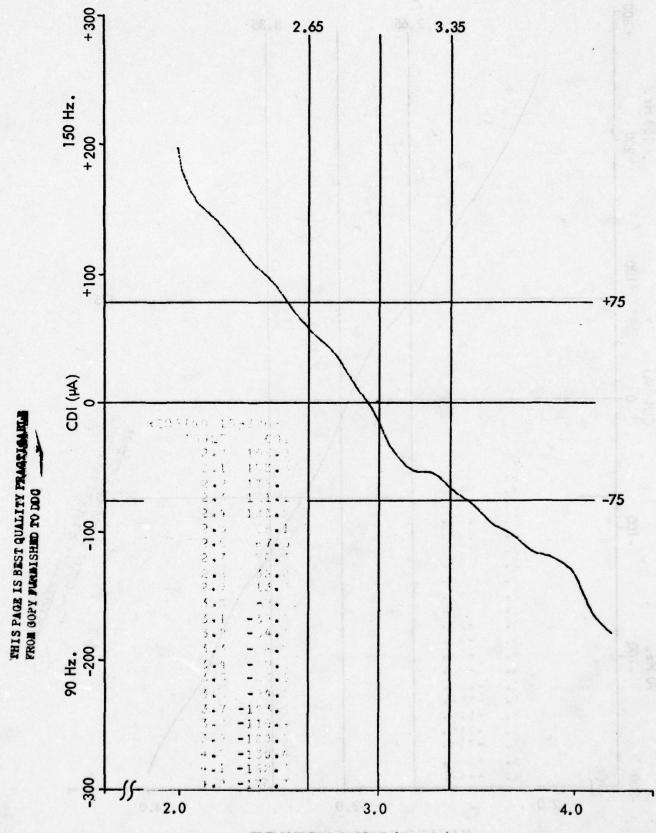


ELEVATION ANGLE (degrees)
Figure 11-449. Approach 15-28, 8° East.

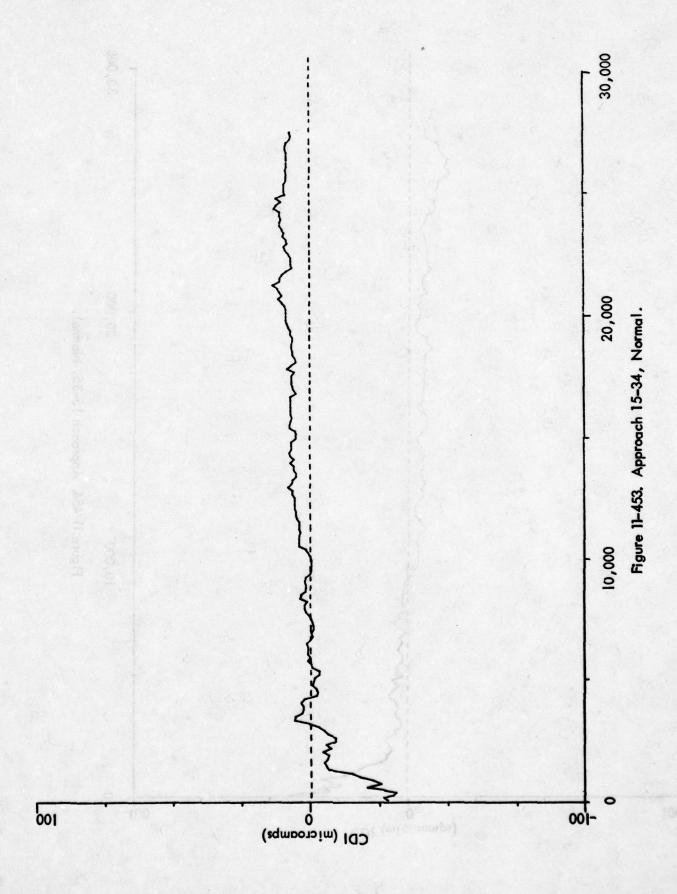


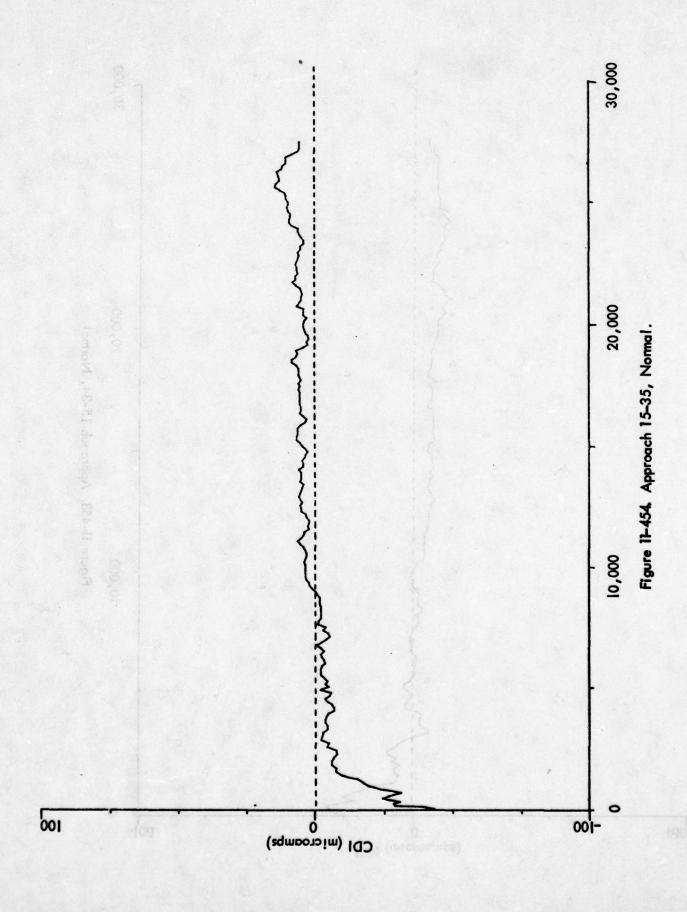


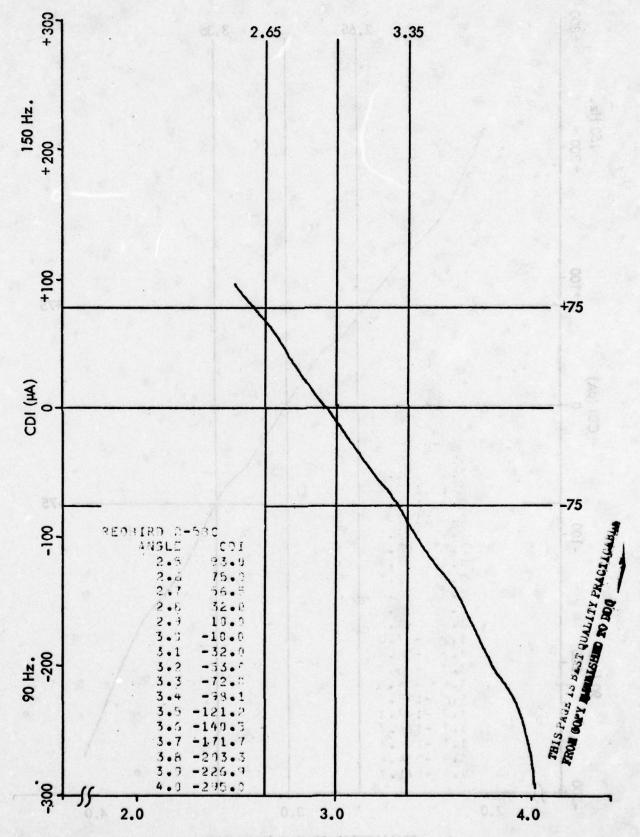
ELEVATION ANGLE (degrees)
Figure 11-451. Approach 15-31, SBO Increased to Sharp Alarm.



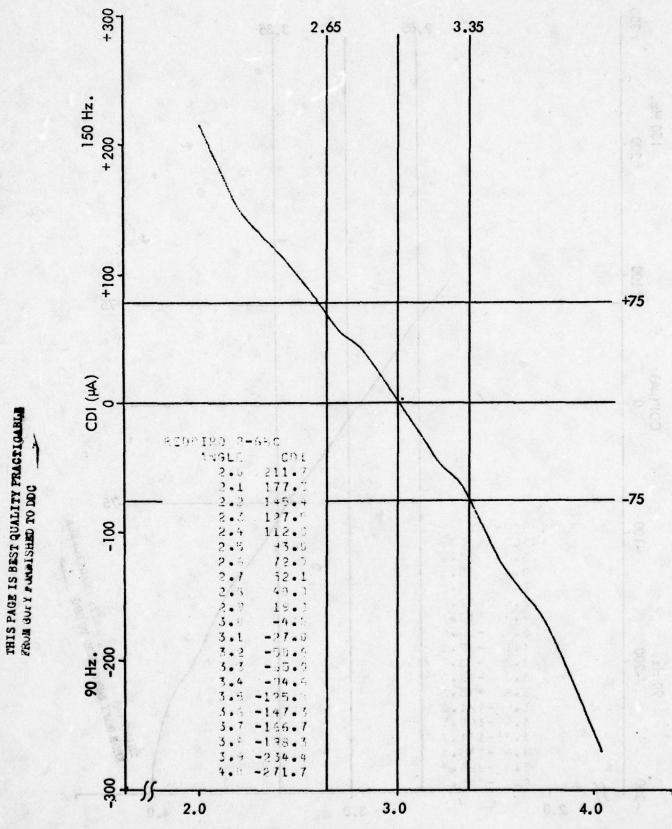
ELEVATION ANGLE (degrees)
Figure 11-452. Approach 15-32, Normal.



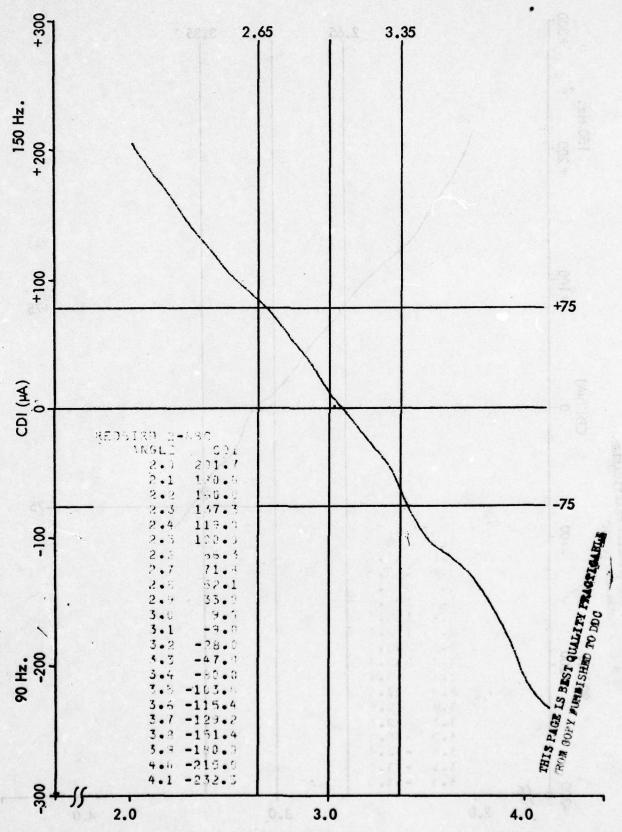




ELEVATION ANGLE (degrees) Figure 11-455. Approach 2-5, Normal.



ELEVATION ANGLE (degrees)
Figure 11–456, Approach 2–6, Normal.
11–622



ELEVATION ANGLE (degrees)
Figure 11-457. Approach 2-8, SBO Reduced to Broad Alarm.
11-623

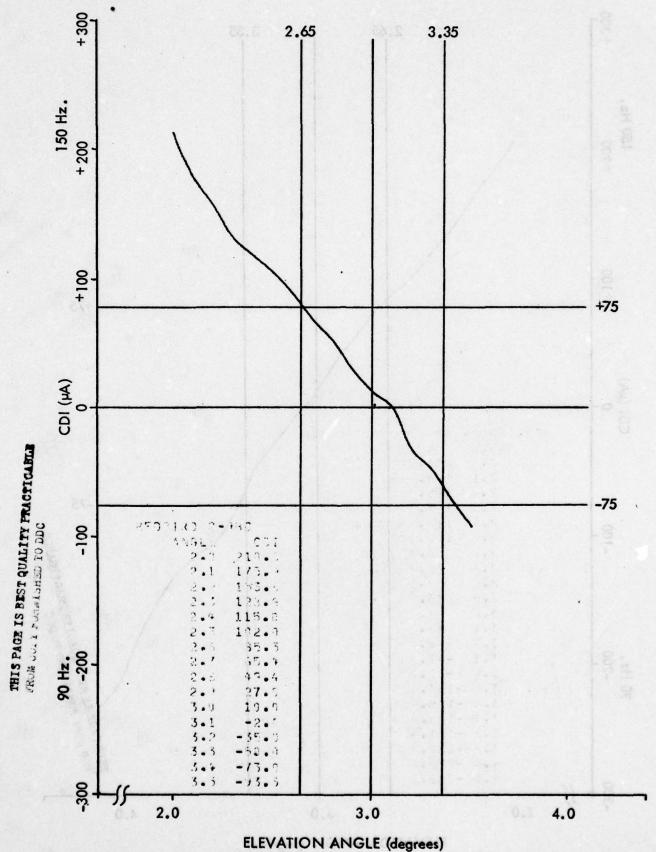
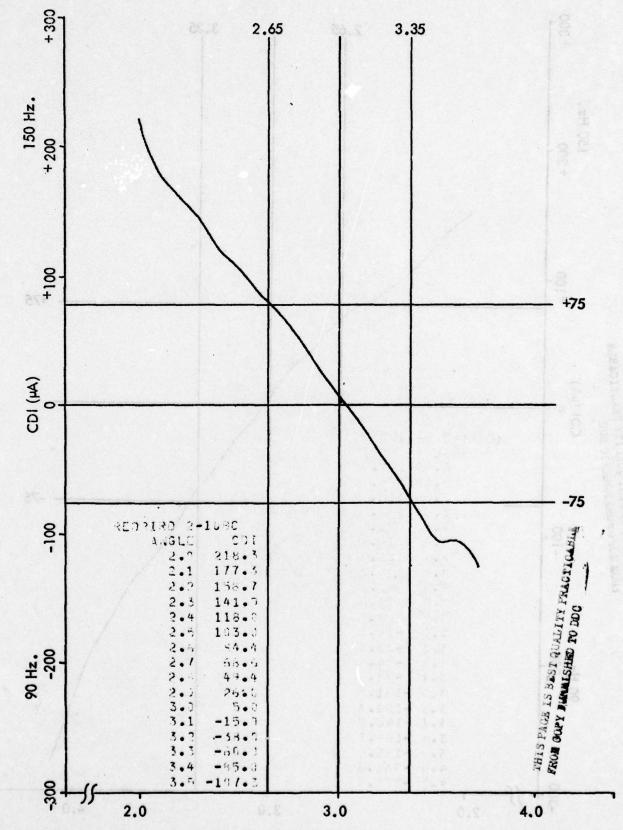


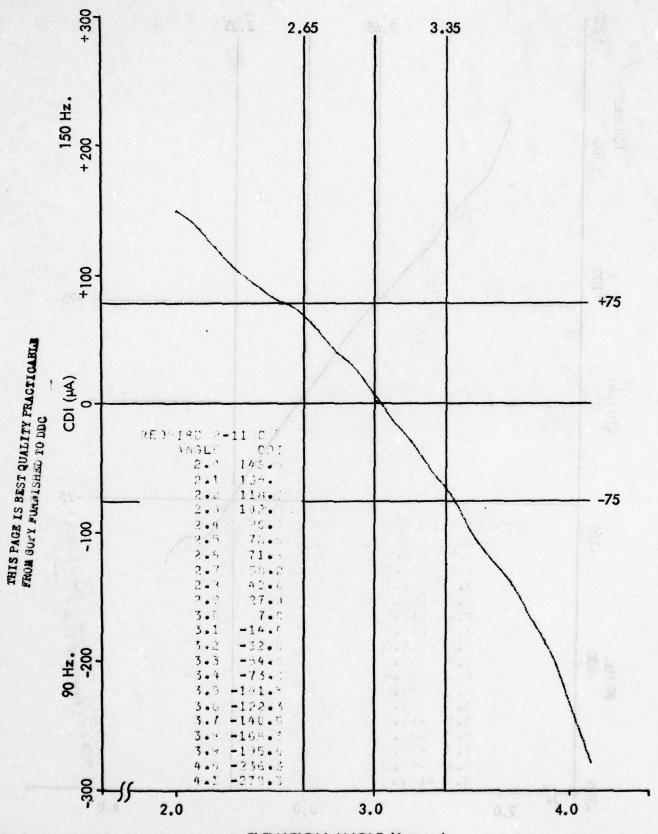
Figure 11-458, Approach 2-9, SBO Reduced to Broad Alarm.
11-624



ELEVATION ANGLE (degrees)

Figure 11-459. Approach 2-10, Normal.

11-625



ELEVATION ANGLE (degrees)
Figure 11-460. Approach 2-11, Middle Antenna Phase Advanced 13°.
11-626

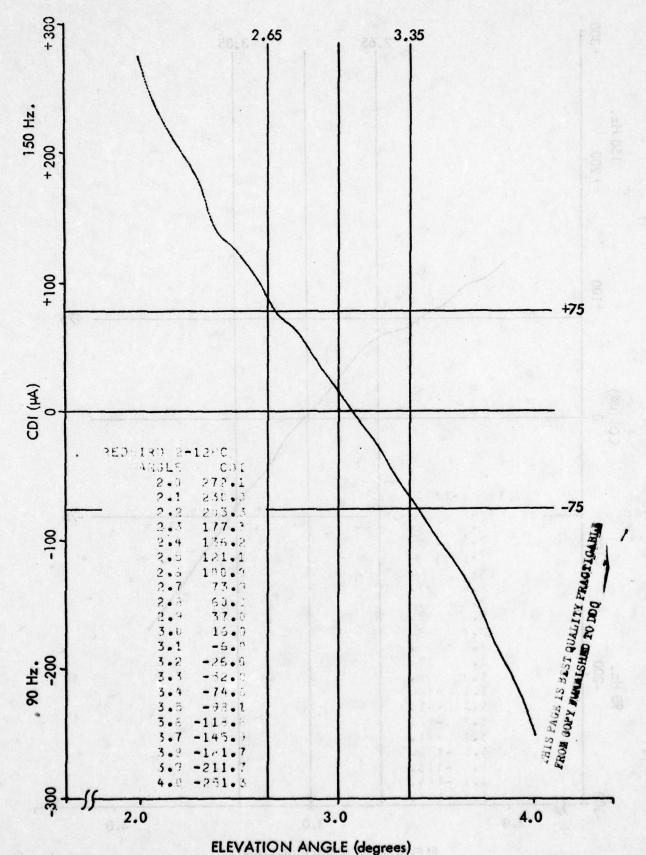
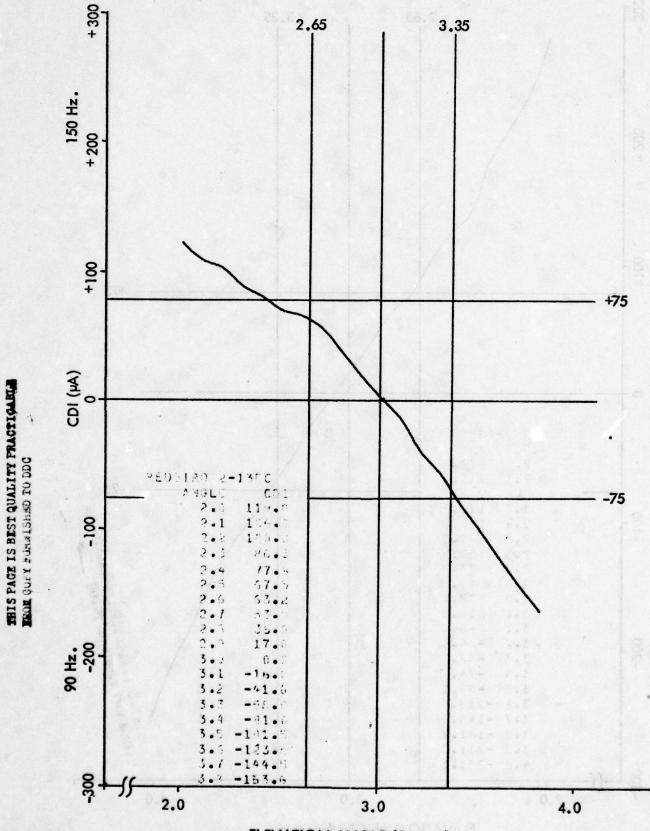
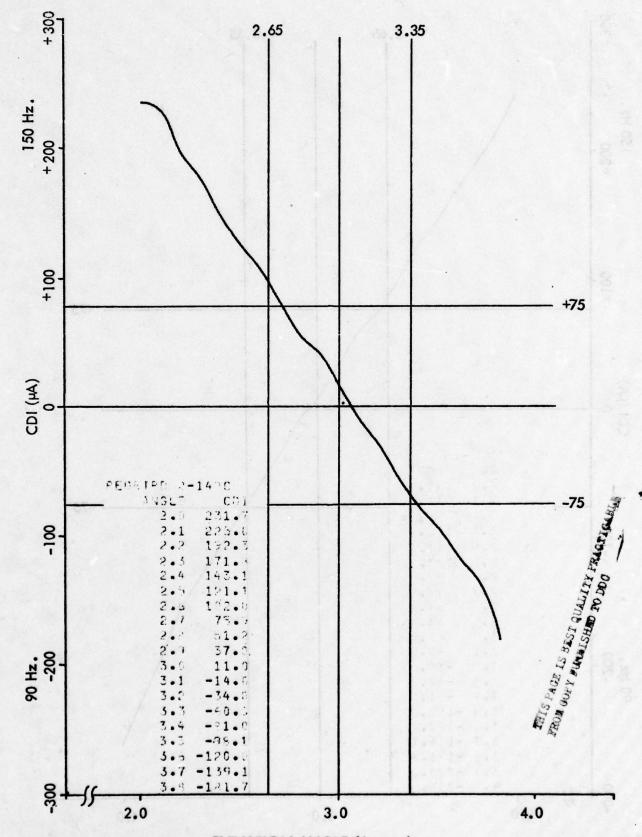


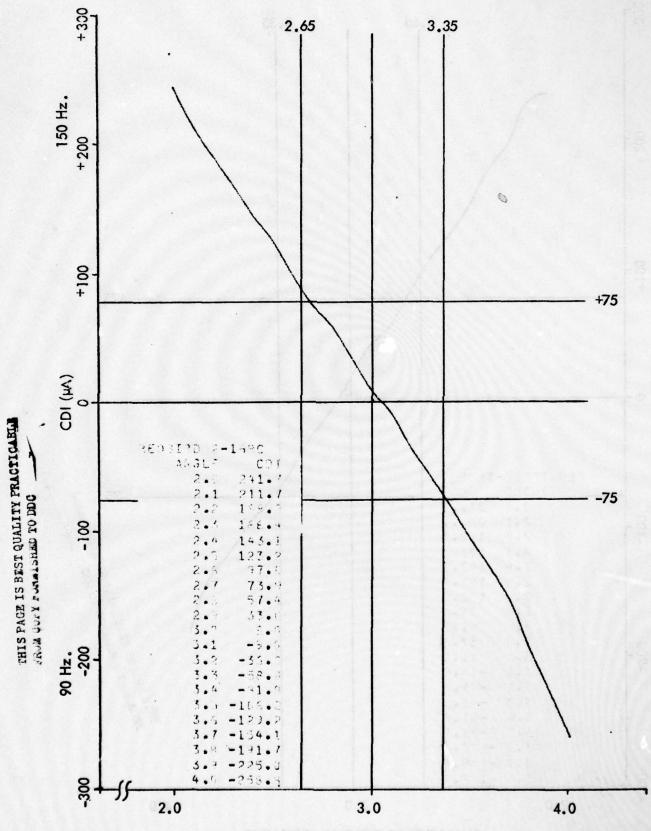
Figure 11-461 Approach 2-12, Middle Antenna Phase Retarded 13°.



ELEVATION ANGLE (degrees)
Figure 11-462, Approach 2-13, Middle Antenna Phase Advanced 18°.



ELEVATION ANGLE (degrees)
Figure 11-463. Approach 2-14, Lower Antenna Phase Retarded 18°...
11-629



ELEVATION ANGLE (degrees)
Figure 11-464. Approach 2-16, Lower Antenna Phase Advanced 15°.
11-630

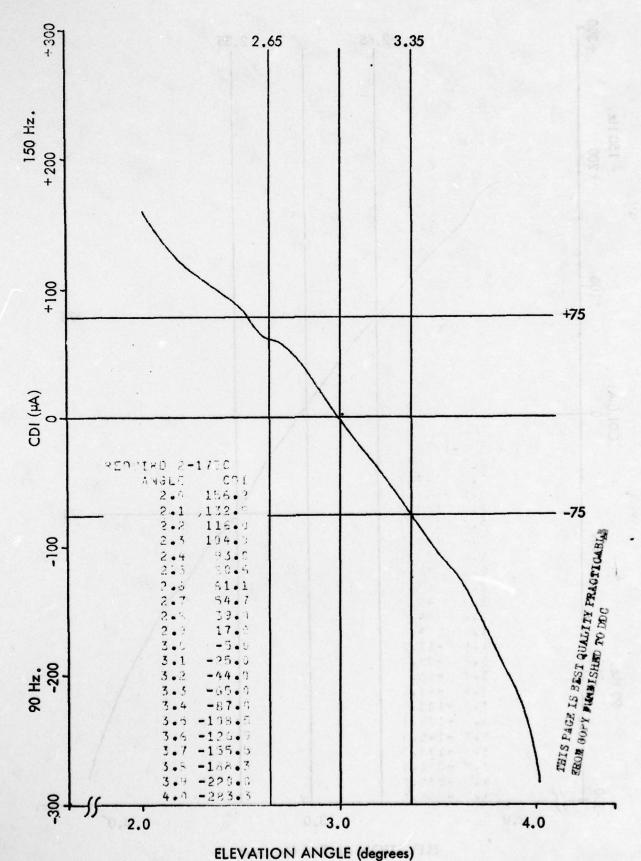


Figure 11-465. Approach 2-17, Lower Antenna Attenuated .5 dB.

11-631

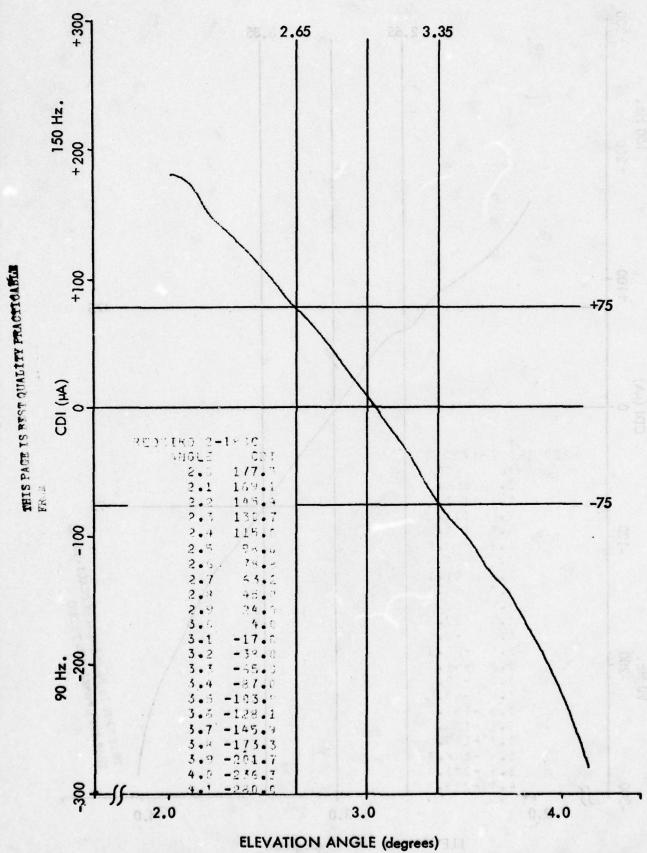


Figure 11-466. Approach 2-18, Middle Antenna Attenuated .5 dB.

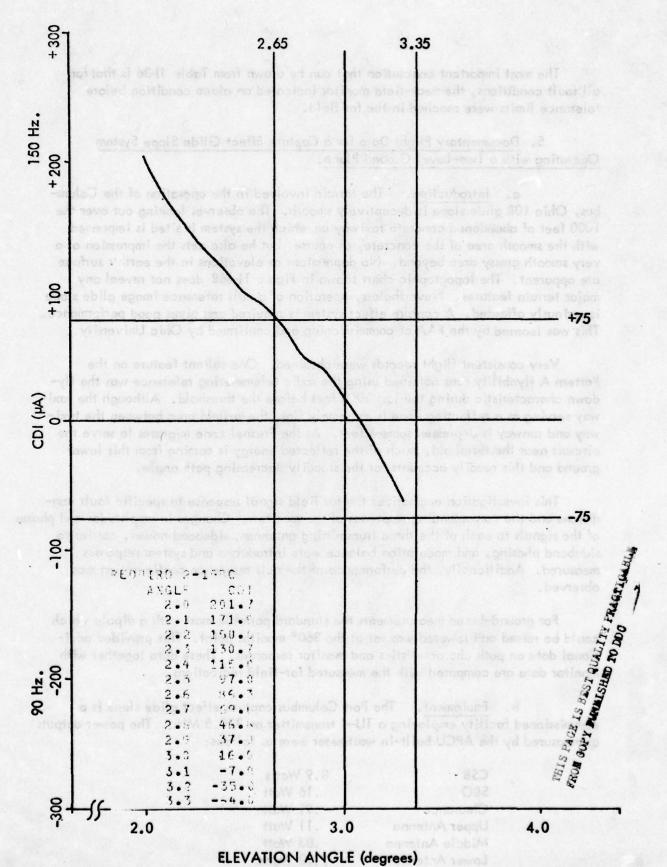


Figure 11–467. Approach 2–19, Lower Antenna Attenuated 1.5 dB.
11–633

The most important conclusion that can be drawn from Table 11-36 is that for all fault conditions, the near-field monitor indicated an alarm condition before tolerance limits were reached in the far field.

- 5. Documentary Flight Data for a Capture Effect Glide Slope System Operating with a Two-Level Ground Plane.
- a. Introduction. The terrain involved in the operation of the Columbus, Ohio 10R glide slope is deceptively smooth. The observer looking out over the 1000 feet of abandoned concrete taxiway on which the system is sited is impressed with the smooth area of the concrete, of course, but he also gets the impression of a very smooth grassy area beyond. No depressions or elevations in the earth's surface are apparent. The topographic chart shown in Figure 11-468 does not reveal any major terrain features. Nevertheless, operation of a null reference image glide slope is seriously affected. A capture effect system is required and gives good performance. This was learned by the FAA at commissioning and confirmed by Ohio University.

Very consistent flight records were obtained. One salient feature on the Pattern A flyability runs obtained using the radio telemetering reference was the flydown characteristic during the last 2000 feet before the threshold. Although the taxiway serving as a reflecting zone is extremely flat, the in-field area between the taxiway and runway is depressed some 4 feet. As the Fresnel zone migrates to serve the aircraft near the threshold, much of the reflected energy is coming from this lower ground and this readily accounts for the steadily decreasing path angle.

This investigation emphasizes the far field signal response to specific fault conditions and the corresponding responses of the monitors. Changes in amplitudes and phases of the signals to each of the three transmitting antennas, sideband power, carrier to sideband phasing, and modulation balance were introduced and system responses measured. Additionally, the performance of the null reference configuration was observed.

For ground-based measurements the standard portable mast with a dipole which could be raised and lowered was set at the 360° monitor point. This provided additional data on path characteristics and monitor responses. These data together with monitor data are compared with the measured far-field indications.

b. Equipment. The Port Columbus capture effect glide slope is a commissioned facility employing a TU-4 transmitter on 330.5 MHz. The power outputs as measured by the APCU built-in wattmeter were as follows:

CSB	8.9 Watts
SBO	.16 Watt
Clearance	.91 Watt
Upper Antenna	.11 Watt
Middle Antenna	.83 Watt
Lower Antenna	2.83 Watts

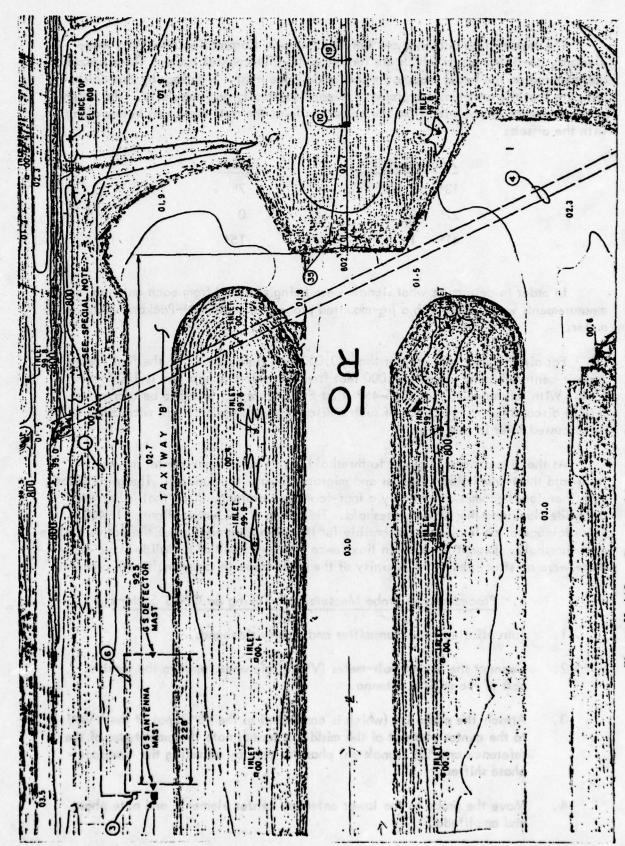


Figure 11-468. Topographic Map of Columbus 10 R Glide Slope Area.

The transmitting antennas are Antenna Products Corporation FA-8976, three element, co-linear arrays which are fed using RG-214 coaxial cable. These antennas are mounted on the heavy standard metal glide slope mast. Sightings by theodolite indicate that the antennas are properly aligned vertically and angularly. The heights of the antennas as measured from the cement base of the mast are given below along with the offsets:

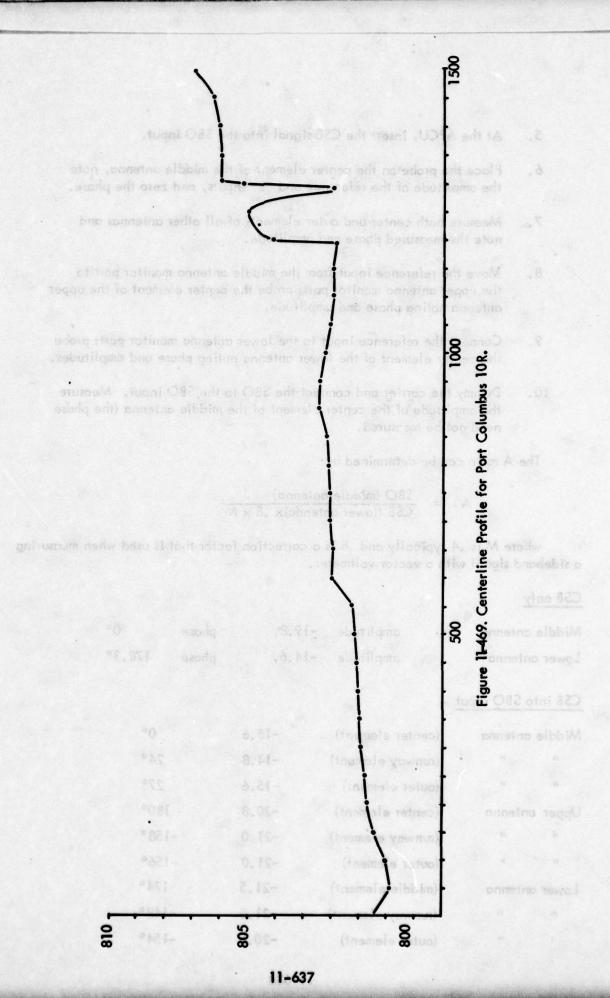
Ante	enna Height	Offset
13'	3 1/2"	7"
271	3"	0
411	the first Parks	15"

In order to determine what signals were being radiated from each antenna, probe measurements were taken with a jig-mounted probe and a Hewlett-Packard vector voltmeter.

For aircraft positions greater than 20,000 feet from threshold, the first Fresnel zone is centered approximately 1,000 feet from the antenna mast and is 1700 feet long. With reference to Figure 11-469 first Fresnel zone is found to be along the terrain discontinuity. Evidence of such a discontinuity seen on flight recordings will be discussed later in this section.

As the aircraft moves closer to threshold, the Fresnel zone center moves in toward the transmitting antennas and migrates toward the runway. The glide slope path therefore becomes affected by a four-foot deep drainage ditch that is between the glide slope and the runway threshold. This ditch is evident in Figure 11-468. This drainage ditch is clearly responsible for the major degradation of the path structure near threshold. Except for a chain link fence 150 feet south of the glide slope array there were no structures in the vicinity of the glide slope to cause multipath problems.

- c. Procedures for Probe Measurement-Taking on CEGS Systems.
- 1. Turn off clearance transmitter and dummy sidebands.
- 2. Connect the vector volt-meter (VVM) reference input to the monitor port of the middle antenna.
- 3. Attach the probe jig (which is connected to the "B" input of the VVM) to the center element of the middle antenna; note the amplitudes of the reference and "B" signals-set phase to zero by adjusting the trombone phase shifter.
- 4. Move the probe to the lower antenna, center element, and note phase and amplitude.



- 5. At the APCU, insert the CSB signal into the SBO input.
- 6. Place the probe on the center element of the middle antenna, note the amplitude of the reference and "B" inputs, and zero the phase.
- 7. Measure both center and outer elements of all other antennas and note the measured phase and amplitude.
- 8. Move the reference input from the middle antenna monitor port to the upper antenna monitor port: probe the center element of the upper antenna noting phase and amplitude.
- Connect the reference input to the lower antenna monitor port: probe the center element of the lower antenna noting phase and amplitudes.
- 10. Dummy the carrier and connect the SBO to the SBO input. Measure the amplitude of the center element of the middle antenna (the phase need not be measured.

The A ratio can be determined by:

where M is .4 typically and .8 is a correction factor that is used when measuring a sideband signal with a vector voltmeter.

CSB only

Middle antenna	amplitude	-19.8,	phase 0°
Lower antenna	amp li tude	-14.6,	phase 178.3°
CSB into SBO input			
Middle antenna	(center element)	-15.6	0°
и п	(runway element)	-14.8	24°
	(outer element)	-15.6	27°
Upper antenna	(center element)	-20.8	180°
	(runway element)	-21.0	-158°
	(outer element)	-21.0	-156°
Lower antenna	(middle element)	-21.5	174°
	(runway element)	-21.5	-148°
	(outer element)	-20.5	-154°

SBO into SBO input

Middle antenna, center element amplitude -33.0

The values presented above give complete information as to what signals were being radiated at the time the measurements were taken. The pertinent data is contained in the individual element measurements; the monitor port readings were taken in order to establish a relationship between the actual radiated signal and the monitor port output.

o vistombergos illie bisway apple brusto edi

The need to measure all three elements of the FA-8976 antenna is due to the fact that the radiated signal from the antenna is a composite of the signals from each of the elements. The equation describing this relationship is as follows:

$$F(\theta) = I_2 + I_1 e^{i\beta d \sin \theta} + I_3 e^{-i\beta d \sin \theta} \cos (\pi/2 \sin \theta)/\cos \theta$$

where \mathbf{I}_1 , \mathbf{I}_2 , and \mathbf{I}_3 are the complex element currents.

For this study, the radiated currents along centerline are the parameters of interest (i.e., $\theta = 0$):

$$F(0) = I_2 + I_1 + I_3$$

The radiated signal along centerline is the sum of the individual element currents. This sum has been computed above and is denoted as the effective radiated current. Taking the above into consideration, the system output relationships can be given by the following table:

Non-septi	CSB	E bho relec	SBO	al and an res
Antenna	Magnitude	Phase	Magnitude	Phase
Upper	0.0	, do	.53	178°
Middle	.55	0°	1.00	0°
Lower	1.0	178.3°	.51	184.2°

Table 11-37. System Outputs, Columbus 10R.

depression in the part threture near threshald due to the drainage ditch between the

d. Terrain and Site Peculiarities. The terrain profile for Port Columbus Runway 10R along centerline is shown in Figure 11–469. As seen in Figure 11–469, the ground slopes upward with approximately a 0.3% grade for 1200 feet in front of the runway surface. Past 1200 feet, the ground elevation abruptly increases about 4 feet and continues to slope upward for a short distance thereafter. The terrain beyond that which is shown in Figure 11–469 is basically flat.

In order to describe the effects of this terrain on glide slope performance, reference will be made to the Fresnel [8] zone locations. These bring the areas on the ground of principal interest for reflections which serve the image system. The size of the elliptical Fresnel zones decreases rapidly and the center moves closer to the antennas as the aircraft approaches threshold.

- e. <u>Data Processing</u>. Information from flight recordings was digitized and stored in the <u>Ohio University IBM Model 370</u> computer. This data was later plotted by a Hewlett-Packard Model 7203A digital plotter under software control of a computer program written specifically for this application. A side-by-side comparison of these graphs and the original flight recordings has been performed to insure accuracy in reproduction.
- f. <u>Documentary Data</u>. The data presented on the following graphs represent the pertinent flight-test results for the Port Columbus, Runway 10R, glide slope facility. These graphs present three particular groups of data, viz, (1) ground data taken with a portable most and portable ILS receiver at the 360° proximity point for the capture effect glide slope (CEGS), (2) flight data from a perturbation study on the CEGS, and (3) flight data from the system configured as a null-reference, glide slope.

One of two graph formats has been used to plot the data. One format gives the course deviation indicator (CDI) current in microamperes versus elevation angle; the other presents CDI versus distance from the runway threshold. The CDI versus elevation angle format is used for plotting ground data and data from Pattern B, level flight along centerline. The ± 75 microamperes and $\pm .35^{\circ}$ reference lines on the level flight formats are for comparing against ideal glide path characteristics, i.e., 0 microamperes at 3.00° , ± 75 microamps at $3.00 \pm .35^{\circ}$. CDI versus distance from threshold formats are used for Pattern A normal approach.

The ground data was taken with the portable mast with a variable-height probe at the 360° proximity point of the upper-lower antennas and measuring the CDI value for varying probe heights. Data points were taken every one-half foot for probe elevations from 4 feet to 13 feet. These were accomplished for every perturbation of the system. These data points were input to a computer program that converted elevation height to elevation angle.

Flight test results from the CEGS show no major terrain effects except for a depression in the path structure near threshold due to the drainage ditch between the glide slope antennas and the runway. (See Figure 11-495).

The null reference system, however, shows pronounced effects due to terrain for aircraft locations on path at a distance greater than 25,000 feet. (See Figure 11–496). As stated in the section on terrain, this aircraft position corresponds to a Fresnel zone on the terrain discontinuity. Also, the null reference shows a noticeable path angle depression near the threshold.

The run number on each plot (e.g., 19-3BC) indicates the day of the month of the test (19), run number that day (3), the type of flight pattern (e.g., A or B), and the initial of the theodolite operator (C).

The graphs of Figures 11–470 through 11–520 present three separate sets of data: (1) flight records from the Port Columbus facility operating normally and with perturbations are shown in Figures 11–470 through 11–494, (2) system response above and below the 360° proximity point corresponding to the flight records of (1) above are given in Figures 11–501 through 11–520, and (3) Figures 11–496 through 11–500 show system performance when configured as a null-reference system.

g. Comparison of Near-Field Alarm Values and Observed Far-Field Response. In addition to the flight data, documentation on integral width monitor response and complete response at the 360° proximity point were recorded. Measurements above and below the 360° proximity point were taken with a portable mast providing CDI versus elevation angle values which enabled path and width angles to be determined. In conventional capture-effect operation, only the path angle is monitored at the 360° proximity point; the additional width information is presented here in order that a better understanding of portable mast measurements will be afforded.

Tabular data from the integral monitor, the 360° proximity point response, and the far-field response are presented in Table 11-38, and a graphical presentation of this data is given in Figure 11-520. The percent alarm limits in Figure 11-520 are for width limits for perturbations in the middle and lower antennas, and the path angle limits for perturbations in the upper antenna. These criteria yield the higher percentage of the two possible alarm indications. Values of greater than 200% alarm for the 360° proximity point are found when width measurements show that the CDI trace does not exceed ± 75 microamperes.

The integral width monitor was capable of responding to all fault conditions that affected path width as can be seen in Figure 11-520. As expected, some perturbations affecting path-only were not seen by the integral width monitor.

Initial perturbations introduced into the upper antenna did not result in adequate response at the 360° proximity point indicating a masking effect caused by excessive clearance transmitter power. As seen in Figure 11-520, proper response was achieved after the clearance transmitter power was reduced. Also seen in Figure 11-520 is that changes in the far-field path width are not accompanied by an equivalent path-width change as measured at the 360° proximity point. This result clearly indicates that portable mast measurements at the 360° proximity point cannot be used to document or verify total capture-effect system performance.

forpe avia bevel karlt a	Near-Field Monitor	tol et eig chia etti	hiro to m	pr be	tot +atto	fur- for equiv	alok.	360° Monitor Point Response	onitor
Foult Condition	Response % Alarm	Path Angle	Width	Structure Angle	% Alarm Angle	% Alarm Width	& *	Path Angle	Width
Normal	0	3.05	.72	2.23	0	0	e/c	3.01	.74
SBO Decreased	180	3.04	-88		5	85	19-6	•	rio a se
Middle +8°	100	3.00	.76	2.29	25	20	19-24	2.95	
Middle +24°	200	3.01	.72	1.70	20	0	19-26	2.96	
Middle - 13°	100	3.03	.79	2.05	2	35	19-23	3.03	.67
Middle - 18°	200	3.12	%	1.96	35	8	19-25		
Lower + 10°	100	3.05	.82	2.11	0	20	19-28	3.05	2
Lower +15°	200	3.07	88.	1.95	10	80	18-31	3.08	2
Lower -14°	901	3.05	.7	2.25	0	25	19-27	2.95	•
Lower -19°	200	3.09	.76	2	20	20	19-29	2.93	18 18 22
Upper + 84°	901	2.76	.75	2.18	145	15	19-34	3.10	2.
Upper -85	901	2.72	.79	2.24	165	35	19-33	•	
Middle -2 dB	128	3.04	.79	2.20	ý	35	19-41	2.99	.82
Middle -3 dB	170	3.07	98.	1.98	01	2	19-43	2.99	.9
Lower -2 dB	114	3.10	.73	2.41	25	2	19-44	2.96	.74
Lower -3 dB	>200	3.10	.67	2.52	25	25	19-45	2.93	8.
Upper -5 dB	100	2.82	8.	2.22	115	64	19-38	3.27	.82
Upper -10 dB	133	2.72	.73	2.20	165	5	19-39	3.40	.82
System Adjust- ment (Clearance -3 dB)	aus thici mucha in dibliw ta se eo dib	n Mega acharan acharan achdra	crest et	sta sens Viges (1 19 Oct.	rigno munico m Malér	# #6 # 1 # 2 !	ahaerit. up A ta	ro el gad aa tear	Pie altigi I Diajoria pet arti d
Upper + 60°	901	2.84	.92		105	100	19-35	3.41	4
Upper - 50°	100	2.83	.79	2.25	011	35	19-37	3.24	8.

Table 11–38. Far-Field Response.

Data taken on the Port Columbus Runway 10R glide slope indicate that conventional capture-effect monitoring (i.e., integral width monitoring and path monitoring at 360° proximity point) is adequate to detect all fault conditions that may appear in the far field if the system is initially set up correctly. Masking of upper antenna faults due to excessive clearance transmitter power is an example of incorrect setup. At the discretion of FAA Maintenance Personnel, the Port Columbus facility was left with the clearance power reduced.

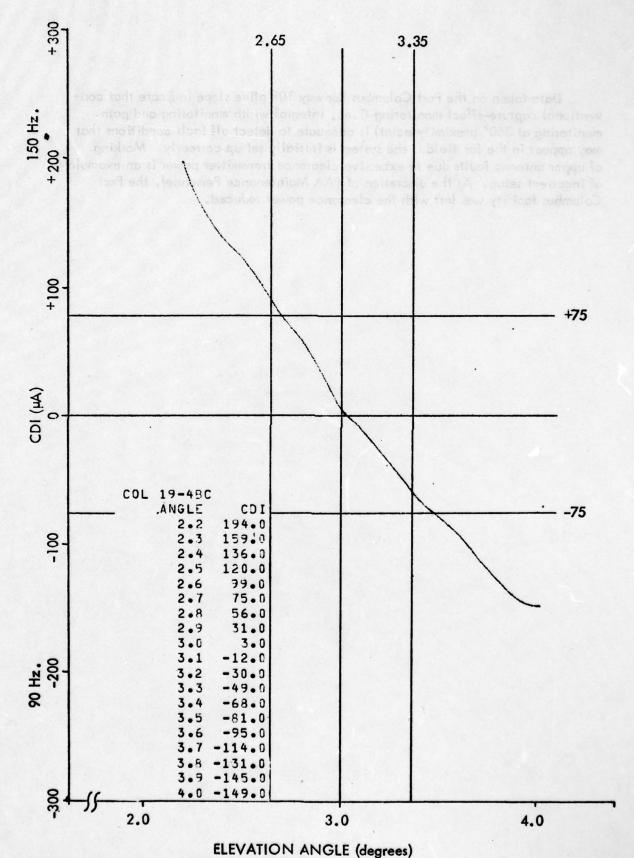
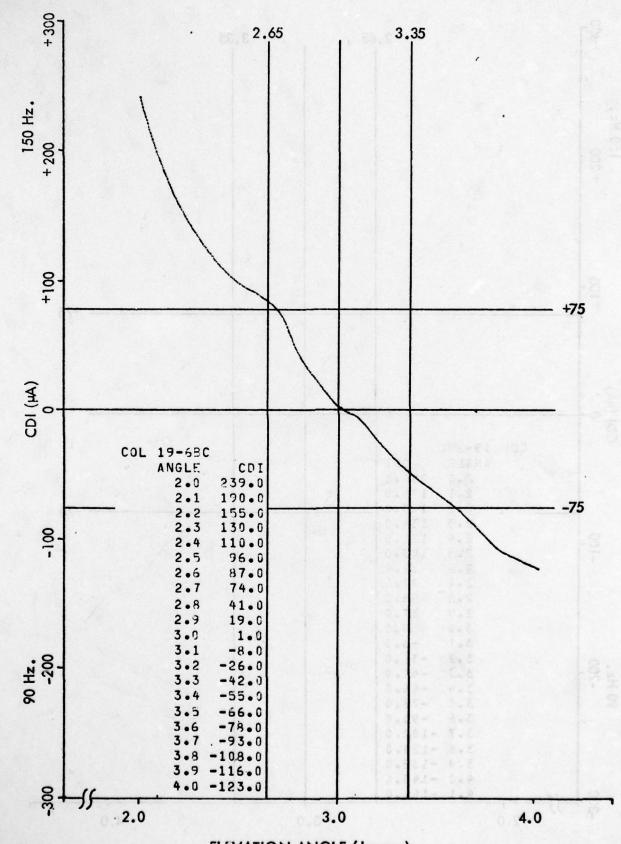
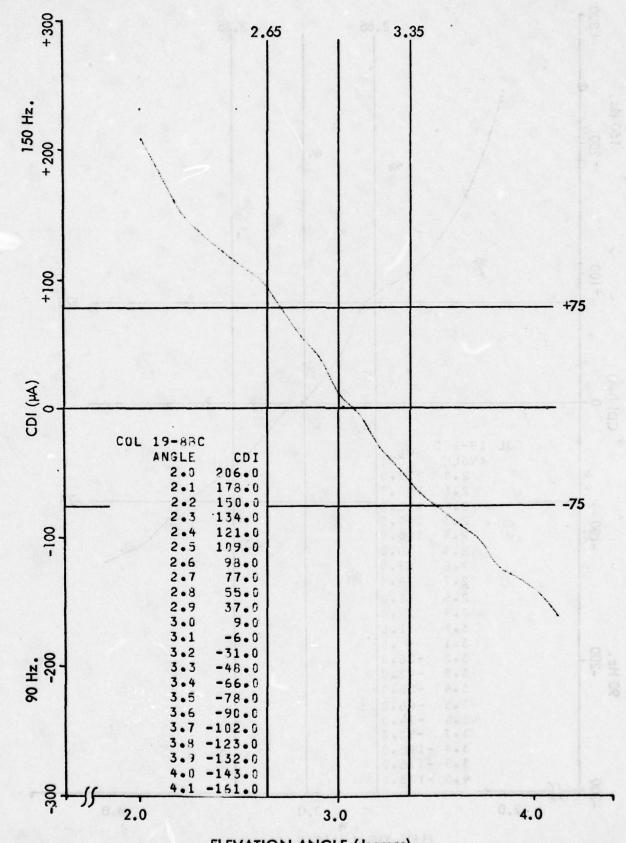


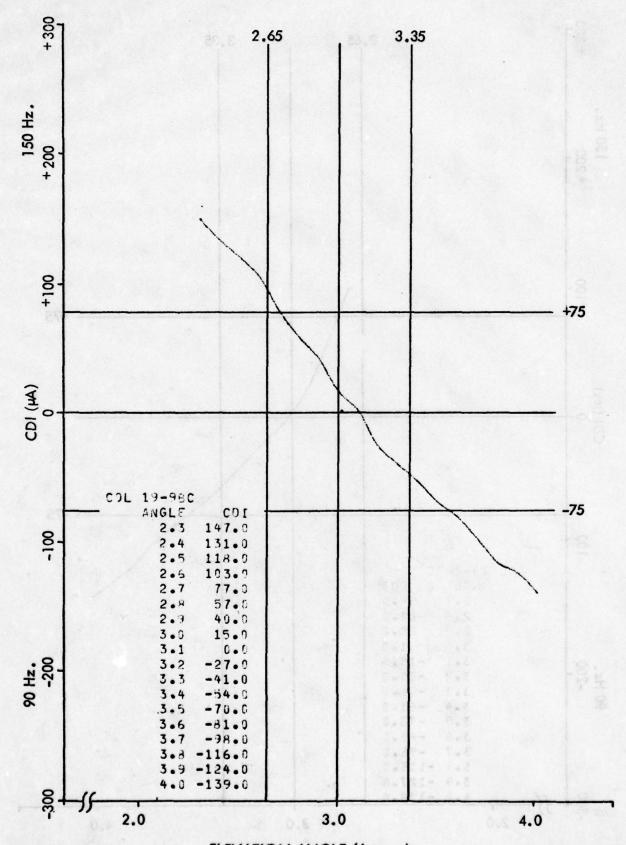
Figure 11-470. Approach 19-4BC, Normal.



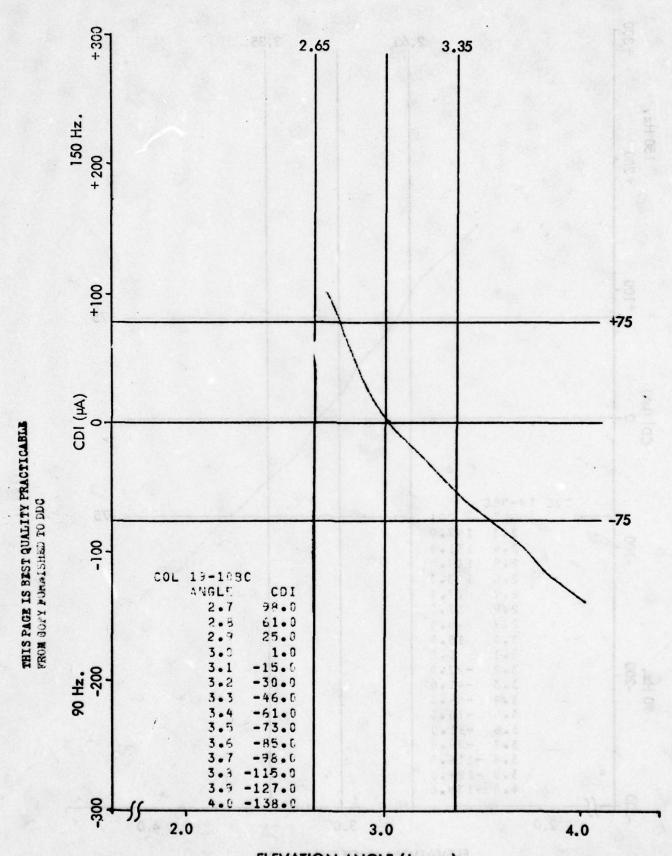
ELEVATION ANGLE (degrees)
Figure 11-471. Approach 19-6BC, SBO Decreased to Broad Alarm.



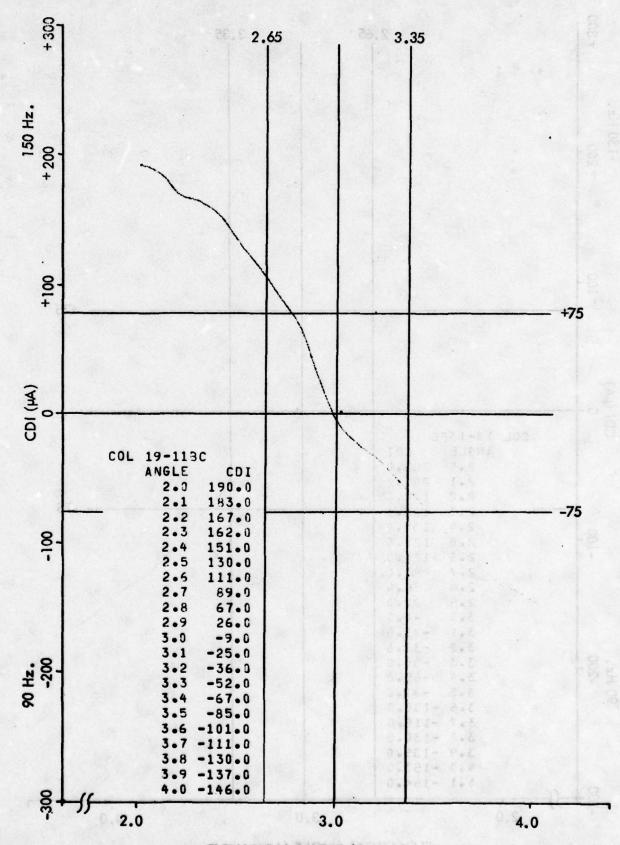
ELEVATION ANGLE (degrees)
Figure 11-472. Approach 19-8BC, Middle Antenna Phase Retarded 15°.
11-646



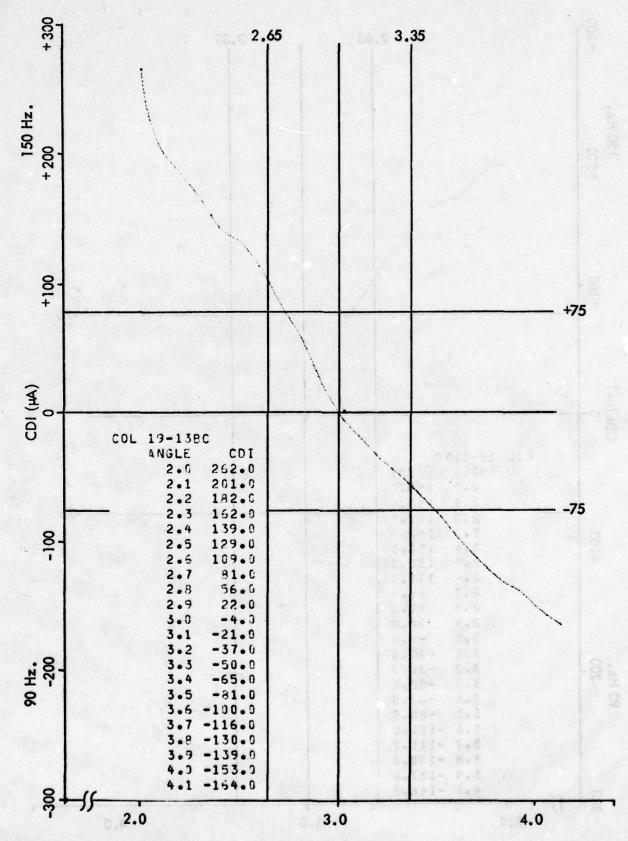
ELEVATION ANGLE (degrees)
Figure 11-473. Approach 19-9BC, Middle Antenna Phase Retarded 15°.



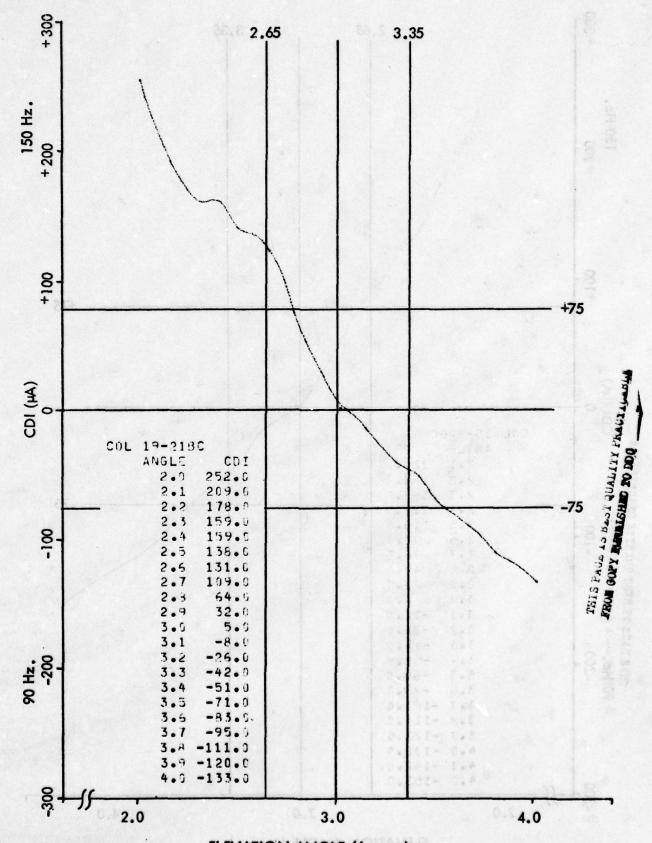
ELEVATION ANGLE (degrees)
Figure 11-474. Approach 19-10BC, Middle Antenna Phase Advanced 15°.



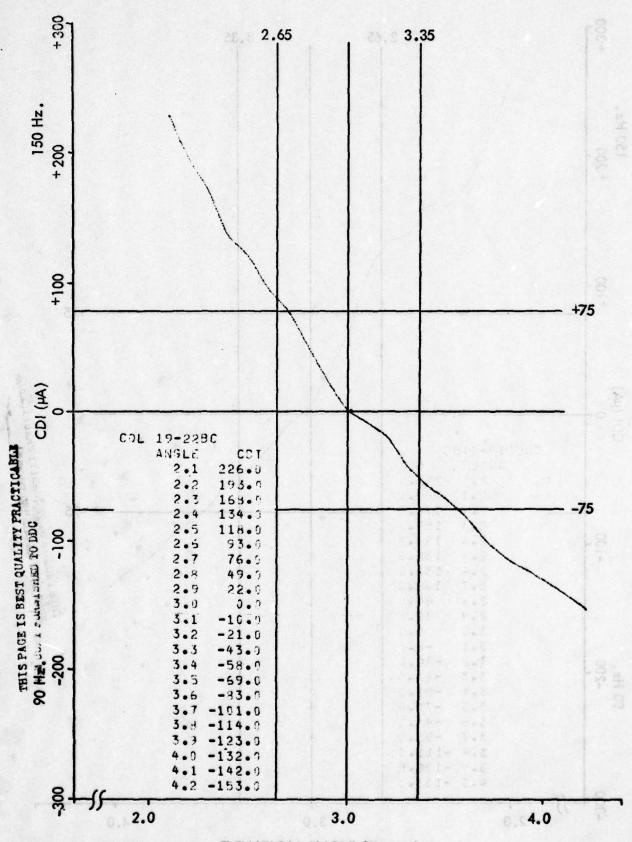
ELEVATION ANGLE (degrees)
Figure 11-475. Approach 19-11BC, Middle Antenna Phase Advanced 15°.



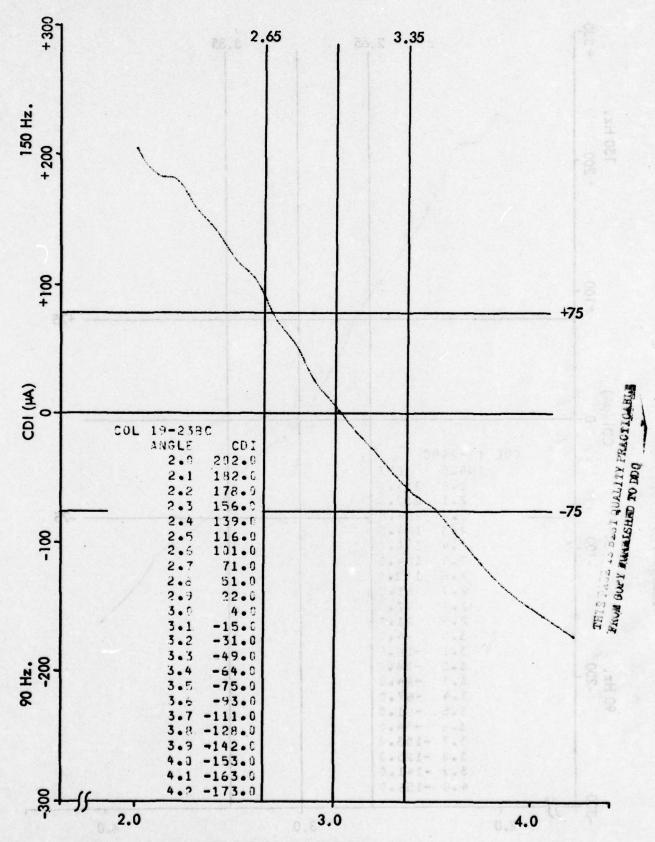
ELEVATION ANGLE (degrees)
Figure 11-476. Approach 19-13BC, Normal, Without Clearance.



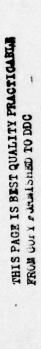
ELEVATION ANGLE (degrees)
Figure 11-47% Approach 19-21BC, SBO Phase Advanced 30°.



ELEVATION ANGLE (degrees)
Figure 11-478. Approach 19-22BC, SBO Phase Advanced 30°.



ELEVATION ANGLE (degrees)
Figure 11-479. Approach 19-23BC, Middle Antenna Phase Retarded 13°.



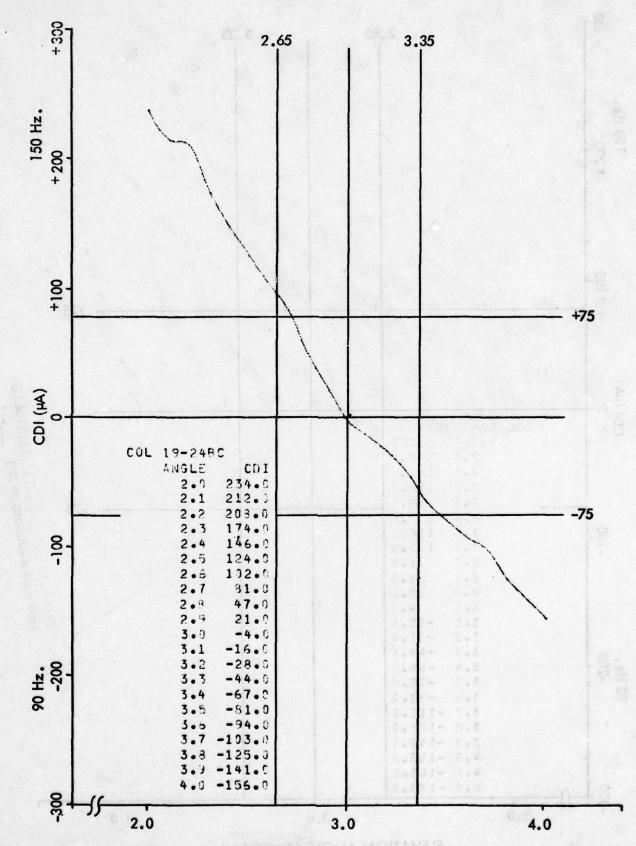
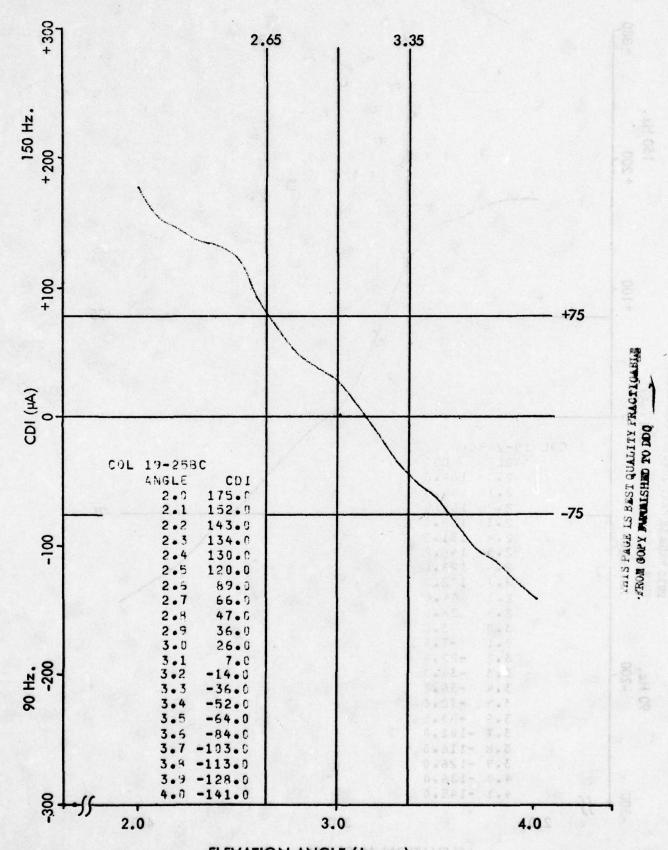
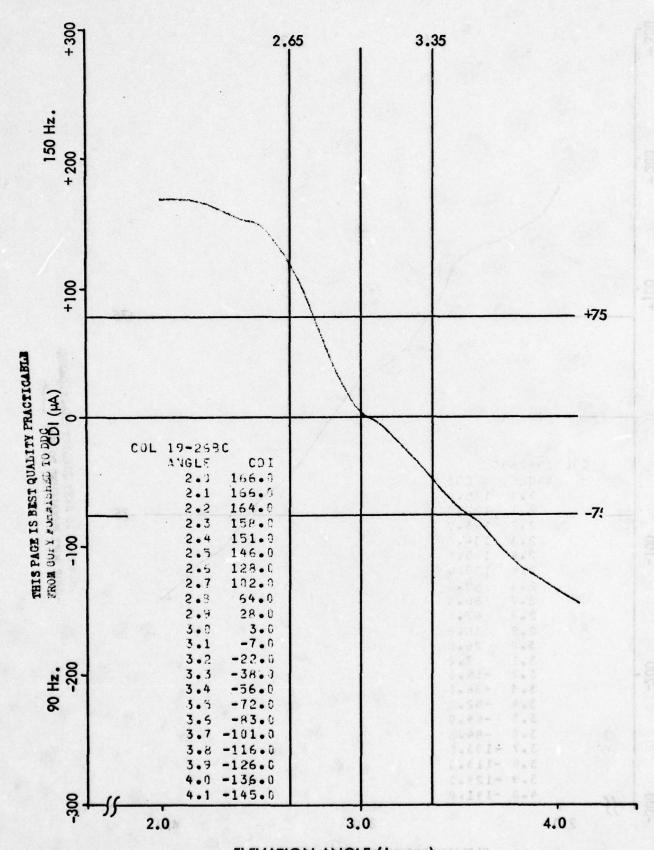


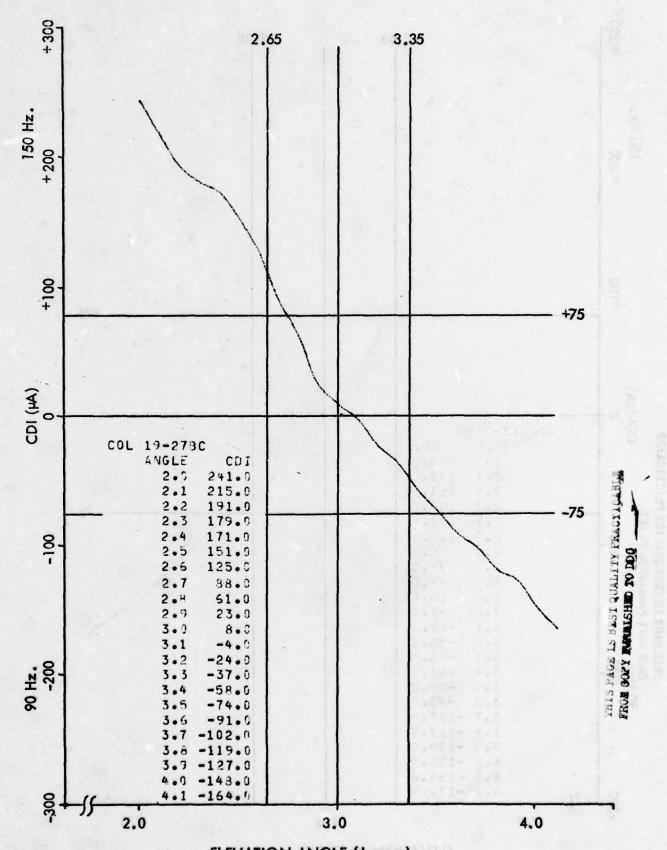
Figure 11-480. Approach 19-24BC, Middle Antenna Phase Advanced 8°.



ELEVATION ANGLE (degrees)
Figure 11–481. Approach 19–25BC, Middle Antenna Phase Retarded 18°.



ELEVATION ANGLE (degrees)
Figure 11-482. Approach 19-26BC, Middle Antenna Phase Advanced 24°.



ELEVATION ANGLE (degrees)
Figure 11-483. Approach 19-27BC, Lower Antenna Phase Retarded 14°.

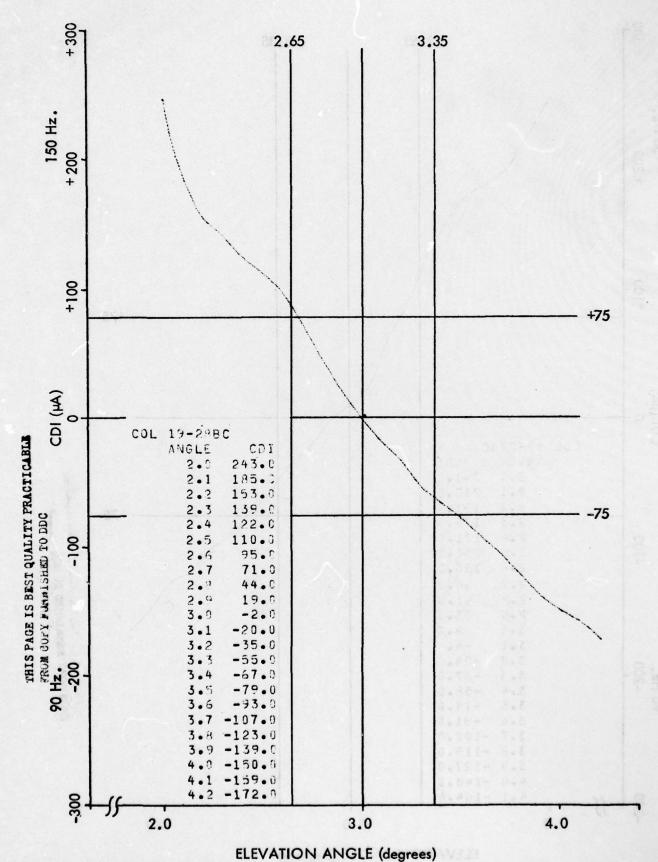
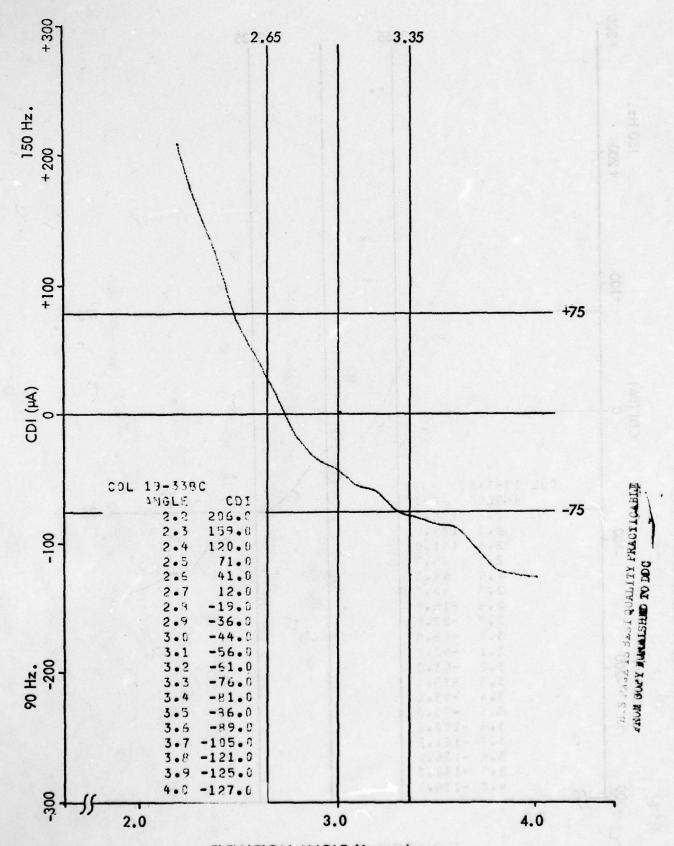
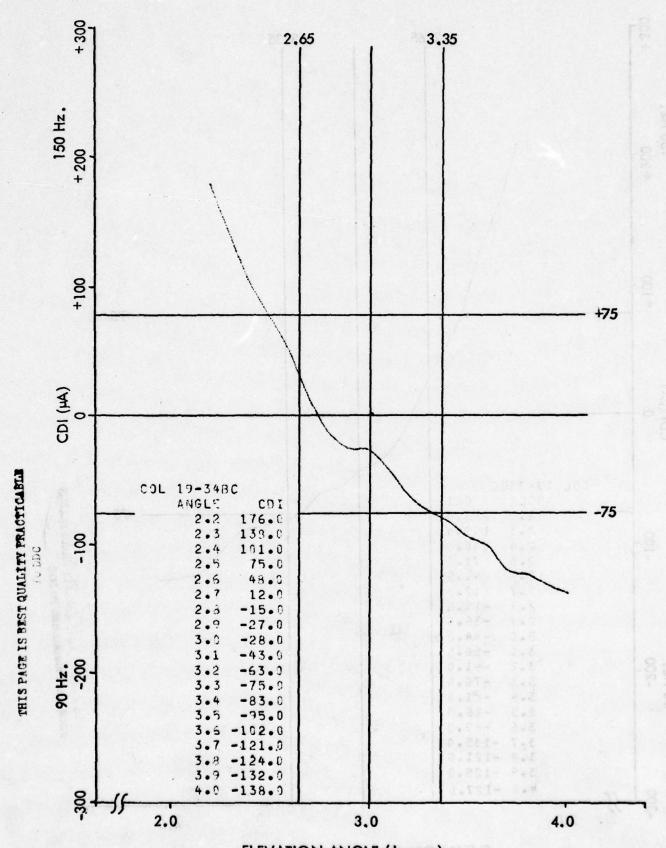


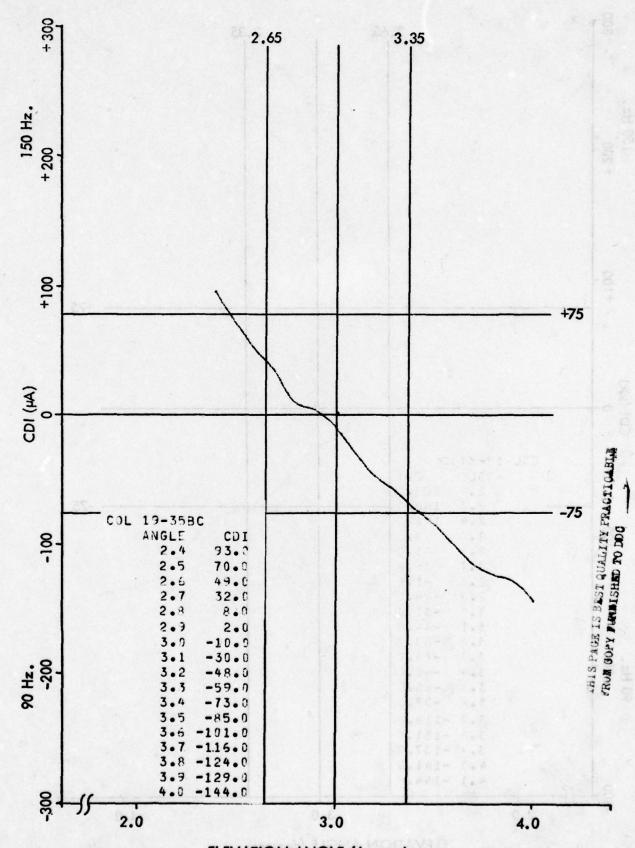
Figure 11-484. Approach 19-28BC, Lower Antenna Phase Advanced 10°.



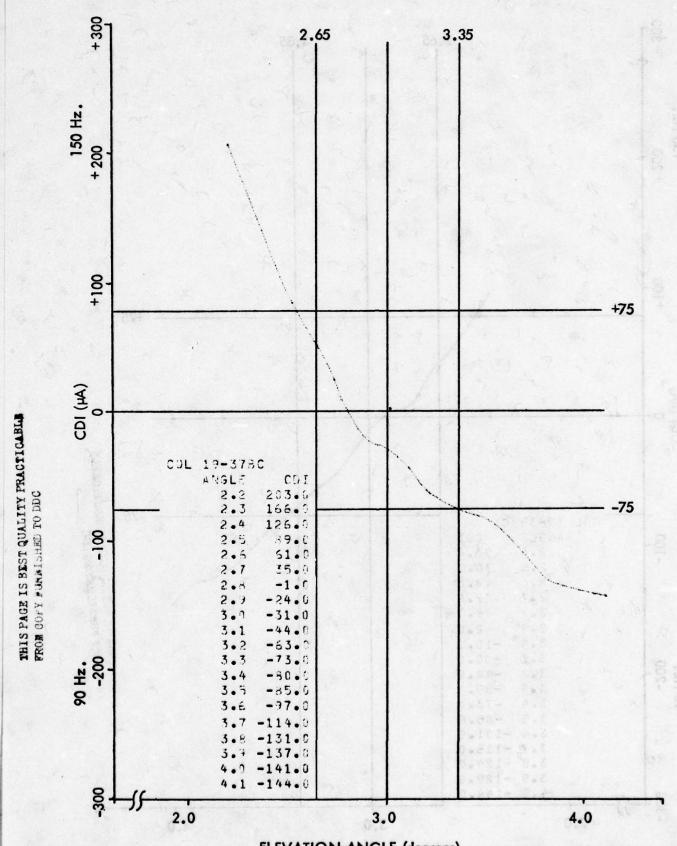
ELEVATION ANGLE (degrees)
Figure 11-485. Approach 19-33BC, Upper Antenna Phase Retarded 85°.



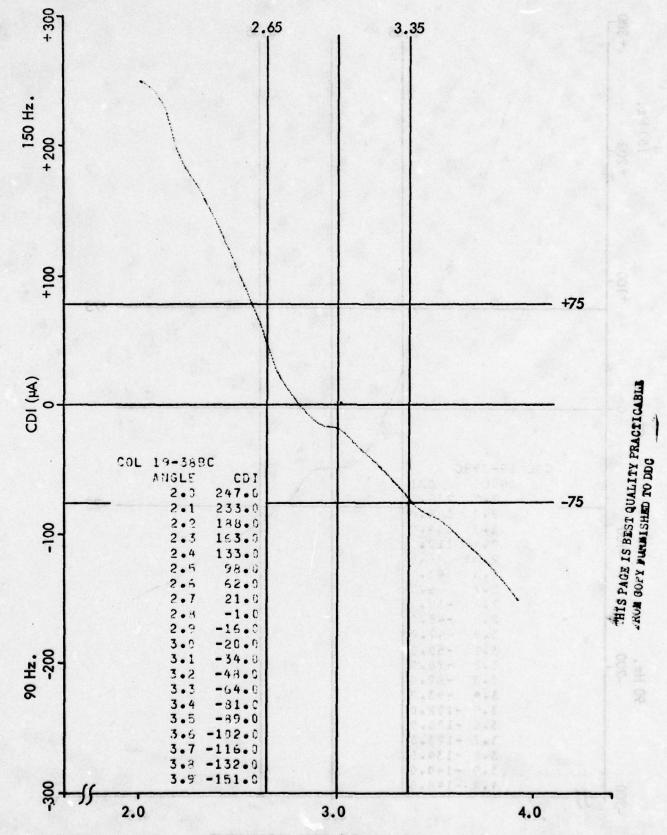
ELEVATION ANGLE (degrees)
Figure 11–486. Approach 19–348C, Upper Antenna Phase Advanced 84°.



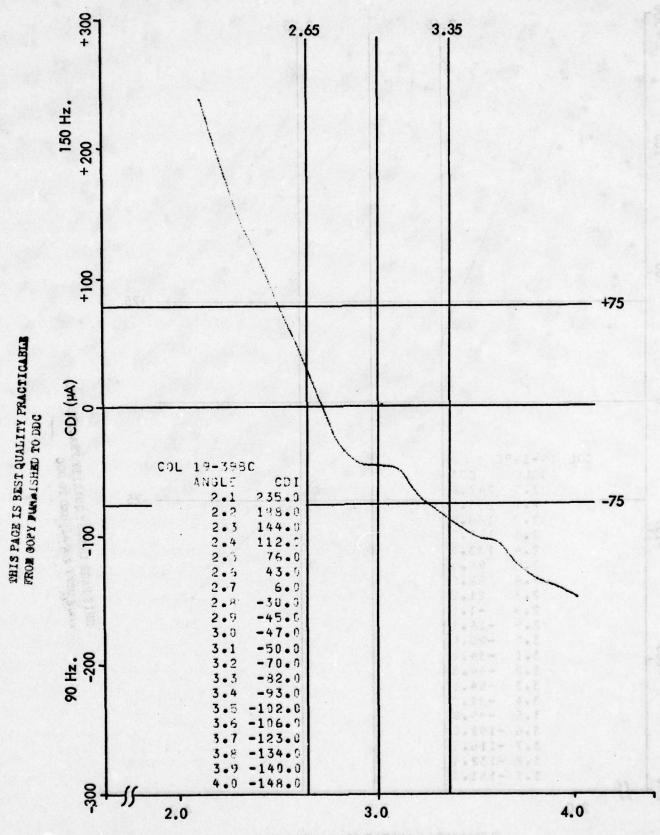
ELEVATION ANGLE (degrees)
Figure 11–487. Approach 19–35BC, Upper Antenna Phase Advanced 60° and 3 dB Attenuation in Clearance.



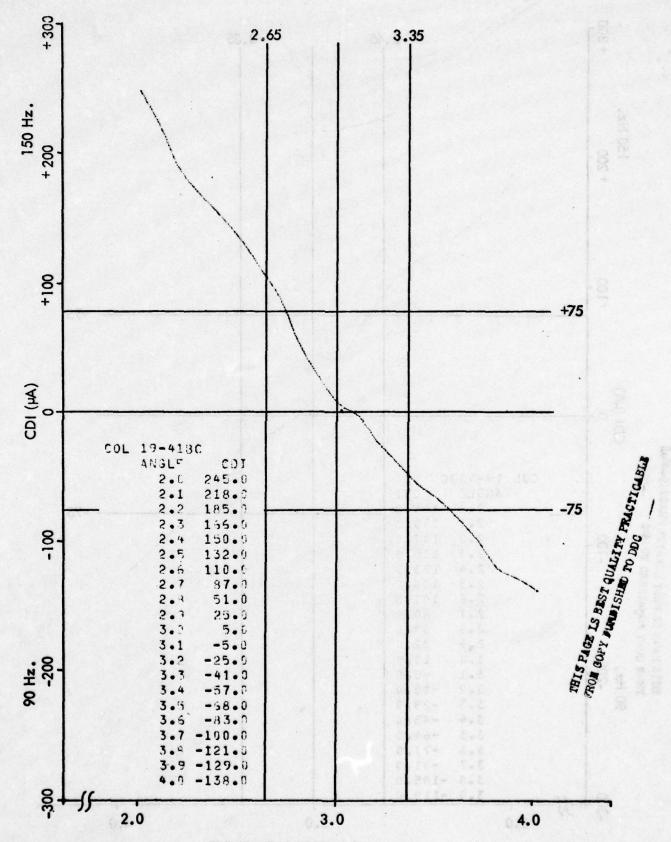
ELEVATION ANGLE (degrees)
Figure 11–488. Approach 19–37BC, Upper Antenna Phase Retarded 58° and 3 dB Attenuation in Clearance.



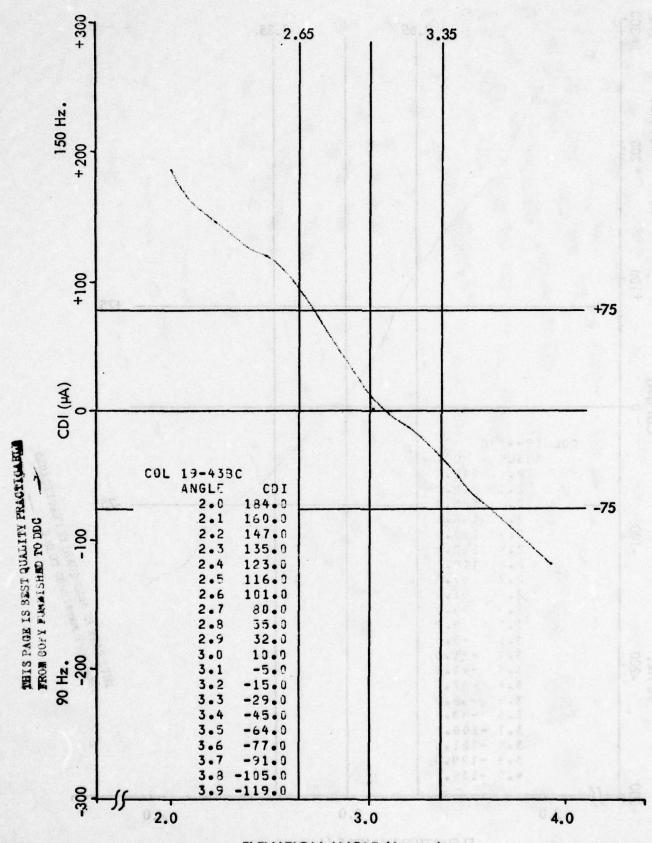
ELEVATION ANGLE (degrees)
Figure 11-489. Approach 19-38BC, Upper Antenna Attenuated 5 dB.



ELEVATION ANGLE (degrees)
Figure 11–490. Approach 19–39BC, Upper Antenna Attenuated 10 dB.
11–664

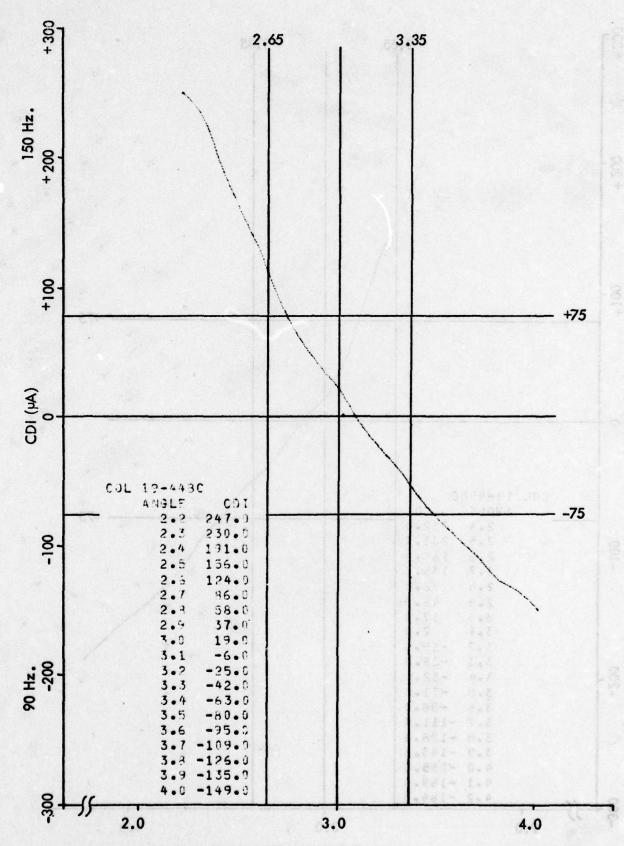


ELEVATION ANGLE (degrees)
Figure 11-491. Approach 19-41BC, Middle Antenna Attenuated 2 dB.

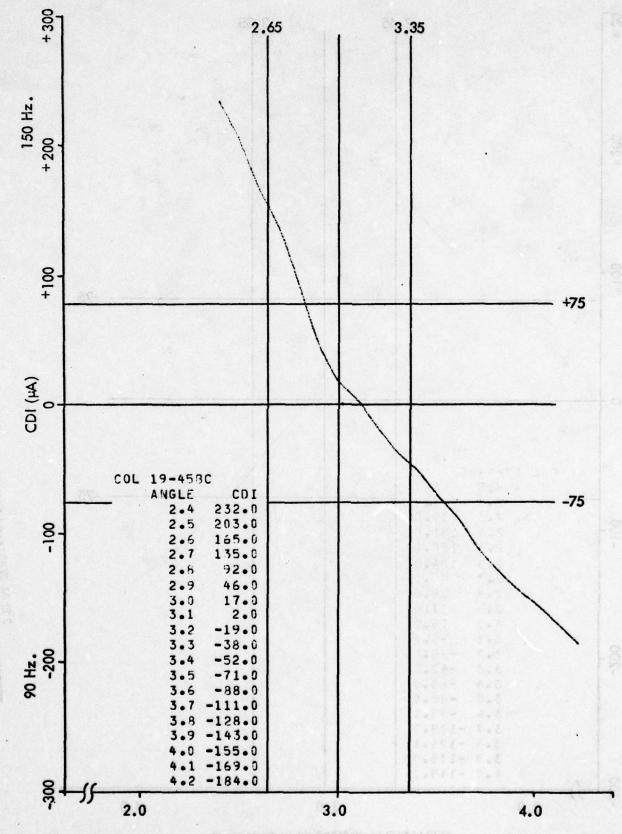


ELEVATION ANGLE (degrees)
Figure 11–492. Approach 19–43BC, Middle Antenna Attenuated 3 dB.

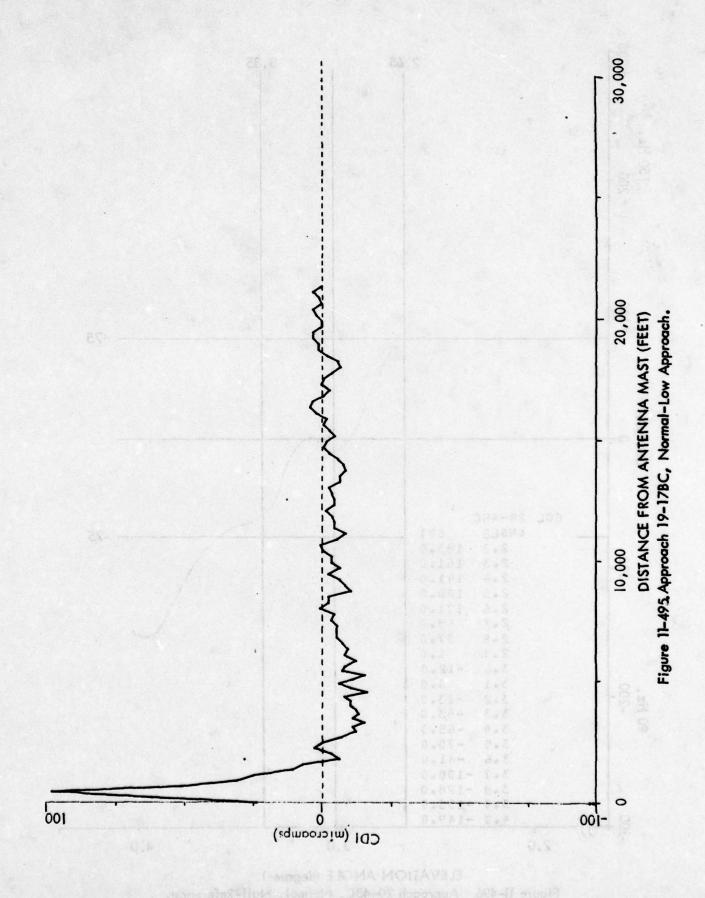


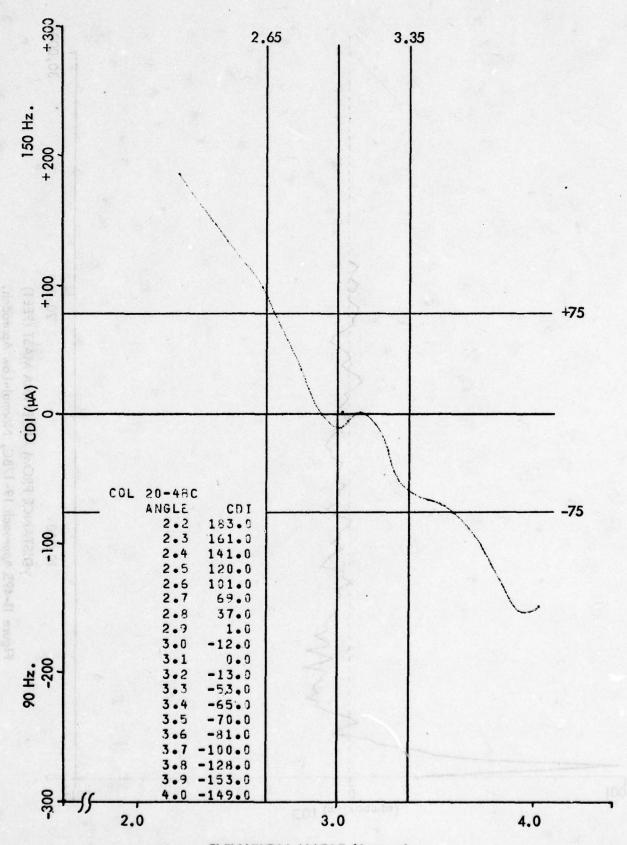


ELEVATION ANGLE (degrees)
Figure 11-493. Approach 19-44BC, Lower Antenna Attenuated 2 dB.



ELEVATION ANGLE (degrees)
Figure 11-494, Approach 19-45BC, Lower Antenna Attenuated 3 dB.





ELEVATION ANGLE (degrees)
Figure 11-496. Approach 20-4BC, Normal, Null-Reference.

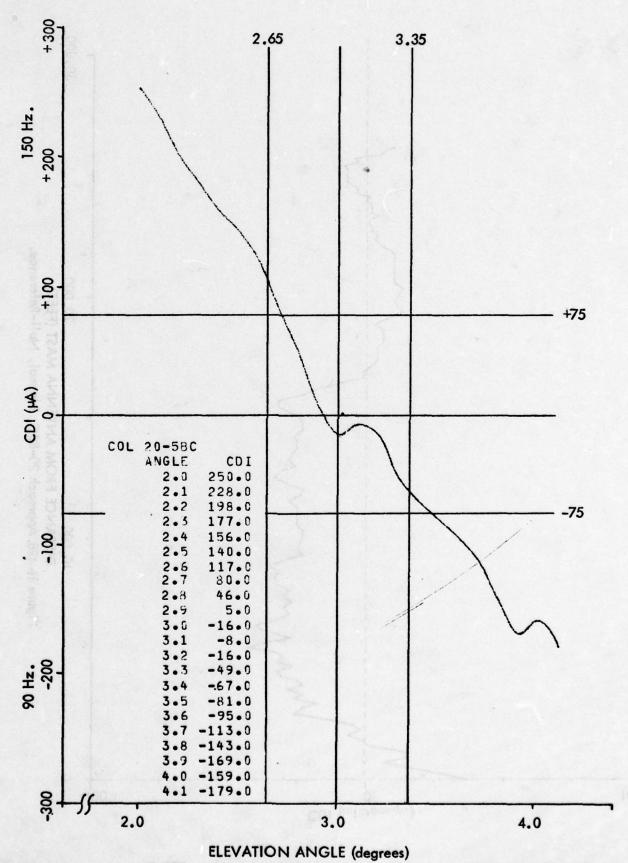
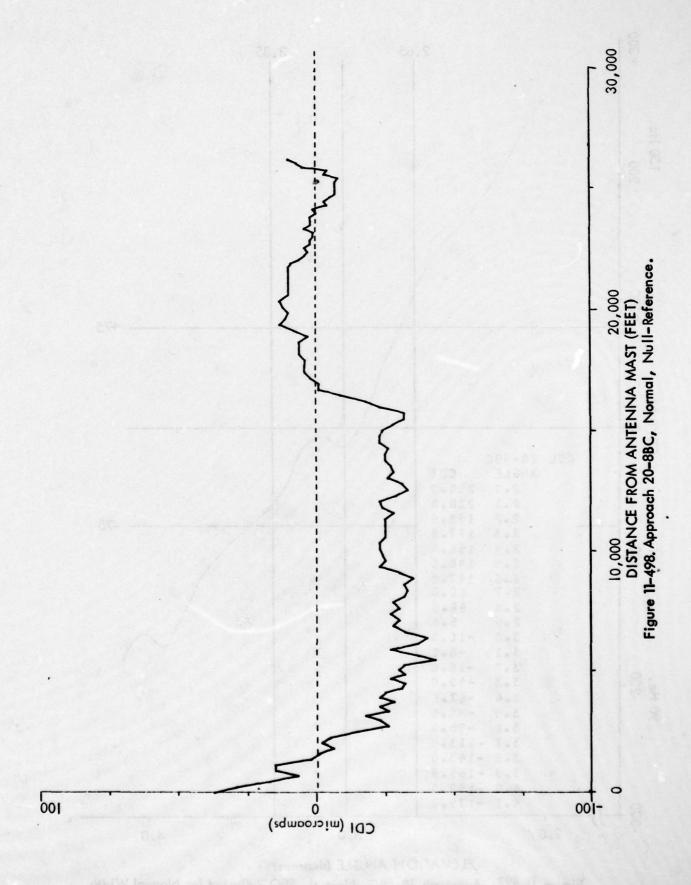
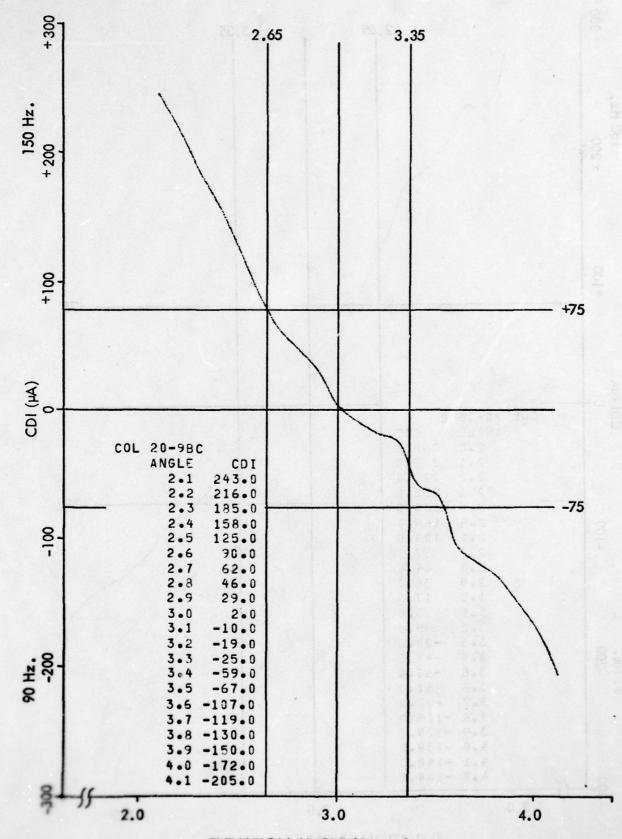
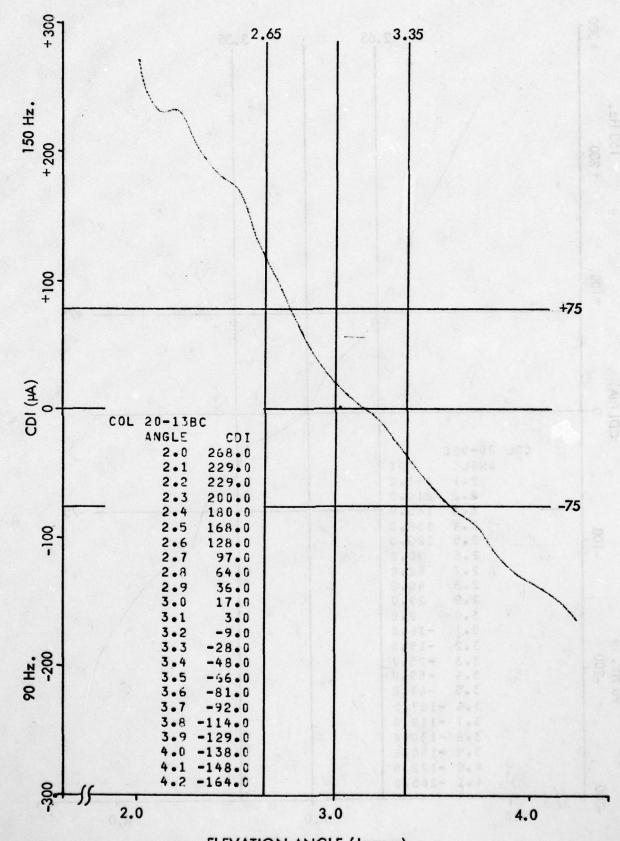


Figure 11-497. Approach 20-5BC, Normal, SBO Adjusted for Normal Width.





ELEVATION ANGLE (degrees)
Figure 11-499. Approach 20-9BC, Normal, Aircraft at 500° AGL.



ELEVATION ANGLE (degrees)
Figure 11-500. Approach 20-13BC, System Restored to Normal CEGS.

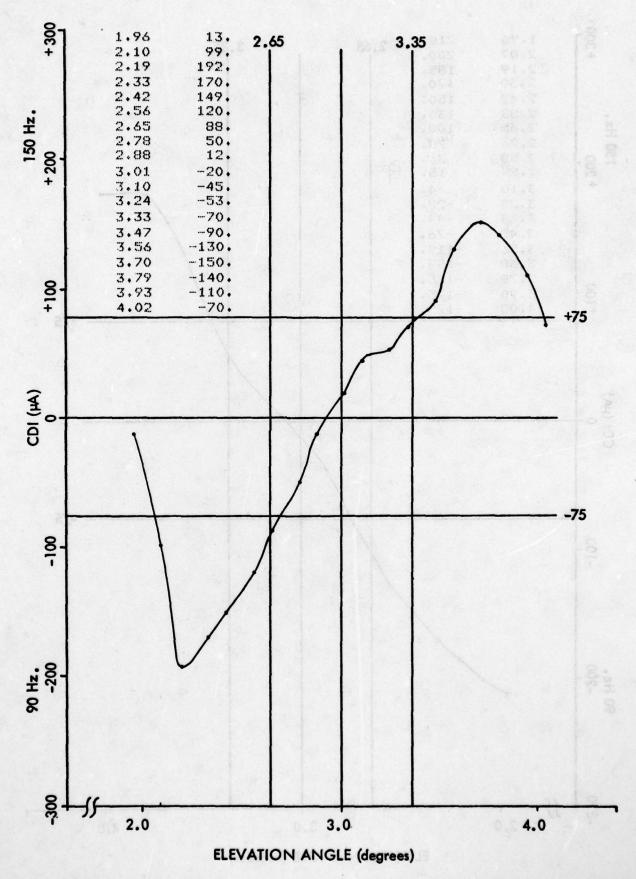


Figure 11-501. Lower Antenna Attenuated 3 dB to Greater than 200% Alarm.
11-675

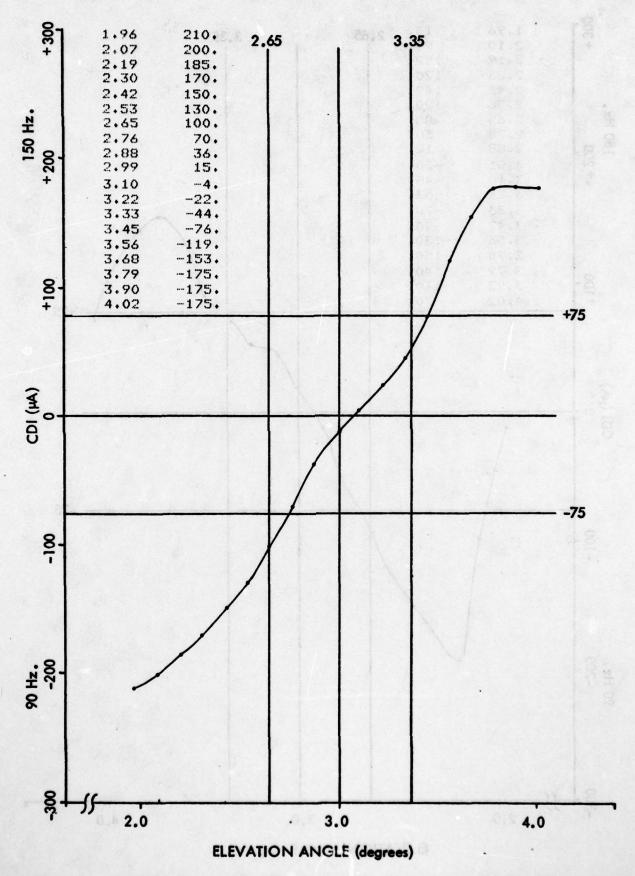


Figure 11-502. Phase of Lower Antenna Advanced 15 Degrees to Twice Alarm.
11-676

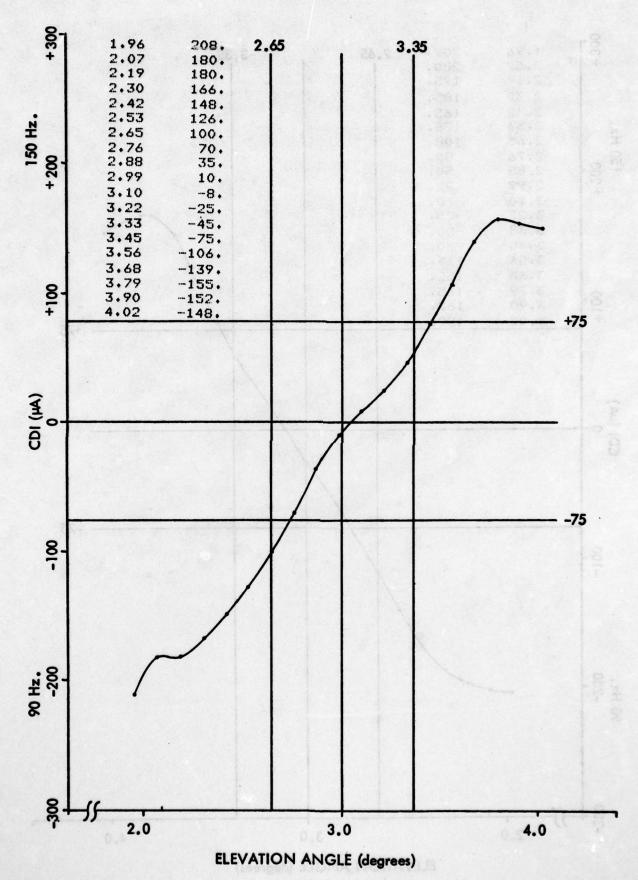


Figure 11-503, Phase of Lower Antenna Advanced 10 Degrees to Alarm.

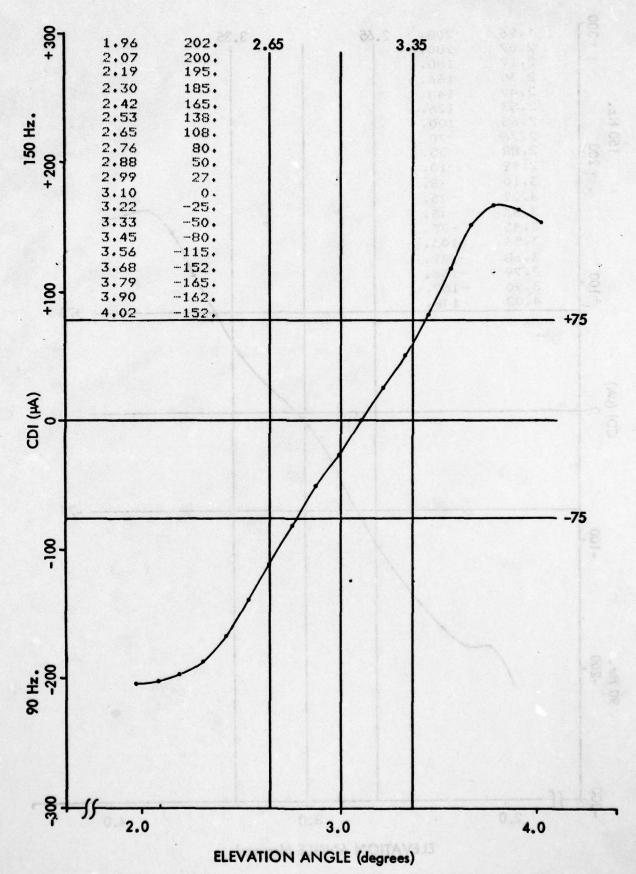


Figure 11- 504. Sideband/Carrier Dephasing; -30 Degrees. 11-678

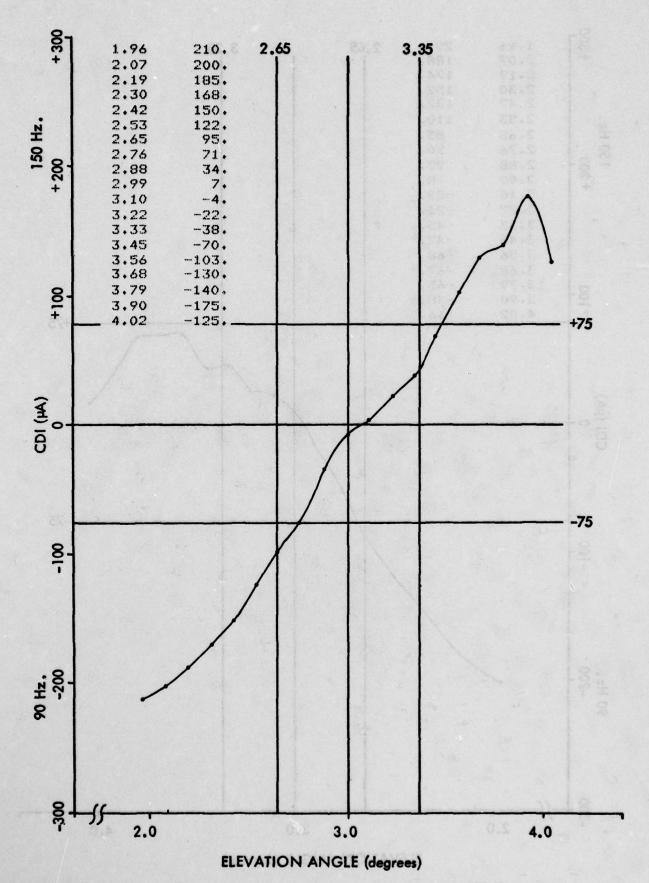


Figure 11-505. Sideband/Carrier Dephasing; +30 Degrees.

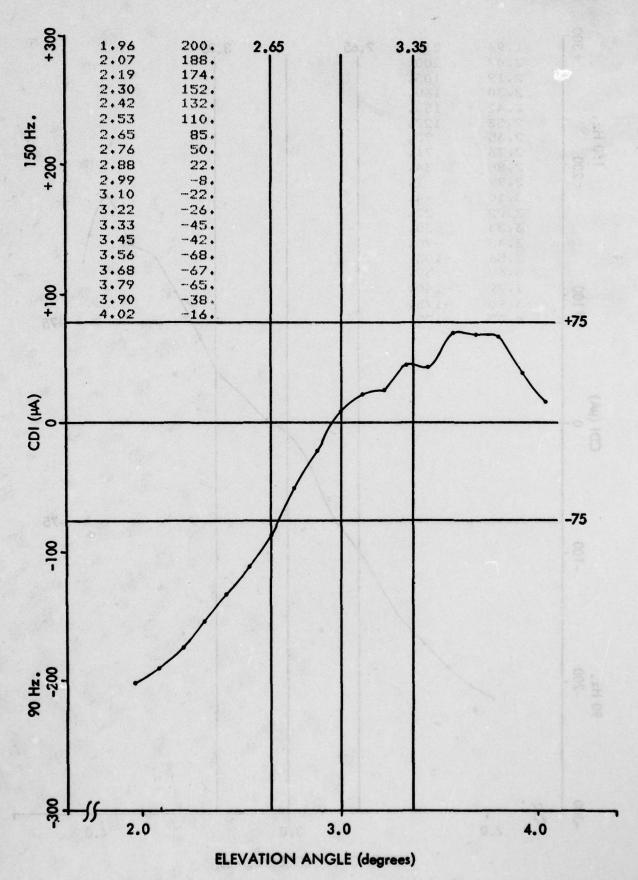


Figure 11-506. Phase of Middle Antenna Advanced 8 Degrees to Alarm.

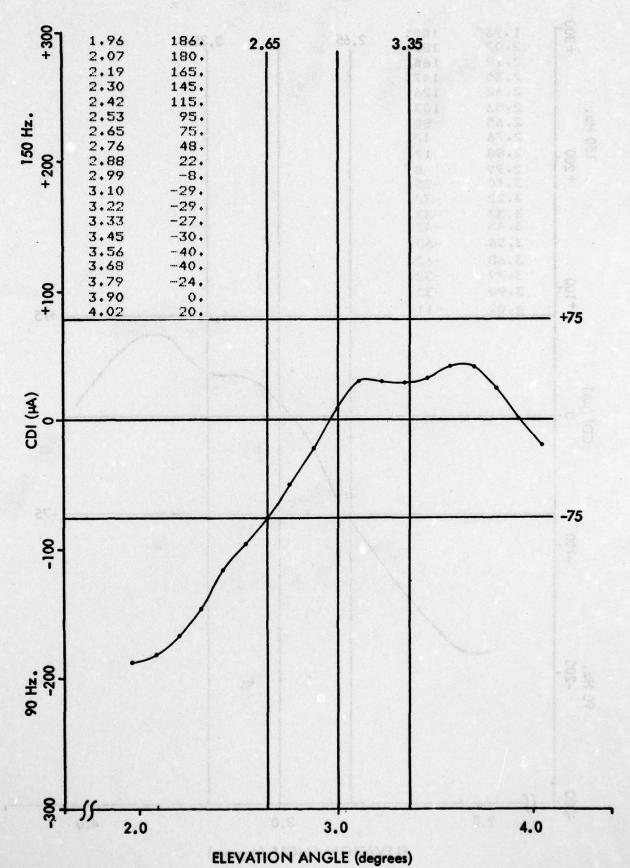


Figure 11-507. Phase of Middle Antenna Advanced 24 Degrees to Twice Alarm.

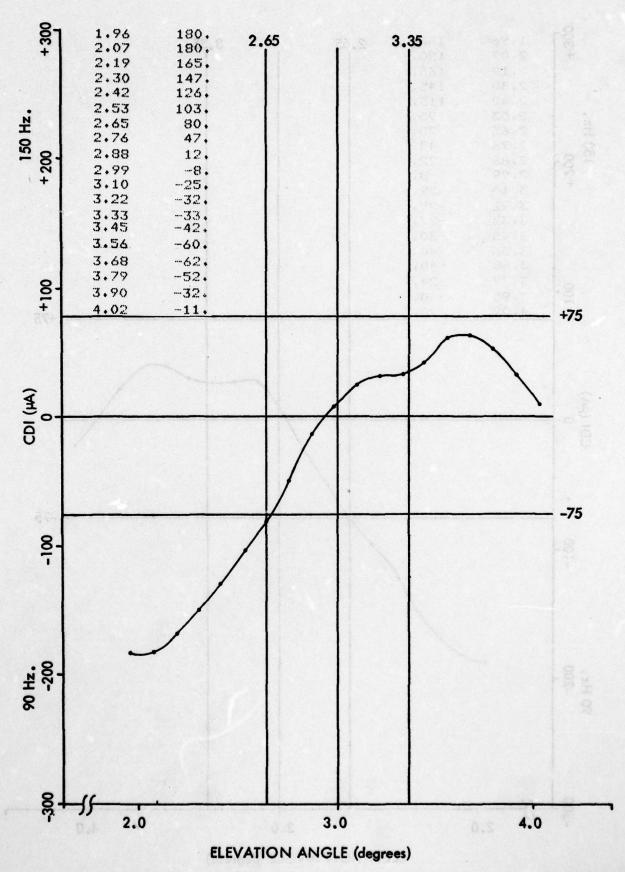


Figure 11-508. Phase of Lower Antenna Retarded 14 Degrees to Alarm.

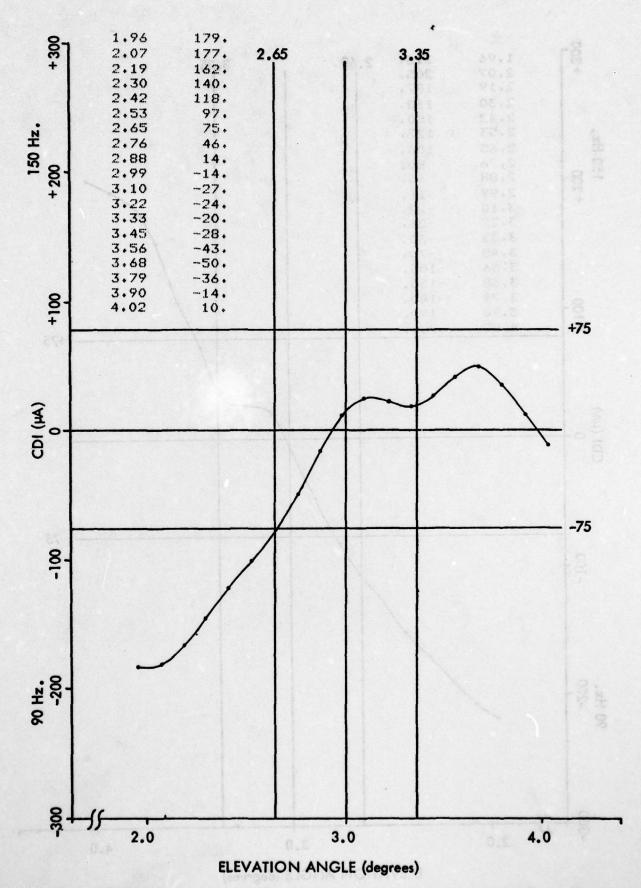


Figure 11-509. Phase of Lower Antenna Retarded 19 Degrees to Twice Alarm.

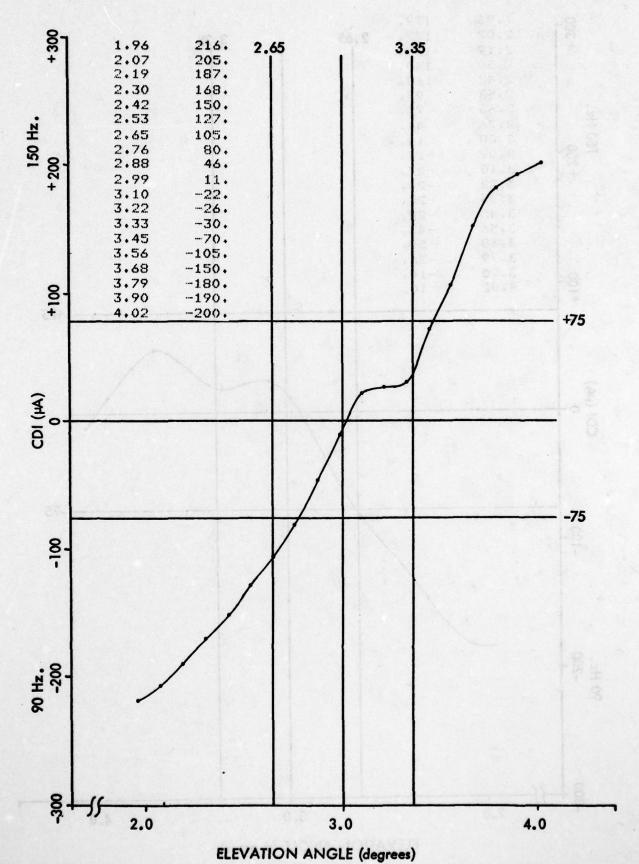


Figure 11–510. Phase of Middle Antenna Retarded 13 Degrees to Alarm.

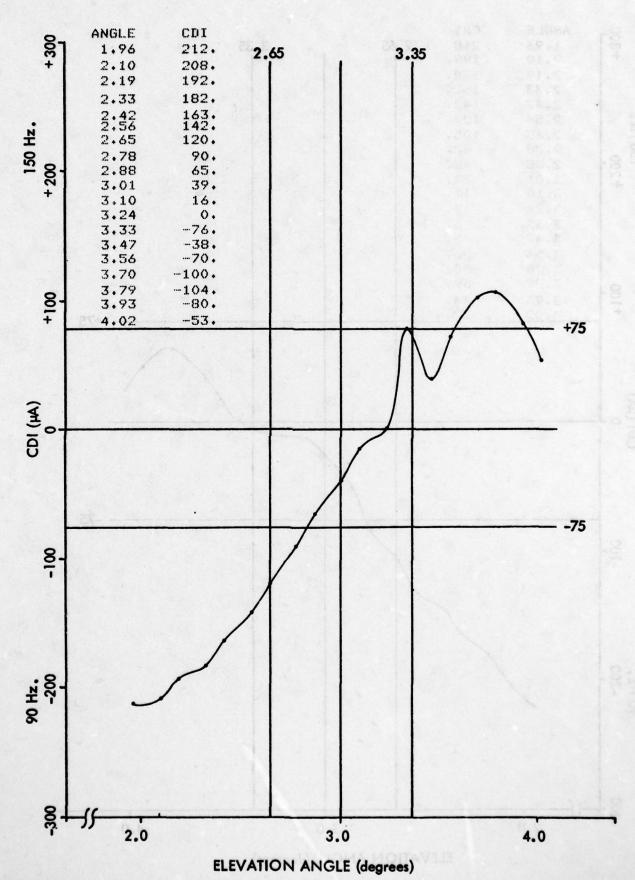


Figure 11-511. Upper Antenna Retarded 50 Degrees to Alarm (Clearance Reduced 3 dB).
11-685

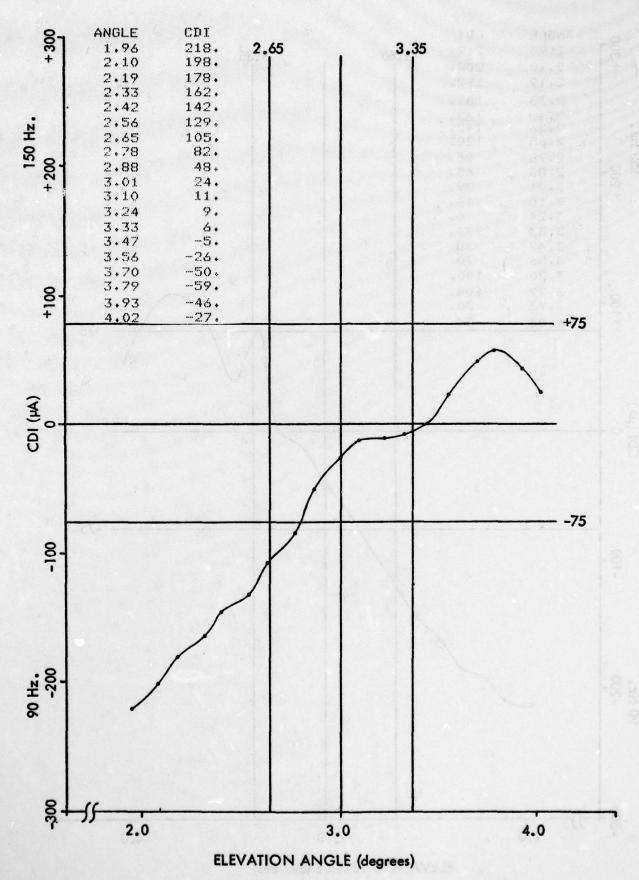
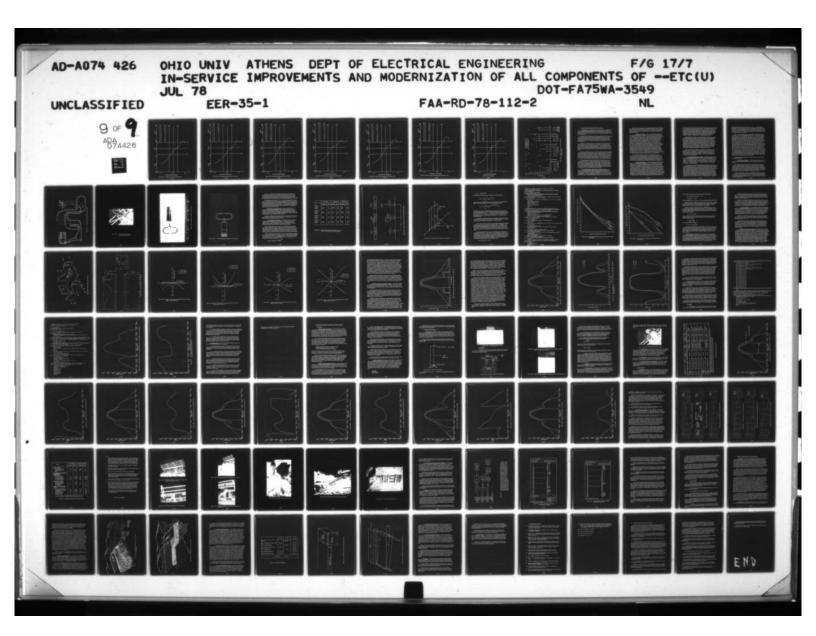


Figure 11-512. Upper Antenna Advanced 60 Degrees to Alarm (Clearance Reduced 3 dB).



9 OF 4 ADA 074426



MICROCOPY RESOLUTION TEST CHART

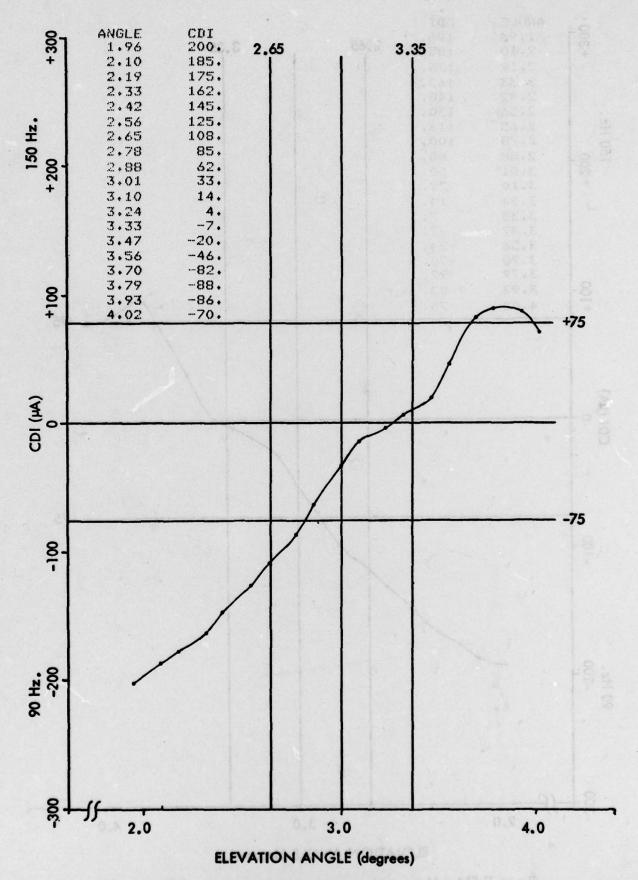


Figure 11-513. Upper Antenna Attenuated 5 dB to Alarm.

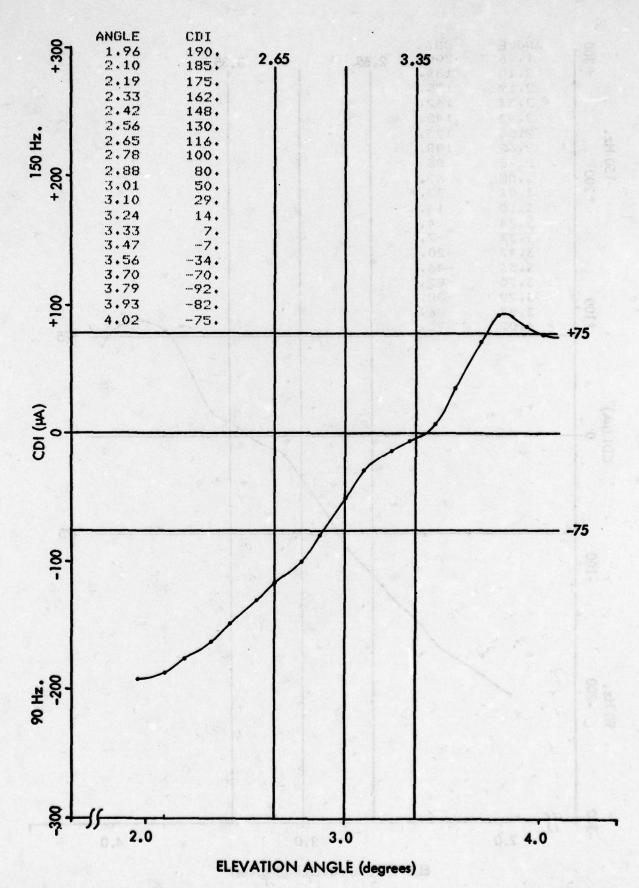


Figure 11-514. Upper Antenna Attenuated 10 dB to 133% Alarm.

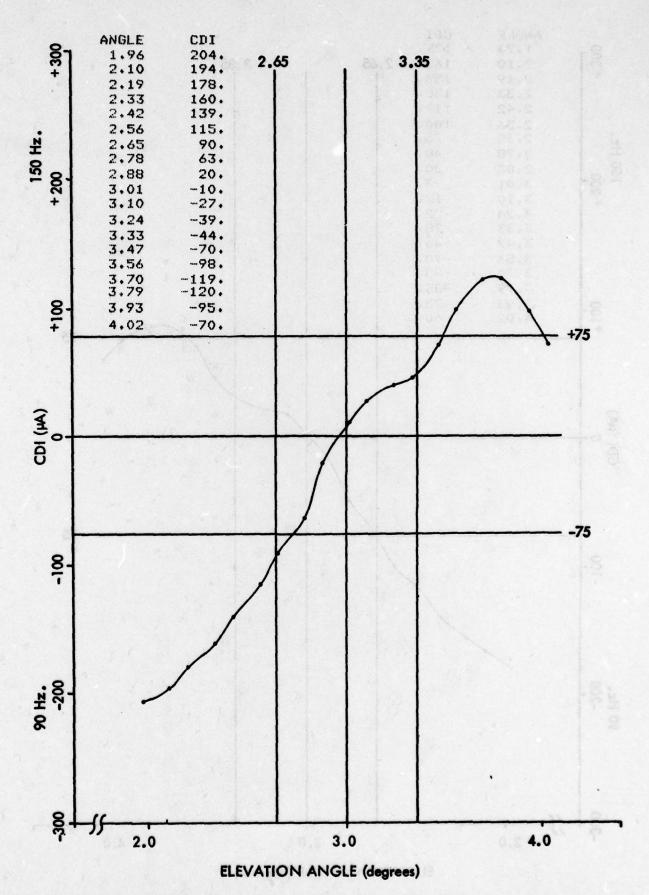


Figure 11-515. Lower Antenna Attenuated 2 dB to 114% Alarm.

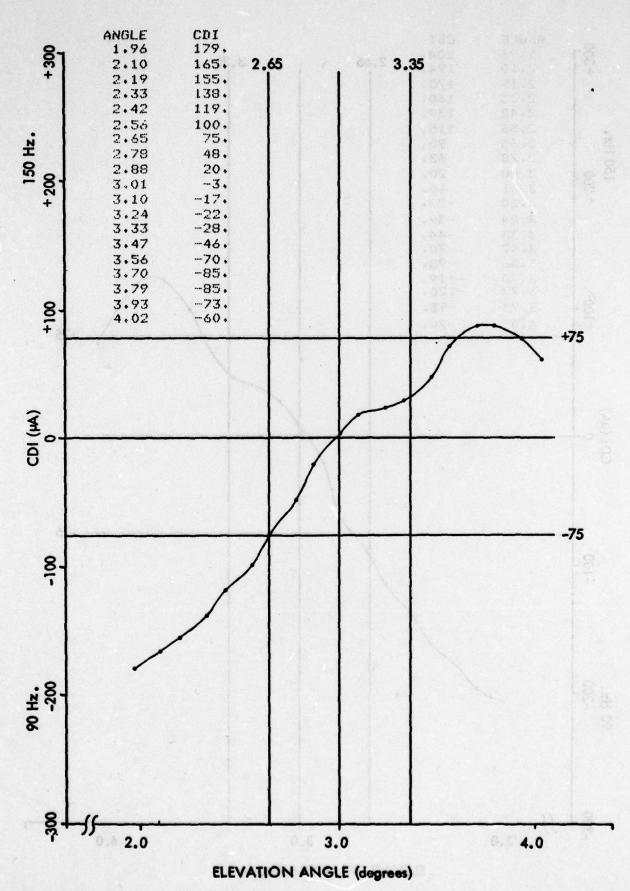


Figure 11-516. Middle Antenna Attenuated 3 dB to 170% Alarm.

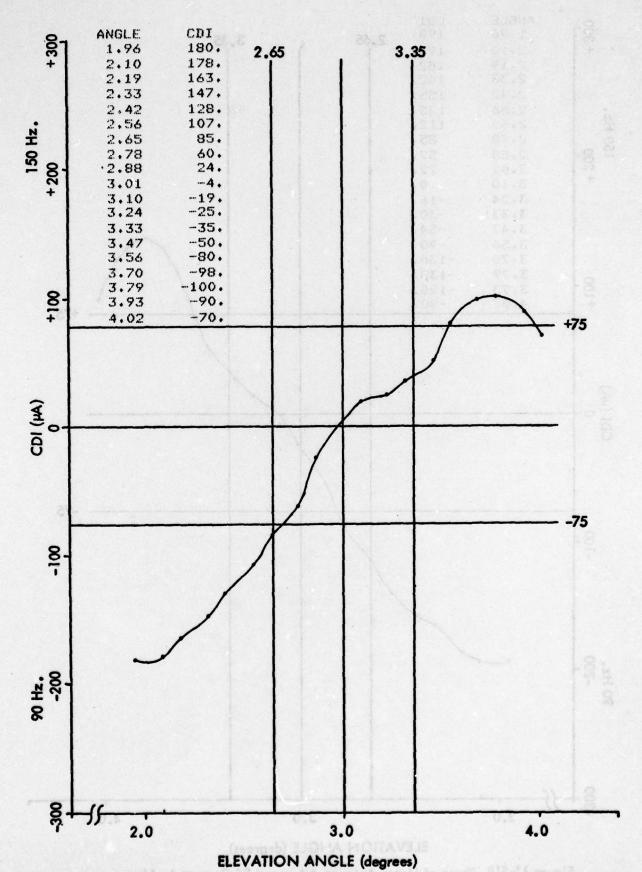


Figure 11-517. Middle Antenna Attenuated 2 dB to 128% Alarm.
11-691

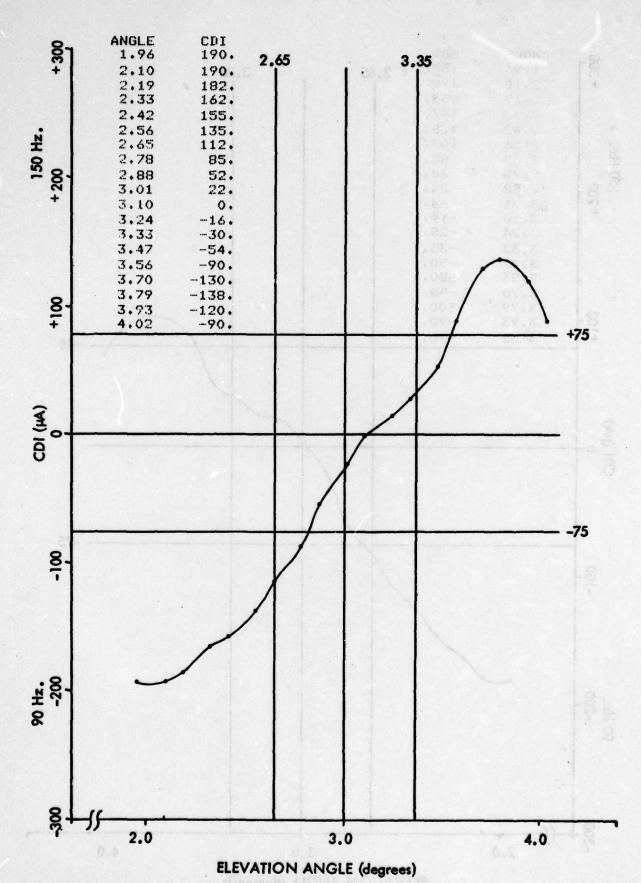


Figure 11-518. Phase of Upper Antenna Advanced 84 Degrees to Alarm.

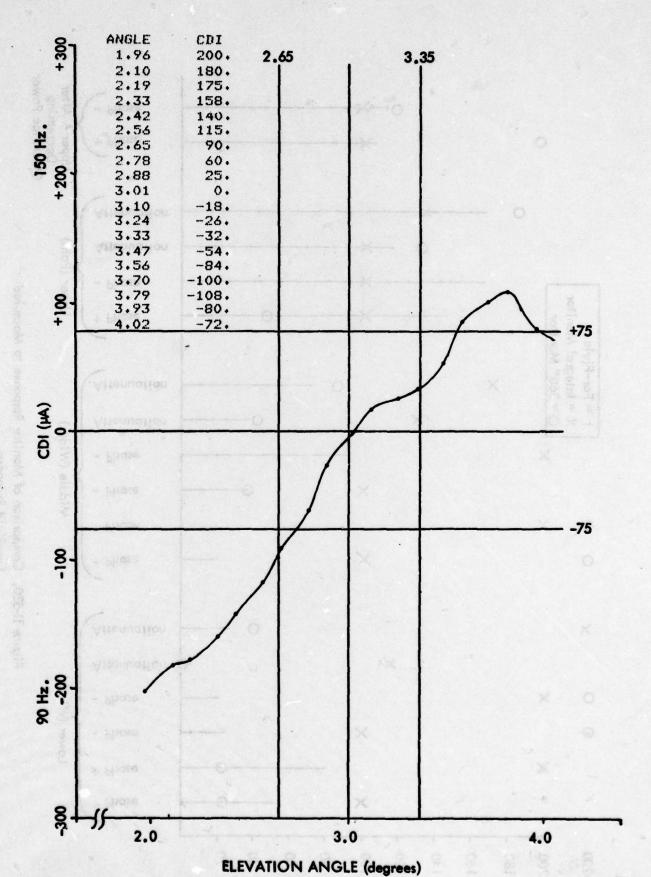


Figure 11-519. Normal Run.

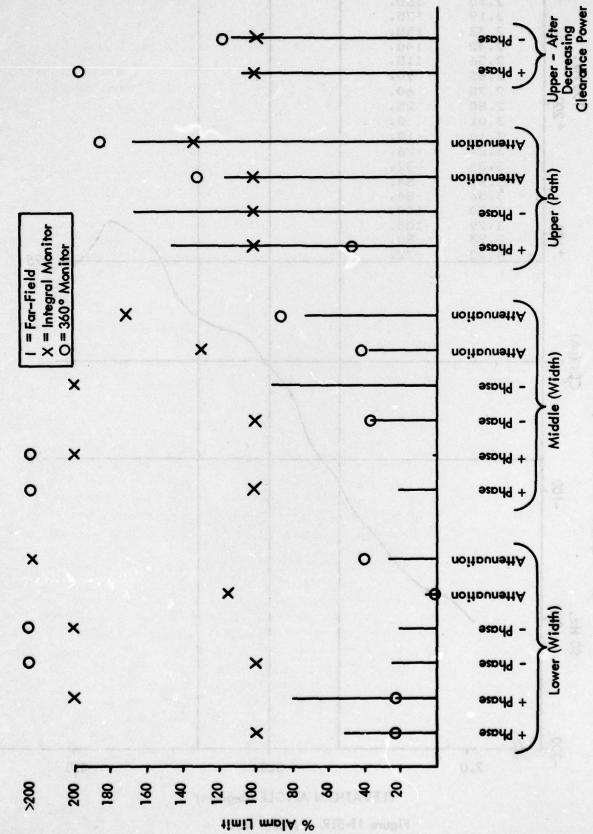


Figure 11-520. Comparison of Monitor Response to Measured Far-Field Response.

J. Measurement and Monitoring of Glide Slope Antennas.

1. Introduction. This section discusses the measurement and monitoring of the phase and amplitude of signals radiated from ILS glide slope antennas. Measurement is considered to be the process of determining the relative phase and amplitude of the signals radiated from each antenna; monitoring refers to signal sampling to allow monitoring of the glide slope.

Measurement of the radiated signals provides documentation of system performance when the antenna positions, ground plane, and transmitter modulation are known. These measurements may be taken with a hand-held probe and a vector voltmeter. A probe jig for positioning the probe has been designed. Measurements taken with a jig-held probe are shown to be significantly more accurate than those taken with a hand-held probe.

The function of integral monitoring is to predict far-field path characteristics based on voltages from the monitor port of each ILS antenna. In an ideal system, these voltages at the antenna monitor ports represent an exact analog of the antenna currents and thus the signals radiated by that antenna. The relationship between the monitor port output and the radiated signal for typical glide slope antennas, and the impact of non-ideal performance on monitoring integrity is discussed in the following sections.

In order to estimate the accuracy with which the phase and amplitude of signals radiated by glide slope antennas must be measured to predict glide path characteristics, a perturbational study was performed on a computer model that simulates a capture-effect system operating on flat terrain. The results of this study establish the relation-ship between a small variation in the antenna currents which relates to measurement error, and the resultant change in the far-field path. Given this relationship, the accuracy with which the far-field path characteristics can be predicted is determined.

The contemporary glide slope transmitting antenna typified by the Antenna Products Company FA-8976 represents a considerably more complex antenna than the bent dipole used in the past. This multi-element antenna, or antenna array, consists of three dipole elements backed by a comer reflector. The monitor voltage for such an antenna is generated by combining sample signals from each array element. This monitor port voltage represents only the signal radiated at one azimuth, usually the antenna centerline, thus suggesting that a fault condition could conceivably exist in the antenna that would not be evident at the monitor port.

2. Relationship Between Radiated Signal and Monitor Port Output. The distinction will be made between ILS system monitoring and the measurement of signals radiated from a glide slope antenna. Measurement can be accomplished via the monitor port if there is a known relationship between the monitor port voltage and the radiated signal. Effective monitoring can be performed only if a change in the radiated signal can be identified by an analogous change in the monitor port voltage.

Single and multi-element antennas are addressed separately since they represent separate antenna types with different factors affecting the monitoring and measurement process. Specimen antennas on which experiments were performed were the Meridian 4360 single-element antenna, and the Antenna Products Company FA-8976 multi-element antenna array.

a. Single-Element Antennas. The Meridian 4360 glide slope antenna is a single-element antenna with a radiator that is fed through a directional coupler. The incident port of this coupler yields an analog of the forward signal to the antenna, while the reflected port of the coupler is an analog of the signal reflected by the antenna. Under ideal circumstances, the antenna would be matched to the transmission line and to free space. In this instance, no power would be reflected by the radiating element and the total radiated signal would be represented by the voltage at the incident port of the directional coupler. Under less-ideal circumstances, an impedance mismatch exists that causes some of the signal sent to the antenna to be reflected back into the transmission line; in this case, the incident port would no longer provide an analog of the radiated signal. Clearly, the incident port of this antenna will provide useful monitoring information only when the reflected port voltage indicates that the radiating element is matched to both the transmission line and to space. Experimental results obtained with the Meridian antenna indicate that the incident port does provide an acceptable analog of the radiated signal when the standing wave ratio (SWR), as determined by the incident and reflected ports, is below 1.1. For SWR's below that value, the incident port was shown to provide an analog of the radiated signal within the measurement accuracy of a jig-held probe that was used to evaluate the monitor port performance.

Four Meridian 4360 glide slope antennas were evaluated in this study. A side-by-side comparison of these antennas shows that the relationship between the incident port output and the radiated signal was consistent from antenna to antenna as measured by a jig-held probe; the SWR for these measurements was below 1.1. Such consistency can permit phase and amplitude measurements of the radiated signal to be made via the incident port when the SWR is determined to be sufficiently low.

b. <u>Multi-Element Antennas</u>. The Antenna Products FA-8976 glide slope antenna is a three-element colinear antenna array. The advantage of using multi-element antennas as opposed to single-element antennas is, of course, that greater directivity can be achieved in the radiation pattern with the multi-element type. Monitoring is accomplished by combining equal signal samples from each array element to generate a single output voltage that is intended to be an analog of the composite signal radiated by the array. Sampling the radiated signal in this manner, however, provides information about the radiated signal only at one azimuth; this azimuth, which cannot be discerned from the monitor port output, corresponds to the azimuth where signals from each array element add in the far field with the same amplitude and phase relationship with which they are summed in the combining network providing the monitor port signal. This azimuth is typically along the antenna boresight since the signals from each element are summed with equal phase to generate the monitor signal. The

monitor, then, observes only one particular azimuth, and there could conceivably exist an out-of-tolerance condition at some other azimuth. For example, if the feed lines of two of the elements were interchanged, the monitor port output would remain unchanged since the combination of signals from the individual elements would not be changed; the composite radiated signal, however, might change considerably depending upon the phase and amplitude relationship of the feed lines interchanged. Although this example is not likely to occur, it does bear out the fact that a fault condition can occur in the far field that is not evident at the monitor port.

Experimental data was taken on 11 FA-8976 glide slope antennas to determine the relationship that exists between the monitor port output and the radiated signal. This relationship was determined by feeding a known signal to each antenna and determining the difference in phase and amplitude between the radiated signal (as determined by a jig-held probe) and the signal at the monitor port. The results of this experiment reveal that the relationship between monitor port output and radiated signal differs considerably (greater than 4 dB in amplitude and 10° in phase) from antenna to antenna. This inconsistency in the relationship between radiated signal and monitor port output does not necessarily indicate a deficiency in monitoring capability since effective monitoring can be performed as long as changes in the radiated signal are appropriately reflected in the monitor port output.

Since the monitor port output does not provide an exact analog of the signal radiated, and the relationship between the radiated signal and the monitor output differs from antenna to antenna, it is undesirable to employ the monitor port of a multi-element antenna to determine the phase or amplitude signals radiated by an antenna. Rather, probe measurement techniques, such as the ones presented later in this section, should be employed.

3. Recommended Measurement Techniques. The equipment required to perform the probe measurements is as follows: 1-VVM (Hewlett-Packard 8405A or equivalent), 1-current induction probe, 2-50 ohm dummy loads, 2-50 ohm coaxial cables of equal length that are long enough to reach from the VVM to the most distant antenna, 1-50 ohm phase shifter, 2-50 Ω tee connectors (H.P. 11536A or equivalent), and 1-50 Ω power splitter (H.P. 11549A or equivalent). Most of these items require N-type cable fittings.

The first procedure that must be performed before taking probe measurements is to adjust zero phase on the VVM. This is accomplished by feeding the A and B channels of the VVM with the same signal and adjusting the "zero" knob of the VVM. This is done by connecting both tee connectors to the outputs of the power splitter and dummying the outputs of the tee connectors. When the power divider input is fed with a signal at the glide slope frequency, this signal will be fed to both tee connectors in phase at the same amplitude; a cable connected to the middle antenna monitor port has proven to be a convenient signal source for feeding the power splitter. With the VVM connected as described above, zero degrees phase shift should be read on the phase meter with the "phase offset" knob on zero; adjustments to attain a zero degree readings should be made with the "zero" knob. The voltage readings on channels A

and B should also be checked to insure that they are of the same magnitude; small differences between the channels (.2 dB) are not uncommon and will not affect the measurements. If larger differences are seen, the VVM probes should be interchanged in the tee connectors; if the difference between the channels remains the same, it is recommended that the VVM be calibrated, as the problem is with the VVM and not the tee connectors or the power splitter.

Figure 11-521 depicts the suggested configuration for making antenna probe measurements. Once the configuration of Figure 11-521 is completed, the measurements can be taken by using the following procedure: (1) turn on the transmitter: for antenna diagnostics, only the frequency of the transmitted signal is of importance (a signal generator at the proper frequency will suffice). In order to measure CSB or SBO ratios, transmit only the signal of interest. (2) Connect the cable from the "A", or reference port of the VVM to the monitor port of the lower antenna and mount the probe in front of the center element of the lower antenna (see Figure 11-522). The probe is connected to the "B" input of the VVM. Zero the VVM phase meter with the "phase offset" knob set at zero by adjusting the phase shifter. Note the signal amplitude in millivolts on the "RMS VOLTS" scale of the VVM. (3) Without removing the cable from the monitor port (since all measurements are being made with respect to the lower antenna, the monitor port output will be the reference for the entire test), move the probe to the other elements of the antenna and note their phase and amplitude values. As an accuracy check, place the probe on the center element again to be sure that the phase and amplitude has not drifted from the values read previously. If drifting has occurred, reset zero and go through the procedure again. (4) Measure and note the parameters of each of the elements of the remaining antennas. Again, after all other measurements are taken, recheck the phase and amplitude of the center elements of the lower antenna to insure that no drifting has occurred. If drifting has occurred, the entire procedure must be performed again.

By performing the above procedure, the relative output of all of the antenna currents can be specified.

4. Hand-Held Probe Performance. Hand-held probes have been and are presently used to determine quantitatively the values of signals being radiated from an antenna.

The probes used for this study are magnetic induction probes that sample the magnetic, as opposed to electric, field near a radiator (such probes are depicted pictorally in Figure 11-523, and schematically in Figure 11-524). These probes are constructed with 1/8 inch outer diameter semi-rigid 50 Ω copper-jacketed coaxial cable, although any small, semi-rigid coaxial cable will be adequate. The constraint on the cable size is that it be several orders of magnitude less than the wavelength so that the probe will have a minimal effect on the fields being measured.

As seen in Figure 11-524, there is a short length of exposed center conductor on the probe. It is across this gap that a potential is created, according to Faraday's Law, due to fields in the vicinity of the probe. This induced voltage represents an analog of currents on the radiating element, [9] and this element current is representative of the radiated signal.

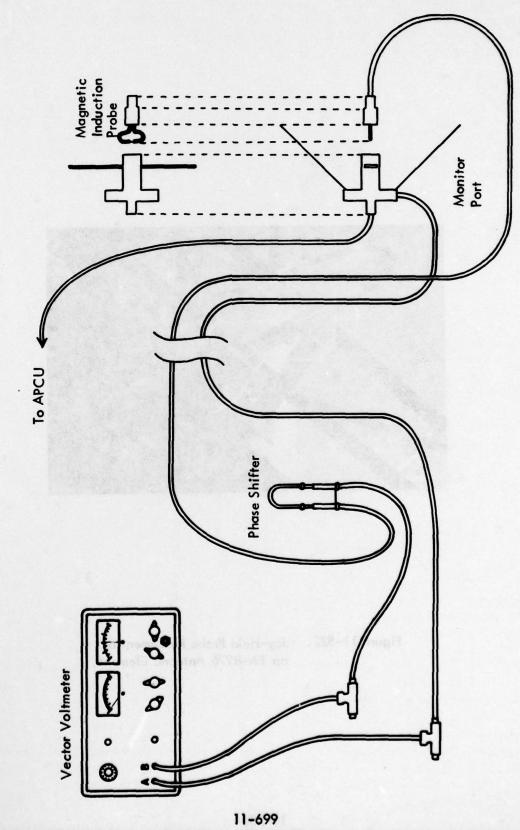


Figure 11-521. Configuration for Making Probe Measurements.

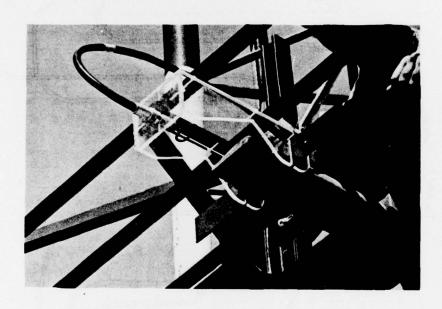


Figure 11-522. Jog-Held Probe Placement on an FA-8976 Antenna Element.

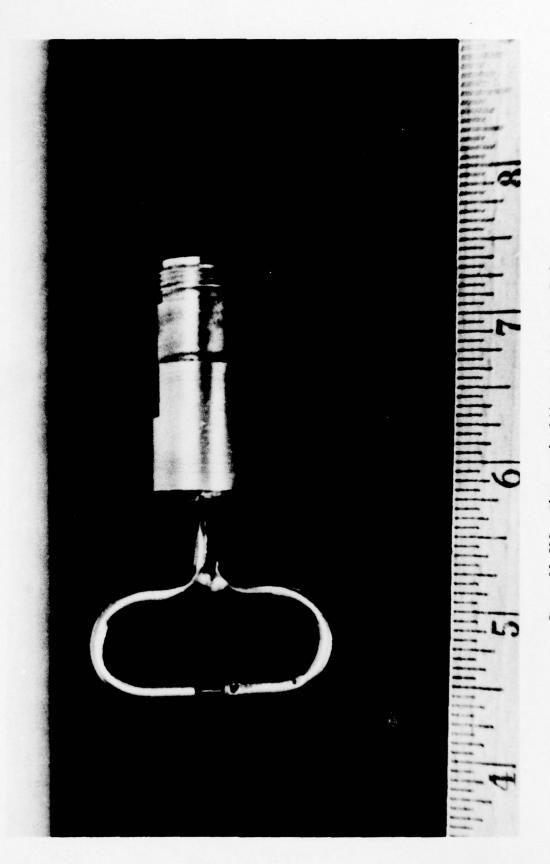


Figure 11-523. Photograph of Magnetic Induction Probe.

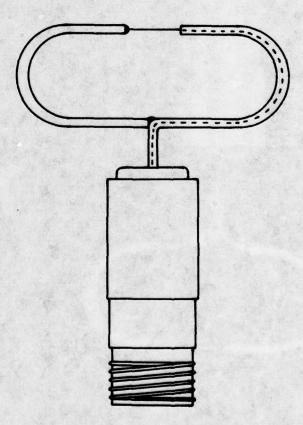


Figure 11-524. Schematic Representation of Magnetic Induction Probe.

Table 11-39 presents probe measurements obtained by four individuals on a commissioned glide slope facility. This data represents a best-case situation as the individuals participating in the experiment were experienced with such measurements and were performing the measurements on an antenna with easy access; similar tests were performed under less ideal circumstances with appreciable degradation in accuracy.

The measurements listed in Table 11-39 are for the three elements on the lower antenna. The "above" and "below" row represent measurements taken on top and underneath the indicated elements; these measurements should be of the same magnitude and of supplementary phase angles. As seen in Table 11-39, the measured amplitude varies by over one-half decibel and the phase by over 10°. Data from other hand-held probe measurements support the contention that the data of Table 11-39 is as repeatable as can be expected using hand-held probes.

5. Development of the Jig-Held Probe. Extensive work with terrain-sensitive glide-slope computer simulations at Ohio University indicated that in order to make accurate predictions concerning glide slope system performance, antenna currents must typically be measured with greater accuracy than has been realized with hand-held probes. This conclusion motivated the development of a simple jig for holding the probe while vector voltmeter readings are made.

Analyses and experiments have been performed to answer the question as to where the probe should be positioned to sample antenna currents with greatest accuracy and without interference from other elements in the array.

a. Probe Placement and Stability. The magnetic field in the vicinity of a radiating element relates directly to the antenna currents generating that field. Induction probes, such as the ones used for this report, sample magnetic fields. Antenna currents can then be determined from probe measurements once the relationship between magnetic fields and antenna currents has been established.

Figure 11-525 shows the basic dimensions of the FA8976 glide slope antenna. Each radiating element of this antenna is electrically one-half wavelength long and employs thin rectangular metal plates for the dipole arms; using such a rectangular plate element instead of a thin wire element allows the element to resonate over a broader range of frequencies. Determination of the magnetic field near these elements involves integrating the magnetic field contributions from each incremental piece of the element.

Numerical integration can be employed to solve the integral defining the magnetic field in the immediate vicinity of a radiating surface by summing the field contributions over all elements of the surface. The coordinate system for the analysis presented here is given in Figure 11-526. Using this coordinate system, the field contribution from any element (x,z) seen at the test point is: [9,10]

$$H_{x}(y)$$
 from element $(x,z) = \frac{I(x,z)e^{-i\beta r}}{r}$

e magni kude e	Outer Dipole		Middle Dipole		Runway Dipole	
r sbutilqaas b ng blan-bash	Amplitude	Phase	Amplitude	Phase	Amplitude	Phase
Subject 1	p I Stall alon	to cleb	ntion first has	disco will	floopque afneros	utcam J
Above Below	-10.5 -10.0	73 112	-11.5 dB -11.5	46° 130	-10.0 -10.0	75° 112
Subject 2	erwich ausgeber Manschau is Ma	eqols al	Alg salmeses	n ensitals	e occureta pro-	est of
Above Below	-10.2 -10.0	75 110	-11.5 -11.5	43 140	-10.0 -10.0	77.5 110
Subject 3	was not named a	a Lamerts	re need would	Temporal meaning	nen servient	
Above Below	-10.3 - 9.8	<i>7</i> 5	-11.8 -11.2	49 140	-10.0 - 9.6	75 109
Subject 4	agretic field in	oriF .yt	House broads	in recombile	o, Prole	
Above Below	-10.3 - 9.8	71 113	-11.8 -11.3	42 141	-10.2 - 9.7	75 112

Table 11-39. Hand-Held Probe Measurements Taken from the Lower Antenna of a Commissioned Glide Slope Facility.

Humanical integration can be employed to solve the integral deficiled, the magnetic

Figure 11-325 shows the basic dimensions of the FARYTO office slope ontenna.

analoys thin rectangular metal plates for the dipate arms, usings undia rectampilar plate

Held in the Immediate vicinity of a reducing surface by summing the field contributions

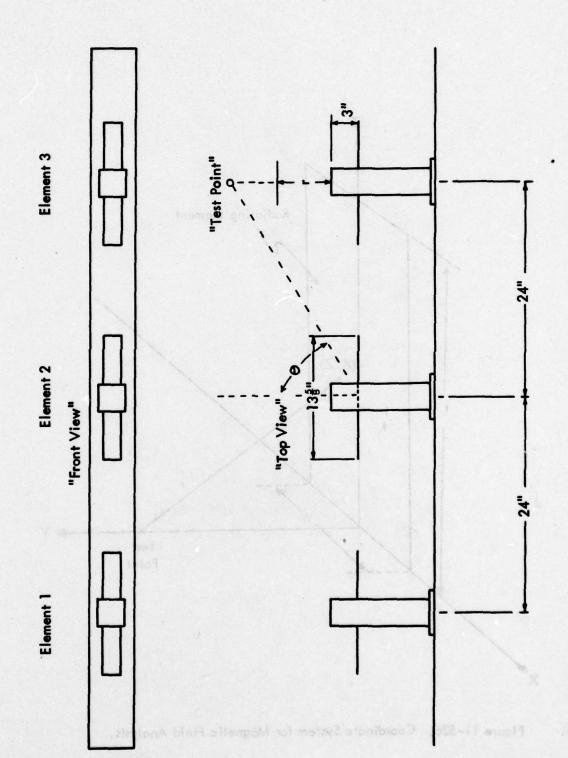


Figure 11-525. Element Dimensions for the FA-8976 Glide Slope Antenna.

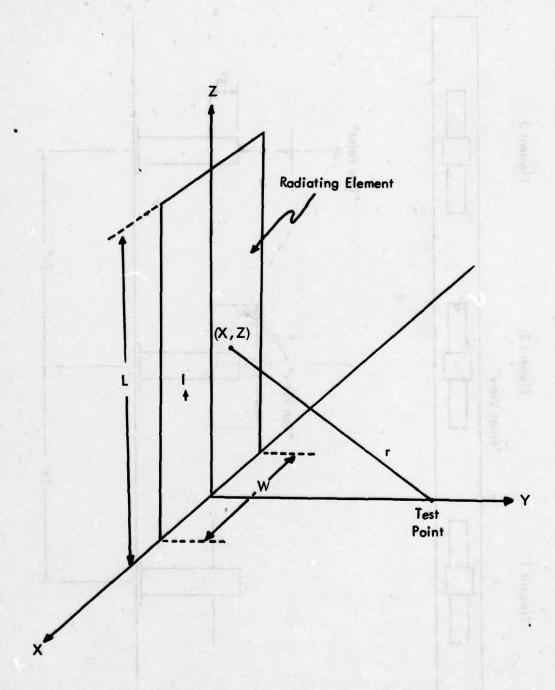


Figure 11-526. Coordinate System for Magnetic Field Analysis.

where
$$r = \sqrt{x^2 + y^2 + z^2}$$

The composite field at the test point is (integrating over all other elements);

$$H_{x}(y) = \frac{1}{4\pi} \int_{-L}^{L} \int_{-\frac{w}{2}}^{\frac{w}{2}} \frac{-i \beta r}{r} dxdz$$

Substituting in for r and recalling that the current distribution for a resonantly excited dipole is sinusoidal (end effects will be neglected) the integral becomes:

$$H_{x}(y) = \frac{1}{4\pi} \int_{-L}^{L} \int_{-\frac{w}{2}}^{\frac{w}{2}} \frac{\cos \beta z}{r} e^{-j\beta \sqrt{x^{2} + y^{2} + z^{2}}} dxdz$$

This integral is evaluated on the following pages with the aid of a computer using numerical integration techniques. [11] This particular integration was performed using the Newton-Cotes formulas. The error in this operation is on the order of the 5th power of the z increment (i.e., the error is on the order of .0148 5 = 7×10^{-10} which is substantially less than the truncation error of the computer). The program is listed on the following page.

Measured values of phase and amplitude versus distance in front of the radiating element are plotted in Figures 11–527 and 528 along with calculated values. The value along the abscissa corresponds to the dimension "r" in Figure 11–526.

As seen in Figure 11-527, there is a close correspondence between the predicted amplitude and the measured amplitude of the magnetic field. (As a reference, 1/R, the intensity/distance relationship for an incremental source, is also plotted.) The divergence of the amplitude of element 2 from elements 1 and 3 for distances greater than 4 inches is due to the fact that the fields from the outer elements (1 and 3) add to the field produced by the center element (2) causing its radiation intensity to appear higher.

The amplitude measurement of an element can best be made in a region where superposition is minimal (i.e., where relative element amplitudes do not change with increasing distance from the element). As seen in Figure 11-527, this region is between 0 and 4 inches. The maximum interference caused by another element in this region would be 13 dB below the amplitude of the element being measured (see Figure 11-526 for the dimensions used in the following calculation): Φ = angle off broadside of the element causing the interaction to the measurement point

$$\phi = \tan^{-1}(24/(3+4) = 74^{\circ}$$

```
C PROGRAM TO EVALUATE THE H FIELD IN FRONT OF A FA8976
C GLIDE SLOPE ANTENNA ELEMENT
C KENT CHAMBERLIN
C AVIONICS ENGINEERING CENTER
C OHIO UNIVERSITY, ATHENS OHIO
REAL*8 Y, H, HMAX, ANG, ANGLE, REF
     CALL HFIELD(3., HMAX, REF)
C ALL CALCULATIONS WILL BE REFERENCED TO 3 INCHES FROM THE ELEMENT
C WHICH CORRESPONDS TO A R OF O INCHES
     DO 10 I=3,15
C Y GOES FROM 3 TO 15 INCHES WHICH REPRESENTS A R OF 0 TO 12 INCHES
     Y=DFLOAT(I)
     CALL HFIELD(Y, H, ANG)
     HDB=20.*DLOG10(H/HMAX)
     ANGLE=ANG-REF
     PRINT 1,Y,HDB,ANGLE
     FORMAT(1X,3(F10.5,5X))
10
     CONTINUE
     STOP
     END
C SUBROUTINE HFIELD YIELDS THE AMPLITUDE AND PHASE OF THE MAGNETIC
C FIELD FOR A GIVEN DISTANCE (Y) FROM THE ELEMENT
SUBROUTINE HFIELD(Y, H, ANG)
     IMPLICIT COMPLEX*16(C)
     DIMENSION CG(4)
     REAL*8 BETA, INCX, INCZ, H, X, Z, PI, EXPON, Y, ZABX, R
     PHASE(C) = ATAN2(AIMAG(C), REAL(C))*180./PI
C PHASE IS A FUNCTION STATEMENT THAT DETERMINES THE PHASE IN
C DEGREES OF A COMPLEX NUMBER
     PI=3.14159265358979
     BETA= . 17682D0
C BETA IS THE PROPOGATION CONSTANT =2*PI/WAVELENGTH
     INCZ=.0148D0
     INCX=.2DO
C INCX AND INCZ ARE THE INCREMENTAL VALUES IN THE X AND Z DIRECTIONS
     CH=(0.D0,0.D0)
      DO 20 J=1,11
     X=-1.DO+DFLOAT(J-1)*INCX
C X IS INCREMENTED FROM -1 TO +1, THE WIDTH OF THE ELEMENT
     DO 20 K=1,400
     DO 10 N=1,4
     Z=DFLOAT((K-1)*3+(N-1))*INCZ-8.88D0
C Z IS INCREMENTED FROM -WAVELENGTH/4 TO +WAVELENGTH/4
     R=DSQRT(Z**2+Y**2+X**2)
C R IS THE DISTANCE FROM THE TEST POINT TO THE INCREMENTAL ELEMENT
     EXPON=-BETA*R
     CEXPON=DCMPLX(0.DO,EXPON)
     CURENT=DCOS(BETA*Z)
C CURENT IS THE CURRENT DISTRIBUTION ON THE ELEMENT
     CG(N)=CURENT*CDEXP(CEXPON)/R
C CG(N) IS THE FIELD CONTRIBUTION FROM THE NTH ELEMENT
     CH=CH+(3.D0*INCZ/8.D0)*(CG(1)+3.D0*CG(2)+3.D0*CG(3)+CG(4))
C THE ELEMENTAL CONTRIBUTIONS ARE SUMMED WITH APPROPERIATE
C WEIGHTING FACTORS
20
     CONTINUE
     H=CDABS(CH)/1.DO
     ANG=PHASE (CH)
```

11-708

RETURN

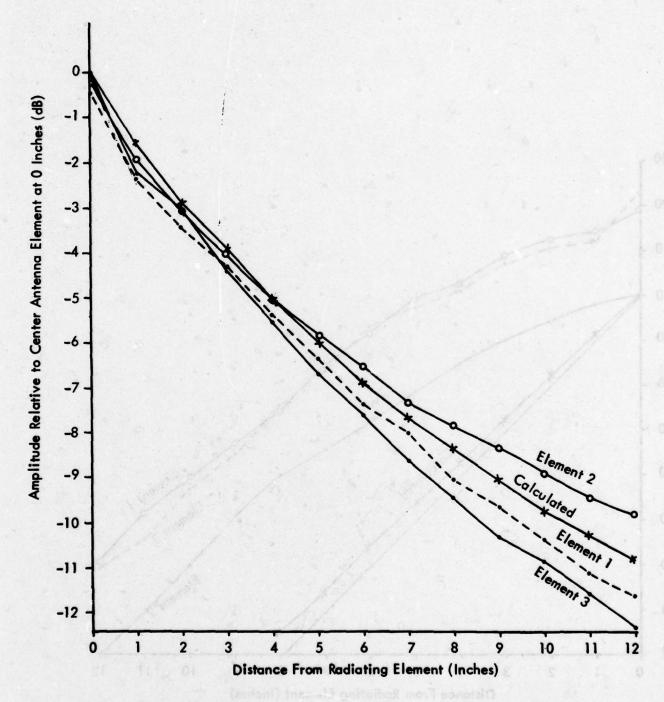


Figure 11-527. Probe Measured Amplitude of Elements of the FA-8976 Antenna Versus Distance.

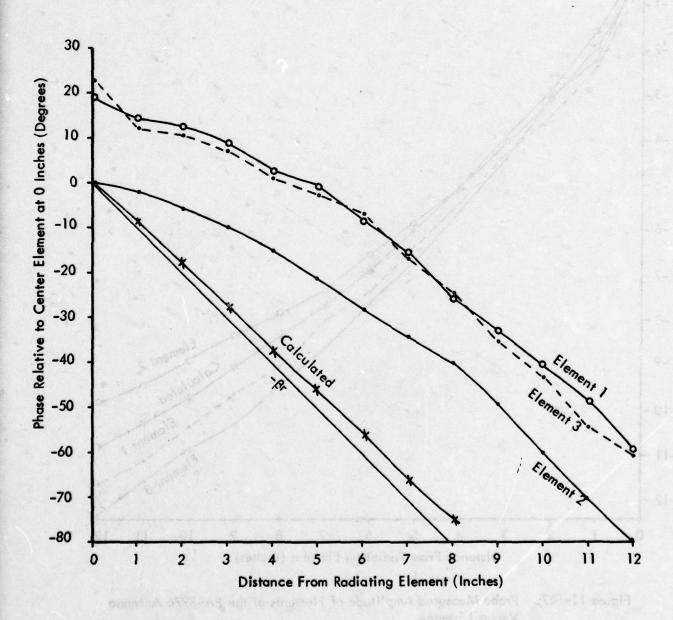


Figure 11-528. Probe Measured Phase of Elements of the FA-8976 Antenna Versus Distance.

The array factor for that angle is (assuming sinusoidally excited elements):

$$AF = \cos (90^{\circ} \sin 74^{\circ})/\cos 74^{\circ} = .224$$

$$20\log_{10}.224 = -13 dB$$

Elemental superposition of this nature is not felt to be detrimental to these measurements.

A graph of the relative phase of the elements is given in Figure 11-527 along with calculated values of phase. The 20° phase shift between end and center elements is to prevent a null from occurring in the antenna pattern in the vicinity of the runway threshold; such a null would occur if the elements were fed in phase.

The 30° discrepancy between the measured and calculated phase may be due to near-zone radiation effects on antenna element currents. This phenomenon occurs for distances from the element substantially less than $\sqrt{2}$ and appears in the form of a phase shift. Taking this effect into account, the apparent element current distribution at small distances becomes:

$$I(z) = (1 + jk) \cos \beta z$$

where z is the distance from the center of the dipole along the element, β is the propagation constant, and k is a constant determined by the antenna impedance (Zo), and Ri the radiation resistance

$$k = \frac{Ri}{4Z_0} = \frac{73}{143} = .51$$

The current distribution then becomes:

$$I(z) = (1 + j.51) \cos \beta z$$

The phase shift introduced by this near zone effect is 27° which may explain the discrepancy between the calculated and observed phase. The calculated and observed phase curves become nearly equal when the zero phase reference is moved to 8 inches since this region is less influenced by the near zone effect. Note that all curves in Figure 11-528 have the same slope $(-\beta r)$ outside the region where the near zone effect is present.

The phase difference between elements 1,2, and 3 as seen in Figure 11-528, does not change appreciably with distance from the radiator with the exception of the first inch. Phase sampling in this area has repeatedly resulted in errors on the order of 5°. Such an error so near a radiating element is not unexpected due to the presence of reflecting surfaces and non-ideal current distributions on the elements. It would appear that, because of phase anomalies near the element, probe measurements should be taken at distances of 2 inches or more to obtain accurate phase readings.

Since amplitude measurements can be made accurately for distances less than 4 inches, and phase measurements can be made accurately for distances greater than 2 inches, it would appear that 3 inches from the element would be an optimum position to make probe measurements. The measurement sensitivity at this point is 5°/inch in phase and 1 dB/inch in amplitude.

A design for a jig capable of holding a probe 3 inches from the radiator is given in Figure 11-529. The critical requirements for any probe jig are that it be capable of holding the probe rigidly and repositioning it accurately in subsequent measurements. The jig shown in Figure 11-529 is constructed from 1/4 inch plexiglas; styrofoam is considered to be more electromagnetically invisible; however, plexiglas offers a more rigid structure and is, therefore, considered more desirable in this application.

b. Experimental Results. As an experiment to determine the repeatability of these measurements, two persons were trained in the use of the VVM and shown how the tests were to be taken; the total training time was less than two hours. Measurements were taken over a two-week period on a daily basis, weather permitting, over a 40°F temperature range with 2 different VVM's. The results of this experiment indicate that a measurement accuracy of 1° in phase and 0.2 dB in magnitude can be realized by personnel with a minimum of training using a suitable probe jig.

One source of error observed in these experimental tests was an uncalibrated and/or cold vector voltmeter. Such sources of error can be eliminated by following the manufacturer's recommendations [13] for calibration and allowing at least one-half hour for warm-up.

Another source of error can be the expansion and contraction of the cables connecting the VVM to the probe and reference signals. This temperature-related phenomenon can appear as an erroneous phase shift in the final measurement unless some form of phase compensation technique is employed. Phase compensation can be accomplished by using equal length transmission lines for the probe and for the reference signal and arranging them so that they are exposed to the same environmental influences.

6. Far-Field Response to Antenna Currents. Since the purpose of this study is to enable judgments to be made concerning glide slope system performance based on measurements of antenna currents, it is important to determine the sensitivity of glide path angle and width to variations in the antenna currents. By employing a computer simulation model that was developed under a previous study, a far-field relationship describing path and width response to changes in antenna currents has been established. This model is for a capture-effect system operating on flat, level terrain. Although it is realized that this sensitivity will change substantially for a non-ideal terrain, the information given by this simulation is considered to give a general indication of what happens in the far field for changes in the transmitter parameters. Graphs depicting these sensitivities are given in Figures 11-530 through 533. Measured values from an earlier study [14] corroborate the information in Figures 11-530 through 533. The abscissa of these graphs represents the parameter that is varied, and the

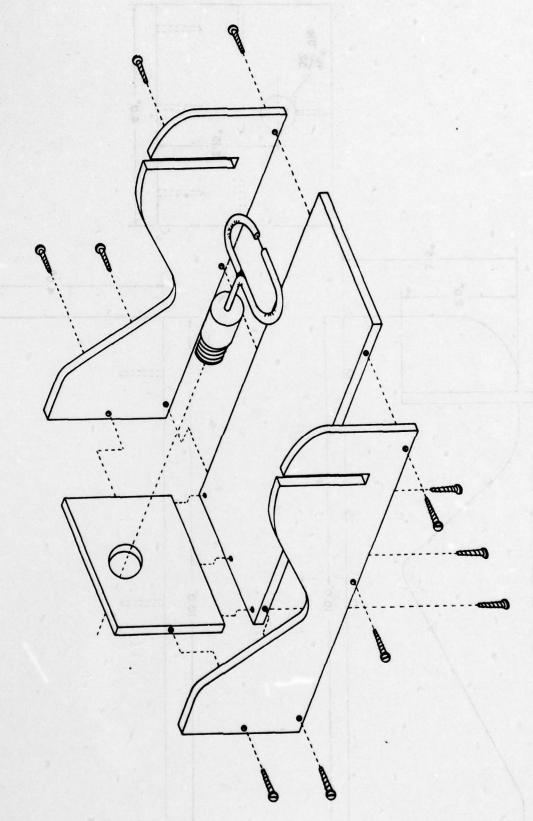
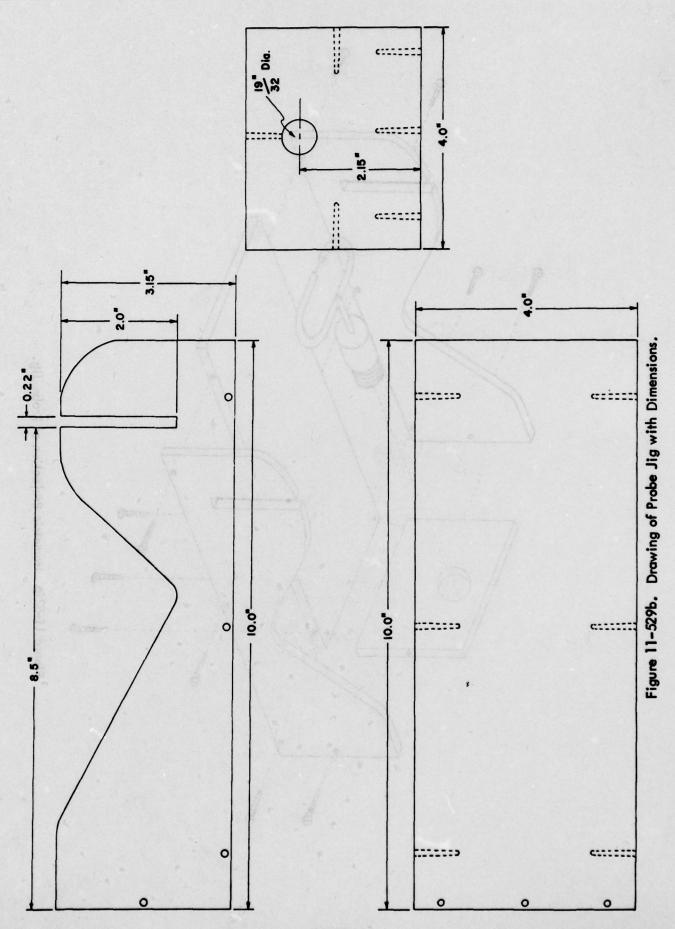


Figure 11-52% Isometric Projection of Probe Jig.



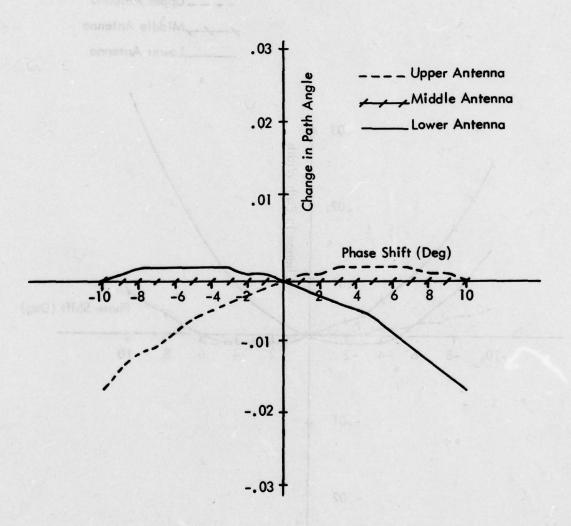


Figure 11-530. Change in Capture Effect Glide Slope Path Angle (3.0°Normal)
Caused by Antenna Dephasing.

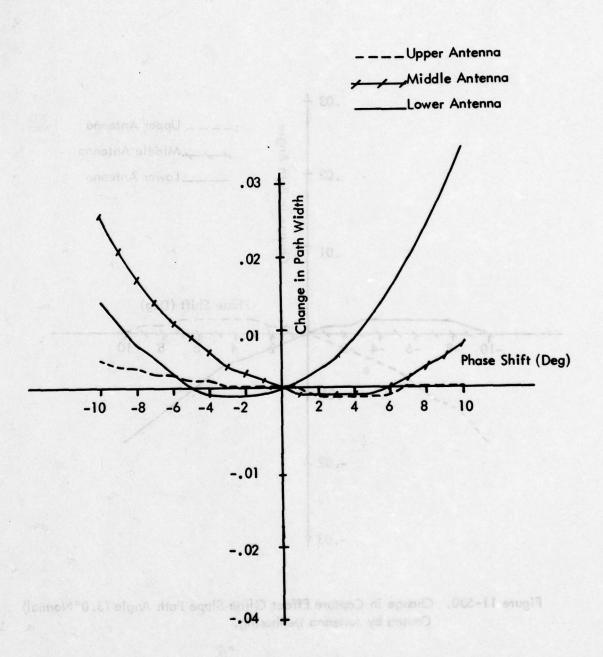


Figure 11-531. Change in Capture Effect Glide Slope Path Width (.7° Normal)
Caused by Antenna Dephasing.

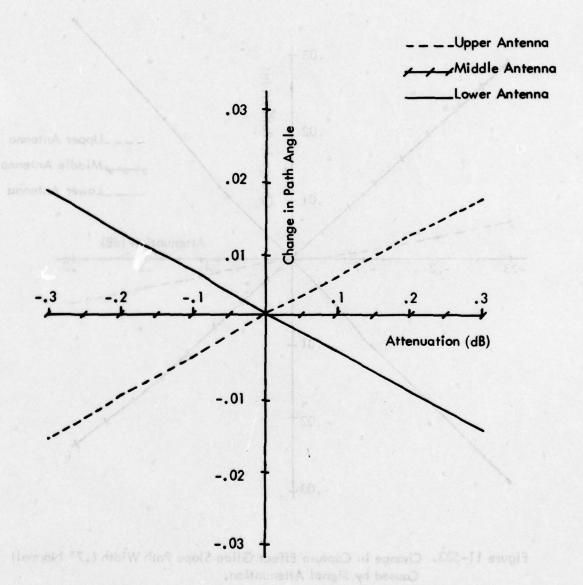


Figure 11-532. Change in Capture Effect Glide Slope Path Angle (3.0° Normal)
Caused by Signal Attenuation.

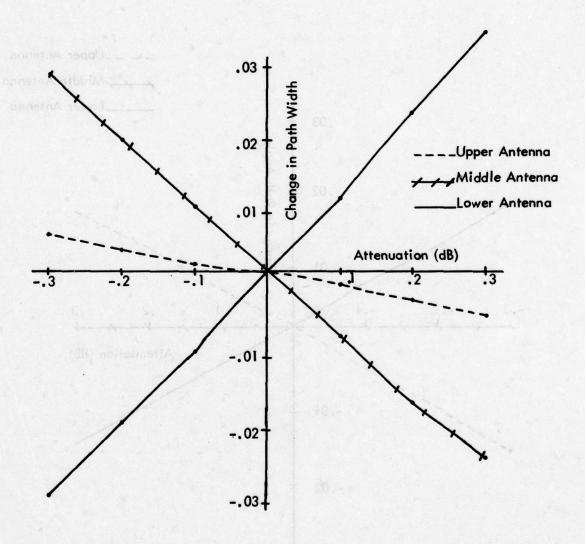


Figure 11-533. Change in Capture Effect Glide Slope Path Width (.7° Normal)
Caused by Signal Attenuation.

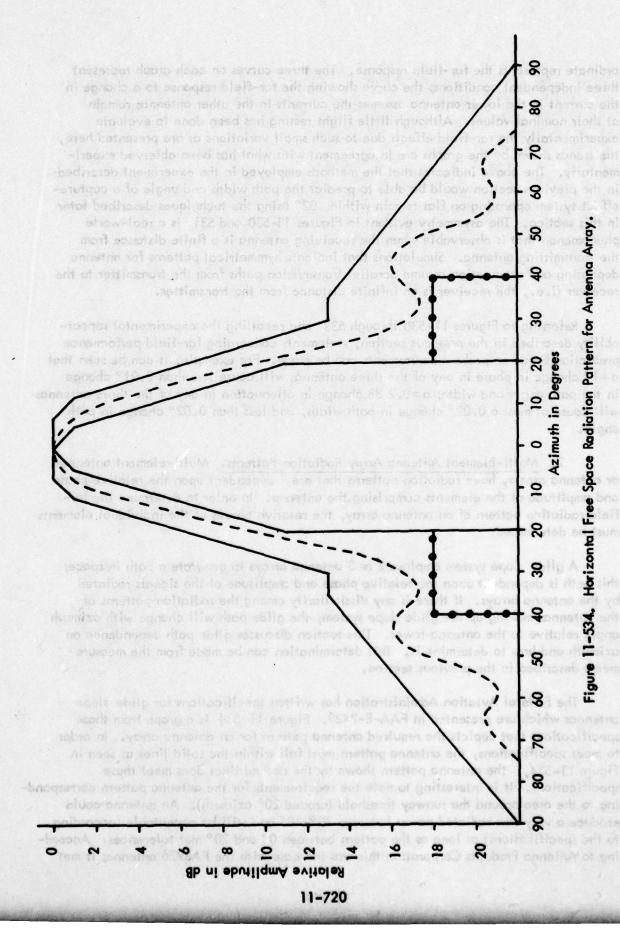
ordinate represents the far-field response. The three curves on each graph represent three independent conditions; the curve showing the far-field response to a change in the current in the lower antenna assumes the currents in the other antennas remain at their nominal values. Although little flight testing has been done to evaluate experimentally the far-field effects due to such small variations as are presented here, the trends shown by the graphs are in agreement with what has been observed experimentally. The above indicates that the methods employed in the experiment described in the previous section would be able to predict the path width and angle of a capture-effect system operating on flat terrain within .02° using the techniques described later in this section. The asymmetry evident in Figures 11-530 and 531 is a real-world phenomenon that is observable when the receiving antenna is a finite distance from the transmitting antenna. Simulations that indicate symmetrical patterns for antenna dephasing and attenuation assume parallel transmission paths from the transmitter to the receiver (i.e., the receiver is an infinite distance from the transmitter.

Referring to Figures 11-530 through 533 and recalling the experimental repeatability described in the previous section, statements concerning far-field performance prediction based on probe measurements can be made. For example, it can be seen that a $\pm 1^{\circ}$ change in phase in any of the three antennas will cause less than 0.01° change in the path angle and width; a ± 0.2 dB change in attenuation in any of the three antennas will cause at most a 0.02° change in path width, and less than 0.02° change in path angle.

7. Multi-Element Antenna Array Radiation Patterns. Multi-element antennas, or antenna arrays, have radiation patterns that are dependent upon the relative phase and amplitude of the elements comprising the antenna. In order to determine the farfield radiation pattern of an antenna array, the relative phases of the individual elements must be determined.

A glide slope system employs 2 or 3 antenna arrays to generate a path in space; this path is dependent upon the relative phase and amplitude of the signals radiated by the antenna arrays. If there is any dissimilarity among the radiation patterns of the antennas making up the glide slope system, the glide path will change with azimuth angle relative to the antenna tower. This section discusses glide path dependence on azimuth and how to determine it. This determination can be made from the measurements described in the previous section.

The Federal Aviation Administration has written specifications for glide slope antennas which are presented in FAA-E-2429. Figure 11-534 is a graph from those specifications that depicts the required antenna pattern for an antenna array. In order to meet specifications, the antenna pattern must fall within the solid lines as seen in Figure 11-534, the antenna pattern shown by the dashed lines does meet these specifications. It is interesting to note the requirements for the antenna pattern corresponding to the area around the runway threshold (around 20° azimuth). An antenna could produce a very low radiated power between 20°-30° and still be acceptable (according to the specifications) as long as the pattern between 0° and 20° met tolerances. According to Antenna Products Corporation this was the case with the FA8976 antenna; it met

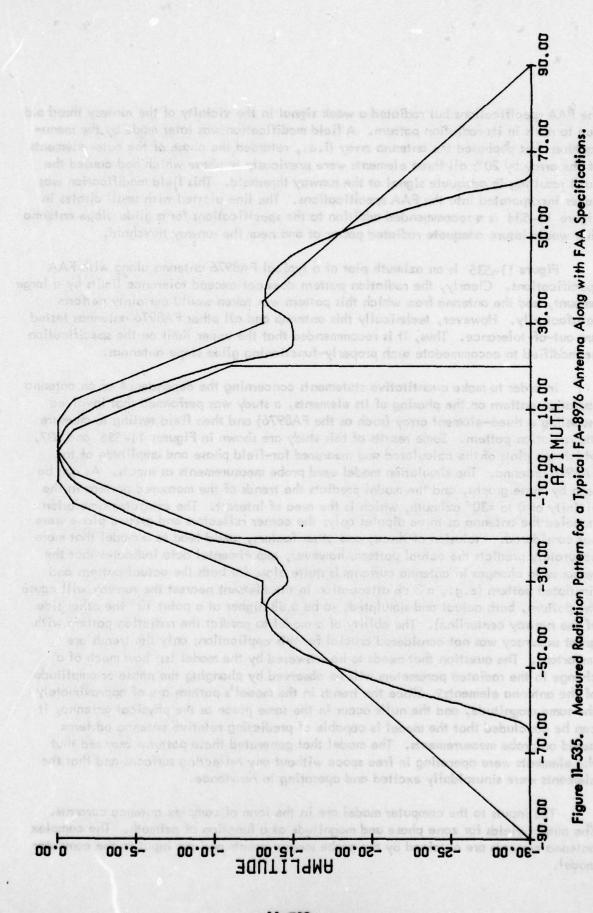


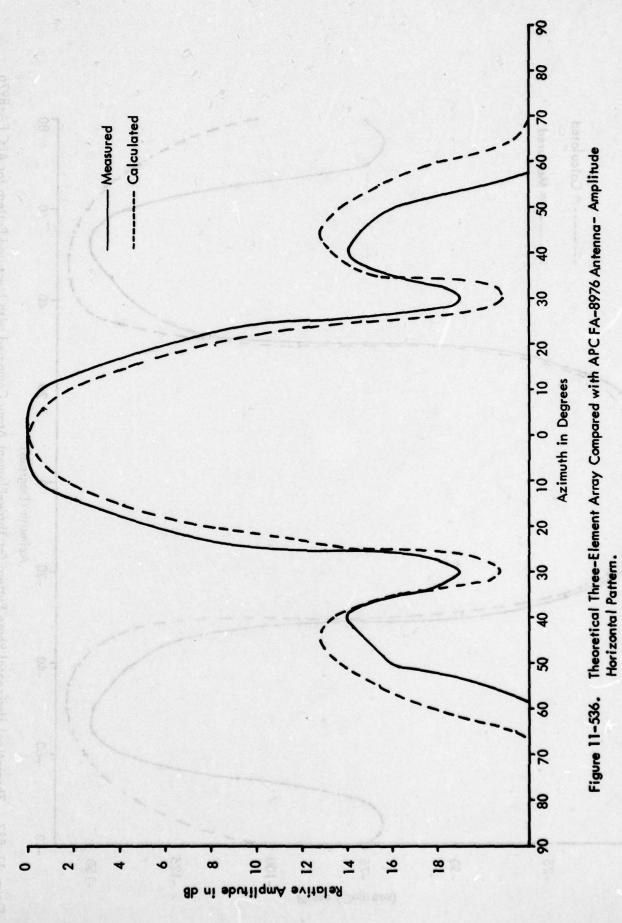
the FAA specifications but radiated a weak signal in the vicinity of the runway threshold due to nulls in its radiation pattern. A field modification was later made by the manufacturer that dephased the antenna array (i.e., retarded the phase of the outer elements of the array by 20°; all three elements were previously in phase which had caused the null) resulting in adequate signal at the runway threshold. This field modification was never incorporated into the FAA specifications. The line plotted with small circles in Figure 11-534 is a recommended addition to the specifications for a glide slope antenna that would insure adequate radiated power at and near the runway threshold.

Figure 11-535 is an azimuth plot of a typical FA8976 antenna along with FAA specifications. Clearly, the radiation pattern does not exceed tolerance limits by a large amount, and the antenna from which this pattern was taken would certainly perform satisfactorily. However, technically this antenna and all other FA8976 antennas tested are out-of-tolerance. Thus, it is recommended that the upper limit on the specification be modified to accommodate such properly-functioning glide slope antennas.

In order to make quantitative statements concerning the dependence of an antenna radiation pattern on the phasing of its elements, a study was performed that involved modeling a three-element array (such as the FA8976) and then field testing to measure the radiation pattern. Some results of this study are shown in Figures 11-536 and 537, which are plots of the calculated and measured far-field phase and amplitude of the FA8976 antenna. The simulation model used probe measurements as inputs. As can be seen by these graphs, and the model predicts the trends of the measured pattern in the vicinity of 0 to ±30° azimuth, which is the area of interest. The computer simulation modeled the antenna as three dipoles only; the corner reflectors and ground plane were not considered. Inclusion of these, and other factors, could lead to a model that more accurately predicts the actual pattern; however, experimental data indicates that the response to changes in antenna currents is quite close for both the actual pattern and simulated pattern (e.g., a 3 dB attenuation in the element nearest the runway will cause the pattern, both actual and simulated, to be 5 dB higher at a point 10° the other side of the runway centerline). The ability of a model to predict the radiation pattern with great accuracy was not considered crucial for this application; only the trends are important. The question that needs to be answered by the model is: how much of a change in the radiated parameters will be observed by changing the phase or amplitude of the antenna elements? Since the trends in the model's pattern are of approximately the same magnitude, and the nulls occur in the same place as the physical antenna, it can be concluded that the model is capable of predicting relative antenna patterns based on probe measurements. The model that generated these patterns assumed that the elements were operating in free space without any reflecting surfaces and that the elements were sinusoidally excited and operating in resonance.

The inputs to the computer model are in the form of complex antenna currents. The output yields far zone phase and magnitude as a function of azimuth. The complex antenna currents are obtained by the probe measurements and are input to the computer model.





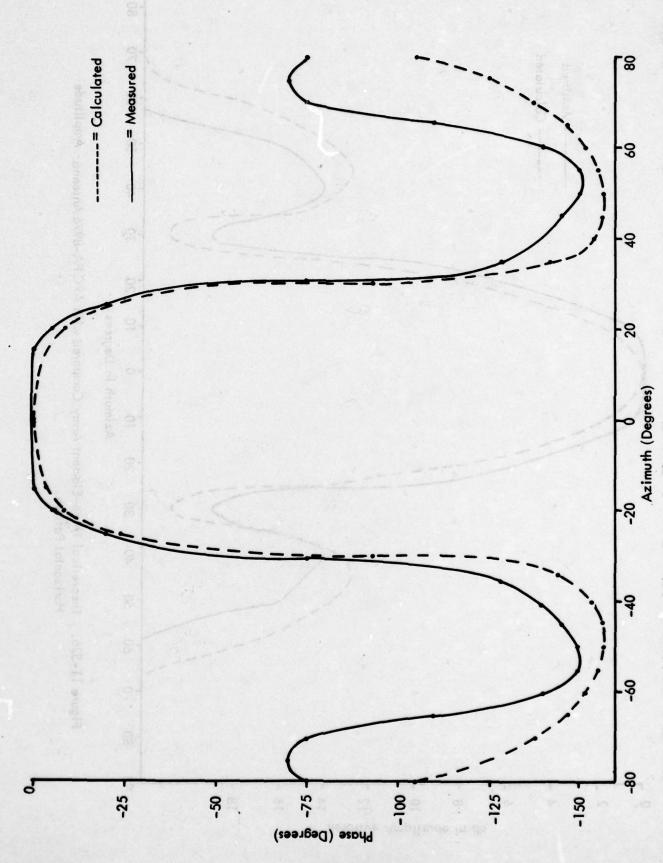


Figure 11-537. Theoretical Horizontal Phase Pattern for Three-Element Array Compared with Measured Pattern for APC FA-8976

The program to simulate the FA8976 antenna is listed on the following pages along with typical output. The program shown in Figures 11-538 and 539 is for the case where one of the outer elements is attenuated 3 dB with no change in phase. As indicated by the program comment statements, inputs to the simulation are measured antenna currents (since there are only 3 input parameters, they are input into the program itself rather than by cards). A measured value may be input to the program by converting from phase and amplitude to a complex value (x + y).

The computer simulation was run for a variety of fault conditions. The three elements of the FA8976 antenna are typically fed at equal amplitudes, with the outer elements in phase with each other and $20-25^{\circ}$ retarded with respect to the center element. Faults were input to the simulation as deviations from these values. The results of this study indicate that phase variations on the order of $\pm 5^{\circ}$ do not greatly affect the far-field parameters; however, attenuation greater than 2 dB greatly alters the antenna pattern. Unfortunately, these values cannot be used as tolerances for antenna diagnostics due to the unknown effect of certain parametric changes when dealing with a non-ideal terrain.

In order to set tolerance limits on antenna element parameter variations, further work is required using a terrain-sensitive glide slope model to determine the relationship between array performance and path characteristics.

8. Antenna Diagnostics. As stated in the previous section, absolute tolerances on antenna element phasing and signal strength cannot be established without further investigation. However, probe measurements can be of significant value for antenna diagnostics since faults that cause system outages are typically large enough to be immediately recognizable.

It is recommended that the probe measurements described earlier be taken on a regular (monthly) basis to establish baseline information for the system. In the event that the system fails, antenna integrity can be determined by comparing baseline measurements with faulted measurements. Information obtained for this report indicates that any antenna fault large enough to cause a system failure will result in a probe measurement variation substantially larger than variations due to measurement errors.

Probe measurements can also be used for system diagnostics, once it has been determined that none of the antenna arrays have failed, by using the measurements to determine the phasing between the individual antennas. Improper phasing due to temperature changes, aging, or moisture in the cables feeding the antennas can be detected easily.

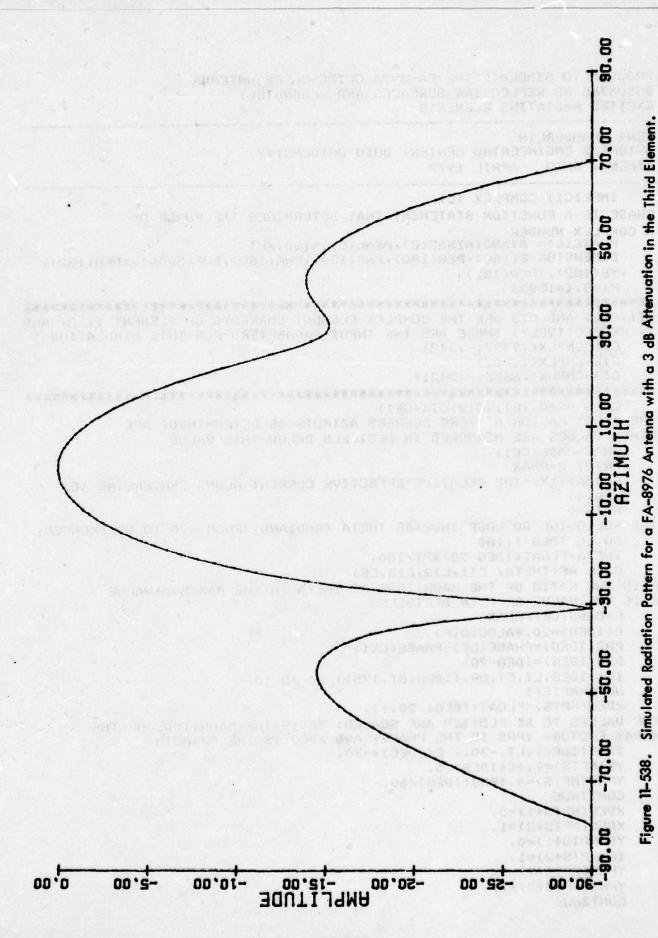
The true test of the probe's capability to aid the technician will be in the field, although information obtained thus far indicates that probe measurements can provide valuable data concerning a system's performance and can be taken without undue effort.

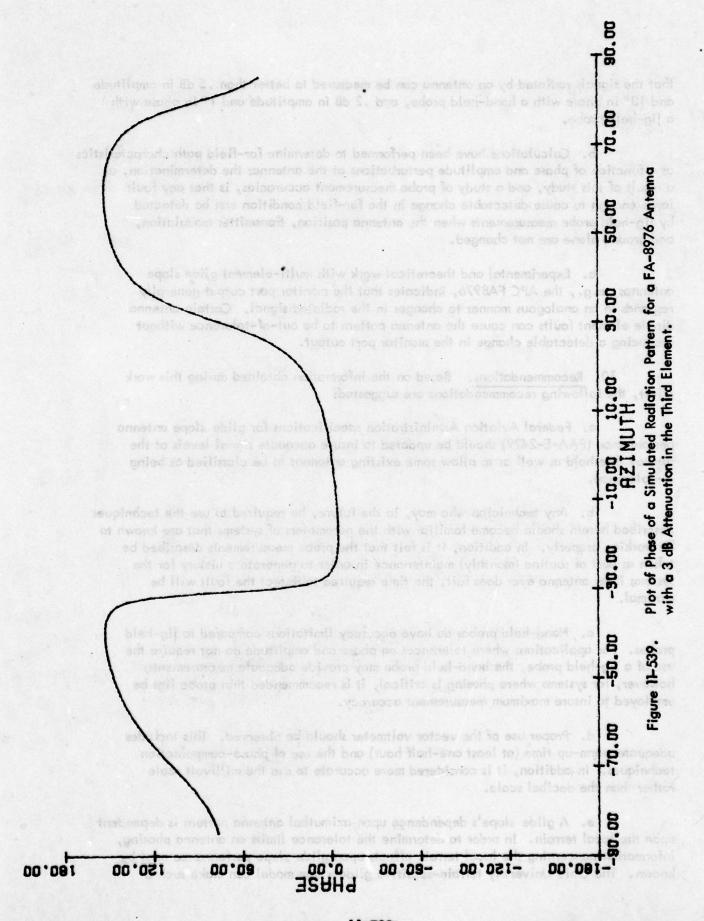
9. Conclusions.

a. An investigation into the use of magnetic induction probes with threeelement corner reflector antennas has been performed; the results of this study indicate

```
C THE FOLLOWING CREATES PLOTS OF THE DATA
    CALL PLOTS (BUF, 20000, 11)
    CALL AXIS(1.,1.,'AZIMUTH',-7,9.,0.,-90.,20.,10.)
    CALL AXIS(1.,1.,'PHASE',5,6.,90.,-180.,60.,10.)
    CALL FLINE(XDEG, YPHS, NPTS, 1, 0, ISYM)
    CALL PLOT(0.,0.,-3)
    CALL AXIS(1.,1.,'AZIMUTH',-7,9,,0.,-90.,20.,10.)
    CALL AXIS(1.,1.,'AMPLITUDE',9,6.,90.,-30.,5.,10.)
    CALL FLINE(XDEG, YE, NPTS, 1, 0, ISYM)
    CALL PLOT(0.,0.,-3)
    CALL PLOT(1.,1.,3)
    CALL PLOT(3.75,4.4,2)
    CALL PLOT(4.,4.4,2)
    CALL PLOT(4.9,6.8,2)
    CALL PLOT(5.15,7.,2)
    CALL PLOT(5.85,7.,2)
    CALL PLOT(6.1,6.8,2)
    CALL FLOT(7.,4.4,2)
    CALL PLOT(7,25,4,4,2)
    CALL PLOT(10,,1,,2)
    CALL PLOT(4.5,1.,3)
    CALL PLOT (4.5,4.8,2)
    CALL PLOT(5.25,6.8,2)
    CALL PLOT(5.5,7.,2)
    CALL PLOT(5.75,6.8,2)
    CALL PLOT(6.5,4.8,2)
    CALL PLOT(6.5,1.,2)
    CALL PLOT(0.,0.,-3)
    CALL PLOT(0.,0,,999)
STOP
    END
C SUBROUTINE AF GENERATES THE ARRAY FACTOR IN PHASE AND AMPLITUDE
FOR THE ANTENNA ARRAY FOR A GIVEN AZIMUTH (THETA) IN RADIANS AND
ANTENNA CURRENTS AS DESCRIBED ABOVE.
SEE TEXT FOR A DESCRIPTION OF THE SUBROUTINE OPERATION
SUBROUTINE AF (THETA, C11, C12, C13, CE)
    IMPLICIT COMPLEX(C)
    PI=3.1415926
    PSI1=(4.*PI/3.)*SIN(THETA)
    PSI3=-PSI1
    CSI1=CMPLX(0.,PSI1)
    CSI3=CMPLX(O.,PSI3)
    CE=(CI2+CI1*CEXF(CSI1)+CI3*CEXF(CSI3))
   >*(COS((PI/2.)*SIN(THETA))/COS(THETA))
    RETURN
    END
```

```
C PROGRAM TO SIMULATE THE FA-8976 GLIDE-SLOPE ANTENNA
 ASSUMING NO REFLECTING SURFACES AND RESONATELY
C
 EXCITED RADIATING ELEMENTS
C
 KENT CHAMBERLIN
C AVIONICS ENGINEERING CENTER, OHIO UNIVERSITY
C ATHENS, OHIO
                APRIL 1977
     IMPLICIT COMPLEX (C)
C PHASE IS A FUNCTION STATEMENT THAT DETERMINES THE PHASE OF
C A COMPLEX NUMBER
     PHASE(C) = ATAN2(AIMAG(C), REAL(C))*180./FI
     DIMENSION E(180), DEG(180), PHS(180), PHA(180), BUF(5000), XDEG(182),
     ,YE(182),YPHS(182)
     FI=3.1415926
C CI1,CI2, AND CI3 ARE THE COMPLEX ELEMENT CURRENTS OF ELEMENT 1, 2, AND
C 3, RESPECTIVELY; THESE ARE THE INPUT PARAMETERS FOR THIS SIMULATION
     CI1=CMPLX(.9397,-.342)
     CI2=CMPLX(1.,0.)
     CI3=CMPLX(.6653,-.2421)
CALL AF(0.,CI1,CI2,CI3,CE1)
C THE ARRAY FACTOR AT ZERO DEGREES AZIMUTS IS DETERMINED; ALL
C OTHER VALUES ARE MEASURED IN DECIBELS BELOW THIS VALUE
     RMAX=CABS(CE1)
     PRINT 2, RMAX
     FORMAT(1X, 'THE RELATIVE EFFECTIVE CURRENT ALONG CENTERLINE IS'
    <,F8.4)
     NPTS=0
C THE FOLLOWING DO LOOP INDEXES THETA (RADIANS) FROM -90 TO 90 DEGREES
     DO 10 IDEG=1,180
     THETA=FLOAT(IDEG-90)*PI/180.
     CALL AF(THETA, CI1,CI2,CI3,CE)
C F IS THE RATIO OF THE MAGNITUDE AT THETA TO THE MAXIMUM VALUE
C E IS THE VALUE OF F IN DECIBELS
     F=CABS(CE)/RMAX
     E(IDEG)=20.*ALOG10(F)
     PHS(IDEG)=PHASE(CE)-PHASE(CE1)
     DEG(IDEG)=IDEG-90
     IF((IDEG.LT.5).OR.(IDEG.GT.175)) GO TO 10
     NFTS=NFTS+1
     XDEG(NPTS)=FLOAT(IDEG)/20.+1.
C THE VALUES TO BE PLOTTED ARE SCALED: YE IS THE MAGNITUDE OF THE
C ARRAY FACTOR, YPHS IS THE PHASE, AND XDEG IS THE AZIMUTH
     IF(E(IDEG).LT.-30.) E(IDEG)=-30.
     YE(NPTS)=7. +E(IDEG)/5.
     YPHS(NPTS)=4.+PHS(IDEG)/60.
10
     CONTINUE
     XDEG(NPTS+1)=0.
     XDEG(NPTS+2)=1.
     YE(NPTS+1)=0.
     YE(NPTS+2)=1.
     YPHS(NPTS+1)=0.
     YPHS(NPTS+2)=1.
20
     CONTINUE
```





that the signals radiated by an antenna can be measured to better than .5 dB in amplitude and 10° in phase with a hand-held probe, and .2 dB in amplitude and 1° in phase with a jig-held probe. b. Calculations have been performed to determine far-field path characteristics as a function of phase and amplitude perturbations at the antenna; the determination, as a result of this study, and a study of probe measurement accuracies, is that any fault large enough to cause detectable change in the far-field condition can be detected by jig-held probe measurements when the antenna position, transmitter modulation, and ground plane are not changed. c. Experimental and theoretical work with multi-element glide slope antennas, e.g., the APC FA8976, indicates that the monitor port output generally responds in an analogous manner to changes in the radiated signal. Certain antenna dipole element faults can cause the antenna pattern to be out-of-tolerance without producing a detectable change in the monitor port output. Based on the information obtained during this work 10. Recommendations. effort, the following recommendations are suggested: a. Federal Aviation Administration specifications for glide slope antenna performance (FAA-E-2429) should be updated to insure adequate signal levels at the runway threshold as well as to allow some existing antennas to be classified as being in-tolerance. b. Any technician who may, in the future, be required to use the techniques described herein should become familiar with the parameters of systems that are known to be working properly. In addition, it is felt that the probe measurements described be taken as part of routine (monthly) maintenance in order to generate a history for the system; if an antenna ever does fail, the time required to detect the fault will be minimal. c. Hand-held probes do have accuracy limitations compared to jig-held probes. For applications where tolerances on phase and amplitude do not require the use of a jig-held probe, the hand-held probe may provide adequate me asurements; however, for systems where phasing is critical, it is recommended that probe jigs be employed to insure maximum measurement accuracy. d. Proper use of the vector voltmeter should be observed. This includes adequate warm-up time (at least one-half hour) and the use of phase-compensation techniques. In addition, it is considered more accurate to use the millivolt scale rather than the decibel scale. e. A glide slope's dependence upon azimuthal antenna pattern is dependent upon the local terrain. In order to determine the tolerance limits on antenna phasing, information concerning the local terrain effects upon glide slope performance must be known. The Ohio University terrain-sensitive glide slope model can make such a 11-730

determination; it is suggested that this model be exercised to determine antenna phasing tolerances for varied terrain configurations.

as the top of the street of Glide Stage Antennas, factly in the history of Uiff glide stages postation in the United States, the street dipole was used exclusively as a source element for the street trained test. The basic dipole clement was madified to become a bent dipole and give broader as invalidation of the provide stage in the top of the street of the stree

Since 1970 at least five different nonufraturers have produced directive glide slope arrays. Three have used the design of three continual dipole elements placed in comman reflectors, it us providing to: elevation as vertices ordered in estimate directivity. Because these three antiques those found common use in commissioned gifab slope systems, it was considered important to investigate in detail their performance characteristics and to take an approximation as expensive and the specific fault consittions. The times extends of concern are:

FASCOT manufactured by Airborne Instrument Laboratories
FASCO manufactured by Scorwell Laboratories
FASCO manufactured by Antenna Francisca Company

the two other directive artennas, are by Meridian Metalonaft, using times auredtype divotes on a baseblate, and the other, a large day tystype mattered by faces instruments, have been or are currently being used for glide stope aparation.

Espherical me three-context reflector type as annot her the provision for abraining a signal complexing narposes. The representativeness of this signal is of parameters in a parameter of the signal is of parameters in a parameter of the signal is of parameters in a constitution of the signal field signal has been excomplished. Additionally a constation between the signal name is and the response of the modifier collibrated by although not heat experimently determined.

by thistery of Stemei Something for Monitorings, Integral manitoring is been found to be a very elective mades of monitoring glids slope system performance. To achieve this type of maniforing selicitationly it is necessary to have a signal sample that it representative of the currents in the nationing elements. Several techniques have been used with the various antennal and these will be electived.

The FAA inclemented a method of signal sampling with the early bent dipole by families a small half food with a wire approximately one inch chave the base plane serving as the religious for the antennas and termination into this plane. This helped solve early problems in monitoring the capture-effect system and also found use when the FAA cramitted to integers accumulated as integers accumulated as integers accumulated as integers.

K. Experimental Investigation of Contemporary Glide Slope Antennas.

1. Introduction.

a. History of Glide Slope Antennas. Early in the history of UHF glide slope operation in the United States, the single dipole was used exclusively as a source element for the signal transmitted. The basic dipole element was modified to become a bent dipole and give broader azimuth signal coverage because it was believed necessary to provide signal to touchdown. When rough path structure became a significant problem in meeting Category II requirements in the late 1960's, concern was given to directing the signal principally into the approach region. Further motivation for directive elements also came from the need for gain if solid state transmitters were to be used.

Since 1970 at least five different manufacturers have produced directive glide slope arrays. Three have used the design of three collinear dipole elements placed in corner reflectors thus providing for elevation as well as azimuth directivity. Because these three antennas have found common use in commissioned glide slope systems, it was considered important to investigate in detail their performance characteristics and to take one in particular and examine its performance under specific fault conditions. The three antennas of concern are:

FA8651 manufactured by Airborne Instrument Laboratories FA8730 manufactured by Scanwell Laboratories FA8976 manufactured by Antenna Products Company

The two other directive antennas, one by Meridian Metalcraft, using three curvedtype dipoles on a baseplate, and the other, a large cavity-type marketed by Texas Instruments, have been or are currently being used for glide slope operation.

Each of the three-corner reflector type antennas has the provision for obtaining a signal sample that can be used for system monitoring purposes. The representativeness of this signal is of paramount importance when considering the integrity of the monitoring. A careful investigation of correlation between the signal sample and the farfield signal has been accomplished. Additionally a correlation between the signal sample and the response of the monitor calibrated by airborne methods has been experimentally determined.

b. <u>History of Signal Sampling for Monitoring</u>. Integral monitoring has been found to be a very effective means of monitoring glide slope system performance. To achieve this type of monitoring satisfactorily it is necessary to have a signal sample that is representative of the currents in the radiating elements. Several techniques have been used with the various antennas and these will be discussed.

The FAA implemented a method of signal sampling with the early bent dipole by forming a small half loop with a wire approximately one inch above the base plate serving as the reflector for the antennas and terminating into this plate. This helped solve early problems in monitoring the capture-effect system and also found use when the FAA committed to integral monitoring of width for the null reference system.

Deriving a representative signal for the multi-elements found in the comer reflector arrays is a more demanding task. To be satisfactory each dipole must be sampled and the resulting signal combined to be representative of an effective current which may be considered the signal source current of the array.

The APC FA8976 antenna makes use of the simplest and most straightforward means of extracting a sample. A coaxial line is brought up to the balun used to stand the dipole off $\frac{1}{4}$ wavelength from the base with the shield terminated on one arm of the balun and the centerconductor penetrating through and terminating on the other. The three lines coming from each dipole are then joined together to give a composite with a non-50-ohm port.

The AIL FA8651 samples signals by terminating the shield of the coax at the base plate bringing only the center conductor to a low impedance point on the balun. This in effect formed a 2-inch diameter square loop with the balun element. The three samples were then combined using a stripline, constant-impedance device for this purpose.

The Scanwell FA8730 makes use of capacitive coupled signal samples from each dipole to represent the dipole currents. The signals are combined to provide a signal at the single port used to feed the monitor circuit.

Another method for signal sampling has been used with experimental antennas. This involves a loop approximately one inch by two inches mounted very close to the gap on the center dipole. (See page 38 of SRDS Report 73-137). In this antenna two loops were used, one for path and one for width monitoring. The dipoles in the experimental antenna were series fed, hence it was believed unnecessary to sample the signals from the end dipoles.

The Meridian dipoles provided signal sample by means of a directional coupler. The sample is representative only when the SWR at the antenna is 1.1:1 or less.

2. Specific Antennas Involved in Tests. Three contemporary, readily available, corner reflector-type antennas were selected for field testing. Of particular concern was the relation between the far-field signal produced by the antenna and the signal sample being provided for monitoring purposes. A dearth of information seems to exist on this subject, so it was deemed important to establish this relationship through carefully controlled experimental measurements. Because of alleged difficulties in field operations with one particular antenna; viz, the AIL FA8651, performance characteristics of this antenna were stressed. The three antenna types considered were:

AIL FA8651 APC FA8976 Scanwell FA8730 Deliberate faults were introduced into the FA8651 antenna and resulting changes in the phase and amplitude of the far-field signals were observed. The principal reference was to a standard $\frac{1}{2}$ wavelength dipole.

3. Measurement and Techniques.

a. Test Range. The antenna test range at Ohio University's Avionics Engineering Center's test facility at the New Tamiami Airport, Miami, Florida was used for all testing. Figure 11-540 shows the layout of this range. Figure 11-541 is a view of the range from behind the antenna under test and Figures 11-543a and 543b are views of the antenna test jig and the far-field dipole receiving antenna respectively from the far-field vector voltmeter position.

This site provided the unobstructed field area necessary for satisfactory testing. Power and support services were conveniently available from the glide slope transmitting buildings nearby.

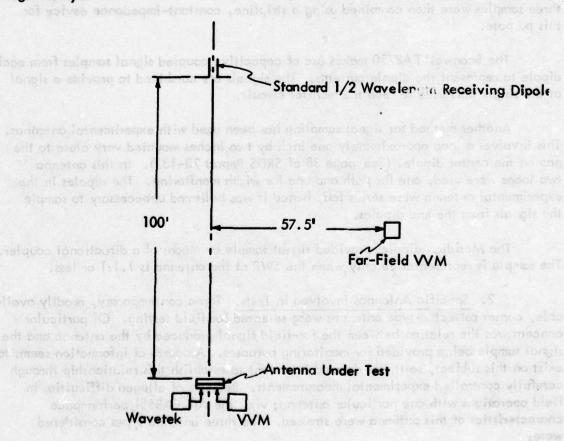


Figure 11-540. Antenna Test Range Layout.

All measurements were made with the reference dipole antenna in position on the supporting mast.

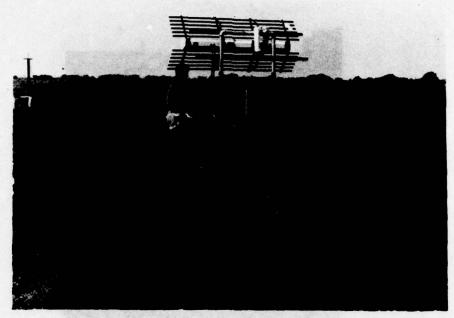


Figure 11-541. The Tamiami Antenna Test Range.

b. Specific Tests.

(1) Impedance, VSWR. Complex impedance and VSWR data were derived from incident and reflected voltage and phase measurements. Figure 11-542 shows the test set-up used to obtain these data.

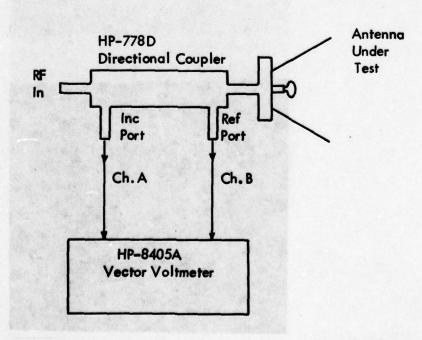


Figure 11-542. Impedance and VSWR Test Configuration.

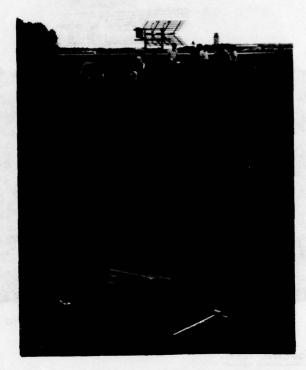


Figure 11-543a. The Antenna under Test as seen from the Far-Field Measurement Position.

Tamiami Test Range, Miami, Florida.



Figure 11-543b. The Far-Field Receiving Dipole as seen from the Far-Field Measurement Point.

The basic reference instrument for collecting data on these as well as most of the other tests was the Model 8405A Hewlett Packard Vector Voltmeter. Two such instruments were used and calibrations can be traced to the National Bureau of Standards through the standards of the FAA Approved Repair Station maintained by Ohio University.

Initially, a calibrated short was used to terminate the directional coupler and obtain a "reference phase difference". This reference phase difference was then subtracted from subsequent phase measurements to arrive at the true phase difference between the incident and reflected port voltages of the directional coupler.

Voltage measurements at the incident and reflected ports of the directional coupler can be used to find the reflection coefficient p from the equation:

$$\rho = 10^{-\frac{v_1 - v_r}{20}}$$

where v_i and v_r are the incident and reflected port voltage levels in dB. Further, the VSWR of the antenna can then be found since:

$$VSWR = \frac{1+\rho}{1-\rho}$$

the VSWR and the phase information can now be plotted on a Smith Chart to find the complex impedance of the antenna being tested.

- (2) Gain. The gain of the antenna under test with respect to a standard dipole was also measured on the test range. With a directional coupler in line, the reference dipole on the antenna test jig was excited. The incident port output of the directional coupler was used as the reference input (channel A) to the far-field vector voltmeter. The output of the standard receiving dipole located in the far field was then measured as channel B on the far-field vector voltmeter. With the same directional coupler in line the antenna under test was excited and the receiving dipole output again measured. The gain of the antenna under test can be seen to be the difference of the two signal levels in decibels.
- (3) Bandwidth. The glide slope frequency range of 329 MHz to 335 MHz was used to examine bandwidth characteristics of the antennas. Once established all further tests were conducted at 332.00 MHz.
- (4) Dipole Currents. The relative phase and amplitude of the individual dipole currents were measured with a hand-held probe and vector voltmeter. With the probe in position the output of the probe was measured as channel B in the vector voltmeter. The manitor output of the antenna was used as the reference input to the vector voltmeter channel A. All amplitude and phase measurements were normalized to the

center dipole. The center dipole, therefore, is always 1.0/0°. Figure 11-544 shows a probe measurement being made an APC FA8976 glide slope antenna with the aid of a jig.



Figure 11-544. Probe Measurements on the APC FA-8976.

- (5) Radiation Pattern. Azimuth radiation pattern plots for both amplitude and phase were made using data taken on the test range. The spacing between transmitting antenna and the receiving dipole was 100 ft. which meets the conventional criterion for the far-field range of $2D^2/\lambda$ or 35ft. Measurements were made every 5° from -90° to +90°. Positive angles on the azimuth plots represent counterclockwise angles from centerline looking down. The monitor output port of the antenna under test was used as the reference input to the far-field vector voltmeter.
- (6) TDR Signature. Time domain response signatures were taken for the input ports of all antennas tested. A Tektronix 1502 TDR Cable Tester was used to obtain the signatures. For all signatures the monitor port was terminated in 50Ω
- (7) No-Fault Monitor/Input Port Relationship. The monitor port output phase and amplitude with respect to the input port phase and amplitude under no-fault conditions was determined for all antennas. This data appears in Table 11-40. The monitor/input port relationship remained constant over a range of input levels from -20 dB to +10 dB.

4. Matrix of Results.

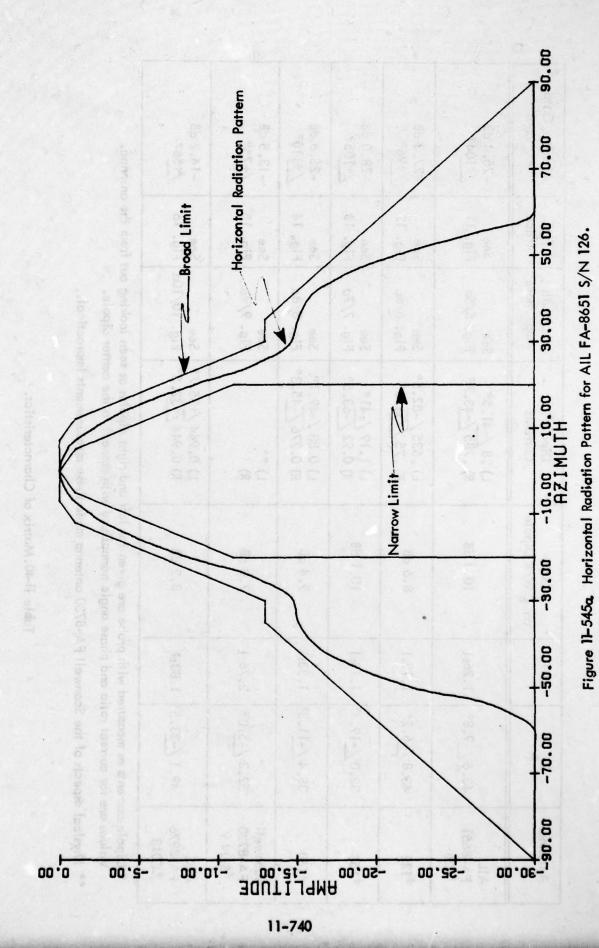
a. Baseline Data. Table 11-40 lists the characteristics of the six antennas tested. These characteristics were derived from data taken on the test range using the techniques described briefly in the previous section. Figures 11-545 through 550 follow Table 11-40 and show the front hemisphere free space radiation pattern phase and amplitude for each of the antennas tested. These may be considered as conventional

Antenna	Z	SWR	Gain on & W/R Dipole	Dipole* Currents	Azîmuth Amp/Phase	TDR	Monitor Output
AIL FA-8651 *126	43.6 /-9.8°	1.26;1	10.4 dB	L) .8 /-41.5° R) .785 /-43.7°	See Fig. 5/5a	See Fig. 11	-25.4 dB /+104°
132	43.8 /-6.2°	1.19:1	8.6 dB	L) .635 /-82.5° R) .75 /-56.5°	See Fig. 6/6a	See Fig. 12	-27°3 dB /+96°
153	33.0 /-19.4° 1.73.1	1.73:1	10.1 dB	L) 1.19 /-41° R) 0.92 /-63.5°	See Fig. 7/7a	See Fig. 13	-28.0 dB /+105°
4160	38.4 /-11.3° 1.33:1	1.33:1	9.4 dB	L) 0.88 /-49.1° R) 0.776 /-45.3°	See Fig. 8/8a	See Fig. 14	-25.6 dB /+110°
Scanwell FA-8730 Fs/N 9	52.3 /-5.0°	2.76:1	7.0 dB	L) ** R)	See Fig. 9/9a	See Fig. 15	-13.5 dB /+75°
APC FA-8976 *C013	49.1 /-33.5 1.88:1	1.88:1	8.2 dB	L) 0.944 /+35.7° R) 0.944 /+32.5°	See Fig. 10/10a Fig. 16	See Fig. 16	-14.2 dB /+56°

* Dipole currents as measured with probe are given for left and right dipoles as seen looking out from the antenna. Values are for current ratio and phase angle normalized with respect to the center dipole.

Table 11-40. Matrix of Characteristics.

^{**} Physical aspects of the Scanwell FA-8730 antenna made these measurements impractical.



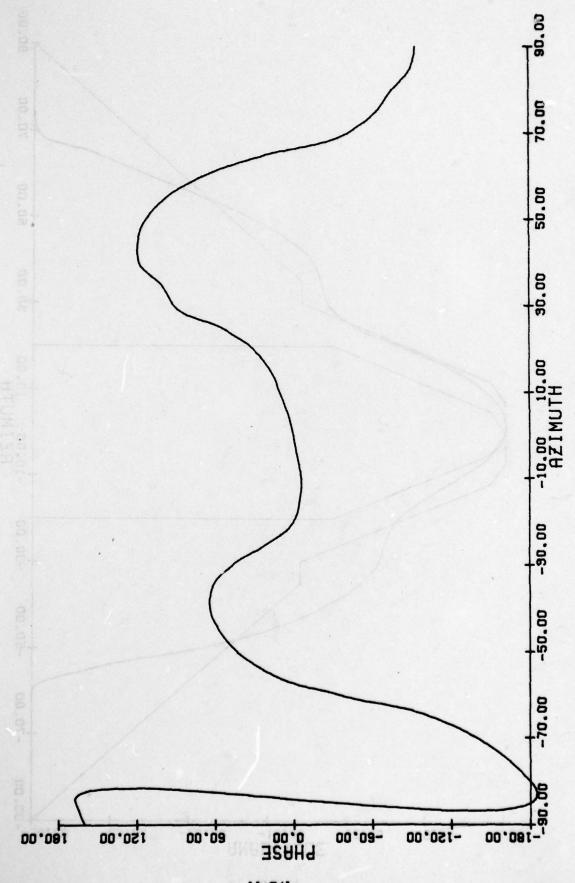
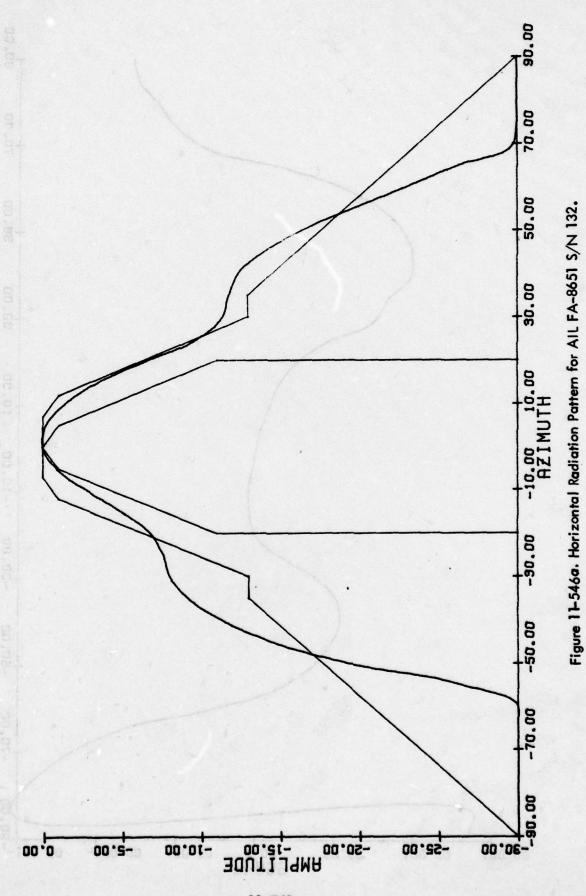
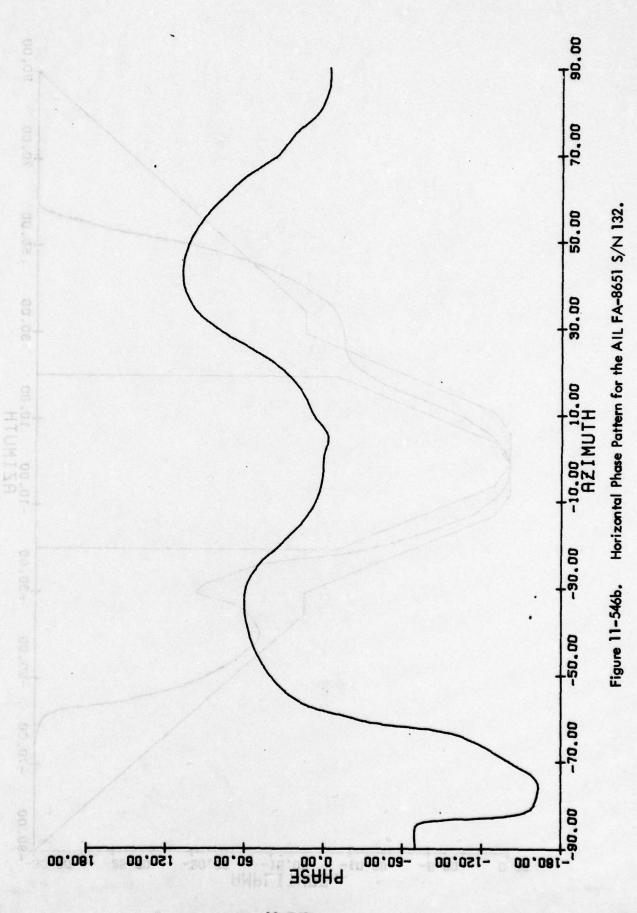
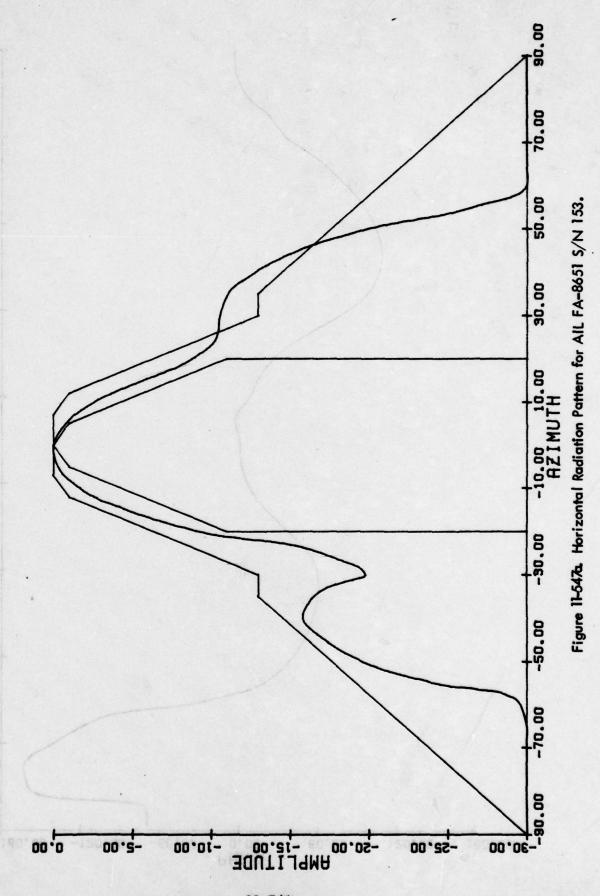


Figure 11-545b. Horizantal Phase Pattern for the AIL FA-8651 S/N 126.



11-742





11-744

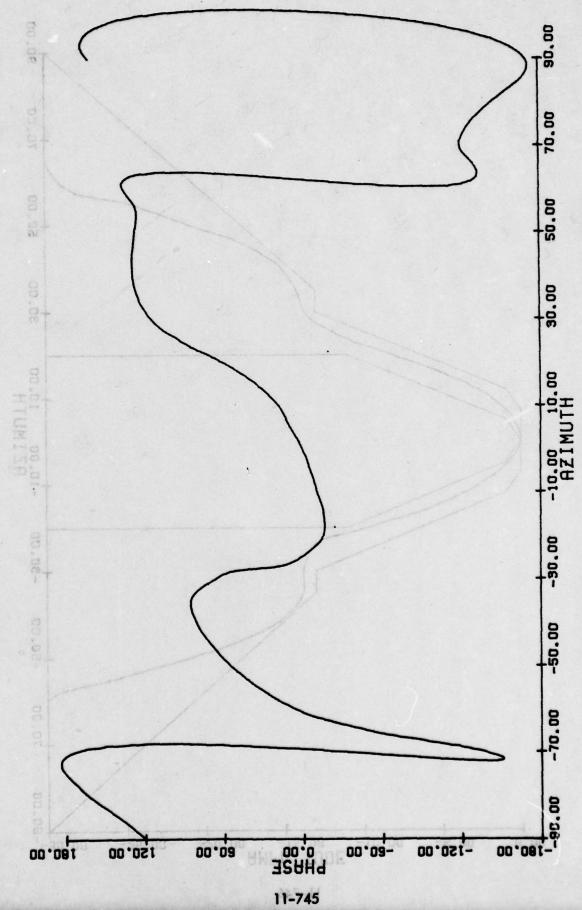
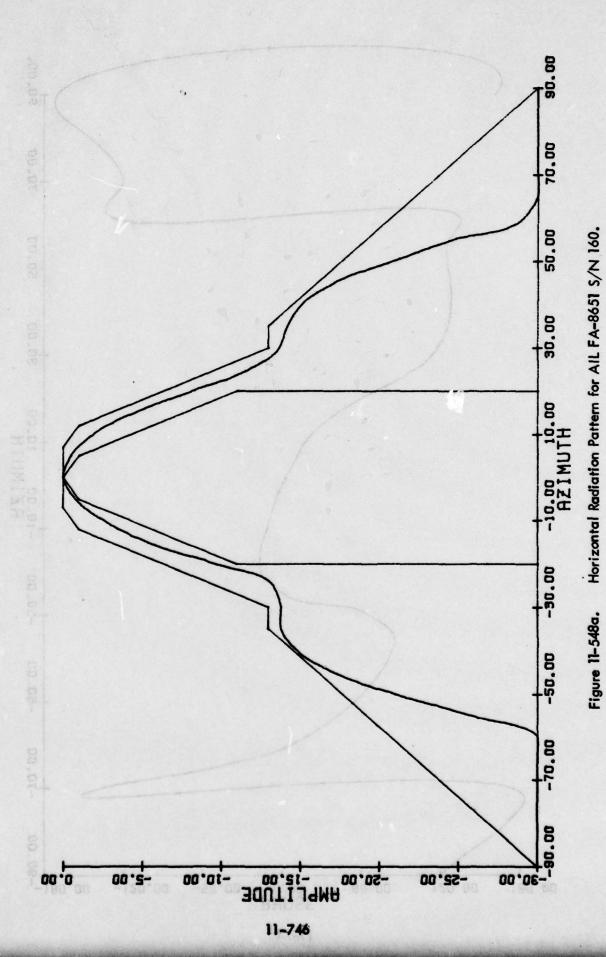
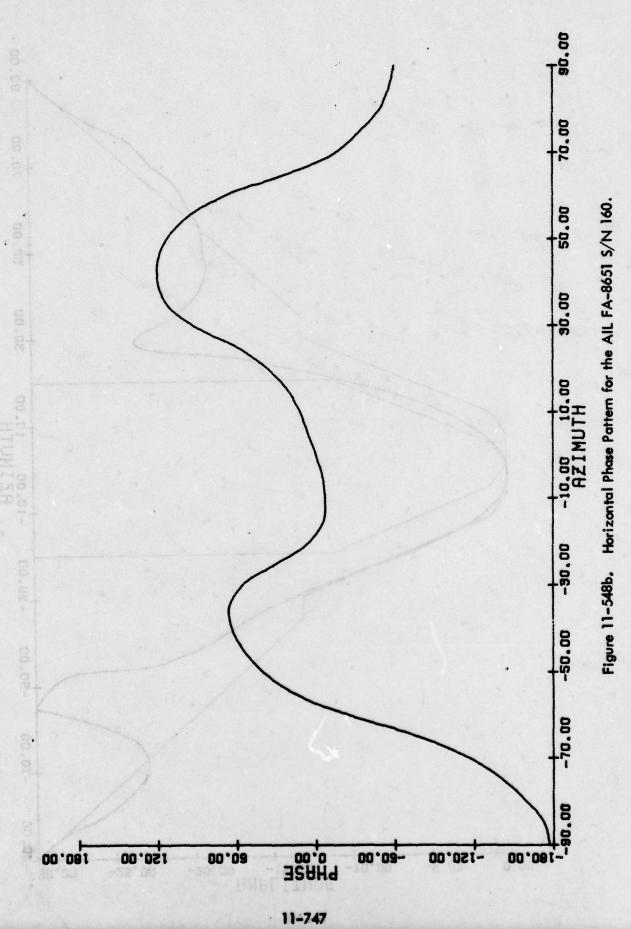


Figure 11-547b. Horizontal Phase Pattern for the AIL FA-8651 S/N 153.





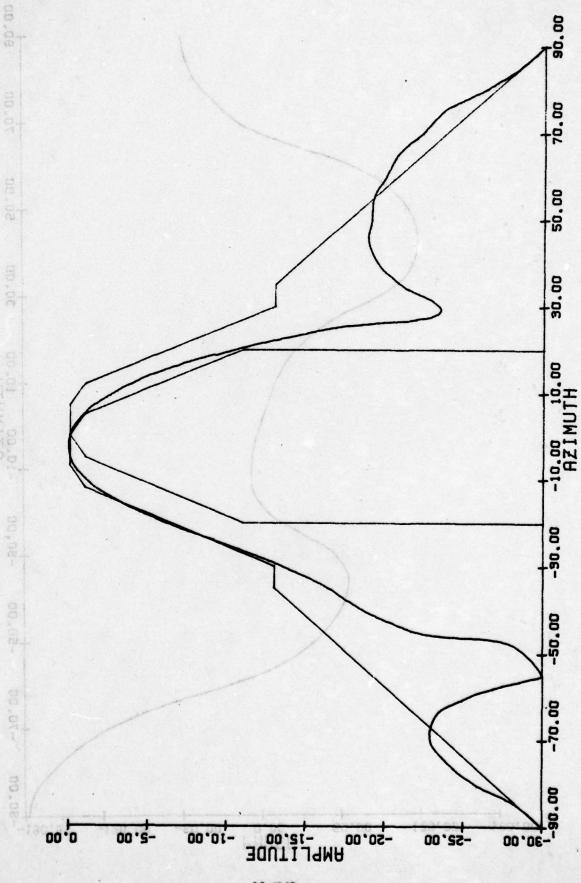
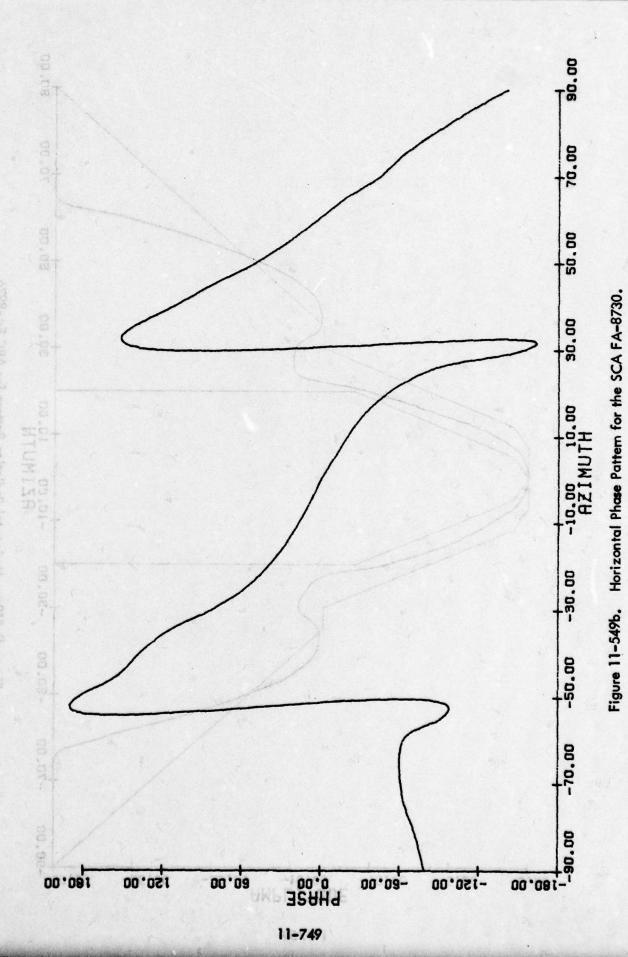
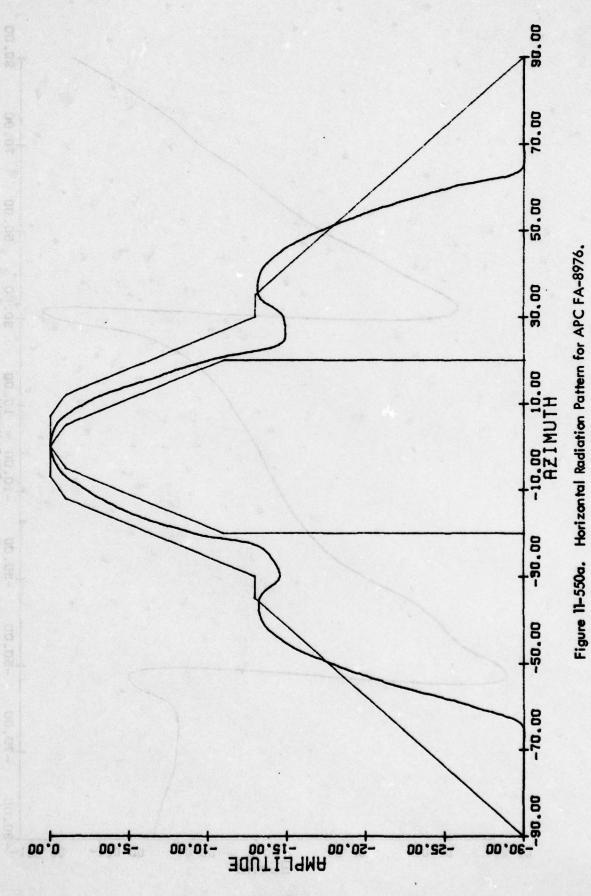
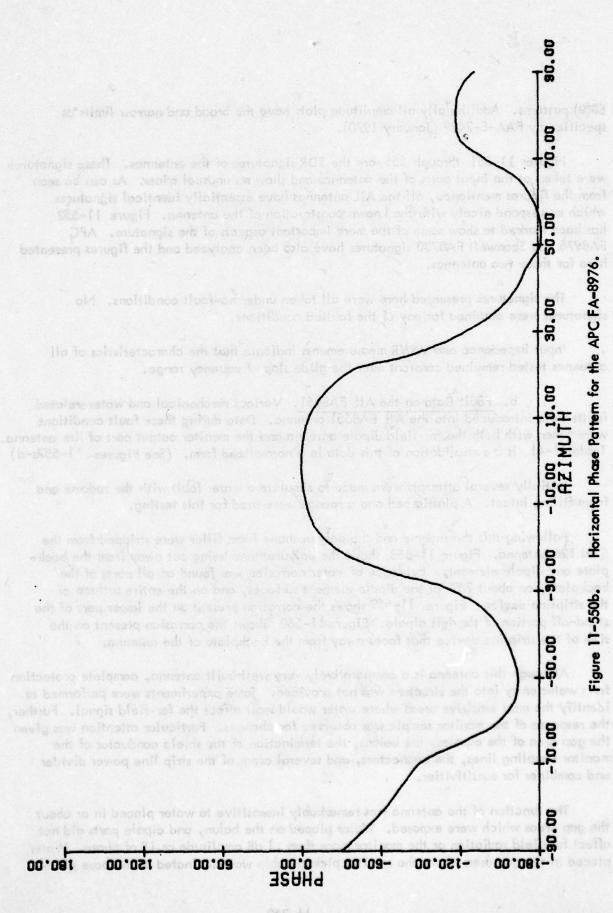


Figure 11-54%. Horizontal Radiation Pattern for SCA FA-8730.





11-750



E9(9) patterns. Additionally all amplitude plots have the broad and narrow limits as specified by FAA-E-2429 (January 1970).

Figures 11-551 through 556 are the TDR signatures of the antennas. These signatures were taken as the input ports of the antennas and show no unusual triats. As can be seen from the figures mentioned, all the AIL antennas have essentially identical signatures which correspond nicely with the known construction of the antenna. Figure 11-552 has been marked to show some of the more important aspects of the signature. APC FA8976 and Scanwell FA8730 signatures have also been analyzed and the figures presented here for those two antennas.

The signatures presented here were all taken under no-fault conditions. No signatures were obtained for any of the faulted conditions.

Input impedance and VSWR measurements indicate that the characteristics of all antennas tested remained constant over the glide slope frequency range.

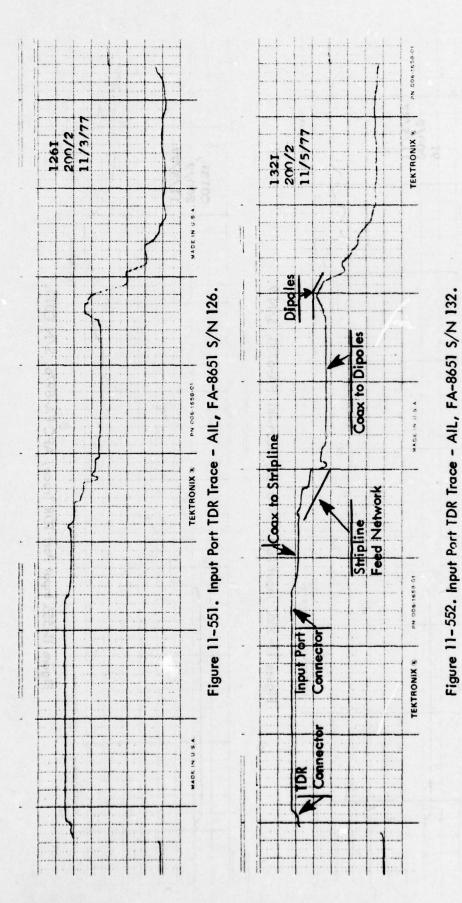
b. Fault Data on the AIL FA8651. Various mechanical and water-related faults were introduced into the AIL FA8651 antenna. Data during these fault conditions were taken with both the far-field dipole antenna and the monitor output port of the antenna. Table 11-41 is a consolidation of this data in a normalized form. (See Figures 11-557a-d)

Initially several attempts were made to simulate a water fault with the radome and foam filling intact. A plastic pad and a sponge were used for this testing.

Following this the radome and the polyurethane foam filler were stripped from the S/N 126 antenna. Figure 11-558 shows the polyurethane being cut away from the backplate and dipole elements. Evidence of water corrosion was found on all parts of the backplate, on about 20% of the dipole element surfaces, and on the entire surface of the stripline device. Figure 11-559 shows the corrosion present on the lower part of the stand-off portion of the left dipole. Figure 11-560 shows the corrosion present on the side of the stripline device that faces away from the backplate of the antenna.

Although this antenna is a comparatively very well-built antenna, complete protection from water entry into the structure was not provided. Some experiments were performed to identify the most sensitive areas where water would most affect the far-field signal. Further, the response of the monitor sample was observed for changes. Particular attention was given the gap area of the dipoles, the baluns, the termination of the shield conductor of the monitor sampling lines, the connectors, and several areas of the strip line power divider and combiner for sensitivities.

The function of the antenna was remarkably insensitive to water placed in or about the gap areas which were exposed. Water placed on the balun, and dipole parts did not affect far-field radiation or the monitor more than .1 dB amplitude or 1° of phase. Water placed in the gap area where the monitor pickup cable was terminated at the base plate



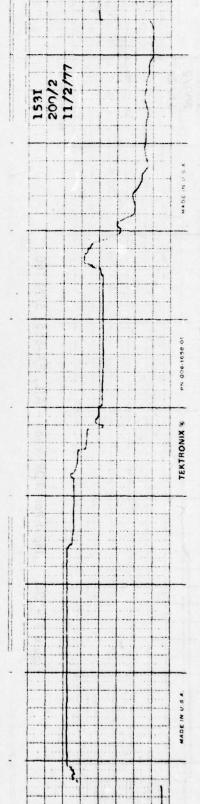
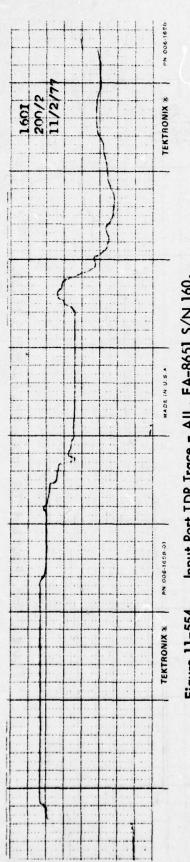


Figure 11-553. Input Port TDR Trace - AIL, FA-8651 S/N 153.



Input Port TDR Trace - AIL, FA-8651 S/N 160. Figure 11-554.

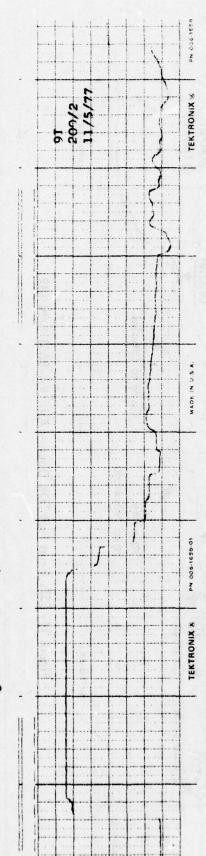


Figure 11-555, Input Port TDR Trace, Scanwell FA-8730, S/N 9.

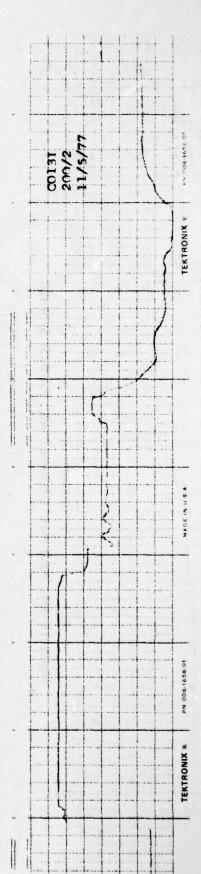


Figure 11-556, Input Port TDR Trace, APC FA-8976, S/N C013.

FAULT	Far-Field Change		Monitor Output Change	
	Amplitude	Phase	Amplitude	Phase
Faults with Radome				
Plastic Bubble Pad Top ¹ Plastic Bubble Pad Front Sponge ²	0 dB 0 0	0 -2.0° 0	0 dB -0.1 0	0 -0.7° 0
Faults without Radome and Poly- urethane Foam Mechanical Faults	io and foldman Appropriation	a o prod ov baves	nde e Vollet e Legit De sof de Legit vollet e	
Right Monitor Discon. Center Dipole Shorted L or R Dipole Shorted Left Monitor Shorted ⁴	0 -4.0° -0.5 0	0 +10.0° -6.0° 0	-3.5 -5.0 -0.8 -0.6	+10.0° +12.6° -3.4° -10.0°
Water Faults on Surfaces				
Plastic Bubble Pad ¹ (3)* Sprayed Water ⁵ (3) Wet Cloth ⁶ (2)	0 0 0	-3.0° 0 0	-0.5 0 0	-1.4° 0 -5°,
Water on the Edge of Stripline Device	centre ed Sha tacks instica to			-10.0°
Water Spray Top Edge (2) WI Top Edge, Bar Loose ⁷ (3) WS Feed Area ⁸ WS Monitor Area (2)	0 -1.4 -0.5	0 -13.0° -5.0°	-0.2 -1.5 -2.2 0	-0.7 -12 -3.5° -2.5°
WI Monitor Area (2) WI Feed Area (3)	0	0	0	-1.0°

^{*} Number in Parenthesis Indicates the Number of Attempts at that Test.

Table 11-41. Normalized Fault Data for AIL FA-8651 S/N 126.

Notes:

- 1. The plastic bubble pad used was a piece of plastic, blistered packing material. Water was injected into the individual bubbles with a syringe. Each bubble received 1 cc of water. 64 bubbles in all were injected with water. The 64 bubbles made up an area 24" x 4.5". This pad was then either taped to the front or top of the radome, or wrapped around the dipole as the appropriate fault description indicates. Figure 11-557a shows one of the bubble pad tests.
- 2. The sponge used was $5" \times 3" \times 1"$ and was soaked with water. The sponge was laid atop the radome.
- 3. The dipole was shorted by placing an N connector across the dipole near the feed point. This is shown in Figure 11-557b.
- 4. Monitor pick-up point was shorted with a test lead to the backplate.
- 5. Figure 11-557c shows the elements of one of the dipoles being sprayed. Even though for all the sprayed water tests enough water was applied to begin to drip off the area being tested, no effects were seen either at the air field or the monitor port output.
- 6. The wet cloth was a piece of 1/2" x 1" material thoroughly soaked and placed right at the monitor pick-off point of the center dipole.
- 7. W1 = Water Injection. Typically 4 cc of water was injected using a hypodermic syringe. Little of the 4 cc of water actually entered the stripline due to the obvious difficulty of forcing water between epoxy board layers. In this particular test one of the bars used in the construction of the stripline case was loosened somewhat. It should be noted that this bar was found to be loose to approximately the same extent when the antenna was disassembled. Figure 11-557d shows water being injected into the feed area.
- 8. WS = Water Spray. This means that the area mentioned for the test was either sprayed with water (until water collected on the surface) or water was poured on the area.

Table 11-41. (Continued).

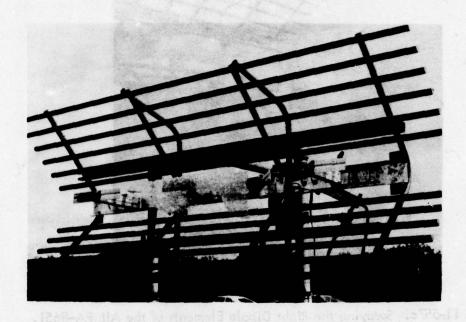


Figure 11-557a. "Bubble Pad" Wrapped Around the Center Dipole of the AIL FA-8651 Glide Slope Antenna.

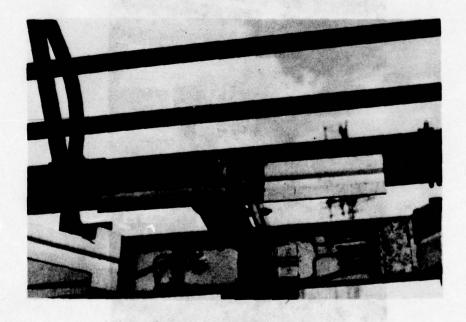


Figure 11-557b. Shorted Center Dipole Test of the AIL FA-8651.



Figure 11-557c. Spraying the Right Dipole Elements of the AIL FA-8651.

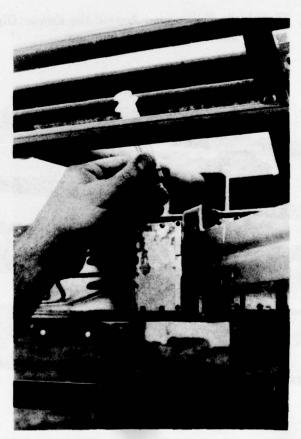


Figure 11-557d. Injection of Water in the Feed Area of the Stripline of the AIL FA-8651.



Figure 11-558. Polyurethane Foam Being Cut Away.



Figure 11-559. Water Corrosion on the Left Dipole of the FA-8651.

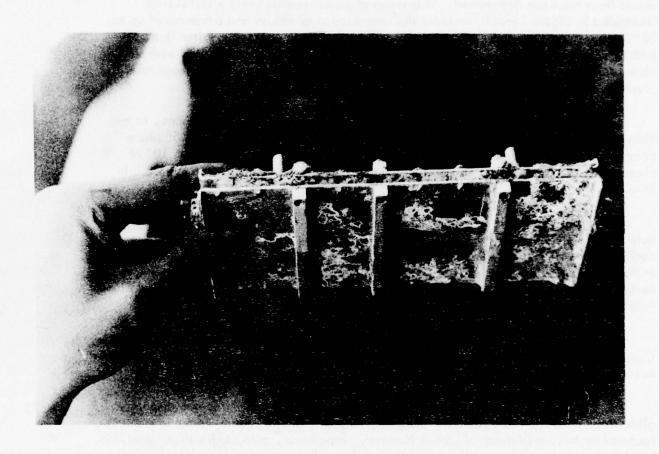


Figure 11-560. Corrosion on the Stripline Device.

did produce noticeable phase changes of 10° but only in the monitor circuits. The far field was unaffected. Water sprayed onto the exposed structure did not significantly affect the antenna operation.

5. Correlation of Signal Samples with Monitor Response. The AIL Mark 1B monitor response to various phase and amplitude faults introduced into the monitor RF return lines has been determined. This series of measurements using a test set-up illustrated in Figure 11-561 includes the introduction of delays and advances of up to 20° in phase and 1 dB and 2 dB attenuations into the lower antenna monitor line. The middle antenna monitor line of the capture effect configuration was faulted with similar phase delays and advances. Tables 11-42 and 11-43 show the results of those tests given in percentage of width alarm.

Further testing showed that combined faults were additive. For instance, combined faults in the lower antenna monitor line of 1 dB of attenuation and a 5° phase delay gave a width indication of 494% of alarm. The same attenuation with 10° of phase delay indicated 538% of alarm. In both cases the monitor was also 3.0 dB into RF alarm.

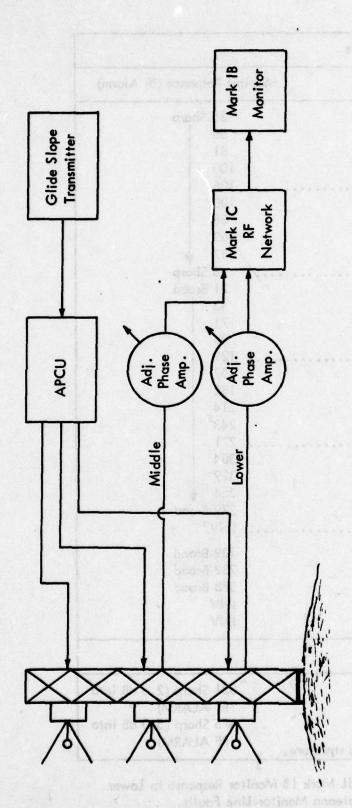
Estimates of the AIL Mark 1B monitor response to various changes in the monitor output port signal of the lower and center antenna in the capture-effect glide slope configuration using the FA8651 antennas can be made with a knowledge of the change in the magnitude and phase of that RF signal. Fault data, e.g., amplitude and phase perturbations, such as appear in Table 11-41, can be translated to percentage of alarm (width) by referring to Tables 11-42 and 11-43.

It should be clearly recognized that this monitor response is not analog in character Correspondence of alarm values with complex RF signal values coming to the monitor must not be expected.

6. Summary. An investigation of the characteristics of three contemporary glide slope antennas has been completed with emphasis on the FA8651 antenna manufactured by AIL, a Division of Cutler Hammer. Impedance, gain, azimuth patterns, bandwidth, monitor port sampling, and time domain characteristics have been experimentally determined. Additionally the FA8651 has been studied under faulted conditions with a Mark 1B monitoring system in operation.

Of particular interest for the FA8651 has been the integral monitor pickup response to specific faults and the Mark 1B monitor interpretation of these pickup signal changes in terms of indicated path-width condition. The tests showed that faults with the antenna element themselves were observable at the pickup output port essentially in analog form compared to the far field; faults in the distribution feed portion of the stripline were also observable in analog form, but faults with the recombining portion of the stripline unit were seen only in pickup sample signals.

Each of the three types of antennas is capable of performing satisfactorily in the presence of incident and residual water on the radomes and external conducting surfaces.



Port, and Possibly at the Input Port. To determine the correlation between capture effect array configuration. The amplitude and phase of the middle Expected to be Evident in the Far-Field Radiation, the Antenna's Monitor and lower antenna monitor lines were then incremented through a range to the monitor port signal and the AIL Mark 1B monitor response, three APC FA-8976 glide slope antennas were installed and operated normally in a A Perturbational Influence Impacting the Glide Slope Antenna May Be obtain the monitor response. Figure 11-561.

Lower Antenna Faults			
Phase Faults (°)	Monitor Response (% Alarm)		
-2	25 Sharp		
-4	50		
-6	81		
-8	100		
-10	106		
-12	100		
-14	88		
-16	69		
-18	37		
-20	6 Sharp		
-22	21 Broad		
-24	43		
-26	71		
-28	96		
-30	129		
-32	157		
-34	182		
-36	214		
-38	243		
-40	271		
-42	304		
-44	329		
-46	354		
-48	379 Broad		
-50	INV*		
+10	139 Broad		
+20	282 Broad		
+30	378 Broad		
+40	INV		
+50	INV		
Attenuation Faults			
1.0 dB	331 Sharp (2.5 dB into		
2.0 dB	RF ALARM) 675 Sharp (5.0 dB into		
	DE ALADAM		
INV denotes inverted struct	ure.		

Table 11-42. AIL Mark 1B Monitor Response to Lower Antenna Monitor Line Faults.

Middle Antenna Faults			
Phase Faults (°) Monitor Response (% Alarm)			
-2	19 Sharp		
81-41 or Vicent epison sons	19 Sharp		
in acceptable that 6-m			
Re-Basila through modificals	7 Broad		
-10	25		
-12	46		
to -14 diseases made even a			
-16			
-18	125 OCTSA-1 bril 123		
-20	154		
-22 was total box wald	of and and 179		
-24	211		
-26	243		
-28	275		
-30	300		
-32	329		
-34 has result on the firm but	nonabilism 357		
-36			
-38 as vibratal ad bas	chample of INV*		
-40	INV		
-42	INV. are an extra floring and		
-44	INV in a select the brack that		
-46	INV		
-48	INV		
-50	Manual of the INV and an address of the control		
+10	nimethal evidence and thearetical confide		
100	1/0 0		
+20	160 Broad		
+30	275 Broad		
+40	375 Broad		
+50	INV		

alle Walls

Table 11-43. AIL Mark 1B Monitor Response to Middle Antenna Monitor Line Faults.

The use of foam materials within radomes, while providing mechanical support, does not provide for critical seals against entry of moisture. With respect to the FA8651 temperature changes apparently open seams in the radome thus allowing moisture to travel by capillary action into critical locations such as the stripline distribution and recombining unit.

SWR values were variable among the antenna specimens from 1.15 to 1.9:1 thus suggesting that a specification should be written that would indicate the maximum allowable value.

Gain of these corner reflector type antennas range from 7 to 10 dB over a one-half wavelength dipole. Azimuth patterns are within acceptable limits. Time domain signatures are straightforward and provide a reference for significant fault observation. Bandwidth characteristics are excellent.

7. Conclusions. Several conclusions have been drawn based on the experimental work performed using the three corner reflector-type antennas; viz, the FA8976, FA8651, and FA8730.

The APC FA8976 antenna offers the simplest and least expensive construction and its design using plastic coverings over the critical feed portions makes use of plastic shields and gravity to prevent water from entering critical areas. The monitor sample, although coming from a non-50 ohm port, does adequately represent changes in the radiated signal.

The AIL FA8651 represents a well-designed antenna from an electrical viewpoint; however, the performance of the antenna also depends on the construction of the foam filling, the space about the antenna elements and the integrity of the weather seal for proper operation. Disassembly of a sample antenna taken from service at Walla Walla, Washington indicates the seal is not always maintained and that water had entered the baseplate and stripline regions, this latter being a most critical region. Two results can occur.

First, moisture in the distribution portion can affect the far-field phase and amplitude. Experimental evidence and theoretical considerations show that this is observable in a near analog manner at the monitor sample port on the antenna. Second, the moisture can affect just the recombining portion of the stripline unit thus causing a disturbance at the monitor port with no evidence of far-field change. As a consequence of this latter, it is reasonable to expect that there will be monitor changes that are unaccompanied by far-field change.

Soaking the medium surrounding the area where the monitor coaxial line shield is terminated in the FA8651 produces significant response at the monitor port. Water injected around the feed points of the dipole have minimal effect on the monitor and the far field.

The antenna performance seems remarkably stable with water directly on the elements. The urethane foam material immediately surrounding the FA8651 antenna elements rejects water injected directly into the foam. Water will rest on the foam surface without penetration. Foam soaked in water will absorb about 75 milligrams of moisture per cc of material. Capillary action occurring between the foam surface and the metallic surfaces appears to be prevalent and leads to problems with the internal stripline device which is not sealed well.

Seals, therefore, become a crucial item in determining long-term characteristics of a given antenna. Designs which minimize the lengths of gaps that must be sealed, which make maximum use of gravity to protect vulnerable areas, which offer greatest rigidity of support for gaps to be sealed and which provide materials with similar coefficients of expansion are regarded as superior.

Water collecting on the outside of the radome and collections of water in amounts greater than moisture content of snow clearly do not degrade antenna performance. The radome provides an effective standoff for foreign materials.

FAA experience tends to indicate that operational problems using the FA8651 antennas occur most often at sites where large daily or seasonal temperature variations are experienced. Materials used in the antennas are known to have different coefficients of expansion; therefore, seals may be expected to open and materials crack thus allowing for penetration of moisture.

8. Recommendations.

- (1) Very careful consideration must be given to preventing moisture from entering critical antenna components such as stripline distribution units and other regions where high electromagnetic field stress is present. Maximum use of gravity should be made to eliminate entry of moisture.
- (2) Areas to be sealed should be rigidly supported and of materials with similar coefficients of expansion.
 - (3) Foam materials must not be used for seals.
- (4) Signal samples should be processed to form an analog of glide slope far-field conditions. This would, in the case of the Mark 1B necessitate a significant but rather simple, inexpensive change in sample signal collection; viz, obtaining the processing of signal from the upper antenna in the capture-effect array.
- (5) A study should be made of the non-analog monitor as it is used in the Mark 1B and other similar systems. The relevance of non-cancellation of the clearance signal to monitoring should be ascertained. Presently the monitoring of width is a function of clearance power level and anomalous monitoring conditions conceivably can occur.
- (6) Additional work is recommended to identify the specific mechanisms causing monitor sample signal perturbation with water in and around the FA8651 stripline device.

L. Minimum Site Preparation for an Image Glide Slope.

1. Introduction. The motivation for this section comes from the need to have airport designers specify minimum terrain modification consistent with providing an acceptable glide slope signal in space and avoid over-specification and unnecessary costs. A site without overdesign will obviously counter many of the claims offered by proponents of microwave systems that contemporary glide slope systems are impossible or too expensive to obtain at many desired locations. The following discussion leads to a step-by-step calculation of cost savings at a generalized, problem site. The most recently available technical information is utilized to work towards an absolute minimum of site preparation. The intent, in part, is to be instructive for airport designers.

There are a number of instrument landing system glide slope sites existing today in the United States where at least \$100,000 could have been saved in site preparation costs if all existing ILS technology had been applied in the design of the site. A major purpose of this section is to provide a more general dissemination of some technical facts which, if applied to problem glide slope sites in the planning stages, can result in substantial savings to the local airport sponsor and the federal government which generally is involved with matching funds.

With but very few exceptions, the more than 500 U.S. ILS glide slope facilities operating in 1975 are of the image type. This means that the essential signal in space provided for the user aircraft comes in part via a reflection from the earth. Theoretical considerations for an image glide slope typically involve assumptions of a flat, smooth, perfectly-conducting ground for the reflecting surface. It is logical, therefore, that many specifications used by designers allow but slight deviations from this ideal. In fact, the allowable limits for the most part have never been determined, with the result being over-specification. It certainly should be clear to most readers that this over-specification can and does lead to excessive and unnecessary costs in preparing an image glide-slope site. These costs come basically and usually from the apparent need to move earth to construct a large level area adjacent to the runway for a reflecting plane serving the glide slope. A review of records of costs for site preparations clearly indicates why many people have come to regard the glide slope as an expensive landing aid; and in certain cases, some conclude it is not justified in spite of its important contribution to safety of aircraft landing operations.

An investigation of more than 22 glide slope facilities has been accomplished in part by visits to the site, and the comments, conclusions, and recommendations of this section are based on this work. The intent is to provide information which will permit image glide slope siting at reasonable cost in spite of limitation in quality of real estate. Present costs are excessive, unnecessary, and increasingly intolerable. National financial resources can better be applied to other aviation requirements such as an increase in the number of facilities and visual aids such as VASIs.

2. General Case. In order to provide the reader with some detailed insight into the conditions which have motivated engineers and planners to expend the large sums of

money for image glide slope sites, a generalized hypothetical case is described. This is, in effect, a composite of the conditions commonly found at so-called difficult sites. The proposed collective modifications have not been experimentally checked and this should be done to ascertain the interaction or dependency. The composite of all modifications is presented to illustrate the principles.

Reference is made to Figures 11-562 and 563. Commonly an airport is encouraged or forced to extend the length of its instrument runway to permit high performance jet aircraft to operate satisfactorily. Since the desired touchdown region on the runway is located approximately 1000 feet inside the threshold, this constrains the glide slope placement to be approximately abeam this 1000-foot region. This placement is thus in a location which is typically requiring extensive fill, for airport runway extensions most often require building up an area rather than cutting. The probability is low that cutting of a hill is required since this hill would have been an obstruction and would have likely eliminated consideration of construction of the runway initially. Frequently then, earth fill is not only required for the runway and protecting shoulders but is necessary for an area to serve the glide slope. Figure 11-562 would suggest that as much as 10 acres of flat surface would be prepared for image glide slope operation. Equating this in dollars can be done as follows. For a fill of an area 1250 feet by 200 feet which represents the excess for the glide slope over just the runway and berm preparation and assuming an average 25-foot deep fill, cost based on a \$1.00 per cubic yard charge is \$231,481 (see Figure 11-560). Certainly some sites might be less, but there are many which have cost more and this is used as a typical case for rolling or hilly country. One should note that new sites being installed at this point in history are probably going to require more preparation and greater costs since the easy sites have been taken in years past and inflation seems to be a continuing trend.

A planner, therefore, currently evaluates the need for a glide slope against such site preparation charges. It is understandable that many negative decisions are made on glide slope installations.

3. Engineering for Minimum Costs. The engineer in our contemporary society must be cost-conscious to be truly effective. Too often in the past, perhaps because government matching funds were available, the proverbial pencil was not sharpened and higher than necessary costs were incurred. Importantly, though, specifications promulgated by the FAA have not always reflected the optimum values when recognizing tradeoffs between the ideal and a practical, cost-effective installation.

First, airborne performance requirements have not until recently been quantified in a scientific manner. [15] Because of this, signal in space requirements and tolerances and set using a valid technical base. As a result, to be safe, a very conservative and has been used in establishing criteria of acceptability for glide slope performance. The past 5 years; unfortunately, these have not been used yet to relax criteria and preparing image glide slope sites. This results in over-specification.

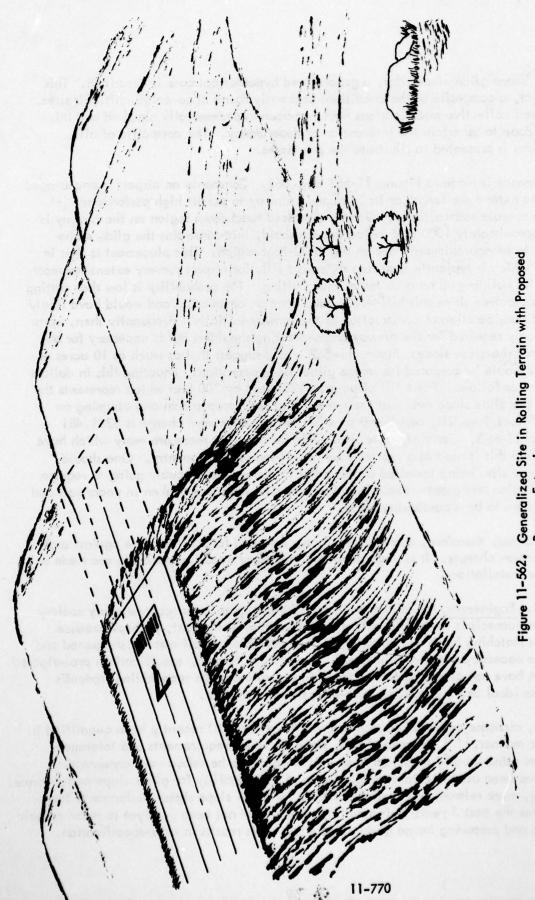
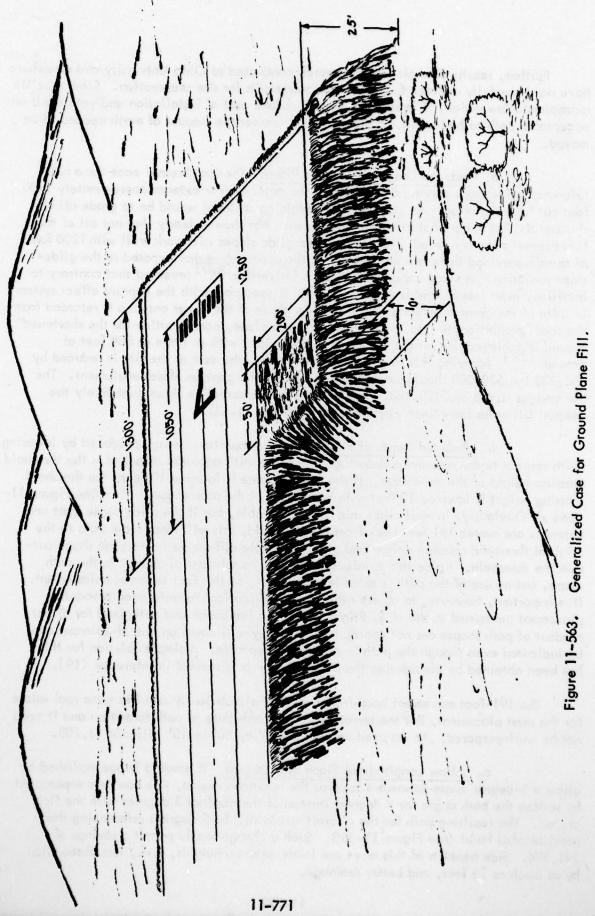


Figure 11–562. Generalized Site in Rolling Terrain with Proposed Runway Extension.



Further, results of engineering research conducted at Ohio University and elsewhere have not been fully utilized for relaxing requirements for site preparation. Some specific examples follow which, if implemented, will reduce cost of installation and yet permit an acceptable path to be formed. Basically each reduces the amount of earth needed to be moved.

- a. Reduced Length of Ground Plane. The first Fresnel zone for a null reference glide slope serving an aircraft at the outer marker extends approximately 1900 feet out from the array. An approach for obtaining an ideal would be to grade all of this terrai. Flat out to that distance. Experience has shown clearly that not all of the first Fresnel zone is needed. Null reference glide slopes will work well with 1200 feet of terrain provided there are no upslopes in the approach region exposed to the glide-slope radiation. A study conducted at Ohio University 10,17 revealed that contrary to intuition, even less ground is required to form a good path with the capture effect system in spite of the greater antenna height. If the phase of the upper antenna is retarded from the ideal proportionate to the shortened ground plane, compensation for the shortened ground is achieved and a satisfactory path is obtained with as little as 800 feet of ground. [18] Applying this to our generalized case, the cost of the site is reduced by \$83,333,but \$30,000 should be added to allow for the capture effect equipment. The net savings would be \$178,148. This is believed conservative since most likely the deepest fill areas have been eliminated (see Table 11-44).
- b. Reduced Depth of Fill. The only important change produced by lowering (with respect to the runway) a smooth ground plane with antennas attached is the threshold crossing height of the on-course. If the ground plane is lowered 10 feet, the threshold crossing height is lowered 10 feet with no change in the path shape. [19] (See Figure 11-564.) Obviously, in most cases this is unacceptable, but if the glide slope mast and antennas are moved 191 feet back from the threshold, this will restore the path to the original threshold crossing height and give negligible difference in the path shape outside the threshold. Inside the threshold there will be substantial change in the path shape, but no use of the path is made in this region, so this fact becomes unimportant. It is important, however, to observe that the specifications for reference theodolite placement contained in the U.S. Flight Inspection Handbook and optimized for direct readout of path shapes are not appropriate, for they will cause an out-of-tolerance to be indicated even though the path in space is acceptable. A simple solution for this has been obtained by considering the pedestal case as discussed in reference [19].

The 191-foot movement back from the threshold obviously requires some real estate for the mast placement, but the terrain does not contribute to path formation and it need not be well-prepared. An assumed volume of 200° by 50° by 10° will cost \$3,703.

c. Allow Longitudinal Slope of 1 Degree. If grading is accomplished to allow a 1-degree slope downward towards the approach region, this can be compensated by setting the path angle for 4 degrees instead of the nominal 3 degrees with the flat ground. The resulting path for the aircraft would still be 3 degrees referencing the gravitational level (see Figure 11-565). Such a change would permit a savings of \$41,374. Side benefits of this move are lower antenna heights, i.e., less obstruction by as much as 15 feet, and better drainage.

3 9 6	Savings	Cost	Balance
Total Fill		\$231,481	
Reduce Length of Ground Plane to 800°	\$83,333	300	\$148,148
Convert to Capture Effect		\$ 30,000	\$178,148
Lower Remaining Ground Plane 10	\$59,259		\$118,889
Build Platform for Mast		\$ 3,703	\$122,592
Allow Longitudinal Slope of 1°	\$41,374		\$ 81,218
Allow Transverse Slope of 2.5°	\$14,814		\$ 66,404

Table 11-44. Budget for Reducing Fill.

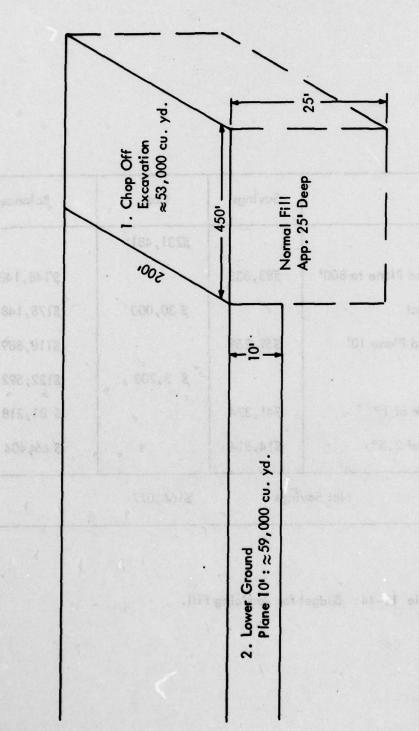
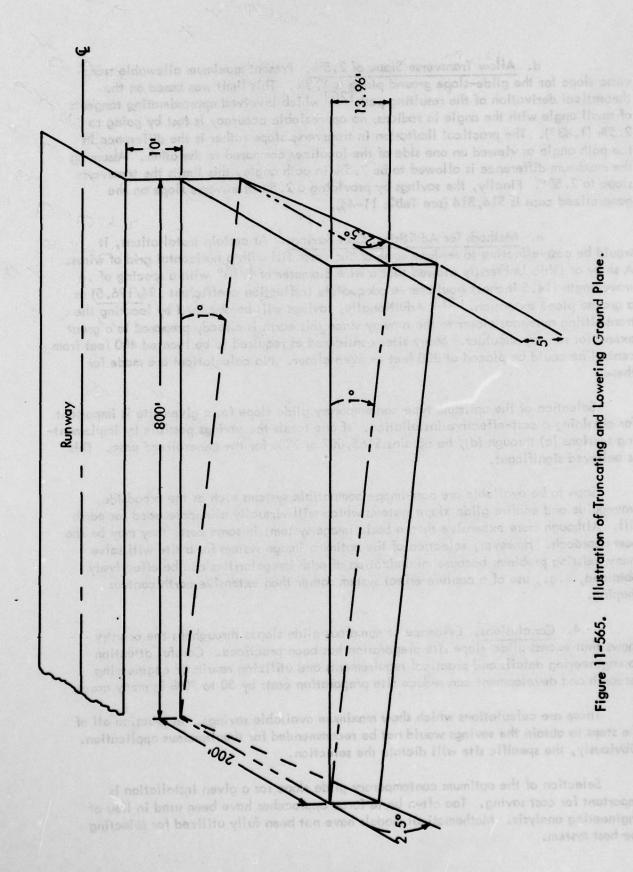


Figure 11-564. Illustration of Truncated and Lowering Ground Plane.



9 Illustration

- d. Allow Transverse Slope of 2.5%. Present maximum allowable transverse slope for the glide-slope ground plane is 1.5%. This limit was based on the theoretical derivation of the resulting path [20] which involved approximating tangents of small angle with the angle in radians; no appreciable accuracy is lost by going to 2.5% (1.43°). The practical limitation in transverse slope rather is the difference in the path angle as viewed on one side of the localizer compared to the other. Assuming the maximum difference is allowed to be 7.5% in path angle, this limits the transverse slope to 2.58°. Finally, the savings by providing a 2.5% transverse slope on the generalized case is \$14,814 (see Table 11-44).
- e. Methods for Additional Cost Savings. At certain installations, it would be cost-effective to replace some of the earth fill with a horizontal grid of wires. A study at Ohio University showed that a wire diameter of 1/16" with a spacing of .4 wavelength (14.5 inches) would serve adequately (reflection coefficient .94/196.5) as a ground plane extension. [21] Additionally, savings will be obtained by locating the transmitting antennas closer to the runway since this earth is already prepared to a great extent for runway shoulder. Many sites considered as required to be located 400 feet from centerline could be placed at 300 feet or even closer. No calculations are made for these.

Selection of the optimum type contemporary glide slope for a given site is important for obtaining a cost-effective installation. If one totals the savings possible by implementing sections (a) through (d), he obtains \$165,007 or 71% for the generalized case. This is believed significant.

Soon to be available are non-image compatible systems such as the broadside, waveguide and endfire glide slope systems which will virtually eliminate need for earth fill. Although more expensive than a basic image system, in some cases they may be the best approach. However, selection of the optimum image system for a site will solve many existing problems because minimization of path irregularities can be effectively obtained, e.g., use of a capture-effect system rather than extensive earth contour shaping.

4. Conclusions. Evidence at numerous glide slopes throughout the country shows that excess glide slope site preparation has been practiced. Careful attention to engineering details and practical requirements and utilizing results of engineering research and development can reduce site preparation costs by 50 to 70% in many cases.

These are calculations which show maximum available savings. In practice all of the steps to obtain the savings would not be recommended for simultaneous application. Obviously, the specific site will dictate the selection.

Selection of the optimum contemporary glide slope for a given installation is important for cost saving. Too often brute force approaches have been used in lieu of engineering analysis. Mathematical models have not been fully utilized for selecting the best system.

Specifications for site preparations currently do not reflect recent engineering advances in ILS technology. FAA specifications as they stand do not show compatibility between what is required for the signal in space and what is required in ground preparation to give those signals. The grading is based on much more stringent signal conditions than currently required.

Costs of some glide slope installations have indicated extravagance when it comes to earth fill in particular. This cannot be tolerated for it can only ultimately result in less availability and reduced safety for the flying public.

5. Recommendations. The FAA should review its specifications for glide slope sites and modify these to reflect current state-of-the-art ILS technology and provide for the most cost-effective installation. Compatibility of all requirements should be insured. Additionally, the FAA should see that these are promulgated to the appropriate areas so that the airport design engineer obtains the information at the earliest possible time.

The FAA should investigate and determine on a scientific basis the minimum distance which antenna masts may be placed with respect to the runway. Also, frangible low mass structures should be developed to enhance safety.

MILL O. A. . cos R. H. McFarland, MThe Effects of Irregulat Contour on theans

Sitting Criteria for Instrugent Landing Systems, Department of Transpositations

Walter, C.H., Traveling Wate Antennas, Dover Publications, Inc., New York,

tilldebrond, Introduction to Numerical Analysis, McGrow-Hill Stok Company.

Vector Voltacias 2405 A Operating and Service Manual, Hewlett-Packard.

Kraus, Antsong, McCarov-Hill, 1200, pp. 461-166.

"Instrument Landing In provement Program, FAA-RD-73-137, Avients Engineering

M. References for Section XI.

- [1] "Preliminary Instructions Two-Antenna End-Fire Glide Slope Array," Section 6.4, Monitor Alarm Limit Setup, Watts Prototype Company, 5615 Vine Street, Alexandria, Virginia 22310.
- [2] U.S. Flight Inspection Manual, OAP-8200.1, Chg. 17, 8/26/70, Section 217.33142(2), p. 217-17.
- [3] Watts, C.B. Jr., "Description of the Endfire Slotted Cable Glide Slope Medium Aperture," Watts Prototype Company, 5615 Vine Street, Alexandria, Virginia 22310, January 1977.
- [4] Bottoms, T.H., H.C. Hurley, L.N. Spinner and J.W. Watt, "A Directional Glide Path," Technical Development Report 336, CAA, Technical Development Center, Indianapolis, Indiana, February 1958.
- [5] McFarland, R.H., "A Flush-Mounted Glide-Path System", IRE Transactions on Aerospace and Navigational Electronics, Vol. ANE-9, Number 4, December, 1962.
- [6] Hill, D.A., and R. H. McFarland, "The Effects of Irregular Contour on Image Glide-Path Systems," Avionics Research Group, Ohio University, Report EER 5-4, September, 1966, pp. 5-31.
- "Instrument Landing System Improvement Program," RD 72-71, Avionics Engineering Center, Ohio University, Athens, Ohio, June, 1972, p. 20.
- [8] Siting Criteria for Instrument Landing Systems, Department of Transportation, Version 67.50.16A, August, 1973, p. 52.
- [9] Kraus, Antennas, McGraw-Hill, 1950, pp. 461-464.
- [10] Walter, C.H., <u>Traveling Wave Antennas</u>, Dover Publications, Inc., New York, 1970.
- [11] Hildebrand, Introduction to Numerical Analysis, McGraw-Hill Book Company.
- [12] Antennas and Radiation Patterns, Manual FV-108-1, Catalogue No. 40203/40204, Department of Transportation, July, 1975.
- [13] Vector Voltmeter 8405 A Operating and Service Manual, Hewlett-Packard, 1501 Page Mill Road, Palo Alto, California.
- [14] "Instrument Landing Improvement Program, FAA-RD-73-137, Avionics Engineering Center, Ohio University, Athens, Ohio, May, 1973, p. 45.

- [15] Hofmann, Lee, Warren F. Clement, Dunstan Graham, Gary L. Teper, Bryon L. Wiscons, David L. Hemmel, Richard H. McFarland, "ILS Glide Slope Standards, Part 1: A Review of Flight Inspection Standards Affecting Landing Performance and Comparison with Limits Evolved from System Analysis," June, 1975.
- [16] Op. cit., RD-72-71, pp. 170-192.
- [17] Op. cit., RD-73-137, pp. 60-75.
- [18] Op. cit., RD-72-71, pp. 60-75.
- [19] Ibid, RD-72-71, pp. 14-29.

XII. INVESTIGATORS AND ACKNOWLEDGEMENTS

This final report has given details of a multifaceted work effort performed by many people nearly all of whom were staff members of the Avionics Engineering Center, Department of Electrical Engineering, College of Engineering and Technology, Ohio University, Athens, Ohio. This team effort has involved personnel at all levels from student interns to faculty and post doctoral personnel. The purpose of this section is to name the contributors, thus providing professional recognition and identifying responsibilities for given sections of work.

In the conduct of the various work efforts many contributions have been received from various sources of the FAA, e.g., the Washington Office, Regional Offices, some Aeronautical Center personnel, and NAFEC flight check teams. Sincere appreciation is expressed for these contributions.

Following are given the names of the investigators who served as principal authors for the reporting of the work.

- Dr. Richard H. McFarland served as project director for all work under this contract. He was personally involved with the data collection monitoring and other efforts for evaluating the Watts Slotted Cable Endfire Arrays at Tamiami, and Rock Springs Wyoming. He participated in and reported results from evaluations of the Alford 14/6 localizer array and the Hollins-Watts slotted cable localizers. Also, he developed criteria for classifying flight check records, developed the capability for obtaining quality flight data using low cost airborne equipment, and suggested minimum grading for poor glide slope sites.
- Dr. Robert W. Lilley supervised and participated in the work which yielded demonstrations of devices to provide range and range-rate information from the localizer, precision location over the marker beacon stations, and touchdown zone wind. He has been assisted in these efforts by Messrs. David Herold and Paul Blasche. He also was the major contributor to the investigation of presentation of remote monitor data for control and display. He served as editor for this report.
- Dr. Robert Rondini performed considerable work on evaluation of the slotted cable localizer and investigation of monitoring of the slotted cable glide slope through the use of specific fault checks.
- Mr. Harry Hooghkirk was responsible for establishing the Tamiami test site and participated in the evaluation of the Alford 14/6 localizer array.
- Professor G.E. Smith edited portions of this final report, analyzed and developed a figure of merit for the Alford 14/6 array, analyzed data on fault effects on the capture effect glide slope and its monitors, and investigated the effects of severely limited terrain on glide slope performance.
 - Dr. Raymond Luebbers has supervised the mathematical modeling effort and contributed

extensively to the mathematical work which yielded predictions of glide slope and localizer performance when affected by the presence of hangars, tides, irregular ground or ships. Further he analyzed effects of carrier sideband leakage into sideband only signal on glide slope performance. He was significantly assisted in this work by Mr. Vichate Ungvichian.

Mr. Kent Chamberlin contributed to the evaluation of the Hollins-Watts slotted cable localizer and the investigation of induction probes for purposes of ascertaining and predicting performance of glide slope arrays. He also participated in data collection and documentation of performance of the Columbus, Ohio, Redbird, Texas, and Addison, Texas, capture-effect glide slope facilities. Finally he was a contributor to the analysis of remote monitoring and display of ILS information.

Mr. George Roth aided in data collection and provided documentary compilations for Tamiami and Lawton, Oklahoma, capture-effect glide slope sites.

Messrs. Edward Boso and Frank Myers developed the computer modeling for the capture-effect system performance in the far-field and at the near-field monitors for the Tamiami site.

Mr. Raymond Croxford designed, fabricated, calibrated, and tested an airborne package for collection of airborne data on the localizers and glide slopes.

Mr. Lawrence Mitchell assisted in the theoretical analysis of glide slope performance when obstructions and imperfect ground planes were present. Also, he provided the design of a 90 Hz phase lock loop and mechanizations for special below path, glide slope monitoring.

Mr. Joe Longworth designed the 90/150 Hz phase measuring device.

Mr. Tran Ban provided the analysis of the Watts slotted cable glide slope theoretical performance in the presence of irregular ground.

Mr. R. Douglas Reeder designed the experiments, collected, and reported the data on the use of the TDR as a tool for non-destructive testing of ILS transmitting systems.

Messrs. Walter Phipps, Aaron Swearingen, Dan Ellis, Richard Zoulek and Ken Davis served as data collection specialists and laboratory technicians.

Report production and administrative support were furnished by Ms. Hope Mills, Mr. Delmar Pullins, Ms. Shirley Wilson and Ms. Roma Beverage, and drafting support by Messrs. John Hayes and William Hoffman.

FAA personnel who have had inputs into this work effort are Mr. H.H. Butts, Mr. Forrest Yetter, Mr. Carl Peterson, Mr. Rial Sloan, Mr. Don MacLeod, Mr. John Alf of the Washington office.

Regional personnel who contributed are Messrs. Micky Lindecker, Richard Corn, Curtis Dove, Richard Seiferth, along with Don Ewing from the Aeronautical Center and Bill Yost from NAFEC.

FAA contractors who assisted were Dr. Clinton Hollins, Dr. Andrew Alford, Mr. Chester Watts, and Mr. Robert Littlepage.

